Tailings beach slope prediction

A thesis submitted in fulfilment

of the requirements for the degree of

Doctor of Philosophy

Tim Fitton

School of Civil, Environmental and Chemical Engineering,

RMIT University

May 2007

Abstract

Tailings (mining waste) disposal is a significant consideration for the mining industry, with the majority of the ore processed in most mining operations ending up as tailings. This creates large volumes of tailings, which must be handled and stored responsibly to avoid potential environmental catastrophes. The most common form of tailings storage facility is the impoundment, where tailings are contained within a basin, with beaches forming around the perimeter of the impoundment and a pond standing in the middle. A relatively new method of tailings storage is to create a 'stack', whereby the tailings solids form a large heap, with the discharge of tailings slurry from the apex of the heap. This method of tailings storage is finding greater popularity as the industry seeks to reduce the amount of water discharged with the tailings, and usually features the discharge of non-segregating tailings slurry that flows turbulently in its own self formed channel down the tailings beach. It is of significant value for mine operators and tailings engineers to be able to predict the shape of the beach that forms in either of these disposal scenarios. The key to being able to do this relies on a method of prediction of the beach slope.

The aim of this work is to develop a method of tailings beach slope prediction for tailings slurries that are sub-aerially discharged from a pipe.

In this thesis a literature review is undertaken, investigating existing methods for the prediction of tailings beach slopes. These methods are validated against relevant industrial and experimental data.

Two separate phases of experimental work have taken place in an effort to investigate tailings deposition behaviour, one at mine sites and the other in a laboratory on a small scale. The methodology and results of this experimental work are presented here.

Three new tailings beach slope prediction models are presented; a simple empirical model enabling quick approximate predictions; an a priori tailings beach slope prediction model based on existing theories of open channel flow, sediment transport and rheology, which is more powerful due to the greater degree of theory in its foundation; and a new semi-empirical model that shares some of the theoretical aspects of the a priori model but offers better predictions due to its empirical calibration to the experimental data.

The experimental results, along with 3 other independently collected sets of relevant industrial and experimental data, are used to validate the beach slope prediction models found in the literature, as well as the new beach slope models presented in this thesis. Statistical evaluation of the performance of all of these models is presented to enable comparison.

Finally, a new beach shape model is presented for the three dimensional geometric forecasting of the beach surface of a tailings stack. Historic tailings discharge data is run through the beach shape model, and the shapes predicted by the model are compared with aerial survey data of a real tailings stack for validation of the shape model. This work not only presents a new method of tailings stack shape prediction, but also a plausible theory for explaining the concavity of tailings beaches. The stack shape model also has the potential to be developed further for the three dimensional modelling of tailings beaches formed in other types of storage facilities, such as impoundments or valleys.

Declaration

I certify that except where due acknowledgement has been made, the work is that of the author alone; the work has not been submitted previously, in whole or in part, to qualify for any other academic award; the content of the thesis is the result of work which has been carried out since the official commencement date of the approved research program; and, any editorial work, paid or unpaid, carried out by a third party is acknowledged.

Tim Fitton

Dedication

I dedicate this work to my parents.

Acknowledgements

I am greatly indebted to Paul Williams for many important reasons, not least of which is his initiation of this research project. Some 20 years ago Paul personally conducted pioneering experimental research into tailings deposition in pursuit of his "holy grail", a method of beach slope prediction. He has since devoted a significant part of his life towards this goal for the good of the mining industry and the environment. Paul and his company, Australian Tailings Consultants, have sponsored this project. He is a proud supporter of tailings research and an expert on the handling and storage of tailings.

I would also like to thank Professor Sati Bhattacharya and Andrew Chryss at RMIT University for their guidance, criticism and supervision of this project. In addition to his significant contribution of academic support, Andrew Chryss has also provided a considerable amount of technical and practical aid to the project, including major input during the experimental aspects of this research.

Anglo Gold Ashanti have provided sponsorship to this research project, both in the form of funding and also in hosting a 5 week experimental campaign at their Sunrise Dam mine site in Western Australia during February and March of 2005.

Wheaton River Minerals also deserves thanks after allowing experimental work to be undertaken at their mine site near Cobar, New South Wales in mid 2004.

During the aforementioned experimental campaigns, significant assistance was provided by certain individuals from Australian Tailings Consultants. I would like to mention Behnam Pirouz, Peter Lam and Alex Walker, who all made valuable contributions. In particular, Behnam Pirouz made a major contribution towards the preparation, design and procurement for the experimental work. Also, thanks goes to Mike Allen from RMIT University for his development of the experimental apparatus.

I would also like to thank Rio Tinto for providing grants for several students to travel to Glasgow, Scotland, to attend the 7th World congress of chemical engineers in mid 2005, amongst which I was fortunate enough to be chosen to represent RMIT University.

I would finally like to thank the Australian Research Council for their support of this APAI linkage project.

Tim Fitton
April 2007

Nomenclature

This list of nomenclature includes symbols that recur throughout the thesis in a number of equations. It does not include symbols that are specific to a particular equation. In such instances where these unique symbols appear, they are defined in the text immediately following the equation.

A	Cross sectional area of flow (m^2)
b	Stream or channel width (m)
C_D	Particle drag coefficient (dimensionless)
C_V	Volumetric concentration (expressed as a fraction)
C_W	Concentration by weight (expressed as a fraction)
D	Pipe diameter (m)
d	Particle diameter, assumed to be d_{50} if not specified (m)
d_{50}	50^{th} percentile particle diameter (m)
d_{85}	85^{th} percentile particle diameter (m)
f_D	Darcy friction factor, sometimes referred to as the Weisbach friction factor (dimensionless)
Fr	Froude number (dimensionless)
g	Acceleration due to gravity (m/s^2)
H	Overall height of a tailings beach (m)
i	Tailings beach slope, equal to the vertical rise / horizontal run (fraction, but normally presented as a percentage)
K	Consistency index fitted to rheogram for the application of a rheological model ($Pa.s^n$)
K_{BP}	Bingham plastic viscosity (Pa.s)
k_s	Bed roughness from the Colebrook-White equation (m)
L	Overall horizontal length of a tailings beach (m)
n	Power used in the application of a rheological model (dimensionless)
n	Roughness coefficient from the Manning equation ($s/m^{1/3}$)
P	Wetted perimeter of channel cross section (m)
Q	Flow rate (m^3/s)
q	Specific flow rate, equal to Q / b. (m^2/s)
Re	Reynolds' Number (dimensionless)
Re_{HB}	Reynolds' Number for a Herschel Bulkley fluid
R_H	Hydraulic radius, equal to A / P (m)
S	Specific gravity of tailings slurry (g/cc)
S_0	Channel bed slope, assuming uniform flow conditions (expressed as a fraction)
s	Ratio of density of solid particles to density of carrier fluid
V	Mean velocity of flow, equal to Q /A (m/s)
V_C	Minimum transport velocity (m/s)
V_s	Settling velocity of a single particle in static carrier fluid (m/s)
x	horizontal distance from discharge point (m)
y	vertical distance from the lowest point on a beach (m)
y	depth of flow (m)
$\dot{\gamma}$	Shear rate applied to a fluid (1/s)
δ	Layer thickness (m)

θ	Angle of repose of a slurry (radian)
μ	Viscosity of a fluid (Pa.s)
ν	Kinematic viscosity of a fluid (m^2/s)
ρ	Density of a fluid, assumed to be slurry density without subscript (kg/m^3)
ρ_l	Density of carrier fluid in a slurry (kg/m^3)
ρ_s	Density of solid particles (kg/m^3)
ρ_m	Density of carrier medium fluid (kg/m^3)
τ	Shear stress (Pa)
τ_y	Yield stress of a non-Newtonian fluid (Pa)

Contents

List of figures

List of Tables

Chapter 1: Introduction

1.1 Background

1.1.1 Tailings production and disposal

Tailings are the leftover rock or soil particles that are discarded from a mining operation after the desired mineral has been extracted. Tailings are also referred to by several other names including tails, tailing, slime, slickens and gangue. A typical commercial mine may produce anywhere from half a million to 40 million tonnes of tailings each year. To give some indication of the scale of current tailings production, Anglogold Ashanti, currently one of the world's largest mining companies, currently has interests in 2 mines in Australia; Sunrise Dam and Boddington. Both are gold mines, with Sunrise Dam producing over 3 million tonnes of tailings last year and Boddington expected to produce over 30 million tonnes upon completion (Ehm 2005). In the case of Sunrise Dam, an average of 3.68 grams of gold was produced for each tonne of ore that was mined, whilst at Boddington this figure was about 1 gram per tonne. With current gold prices and mining and processing technology enabling such low grade ore to be economically viable, the mining industry looks to continue in its production of massive quantities of tailings. In Australia alone, it is estimated that there are 600 tailings storage facilities currently in operation (Engels 2006), so it can be appreciated that tailings production is a massive issue all over the world.

Tailings particles are typically less than a millimetre in diameter as a result of mechanical crushing and grinding, and are usually mixed with water to form a slurry. The reason for this is for the processing of the ore, which usually takes place in an aqueous environment to enable chemical extraction of the minerals. Depending on the ore composition and the type of process used at the mine to extract the desired minerals from the ore, tailings slurry may contain heavy metals and toxins such as cyanide. Some tailings types can also generate acid through oxidation of sulphides contained in the tailings. Disposal of the tailings slurry is economically achieved by pumping the slurry through a pipeline to a dumping site. In the past this disposal has been done in the most economical fashion possible; sometimes discharging directly into the nearest river, ocean or local depression with the obvious

objective of simply getting rid of the tailings. In recent times legislation has been passed in many countries to supersede such practices with more environmentally friendly alternatives in order to curb potential damage to the environment. Growing pressure has been applied internationally by various organisations such as the United Nations Environmental Programme (UNEP), the World Bank and the International Monetary Fund (IMF) to improve the environmental impact and attitudes of global mining companies and governments. Beyond this, many mining companies have recognised the concepts of social and environmental responsibility and "licence to operate", and are actively seeking to maintain and even improve on current "world best practice".

1.1.2 Tailings impoundments

Impoundments are the most commonly used modern tailings storage facility (TSF), in which the tailings slurry is contained within a basin that is created by the construction of dam structures. In flat terrain it is necessary to build an impoundment cell (often referred to as a "paddock dam", "ring dyke" or "turkey's nest"), which has dams forming the full perimeter of the impoundment. The word "dam" is often misused in this context in describing the entire impoundment, when in fact the dam is the wall that acts as the containment boundary. In mountainous terrain, the local topographic features can often provide natural boundaries for the major part of the impoundment if a suitable location is chosen, potentially enabling the construction of a relatively small dam to close a large basin off. In many cases these dams are built from earth or rockfill, whilst in some, methods have been developed for building the dams from tailings or the coarse fraction of the tailings. In a typical impoundment storage facility the tailings slurry is discharged from many pipe outlets (called spigots), which are arranged at intervals around the perimeter of the impoundment. The solid particles in the slurry typically settle soon after they are discharged from the spigot, and together they form a beach at the point of discharge that slopes towards the middle of the impoundment. Over time, the beach generated by each spigot builds up in height, length and width until it eventually merges with the beaches of the neighbouring spigots, and ultimately the entire perimeter of the impoundment has one long beach. With the constant build up in height of the beach, it is necessary to periodically lift the spigots and their supplying pipelines higher in order to prevent them from being buried in tailings. The slurry water, often referred to as decant water or super-natant water, runs downhill into the middle of the impoundment to form a pond. In many

mining operations this pond water is pumped back to the process plant for reuse. Most impoundment dams are built incrementally, starting off low and periodically being built higher in stages in order to spread the cost of this considerable capital expense over a longer term, particularly in light of the fact that the impoundment is usually set up before the mine is producing any income. At the end of life of the mine, environmental regulations often dictate the "rehabilitation" of the tailings storage site, whereby the mining company is expected to cap the site and revegetate it.

Figure 1. Photograph of a tailings impoundment during a downstream raise of the dam

Despite considerable improvement on previous forms of uncontained disposal techniques, impoundments still present some significant environmental and safety risks. From an environmental perspective, there is the real potential for toxic contaminants to seep into the underlying soil and enter subterranean aquifers that can carry it further away to damage the environment. This has led to regulations governing impoundment permeability limits. There is also the potential for the dam to leak, which has led to engineered solutions such as toe drains and seepage monitoring programmes. The worst scenario is the potential for a dam to fail structurally. This has occurred in dozens of instances over recent decades as a result of earthquakes, rainfall events that caused the impoundment to fill and overflow with rapid erosion of the dam occurring as a result, from poor construction of the dam in the first place, or from operational negligence in which the impoundment has been simply overfilled with tailings slurry. In any of these dam failures, there is the potential for the tailings contained within the dam to liquefy and flow out of the impoundment through the point of failure. The requirement for impervious conditions at impoundment boundaries leads to the entrapment of water, which may be desirable from a seepage point of view, but has the serious side effect of keeping the stored tailings in a condition that is more conducive to liquefaction in the event that the impoundment retaining structure should fail. This has happened in catastrophic proportions in several instances, with tailings mud flows of several meters in depth running down valleys to completely bury entire villages, killing hundreds of

people and causing untold environmental and property damage (UNEP 2005). A short listing of some of the deadliest dam failures in recent decades would include: Bulgaria 1966, 488 people killed. Zambia 1970, 89 people killed. USA 1972, 125 people killed. Italy 1985, 268 people killed. South Africa 1994, 17 people killed. China 2000, 15 killed and 100 missing. Between the years 2000 and 2006 there have been 14 serious dam failures registered on the United Nations Environment Programme listing.

Impoundments also present an engineering problem when the final stage of rehabilitation is reached. The impervious basin, combined with the permanent presence of a pond on the tailings surface, means that most of the deposited tailings are located below the phreatic surface (water table). This inhibits the drying of the tailings, particularly when the mine is located at a site where rainfall has a net positive effect over evaporation. This saturation results in the contained tailings having a low strength, which makes it very difficult to operate earthworks equipment on the surface of the tailings impoundment to spread topsoil. Persistent rainfall can prevent the rehabilitation effort and cause it to drag out for years.

For an impoundment type of tailings storage facility, the ability to predict the beach slope is important for the following purposes:

- Designing the dam structure. The slope of the beach will determine the necessary height of the dam, and to a lesser degree, the pressure acting on the dam, both from the static weight of the solids as well as the hydrostatic pressure within.
- Determining the freeboard storage volume of the impoundment. This freeboard volume is defined as the remaining storage capacity of an impoundment that can safely be used without breaching of the dam occurring, and it must provide adequate storage capacity for rainfall runoff after a major storm event as well as future tailings.
- Planning the periodic raising of the dam as the impoundment fills up

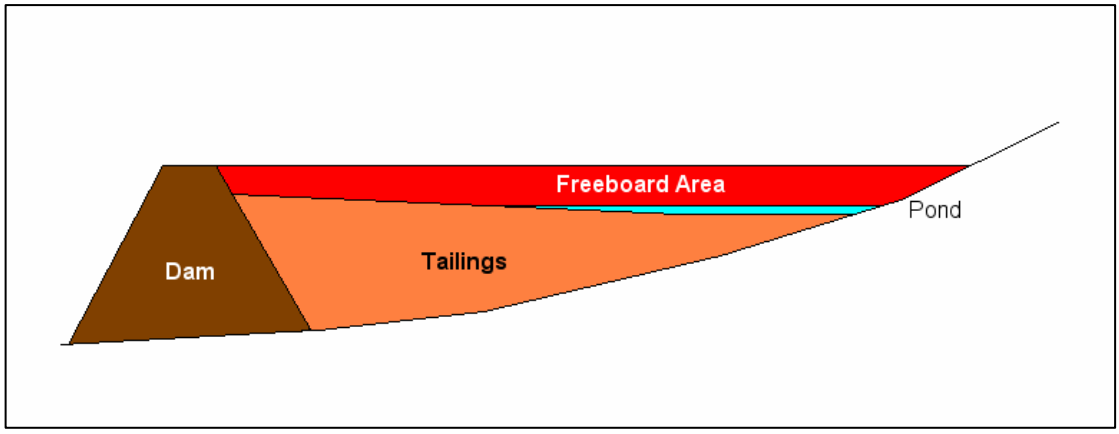

Figure 2. Diagram of relevance of beach slope in an impoundment

1.1.3 Tailings stacks

Robinsky (1975) proposed an alternative form of tailings storage facility that he called Tailings Management System (TMS), which is now more commonly referred to as a tailings stack or a Centrally Thickened Discharge (CTD) scheme. In a tailings stack facility the tailings slurry is discharged from a single elevated point above a flat plain to form a conical hill. Depending on the topography, a dam may not be required for containing the slurry, but some form of perimeter bund or drain is required to collect rainfall runoff and slurry bleed water to prevent it from being allowed to run into the surrounding environment. A separate pond for this runoff is therefore required, which can be used for recycling of the collected water if needed. On the stack surface, the tailings slurry will typically spread in thin layers of about 5 to 10 centimetres depth in local regions, with each layer typically sitting exposed for some days before being covered up by the next layer. This deposition process will be discussed in some detail later in this chapter. It is noted that these thin layers of deposited tailings are able to dry out considerably from natural evaporative processes, which brings some major benefits to this type of tailings storage facility. Firstly, the relative dryness of the stack means that there is minimal leaching of toxins into the underlying soil (Williams & Seddon 1999). Secondly, this typically low moisture content gives the stack considerable strength to support itself and withstand earthquakes or general structural incompetence failures (Fourie 2006). This aspect presents a massive advantage when the stack surface gets rehabilitated upon cessation of mining, due to its structural integrity to support earthworks machinery. Another aspect of tailings stacks that give them an advantage over impoundments is the stability of the stack resulting from the gentle slope of the surface. By comparison, though the tailings in an impoundment are relatively flat, the impounding dam is

relatively steep, so that if the contained tailings in both TSF's were to liquefy in the event of an earthquake (presuming the moisture content in both facilities was sufficiently high to enable liquefaction to occur), the impoundment would present a significantly greater risk of flowing due to the higher potential energy of its shape. Investigation of this topic by Fourie (2006) found that a tailings stack typically has a beach slope that is flatter than the angle of repose adopted by liquefied tailings that have come to rest. Finally, one of the major advantages of tailings stacks over impoundments is the economic benefit in certain circumstances. A major expense in the initial establishment of a tailings stack is a thickener that can process the total mine output to the required discharge concentration, but with an impoundment on the other hand, the major capital cost is the initial construction of a dam. In situations where water is scarce (and therefore expensive), tailings stacking presents enormous potential for reducing water losses and operating costs.

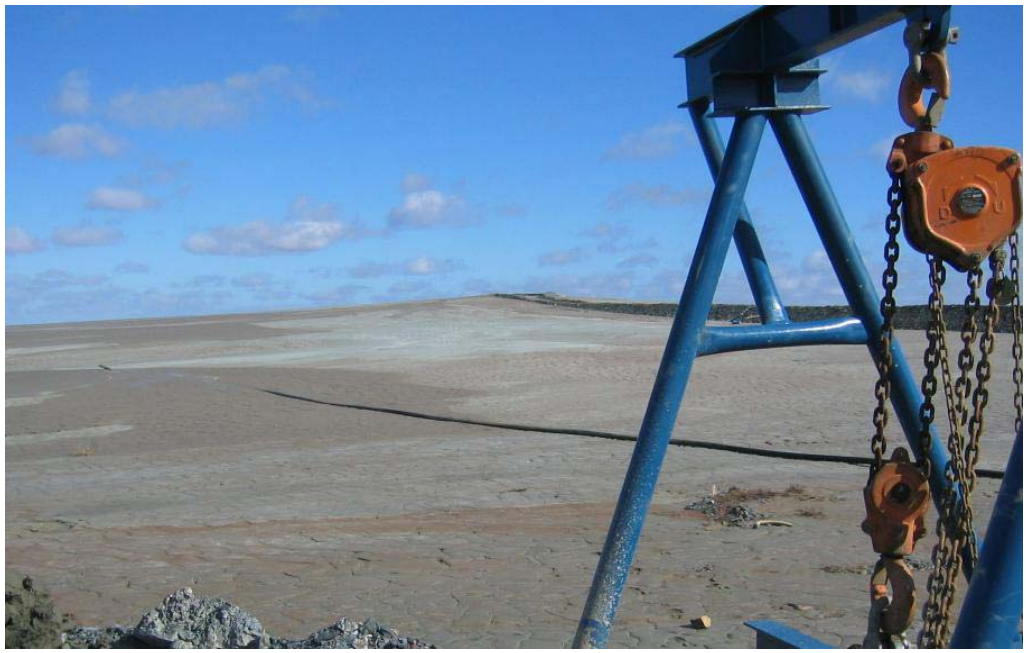

Figure 3. Photograph of the Peak mine tailings stack, near Cobar, New South Wales

In the case of a tailings stack, the ability to predict the beach slope becomes even more critical than an impoundment for the following reasons:

- Determining the height of the stack. This will dictate the storage capacity of the stack.
- Forecasting the required land surface area to accommodate the stack.
- Designing the perimeter bund. It is necessary that the bund is sized to retain decant water as well as rainwater runoff, the volume of which is dictated by the surface area of the stack.

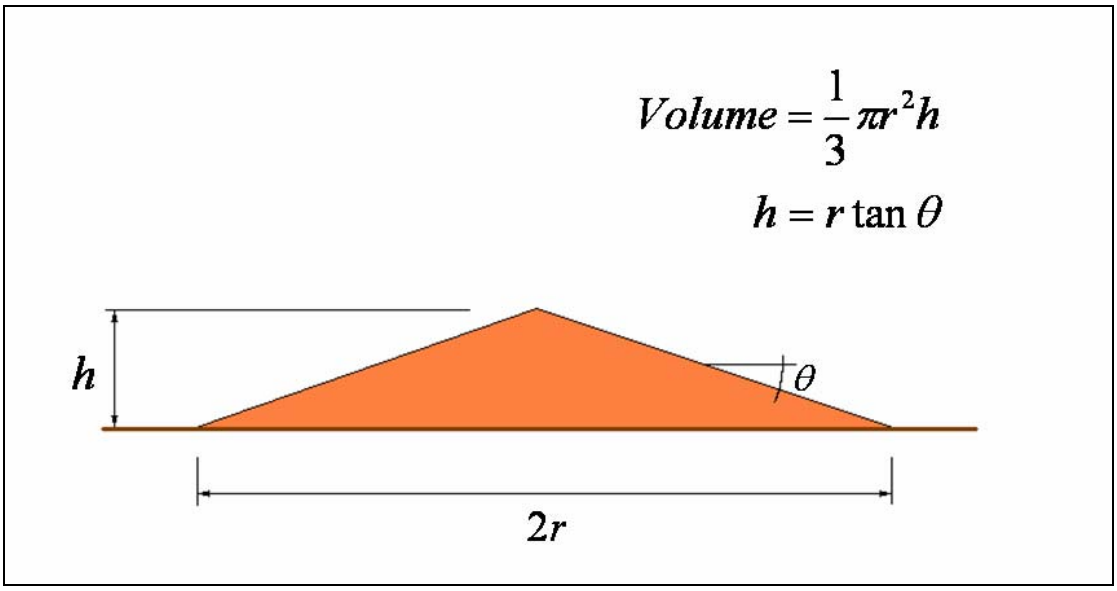

Figure 4. Diagram showing the relevance of beach slope on a tailings stack

When a tailings stack is constructed on sloping ground instead of flat ground, this type of tailings storage facility is commonly referred to as a "down-valley discharge" (DVD) scheme. In such cases it becomes even more critical to be able to accurately predict the beach slope of the tailings because this can determine the feasibility of the entire scheme.

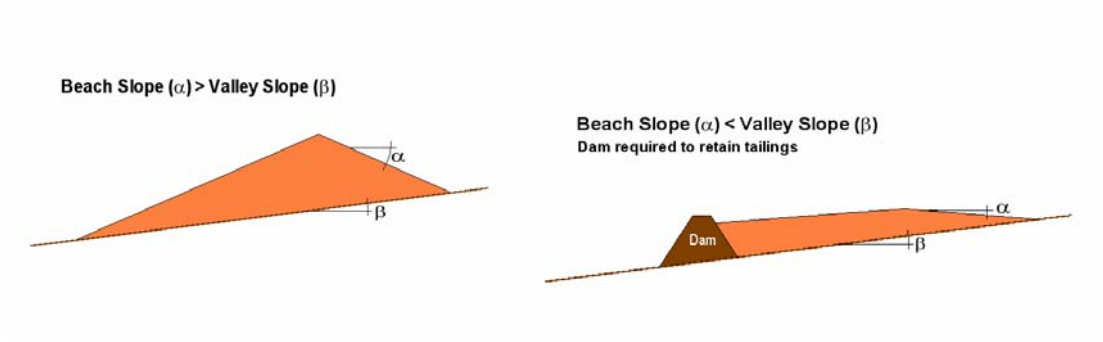

Figure 5. Down valley discharge schemes, showing two possible configurations

As a general note it is fair to say that beach slope prediction is much more relevant in the context of stacks than it ever has been in the past with impoundments. This can be asserted on the basis that most operators of impoundments have not had to consider the tailings beach slope per se; rather they have been more concerned with the surface level in terms of the risk of the dam being breached by tailings or stormwater. In most impoundments the beach slope has been almost flat anyway, and with the pond

surface considered in the overall cross section of the impoundment, it can be appreciated that the contents of an impoundment are often regarded as being flat from an operational point of view.

1.1.4 Dry stacked tailings

Another term, "dry stacked tailings", is sometimes seen in the literature. Though this term is not to be confused with dry tailings or a tailings stack, it has already been adopted for describing two very different forms of tailings storage methods:

The first definition of dry stacked tailings is a recently introduced form of tailings storage in which tailings slurry is pumped into a bounded flat paddock until a thin layer covers the entire area (Glenister & Abbott 1989; Sofra & Boger 2001). The discharge is then stopped for a long period, during which time a significant fraction of the contained water is able to evaporate. Whilst the evaporation phase is in progress, the tailings slurry being produced by the mining operation is sent to another paddock. It can be seen that this form of tailings disposal requires several paddocks to enable the production to continue uninterrupted, and it also requires a relatively higher degree of maintenance and monitoring than some other disposal schemes. It has gained some following in the alumina industry due to the relatively flat-beaching nature of bauxite tailings, which is often referred to as "red mud".

The second definition of dry stacked tailings sees the tailings slurry dewatered with drum filters to the point that it becomes a cake that can no longer be pumped through a pipe (Davies & Rice 2001). This cake still carries moisture, but at a content below saturation. This dried tailings cake requires haulage with trucks or conveyor systems to its storage facility. Three examples were presented by Davies and Rice where this system has been adopted in Canada, Alaska and Chile.

1.1.5 Underground and in-pit storage

In some rare cases it is possible to pump tailings into an open cut pit or an underground mine that has been mined out, but this is not typical because in most cases the mining operations (or access to them) are still ongoing at these sites. In underground discharge, the beach slope has significance, since it is

desirable to have steeply beaching tailings in areas that have been mined out so that other areas that are still being worked are not flooded with tailings. Beach slope is not so important for disposal in a pit, since the desired result is a flat surface with high strength for earth moving equipment to run on for the rehabilitation of the site.

1.1.6 Submarine and riverine tailings disposal

The act of deliberately discharging tailings slurry into an ocean or river still goes on to this day in several major mining operations in the South East Asian region, despite the controversial impact that this has on the environment. Various investigations of this topic have generated support for both sides of the argument of whether this form of tailings disposal is damaging to the environment, and whilst the International Council of Mining and Metals supports submarine and riverine tailings disposal in certain situations (ICMM 2005), the governments of many of the western nations outlaw it.

1.2 Classification of tailings

In terms of their potential behaviour on a beach, tailings can be categorised into 4 main groups:

- Dry tailings
- Segregating slurry
- Non-segregating slurry
- Paste

Some effort will be made here to define each of these 4 groups.

1.2.1 Dry tailings

"Dry tailings" are essentially tailings that are not mixed with water to form a slurry or paste. One such example of this can be found in some mining operations where a method of mineral extraction called "heap leaching" is adopted, in which the ore is dumped in a big heap and chemicals are periodically sprayed on top of it that leach the mineral from the ore and drain down through the heap under

gravitational forces. This “pregnant” leachate is collected by a drainage system that underlies the heap, and is then refined. In heap leaching operations, the remaining ore is not usually referred to as tailings, but instead is called “residue”. Heap leaching operations will continue to produce leachate for years after the spraying ceases, so unlike other mineral processing methods, it is difficult to define the exact point when the ore becomes residue in a heap leaching facility, but one logical definition would be the moment that the mining company stops collecting the leachate.

Small scale mining ventures often create dry tailings, where the miner sifts through the dirt mechanically to find his treasure. This was typical centuries ago in gold and diamond mining, and still continues in some non-commercial mines and smaller gemstone mining operations. The majority of commercial mining operations currently underway do not produce dry tailings.

1.2.2 Segregating tailings slurry

Segregating tailings slurry is a mixture of rock (or soil) particles and water, in which the larger particles will preferentially settle out before the smaller ones. These slurries are typically of low concentrations.

1.2.3 Non-segregating tailings slurry

Non-segregating tailings slurry is similar to segregating slurry, but with one critical difference; the large and small particles are seen to settle at the same rate. Non-segregating slurries are typically more concentrated than segregating slurries, but since the transition point from segregating to non-segregating behaviour is dependant on the mineralogy ore, it is possible for a segregating slurry of one ore type to have a higher solids concentration than a non-segregating slurry of another ore type. However, any given segregating slurry can be thickened to be a non-segregating slurry with the removal of water. The point that separates segregating and non-segregating slurries is known as the segregation threshold.

1.2.4 Paste tailings

The definition for paste is not so clear, with many people in the industry often using this term very imprecisely in describing what others might recognise as thickened slurry. What can be said definitively is that paste is created by removing water from slurry. Some attempts have been made to define the boundary between slurry and paste with a definite yield stress value or a viscosity value or a slump value (Newman et al. 2001). Other more subjective definitions are: "paste is too thick to be pumped with centrifugal pumps, and so requires positive displacement pumps" and "paste will not settle in a pipe" (Theriault et al. 2003). Paterson (2004) stated that paste "…can be transported at low velocities without particles settling on the pipe invert. On deposition there is very little, or no, bleed water from the mixture…" These industry definitions are developed from a practical point of view in terms of transporting the material and avoiding the blockage of pipelines. In this work, paste will be defined as a mixture that does not bleed water, in which particles do not settle further, based on the definition provided by Paterson.

1.2.5 Thickened tailings

The term "thickened tailings" is used to describe tailings slurries that have been concentrated by the removal of water, though in the past this term has also been used to describe non-segregating slurry (Robinsky 1975, 1978). Strictly speaking, thickened tailings could include segregating slurries, non-segregating slurries or paste, so it can not be regarded as a discrete category for engineering purposes like the other 4 types of tailings. In industry the concentration of a slurry is usually achieved in a thickener, which is essentially a cylindrical tank with a conical base that acts as a settling pond, usually with a mechanical raking device continuously rotating about its central vertical axis to provide egress paths to assist trapped water to escape from the settling mass of solid particles. Often flocculating agents and coagulants are added to the slurry to speed up the settling process. Sometimes filtering devices (such as disc filters, belt presses and centrifuges) are used instead of thickeners (or in conjunction with thickeners) for thickening the tailings slurry by pressing against filter screens to extract water. In recent years the design of thickeners has evolved to enable higher concentrations of slurry to be created, with the tank bases being shaped as steep cones to increase the depth in the

thickener and thus force more water out of the mixture with greater compressive force. Both of these thickening devices are capable of producing paste or thickened tailings.

1.3 Beach slopes

By convention, tailings beach slopes are usually expressed as a percentage, rather than an angle or a fraction. The percentage is calculated as 100 times the vertical rise over the horizontal run, so that a beach with 1 meter of vertical rise over 20 meters of horizontal run would have a 5 percent slope. Typical beach slopes seen in non-segregating tailings storage facilities vary between 1 and 5 percent (Williams & Seddon 1999), whilst in a segregating tailings storage facility the average beach slope is typically less than 1 percent (Morris & Williams 1999), though near to the discharge point the local beach slope is often steeper. (Blight & Bentel 1983) For a paste, the slope of the deposit formed is expected to be significantly steeper than that of a tailings slurry, with experimental results showing that small samples of paste can yield slopes of up to 19 percent (Sofra & Boger 2002), though the discharge of such viscous paste onto a tailings beach is generally not viable or practical.

1.4 Beach profile and concavity

In all cases of large scale tailings disposal, tailings beaches are found to be concaved in profile, with the amount of curvature varying from one case to the next. In some cases the degree of concavity is so low that the beach is almost linear in profile, but it has been shown that beaches formed by the discharge of segregating slurry exhibit greater concavity than those formed by non-segregating slurry.(Robinsky 1978; Williams 2001)

1.5 Application of tailings types

In the majority of mining operations, tailings slurry is thickened to a point below the segregation threshold and discharged to an impoundment. In such cases the thickening effort is driven by the desire to recover some of the water and the costly chemicals contained within it for recycling. In some other cases there is no thickening done on the tailings slurry.

Tailings stack type facilities, of which there are only about 20 or so currently operating in the world, receive non-segregating tailings slurry in the majority of cases. This is done to minimise water consumption from evaporative losses and to achieve a relatively steep beach slope.

Paste tailings is used for underground backfill in some mines. The reason for this is that it can be used as structural fill in underground stopes following the addition of cement to the paste. This allows miners to dig out surrounding rock that would otherwise have collapsed without the support of the cemented tailings. Furthermore, its steep angle of repose allows it to be used in local areas in an underground mine with low risk of the tailings flowing into other working parts of the mine.

The discharge of paste tailings in an above ground storage facility is very rare for several practical reasons. Firstly, paste production technology is relatively new. Secondly, at most mine sites the cost of producing and transporting tailings paste to a dumping site is higher than the cost of the water that is otherwise lost in tailings slurry. Thirdly, though the steeper beach slopes that could be gained by discharging paste would reduce the footprint of an above ground tailings storage facility, at a typical remote mine site the land space saved is not of sufficient value to warrant the cost of paste production. Another less obvious reason for the rarity of paste discharge in above ground facilities is the reduced structural stability of the deposit formed if steep slopes of 19% or more are gained.

1.6 Tailings beach formation from non-segregating slurry

The following description of tailings beach formation is based on the author's own observations of non-segregating tailings slurry flowing down the surface of the conical tailings stack of the Sunrise Dam gold mine in Western Australia in February 2005. During this period, the flow rate and water content of the discharged slurry could be adjusted.

A tailings beach builds up under the arrival of many thinly spread deposits of tailings, each caused by the supply of tailings to some location on the beach surface by a self-formed channel. At the end of a channel the tailings can be seen to disperse in a wide flat sheet a few inches thick, but over time the channel gradually advances in length along the top of this freshly deposited sheet at the rate of

approximately 5 metres per minute, enabling the tailings to gradually spread further from the point of discharge. The direction taken by the sheet flow is essentially dictated by gravity as the tailings runs along the path of least resistance, but the deposited location and depth of this material dictates the future path of the self-formed channel, as it is necessary for this freshly deposited tailings to form the sides of the new channel. Eventually the channel experiences a bank-up effect when the sheet flow builds up in an area that is flatter than the channel slope, at which time the channel will suddenly adopt a completely new path from some point upstream. It was found that concentrated slurry will deposit near the top of the beach at a steep slope, while diluted slurry will run further away at a flatter slope. It was also found that a low flow rate will see the channel run at a steep slope, with the sheet deposition occurring near the top of the beach also at a steep slope, while a large flow rate will cause the channel to adopt a flatter slope, thus resulting in deposition further away at a flatter slope.

An interesting phenomenon was observed when a relatively steep beach formed at a low flow rate was eroded by a channel flowing at a much higher flow rate. The new channel cut itself a canyon, getting deeper and deeper into the underlying beach. The channel also formed many small waterfalls along its route, and these waterfalls gradually moved upstream as the turbulence created at each one undermines the channel bed immediately upstream of it.

This deposition behaviour corresponds to that which was observed and documented by Williams and Meynink (1986) during a series of tailings slurry stacking experiments in New Guinea, in which the slurry was discharged onto a flat plane and observed to form a large puddle that spread in all directions for some time before the flow suddenly confined itself to its self-formed channel to ride over the top of the freshly deposited tailings towards the outer edge of the puddle to propagate further. Near the edge of the puddle the channel flow once again ‘broke out’, reverting to sheet flow.

This behaviour may better be described in terms of resistance to flow. Sheet flow will occur while there is little resistance against the flow being able to push the boundaries of the puddle larger. The self confinement to a channel will occur when the amount of resistance to forming the channel is less than the amount of resistance to spreading the puddle boundaries.

Williams & Meynink (1986) asserted that this channel slope dictates the overall slope of the tailings beach formed. The author's own observations of deposition behaviour on the Sunrise Dam tailings stack support this assertion.

It follows from this that the prediction of a tailings beach slope stems from predicting the slope of the channel of tailings slurry that runs down the beach.

1.7 Statement of the problem

At present there is no satisfactory method available for the prediction of tailings beach slopes that are generated by the discharge of non-segregating tailings slurry. This makes the design and management of tailings storage facilities more difficult, particularly for tailings stacks and down-valley discharge schemes, where the predicted beach slope is a critical design parameter.

1.8 Aim

The aim of this work is to develop a method of predicting the slope of the beach that forms when a tailings slurry is sub-aerially discharged from a pipe.

1.9 Thesis structure

The work presented here is structured in the following manner:

- Literature Review (Chapter 2). The literature that specifically addresses the topic of tailings beach slope prediction will be discussed, as well as other related literature of relevance.
- Approach to the problem (section 3.1). Some discussion of the physical processes that are relevant to tailings beach slopes will establish an approach for the experimental work.
- Experimental work done (Chapter 3)
- Validation of beach slope models presented in the literature (Chapter 4). The beach slope models found in the literature are applied in predicting slopes to compare with 5 different sets

of data, 2 of which contain beach slope data and the other 3 containing relevant experimental data.

- Creation of a simple empirical beach slope model (Chapter 5). This model is based on an empirical fit to new experimental data.
- Development of a new a priori channel equilibrium slope model (Chapter 5). A model is developed that is based on previously established work done by others in related fields.
- Creation of a new semi-empirical equilibrium slope model (Chapter 5). This model features some aspects of the a priori model, but with empirical calibration from new experimental data.
- Validation of the new a priori and empirical models (Chapter 5). The new models are tested against the same 5 sets of experimental data that were used in Chapter 4 to validate other models from the literature.
- Review of three-dimensional tailings beach modelling methods (Chapter 6).
- Creation of a new three-dimensional tailings stack shape model (Chapter 6)
- A summary of new contributions and findings arising from this work is presented (Chapter 7)
- Conclusions are drawn from the work presented in the thesis (Chapter 7)
- Recommendations are presented for future research in this field (Chapter 7)

Chapter 2: Literature review

There is a substantial amount of literature that focuses specifically on the prediction of tailings beach slopes, but the various approaches applied to the problem causes this literature to fall into several categories. There is also an amount of related literature that does not specifically focus on tailings beach slope prediction, but is still very relevant to this work. In an attempt to apply some logical structure to this literature review, the literature is presented in the following order:

- 2.1 Tailings beach slope prediction
    - 2.1.1 Empirical equations fit to real tailings beaches
    - 2.1.2 Empirical equations fit to miniature tailings beaches
    - 2.1.3 Empirical equations fitted to open channel flume experiments
    - 2.1.4 Tailings stacking experiments
    - 2.1.5 Theoretical approaches
    - 2.1.6 Tailings beach profile prediction
- 2.2 Hydraulic fill studies
- 2.3 Geological investigations of alluvial fan deposits
- 2.4 Prediction of spillage from a tailings dam failure
- 2.5 Slump of tailings pastes

Rheology

It is appropriate to introduce the science of rheology at this point, since it does appear in various forms in a number of the references visited in this literature review. Rheology is the study of flowing matter, such as liquids, slurries, emulsions, and melts. Rheology describes the deformation of such matter when it is subjected to external shear forces. Laboratory instruments called rheometers have been developed to experimentally investigate the deformation of such matter under measured rates of shear.

Some fluids, such as water, exhibit Newtonian behaviour, in which case the shear stress in the fluid is uniformly proportional to the applied rate of shear. When the shear stress is plotted against the applied shear rate, the resultant graph is known as a rheogram. Newtonian fluids appear as straight lines that intersect the origin of a rheogram, the slope of which give the viscosity of the fluid. Non-Newtonian

fluids will either exhibit a yield stress, non-linear viscosity characteristics, or both. Yield stress is an internal property that enables a fluid to resist deformation up to a certain point, effectively enabling it to behave as a solid while it is subjected to stresses that are less than the yield stress. Typically a tailings slurry will exhibit both yield stress and varying viscosity at different shear rates, which firmly places it in the realms of a non-Newtonian fluid.

Rheological modelling

Numerous rheological models have been proposed for the purpose of mathematically describing the rheological characteristics of a fluid. Such models provide a means by which various aspects of a fluid's rheological behaviour can be taken into account in the mathematical modelling of various fluid dynamics related processes, and many such examples can be found in this literature review. Three commonly used rheological models are the Bingham plastic, power law, and Herschel-Bulkley models. Each of these three empirical rheological models is described below:

Bingham Plastic model

This model suits a fluid with a yield stress and linear viscous behaviour. The equation for the Bingham Plastic model is as follows:

$$\tau = \tau_y + K\dot{\gamma} \qquad (37)$$

where τ is the shear stress (Pa), τ_y is the yield stress (Pa), K is the Bingham plastic viscosity (Pa.s) and $\dot{\gamma}$ is the shear rate applied to the fluid (1/s).

Power Law model

This model suits a fluid without yield stress that exhibits non-linear linear behaviour. The equation for the Power Law model is presented below:

$$\tau = K\dot{\gamma}^n \qquad (38)$$

where τ is the shear stress (Pa), K is the Power Law consistency index (Pa.s^n), n is a power and $\dot{\gamma}$ is the shear rate applied to the fluid (1/s).

Herschel-Bulkley model

This model suits a fluid with a yield stress that exhibits non-linear viscous behaviour. The equation for the Herschel-Bulkley model is presented below:

$$\tau = \tau_y + K\dot{\gamma}^n \qquad (39)$$

where τ is the shear stress (Pa), τ_y is the yield stress (Pa), K is the Herschel-Bulkley consistency index (Pa.s^n), $\dot{\gamma}$ is the shear rate applied to the fluid (1/s) and n is a power. This model is essentially the combination of the previous two. It carries an extra empirical parameter compared to each of the other two, but has the advantage of combining non-linear viscous behaviour with a yield stress, which neither of the other two models can do.

The graphical presentation of these three models allows a better comparison of their characteristics.

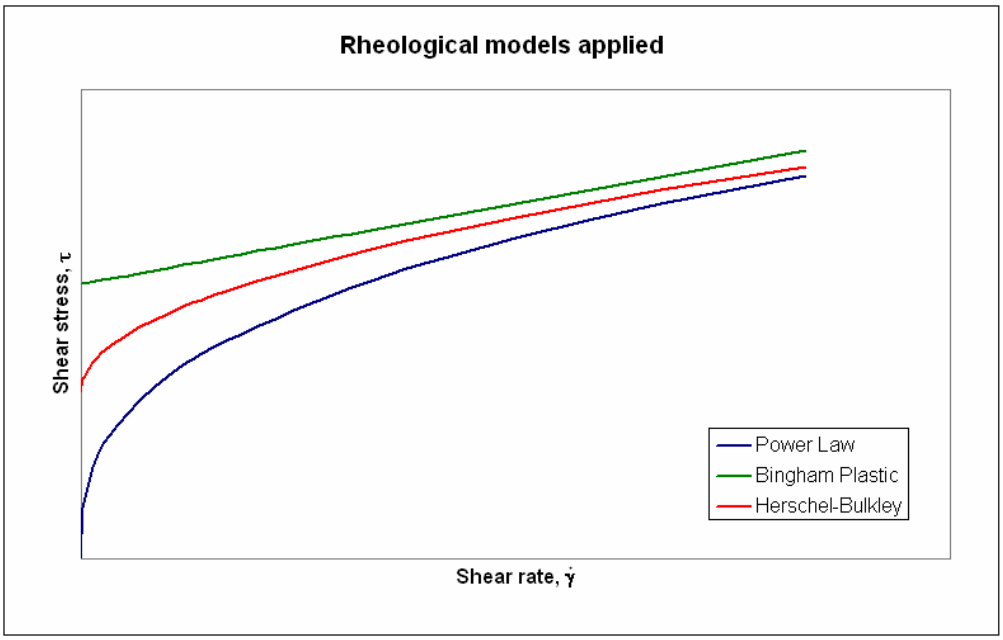

Figure 6. Graphical comparison of the Power Law, Bingham Plastic and Herschel-Bulkley rheological models.

2.1 Tailings beach slope prediction

Some work has been presented in recent decades featuring attempts to develop a reliable means of predicting tailings beach slopes. Most of the earlier work done in the field of tailings beach slope prediction was focused on predicting the beach surface and particle distribution profiles in a tailings impoundment context, where the tailings slurries were generally segregating. This segregation caused the coarse particles to deposit nearer to the discharge points, which are typically positioned along the crest of a dam. These coarse particles had a relatively high permeability, so one of the major motives for the above research was based around modelling the phreatic (hydraulic) surface profile to analyse the hydrostatic pressure on a dam. This segregating characteristic would also result in variation of the strength and compressibility of the beach as a function of the radial distance from the discharge spigots, which was also of interest in the contexts of evaluating the feasibility of upstream raising of the dam and of rehabilitating the area (Williams & Morris 1989). Beach slopes were of a lesser interest in being used to calculate the freeboard volume of an impoundment for rainfall containment and future tailings storage capacity, because the typically flat slopes of tailings beaches in impoundment situations have a relatively minor effect on the freeboard volume when compared to the remaining freeboard of the dam above the discharge spigots. More recently with tailings stack disposal methods becoming more popular, there has been a greater interest in beach slope prediction. A review of this beach slope literature is presented here.

2.1.1 Empirical equations fit to real tailings beaches

A logical starting point in the pursuit of a tailings beach slope prediction method is to examine some real tailings beaches and try to fit an empirical equation to their shape. Several such empirical approaches have been presented. It should be noted here that all of these methods are based on measuring the overall height and overall length of a tailings beach in an impoundment, and presenting the overall slope as the ratio of these two values. The overall height of a beach is usually deduced from the difference in elevation between the spigots and the pond, when in reality the spigots may be situated quite some distance above the actual beach. For this reason, some care should be taken in accepting overall slope figures at face value, given that in some cases the overall height may be only

two or three times greater than the drop from the spigots. It is therefore necessary to check the cross sectional profile points to be sure that there is not some very high point at the head of each beach.

Melent'ev et al. (1973) proposed the following equation for predicting the overall slope for a concaved tailings beach:

$$\frac{H}{L} = 0.15 C_V^{1/3} \left(\frac{d_{50}}{h^*} \right)^{1/6} \quad (1)$$

where H is the overall height of the beach, L is the overall length of the beach, C_V is the solids concentration of the incoming tailings slurry, d_{50} is the median particle size, and h^* is the stream depth associated with the scour velocity of clear water. It was also stated that this equation could be used to calculate the slope of the beach at any specific point, provided the input parameters were known for the slurry at that particular point. An expression was provided for calculating h* as follows:

$$h^* = \frac{Q_W}{V_H b} \quad (2)$$

where Q_W is the water flow rate, V_H is the stream velocity for no erosion to occur, b is the stream width.

The use of the word “scour” suggests that the process of tailings beach formation is caused by the tailings flow eroding solid particles from the bed in a scouring process, which would be entirely contradictory to what has been observed by later workers, and indeed to the physics of beach formation.

Robinsky (1975) presented a landmark paper in 1975 that first introduced his idea of tailings stacking. Though this paper was predominantly conceptual in its introduction and promotion of this new idea, he was able to draw on practical experience that had been gained in the establishment and operation of the world’s first tailings stack facility that he had engineered at the Kidd Creek mine in Canada, as well as some proprietary laboratory research that he had conducted. In this paper Robinsky did not present any

equations or hard numbers relating to beach slope prediction, but he did make some interesting qualitative comments about the depositional behaviour of tailings from its hydraulic discharge as a slurry; Firstly he stated that the solids concentration is an important factor in the prediction of tailings beach slopes. Secondly, he listed the gradation of solid particles as being an important factor. Thirdly, he stated that the flow rate has an effect on the beach slope, with lower flow rates yielding steeper beach slopes. To further substantiate this third statement, he added that the (7500 dry tons per day) discharge of tailings onto the Kidd Creek stack is split into 24 streams in order to achieve steeper beach slopes. Finally he added temperature and pH as other parameters that have a lesser effect. He concluded his paper by saying that the best way to predict the beach slope is to perform laboratory experiments in conjunction with field tests.

It is worth noting that Robinsky's statement about the effect of flow rate went largely unnoticed for some years. The splitting of flow to produce steeper slopes at Kidd Creek has since been done at other mine sites many years later, but there has most definitely been an element of reinventing the wheel amongst these more recent experiences, evident in the time taken to implement this change.

In a later paper Robinsky (1978) provided some more detailed information about tailings deposition that was not presented earlier. Of greatest interest was a plot of concentration vs beach slope based on some in-house laboratory tests that he had performed on copper tailings. Robinsky did not present any equivalent plot for the effect of flow rate on beach slope because he regarded the slurry concentration as the factor "most practical to control". However, it was stated that "the volume of flow can affect the build-up of slopes by as much as one-half to one percent", a rather down-graded statement when compared to his comments on flow rate in his previous paper. Since an equation was not presented for the prediction of beach slopes, Robinsky's concentration vs beach slope graph has been presented here instead:

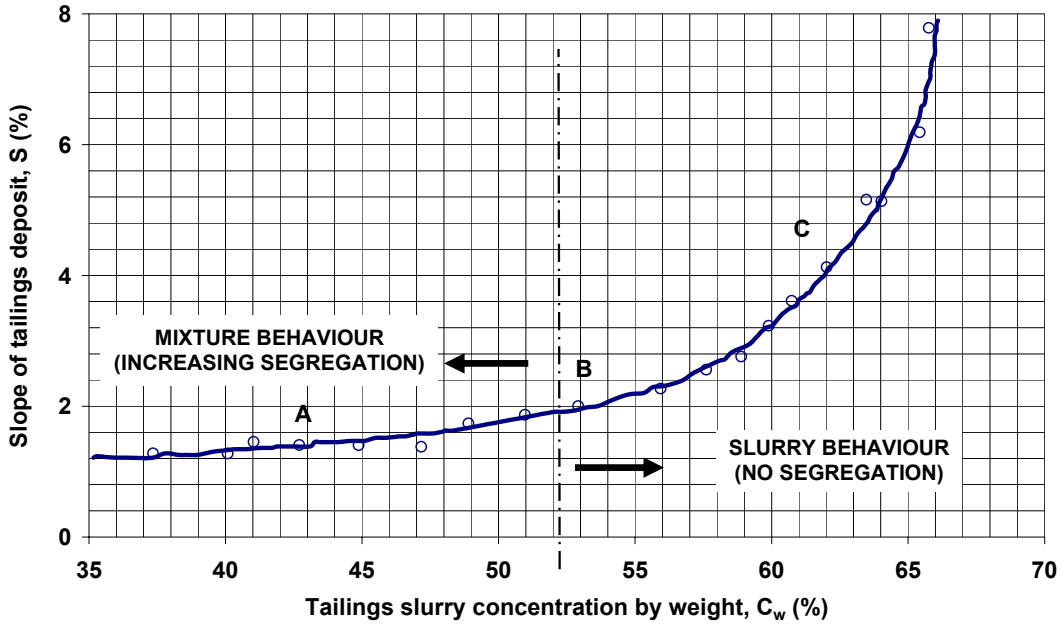

Figure 7. Plot of S vs C_W presented in Robinsky (1978)

No details were provided about the laboratory tests done to generate this data. Furthermore, it is not known whether this equation represents an empirical fit to the slope of actual tailings beaches as a factor of lab test results done with the corresponding slurries.

Wates et al. (1987) reported that the slope of a tailings beach was dictated by the slurry specific gravity, and not particle size. To support their claim they presented a plot of slurry specific gravity vs beach slope for some field data that they had collected from "a number of mines", which showed a strong trend, though they mysteriously refused to accept the validity of the data fit in stating "The variations are too great to distinguish any definite relationship between slurry relative density and beach slope but the trend is clearly evident." No equation was provided for the line of best fit drawn on their graph, which is reproduced here as Figure 8.

It is noted that the title of the work presented by these authors, "The effect of relative densities on beaching angles and segregation on gold and uranium tailings dams" indicates that they were working with segregating slurries, at least with some of the tailings slurries tested. However, no new data was presented by Wates et al. to suggest the factors that effect segregation, nor was any data presented to show that segregation was even occurring on the beaches observed. Instead, they stated that

segregation does not occur on a gold or uranium tailings beach without providing any evidence to support this claim.

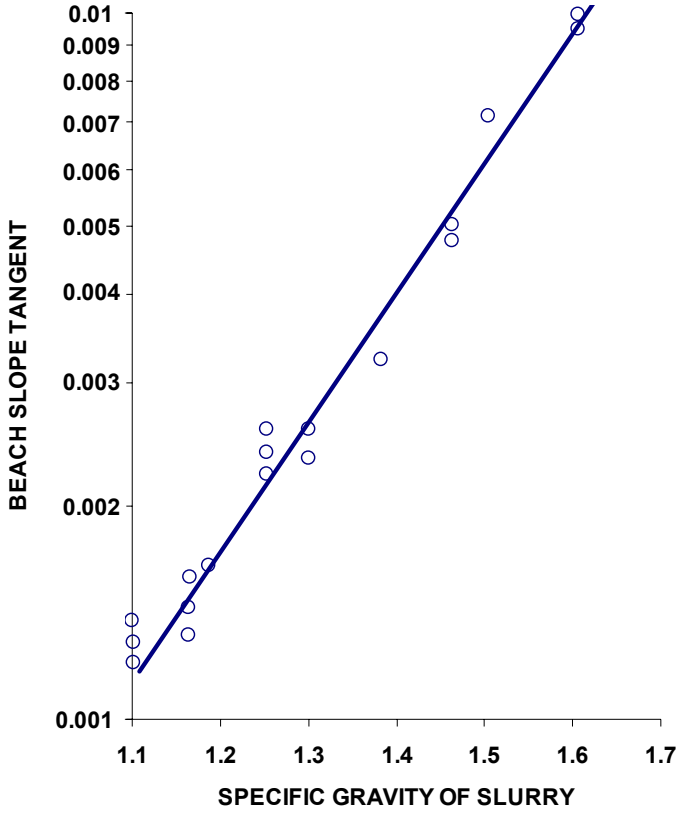

Figure 8. Graph of beach slope vs slurry specific gravity presented in Wates et al. (1987)

The US Bureau of Mines undertook an investigation into the beach characteristics of tailings with a focus on the construction of safer, more stable tailings dams. (Boldt 1988) This investigation took place in 3 phases, with the first being the survey and monitoring of tailings beaches at 18 different mines in the United States, the second being laboratory flume experiments, and the third being larger scale tailings discharge experiments at mine sites. The focus of this investigation was on the structural stability of hydraulically placed tailings, nominally in predicting the particle sorting as a function of distance from the spigots, but there was consistent recording of beach slopes throughout the research.

Boldt's work was very statistically orientated. There is a negligible attempt to present any form of literature review or research in the report, and virtually no consideration of physical principles involved in the tailings depositional process. Boldt has listed all the surveyed data in table form in the report, and made some statistical analysis into 119 linear correlations between various measurements recorded.

Many of the correlations are ridiculous in their contexts (flow rate vs cohesion of the deposited material for example, or specific gravity of the solid particles against the percentage passing the size 50 sieve), so most of them are statistically insignificant with one exception: Flow rate vs beach slope for the full scale deposition trial data, which scored an R^2 value of 0.958. The linear fit equation presented for this correlation is as follows:

$$i = 1.98 - 0.0043Q \tag{3}$$

where i is the beach slope (%) and Q is the flow rate expressed in US gallons per minute.

Pinto & Barrera (2002) published an empirically derived equation for predicting the slope of a segregating tailings beach, based on data that was logged from 6 Chilean copper mines. Their equation is as follows:

$$i = 0.009(s-1)^{15.6}\frac{C_W^{\,1.38}}{P^{0.86}} \tag{4}$$

where i is the average slope of the beach (%), s is the ratio of the specific gravity of the solids to that of the water in the slurry, C_W is the solids concentration by weight (fraction), and P is the dry tonne production rate (kt per day).

There is no particle size term in the equation (such as the median particle diameter). Pinto and Barrera found in their fitting of a curve to their data that the particle size appeared to have a virtually negligible effect, so they decided to simply drop it from the equation.

The sensitivity of the Pinto and Barrera equation with respect to the slurry specific gravity (G) is noted. This parameter is raised to the power of 15.6. This is a particularly unforgiving aspect of Pinto and Barrera's equation, since slightly different values will produce extraordinarily differing results.

2.1.2 Empirical equations fit to miniature tailings beaches

A considerable proportion of the attempts to predict tailings beach slope are based on the use of laboratory flumes to experimentally model the behaviour of a full scale tailings beach. (Blight 1987; Blight et al.1985; Boldt 1988; Fan & Masliyah 1990; Fourie 1988; Kupper 1991; Ribeiro & Assis 1999; Wates et al. 1987) It must be made clear that in some of these works the word "flume" is referring to a rectangular tank that looks more like a large fish tank. In many of these cases the walls of the tank are clear to enable external observation of the deposition of particles inside, and the base is typically flat without any inclination above horizontal. In most of these "fish tank" style flumes the slurry is admitted at one end at a very low flow rate (a few litres per minute, for example) and allowed to deposit particles on the floor of the flume to gradually build up a mini "beach". In some cases these flumes have a discharge outlet at the opposite end of the tank to allow the decant water to exit, but in others the tank is sealed so that the decant water forms a pond at the downstream end of the flume.

Blight et al. (1985) conducted laboratory experiments, running tailings slurry down a 1.82 meter long flume and forming a sediment deposit in the flume in an effort to apply it in a predictive context. They found that the overall slope of a tailings beach is affected by three factors: the solids concentration of the slurry (higher concentrations produce a steeper beach slope), the size of the solids particles (larger particles produce a steeper beach) and the origin of the tailings. This last factor is the most difficult to quantify, since it is likely to cover a combination of other unnamed factors such the mineral properties, clay content, rheology, specific gravity, chemical effects from the mine processing etc.

Unfortunately however, they found that the overall slope of the laboratory flume beaches did not show any resemblance to the overall slope of an actual tailings beach, so they were unable to develop a method of predicting beach slopes.

It is worth noting here that their small scale laboratory test apparatus was filled at a very low discharge rate that was not discussed, an omission that would suggest that the effect of different flow rates was not investigated or appreciated.

Wates et al. (1987) stated the slope of a tailings beach was dictated by the slurry concentration, and not particle size. As well as presenting a plot of concentration vs beach slope for field data from actual tailings beaches, they also presented experimental laboratory data to further lend support to this theory, but the trend was very weak. Their experimental data was gathered using a 10 meter long "fish tank" style flume, with two different types of tailings slurry being used; gold and uranium. The flume data loosely suggested that the beach slope increased as the concentration increased. No empirical equation was fitted to the data.

Blight (1987) presented some remarkable findings from some experiments with fly ash slurry in which it was observed that the slurry beached at its steepest slope of 5% at a concentration of 40% solids, with higher concentrations yielding dramatically flatter slopes. Blight theorised that this particular concentration marked the transition between a "particle settling" flow regime and a "mud flow" regime. Blight asserted that the "mud flow" regime was what applied to the type of "dams" that Robinsky had described in his 1978 paper. Only one type of slurry was discussed in this context, and similarly to Blight's previous 1985 paper, the flow rate was again not stated, but extraordinarily, Blight then made the claim that a higher flow rate would result in a shift of the transition concentration to a lower value, because he expected a greater depth of flow to occur on the beach, which would therefore provide "less opportunity for a particle settling regime to become established". This last comment is remarkably unfounded on the basis of any of the information presented in Blight's paper.

Fourie (1988) reported on an investigation of the use of a small scale fish-tank type flume for the prediction of beach concavity in this paper. Experiments were performed in a laboratory flume of the same dimensions as that of Blight et al. (1985), but using three different tailings slurries; bauxite, nickel ore and coal. Fourie presented experimental findings to suggest that the concentration of a slurry affected the overall slope of a beach, but no empirical equation was presented on the basis of this experimental data for the prediction of tailings beach slopes (actual or miniature). It is of interest to note that Fourie reported a slurry flow rate of 30 litres per hour into his flume for all of his experiments. It is apparent that no other flow rates were tested, so the effects of varying the flow rate were not investigated.

Boldt (1988) presented experimental data that was collected during flume experiments as part of an investigation into tailings beach characteristics that was conducted by the US bureau of mines. The timber flume used was referred to as a "deposition trough", with a length of 40 feet and a width of 2 feet. It is believed that the flume remained horizontal for all of the runs presented. Tailings slurry from two different mines was discharged through a 1-1/4 inch pipe at exit velocities ranging from 4 to 9 feet per second (flow rates equivalent to 1.0 to 1.7 l/s) into the flume at concentrations ranging between 20% and 50% solids by weight. Boldt attempted to find correlations between pairs of experimentally measured parameters, but no strong correlations were found from the flume data. It is fair to note however, that one of the stronger of these correlations (with an R^2 value of 0.57) is that between flow rate and beach slope. An even stronger correlation was calculated for the horizontal distance vs percent passing a size 200 sieve, which suggests segregation was occurring in the flume.

Fan & Masliyah (1990) conducted experiments in a 4.87 meter plexiglass flume using sand and water mixtures varying from 3.1% to 5.9% by volume. It is noted that these concentrations are very low in comparison to those used in industry. Their results yielded consistently concave profiles of beaches. Like the other miniature beach investigators, these workers found that the beach slope could not be predicted from their experimental trials.

Kupper (1991) conducted a series of experiments in a 6.1 meter plexiglass flume with 3 different types of sand to investigate the effects of variation in concentration, flow rate and grain size distribution on the resulting overall slope of the deposit, which was referred to as the equilibrium slope. Slurry concentration was varied between 1.5 and 40.5% by weight and the flow rate was varied from 5 to 20 litres per minute.

After compiling some results from similar tests performed by other workers, Kupper proposed an empirical formula for predicting the overall slope i_{av} of a tailings beach as follows:

$$i_{av} = 5\sqrt{\frac{A\sqrt{g\left(\frac{\rho_s}{\rho_l}-1\right)}\sqrt{d_{50}}C_w}{Q}} \qquad (5)$$

where: A is the cross-sectional area of the discharge pipe (m^2)

C_w is the slurry solids concentration by weight (%)

d_{50} is the median grain diameter (m)

g is the acceleration due to gravity (m/s)

Q is the flow rate at the discharge point (m^3/s)

ρ_s is the density of the solid particles (kg/m^3)

ρ_l is the density of the carrier fluid (kg/m^3)

One point that should be noted about Kupper's formula is that it does not contain any terms that represent the individual ore type characteristics other than the specific weight of the solids and the median particle diameter. This could be seen as an advantageous aspect of her formula from an application point of view, since these ore-specific parameters are generally more complex and difficult to quantify experimentally. However, in the pursuit of accurate beach slope predictions, this must be seen as a disadvantage of the Kupper formula, since it has been demonstrated by several workers that the ore type has a significant effect on the beach slope (Blight et al. 1985; Fourie 1988).

Another point to note about Kupper's work was her use of the term "equilibrium slope" in a context that was not consistent with others. This was a difference that was acknowledged by Kupper when she cited other work in which the term was used in a sediment transport channel flow context, but she felt that her application of the term was warranted because she argued that erosion and deposition were in equilibrium with one another on a miniature beach in a fish-tank flume.

There are some interesting points to be noted about Kupper's work. Firstly, there is some discussion on segregation and its relevance to beach slopes and concavity. Citing the work of Fourie (1988), Kupper states that non-segregating slurries exhibit different beaching characteristics to segregating

slurries, noting the profiles observed by Fourie being convex upward instead of concave. This is one of the earliest published forms of recognition of this effect.

Kupper's work also bears some focus on spigot diameters, evidently implying that the exit velocity is relevant to the beach slope and shape. This is consistent with the work of Boldt, who also investigated spigot exit velocity in relation to the beach slope. Kupper even went so far as stating that the height of the spigot above the beach and the angle of the spigot relative to the beach can change the velocity of the flow at the upstream end of the beach, but failed to present any evidence to support this claim.

From this discussion of the mechanisms of particle transport, it is evident that Kupper has an appreciation for the effect of the channel flow behaviour of tailings slurries in the grander context of beach formation. This is significant, since up to that time many other researchers of tailings beach slopes had either ignored the channel flow behaviour of tailings, or otherwise not noticed it at all. The then previously published works of Fourie, Blight et al., Fan & Masliyah and others made no mention of the channel flow behaviour of tailings slurry, and the experiments described by these workers also showed a complete disregard for any effects that this channel flow may have in the formation of a tailings beach.

2.1.3 Empirical equations fitted to open channel flume experiments

Around 2003 an experimental project was commenced to study the open channel flow of tailings, with the objective of investigating the relationship between the open channel flow characteristics of the slurry and the beach formed by the same slurry. Behnam Pirouz was the first PhD student taken up with this project, which involved consultant Andrew Chryss of RMIT University. A 10 meter long flume was constructed for the testing of tailings slurry at mine sites.

The initial experimental campaign with the flume took place in April of 2004 at the Peak gold mine in Cobar, New South Wales, Australia. The flume had a rectangular cross section 1 meter wide and 500 mm deep. The plan was to fill the flume with tailings slurry and wait until a channel formed on top of a settled bed of tailings. This was achieved three times during the week-long campaign, and on each

occasion the channel took many hours to form, and was highly sensitive to any probing with gauging instruments. Such probing caused the destruction of the channel due to the turbulent disturbance of the probe's immersion overcoming the relatively weak interstitial shear stresses holding the tailings particles in place, ultimately eroding the structurally sensitive channel banks. It was decided that such experiments were not viable, and the flume was modified to attempt a different approach. Details of this initial experimental campaign can be found in the Behnam Pirouz's PhD thesis (Pirouz 2006).

The flume was modified with the installation of a 10 meter long semi-circular plastic channel, so that the channel boundaries were now rigid. Two mine sites were visited with this new flume. Tim Fitton, the author of this thesis, was present at both sites. Pirouz was present at the first site only. Details of this experimental work can be found in Chapter 3.

The data gathered from this work generated several empirically calibrated tailings beach slope prediction models, each of which predicted the slope of a self formed channel of tailings that occurs on a tailings beach, with the assertion that this channel slope dictated the beach slope. Three such models were published, and will be described here.

Chryss et al. (2006) presented a tailings beach slope model that was based on open channel fluid dynamics, stable channel dynamics and rheology. The application of this model entailed the simultaneous solution of 3 equations, the first one of which predicted the cross sectional shape for a channel:

$$x = y_0(h_0(y/y_0)^{0.5} + h_1(y/y_0)^{1.5} + h_2(y/y_0)^{2.5}) \quad (6)$$

where x and y are Cartesian co-ordinates for channel cross-sectional profile, h_0, h_1 and h_2 are geometric constants, and y_0 is the maximum depth of flow in the channel. In the initial conference paper publication of the Chryss et al. model, the 3 geometric constants were not discussed in detail, but were instead noted as being a function of the underlying tailings making up the bed of the channel. From private communication with Andrew Chryss that is presented in Appendix L, the following equations are reported:

$$h_0 = (2/t^2 - 2)^{0.5} \quad (7)$$

$$h_1 = 1/6(2/t^2 - 2)^{0.5}(-1/t^2 - (t^2 - 1)/(4t^2))/(1/(2t^2) - 1/2) \quad (8)$$

$$h_2 = 1/5(2/t^2 - 2)^{0.5}((0.5(1/(2\,t^2) - (3 + t^2)/(8t^2))/(1/(2t^2) - 0.5) \ldots$$
$$-(-1/t^2 - (t^2 - 1)/(4t^2))^2/(8(-0.5 + 1/(2 * t^2))^2))) \quad (9)$$

$$t = \frac{\tau_y}{(\rho g y_0)} \quad (10)$$

where t is the non-dimensional mass yield stress of the bed material, τ_y is the yield stress of the bed material, ρ is the density of the bed material, and g is gravitational acceleration.

The second equation as presented in the Chryss et al. paper predicted a 2 dimensional velocity profile for open channel flow at its centreline:

$$v(y) = V + 1/\chi(gR_hS_0)^{1/2}(1 + \ln(y/y_0)) \quad (11)$$

where $v(y)$ is the axial velocity in a channel at a depth y metres above the channel bed, V is the mean axial velocity, χ is the Von Karman constant, R_h is the hydraulic radius, and S_0 is the slope of the channel. A graph was provided in the paper for the determination of an χ value as a function of the concentration of the slurry flowing in the channel.

The third equation from the Chryss et al. paper is the Manning equation for open channel flow:

$$V = \frac{1}{n} R_h^{2/3} S_0^{1/2} \quad (12)$$

where R_h is the hydraulic radius and S_0 is the channel slope. It was suggested that an assumed value of 0.0081 s/m$^{1/3}$ be used for Manning's n, based on an empirical fit to the flume data.

This model was not validated with any experimental data because of the requirement for the bed concentration as an input parameter, of which no experimentally measured data was known. In its previously published form this model was not able to be applied, due to the omission of the empirical constants in the first equation. As presented here, the application of the Chryss et al. model is now possible.

Fitton et al. (2006) presented a semi empirical model for the prediction of tailings beach slopes, based on open channel fluid dynamics, rheological modelling and an empirical fit to the flume data that is presented in Chapter 3. An empirical equation was presented for predicting the depth of flow in a channel of tailings slurry as a function of the flow rate:

$$d = 12.2Q^{0.6} \tag{13}$$

where d is the depth of flow in the channel (expressed in millimetres), and Q is the flow rate in litres per second. From this predicted depth, the channel cross sectional area and wetted perimeter was calculated on the basis of an assumed shape, with the ratio of the area over the wetted perimeter equalling the hydraulic radius of the channel. Fitton et al. then presented the following equation for calculating the channel slope:

$$i = 100 \tan \arcsin \left(\frac{0.073V^2}{\left[\frac{8\rho V^2}{\tau_y + K\left[\frac{2V}{R_H}\right]^n} \right]^{0.25} 2R_H g} \right) \tag{14}$$

where i is the beach slope (%), V is the mean velocity of flow in a channel of tailings slurry (m/s), ρ is the slurry density (kg/m^3), R_H is the hydraulic radius of the channel (m) and g is the acceleration due to gravity (m/s^2). τ_y, K and n are rheological parameters of the slurry as determined through the fit of the Herschel-Bulkley model to rheological data measured for the slurry experimentally, where τ_y is the yield stress of the slurry (Pa), K is the consistency index (Pa.s^n) and n is a power with no units.

Pirouz (2006) presented a semi-empirical model for the prediction of tailings beach slopes that was also based on predicting the slope of a self formed channel on a beach. The theoretical aspect of Pirouz's work was the application of energy dissipation equations, whilst the empirical aspect of Pirouz's method focused on experimentally measuring the "zone settling rate" of a slurry, which is defined as the speed of the linear part of the settlement curve for the interface that forms between the decant water contained in the slurry and the particles that settle out. The zone settling rate is determined in a lab under still conditions, in which a sample, typically of some litres in volume, is monitored as it settles in a wide bowl with a flat base and vertical sides. A typical zone settling rate for a tailings slurry would be about 5 millimetres per hour, but this is higher for a more dilute sample of the same slurry.

The crux of this empirical component of Pirouz's model is a fairly weak 8 point correlation between Reynolds number values for one type of tailings slurry in channel flow plotted against zone settling results for samples of the same slurry in still conditions in a lab. He uses this correlation to suggest that the zone settling rate can be used to predict the Reynolds number "required to create that amount of turbulence in the flow". One must question the rationale for correlating these two very different independently measured quantities. Furthermore, even if one were to accept the connection, more data for another type of slurry would be of significant value in adding strength to the trend, but none is presented.

To enable this model to be applied without performing zone settling experiments, Pirouz presents a chart for predicting of the zone settling rate for a slurry, based on the slurry concentration and the depth of flow of the slurry in an open channel. This chart associates the initial depth of the zone settling test with the depth of flow in the channel. This is a questionable connection between two very independent quantities, seemingly on the basis that they are equal scalar quantities.

The Pirouz slope prediction procedure refers to "*VI*" in the "Stable Channel Section Equations" in Appendix C, but it was found that Appendix C did not feature any equation with a *VI*. The only equation that calculates a velocity requires input values for Manning's *n* and the channel slope, which would not enable the prediction of a beach slope. It was found that Pirouz's prediction procedure was not sufficiently clear to enable its application.

Another aspect of Pirouz's model makes it potentially difficult to apply; Pirouz suggests the experimental measurement of the submarine angle of repose of tailings in order to predict a channel cross sectional shape in accordance with a method set forth by the US Bureau of Reclamation. There are some problems with this suggestion in the context of tailings slurry however: The USBR graph presented by Pirouz shows a particle size range of 0.2 to 4 inches, whereas the particles of Pirouz's slurry had a median grain diameter of 8 microns, some 600 times smaller than the smallest USBR particle. Even if one were to assume that the USBR rationale could still apply under these conditions, the suggested method of dropping particles into clear water in a container to sink to the bottom and form a cone would take a long time when the median particles are only 8 micron in diameter. The handling of individual particles of that size would also pose significant difficulty and tedium. However, beyond these practical limitations of Pirouz's approach, he has also defied his own aversion to clear water conditions, which he made clear when he dismissed sediment transport approaches earlier on in his thesis for this reason.

Pirouz has tested no independent data for the validation of his model. Only 3 graphs are presented, each with only 8 points of data shown, the same 8 points of data that have been used in generating the empirical fit that the Pirouz model is based upon.

In its presented form, the Pirouz model can not be applied. The equations to be used are not apparent, and the challenge of measuring the angle of repose of tailings particles under water imposes a significant obstacle in the way of its application.

2.1.4 Tailings stacking experiments

Others have conducted large scale tailings discharge experiments to more specifically analyse the formation of tailings stacks (Williams & Meynink 1986).

Williams & Meynink conducted an experiment in which approximately 47,000 tonnes of thickened copper tailings was discharged onto a large flat area over a period of about 45 days to create a large stack. Simultaneously they poured smaller stacks with the same tailings at a smaller flow rate nearby, in an attempt to compare the geometry of the large and small stacks. They found that the small stacks did not resemble the large one, neither in slope geometry, nor in the curvature of the resultant beach profiles.

Williams & Meynink also made the following observations about the slurry deposition process: The slurry will initially fan out to cover a wide area until a certain resistance to further dispersion is achieved. The tailings will then confine itself to a self-formed channel that runs on top of the recently deposited fans, to travel to the outlying reaches of the deposit. The slurry is then seen to disperse in the same wide thin fans to deposit in that new frontier. Eventually this new deposit will reach a resistance point, and the self formed channel will advance across the top of this area to move even further along. It was noted that the slope of the self-formed channels is less than the slope of the fan flows. Due to this observed channel transport of the non-segregating tailings it was suggested that the slope of the self formed channels were defining the overall slope of the tailings beach.

Williams & Meynink presented an empirical formula for predicting the slope of the self forming channel, as follows:

$$S = \frac{8.81 C_W \overline{W}_c}{K} \tag{15}$$

where S is the slope of the channel (%), C_W is the solids concentration (% w/w), $\overline{W_c}$ is the mean fall velocity of the mixture (m/s) at the concentration C, and K is the "transport constant", an empirical constant that is fitted to a particular tailings slurry (m/s).

Despite the apparent simplicity of this approach, it was found that Williams & Meynink's formula was not reliable in predicting this channel slope. The transport constant K was not an easily derived parameter, as it must define so many characteristics of a given slurry. Williams & Meynink initially proposed that the transport constant could possibly be universal in its application to all tailings slurries, but it was later found that different slurry flows have different transport constants. (Williams 2005)

2.1.5 Theoretical approaches

Attempts have been made to produce more theoretically based tailings beach slope models through the prediction of the angle of repose from a geomechanics slope stability approach (Blight & Bentel 1983), prediction of energy dissipation in a turbulently flowing channel (McPhail 1994; McPhail & Blight 1998; Pirouz 2006), and application of sediment transport theory in a river bed load context (Morris 1993; Morris & Williams 1996, 1997a).

Blight & Bentel (1983) investigated the angle of repose that resulted from the discharge of non-segregating slurry. They chose to do this by applying the geotechnical design approach of infinite slope stability analysis, presenting the following equation for predicting the angle of repose, θ:

$$\theta = \arcsin\left(\frac{\tau_0}{\rho g \delta}\right) \tag{16}$$

where τ_0 represents the yield stress of the tailings, ρ is the tailings density, and δ is the layer thickness. It is noted that this equation is a form of Du Boys' equation, though this was not acknowledged in Blight & Bentel's paper.

Blight & Bentel then went about experimentally validating this approach in a rather novel way by conducting laboratory experiments in which a 5 mm thick layer of non-segregating slurry was spread evenly across a pane of glass, with the pane then tilted until the slurry slid down its surface. The presented plots of tilted plane experimental results alongside the model curve did provide good support to the theoretical model. However, Blight & Bentel were not able to show that this approach could be extended to actual tailings beaches, despite having field data on hand, because their model predicted slump failure for a high density thickened tailings, which, according to their reference Robinsky, formed a linear beach. They had collected field data in which actual tailings beaches at 6 platinum tailings dams as well as individual gold, copper and diamond tailings beaches were measured, but the slurry discharged onto these 9 concaved beaches was segregating in all cases.

Cross-sectional profiles for the 6 platinum beaches were presented in the paper, with the overall beach slopes (total height divided by total length) ranging between 0.044 and 0.021. No empirical beach slope equation was presented on the basis of this data.

There was no acknowledgement of the channel flow behaviour of a tailings slurry in Blight & Bentel's paper, and their experimental approach shows that they were completely focused on sheet flow of tailings slurry.

One comment that must be made about the described experimental technique is that it is unrealistically affected by the smoothness of the glass surface when compared to a tailings beach surface, let alone the effect of any seepage, absorption or suction of water that might occur on a layer of tailings, which will not occur on glass. The astonishing aspect of this is the comment by Blight & Bentel that their experimental data "probably represent the lower limit to the inclinations corresponding to [the] equation".

It is noted that the experimental results presented by Blight & Bentel only mentioned layer thicknesses of 5 mm. It is wondered if they tried layer thicknesses other than 5 mm, and if so, why this data was not presented.

Blight et al. (1985) presented an amendment to the slope equation previously presented by Blight & Bentel (1983) : it is stated that the angle of repose equation was incorrectly presented without a factor of 2 multiplied with the repose angle θ, which thereby yields:

$$2\theta = \arcsin\left(\frac{\tau_0}{\rho g \delta}\right) \tag{17}$$

This amendment now renders equation 17 to be in contradiction with DuBoy's equation.

One critical problem with this equation as identified by Blight et al. is the definition of δ, the depth of each layer of tailings, since it is not known in a tailings beach situation. Furthermore, the authors then presented experimental data with known layer depths to demonstrate that the slope equation was inadequate in a predictive capacity anyway, concluding the exercise by stating that the beach slope can not be predicted from the laboratory measurement of the yield stress of the slurry.

McPhail (1994) presented a new approach to beach formation based on the principles of energy conservation. For predicting the beach profile, his work presented the following series of equations:

$$y = y(x + \Delta x) + S_B(x)\Delta x \tag{18}$$

where $S_B(x)$, the slope of the beach at point x is given by:

$$S_B(x) = -\frac{(1 - \exp^{-\mu P_0})}{L\mu \exp^{-\mu P(x)}} \tag{19}$$

where $P(x)$, the stream power at point x is given by:

$$P(x) = -\frac{1}{\mu}\ln\left[(1 - \exp^{-\mu P_0})\frac{x}{L} + \exp^{-\mu P_0}\right] \tag{20}$$

where P_0, the stream power at the plunge pool is calculated by:

$$P_0 = \rho q \frac{v^2}{2} \tag{21}$$

and μ, a constant, is solved from the following equation:

$$S_0 = -\frac{(1-\exp^{-\mu P_0})}{L\mu \exp^{-\mu P_0}} \tag{22}$$

where S_0 is the initial slope of the beach, L is the length of the beach, v is the velocity in the plunge pool, and x and y are the horizontal and vertical coordinates along the beach profile respectively.

It quickly becomes apparent that this approach is very difficult to apply in predicting the profile of a tailings beach because some of the input parameters are practically impossible to calculate or measure in the first place. You must know the initial slope of the beach and then nominate a length for your beach. If you knew these things to begin with you would not go to all the trouble of predicting a profile. Besides these two parameters, it is also necessary to know the velocity in the plunge pool. This is a remarkable feat, to be able to state the velocity of a fluid in such a turbulently chaotic environment. This thereby limits the value of McPhail's approach.

2.1.6 Tailings beach profile prediction

In the investigation of the slope of tailings beaches, it is generally observed that the tailings beaches are usually concave in cross-section, though the degree of concavity from one beach to the next can vary considerably. This has led to more specific research being done in an effort to predict the cross-sectional shape of a tailings beach, which is commonly referred to as the beach profile. Though this work is highly relevant in the greater context of predicting tailings beach shapes, strictly speaking it is a diversion from the topic of predicting beach slopes. In some of the literature discussed in this section, it has been found that the pursuit of a method of tailings beach profile prediction has shifted the

research focus completely away from the topic of tailings beach slopes. However, the work presented in this field to date deserves some discussion here for obvious reasons.

Melent'ev et al. (1973) presented the concept of "the Master Profile". Through the comparison of several tailings beaches, they asserted that the cross sectional profile of any hydraulically deposited tailings beach could be found to follow a dimensionless "master profile" as per the following equation:

$$\frac{y}{H} = \left(1 - \frac{x}{L}\right)^n \tag{23}$$

where y represents the vertical distance from the lowest point of the beach, H is the overall height of the beach, x is the relative distance along the beach from the discharge point, L is the overall length of the beach and n is a fitted power that describes the curvature of the beach.

Robinsky (1975) did presented two conceptual theories to explain the resultant profile of a tailings beach. Firstly he stated that tailings streams bifurcate as they run down a beach, a process that he deemed to be the inverse of the natural behaviour of rivers as they merge. In drawing this river analogy further, he stated that in nature the smaller tributary streams have steeper gradients than the wider trunk stream that they flow into. By this rationale he stated that the diminishing sized streams on a tailings beach should have steeper slopes than the primary channel, resulting in an overall convex profile of the tailings beach. However, Robinsky then went on to say that the sheet flow aspect of tailings deposition essentially resembled the alluvial fan behaviour of many geological sedimentary deposits, in which a concave profile is always observed. From these two processes he decided that the overall effect would be a straight beach with no curvature, or else one with slight concavity.

Robinsky (1978) later presented another theory for explaining the concavity of a tailings beach. He introduced the concept of a segregation threshold. He used this to explain the relevance of segregation on the beaching of tailings, asserting that segregating slurry will produce a beach with significantly greater concavity than non-segregating slurry. Segregating slurry will deposit the larger particles near to the discharge point, whilst a non-segregating slurry will drop all particles uniformly along the length

of the beach. He presented Particle Size Distribution (PSD) data to support this finding, generated from tailings samples that were taken from various points along the Kidd Creek stack beach after segregating and non-segregating slurries were discharged for several months respectively.

Robinsky claimed that a non-segregating slurry will create a linear beach with a slope that is "close to the natural angle of repose of the slurry", but then went on to say that the 3680 foot-long beach at Kidd Creek exhibits a concavity of some 2 to 3 feet. He claimed that this concavity was due to the viscosity of the tailings decreasing slightly over the 3680 foot distance because of water entering the slurry from the underlying tailings, which is squeezed out by the weight of the newly deposited tailings.

Blight & Bentel (1983) presented dimensionless profiles of actual tailings beaches that were surveyed at some 9 impoundments to show that all of them could be reasonably described by the Master Profile equation of Melent'ev et al. (1973) (equation 23), providing the value of n was known. It is noted however, that there is a distinct absence of any mention of Melent'ev et al. in this paper, despite subsequent publications by Geoff Blight acknowledging Melent'ev et al. as being the creators of the Master Profile equation and concept. It is noted however, that in order for the Master Profile concept to be applied in a predictive context, not only does the power n need to be quantified, but also the elevations of both the apex and toe of the beach, as well as the overall length of the beach. These workers also reported that the degree of curvature of a beach increased with an increase in particle size.

Blight et al. (1985) presented a study of the ability for laboratory scale tailings beach tests to predict the degree of concavity of a tailings beach. A flat bottomed plexiglass flume of about 1.8 meters in length and 0.6 m in width was used, which essentially resembled a fish tank. Their flume had a spigot at one end for the introduction of tailings slurry, and a decant outlet at the other for drainage of the liquor. These workers tested 4 different types of tailings slurry in their flume; gold, copper, diamond and platinum. They asserted that a normalised dimensionless profile could be generated from a small scale flume test, which would enable the determination of a value of n in the master profile equation (equation 23).

Smith et al. (1986a, 1986b) undertook a field investigation of tailings beach profiles in which 6 different types of tailings beaches were considered; molybdenum, silver, gold sulphide, platinum, uranium and copper. Mine sites were visited, and full sized tailings beach profiles were surveyed. In both of their 1986 papers, Smith et al. claimed to have developed a method for predicting beach slopes, but in fact their prediction procedure merely prescribed the use of either a power law or an exponential profile fit equation to predict the dimensionless beach profile. In either case, an empirical factor was provided to account for an expected degree of curvature, but neither of the two equations actually calculated the beach slope. It must be said that their frequent use of the word "slope" was highly misleading. Their empirically prescribed power of 1.65, and the equivalent alternative exponential factors for the exponential fit were not ideal, but instead, merely an average value of those fitted to the beach profiles. This was hardly a major advance on Melent'ev et al. (who initially proposed the power law fit with a power of 1.6), with the exception of the exponential equation being proposed as an alternative, with a procedure presented for determining when it is more appropriate to use.

Williams & Meynink (1986) found qualitatively that hydraulic sorting caused concavity on the basis of the collected data and observations of their tailings stacking trials, though there was no attempt to present any quantitative relationship between the two.

Wates et al (1987) suggested that the curvature of a tailings beach is caused by the decrease in concentration of the slurry as it progressively loses solid particles during its journey down the beach, rather than from the sorting of particles as they segregate down the beach. They claimed that this phenomenon was evident from their flume experiments, but such evidence was not presented in the paper.

Fourie (1988) reported on his own attempt to repeat the experimental findings of Blight et al. (1985). He performed experiments in a laboratory flume of the same dimensions as that of Blight et al, but using three different tailings slurries; bauxite, nickel ore and coal. Fourie found that his miniature beaches were all convex in shape, rather than concave as observed by Blight & Bentel. He explained this as being the result of his tailings "having relatively higher solids content and to the gap graded

nature of bauxite tailings". Fourie also observed that different concentrations of slurries produced miniature beaches with the same normalised profile.

Williams & Morris (1989) investigated the profile of a tailings beach, based on principles of river bed hydraulics and sediment transport theory. They proposed a new method of defining the beach profile, based on an equation presented by Shulits in 1941 for the prediction of the longitudinal profile of natural river beds:

$$S = S_0 \exp\left(-\omega \frac{x}{L}\right) \tag{24}$$

where S is the slope of the river profile at a horizontal distance x beyond the highest point of reference, S_0 is the initial slope of the river, L is the length of the river, and ω is a constant, calculated with the following equation:

$$\omega = \ln\left(\frac{S_0}{S_L}\right) \tag{25}$$

where S_L is the slope at the far end of the river, where $x = L$.

Williams & Morris showed that these equations provided a good fit to their own data as well as that of Blight & Bentel (1983), which was a better fit than that achieved by Blight & Bentel in their application of the Melent'ev et al. Master profile equation. However, despite this successful demonstration, Williams & Morris' approach provides no further insight into tailings beach slope prediction. They simply showed that the concaved profile of a tailings beach more closely follows the shape of an exponential function than that of a power law function. However, this work was not new, since Smith et al. (1986) had already proposed a similar exponential equation three years earlier.

In the mid 90's Morris & Williams set about conducting a range of flume experiments to investigate the applicability of laboratory flume experiments in determining the parameters used in his model;

nominally the final and initial slopes of a beach. In 1996 they released a paper discussing the flume experiments and their subsequent findings: flume experiments do not gain a reasonable resemblance to actual tailings beaches (Morris & Williams 1996). They did, however, claim that the parameter ω (equation 25) could reasonably be gained from the flume experiments, thereby enabling the experimental prediction of beach curvature. This claim echoed the findings of Blight et al (1985), reported some 11 years earlier.

Morris & Williams concluded that the initial slope of a beach was the only parameter left that prevented the applicability of their model for predicting beach profiles. They suggested that it would be worthwhile to investigate the processes that take place in a plunge pool, to better understand the behaviour of tailings beach deposition at its upstream end. If a method could be developed that accurately predicts the initial slope of a beach, then with simple flume experiments the rest of the beach profile could be predicted, using the model proposed by Williams & Morris in 1989.

Beyond their research into the profiles of tailings slurries, in the mid 90's Williams & Morris also analysed some full scale beach profiles that were generated through the co-disposal of tailings slurry mixed with larger sized unprocessed waste rock. They found that their same river profile equation fitted co-disposal beach data as well. (Morris & Williams 1997b, 1997c)

Fan & Masliyah (1990) proposed a "theoretical" model for predicting the profile of a tailings beach, which could be simplified to a similar form of equation to that proposed by Melent'ev et al. (1973). Like previous workers who investigated the "Master Profile" concept, the approach of Fan & Masliyah also required that the height and length of the beach be known, and used an empirically derived constant to dictate the degree of concavity of the beach.

Kupper (1991) made some interesting observations about the cause of beach concavity. She presented some evidence to refute the claim that particle sorting is the cause, but then suggested that concavity is instead due to two factors: the change in concentration of the bed load layer of the slurry that is flowing down the beach in a channel, and the seepage of water from the slurry at the upper section of the beach and seepage of water into the slurry at the lower sections of the beach.

Chryss et al. (2006) suggested that beach profile concavity is caused by a change in the density of the underlying tailings material, with this variation in bed density resulting in different channel shapes occurring on a tailings beach, this in turn causing a different equilibrium slope of the channel.

Fitton et al. (2006) asserted that variation in slurry discharge parameters would cause concavity of a tailings beach, on the basis that low flow rates or high concentrations would result in steep deposits located near the discharge spigots, and high flow rates or low concentrations would leave flatter deposits far from the discharge outlet. The superposition of numerous such deposits would ultimately create a concave profile.

2.2 Hydraulic fill studies

Related work has been done on sand-water mixtures in the context of predicting the slope of beaches formed the hydraulic discharge of dredged sand (Winterwerp et al. 1990).

Winterwerp et al. (1990) conducted a series of flume experiments to analyse sediment deposition in the flow of a sand-water mixture. Their work did not focus on tailings, as they were instead conducting a laboratory investigation of the recent hydraulic fill land reclamation activities taking place in the Netherlands. They conducted experiments with a small flume of 1.5 m length and a large flume of 9 m length, whilst also collecting a set of data from full scale field measurements from a dredging fill site.

Of critical importance to the Delft team was the concept of an “equilibrium slope” in the channel flow of the sand-water mixture, whereby the erosion of the underlying bed is equal to the deposition of new sediment, therefore cancelling each other out and resulting in a total transport scenario. These workers suggested that the slope of the hydraulically deposited beach of sand was defined by this channel equilibrium slope, in the same context that Williams & Meynink suggested the same aspect of tailings beach formation.

Winterwerp et al. presented an empirically modified equation for the prediction of the equilibrium slope of an open channel of sand and water in turbulent flow, based on a modified form of the sediment

transport formulation of Engelund-Hansen to gain a better fit with their data. This equation was as follows:

$$i_{eq} = \left[\frac{(s-1)^2 d_{50}}{0.20} C_V (1-C_V)^2 \right]^{0.6} \left[\frac{f_D g^2}{8} \right]^{0.1} q^{-0.4} \qquad (26)$$

where s is the ratio of the density of the solids to the density of the carrier fluid, d_{50} is the median grain diameter, C_V is the volumetric concentration, f_D is the Darcy friction factor and q is the specific flow rate, equal to the channel flow rate divided by the channel width.

It was found by Winterwerp et al. that this equation vaguely fitted some of their large scale flume data, but not so for the small scale data or the field data.

Winterwerp et al. also presented a completely empirical equation of best fit to their data as follows:

$$i_{eq} = \left[0.0056 \frac{d}{d_{ref}} - 0.0045 \right] q^{-0.45} \qquad (27)$$

where d is the representative grain diameter, d_{ref} has a constant value of 65 μm, and q is the specific flow rate, equal to the channel flow rate divided by the channel width.

Winterwerp et al.'s empirical equation makes no reference to the concentration of the sand-water mixture, which infers that the concentration has no significant effect on the channel equilibrium slope.

The findings of Winterwerp et al. were very interesting in relation to the effect of the scale of the flume used. They exercised a very rigorous approach to their flume experiments, using modern and accurate measurement techniques to collect their data. Due to the close similarity of our experimental methods to theirs, it is well appreciated how difficult such measurements are to gather, and more critically, how subjective the results can be depending on the experimenter. For this reason, comparisons of the

various experimental programmes of Winterwerp et al. can be said to be of considerable power, because the three different types of experiments were all run by the one group of experimenters. It is noted that the smaller of their two laboratory flume rigs presented data that was apparently random and demonstrated no obvious trend. The data collected in the field also defied any trend as a result of the difficulty in being able to physically collect the data on site.

2.3 Geological investigations of alluvial fan deposits

Sedimentary geologists have also presented field studies done on alluvial fan deposits with empirically "calibrated" fan profiles (Parker et al. 1998a, 1998b; Sun et al. 2002), with corroborated laboratory experimental work being done in an attempt to develop a small scale test method for predicting alluvial deposition (Whipple et al. 1998). These workers had a broad focus that aimed to model all fluvial fan depositional processes, from the slow, massive scale morphology of river deltas and vast flood plains to the relatively smaller scale build up of tailings beaches. In the work presented by this group, a large scale investigation of tailings beaches took place at the "Rolling Stone" mine in Minnesota, USA, over several years during the 1990's. The data collected from this investigative work was used to calibrate a model that was presented in the other of two companion papers in 1998.

The following equation was presented in the 1998 paper by Parker et al. for predicting the slope of an alluvial fan deposit:

$$S = \left[R^{-1/2} \alpha_S^{-1} \alpha_b^{(3+2p)/2} \alpha_r \left(\frac{\alpha_b}{R} - \tau_c^* \right)^{-n} \left(\frac{Q_{S0}(1-\hat{r})^2}{Q_W} \right) \right]^{1/(1-p)} \qquad (28)$$

where R is the submerged specific gravity of the sediment, α_S is the sediment transport coefficient, α_b is the flow channelization coefficient, p is the hydraulic resistance exponent, α_r is the hydraulic resistance coefficient, τ_c is the sediment transport critical shields stress, n is the sediment transport exponent, Q_{S0} is the flow rate of sediment, $\hat{r}$ is the dimensionless radial distance from the apex of the fan (equal to the radial distance divided by the length of the fan) and Q_W is the flow rate of water.

In three of the cited papers, this model has been applied in various contexts. In the 1998 experimental paper, the model was calibrated against the recorded data for the Rolling Stone mine tailings dam. In the 1998 paper by Whipple et al., the model was tested against small scale fluvial experimental data that was generated in two 3-dimensional laboratory experiments. In the 2002 paper by Sun et al., the same model was once again tested, but on this occasion, against some large scale data for the morphology of the fan delta of the Yellow River, China. In each of these 3 papers, different values have been adopted for the various coefficients and exponents in the equation, so the respective values nominated for each paper are presented in Table 1.

	α_s	α_b	p	α_r	τ_c	n
Parker et al. 1998	16.3	3.6	0	10	0	2.5
Whipple et al. 1999	16	0.237	0.167	6.95	0.132	1.8
Sun et al. 2002	11.25	2.97	0	15	0	2.5

Table 1. Assigned values for parameters in the Parker et al. equation

2.4 Prediction of spillage from a tailings dam failure

A model was developed for the prediction of the mass flow of tailings from a failed embankment. (Jeyapalan et al.1983a, 1983b) This model predicted the speed and the geometry of an avalanche type flow as it poured out through the breach in the basin. Jeyapalan et al. conducted flume experiments with a 6 ft long x 1 ft wide fish tank type flume, in which viscous oil was used as an analogue to the tailings. A volume of oil was confined at one end of the flume behind a vertical wall located 4 ft from the far end. The wall was quickly removed vertically to release the oil, which then spilled forward in a tongue-like shape that was periodically photographed with a clock in view. The speed of the tip of the tongue, and the height of the tongue were predicted very well by the model presented by Jeyapalan et al. However, the point at which a tailings flow stops, which Jeyapalan et al. referred to as the freezing point, was not predicted for the presented flume experiments, because the freeze time predicted by the model required the tailings to have a yield stress. The oil used in his flume did not have a yield stress, so the flow did not reach a freezing point, and the fluid eventually levelled out to a uniform depth in the base of the experimental tank.

Jeyapalan et al. did not focus on the prediction or formation of tailings beach slopes, nor did they create their model with this objective in mind. These workers did not consider the channel flow mechanism that causes tailings deposition on a beach. Their model was not based on the continuous discharge of tailings slurry from a spigot. For these reasons, the Jeyapalan model is not investigated further for the modelling of tailings beach slopes. However, the Jeyapalan et al. model is discussed here because of its relevance to other work done using similar physical concepts, but with a view to predicting tailings beach slopes, such as the work of Blight & Bentel (1983) and that of Sofra & Boger (1996).

2.5 Slump of tailings pastes

Research was also recently done to model the slumping behaviour of tailings pastes (Nguyen & Boger 1998; Pashias et al. 1996; Sofra & Boger 2001) and other "yield stress fluids" (Coussot et al. 1996), with much research done on the rheology of tailings slurries (Clayton et al. 2003; Nguyen & Boger 1998)

Pashias et al. (1996) attempted to characterise the slumping behaviour of yield stress fluids, with a particular focus on tailings pastes. These workers conducted research in the rheology of yield stress fluids in an attempt to investigate any relation between the slumping behaviour of the fluid and the yield stress of the fluid. They explored the applicability of the standard slump test – a commonly used basic field test for gauging the flow behavior of wet concrete – for measuring the yield stress of tailings slurry and other yield stress fluids. They found that the slump test was highly applicable in this capacity, and was thus able to lead to a simple alternative test for the determination of the yield stress of a fluid. They then posed the notion of a "50 cent rheometer" on the basis of the standard slump test cone being replaced with a cylinder that could be served with the use of a short piece of pipe, such as the mid-section of a soft drink can.

Coussot et al. (1996) investigated the flow of a finite volume of a yield stress fluid on an inclined plain. A fully theoretical approach was taken in developing a 3 dimensional model, and experimental results were gathered through experimentation with kaolin clay slurries on an inclined plane. It was stated

that the longitudinal profile of a finite blob of yield stress material could be described with the following equations:

$$D = H - \ln|1 + H| \tag{29}$$

$$D = \rho g d (\sin\theta)^2 / \tau_c \cos(\theta) \tag{30}$$

where D is the dimensionless distance from the leading edge of the deposit, H is the dimensionless height of the deposit, ρ is the density of the slurry, g is the acceleration due to gravity, d is the distance from the leading edge of the deposit, θ is the angle of the underlying plane and τ_c is the yield stress of the slurry. It can be seen that this equation, like that of Blight & Bentel (1983), also equates to DuBoy's equation.

The experimental data provided excellent validation to their model, though it was found that their model, when applied to the prediction of the slump of wet concrete on a flat plane, overestimated the spread of the concrete.

Sofra & Boger (2001) investigated experimental flume tests on a small scale to measure the angle of repose exhibited by 3 different tailings pastes at various concentrations and slopes. The test was done in such a way that a discrete paste sample was released from a container at the head of the flume rig by the removal of a sluice gate, similarly to the experiments done by Jeyalapan et al. (1983b). The paste would then run down the slope a certain distance and stop before it reached the bottom of the ramp. The slope at the toe of the flow would then be measured. They presented their findings graphically, and found that the following relationship could predict the angle of repose of a paste flow down an inclined plane:

$$\theta = f\left(\frac{\tau_y \eta}{\rho^2 W^2 g v}\right) \tag{31}$$

where: θ is the angle of repose (in degrees)

τ_y is the yield stress (Pa)

η is the viscosity (Pa.s)

ρ is the slurry density (kg/m^3)

W is the width of the inclined plane (m)

g is the acceleration due to gravity (m/s^2)

v is the initial velocity of the flow (m/s)

From the graph that was presented in their paper, a gradient of 2.667 x 10^6 has been calculated for the line of fit for their data, producing the equation:

$$\theta = 2.667 \text{ x } 10^6 \left(\frac{\tau_y \eta}{\rho^2 W^2 g v} \right) \qquad (32)$$

Despite their claim that their model predicted tailings beach slopes, the approach of Sofra & Boger was not relevant to the formation of a tailings beach. Like Jeyapalan et al. in their modelling of tailings dam failures, these workers did not consider the channel flow mechanism that causes tailings deposition on a beach, nor did Sofra & Boger consider the continuous discharge of tailings slurry from a spigot either. Both of these processes are essential in the formation of a tailings beach.

Another incompatibility between the approach of Sofra & Boger and the process of tailings beach formation was the comparatively high viscosities of the pastes tested by Sofra & Boger. The range of yield stress values exhibited by the pastes tested by Sofra & Boger was between 17 and 210 Pa, while tailings slurries discharged on a beach typically exhibit yield stress values between 0 and 30 Pa. A paste with a yield stress value of 200 Pa would not be viable for discharging onto a tailings beach for a number of reasons: it would be very expensive to pump; it would not spread out in thin layers to dry and gain strength; it would pose a significant threat of slump failure because of this low development of strength; and it would quickly bury the discharge spigots.

It is noted that the work of Blight & Bentel (1983) could also be included in this section. Instead of considering the shape formed by a yield stress fluid, Blight & Bentel were solely interested in the angle of repose of an evenly spread layer. It can be seen that their equation for the angle of repose (equation 16) is very similar to that presented by Coussot et al. (equation 30).

2.6 An ongoing problem

Unfortunately, much of the work discussed above can not be regarded as presenting a reliable, general, and easily applied method of tailings beach slope prediction. Some of the models are not accurate, as will be shown. Some of the models are not simple to apply. Some of the models are limited in either catering to such a specific tailings discharge situation (such as a limited ore type, or for very low segregating concentrations or for very high concentrations), and others are impossible to apply without knowing an "initial" beach slope, effectively defeating the purpose of the exercise. Many authors seem to have taken the path to profile prediction instead of slope prediction; despite their own admission of there being the need for a slope prediction method, and some workers seem to have incorrectly proclaimed their research to be on tailings beach slopes when in fact it was not.

In consideration of numerous observations the of tailings discharge behaviour in real tailings storage facilities (Pirouz 2006; Williams & Meynink 1986) as well as the author's own observations that are noted in section 1.6, it becomes apparent that many of the previous workers have incorrectly identified the mechanisms that take part in the formation of a tailings beach.

This incorrect identification is most evident with the number of miniature scale "fish tank" flume experimenters (Blight et al. 1985; Boldt 1988; Fan & Masliyah 1990; Fourie 1988; Kupper 1991; Ribeiro & Assis 1999; Wates et al. 1987; Williams & Morris 1989), in which the channel flow behaviour of hydraulically discharged tailings slurry never actually occurs in their flumes because of the minute flow rates that are being applied. Low flow rates were adopted in an order to allow the tailings particles to gently settle inside the flume to form a deposit, with many of these experiments conducted at very low concentrations. In many of these cases it appears that the workers are not aware of the critical influence of the naturally occurring channel formation. Though it could be said that fish

tank exercises enable the observation of particle deposition in a controlled environment, it is critical that the process being observed in the flume can be correctly identified in full scale tailings discharge if it is to be claimed as a method of tailings beach modelling. The work of Fourie (1988) provides a good example, in which a non-segregating slurry is producing convex profiles in his flume, to his surprise. Many of the other miniature flume experimenters also seem to make a similar assumption that the mini "beach" forming in their flumes is just that; a mini beach. It was evident that they expected that their mini beach could be scaled up in some way to produce some meaningful information about the full scale behaviour of a tailings discharge scenario. When it became evident that the flume beaches were not giving realistic slopes, they tried to apply their flume experimental data to the prediction of beach profile curvature instead. It has not been said that fish tank flume deposits are not miniature beaches, but it should have been, and it is being said right now. Fourie's findings should have led these workers to consider this possibility. Until Fourie's work, most of the previous studies observed concave deposits, which were comparable to real tailings beaches, even if the slopes were not. With Fourie's finding, not only the fact that fish tanks don't form mini versions of real tailings beaches should have been realised, but also, it should then have been realised that the degree of curvature of the deposit formed inside a fish tank flume is not indicative of the degree of curvature of a full sized tailings beach either.

Another interesting comment to be made about some of the articles presented earlier on in the literature, such as those by Fourie (1988) and Blight (1987), is that no apparent regard has been made for the rheology of a slurry. Instead, all focus is on the solids content. Fourie is blatant in his comparison of different types of slurries on the basis of solids contents, without any regard for the possibility that a coal slurry at a given concentration might exhibit different flow characteristics to a nickel ore slurry at the same concentration.

Another example of the incorrect identification of the processes of tailings beach formation can be found in the work of Sofra & Boger (2001). These workers experimented with tailings pastes, observing the rapidly occurring slump of a measured quantity of paste being released on an inclined ramp. They claimed that these experiments were creating miniature versions of thickened tailings

beaches, but once again, this was an example of tailings researchers failing to consider the physical processes that take place on a tailings beach.

The theoretical approaches of Morris and McPhail can both be seen to appreciate the critical effect of the self formed channel of tailings on the resulting beach slope. Not only do both these workers note the occurrence of channels on a tailings beach, but they also tackle their respective beach slope models from a channel flow perspective. Unfortunately however, neither of their respective models offered a means of beach slope prediction.

Blight (1994) reviewed some of the work to date that had been achieved in the field of tailings beach modelling, and made the following statement: "At present there is no rational or adequate empirical method for predicting the average gradient for a beach". Later on in the same work Blight stated, "At present there appears to be no satisfactory expression for predicting the average beach slope". This sentiment was resounded more recently by Pinto and Barrera (2002) upon a further updated review of literature pertaining to tailings beach slope prediction.

From the literature reviewed here, some effort will be made to validate each of the slope prediction models against new experimental data as well as some independently collected experimental data and full scale tailings beach slope data. This work will be presented in Chapter 4.

All of the work that has been discussed in this chapter has focused on the prediction of tailings beach slopes (or the slope of some related material) in a two-dimensional context. Later in this thesis the three dimensions of a tailings storage facility are considered, with Chapter 6 presenting some discussion and modelling of three-dimensional tailings beaches.

Chapter 3: Experimental Work

3.1 Experimental Rationale

In section 1.6 it was reported that a non-segregating tailings slurry forms its own channel as it runs down a tailings beach. This process has been observed and described by Williams & Meynink (1986), Pirouz et al. (2005) and Fitton et al. (2006). These authors all asserted that the channel runs at a slope that is sufficient to keep all the slurry particles transported downstream, but not so steep as to erode the underlying beach. All of these authors suggested that the channel slope dictates the slope of the tailings beach. Documenting some related experimental work with sand-water mixtures, Winterwerp et al. (1990) referred to this critical slope of the channel as the "equilibrium slope", named as such because it was sufficiently steep to enable the transport of all of the slurry particles whilst not being so steep as to erode the underlying bed of deposited particles, thereby effectively placing the opposing effects of erosion and deposition in equilibrium.

The experimental phase of this research project set out not only to investigate this channel flow behaviour of tailings slurry, but to generate some useful data to allow quantitative analysis to be done. In order to gather such data, a flume was seen to provide a useful means for simulating the open channel flow of tailings slurry at a variety of slopes, flow rates and concentrations, with an approach similar to that of Winterwerp et al. (1990). Unlike monitoring the discharge of slurry down an established beach like the work described by Boldt (1988), the use of a flume presented two major advantages: firstly, it enabled the testing of differently sloped channels; and secondly, the flume allowed good access to the channel for probing and close measurements to be made of velocities, concentrations, depths, and channel width.

3.2 Experimental Programme

Two major experimental phases were undertaken for this project. The first phase consisted of large scale field experiments that were conducted at two mine sites in Australia. The first experimental campaign took place from 24th May to 1st June 2004 at the Peak Gold Mine in Cobar, New South

Wales; and the second occurred between 17th February and 17th March 2005 at the Sunrise Dam Gold Mine, in Western Australia. The second phase of experimental work was undertaken between 31st January and 7th March 2007 at RMIT University in Melbourne, Australia, using a small scale flume.

3.3 Phase 1: Large scale field experiments

3.3.1 Experimental Objectives

The primary objective of the experimental work was to observe the equilibrium slope of tailings slurry running down a flume of adjustable slope so that the effects of changing the slurry concentration and flow rate could be observed. Numerous secondary objectives were also planned, such as the measurement of velocity and density at specific points within the flow. Taking velocity measurements across the flume at a particular cross section would allow the velocity profile at this cross section to be constructed, which could then provide significant evidence in identifying whether the flow was turbulent or laminar under equilibrium slope conditions. As well, velocity and depth measurements taken at various points along the length of the flume would indicate whether uniform flow conditions had been reached in the flume. Density measurements taken at specific points within the flow would enable the plotting of density profiles with respect to depth. This could then provide evidence of settling behaviour of the particles in the slurry, as well as some further indication of turbulent or laminar flow conditions. Sampling of slurry from specific locations within the flume was another objective of the large scale experimental work. Particle size analysis of these slurry samples would then provide an indication of segregation occurring in the flume. Rheological measurements of the tailings slurry at various concentrations was also planned. This rheological testing would allow the non-Newtonian nature of the fluid to be characterised with flow models in later analysis. Another experimental objective was to measure the cross sectional shape of self-formed tailings channels. The channel shape is not only required for calculating parameters that are essential to the analysis of open channel flow, but also for confirming that the adopted cross-sectional shape of the flume is representative of the channels that occur on a tailings beach.

Interesting and relevant anecdotal and qualitative data could also be gleaned from these field campaigns too, through a number of avenues:

- Observations of tailings discharge, transport and deposition on the beach. This behaviour could be observed for the slurry discharged from the processing plant as well as for the modified outflow from the flume.
- Advice and experience passed on from the operations personnel at the mines.

3.3.2 Flume for large scale field experiments

On the basis of the experimental rationale (Section 3.1) and objectives (Section 3.3.1), a flume was designed and constructed for the large scale field experiments. The flume was designed to emulate the flow conditions experienced by tailings slurry that is flowing in self formed channels on a tailings beach as closely as possible. It was intended that the flume would enable the testing of tailings slurry being directly discharged at the mine site at a flow rate that is typical of that discharged from a spigot onto a tailings beach, so it was necessary for the flume to be reasonably sized to achieve this. From studying the sizes of self-formed channels on tailings beaches, a flume length of 10 meters was chosen on the basis that it would be sufficiently long to enable the development of uniform flow. This figure was calculated from the work presented by Shenoy & Mashelkar (1983), in which it was reported that the entrance length for fully developed turbulent flow was $13D$ for flow with a Reynolds number of 6000, and greater for higher Reynolds numbers, where D is the diameter of the pipe. It is expected that the Reynolds numbers encountered in the flume will be between 1000 and 5000, so this figure of $13D$ should provide a conservative estimate for the entrance length. Applying the geometric conversion of $D = 4R_H$ (where R_H is the hydraulic radius of the channel), it is calculated that the entrance length for turbulent flow in a channel with a Reynolds number of 6000 would be equal to $52R_H$. The hydraulic radii of the channels found on tailings beaches range from 15 to 50 mm for flow rates ranging between 2 and 25 litres per second. Therefore, the development length required in the flume was calculated to be between 0.8 and 2.6 meters for flows of these magnitudes. The exit length (the downstream section affected by a gradual decrease in depth as a result of the increase in surface velocity) in the flume was also considered in the design. Yen (2003) suggested an exit length that was half of the entrance length for laminar open channel flow, while Bhagoria et al. (2001) used an exit length half the entrance length

for an experimental air duct system flowing turbulently. On this basis, it was conservatively assumed in this work that the exit length would be equal to the entrance length; ie, 2.6 m for the maximum design flow rate. The length of 10 metres would therefore be sufficient to provide a test section of fully developed flow some 4.8 to 8 metres in length in the mid section of the flume.

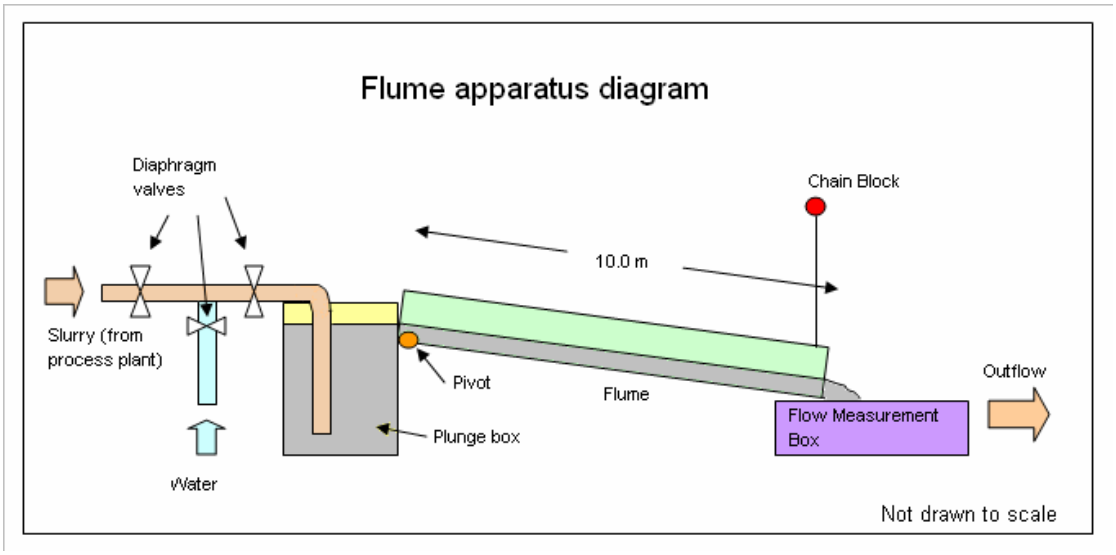

Figure 9. Flume apparatus diagram (grey areas indicate slurry flow profile)

Figure 10. Side view of the flume

Figure 11. Photo of the flume from above whilst flowing at an equilibrium slope

3.3.3 Channels for the flume

The choice of two semi-circular channels of 425 mm internal diameter and 340 mm internal diameter for the flume channels was based on measurements taken of self formed channels at Peak Gold Mine in Cobar, as well as the commercial availability of pipes of suitable size. In channels with soft boundaries, a concentration probe was used to determine the effective boundaries by logging slurry concentrations at specific depths and lateral positions at a given cross-section. It was found that the concentration increased suddenly at a specific depth, which was deemed to be the bed of the channel. This data was used to generate cross-sectional profiles for these channels. It was also found that dry beds of old channels no longer flowing could provide some useful channel shape data with greater ease, since a ruler could be used instead of the blind probing technique used for flowing channels. However, in such cases there was uncertainty imposed by tailings that had remained in the channel upon the cessation of flow. Some efforts were made to scrape the leftover tailings from the channel in an attempt to expose the stiffer bed material. Upon consideration of the cross sectional shapes of these self-formed channels, it was found that the arc formed by part of the circumference of a suitably sized pipe approximated the shape of a typical self-formed channel. A selection of the measured self-formed channel profiles with superimposed pipe arcs appear in Figure 12. The interior surfaces of the artificial

channels were lined with coarse sand, which was intended to capture some settled tailings particles to provide an equivalently rough boundary to that which would be found in a self-formed channel. The final consideration in the emulation of the channels on a tailings beach was the aspect of seepage and permeability from the channel boundaries. It was felt that the rate of seepage into the underlying tailings on a tailings beach was sufficiently low compared to the flow rate of the channel to enable this effect to be ignored in the flume. Having considered the aspects of channel length, shape, roughness and permeability in the flume, it is asserted that the flow conditions in the flume would be effectively equivalent to that experienced in a self-formed channel on a tailings beach.

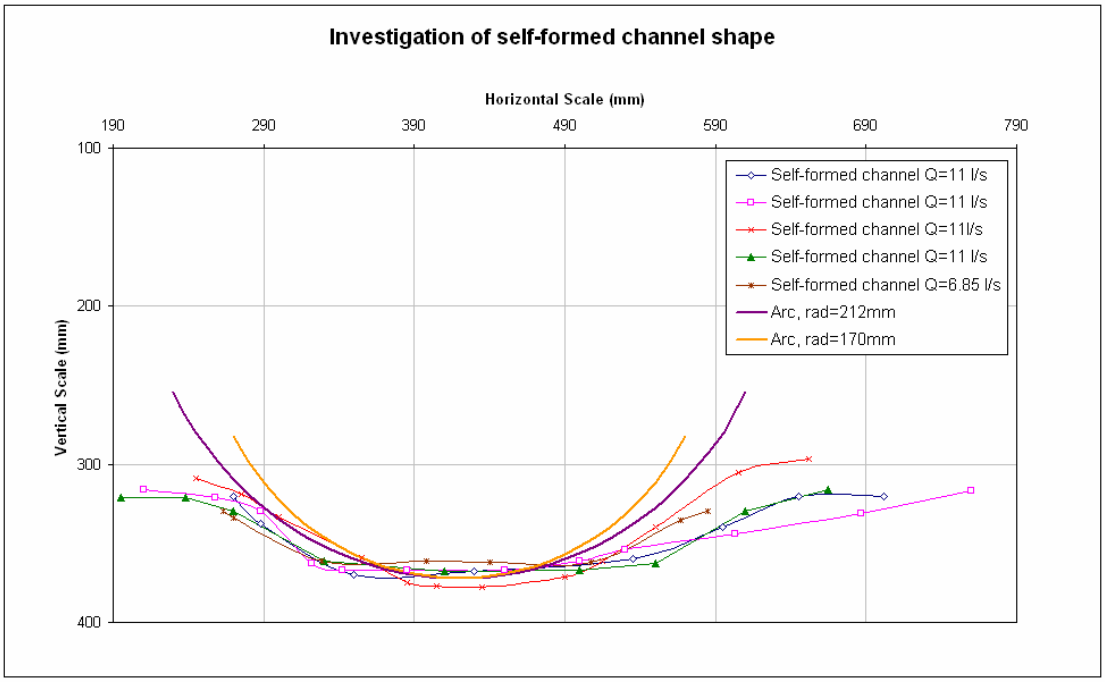

Figure 12. Investigation of self-formed channel cross sectional shapes at Cobar

3.3.4 Tilting mechanism for the flume

Two supporting trestles and chain-block enabled the tilting of the flume to slopes between horizontal and 7% below horizontal (meaning that the downstream end of the flume could be lowered as much as 0.7 meters below the elevation of the upstream end). A photograph of the trestle and chain block is presented in Figure 13. The calibration of the slope of the flume was achieved with the use of an automatic level.

Figure 13. Trestle at downstream end of flume with chain block for raising/lowering of flume

3.3.5 Slurry feed system

A plunge box was located at the upstream end of the flume. Fresh tailings slurry was supplied to the plunge box through a 150mm diameter High Density Polyethylene (HDPE) pipe with an outlet about 20 cm above the plunge box floor. A diaphragm valve was installed in the pipe to allow adjustment of the flow rate of tailings slurry. Approximately 20 m upstream of the plunge box, a second HDPE pipe carrying water was connected to the tailings supply line to allow dilution of the slurry feed. This enabled testing of various concentrations of slurry in the flume. The plunge box was designed to introduce the slurry into the channel as weir overflow, with as much dissipation of the exit velocity from the feed pipe as possible.

3.3.6 Flow measurement system

At the downstream end of the flume a flow measuring box was placed to facilitate measurement of the flow rate by means of an opening gate, a level indicator and a stopwatch, all of which enabled the recording of the time taken for the flume discharge to fill a specific volume. The dimensions of the box were 1.20 m length, 1.00 m width and 0.50 m height, but the full height of the box was never used for flow measurements for a number of practical reasons: firstly, the base of the box constantly collected a

build-up of settled tailings particles that required periodic shovelling out, so the measurement was always started a few centimetres above the base to avoid any geometric intrusion of deposited material. A basic depth gauge marked in 10 cm intervals was placed in the box to enable depth measurement from a reasonable point above the base of the box. Another reason the full height of the box was never used was because of spillage in times of high flow rates, with slurry violently splashing out of the box as the lip was reached. Finally, for the lower flow rates, a depth of 10cm was sufficient, since the time taken to fill a 10 cm horizontal section of the box at 3 litres per second would be 40 seconds.

Figure 14. Flow measuring box with gate open (left) and closed (right)

3.3.7 Equilibrium slope measurement

The primary aim of the experimental work with the flume was to determine the equilibrium slope for a given flow regime. Each flow regime was defined by a nominated flow rate and concentration. By trial and error the slope of the flume would be adjusted until an equilibrium slope for each flow regime was found. The means by which an equilibrium slope was determined depended on the presence of deposited slurry particles on the flume bed. If particles were found to settle on the flume bed, then the current slope was deemed too flat, and the downstream end of the flume was lowered. If no sedimentation was observed after 20 minutes of steady flow, then the slope was deemed to be too steep, and the downstream end of the flume would be raised. Eventually these converging upper and lower limits would lead to an equilibrium slope, with the entire process typically taking a few hours. This approach was essentially the same as that used by Winterwerp et al. (1990) in their experimental research with channel equilibrium slopes of sand-water mixtures. The means by which deposition was

detected consisted of 3 measurements; periodic monitoring of the surface levels, periodic 'feeling' of the channel bed by hand, and in the case of extreme deposition of sediment, visual observation of a significant rise in the surface level of the flow in the flume in the region of deposition.

The upper limit of the slurry concentration available for a flow regime was dictated by the concentration of the raw tailings slurry being supplied by the process plant, but achieving lower concentrations was possible whilst the supply of water to the flume was available. Flow rate upper limits were dictated by the pressure available in the tailings supply line, but furthermore, achieving large flow rates at low concentrations was also limited by the available pressure in the water supply line. A lower limit to concentrations was imposed by the mine operators at both mine sites who requested that very low slurry concentrations be avoided in the interests of minimising erosion to the established tailings beach. This request thereby prohibited the running of clear water through the field flume. Some attempt has been made to address this lack of clear water data during the validation of open channel flow models by considering a separate set of experimental data that consists solely of clear water runs in a similarly large scale flume, which is discussed in section 5.2.5.

In total, some 9 equilibrium slopes were recorded during the Cobar programme, while 41 were observed during the Sunrise Dam programme. These equilibrium slope results are presented graphically in Figure 15. A numerical summary of these equilibrium slopes is presented in Table 14 of Appendix A, whilst a full record of all the chronologically logged measurements from the Sunrise Dam experimental campaign can be found in Table 15 of Appendix A.

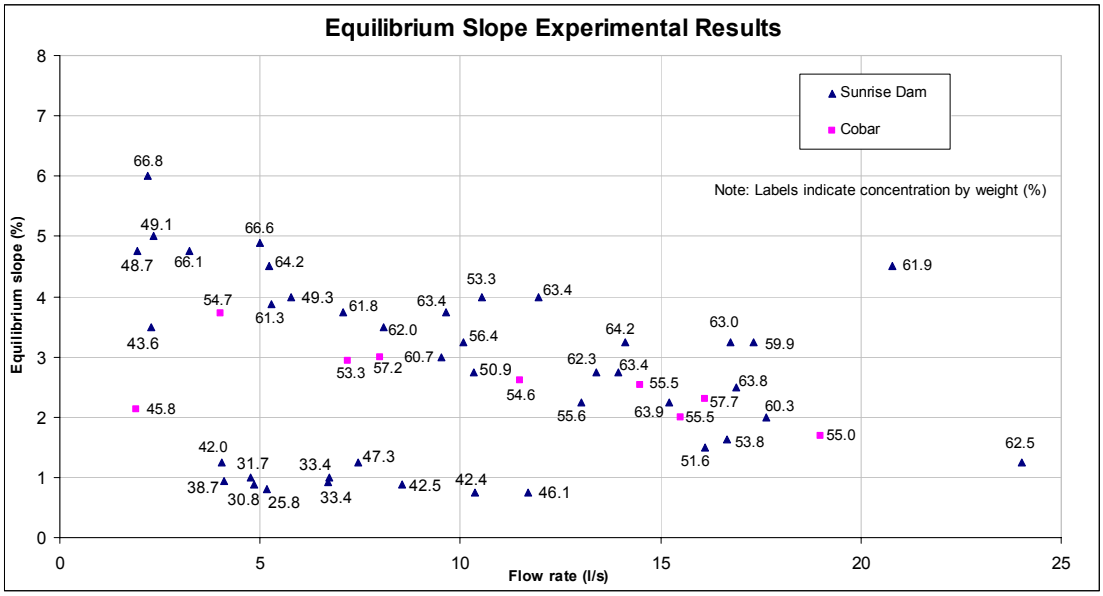

Figure 15. Equilibrium slope results from the two experimental large scale field campaigns

The equilibrium slope results presented in Figure 15 suggested the following points:

- Below a certain concentration, it was evident that segregation was occurring in the flume, resulting in significantly reduced equilibrium slopes. The group of points that appear in the bottom left region of the graph all resulted from segregating regimes of flow. In these segregating flow regimes, touching of the channel bed with one's fingers found that the sedimentation that occurred in the flume below the equilibrium slope was different to that observed in the other flow regimes, in that they produced a hard deposit of large particles near to the downstream end of the flume, while the other non-segregating regimes typically produced a soft slimy deposit of smaller particles near the upstream end or the middle of the flume at slopes flatter than equilibrium.
- Equilibrium slopes are inversely proportional to the flow rate. High flow rates result in low equilibrium slopes; low flow rates give steeper equilibrium slopes.
- Low concentrations would appear to yield flatter equilibrium slopes than higher concentrations. This trend is not as strong as the effect of flow rate on the channel equilibrium slope.
- At low flow rates the effect of segregation reduces. It can be seen that flow rates below about 3 litres per second allowed some slurries of relatively low concentrations to reach steeper equilibrium slopes than the other segregating runs did at higher flow rates. This finding has

significant implications with respect to flume tests at flow rates below about 3 litres per second, and presents another critical issue for those working with experimental flumes with flow rates much lower than this value.

3.3.8 Local depth measurements

Depths of flow were measured at specific points along the flume for two reasons:

- To detect solids deposition in the flume, which causes a rise in surface levels
- To construct surface profiles along the length of the flume, thereby checking for fully developed uniform flow.

These depth measurements were made using a steel ruler, measuring the distance from the fluid surface to fixed points above the fluid surface. The offset distances to the flume bed from these fixed points were also noted so that the depths could be deduced. This method enabled the depth measurements to be made without immersing the ruler (or any other instruments) into the flowing slurry.

Figure 16. A depth measurement being read

3.3.9 Local velocity measurements

Velocities were measured at specific points within the flume flow for two reasons:

- To construct velocity profiles at a specific cross section in the flume, which then provides evidence of laminar or turbulent flow conditions
- To measure velocities at various points along the length of the flume, which can test for fully developed uniform flow

Measurement of fluid velocities at specific locations within the channel flow was enabled through the use of a Delft E-30 velocity probe, which generates an electromagnetic field from 5 electrodes mounted in the bottom surface of an ellipsoid head some 33 mm in diameter and 11 mm thick. The probe senses fluid motion in this electromagnetic field in a region reaching out about 5 mm from the electrodes, with an operating range of 0 – 2.5 m/s. (Delft 2006) Due to the requirement for all 5 electrodes to be immersed in the fluid without any air interaction at the surface, it was found that the E-30 probe could not measure fluid velocities at depths less than about 5 mm. It was also found that the width of the ellipsoid head of the probe prevented velocity measurements from being taken within about 17 mm of the boundaries of the half pipe, though near the centreline, measurements could be taken close to the channel bed because the probe sensors could get close to the channel bed.

A traversing jig was fabricated by Mr Mike Allen at RMIT University for holding either the velocity probe or the density probe in place whilst it was taking measurements, which enabled vertical positioning of a probe to 0.1 mm of a desired depth and lateral positioning to 1 mm due to the inclusion of a digital calliper on the vertical dipping mechanism and a tape measure rigged to the lateral traversing mechanism.

Figure 17. Traversing jig with the velocity probe attached. Note that slurry flow is very low.

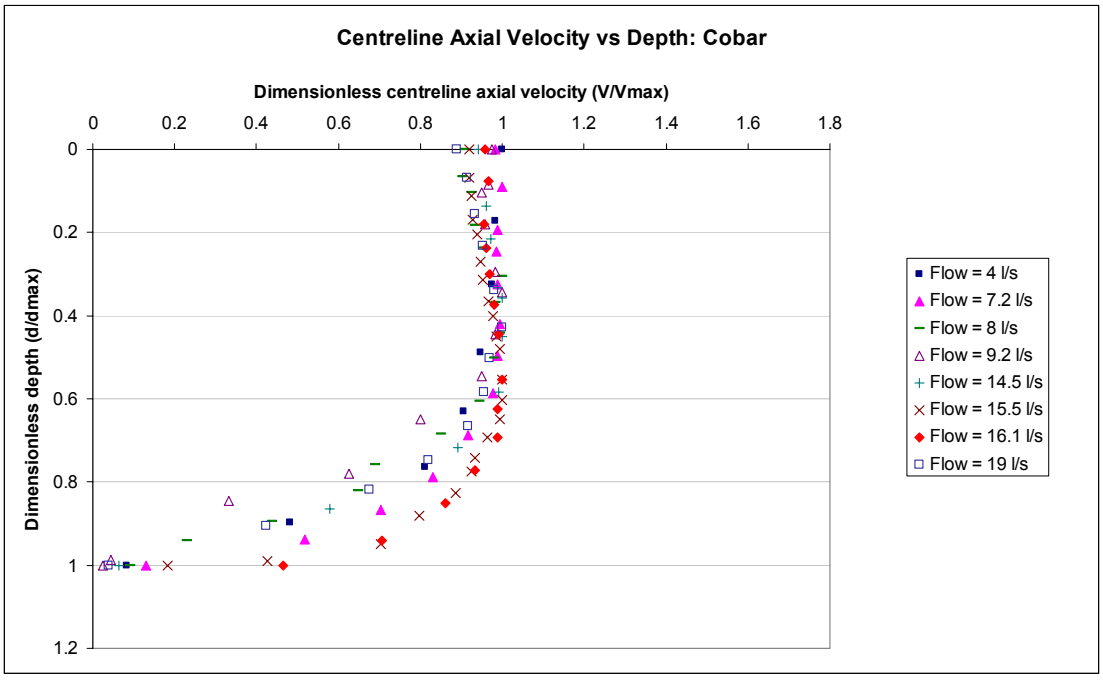

Figure 18. Axial velocity profiles recorded for 8 different flow rates at Cobar

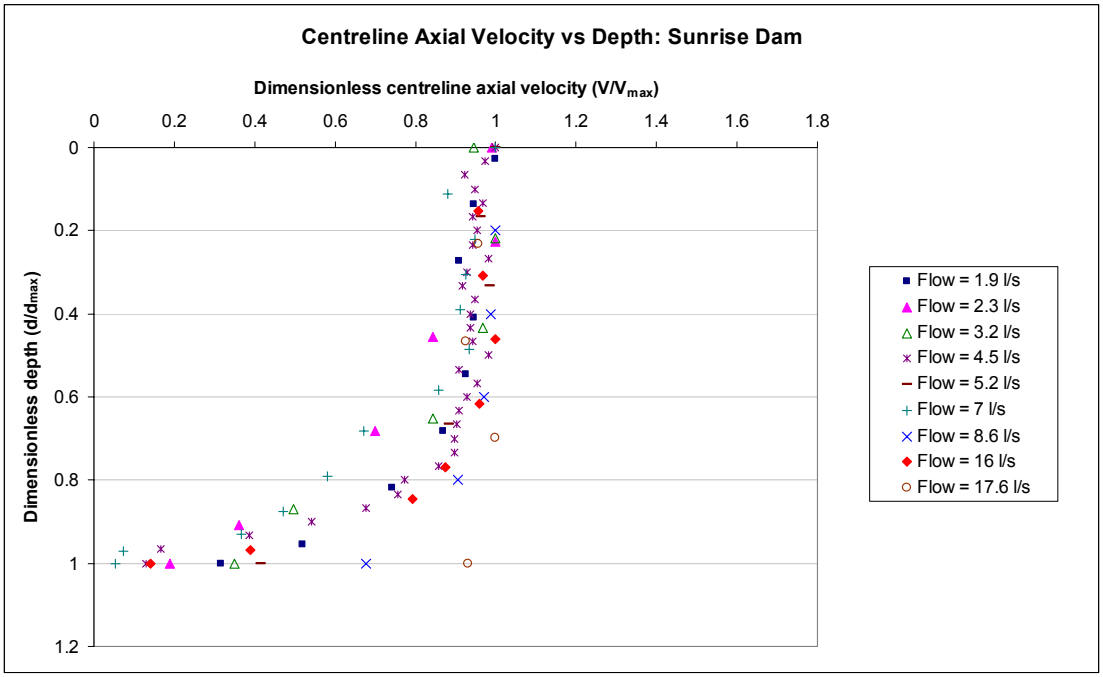

Figure 19. Axial velocity profiles recorded for 9 different flow rates at Sunrise Dam

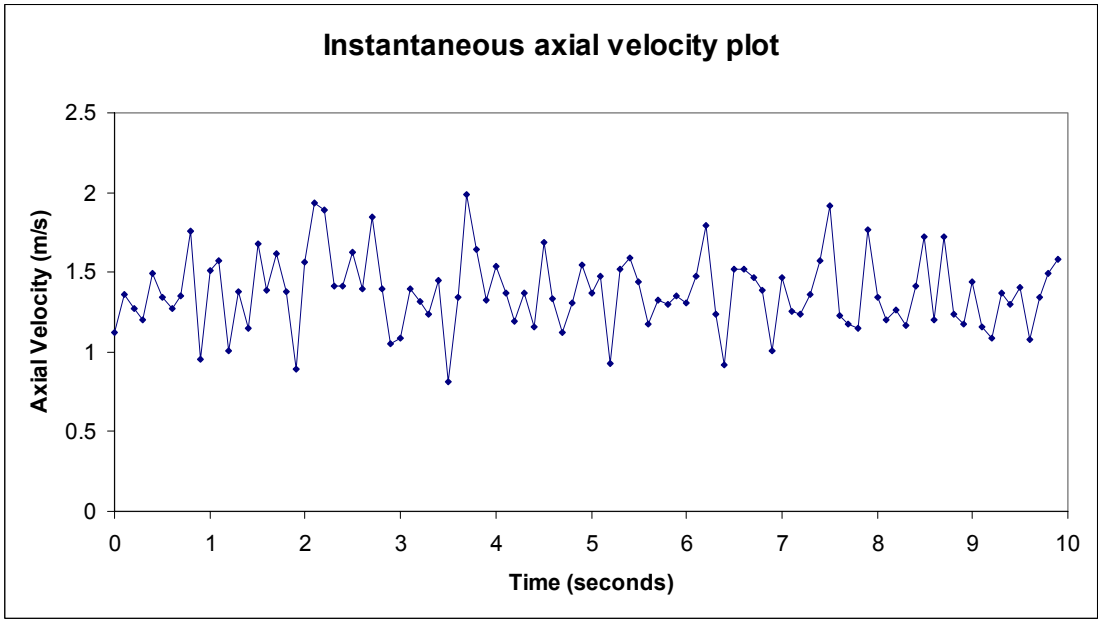

Figure 20. Raw axial velocity data collected by the velocity probe at a rate of 10 Hz.

The velocity–depth profiles presented in Figures 18 and 19 show that the axial velocity at any cross section within the flume at either mine site typically decreases rapidly with depth in the bottom 20% of the depth, but the top 80% can vary from gently decreasing velocity with depth, to uniform velocity distribution, to a bulging profile with the maximum velocity occurring approximately 20% of the depth down from the surface. These plots provide evidence of turbulent flow occurring in the flume, since

under laminar flow conditions one would expect to see a steady linear drop in velocity with depth. The velocities presented here are time averaged points, measured over a 30 second period at the rate of 10 Hz. This was necessary because the measured instantaneous velocities fluctuated significantly as a result of the turbulence in the channel. An example of this behaviour can be seen in Figure 20, where a 10 second stream of raw velocity data gathered by the velocity probe is presented, featuring significant fluctuations in the individual readings that were being recorded every tenth of a second. These readings strongly indicate the presence of turbulent eddies travelling past the probe sensors.

3.3.10 Local concentration measurements

Measurement of fluid density at specific locations within the channel was enabled with the use of a Delft Conductivity Concentration Meter (CCM) probe whilst the electrical conductivity of the fluid remained below a maximum operating value of 60 mS/cm. This probe measured the conductivity of the slurry with the transmission of a current across 4 electrodes mounted in a 10 mm x 2 mm probe tip, with an attached resistance meter used to calculate an effective slurry concentration after calibration with a sample of decant water extracted from the slurry. (Delft 2006) Unfortunately the conductivity of the decant water used in the tailings slurry at Sunrise Dam gold mine was some 5 times greater than the operating limit of the CCM probe, thereby prohibiting its use at that mine site. The complete set of concentration profiles recorded at Cobar appears in Figure 21.

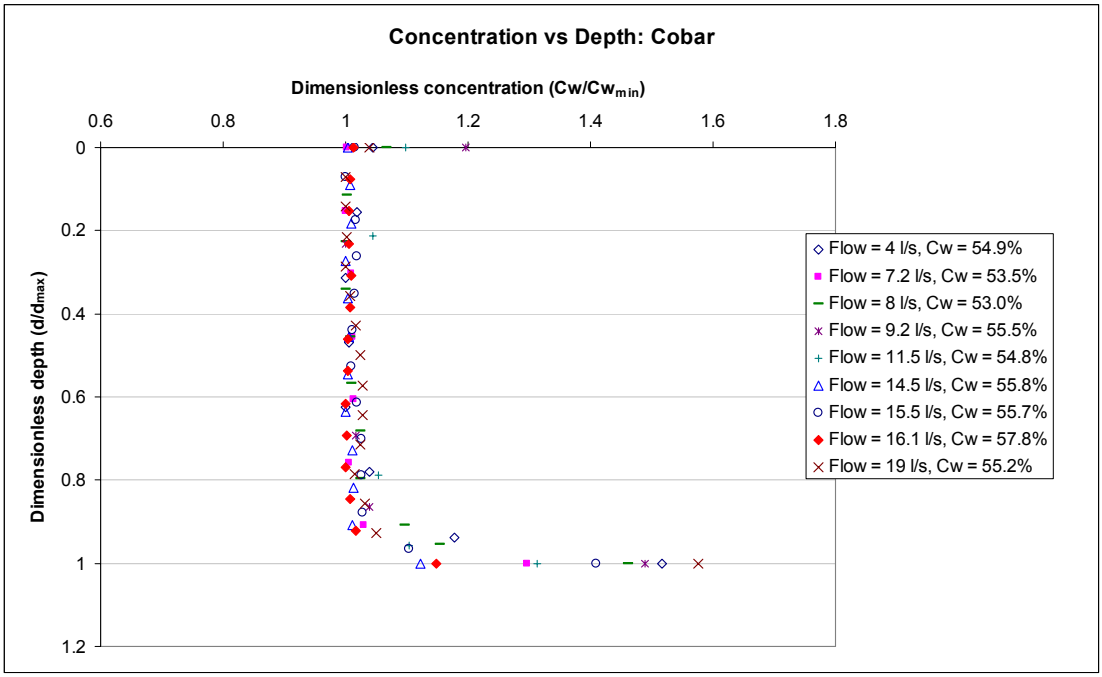

Figure 21. Conductivity Concentration Meter (CCM) probing of the flume at Cobar for 9 different flow rates

The solids concentration of the slurry at all of the measured cross sections in the flume appears to be uniform throughout the upper 90 percent of the depth of flow under equilibrium slope conditions, with the bottom 10% of depth increasing rapidly. (Figure 21) It is thought that this rapid increase in concentration is due to the higher concentration of particles expected to exist in the laminar flowing boundary layer of the channel, though it may alternatively be the result of the probe simply being too close to the channel base, thereby generating artificially high concentration values. Figure 21 clearly demonstrates a homogeneously mixed profile for the major portion of the depth in the channel, which would suggest a lack of segregation of particles. This would also suggest that the flow is turbulent across most of the cross-section, with the turbulence sufficient to keep all the particles evenly scattered across the full depth of the channel.

3.3.11 Concentration measurement of flume discharge

On-site measurement of slurry concentration was enabled with the use of a Marcy density scale (shown below in Figure 22). This is a sprung scale with a bucket of known volume hanging from it. The bucket is filled to the same level every time, ensured by means of two overflow outlets. Marcy gauge

readings were later adjusted by calibration with more accurate data gained from oven dried samples of slurry.

Figure 22. Marcy density scale (left) and 1 litre plastic bucket with notch weirs (right)

Samples of the two tailings slurries were dried in an oven at 100°C for 12 hours to calibrate the Marcy scale readings with accurate total solids (T.S.) concentrations of the slurries. Samples of decant water from the slurries were also oven dried to determine the concentration of dissolved solids (D.S.) present in each.

For the Cobar tailings, the decant water was found to contain 0.78% w/w dissolved solids, giving it a specific gravity of 1.00. The total solids was found to be uniformly 3.5% less than the Marcy readings across the range of concentrations tested, which can be expressed as:

$$T.S._{Cobar} = Marcy - 3.5 \qquad (33)$$

The Sunrise Dam decant water contained 19.1% w/w dissolved solids, with a specific gravity of 1.15, whilst the total solids fit the following linear relationship against the corresponding Marcy data:

$$T.S._{Sunrise\ Dam} = 1.3589 \times Marcy - 19.267 \qquad (34)$$

The C_W data presented in Figure 15 (and Table 14 in Appendix A) and has been corrected from the raw Marcy readings that were recorded on site, using the applicable one of equations 33 and 34 and the following equation:

$$C_W = T.S. - \frac{D.S.(100 - T.S.)^2}{100^2} \quad (35)$$

where all values, including C_W, are expressed as percentages, or otherwise;

$$C_W = T.S. - D.S.(1 - T.S.)^2 \quad (36)$$

where all values, including C_W, are expressed as decimal fractions.

3.3.12 Particle size analysis

Particle Size Distribution (PSD) analysis was undertaken in both experimental programmes in an attempt to detect the possible presence of segregation (hydraulic sorting) within the 10 metre length of the flume. Using a modified syringe, fluid samples were extracted from the flume 10 mm below the channel surface and 10 mm above the channel bed at 3 positions along the length of the flume. Samples were also collected from the plunge box as control readings. The samples were later tested using a Malvern Mastersizer X to generate particle size distribution curves. This particle sizing instrument determined the size of particles in a highly diluted fluid sample by means of laser beam photons being scattered as they travel through a sample of the fluid. The makers of the instrument claim it can measure particle diameters in a range of 0.1 μm to 600μm. (Malvern Instruments 2007) This operating range makes this instrument ideal for the particle size analysis of tailings slurries, with particles typically falling well inside this size range.

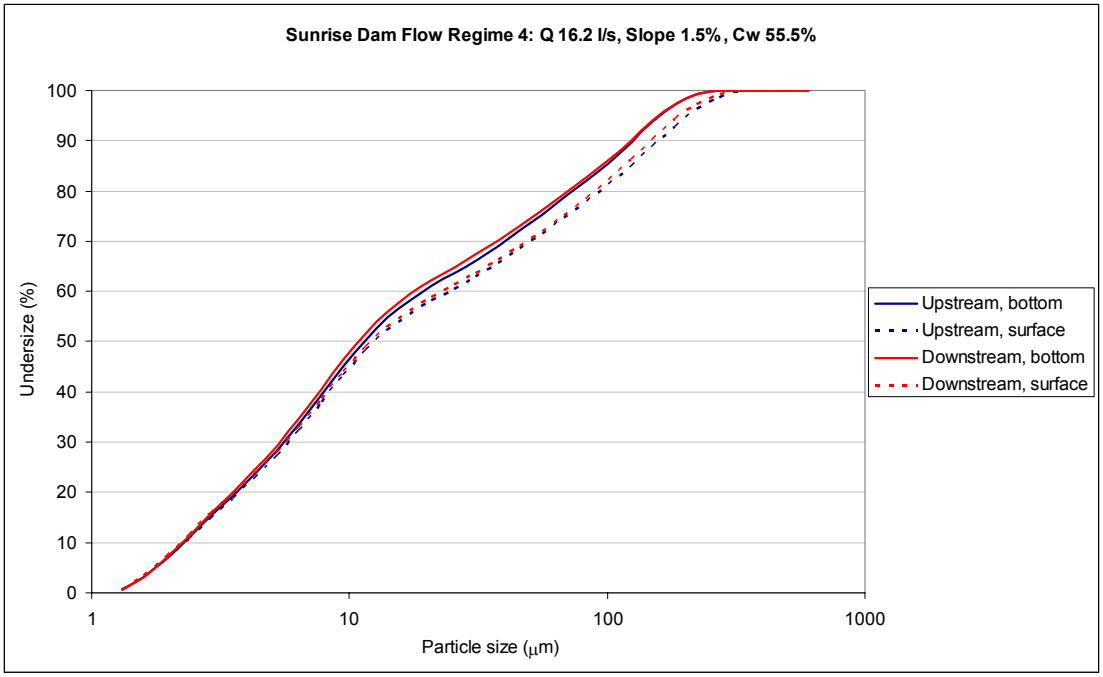

Figure 23. Particle Size Distribution curves for one of the non-segregating equilibrium flow regimes at Sunrise Dam

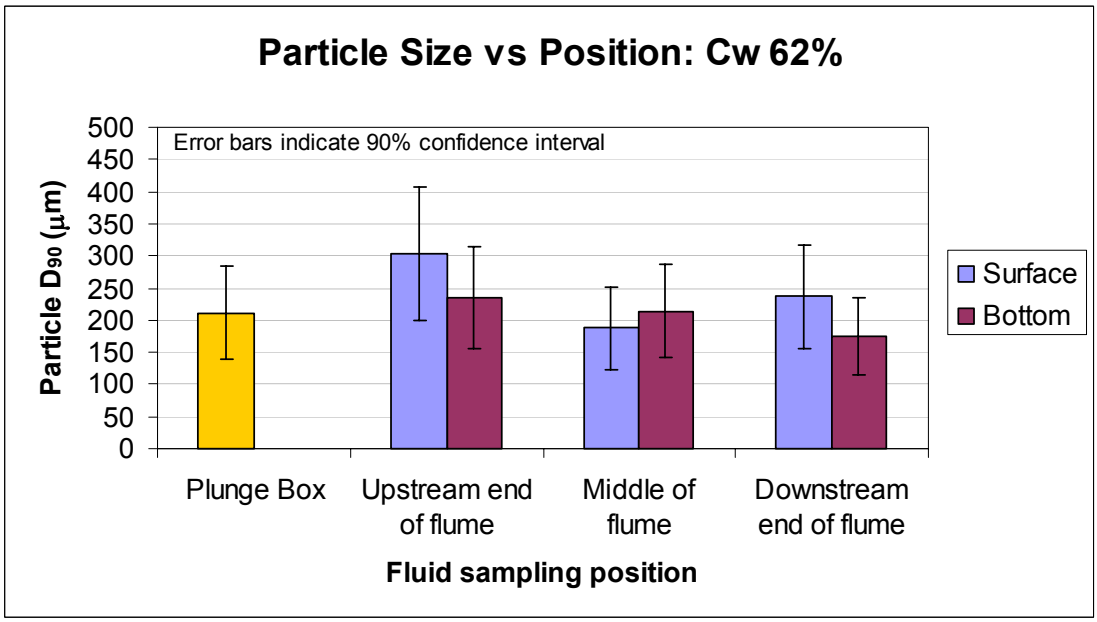

Figure 24. Particle Size (90th percentile) vs. position and depth in the flume for a non-segregating flow regime at Sunrise Dam

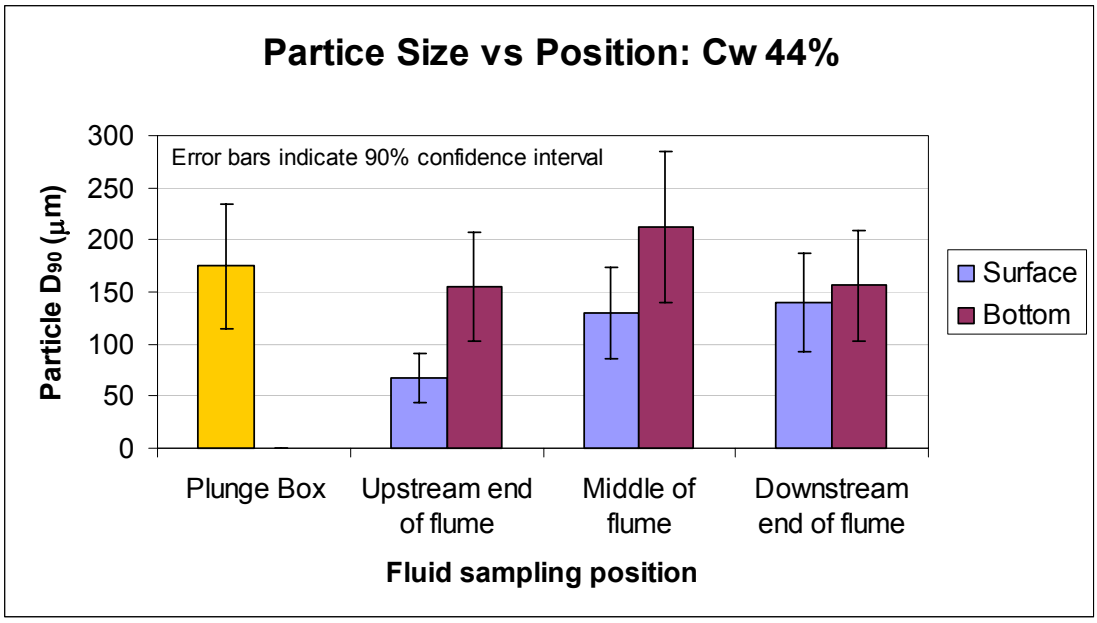

Figure 25. Particle Size (90th percentile) vs. position and depth in the flume for a segregating flow regime at Sunrise Dam

Particle size distribution (PSD) analysis (Figures 23, 24 and 25) showed that for non-segregating regimes the distribution of particles within the flume generally remained the same, irrespective of depth or distance travelled (Figures 23 and 24). This suggests that there was no segregation (hydraulic sorting) occurring in the flume at these concentrations. However, where segregation was detected in the flume (when the hard deposits of particles formed near the downstream end of the flume as described in section 3.3.7), the PSD analysis supported this, with consistently larger particles seen near the bottom of the flume than at the surface at all positions along the length of the flume (Fig 25). Further evidence of this segregating behaviour can be seen in Appendix B.

It was found that the Sunrise Dam tailings particles had a mean d_{50} value of 16 µm, while the mean d_{50} for Cobar was found to be 7.8 µm. Mean d_{85} values were 140 µm for Sunrise Dam and 51 µm Cobar respectively.

3.3.13 Rheological analysis

Rheometric analysis was performed on samples of the two tailings slurries at a number of concentrations to determine the viscous behaviour of these slurries over a range of shear rates that

would enable the fitting of rheological models as a function of concentration for further analysis of these fluids with open channel theory.

Rheological analysis of the tailings slurry at the Peak mine in Cobar was achieved with the use of a portable Thermo-Haake VT550 rheometer with MV2 bob and cup measurement system. This instrument is classed as a Couette rheometer (or concentric cylinder rheometer), implying that it shears a fluid sample in the annular space that is formed between a cup and a cylindrical bob that is inserted into the cup and rotated about its vertical axis. The MV2 bob has a vertical length of 60 mm and a diameter of 18.4 mm, with the annulus to the inner surface of the cup being 2.6 mm. The shear rates applied to the slurry ranged from 0.48 to 595 1/s, and the slurry was kept at a temperature of 36°C, which was representative of the temperature of the slurry in the flume. The concentrations of slurry tested were (in % w/w) 58.1, 55.3, 52.2, 48.8 and 44.4, which covered the range of slurries run through the flume at Cobar.

The rheometric analysis of the Sunrise Dam slurry was done with a Contraves Rheomat 115 Couette rheometer, using a 45 mm diameter bob with vertical grooves etched into the surface to reduce slip. The length of the bob was 68 mm, and the annulus to the inside surface of the cup was 1.89 mm. The shear rates applied to the slurry in the Rheomat 115 rheometer ranged from 0.1 to 400 1/s, and the slurry was kept at a temperature of 36°C, which was again representative of the temperature of the slurry in the flume at Sunrise Dam. The concentrations of slurry tested were (in % w/w) 65.9, 60.6, 56.7, 52.0, 47.2 and 44.9. It is noted that a few of the flow regimes tested in the flume featured concentrations that lay below this figure of 44.9%, but it can be seen from Figure 27 that the shear stress values of the Sunrise Dam tailings slurry are very low below concentrations of 47%. The higher shear rates exerted by the rheometer on these weaker concentrations caused turbulence in the sample, producing shear stress data that was inaccurate. For this reason the rheogram data for the 47.2% and 44.9% concentrations was removed for shear rates above 100 1/s, and for the same reason concentrations below 44.9% were not tested. The calculation of rheological parameters for these lower concentrations was done by extrapolation from the higher concentration data. Figure 15 shows that flow regimes with concentrations below 44.9% w/w all yielded relatively flat equilibrium slopes around 0.8%, so it is asserted that this extrapolation of rheological parameters for the slurries with

concentrations below 44.9% w/w would incur negligible errors in the overall predictions of beach slope.

Rheometric correction

Some effort was made to apply corrections to the rheometric data to allow for the inaccuracy of the reported shear rate from a Couette rheometer in which a Non-Newtonian fluid is tested, but this correction was found to be significantly smaller than the experimental error. It was thus deemed that the rheometric correction added no value to the data. This topic is discussed in more detail in Appendix N.

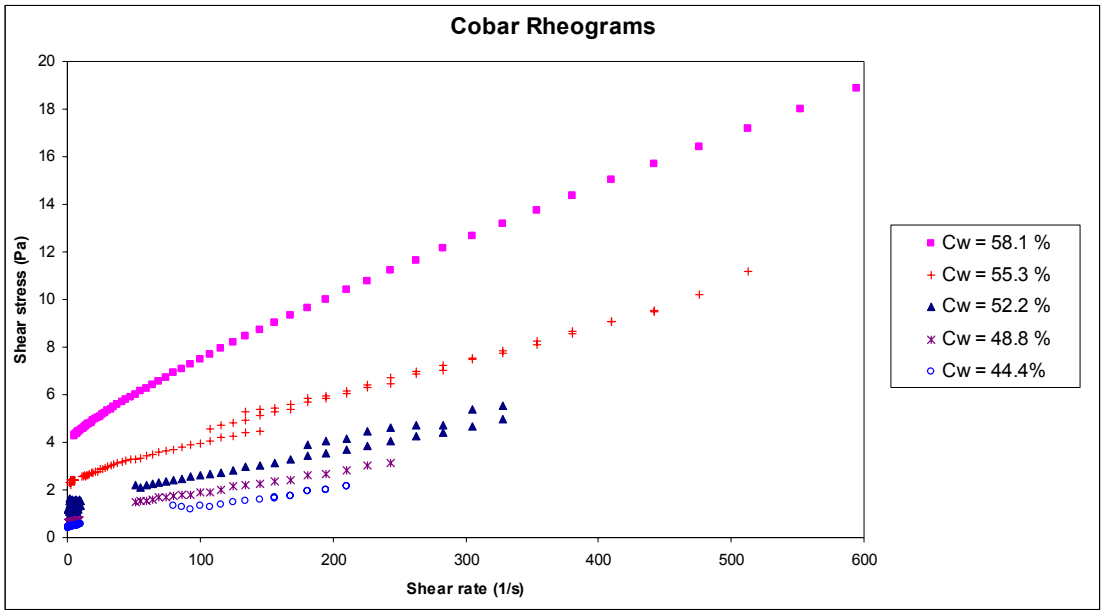

Figure 26. Rheogram for various concentrations of Cobar tailings slurry

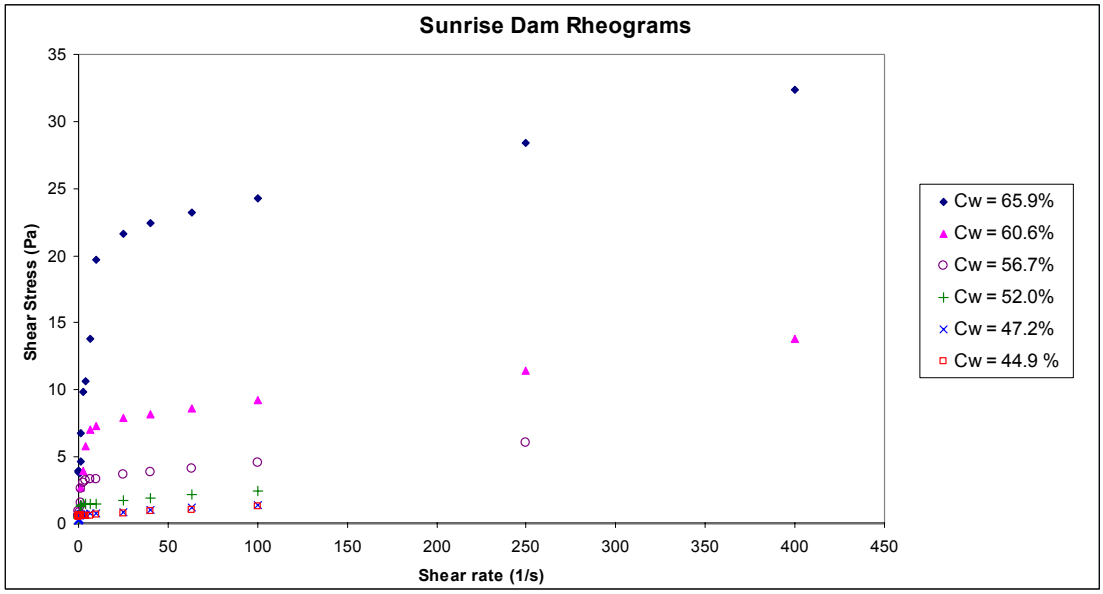

Figure 27. Rheogram for various concentrations of Sunrise Dam tailings slurry

The rheological testing done on each of the tailings slurries has been presented above in the standard shear rate vs shear stress plots commonly referred to as "rheograms" (Figures 26 and 27). These rheograms show that both slurries exhibit yield stresses and shear thinning behaviour. It is also apparent that the rheological behaviour of both of the tailings slurries from these two mines is similar for equivalent concentrations. An effort to elucidate this comparison further takes place in Figure 28, below.

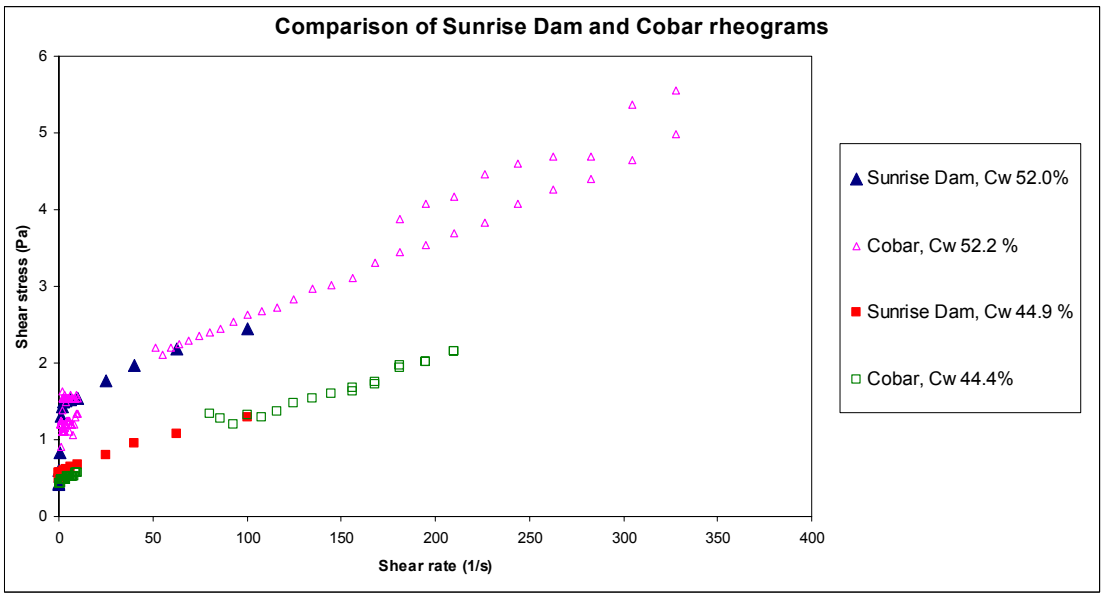

Figure 28. Comparison of Sunrise Dam and Cobar rheograms for two similar concentrations that were tested.

Figure 28 shows a very close similarity in the rheological behaviour of the two mineral slurries with respect to concentration. This similarity could lead to the belief that all tailings slurries of a specific solids concentration exhibit the same flow behaviour, in a similar fashion to that taken by some early workers in the field (Blight 1987; Fourie 1988). However, this has been shown to be an inaccurate generalisation by later workers (Coussot et al. 1996; Sofra & Boger 2000).

Rheological modelling

Several slope prediction models required the input of rheological parameters (such as the Blight & Bentel equation (equation 17) and Sofra & Boger equation (equation 32), amongst others). In such cases the rheological data gained in the experimental work was used. The conventional approach used for applying experimentally recorded rheology data is to fit an empirical rheological model to the data to enable the interpolation of shear stress values as a function of the applied shear rate. The Bingham plastic and Herschel-Bulkley rheological models were both applied to the rheology data measured for the two tailings slurries. Some introduction of these models can be found in Chapter 2.

Beyond fitting these rheological models to each rheogram as a function of the applied rate of shear, various concentrations of slurry that were tested in order to allow the rheological model parameters to be characterised as a function of the slurry concentration. This would enable a rheogram to be predicted for that same slurry as a function of the slurry concentration. The weight concentration was used here for these parameter fit equations (as opposed to the more universally translatable volumetric concentration) because the fit equations were not posed as being globally effective empirical models. They were merely applied for the same slurry to interpolate within the range of concentrations that were tested.

Some care was taken to fit the rheological models to the shear rate range that is of interest to the open channel flows that occur on a tailings beach. The experimental data was used to back-calculate the effective shear rate in the open channel flows that were monitored in the flume. The shear rate was found to be typically between 40/s and 140/s. This work is presented in Appendix O.

Herschel-Bulkley parameter fits

For both the Sunrise Dam and Cobar tailings slurries, the Herschel-Bulkley model curve in Figure 6 resembled the rheograms for these slurries (Figures 26 and 27) more than either of the other two curves presented in Figure 6. The fitting of Herschel-Bulkley parameters to these rheograms was executed by inscribing a curve over each set of concentration data presented in Figures 26 and 27, with the equation of each curve following the format of the Herschel-Bulkley equation (equation 39). For each curve, values for the τ_y, K and n were selected to provide the best fit to the experimental data. These τ_y, K and n values were then plotted against the respective C_W value of the parent data set, as shown in Figures 29 and 30. Equations were then fitted to these parameter charts which would enable the calculation of values of τ_y, K and n for other concentrations of slurry that were not tested in the rheometer.

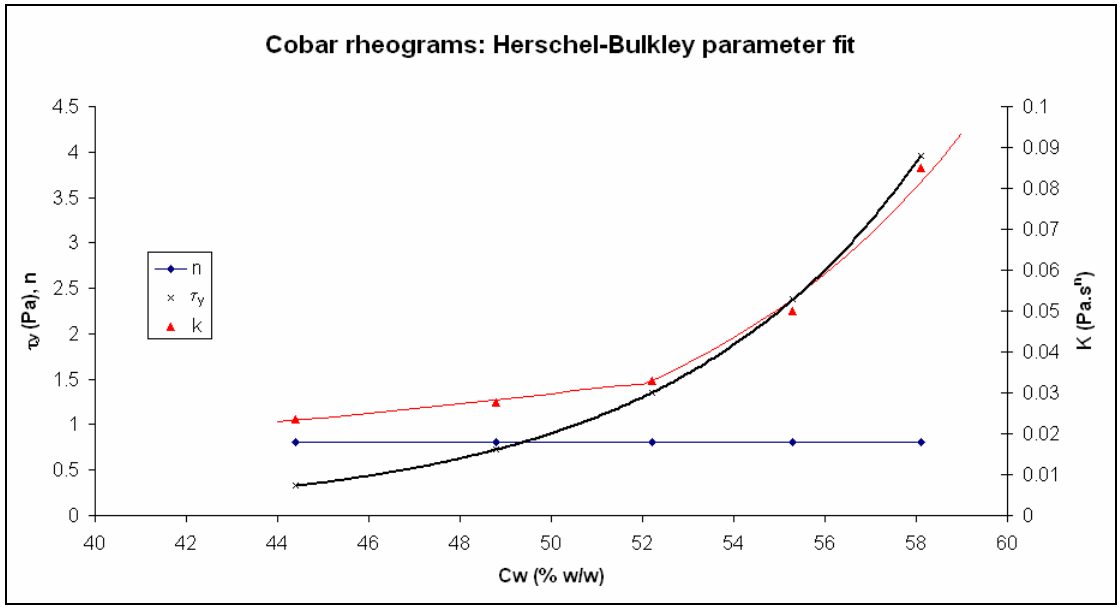

Figure 29. Cobar: Herschel-Bulkley parameter fits as a function of slurry concentration

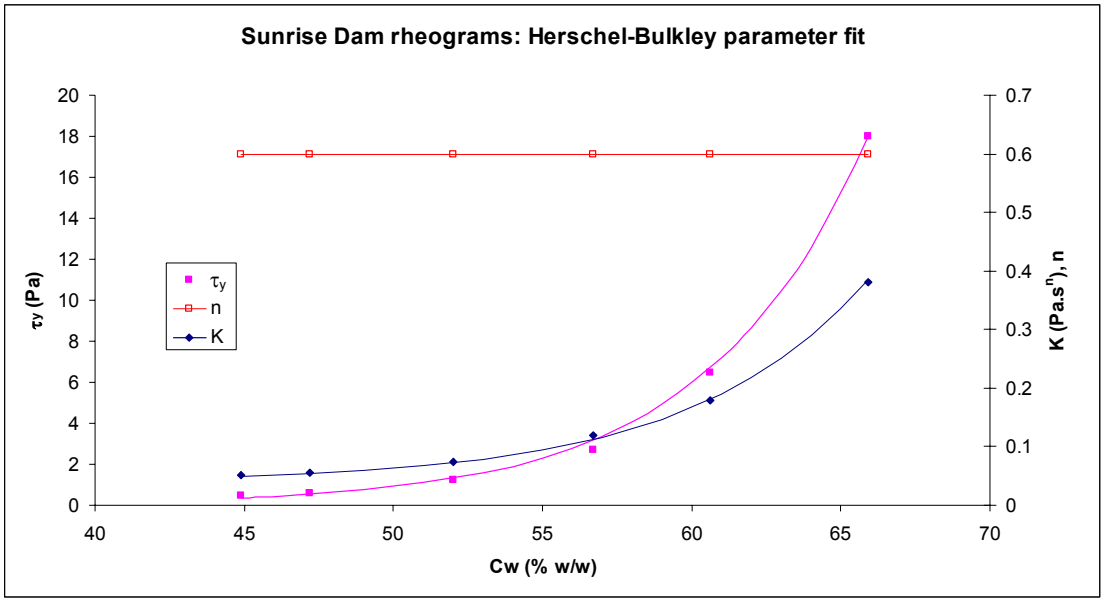

Figure 30. Sunrise Dam: Herschel-Bulkley parameter fits as a function of slurry concentration

For the Cobar rheograms, the following Herschel-Bulkley parameter fit equations were gained:

$$\tau_y = 0.0001\mathrm{e}^{0.1822C_W} \quad (40)$$

$$K = 0.0033\mathrm{e}^{0.0438C_W}, C_W < 52\% \quad (41a)$$

$$K = 0.000011\mathrm{e}^{0.1531C_W}, C_W \geq 52\% \quad (41b)$$

$$n = 0.8086 \quad (42)$$

For the Sunrise Dam slurry the Herschel-Bulkley parameter fit equations are as follows:

$$\tau_y = 0.000075\mathrm{e}^{0.188C_W} \quad (43)$$

$$K = 0.04 + 0.0000047\mathrm{e}^{0.17C_W} \quad (44)$$

$$n = 0.6 \qquad (45)$$

The Herschel-Bulkley fit curves that these sets of equations generate are presented graphically as an overlay to the Sunrise Dam and Cobar rheograms in Figures 31 and 32.

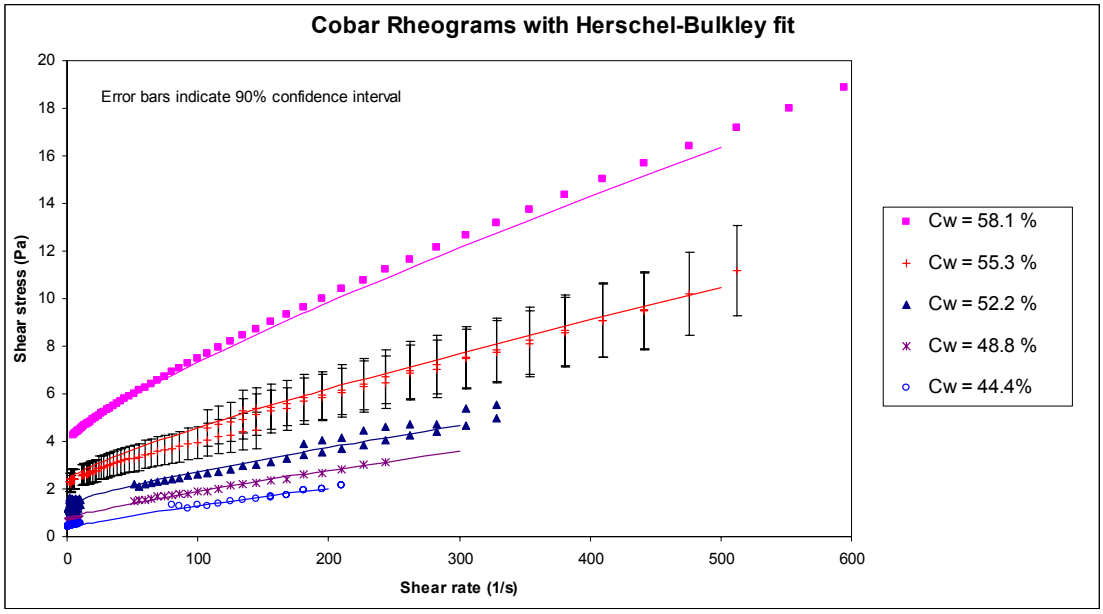

Figure 31. The Cobar rheograms overlaid with Herschel-Bulkley fit curves.

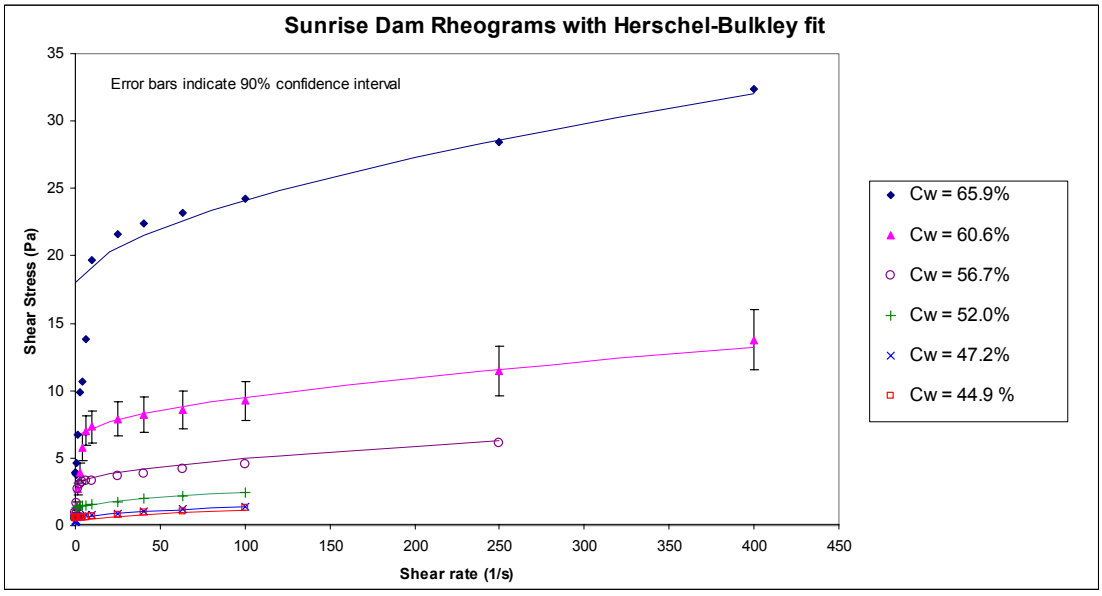

Figure 32. The Sunrise Dam rheograms overlaid with Herschel-Bulkley fit curves.

Bingham model parameter fits

In the cases of the Blight & Bentel model, the Sofra & Boger model and also for some of the work done in the development of a new beach slope model, it was necessary to generate Bingham model parameter fits. A similar approach was used as that described above for the Herschel-Bulkley fits, but using the Bingham equation (equation 37) instead. The parameter fits appear in Figures 33 and 34.

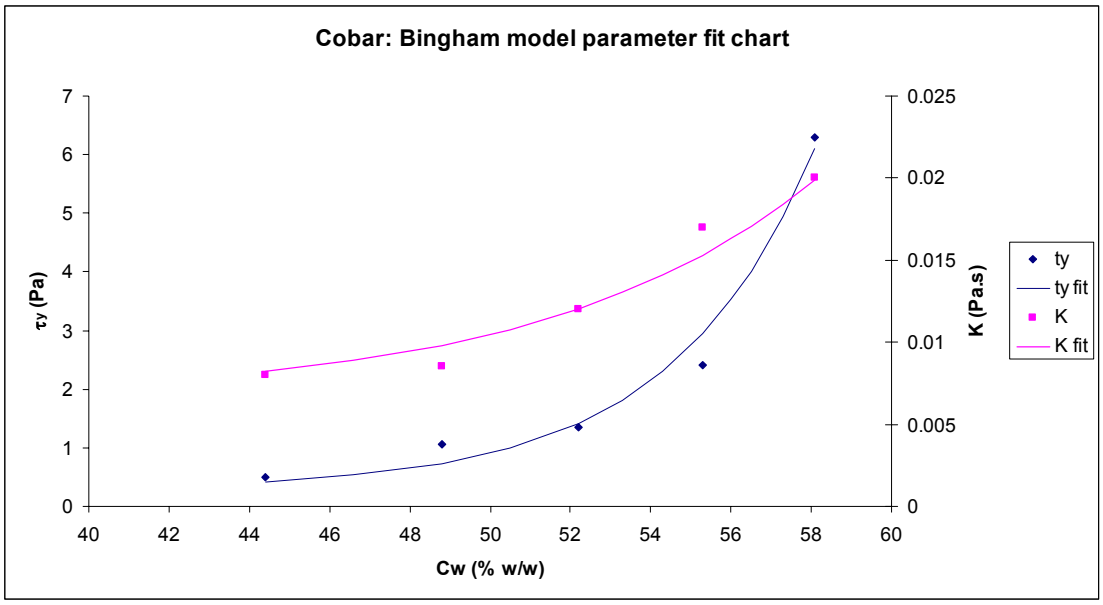

Figure 33. Bingham model parameter fit chart for the Cobar rheograms

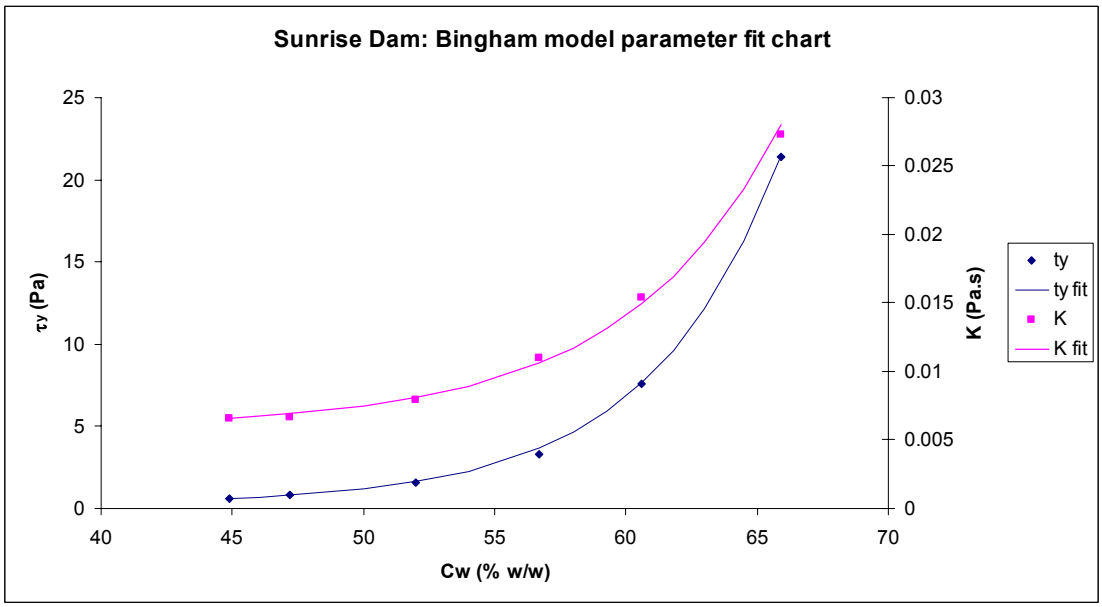

Figure 34. Bingham model parameter fit chart for the Sunrise Dam rheograms

The Bingham model parameter fits for Cobar tailings were as follows:

$$\tau_y = 4\times10^{-7}\,e^{0.28C_W} + 0.3, \quad C_W > 57\% \qquad (46a)$$

$$\tau_y = 5\times10^{-7}\,e^{0.28C_W} + 0.3, \quad C_W < 57\% \qquad (46b)$$

$$K = 4\times10^{-6}\,e^{0.15C_W} + 0.0065, \quad C_W > 57\% \qquad (47a)$$

$$K = 2.2\times10^{-6}\,e^{0.15C_W} + 0.0065, \quad C_W < 57\% \qquad (47b)$$

The Bingham model parameter fits for Sunrise Dam tailings were as follows:

$$\tau_y = 0.00004e^{0.2C_W} + 0.3 \qquad (48)$$

$$K = 3\times10^{-6}\,e^{0.135C_W} + 0.005 \qquad (49)$$

The Bingham model fit lines that these sets of equations generate are presented graphically as an overlay to the Cobar and Sunrise Dam rheograms in Figures 35 and 36.

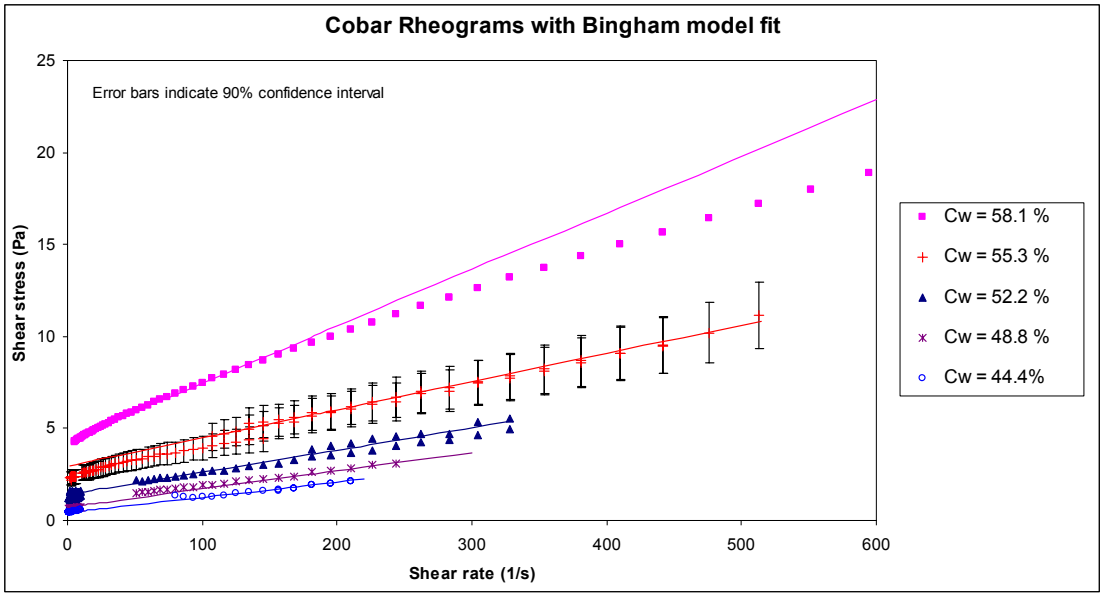

Figure 35. The Cobar rheograms overlaid with Bingham model fit lines.

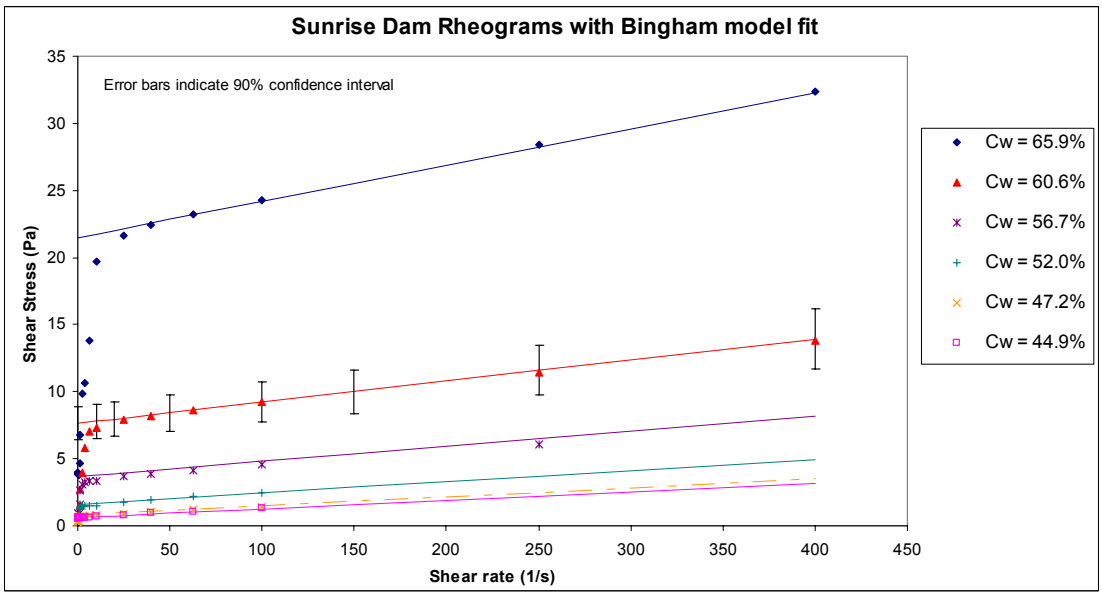

Figure 36. The Sunrise Dam rheograms overlaid with Bingham model fit lines.

3.3.14 Segregation threshold testing

Segregation threshold tests were conducted on samples of tailings slurry from both mines. The importance of the segregation threshold and its effect in the formation of tailings beaches has been identified as critical, with segregating slurries forming much flatter beaches than non-segregating ones due to the deposition of the large slurry particles shortly after exiting the discharge points. (Robinsky

1978) It was deemed appropriate to measure this segregation threshold so that this assertion can be tested.

At present there is no standard laboratory test for determining the segregation threshold of a slurry, so some workers have developed their own in-house testing procedure for achieving this. (Pirouz et al. 2006) This test involves the preparation of different concentrations of the slurry which are each left to settle in a suitably sized container under static conditions. Some time later a pipette is used to extract samples from the lower and upper regions of settled bed, with particle sizing then being done on the two samples. Comparison of these two samples for each tested concentration of slurry then enables the determination of the concentration at which segregation no longer takes place, which is deemed to be the segregation threshold. Further research has since been conducted by Pirouz et al. to investigate the effects of shear on the segregation threshold, which has found that the shearing of a slurry raises the segregation threshold from the value gained in their static segregation threshold test.

The static segregation threshold tests provided the following results:

Peak (Cobar) tailings slurry: 42%

Sunrise Dam tailings slurry: 47%

It is shown in Pirouz et al. (2006) that the same slurry from Cobar experienced segregation at up to 52% solids when subjected to a high amount of shear.

It is of interest to note the equilibrium slope plot (Figure 15) with the static segregation threshold results in mind. It can be seen that the effective segregation threshold for the Sunrise Dam slurry appears to lie between 47.3% and 49% on the basis of the distinct separation of the two groups of equilibrium slope data, whilst for the Cobar tailings this effective segregation threshold appears to lie between 46% and 53%.

This finding reflects on the sheared segregation threshold tests that were documented by Pirouz et al., and suggests that the static segregation threshold is of little value when considering the open channel flow of a slurry. Unfortunately though, the method of shearing in Pirouz et al.'s sheared segregation

experiments was geometrically quite complex, and thus does not lend itself to quantitative analysis to be compared with other quantifiable forms of shear, such as the shear induced by the channel flow. From this, it must be said that the effective segregation threshold of these two slurries is presently indeterminate with the application of the ATC laboratory segregation threshold test, since the shearing of the slurry in the segregation threshold test needs to be of the same magnitude as that which would be presented in the flume for these test results to be comparable with the flume results.

As a result of this uncertainty in the determination of the effective segregation threshold of our slurries, other methods have been considered. It was noted in section 3.3.7 that the presence of segregation in the flume appeared evident on the basis of the depositing particles forming a hard sandy deposit near the downstream end of the flume. This could be identified as a method of detection of segregation, though it makes the task of defining the segregation threshold quite onerous. It would be of significant value to be able to run a simple laboratory test with a small sample of the slurry, instead of going to the considerable effort of conducting full scale flume experiments.

The separate grouping of the equilibrium slope data as noted above presents an inferred indication of segregation, though this involves even more effort than the previously identified method, since this would require numerous flow regimes to be tested in a flume. This issue demonstrates a significant need for further development in the testing of segregation threshold of slurries.

On the basis of the findings discussed here, the effective segregation threshold for the Cobar tailings slurry will be defined as 48%, and for Sunrise Dam the threshold will also be defined as 48% w/w. These definitions will be used in subsequent chapters in classifying the individual flow regimes into the two categories of non-segregating and segregating regimes.

3.3.15 Unhindered settling velocity testing

Unhindered settling velocity tests were undertaken at RMIT University in order to calculate drag coefficients of tailings particles. These tests entailed dropping a single coarse Cobar tailings particle

into clear water contained in a measuring cylinder of 36 mm internal diameter and 305 mm in height to observe the terminal settling velocity of the particle. A stopwatch was used to time each descent over a vertical distance of 200 mm that commenced some 80 mm below the water surface. These coarse particles were separated from the slurry by diluting a slurry sample and pouring the light fraction off the top. It was assumed that the diameter of each of these particles was equal to the 85th percentile diameter (d_{85}), which was measured to be 51 μm during the particle sizing work documented in section 3.3.12. Thirty-six repeat runs were conducted, with the mean settling velocity being 0.028 m/s.

3.3.16 Static settling tests

A series of experiments were conducted at RMIT University, which monitored the settling of Sunrise Dam tailings slurry under static conditions for 24 hours. After this time, an obvious division between the settled material and the clear decant water could be seen. The depth of this section was measured and the corresponding volume calculated. Various concentrations were tested, with results presented in Table 2:

Initial Concentration, Cw	% w/w	64	57.5	51.1	46.7	41.9
Total volume	ml	433	433	433	433	433
Final free water volume	ml	66.5	92.8	99.8	124.9	146.8
Water loss (W.L.)	% v/v	15.4	21.4	23.0	28.8	33.9
Final settled concentration	% w/w	70.8	67.0	60.9	59.0	56.2

Table 2. Results of Sunrise Dam tailings 24 hour static settling tests.

3.3.17 Slurry discharge and deposition observations

During the Sunrise Dam experimental programme, on site stack observations indicated an apparent lack of any bifurcations in the self-formed channels on the stack. Several self-formed channels were photographed from their point of inception to their lower reaches further down the beach at Sunrise Dam, with no evidence of a single stream splitting into two.

3.4 Phase 2: Small scale laboratory experiments

3.4.1 Experimental Objectives

The objective of the small scale flume experiments was to measure equilibrium slopes for analogue Newtonian and Non-Newtonian slurries with smaller channel geometry, lower flow rates and much lower solids concentrations than those tested in the large scale experiments that were documented in section 3.3. The use of a much smaller channel section would not only allow the effects of scale to be examined, but also it was seen that different channel cross-sectional shapes could be considered. Though both flumes had channels of circular cross-section, the surface levels in the small flume were expected to run around the half full mark of the circular pipe, whereas in the field flume most of the surface levels were running at depths about 5 to 20% of the pipe diameter. Thus, the range of channel shapes covered between these two experimental phases would go from semi-circular down to very wide, shallow segment shapes. This was expected to cover the full range of possible self-formed channel shapes on a tailings beach. Investigating the effect of different sized particles on the equilibrium slope was also an objective of the small scale flume experiments. Examining this effect in the field flume was not possible, since the slurry particles could not be changed from one run to the next. It was seen that the small scale flume data would enable a more general and powerful means of validating the models presented in the thesis.

3.4.2 Small flume apparatus

The main component of the small scale flume apparatus was a straight transparent glass pipe of 50 mm internal diameter and 5.4 metres length, which was run partially full at all times to ensure open channel flow conditions. A T-piece fitting on the upstream end of the glass pipe performed the functions of a plunge pool and an entrance weir to minimise the entrance velocity into the flume (see Figures 39 and 40). The flume could be tilted to slopes between horizontal and 8%. A progressive cavity pump was used to circulate the artificial slurries through the flume, with a flow capacity of 2 to 24 litres per minute. Flow measurement, density measurement and temperature measurement was enabled by a Micro Motion F-Series F050 Mass and Volume Flow and Density Sensor coriolis meter, located

immediately downstream of the pump. A schematic diagram of the small scale flume apparatus is presented in Figure 37, while several photographs of the flume apparatus appear in Figures 38 to 41.

To check that the flume length of 5.4 m was sufficient to enable a test section that was free from end effects, the same approach was applied as was used in section 3.3.2, in which the figure of 13D presented by Shenoy & Mashelkar (1983) was used to calculate the entrance length. This figure was for fully developed turbulent flow with a Reynolds number of 6000, where D is the diameter of the pipe. Greater entrance lengths were required for higher Reynolds numbers, according to Shenoy & Mashelkar. It is expected that the Reynolds numbers encountered in the flume will be less than 6000, so this figure of 13D should provide a conservative estimate for the entrance length. Applying the geometric conversion of $D = 4R_H$ (where R_H is the hydraulic radius of the channel), it is calculated that the entrance length for turbulent flow in a channel with a Reynolds number of 6000 would be equal to $52R_H$. The range of possible hydraulic radii for a partially filled 50 mm pipe will vary from 0 to a maximum of 15 mm when the pipe is about 81% full. For the maximum permissible flow rate, the entrance length required in the flume was calculated to be 0.8 meters. The exit length (the downstream section affected by a gradual decrease in depth as a result of the increase in surface velocity) in the flume was assumed to be equal to the entrance length, on the same basis that was adopted in section 3.3.2. This analysis would suggest that the 5.4 m length of the flume is adequate in allowing for end effects, since it should provide a test length of fully developed flow at least 3.8 metres long.

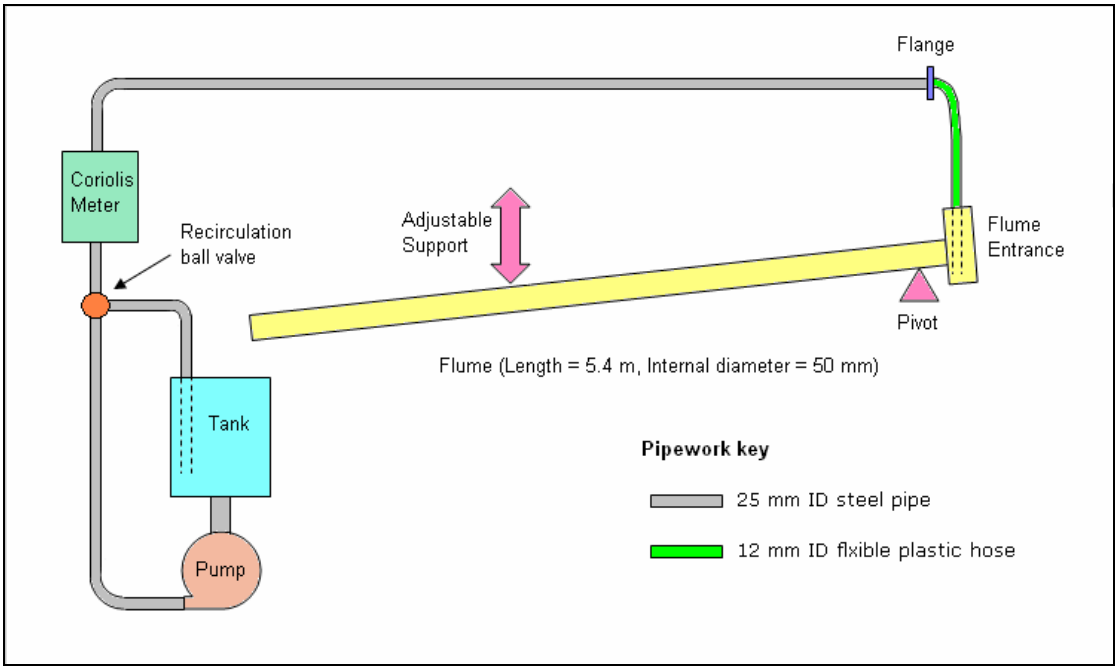

Figure 37. Diagram of small scale flume

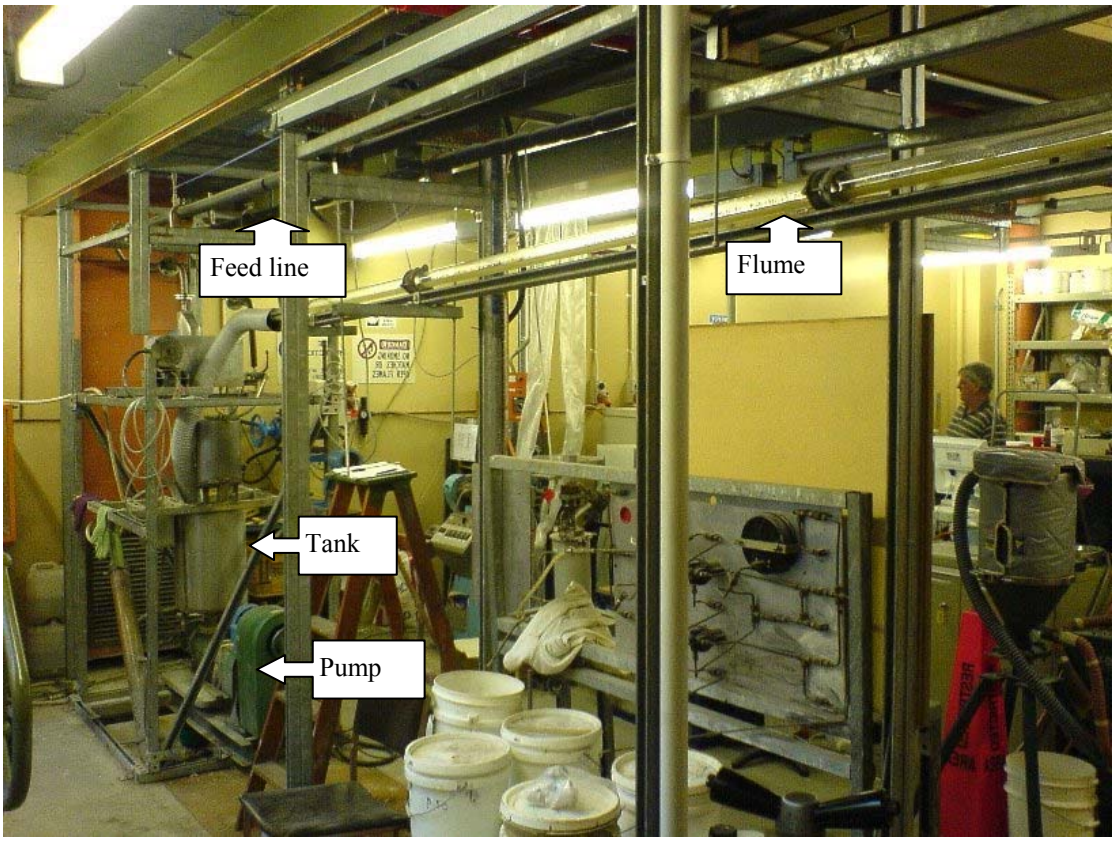

Figure 38. Photograph of small scale flume, showing the downstream end and pump

Figure 39. Photograph of flume, taken from the upstream end

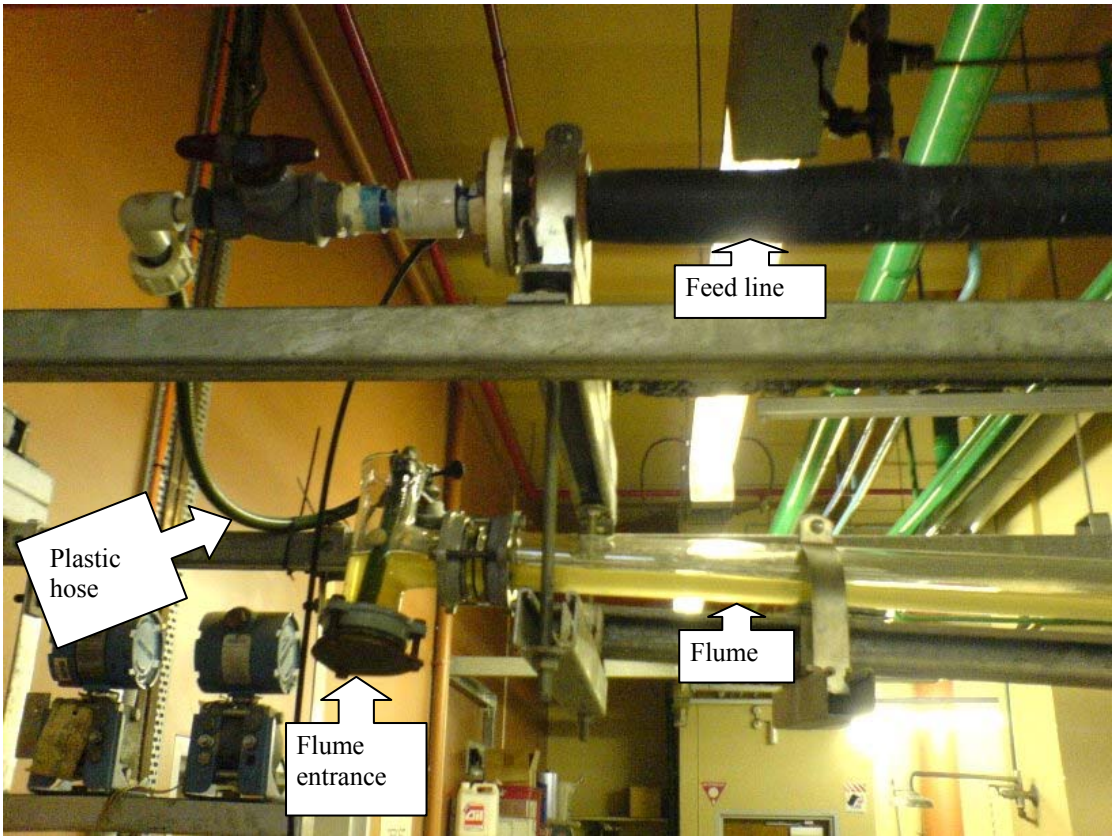

Figure 40. Photograph of flume entrance

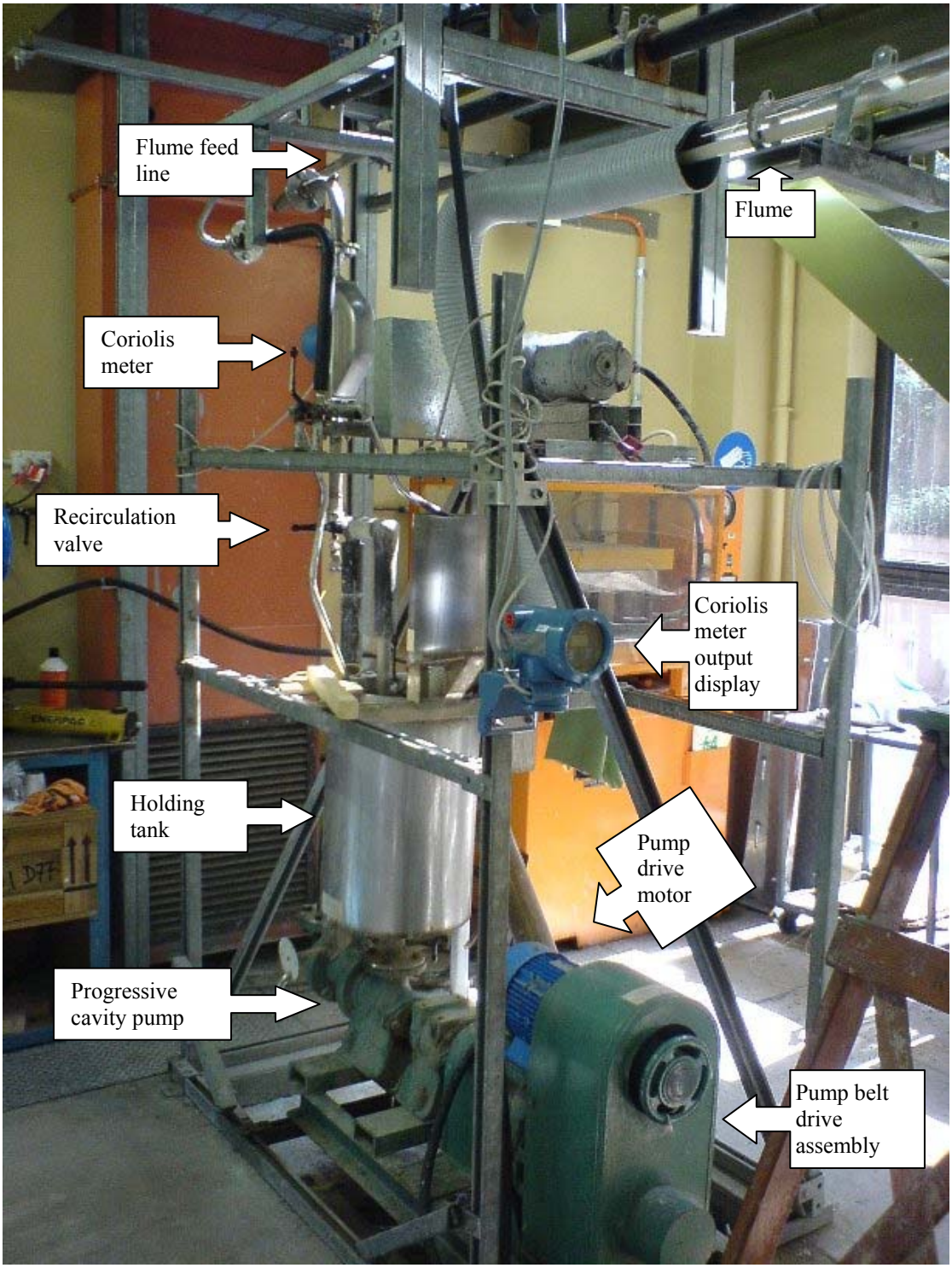

Figure 41. Photograph showing the pump, holding tank and coriolis meter

3.4.3 Experimental procedure

A measured volume of fluid was poured into the holding tank of the flume system with a measured quantity of particles added to the fluid to create an analogue slurry. The pump was then run at full speed, with the recirculation valve used to divide the flow to send some slurry into the flume, and divert the remainder back into the holding tank. This was found to be better than the alternative of leaving the recirculation valve fully open all the time and setting the pump at different speeds for two reasons; at low pump speeds the pump was observed to gradually change speed over time; and deposits of particles formed in the bottom of the tank around the discharge outlet at its base. With the pump running at high speeds it was found that fluctuations in the flow rate were minimised, and solids deposition in the tank was avoided due to the turbulent disturbance in the tank caused by the fluid returning from the recirculation line and the flume discharge. As well, the pump caused a significant amount of vibration to the tank at high speeds, which also appeared to reduce solids deposition there. Once uniform flow was established in the flume, monitoring for particle deposition in the flume was achieved by visual observation through the transparent glass pipe. Like the large scale flume experiments conducted at Sunrise Dam and Cobar, these experiments set out to determine the flattest flume slope at which deposition did not occur. To find an equilibrium slope, the flume was initially set at a fairly steep slope, and flow rate was kept constant as the flume was incrementally raised to yield flatter slopes. Once the slope was flat enough to allow one or more stationary deposits of particles to form in the flume, this particular slope would be deemed to be the equilibrium slope.

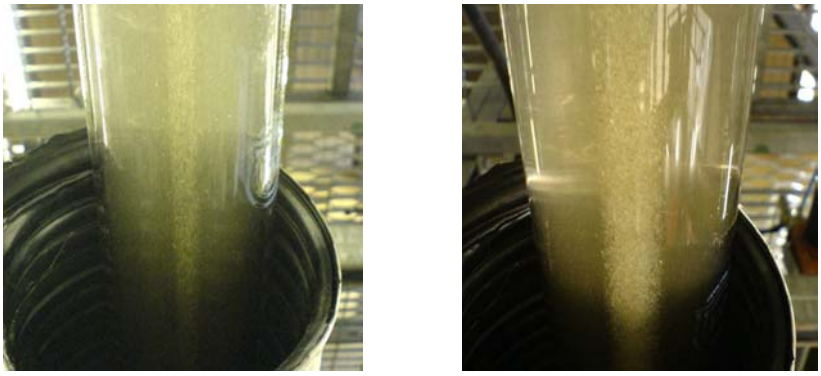

Figure 42. Photographs taken from below the flume looking up at the invert. The left picture shows a rolling bed in which all of the particles are still mobile. The right picture shows a larger, deeper bed, in which the particles lying on the base of the pipe are stationary, whilst the particles above are still moving downstream, thus forming a sheared bed.

At this point, a new flow rate could be tested, with the search for another equilibrium slope starting over again. Once a given fluid was found to have generated a sufficient amount of equilibrium slope

data, a 200 ml sample of the fluid was extracted from the tank and tested in a rheometer for the fitting of a rheological model later on.

The slope of the flume was initially calibrated using a laser level, which allowed subsequent slopes to be calculated on the basis of a single vertical offset measurement from a fixed point. The actual slopes were then deduced later on from the vertical offset data.

The depth of flow in the flume was measured from outside the glass pipe with a steel ruler. Depth readings were repeatedly taken from either side of the flume for any one measurement to ensure that parallax errors were avoided. It was observed that the glass pipe incurred refractive errors in these depth measurements, particularly when the depth was very low or very high. These refractive errors were systematically addressed by a separate series of optical experiments, in which a small vertical scale was set up inside the glass pipe, with the steel ruler used outside the pipe to measure the apparent depth in relation to the actual depth shown by the small scale inside the pipe. A mathematical expression was later fitted to this data empirically to enable all of the flume data to be corrected for refractive errors later on. This work is presented in Appendix I.

Fourteen different fluids were run through the small flume; water, 11 concentrations of carboxymethylcellulose (CMC) mixed with water; and 2 concentrations of carbopol mixed with water. The CMC and carbopol solutions both demonstrated non-Newtonian behaviour. Three different groups of particles were used in the experiments; “coarse”, “fine”, and “mid”. The “mid” crushed glass particles were open graded with a median size of 560 μm. The “coarse” particles were extracted from the “mid” population, taking all those caught in a 1000 μm sieve. The median particle diameter of the “coarse” particles was estimated at 1400 μm. The “fine” particles were also extracted from the “mid” population, taking the particles passing a 420 μm sieve but retained in a 250 μm sieve. The median particle diameter for these “fine” particles was calculated to be 335 μm.

3.4.4 Equilibrium slope testing

The small scale flume experiments generated some 95 equilibrium slopes. This data is presented both in graphical form below in Figure 43. A tabulated form of the data is presented in Appendix H.

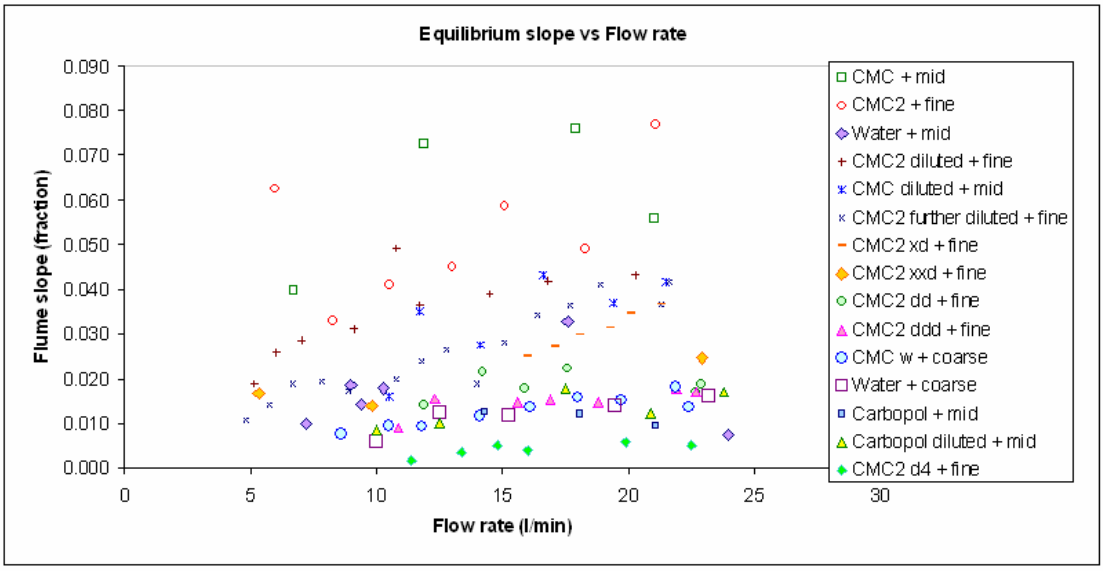

Figure 43. Plot of equilibrium slope data gathered in the small flume. The legend shows the fluid name + particle size

Figure 43 shows the equilibrium slope results for the small scale flume experiments. Various slopes were generated for each fluid as a function of the nominated flow rate and the presence of depositing particles in the channel bed, as per the procedure presented above in section 3.4.3. Some important findings can be listed from the data presented in Figure 43:

Increasing the flume slope to be steeper than the equilibrium slope caused a bed to be washed away, while decreasing the slope to be flatter than the equilibrium slope caused a bed to form. This finding was consistent with the behaviour observed in the large flume.

Increasing the viscosity of the carrier fluid resulted in steeper equilibrium slopes. This was also consistent with the results gained in the big flume.

Increasing the particle size caused steeper equilibrium slopes. This finding was not tested in the large scale flume due to the inability to alter the particle size during that work, but it is consistent with the

findings of others (Durand 1953; Oroskar & Turian 1980; Wasp et al. 1977), who observed that large particles required a higher mean velocity to remain in suspension. In the flume the steeper slopes invoked higher mean velocities, evident from the decrease in depth with an increase in slope.

Increasing the flow rate resulted in steeper equilibrium slopes. This was a curious finding that was both counter-intuitive and completely opposite to the behaviour observed in the large flume. Once a sediment deposit had formed in the flume, the flow rate could be decreased and the sediment was seen to remain, which was consistent with the behaviour of the large flume. When the flume was steepened to allow the deposited sediment to wash away, it would wash away as expected. However, when the flume was incrementally lifted to determine the equilibrium slope for this new flow regime, it was found that a stationary bed would form at a flatter slope than the previous bed formed at the greater flow rate. This behaviour was opposite to that observed in the large flume, so a considerable amount of time and effort was spent investigating this phenomenon. It was soon realised that the particle concentration effectively decreased at low flow rates. It was observed that the particles "disappeared" from the system at low flow rates, particularly when non-viscous fluids were being run. It is thought that these absent particles were depositing in the 25 mm steel pipe that feeds the flume. Confirmation of this suspicion was provided when the flume was set at a flat slope with a low flow rate for a prolonged period, and then the pump speed was increased to enlarge the flow rate. Suddenly the flume would be laden with a bed of particles some 20 mm deep. It was also observed that this particle deposition in the feed line caused the larger particles to be preferentially retained over the smaller ones. It was observed that a flow rates around 20 litres per minute were sufficient to avoid this effect.

Correction of concentration values

A separate series of experiments were conducted to investigate this effect in a bid to empirically quantify the particle capturing effect as a function of flow rate. These experiments took place in two phases; the first phase saw the flow rate adjusted every minute or so, with the corresponding fluid density value read off the coriolis meter almost immediately after each change in flow rate. The second phase allowed some 5 minutes for the flume to run before the density was recorded, thus enabling more time for the concentration to stabilise throughout the flume system. The results of these experiments are presented below in Figure 44, with an empirically fit equation superimposed onto the same graph.

The volumetric concentration (C_V) for each experimental run was determined using the following equation:

$$C_V = \frac{\rho - \rho_W}{\rho_S - \rho_W} \tag{50}$$

where ρ is the mixture density, equal to 1000 times the fluid specific gravity displayed by the coriolis meter, ρ_W is the density of the water and ρ_S is the density of the glass particles (assumed to be 2650 kg/m^3). Since it is well understood that the density of water varies depending on its temperature, the water density was calculated using the following empirical equation:

$$\rho_W = 1000(1.00025 - T^2/195000) \tag{51}$$

where T is the water temperature in degrees Celsius. This equation is based on a fit to table of water density data that can be found in Appendix K.

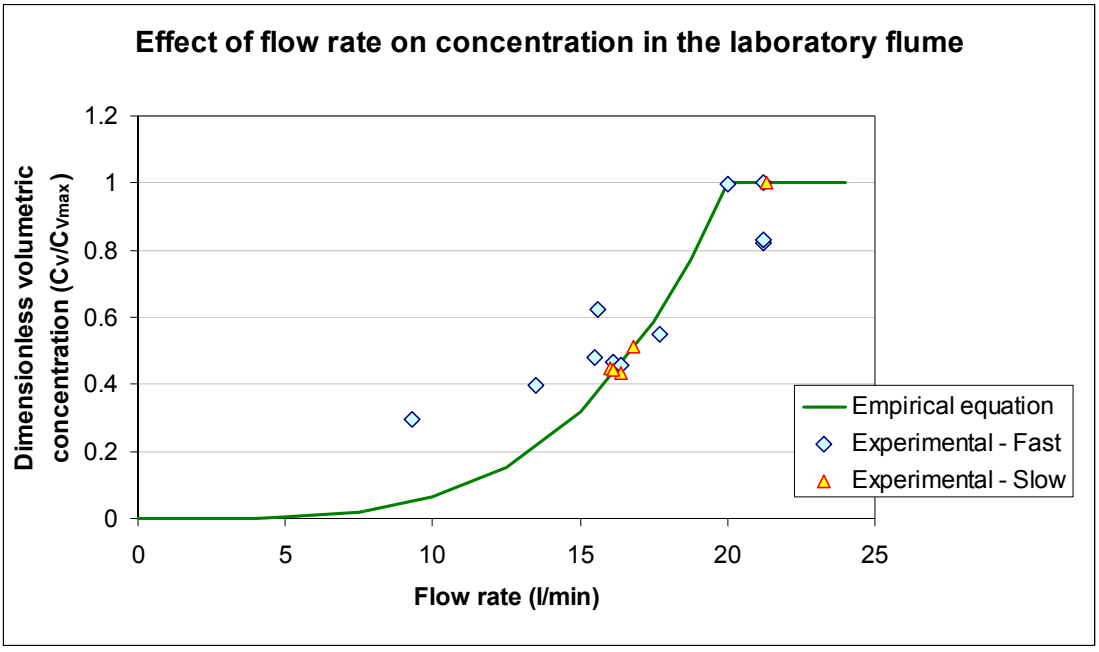

Figure 44. Plot of concentration as a function of flow rate in the small scale laboratory flume. The "fast" points were measured about 30 seconds after a flow rate was set, while the "slow" flow rates allowed the system some 5 minutes to adjust before the concentration was read.

The equations of the empirically fitted curve are as follows:

$$\frac{C_V}{C_{V\max}} = \frac{Q^4}{160000} \qquad 0 < Q < 20 \text{ l/min} \qquad (52)$$

$$\frac{C_V}{C_{V\max}} = 1 \qquad Q \geq 20 \text{ l/min} \qquad (53)$$

Equation 52 relates the concentration to the flow rate with a power of 4. Since the particles were being captured in a pipe with a fixed cross-sectional area irrespective of the flow rate, equation 52 would imply that the concentration can also be related to the velocity by a power of 4. Previous research into particle transport in pipes found the same mathematical relationship. An empirical fit to data presented by Wasp et al. (1977) showing the minimum transport velocity for slurries of various concentrations in a pipe is presented below:

$$V_C = 3.8 C_V^{1/4} \left(\frac{d}{D}\right)^{1/6} \left[\frac{2gD(\rho_s - \rho_l)}{\rho_l}\right]^{1/2} \qquad (54)$$

Where V_C is the minimum transport velocity for a slurry without depositing particles on the pipe bed, C_V is the volume fraction of solids, d is the particle diameter (m), D is the pipe diameter, ρ_S is the density of the solid particles, and ρ_l is the density of the carrier fluid.

The power of ¼ applied to the concentration term in equation 54 relates the concentration to the flow rate by the same power of 4. With this confirmation of the trend observed in the experimental findings in the small flume, equations 52 and 53 have been used to calculate effective concentration values for the small scale flume data.

3.4.5 Particle Size Analysis

Sieve analysis of the "mid" crushed glass particles was carried out to generate a particle size distribution curve for the open graded material.

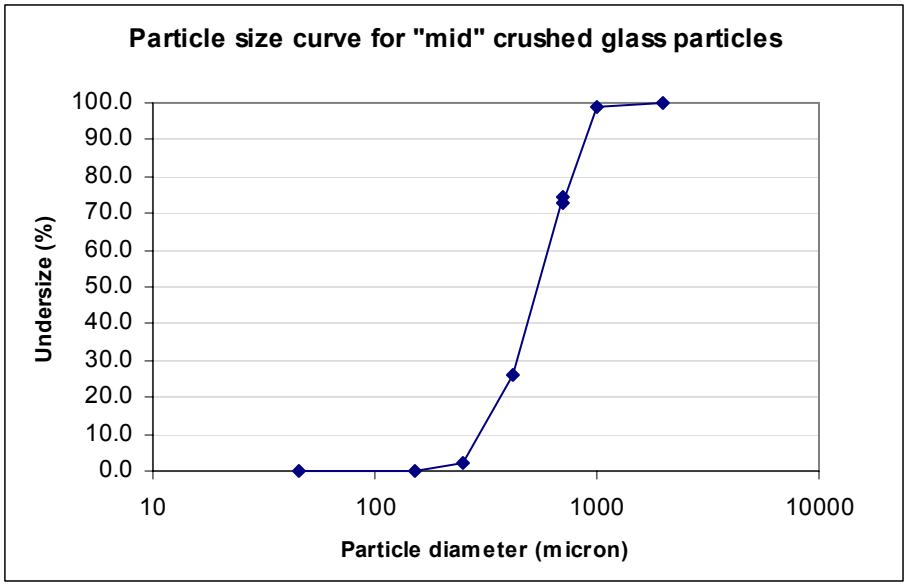

Figure 45. PSD curve for the "mid" particles.

Figure 45 shows that the median particle diameter (d_{50}) for the "mid" population of particles was about 560 μm, the 10 percentile diameter (d_{10}) was about 200 μm and the 90 percentile (d_{90}) about 800 μm. The "fine" and "coarse" particles were extracted from the "mid" population with sieves, with the "fine" group consisting of particles passing a 420 μm sieve that were caught in a 250 μm sieve, and the "coarse" group consisting of particles passing a 2000 μm sieve that were caught in a 1000 μm sieve. The d_{50} for the "fine" particles is estimated to be 335 μm, and the d_{50} of the "coarse" particles is estimated to be 1400 μm.

3.4.6 Unhindered settling tests

Settling tests were undertaken to determine the drag coefficients of the glass particles. These tests were done in water in a large glass measuring cylinder some 500 mm high and 73 mm in bore. 24 particles from each of the 335 μm and 1400 μm median diameter populations were tested.

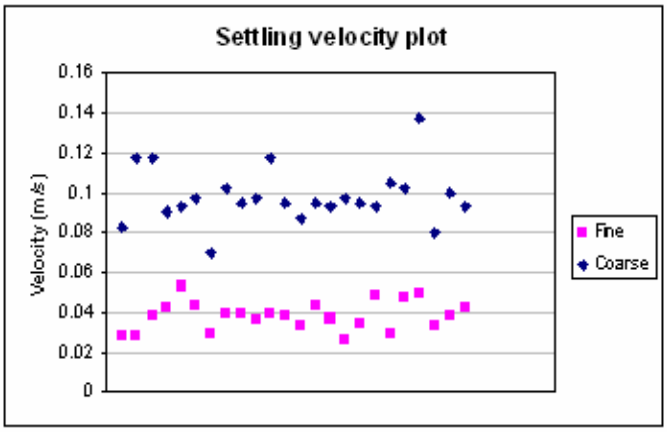

Figure 46. Velocities measured in the unhindered settling tests.

Figure 46 shows that the fine particles (d_{50} 335 μm) had a mean unhindered settling velocity of 0.04 m/s, and the coarse particles (d_{50} 1400 μm) had a mean unhindered settling velocity of 0.1 m/s.

3.4.7 Rheological Analysis

The 13 non-Newtonian fluids that were run through the small scale flume were rheologically tested in a Contraves Rheomat 115 Couette rheometer. Rheograms for 4 of these fluids are presented in Figure 47, with the rheological model curves inscribed on the same graph. The Herschel-Bulkley model parameters for all 13 fluids are presented in Table 3. Individual graphical fits of the rheological model curves for all 13 of the non-Newtonian fluids are presented in Appendix J.

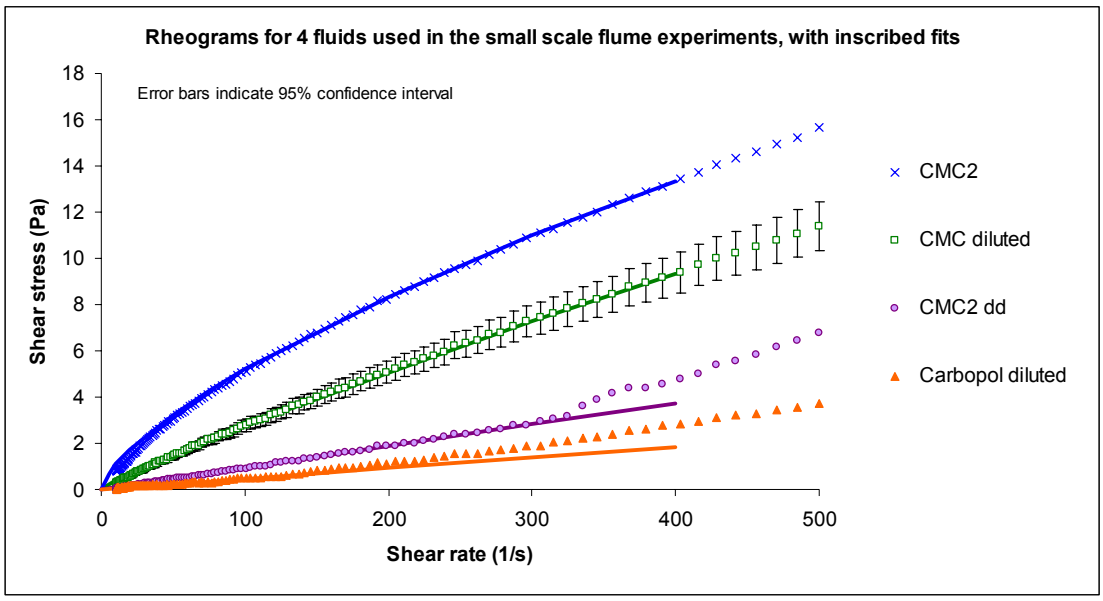

Figure 47. Rheograms for 4 of the non-Newtonian fluids run through the small flume, with the rheological model fit curves inscribed.

Figure 47 shows rheograms for 4 of the non-Newtonian fluids tested in the small flume, with the rheological model fits inscribed for each of the four data sets. Error bars are presented on one fluid for a 95% confidence interval, showing that the rheological model fit is well within these error limits. It is noted that the rheological data suggests that shear thickening is occurring in the CMC2 dd fluid at a shear rate of 320/s and also in the Carbopol diluted fluid at about 150/s, because of the increase in slope of the rheometric data beyond these shear rates. This is not the case however, as this increase in slope is actually an artefact that is caused by turbulent vortices forming at the bob surface, which occurs with low viscosity fluids being sheared at high rates. (Chryss & Pullum 2007)

Fluid name	Parameter fits for Herschel-Bulkley model		
	ty	K	n
Carbopol	0.1	0.008	1
Carbopol diluted	0.02	0.0045	1
CMC	0	0.196	0.7
CMC diluted	0	0.048	0.88
CMC2	0	0.227	0.68
CMC2 diluted	0	0.11	0.77
CMC2 further diluted	0	0.072	0.82
CMC2 xd	0	0.051	0.86
CMC2 xxd	0	0.027	0.92
CMC2 dd	0	0.0105	0.98
CMC2 ddd	0	0.0073	1
CMC2 d4	0	0.003	1
CMC w	0	0.004	1

Table 3. Herschel-Bulkley parameters for the 13 non-Newtonian fluids tested in the small flume.

3.4.8 Discussion of small scale flume experiments

At slopes just below deposition, particles could be seen to roll along the pipe invert. This behaviour was useful as a precursor to an equilibrium slope. However, in viscous fluids it could be seen that a sheared bed replaced the rolling bed that was apparent for non-viscous fluids. In viscous fluids the flow was less turbulent. The surface was smooth, with no waves. This made the measurement of the fluid depth relatively easy. Even the pipe joints didn't cause surface disturbance for highly viscous fluids. Subsequent analysis of these flows confirmed our observations that they were laminar. For turbulent flows with rough surfaces, the accurate measurement of the depth of flow was made more difficult, inevitably introducing greater errors into the measurement.

In laminar flow conditions, a different type of equilibrium flow was occurring, with a different transport mechanism moving the particles. In turbulent flow the particles were spread throughout the flow cross-section as they were swept up by eddies. In laminar flow the particles settled to the bottom of the channel, but they were able to roll or slide along the channel bed while the slope was sufficiently steep to overcome the friction between this moving bed and the channel surfaces.

Graham et al. (2002) experimentally demonstrated that solid particles will settle in laminar flow in horizontal pipes. Slatter (2004) reported that such pipelines running in laminar conditions will inevitably experience blockage from this settlement. It has been suggested that such a pipeline could be kept running at a sufficiently high pressure gradient to overcome the friction force between the sliding bed and the pipe surface. (Cooke 2002) In an open channel the slope of the bed is equal to that of the hydraulic grade line under fully developed uniform flow conditions, which is in turn equivalent to the pressure gradient in a pipeline. It is therefore posed that such laminar flows could also be used to transport particles in channels via the same sliding mechanism, providing a sufficiently steep channel slope is maintained. The experimental data presented here supports this claim, though it is suspected that the slope required for this sliding transport would need to be steeper as the length of the channel increases. Further experimental evidence of this could be gained through the use of open channel flumes of various lengths.

One problem that was experienced in the small flume was the gradual introduction of foreign matter into the fluid over time. This foreign matter was thought to be dirt, rust, and clay particles deposited from previous experimental work being eroded from the inside surfaces of the pipes and pump by the relatively abrasive glass particles being used in this work. This foreign matter not only caused the fluids to get dirty (thereby impeding the view of the glass particles), but also introduced new smaller particles into the system, which may have deposited in the flume and prematurely invoked the deposition of the glass particles at slopes steeper than equilibrium.

3.5 Errors in experimental results

Experimental errors have been approached from two directions in this analysis; firstly statistical analysis of the data was undertaken to estimate the random error for each variable, then secondly an estimation of the instrument errors and human errors took place for all the measured variables.

3.5.1 Random error analysis

Statistical analysis of samples of the measured data took place to estimate the random variability of the parameter in question. In order to undertake this analysis it was necessary to have multiple readings of a randomly variable quantity to be able to check its repeatability. For most of the measured variables this data was available. However, in the case of the flume equilibrium slope data, these repeated measurements were not available for a number of reasons. Firstly, the amount of time required in arriving at a single equilibrium slope measurement was prohibitive because the ability to keep the flow rate and concentration constant long enough to record one equilibrium slope was difficult. Often these input variables changed abruptly before an equilibrium slope had been reached, forcing the abortion of a flow regime before the experiments had reached a result, even if some 3 or 4 hours had already been spent with that particular flow regime. These sudden changes were encountered fairly frequently as a result of changes in the upstream processing operations, and were completely beyond the control of the experimenters. Secondly, the ability to set the flow rate and concentration to precise values was very difficult with the slurry feed system being used, and took a considerable amount of time to achieve. Each time the slurry valve was adjusted, it would take several minutes to measure the flow rate, with the fluid levels in the flume and plunge box also needing some time to stabilise in reaction to the change. The ability to set the slurry concentration to a precise value was much more difficult than the flow rate, because it was necessary to adjust the valves on both the slurry feed line and the water feed line to do this. Once these valves had been adjusted, the time taken to measure the new concentration was considerable, even though a Marcy scale reading can be made in a matter of only a few minutes, because adequate time had to be allowed for the new incoming slurry to mix with the slurry remaining in the plunge box from the previous regime to bring the prevailing concentration in the flume to the new value. Finally once the desired concentration had been reached, the flow rate would usually be completely different from its initially established value. Correcting the flow rate would usually upset

the concentration, and vice-versa. Hence, repeating a specific flow regime with this slurry feed system was practically impossible, making the repeat measurement of an equilibrium slope too difficult and time consuming to attempt. The flow rate, concentration, rheological measurements and particle size measurements were repeatable though, so these variables were analysed for random errors. The results of this random error analysis are presented graphically in Figures 48 to 55. A summary of the random errors is presented in Table 4, with the details of the analysis presented in Appendix G.

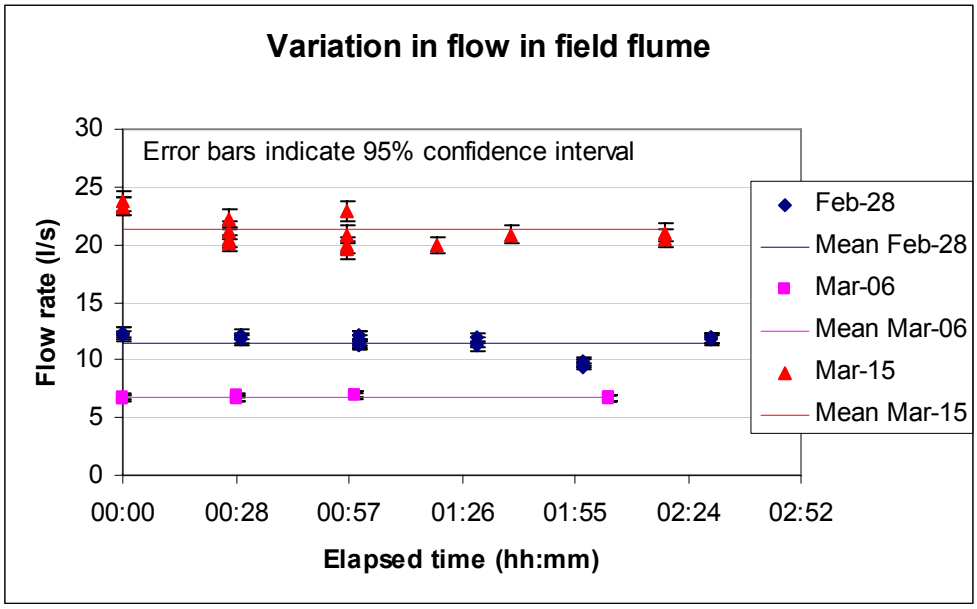

Figure 48. Random error plot for flow rates measured in the field flume

Figure 48 shows a significant amount of variation in measurements for the high flow rate data recorded on the 15th of March. This is due to the difficulty in measurement of the flow rate at high flow rates, which is discussed in section 3.5.2, where the instrument and human errors are estimated.

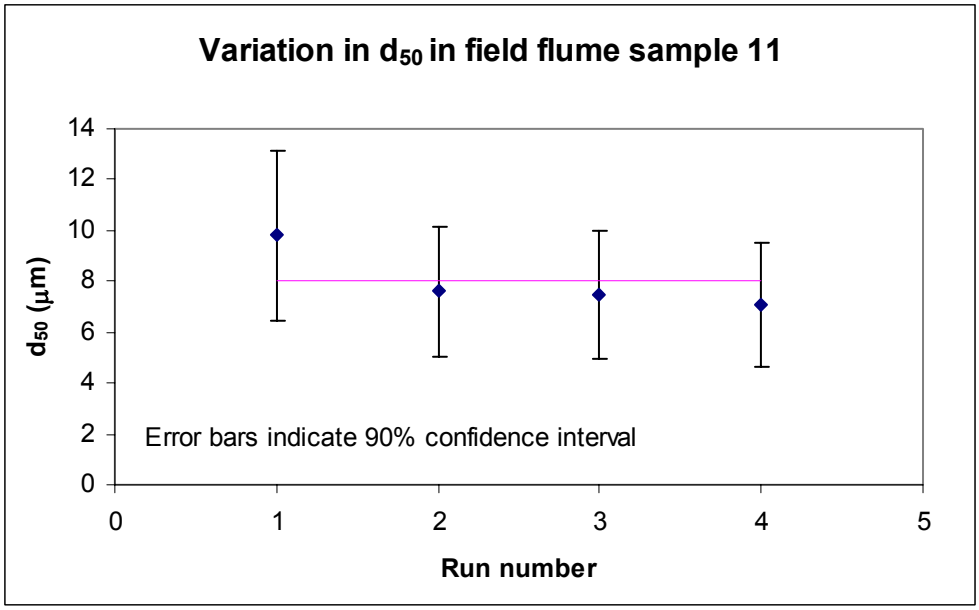

Figure 49. Random error plot for median particle diameters measured in 4 repeat particle sizing runs for one sample extracted from the field flume

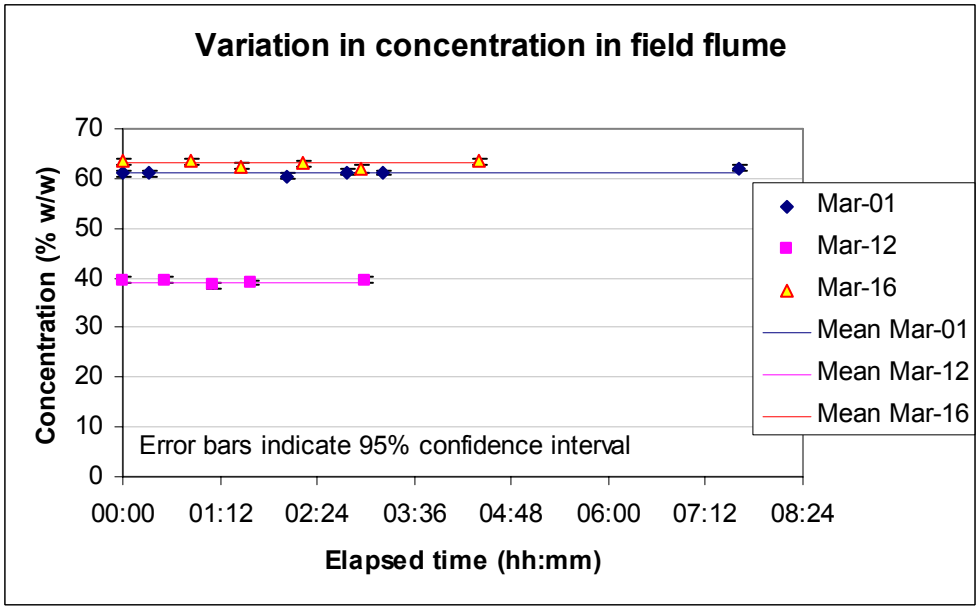

Figure 50. Random error plot for concentrations measured in the field flume

Figures 49 to 55 all show consistency and stability in the measured data, with the mean values for each data set sitting within the error bar range of each observed data point.

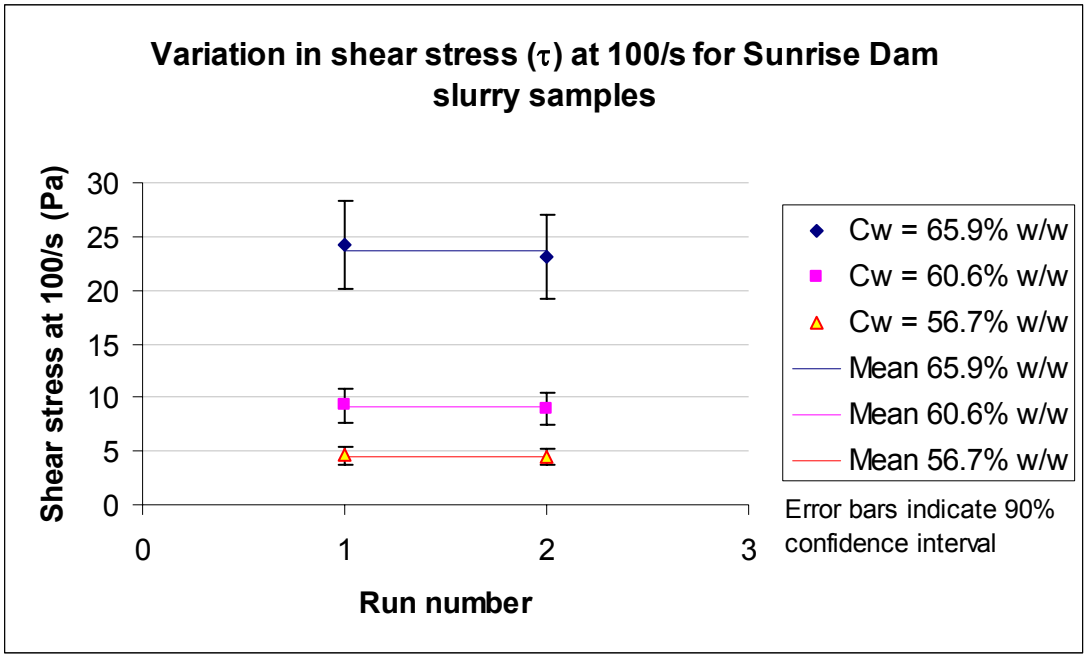

Figure 51. Random error plot for shear stresses measured in the Contraves rheometer while testing slurry samples from Sunrise Dam

Figure 51 compares the shear stresses measured by a rheometer at the shear rate of 100/s for 3 different concentrations of slurry from the Sunrise Dam mine that were each tested twice. This graph shows that the rheometry data was repeatable within the 90% confidence limits calculated for the data.

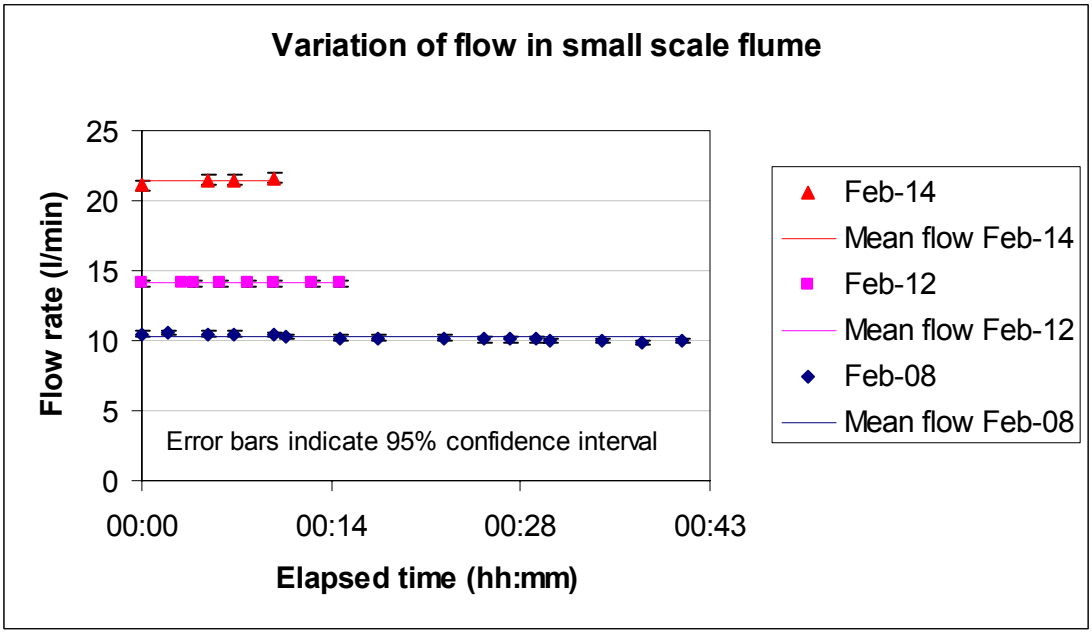

Figure 52. Random error plot for flow rates measured in the small laboratory flume

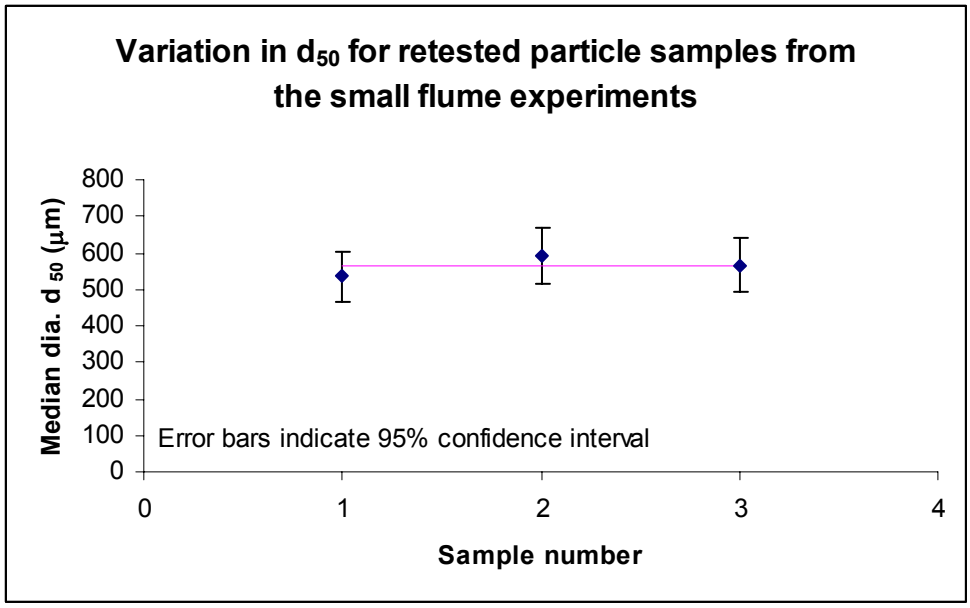

Figure 53. Random error plot for median particle diameter (d_{50}) measured by sieve analysis for the small laboratory flume experiments

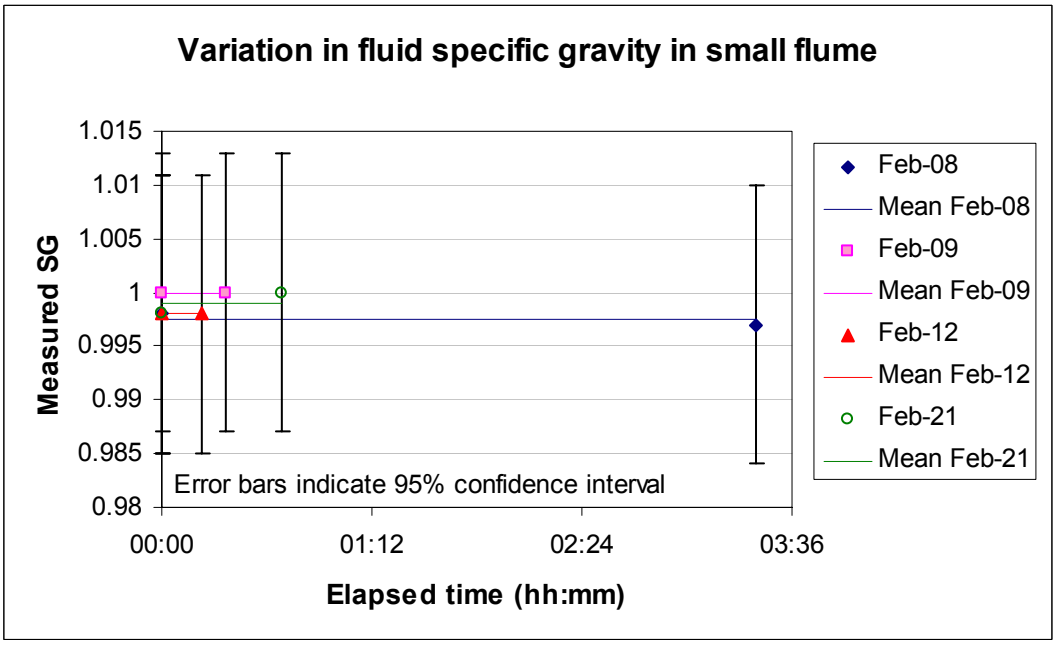

Figure 54. Random error plot for fluid specific gravity measured in the small laboratory flume

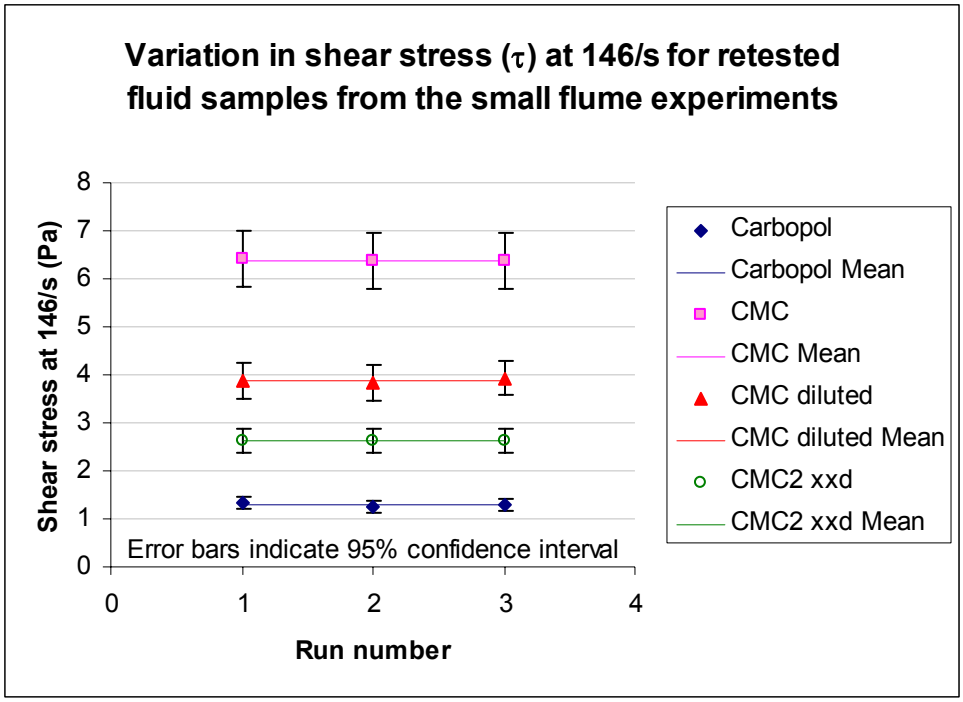

Figure 55. Random error plot for shear stresses measured in the Contraves rheometer while testing fluid samples used in the small laboratory flume

Figure 55 compares the shear stresses measured by a rheometer at the shear rate of 146/s for 4 different fluids that were each tested three times. This graph shows that the rheometry data was repeatable within the 95% confidence limits calculated for the data.

Field flume experiments			Laboratory flume experiments		
Parameter	Confidence interval	Error	Parameter	Confidence interval	Error
Flow rate, Q	95%	± 3.6%	Flow rate, Q	95%	± 1.7%
d_{50}	90%	± 34%	d_{50}	95%	± 13%
C_W	95%	± 1.5%	Specific gravity	95%	± 1.3%
τ at 100/s	90%	± 17%	τ at 146/s	95%	± 9.3%

Table 4. Summary of the random errors for four key variables in both experimental phases.

The random error summary presented in Table 4 shows that the d_{50} data are statistically variable from one measurement to the next, particularly for the field flume slurry particles. It is believed that this is due to the sensitivity of the particle sizer to the sampling technique used when the particles are introduced to the apparatus. The rheometric data also shows some significant inconsistency between shear stress measurements, particularly for the tailings slurries used in the field flume experiments. It is believed that this random error for the mineral slurry data is due to the settling of particles in the

rheometer cup, which reduces the effective concentration of the material, thereby reducing the shear stress experienced by the rotating rheometer bob that is suspended above the bottom of the cup.

3.5.2 Instrument error and human error analysis

The value recorded for each variable during the experimental work was determined by measuring one or more quantities. The temperature of the slurry in the field flume for example, was determined with only one measurement from a thermometer. By comparison, measuring the flow rate in the field flume was more complicated. The time taken for the flow measuring box to be filled had to be measured. This was achieved with the use of a hand-held digital stopwatch, which presented a reading that was accurate to a hundredth of a second. However, the human error in reaction time was much larger than 1/100 of a second, and needed to be quantified. Then the dimensions of the flow measuring box had to be measured. This was achieved with a tape measure, which had its own accuracy. Then the effect of waves in the fluid surface had to be considered, since the stopwatch was stopped once the fluid surface reached a certain level. These 4 sources of error were all affecting the measurement of the flow rate, and needed to be considered in the determination of the measurement error for this variable.

The accuracy of the individual measurements contributing to the logging of each recorded variable were estimated. Many of these estimates were based on the resolution of the instrument (eg. a ruler with a millimetre scale has a measurement accuracy of ±1 mm). For each variable, a worst-case investigation was then conducted, in which the combined measurement error was calculated by compounding all the possible measurement errors from the contributing sources of instrument or human error for that variable. For each combination, each of the relevant instrument or human errors were skewed to their maximum or minimum possible measured values to present a compound error. Once all of the combinations had been calculated for each variable, the one that yielded the largest error was adopted as the measurement error for that variable. Table 5 presents the estimated accuracy for each discrete measurement that was required for quantifying a variable, as well as the calculated measurement error for the variable. The worst case investigation can be found in Appendix G.

Variable	Error	Description of measurement	Accuracy
Field flume experimental measurements			
Depth	± 1mm	Ruler with 1 mm graduations	± 1 mm
Flow	± 14.6%	Stopwatch accurate to 0.1 sec	± 0.1 s
		Human error associated with fast/slow timing in hitting button	± 0.14 s
		Tank with base area 1.20 m x 1.00 m	± 0.01 m
		Depth gauge accurate to 1 cm due to surging wave action in tank at flows < 12 l/s	± 0.01 m
		Depth gauge accurate to 2 cm due to surging wave action in tank at flows > 12 l/s	± 0.02 m
Slope	± 0.05% slope	Initially marked on A frame in texta using an automatic level	± 2 mm
		Accuracy of level and human error in usage (± 1.5 mm in 1 km)*	± 1 mm
		Calibration of level? Perfomed 3 point check. OK.	
		Staff accuracy assumed beyond question. Base kept clean.	
		Parallax error when reading texta marks on A frame	± 2 mm
		Potential for flume channel section to twist, thereby distorting line of sight	
Concentration	± 0.8%	Marcy gauge used on site, then later checked against oven dried samples.	± 5 ml
		Gauge dial can be read to 0.1 % w/w	± 0.1% w/w
Temperature	± 1° C	Mercury thermometer with 1° graduations	± 1° C
Particle size	± 1%	Laser particle sizer used. **	± 1%
Laboratory flume experimental measurements			
Depth	± 1mm	Ruler with 1 mm graduations	± 1 mm
Flow	± 0.15%	Coriolis meter used***	± 0.15%
Slope	± 0.07% slope	Initially measured levels to frame using tape measure and laser level	± 2 mm
		Measurement of gap between support and frame using tape measure	± 2 mm
Concentration	± 1.0 kg/m^3	Coriolis meter used***	± 1.0 kg/m^3
Temperature	± 1° C	Coriolis meter used***	± 1° C
Particle size	± 5%	Endecott sieves used	± 5%
Measurements common to both experimental phases			
Rheology	± 1%	Rheometer accuracy	± 1%

*Nikon-Trimble AP-8 Level specification, http://www.nikon-trimble.com/a_levels/index3.htm
**Malvern Mastersizer 2000 specifications, http://www.malvern.co.uk/LabEng/products/Mastersizer/MS2000/mastersizer2000.htm
***Micro Motion® F-Series Mass Flow and Density Meters specification

Table 5. Summary of instrument errors and human errors for recorded variables.

Table 5 shows that the measurement of flow rate in the field flume presented a significant source of error at ±14.6%. This reflects on the comment made in section 3.5.1 about the scatter in flow data that was presented in Figure 48, where it was noted that the data exhibited significant variation that exceeded the calculated random error. The other measurement error statistics presented here suggest that the remaining variables are not susceptible to such significant measurement errors.

Chapter 4: Validation of beach slope models from the literature

In this chapter, an attempt has been made to test each of the beach slope prediction models presented in the Chapter 2 literature review against the following five data sets:

- Large scale field flume data collected at Cobar and Sunrise Dam (presented in Chapter 3)
- Small scale laboratory flume data collected at RMIT University (presented in Chapter 3)
- Stack data, featuring historic tailings discharge data and aerial survey data from the Cobar and Sunrise Dam tailings stacks (discussed in section 4.1)
- Australian Tailings Consultants (ATC) case history data set (discussed in section 4.2)
- Small scale alluvial fan experimental data (discussed in section 4.3)

The last three of these data sets were independently collected by other workers, and will be described here.

4.1 Stack data from Cobar and Sunrise Dam

4.1.1 Survey data

At both of the gold mines where the experimental programmes took place, the respective operating companies have maintained a practice of periodically carrying out aerial surveys of their tailings storage facilities in an effort to monitor the deposition behaviour of their tailings and subsequently plan and manage any future expansion work that may be required. This survey data has been made available, and is presented in Appendix D. The survey data was used to calculate average beach slopes for each of these two stacks. In Figure 56 a section of the survey plan of the Sunrise Dam tailings stack is presented, with dashed red lines inscribed in the directions of the four compass points from the apex of the stack. Beach surface profiles were then constructed along each of these 4 lines, based on the elevation contours that are crossed by the inscribed dashed red lines. The elevations along these four profiles were then averaged with respect to radial distance to produce the "averaged profile" for the

stack. These profiles are shown in Figure 57. This profiling of the stack survey data was undertaken for both of the tailings stacks for a number of surveys that were logged over time.

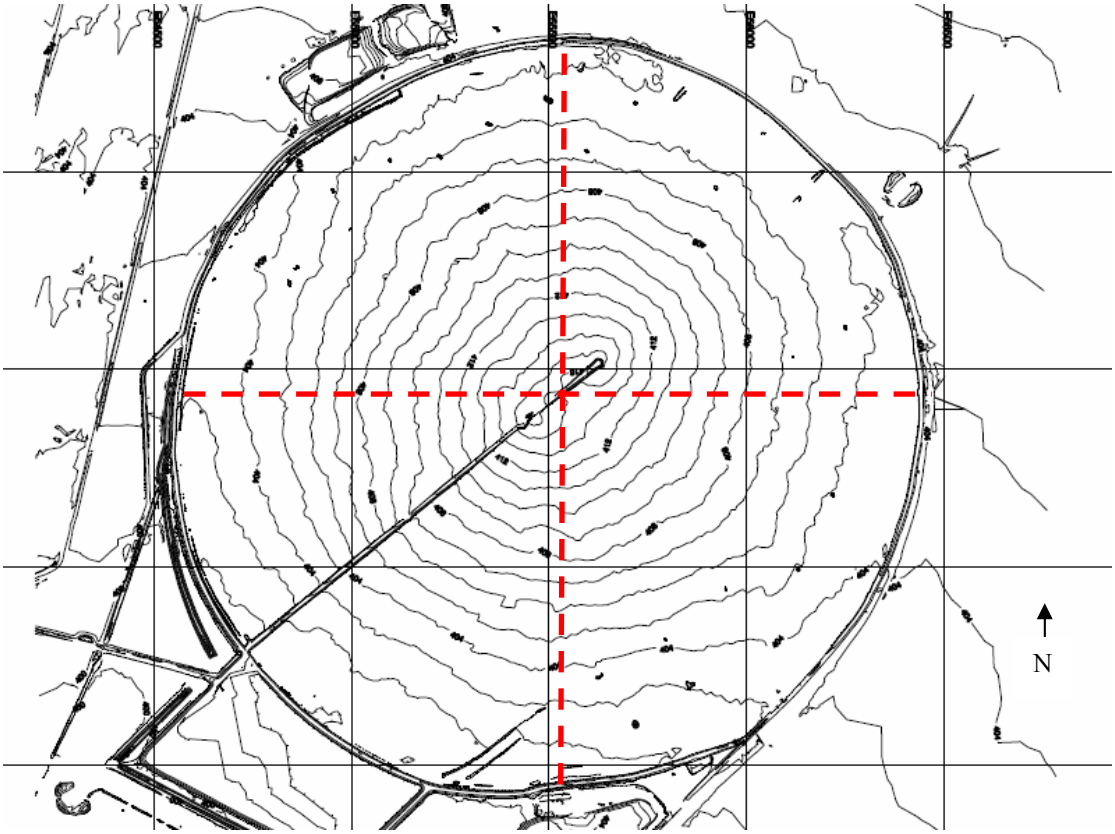

Figure 56. Aerial survey plan of Sunrise Dam tailings stack with inscribed lines along which cross-sectional profiles were constructed

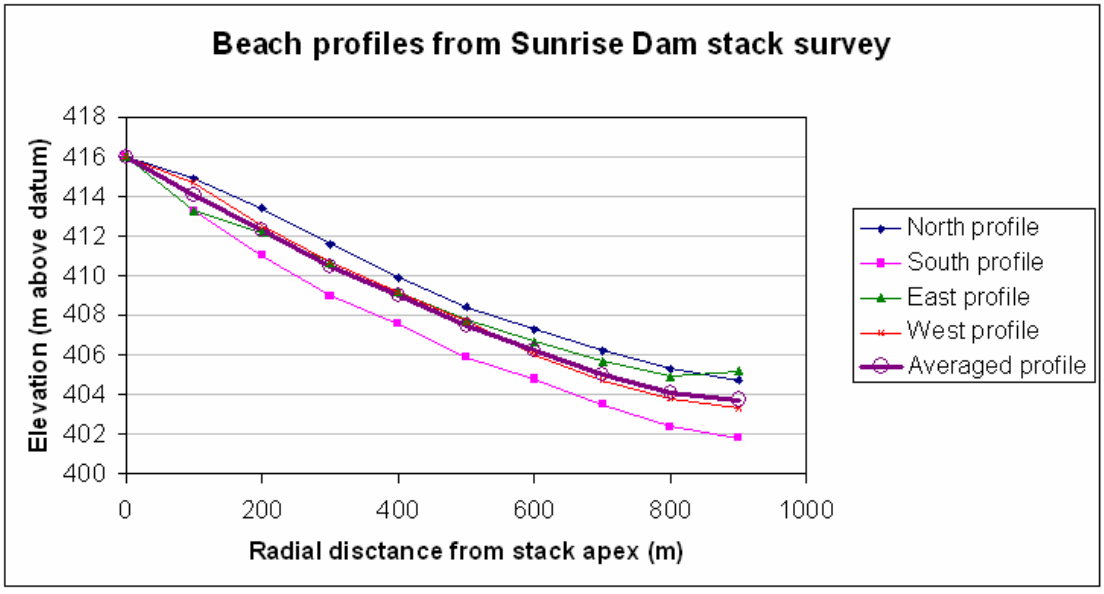

Figure 57. Beach profiles constructed from the Sunrise Dam stack survey plan

The averaged profiles were then used to calculate average beach slopes for the upper third, middle third and lower third of each stack, with each third defined on the basis of the horizontal radial distance from the stack apex.

4.1.2 Tailings discharge data

At both of the gold mines where the experimental programmes took place, the respective operating companies also maintained records of the tailings discharge to their respective tailings storage facilities. In the case of the Peak gold mine in Cobar, this data has been reported as monthly totals, whereas the Sunrise Dam gold mine data has been reported as daily totals. This discharge data can be found in Appendix E.

A summary of the historic tailings discharge and beach slope data provided by the two mining companies is presented in below in Table 6, together forming the stack data set.

Date	No. spigots	Dry production rate (tons per month)	Tailings Beach Slope, % upper third	middle third	lower third	Cw %
Cobar stack slope measurements						
18-Mar-02	1	45,000	2.3	1.6	1.1	53
17-Oct-02	3	46,000	3.6	2.2	1.6	53
14-Mar-03	3	42,000	4.2	2.8	2.2	53
Sunrise Dam stack slope measurements						
01-Dec-01	1	250,000	1.3	1	0.35	60
01-Dec-02	3	300,000	1.95	1.15	0.85	60
31-Dec-03	3	300,750	2.5	1.5	0.8	60
31-Dec-04	5	301,000	2.4	1.5	0.9	60

Table 6. Summary of mine discharge and beach slope data, which together form the stack data set. Note that "No. spigots" indicates the number of discharge points used at a given date.

In order to process the mine data it was necessary to determine the mean slurry flow rate from each spigot. This was achieved with the following equation:

$$Q = \frac{((100\,\mathrm{M}/C_W - \mathrm{M})/\rho_W + \mathrm{M}/\rho_S)}{2635N} \qquad (55)$$

where Q is the mean flow rate from a spigot (in l/s), M is the dry solids mass production rate (t/month), N is the number of spigots, C_W is the concentration by weight (%), ρ_S is the unit weight of the solids and ρ_W is the unit weight of the carrier fluid. It is noted that for both the Cobar and Sunrise Dam slurries the solids density (ρ_S) was 2800 kg/m^3, whilst the carrier fluid densities (ρ_W) were 1000 kg/m^3 for Cobar and 1150 kg/m^3 for Sunrise Dam as a result of differing amounts of dissolved salts.

4.2 Australian Tailings Consultants case history data set

This data set contains tailings beach slope data set that has been compiled over a period of some 20 years by Australian Tailings Consultants (ATC). The data set features 17 full scale tailings beaches from some 8 different mines, with some of these beaches occurring in tailings impoundments and others on stacks.

The majority of the data contained in the Australian Tailings Consultants case history data set has been suppressed from publication here due to its commercial sensitivity. The full data set contains slurry flow rates, concentrations, rheology and particle size data amongst other information that has been made available to the author for this analysis, but permission to publish all this data has been denied. Only the following data has been permitted for publication:

Site	Beach slope S %
Bougainville:	
large scale test	0.8
small scale test 1.	2.7
small scale test 2.	2.1
CSA, Cobar	0.5
	0.74
Elura: No.1 stack	1.65
No.2 stack	1.35
Kelian	0.73
	0.5
Union Reefs	0.9
	0.56
	0.75
Westralian Sands Trial	5.75
Century: Bulk Sample plant 1	1.55
Bulk Sample Plant 2	0.75
Full Scale Production	0.9
Miduk	2.4

Table 7. Limited selection from the Australian Tailings Consultants case history data set.

4.3 Experimental alluvial fan data set

As part of a research project investigating the geological formation of alluvial fan deposits, Whipple et al. (1998) presented a series of experiments in which small scale fan deposits were formed in a laboratory by discharging dilute slurries onto a flat floor at the intersection of two vertical surfaces to produce a deposit resembling the quadrant of a cone by way of solid particles settling on the floor and stacking up over time. These workers noted the existence of channel flow occurring on the surface of the deposit, with the channel periodically changing its course with similar behaviour to that observed on tailings beaches. A weir defined the outer extents of the deposition area, enabling the slurry flow to be left running long enough for the deposit to develop a stable profile through the processes of erosion and deposition taking place simultaneously, with the overflow running over the weir. 51 such runs featuring coal and sand slurries were presented, with volumetric fractions of the slurries varying between 0.0066 and 0.063, discharge rates varying from 0.11 to 0.48 litres per second, median particle sizes ranging from 70 to 550 μm and particle densities ranging from 1350 to 2650 kg/m^3. Average beach slopes observed ranged from 0.8% to 13%. Two deposition areas were used, with one having the weir set at a radius of 2.1 m from the discharge point, and the other set at a radius of 5.2 m.

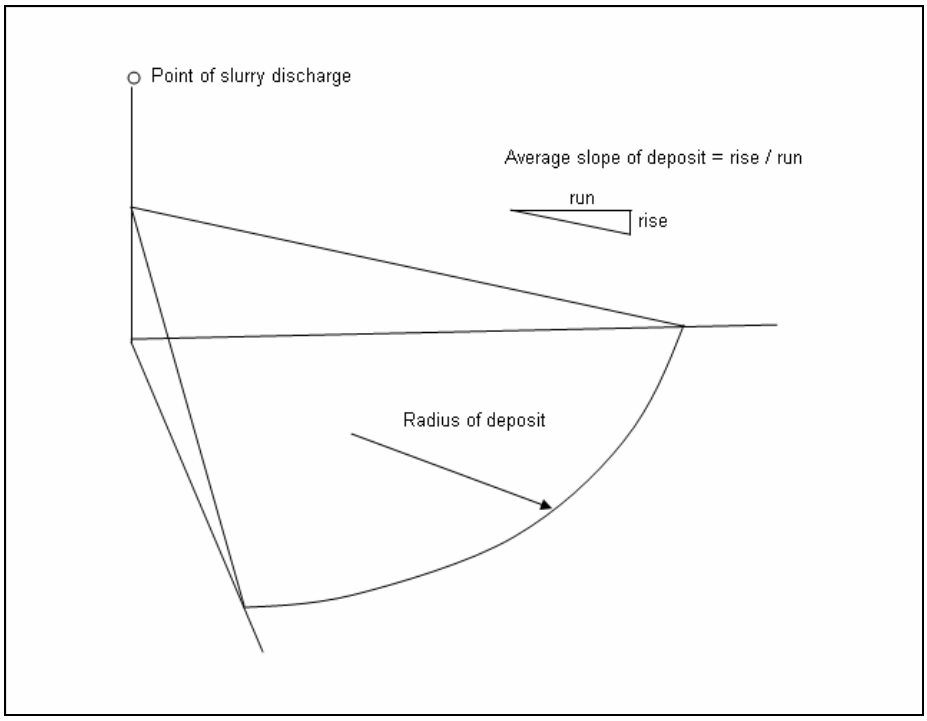

Figure 1. Diagram of the Whipple et al. alluvial fan experiments.

The relationship between tailings beaches and alluvial fans

Of keen relevance in this work is the relationship between tailings beaches and alluvial fans. Whilst there already exists some acknowledgement of this relationship in the literature, the majority of the research presented specifically on tailings deposition makes no reference to the geologically equivalent process of alluvial fan deposition. In a geological investigation of alluvial fans conducted by Whipple et al. (1998), these workers attempted to model the alluvial fans that have formed the Kosi River delta in India, a geological feature that runs approximately 200 km in length and width. In a companion paper (Parker et al. 1998b) these same workers identified the process of tailings beach formation as being a fast-tracked equivalent to that of much larger scale alluvial fan formation that takes place over thousands (or millions) of years. They presented a detailed investigation of the "Rolling Stone" mine tailings basin in Minnesota, United States. The tailings beaches in this basin were also modelled by these workers using the same complex empirical approach. The work presented in the laboratory experiments by Whipple et al. (1998) was the third paper that sprouted from this same investigative project, with the same complex empirical approach once again applied to this work in an attempt to model the small scale laboratory deposits. The work presented in these three papers added a considerable amount of support to the notion that the channel slope dictates the slope of the deposit formed; a theory well subscribed to by numerous other workers in the field of tailings beach slopes such as Williams & Meynink (1986), Kupper (1991), Morris & Williams (1993), McPhail (1994), and Pirouz (2006). This theory had also been proposed by Winterwerp et al. (1990) in their modelling of hydraulic fills in a dredging context. However, despite this work clearly illustrating the connection between tailings beaches and alluvial fans, there was no attempt to apply tailings beach slope models to the prediction of the slope of the alluvial fans.

One issue that deserves some consideration here is the apparent similarity between the alluvial fan experiments and other small scale deposition experiments that have been referred to in Chapter 2 as "fish tank" flume experiments. In section 2.6, these experiments were condemned as being inappropriately associated with tailings beaches, yet here an experimental approach that may seem to be somewhat similar is being hailed as relevant. In response to this point, it is vital that the importance of the open channel flow of slurry is recognised in the formation of a tailings beach. In the "fish tank" flume experiments a channel did not form, both due to very low discharge rates tested, as well as the

use of diffusers and other flow splitting devices to avoid any channelization of the discharge. However, in Whipple et al.'s alluvial fan experiments the channel flow behaviour was well documented and appreciated as the mechanism behind the formation of an alluvial fan.

4.4 Application of slope prediction models

For various reasons, some of the beach slope prediction models presented in the literature could not be applied towards making a prediction. In most other cases it was necessary to make certain assumptions about the input parameters in order to apply the model. A case-by-case discussion of the attempted application of each model follows, with each model appearing in chronological order with respect to its date of publication.

The models by Williams & Morris (1989), McPhail (1994) and Pirouz (2006) could not be applied in the model validation exercise. The Williams & Morris model (equation 24, discussed in section 2.1.6) and the McPhail model (equations 18 to 22, discussed in section 2.1.5) both required an initial slope value to predict an overall slope. Beyond the fact that this initial slope data was not known, it was seen that the requirement for the initial slope as an input parameter defeated the purpose of the exercise. The Pirouz model was not applied because its constituent equations were not clear. This issue has been discussed in some detail in section 2.1.3.

Fit plots

For each model tested in the chapter, the results of the predictions have been displayed graphically in a fit plot, with the measured slopes running along the horizontal axis and the predicted slopes up the vertical axis. The fit plot of this type has been chosen because the input parameters of all the models differ, so the simplest criterion for graphically displaying the predictive ability of each model lies in the comparison of the predicted slope against the measured slope. This criterion makes all of the plots directly comparable with one another, allowing simple comparison of one model against another.

Each fit plot features an "ideal 1 to 1 line", which would be mathematically expressed as $y = x$ on an ordinary set of Cartesian axes. The ideal 1 to 1 line is not the prediction of the model, nor is it a graph

of the model. It is an arbitrary line that indicates a perfect prediction. A perfect model will predict all slopes to be identical to the observed slopes (assuming that the data is accurate), resulting in all points being plotted along the ideal line.

4.4.1 Melent'ev et al. 1973

The Melent'ev et al. (1973) slope prediction model appears in Chapter 2 as equations 1 and 2, which are restated below:

$$\frac{H}{L} = 0.15 C_V^{1/3} \left(\frac{d_{50}}{h^*} \right)^{1/6} \quad (1)$$

where H is the overall height of the beach, L is the overall length of the beach, C_V is the solids concentration of the incoming tailings slurry, d_{50} is the median particle size, and h^* is the stream depth associated with the scour velocity of clear water. An expression was provided for calculating h^* as follows:

$$h^* = \frac{Q_W}{V_H b} \quad (2)$$

where Q_W is the water flow rate, V_H is the stream velocity for no erosion to occur, b is the stream width.

In order to apply these two equations, the following assumptions were made:

- For calculating V_H, Melent'ev did not present any equation or preferred method, so I will use data from Table 6-3 in Abulnaga (2002), titled "Permissible Canal Velocities (after Fortier et al., 1925)". Under the category "Alluvial silts when colloidal" a maximum permissible canal velocity of 1.15 m/s is shown. This value will be adopted to satisfy Melent'ev et al.'s "non-erosive stream velocity" on the basis that it represents a reasonable experimentally measured estimate of the maximum velocity that can be handled by a silt lined canal without erosion occurring.
- It is assumed that Q_W is the slurry flow rate in this exercise.

- For the flume data, the channel width can be calculated using the depth and the known cross-sectional shape of the plastic half-pipe. For the other data, since the channel shape is not known, it is assumed that the stream width, $b = 29.137Q + 116.07$. This empirical equation is based on a linear fit to the self formed channel data presented in Figure 5 of Pirouz's 2006 thesis, in which the flow rates and corresponding channel widths were measured for three self formed channels of tailings slurry. The empirical fit is presented below in Figure 58.

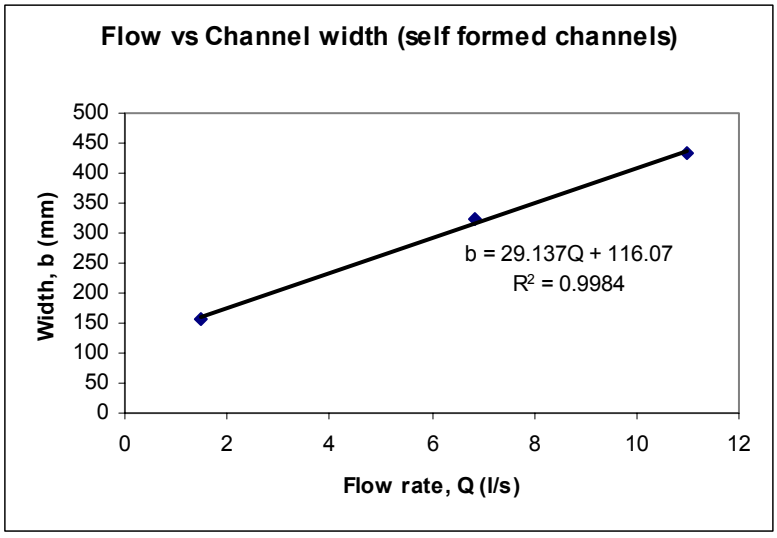

Figure 58. Fitting of linear equation to 3 points of data relating the channel width to the flow rate

The fit plot for the Melent'ev et al. beach slope model is presented below in Figure 59. This graph presents each predicted slope against its measured equivalent, with the measured slopes plotted along the horizontal axis and the predicted slopes plotted along the vertical axis. For a model that predicts perfectly, we would expect to see all of the data points fall on the ideal 1 to 1 line.

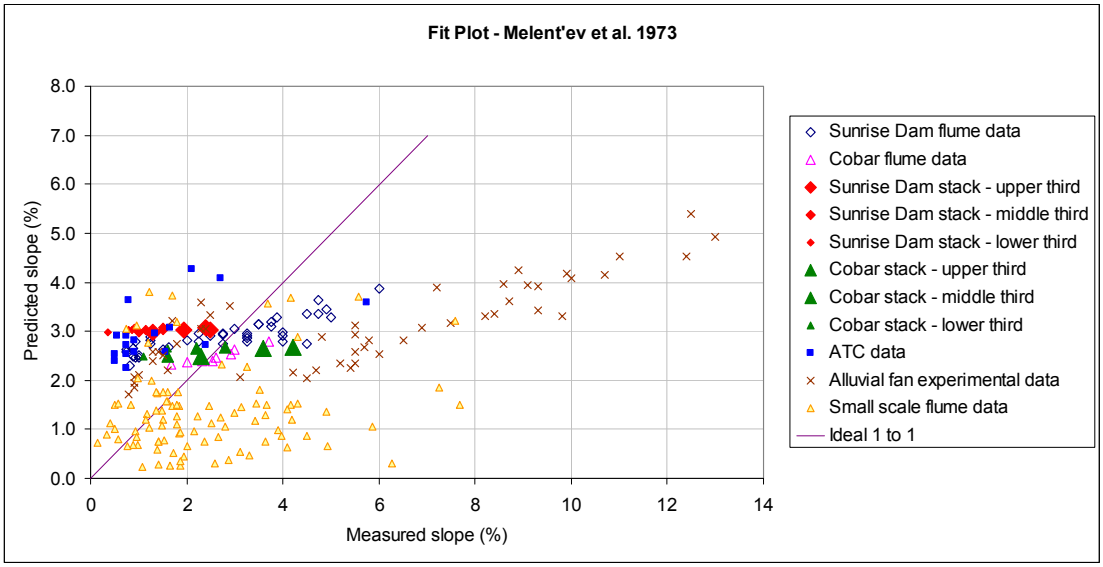

Figure 59. Fit plot of the Melent'ev et al. 1973 beach slope model

Figure 59 shows that the Melent'ev et al. beach slope model has not predicted particularly well with any of the 5 data sets, since none of the data sets show a strong alignment with the ideal fit line. However, it can be said that this model is predicting slopes of the same order of magnitude as the observed slopes in almost all cases.

4.4.2 Robinsky 1978

The graph presented below in Figure 60 has been reproduced from Robinsky (1978). A curve has been superimposed over the graph as a fit to Robinsky's data points.

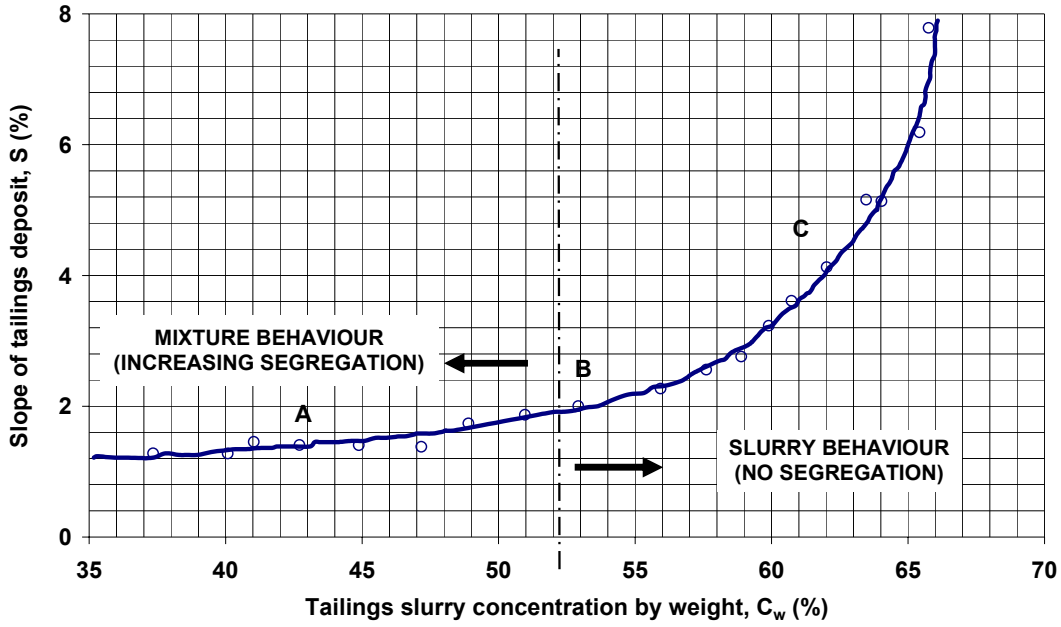

Figure 60. Robinsky's S vs Cw plot, with superimposed fit curve (Robinsky 1978)

The equation for this fit is as follows:

$$i = 3e^{0.17(C_W - 62)} + 1.3 \qquad (56)$$

where i is the beach slope as a percentage and C_W is the solids concentration by weight as a percentage. It is acknowledged that Robinsky never claimed that the slurry concentration was the sole factor influencing tailings beach slopes, so this equation is not reported here as a beach slope prediction model endorsed by Robinsky; it is simply a mathematical fit to the graph presented by Robinsky.

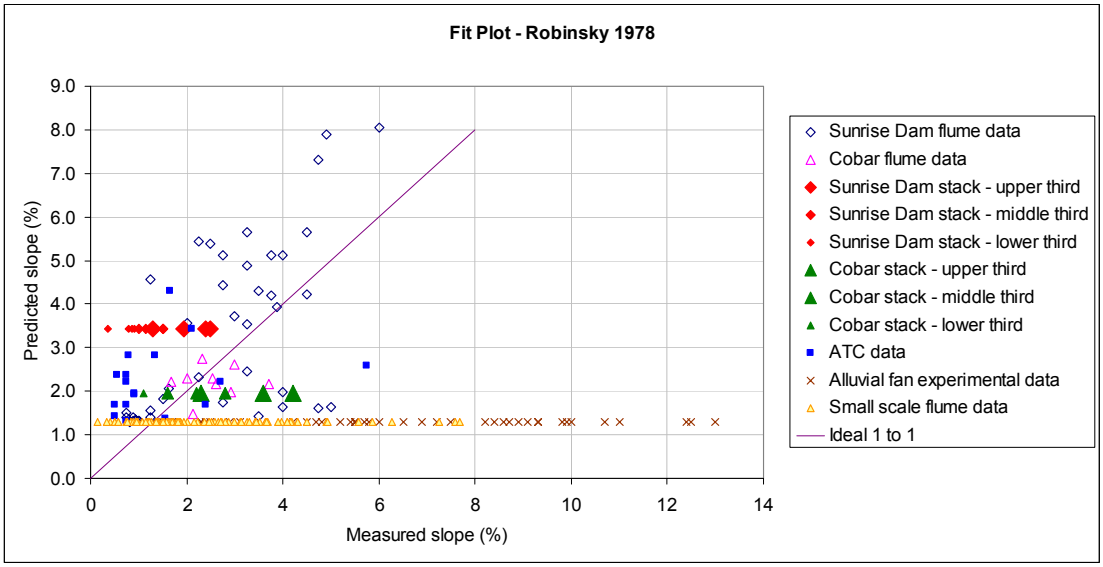

Figure 61. Fit plot of the Robinsky 1978 experimental beach slope vs concentration chart.

Figure 61 shows that equation 56 is constantly predicting a slope of 1.3% for the alluvial fan data and the small scale pipe loop data, both of which feature slurries with concentrations below 40% w/w. These low predictions are consistent with the graph presented in Robinsky (1978), reproduced above as Figure 60. It is noted though, that the lowest plotted point on Robinsky's graph was for a slurry with a concentration of 37% w/w, so any values below this are clearly outside of the range of data reported on by Robinsky. Despite this point though, most of the alluvial fan data and a significant number of points in the alluvial fan data sets were actually observed to run at slopes greater than 1.3%, even though they had solids concentrations well below 40%. The cause of the steeper slopes observed with these data points was the very low flow rates of the slurries, but because equation 56 is completely insensitive to the flow rate, the predictions are poor. It must be restated that equation 56 was not presented by Robinsky as a beach slope model. It is simply a fitted equation to a plot that Robinsky presented. Likewise, it must also be iterated that Robinsky suggested that flow rate affected the beach slope, but he did state that the slurry concentration was the main factor dictating the beach slope.

For the other three data sets (those being the field flume data, the stack data and the ATC data set) it can be seen that equation 56 is predicting slopes of the same order of magnitude as the observed slopes, but none of these data sets show any significant alignment with the ideal fit line. Therefore it must be concluded that equation 56 is not sufficient for predicting beach slopes, with the main cause thought to be its lack of consideration of the flow rate.

4.4.3 Blight & Bentel 1983

Blight & Bentel's 1983 equation was amended by Blight et al. (1985), and appears in Chapter 2 as equation 17:

$$2\theta = \arcsin\left(\frac{\tau_0}{\rho g \delta}\right) \qquad (17)$$

where θ is the angle of repose of the slurry (expressed in radians), τ_0 is the yield stress of the tailings, ρ is the tailings density, g is the acceleration of gravity, and δ is the layer thickness. This equation was developed for the prediction of the slope adopted by a widespread sheet of tailings slurry when it stops flowing, though it was validated with experimental data featuring slopes at which a thin sheet of tailings slurry of known depth will start flowing.

The following assumptions were made in the application of the Blight & Bentel model:

- δ, the layer thickness, assumed to be 0.05 m. This is a reasonable sheet flow layer thickness as observed on tailings beaches.
- τ_0 assumed to be the Bingham yield stress.

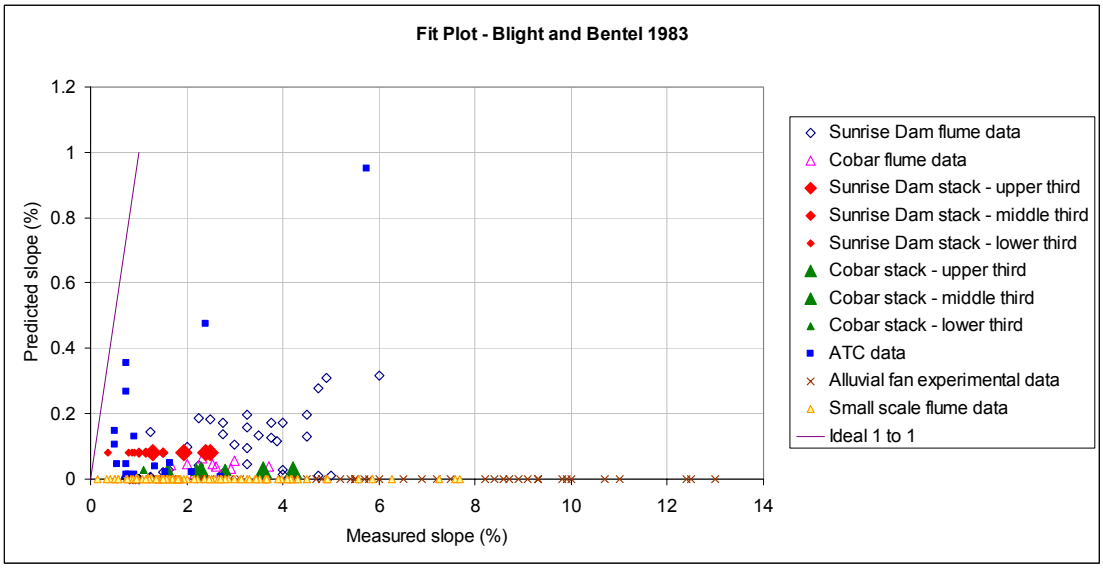

Figure 62. Fit plot of the Blight & Bentel 1983 model (amended 1985).

Figure 62 shows that the Blight & Bentel model predicts very poorly in relation to all 5 sets of data. The predictions for the alluvial fan data and the small scale flume data are particularly poor, but this can be attributed to the zero values of yield stress found in these two sets of data. All of the alluvial fan data points were assumed to have no yield stress value, since it is expected that sand-water mixtures, all of which had volumetric concentrations of 6% or less, will have none. Most of the fluids used in the small scale flume experiments exhibited zero yield stress values when they were tested in a rheometer. Some of the rheometry data from these fluids can be seen in Figure 47 in section 3.4.7.

Further consideration of the poor predictive performance of this model leads to the obvious conclusion that the two sets of experimental flume data used to validate the model was channel flow data, which most definitely did not resemble the sheet flow behaviour considered by Blight & Bentel.

This exercise proves that sheet flow behaviour is not what dictates the slope on a tailings beach. On this basis, it could be said that the Blight & Bentel model should not have been included in this exercise, but its inclusion was deliberate because the Blight & Bentel model was presented as a beach slope model for thickened tailings schemes, specifically in the context presented by Robinsky (1975). It is conclusively shown here that the Blight & Bentel model does not predict beach slopes for such schemes, especially since the majority of the data points contained in the ATC data set pertain to this type of tailings storage method.

4.4.4 Williams & Meynink 1986

The Williams & Meynink equation appears in section 2.1.4 as Equation 15. It is repeated here:

$$S = \frac{8.81 C \overline{W}_c}{K} \tag{15}$$

where S is the slope of the channel (%), C is the solids concentration (% w/w), $\overline{W}_c$ is the mean fall velocity of the mixture (m/s) at the concentration C, and K is the "transport constant", an empirical constant that is fitted to a particular tailings slurry (m/s).

The following assumptions were made in order to apply this equation:

- K, the transport constant, is equal to 0.63 m/s. This is consistent with Williams and Meynink's application of the equation.
- $\overline{W_c}$, the mean fall velocity of the mixture, is equal to the hindered settling velocity of a single particle of size d_{50} in the slurry. From Wasp et al. (1977) equation 3.9,

$$V_S = \left[\frac{4g(\rho_s - \rho_l)d}{3C_D\rho_l} \right]^{1/2} \quad (57)$$

where: V_S = unhindered settling velocity

g = acceleration to gravity

ρ_s = density of solid particle

ρ_l = density of carrier fluid

d = diameter of particle

C_D = drag coefficient of particle

$$\frac{V_S}{w_{ot}} = e^{4.5} \quad (58)$$

where: w_{ot} = hindered settling velocity

e = volume fraction of voids

- For the slurries used in both phases of flume experiments, the unhindered particle settling velocity was measured experimentally (see sections 3.3.15 and 3.4.6). Equation 57 was used to calculate drag coefficients for these particles using these settling velocity measurements.
- For the data from the other 3 data sets, it was assumed that C_D = 0.45, as recommended by Ishii & Zuber (1979)

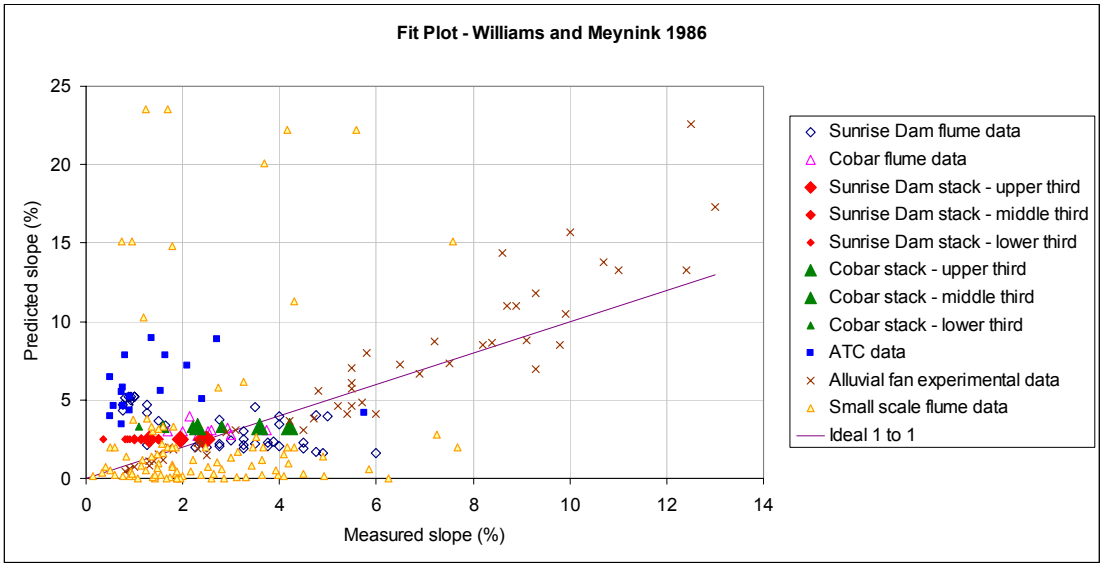

Figure 63. Fit plot of the Williams and Meynink 1986 model

From Figure 63 it is of interest to note the relatively good predictions of the slopes observed in the alluvial fan data set. The predictions of the beach slopes on the upper thirds of both the Sunrise Dam and Cobar stacks are also relatively good. The other data sets were not predicted so well, though the magnitudes of the predictions of the field flume data are reasonable. The small scale flume data shows a significant amount of scatter here, while the ATC data set is generally predicted at slopes 3 or more times steeper than those observed.

4.4.5 Wates et al. 1987

Wates et al. (1987) presented a graph that showed a strong trend between the specific gravity of a slurry and the beach slope that is formed by its discharge. The graph contained data that was gathered from measurements of full-sized tailings beaches. An attempt has been made here to fit an empirical equation to the plot presented by Wates et al.:

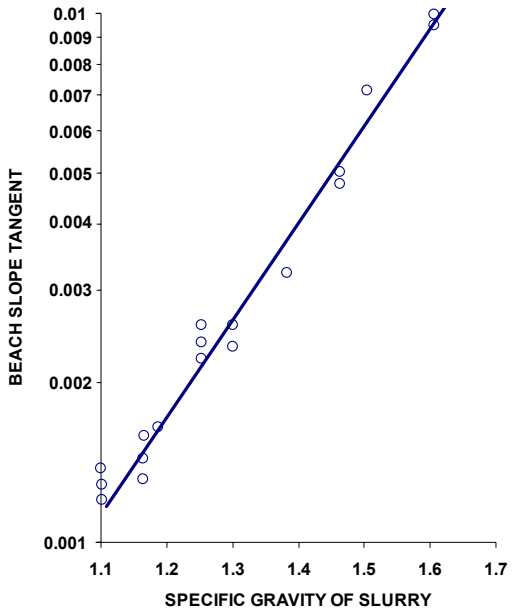

Figure 64. Wates et al.'s graph with superimposed line of best fit (Wates et al. 1987)

The equation for this line of best fit is as follows:

$$i = 9.3 \times 10^{-6} e^{4.35S} \tag{59}$$

where i is the beach slope and S is the specific gravity of the slurry.

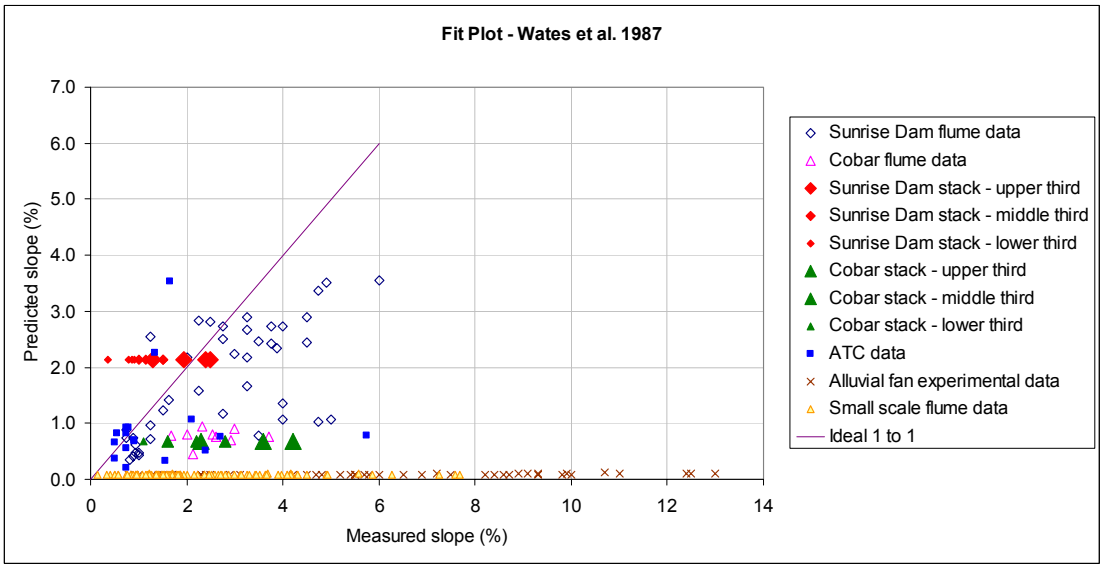

Figure 65. Fit plot of the Wates et al. 1987 beach slope vs density graph

Figure 65 shows that equation 59 is predicting poorly against all five data sets, particularly in the cases of the small flume data and the alluvial fan data. The main problem with equation 59 is its lack of consideration of the flow rate, which was observed to be the most important factor affecting tailings beach slopes during the experimental work featured in Chapter 3. This omission can be cited as the dominant reason for the poor predictive performance of equation 59, particularly in the cases of the small flume data and the alluvial fan data, where the slurry flow rates are well below the flow rates that would have been observed by Wates et al. in their gathering of the field data that they have presented in their graph (Figure 64).

Another reason for the poor slope predictions against the small flume data and the alluvial fan data presented in Figure 65 is that Wates et al.'s field observations were of segregating slurries that were discharged at high flow rates. This gave them flat beach slopes below 1% slope. For the slurries observed by Wates et al. with specific gravity values between 1.1 and 1.2, beach slopes below 0.2% slope were measured. By comparison, the data contained in the small flume and alluvial fan data sets had specific gravity values between 1.0 and 1.1, which is just below the range of specific gravity values observed by Wates et al. as presented in their graph (Figure 64). Clearly it would be expected that these data points would produce beach slopes well below 0.2% if these slurries were to behave consistently with Wates et al's data. However, the very low flow rates used in the small flume and alluvial fan experiments overrode the effect of concentration that Wates et al focused on in their field measurements. To their own demise, Wates et al. did not consider the effect of flow rate in their work, instead citing flow rate among "other factors which cannot be considered in detail in this paper", despite their acknowledgement of the claim of Robinsky (1975), "that reducing the flow rate can increase the slope of a beach".

4.4.6 Boldt 1988

The Boldt equation is presented in section 2.1.1 as Equation 3:

$$i = 1.98 - 0.0043 Q_{USG} \qquad (3)$$

where i is the beach slope (%) and Q_{USG} is the flow rate expressed in US gallons per minute.

No assumptions were necessary in applying this equation.

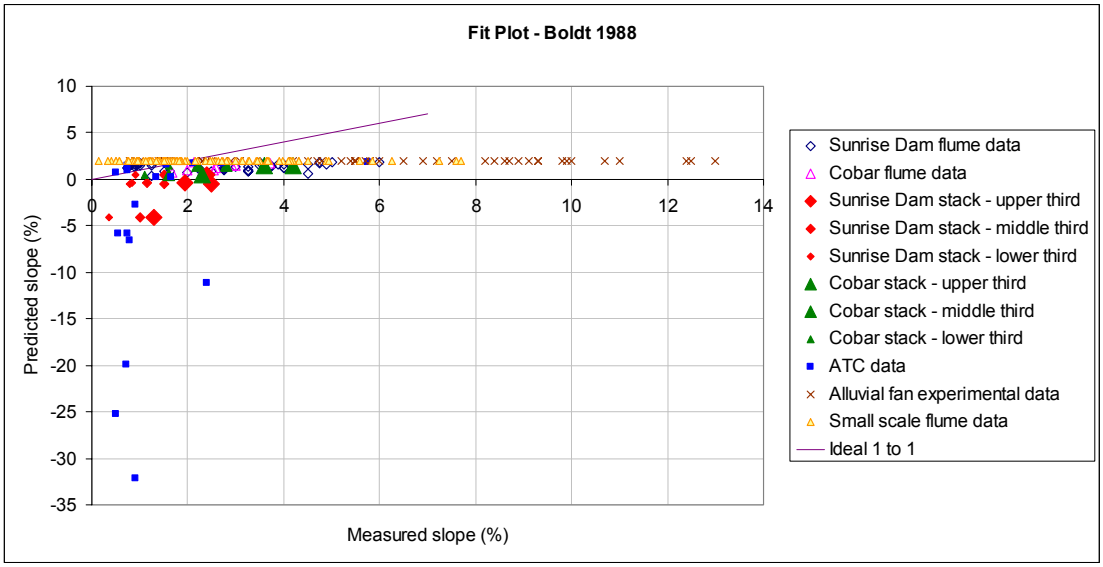

Figure 66. Fit plot of the Boldt 1988 beach slope vs flow rate graph

Figure 66 shows that the Boldt equation predicts very poorly against all five data sets. Of particular note are the negative predictions for the Sunrise Dam stack data and the ATC beach slope data. These negative predictions occurred because some of the flow rates presented in these two data sets were considerably larger than the maximum flow rate tested in the field trial experiments of Boldt. Though Boldt did not list the range of flow rates tested in the field trials, it can be seen that Boldt's equation (equation 3) will predict negative slopes for any flow rate below 460 US gallons per minute (29 litres per second), so it is reasonable to assume that Boldt's field trial experiments did not test any flow rates greater than this value.

Another problem that is evident in Figure 66 is the constant slope predictions of about 2% for the small scale flume data and the alluvial fan data. This issue arises because the flow rates reported in these two data sets are lower than the smallest flow rate tested by Boldt. It can be seen that the beach slopes predicted by equation 3 will approach 1.98% as the flow rate approaches zero.

Boldt's equation is clearly too limited in its range of beach slopes, since it can not possibly predict any slopes steeper than 1.98%. However, a more significant limitation of Boldt's equation is its complete insensitivity to any other factors such as concentration, rheology or particle size, all of which were observed to have an effect on the beach slope during the experimental work presented in Chapter 3.

4.4.7 Winterwerp et al. 1990 – Semi-empirical equation

This equation is presented as Equation 26 in section 2.2, and is repeated below:

$$i_{eq} = \left[\frac{(s-1)^2 d_{50}}{0.20} C_V (1-C_V)^2 \right]^{0.6} \left[\frac{f_D g^2}{8} \right]^{0.1} q^{-0.4} \qquad (26)$$

where i_{eq} is the equilibrium slope of a channel of slurry, s is the ratio of the density of the solids to the density of the carrier fluid, d_{50} is the median grain diameter, C_V is the volumetric concentration, f_D is the Darcy friction factor and q is the specific flow rate, equal to the channel flow rate divided by the channel width.

The biggest challenge in applying this model is the determination of a value for f_D, the Darcy friction factor. Winterwerp et al. did not present any analytical method for calculating an f_D value, but instead assumed a value of 0.035 as an empirical fit to their experimental data. In Chapter 5 a method is developed for the prediction of an f_D value for a loose boundary channel flow scenario, but strictly speaking, that work is not part of the model that Winterwerp et al. presented, so it will not be used here. Instead, the same approach will be taken as that which Winterwerp et al. adopted, with an f_D value of 0.035 assumed in order to apply this equation.

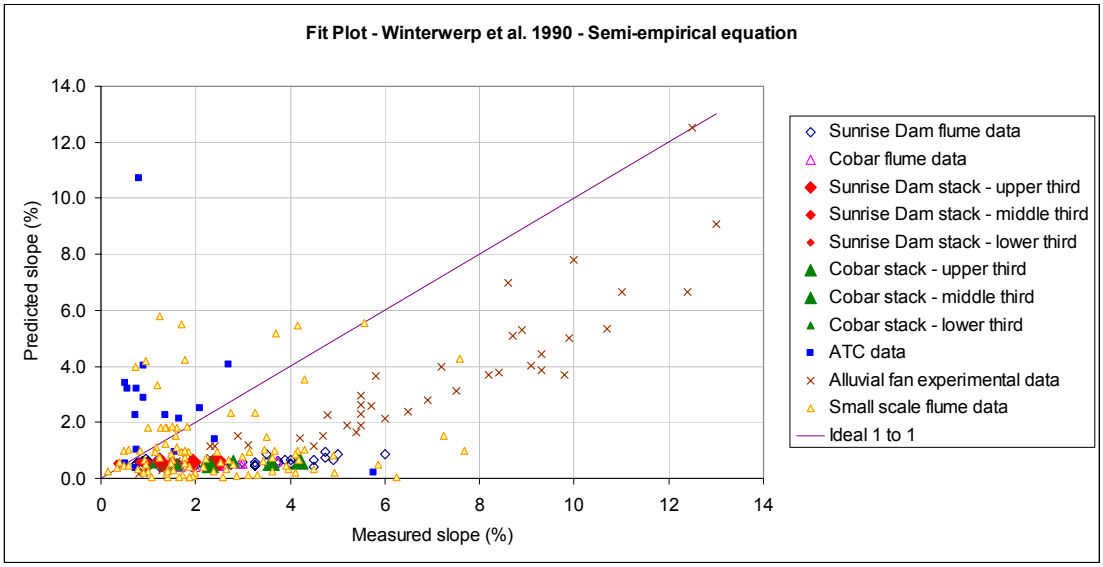

Figure 67. Fit plot of the Winterwerp et al. 1990 semi-empirical equation

Figure 67 indicates that the Winterwerp et al. semi-empirical equation is predicting poorly for all of the data sets. One of the obvious possible causes for this is the assumed f_D value of 0.035. In order to investigate this possibility, an exercise was undertaken to calculate the f_D values for each of the 50 equilibrium slopes that were recorded in the field flume experimental work. It was found that the mean f_D value for the 50 field flume experimental runs was 0.050, with a 95% confidence limit of 0.0054 either side of the mean. The effect of this different f_D value can be quantified by calculating an equilibrium slope with equation 26 using an f_D value of 0.035, and then repeating the exercise with an f_D value of 0.05. The difference is that the latter figure will cause the predicted slope to be 1.036 times steeper than that of the former. It can be seen that the predictions for the field flume data set on Figure 67 are all around 0.5% slope, which is well short of the observed slopes for these points. The adoption of an f_D value of 0.05 instead of 0.035 will raise a prediction of 0.50% slope to a value of 0.52%. This conclusively proves that the assumed f_D value of 0.035 is not the cause of the poor predictions by the Winterwerp et al. semi-empirical model, since it is evident that this model is quite insensitive to this parameter with a power of 0.1 directly applied to it.

Upon closer inspection of Winterwerp et al.'s experimental data it can be seen that the range of concentrations tested reached from 0 to 40% v/v, which is comparable to that tested in the field flume experiments documented in Chapter 3. The range of specific flow rates (the flow rate divided by the

stream width) ranged from 0.05 to 0.15 m^2/s, which is also comparable to that measured in the field flume experiments, which ranged from 0.01 to 0.08 m^2/s.

Since Winterwerp et al.'s experimental data range is so similar to that gathered in the field flume experiments, it is possible to make some comments about equation 26 in terms of the powers that have been applied. Firstly, the power of -0.4 that has been applied to the specific flow rate, which is derived from the Engelund-Hansen equation cited by Winterwerp et al., is seen to provide a reasonable fit to the data gathered in the field flume experiments, which was best fitted by a power of -0.5. However, the power of 0.6 applied to the first term of equation 26 is where these two data sets differ, since it was found that the concentration values of the field flume data were best related to the channel equilibrium slope with a power of 2. It is therefore concluded that it is this power that has caused the poor predictions of equation 26 in relation to the field flume data.

4.4.8 Winterwerp et al. 1990 – Empirical equation

This equation is presented as Equation 27 in section 2.2. It is restated below:

$$i_{eq} = \left[0.0056 \frac{d}{d_{ref}} - 0.0045 \right] q^{-0.45} \qquad (27)$$

where d is the representative grain diameter, d_{ref} has a constant value of 65 μm, and q is the specific flow rate, equal to the channel flow rate divided by the channel width.

In applying this model, d_{50}, the median grain diameter, was assumed in place of d, the representative grain diameter. This is consistent with Winterwerp et al.'s application of the equations in their work. The fit plot generated by this equation is presented below as Figure 68:

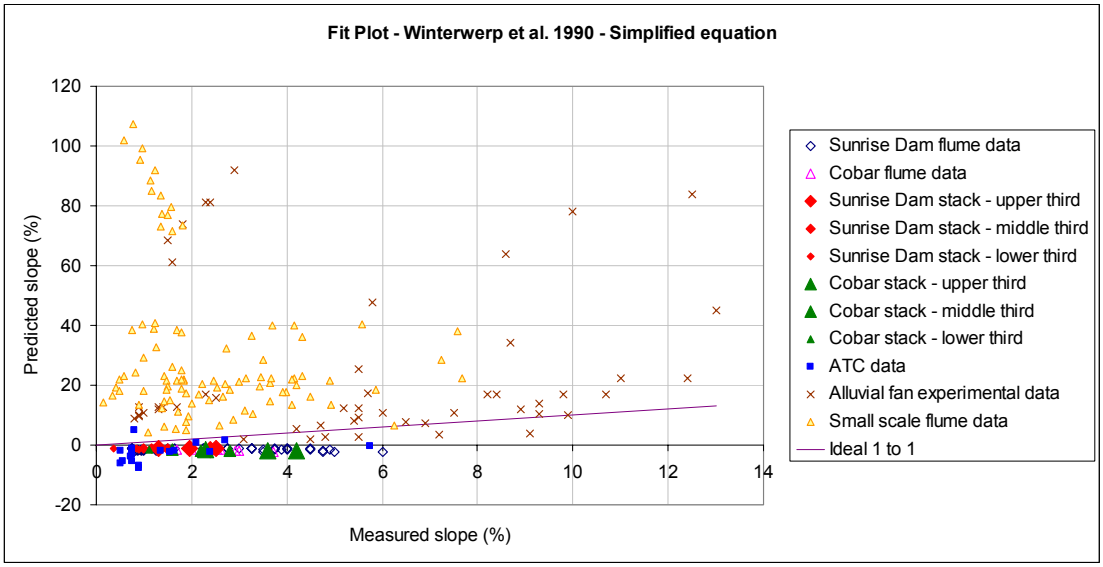

Figure 68. Fit plot of the Winterwerp et al. 1990 simplified empirical equation

It is noted that the Winterwerp et al. 1990 empirical equation (equation 27) predicts negative beach slopes because of the combination of its empirically calibrated d_{ref} constant of 65 μm that forms the denominator under the median particle diameter of the slurry in question (which happens to be greater than the median grain diameter for both of the slurries tested here), and the value of 0.0045 then being subtracted from the product. This crude empiricism effectively causes negative predictions for any slurry with a median grain diameter less than 52 μm, which is a severe limitation of this model. Winterwerp et al.'s experimental data contained d_{50} values ranging between 120 – 235 μm, which explains how they have developed this aspect of their model.

It is interesting to note that Winterwerp et al. gained a power of -0.45 as an empirical fit to the specific flow rate values in their data. This compares favourably with the point raised in section 4.4.7, where it was noted that the field flume data was fitted best with a power of -0.5. This supports the trend that was observed between flow rate and slope in the field flume.

4.4.9 Kupper 1991

This empirical equation presented by Kupper appears as Equation 5 in section 2.1.2. It is repeated below:

$$i_{av} = 5\sqrt{\frac{A\sqrt{g\left(\frac{\rho_s}{\rho_l}-1\right)}\sqrt{d_{50}}C_w}{Q}} \quad (5)$$

where: i_{av} is the overall slope of a tailings beach, defined as the height over the length

A is the cross-sectional area of the discharge pipe (m^2)

C_w is the slurry solids concentration by weight (%)

d_{50} is the median grain diameter (m)

g is the acceleration due to gravity (m/s)

Q is the flow rate at the discharge point (m^3/s)

ρ_s is the density of the solid particles (kg/m^3)

ρ_l is the density of the carrier fluid (kg/m^3)

Kupper's approach was focused on the exit velocity of the slurry from a spigot, with the pipe diameter being a required input in the equation. For the field flume data, the small flume data and the stack data for the Sunrise Dam and Cobar stacks, the following pipe sizes were known:

- Pipe internal diameter for the field flume = 150 mm
- Pipe internal diameter for the small laboratory flume = 12 mm
- Spigot internal diameters for the Cobar stack = 200 mm
- Spigot internal diameters for the Sunrise dam stack = 300 mm

For the other 2 data sets the respective pipe diameters were not known, so the cross-sectional area of the pipe was calculated using an empirical equation that was generated by fitting a curve to a plot of flow rate vs cross-sectional area of flow in a channel, derived from the field flume data set. This approach was warranted on the basis that the A term in the Kupper equation (equation 5) is divided by the flow rate, Q, which could otherwise be stated as the mean velocity of flow. This empirically generated equation would therefore enable a calculated estimate of the velocity that flows in the channel, which is seen as a far more relevant quantity than the velocity of the slurry as it exits a pipe, which could have a wide range of values depending on the spigot diameter. It is argued that the pipe exit velocity is irrelevant compared to the channel velocity anyway, since whatever velocity the slurry

maintains in the pipe will be drastically changed once the slurry enters some sort of plunge pool or other point of velocity dissipation upon exiting the pipe.

The plot of flow rate vs cross-sectional area of flow for the field flume data is presented below as Figure 69, with a power equation fit to the data for predicting the cross sectional area as a function of the flow rate. The equation of this curve is:

$$A = 0.0017Q^{0.7154} \tag{60}$$

where: A is the cross-sectional area of the flow (m^2)

Q is the flow rate (m^3/s)

The coefficient of determination (R^2) for the fit of this curve to the data is 0.87.

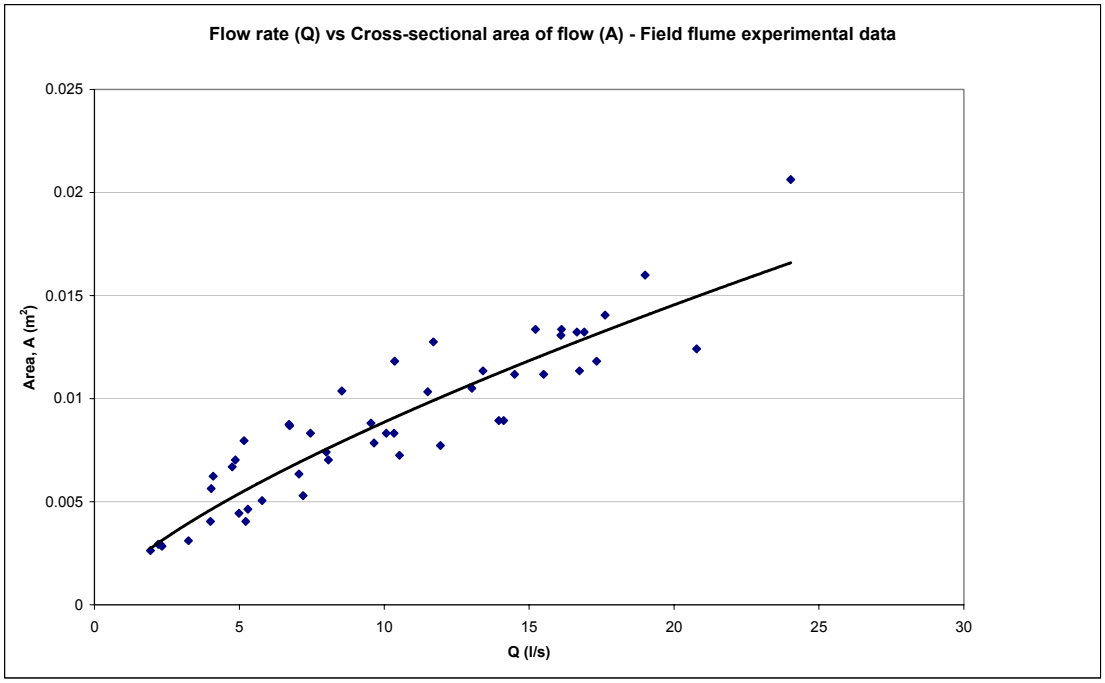

Figure 69. Plot of flow rate against cross-sectional area of flow for the field flume experimental data, with a line of best fit inscribed for estimating A as a function of Q.

The fit plot generated by the application of the Kupper model (equation 5) to predict the slopes observed in the 5 data sets is presented below as Figure 70.

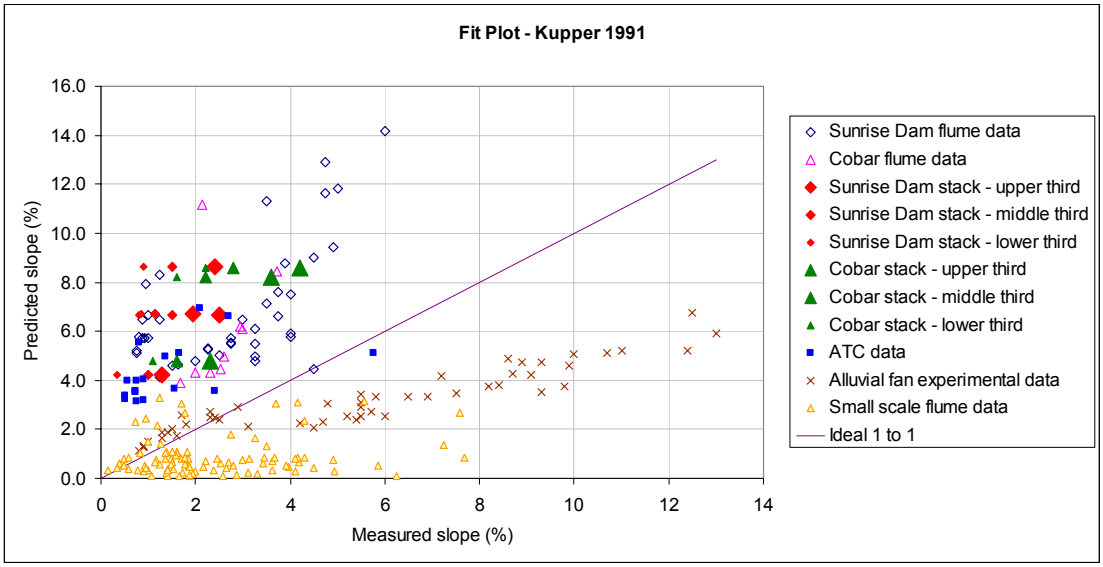

Figure 70. Fit plot of the Kupper 1991 empirical model

Figure 70 shows that the Kupper model predicts poorly for each of the five data sets. For the low concentration slurries tested in the small scale flume and those tested in the alluvial fan experiments, the Kupper model generally predicts flatter slopes than those observed for the same data. The other data sets are generally over-predicted.

Kupper's experimental work tested slurries with concentrations ranging from 1.5 to 40.5% w/w. While this range does share some overlap with all of the five data sets presented in Figure 70, most of the tailings slurry data from the ATC data set, the stack data set and the field flume data set had concentration values greater than the maximum value tested by Kupper, so it is concluded that the steep slope predictions by Kupper's model against these data sets arose from this limitation. As for the small scale flume data and the alluvial fan data, most of the concentration values from these data sets fell inside also range tested by Kupper. The range of flow rates tested by Kupper ranged from 5 to 20 litres per minute, which is very similar to the range tested in the small scale flume experiments. However, Kupper's method of measuring an equilibrium slope was unlike those used in the flume experiments documented in Chapter 3, but was instead of the "fish-tank" style of experiment, in which a deposit of sediment was formed in a tank-like flume through the discharge of slurry at one end of the tank. It must be concluded that Kupper's equation, being a fit to the results observed in a series of "fish-tank" type experiments, provides strong evidence to support the argument stated in section 2.5, that such flumes do not produce slope data that is relevant to tailings beach slopes.

4.4.10 Parker et al. 1998

The model presented by Parker et al. is shown in section 2.3 as Equation 28, with Table 1 accompanying it to show the respective empirical parameters used by Parker et al. in developing this equation. This model predicts S, the slope of a concaved alluvial fan for any radial distance from the head, and is presented below:

$$S = \left[R^{-1/2} \alpha_S^{-1} \alpha_b^{(3+2p)/2} \alpha_r \left(\frac{\alpha_b}{R} - \tau_c^* \right)^{-n} \left(\frac{Q_{S0}(1-\hat{r})^2}{Q_W} \right) \right]^{1/(1-p)} \quad (28)$$

where R is the submerged specific gravity of the sediment, α_S is the sediment transport coefficient, α_b is the flow channelization coefficient, p is the hydraulic resistance exponent, α_r is the hydraulic resistance coefficient, τ_c is the sediment transport critical shields stress, n is the sediment transport exponent, Q_{S0} is the flow rate of sediment, $\hat{r}$ is the dimensionless radial distance from the apex of the fan (equal to the radial distance divided by the length of the fan) and Q_W is the flow rate of water.

An $\hat{r}$ value of 0.165 has been used so as to predict the beach slope one sixth of the way along the beach from the discharge point, to predict an indicative beach slope for the upper third of the beach. The values used for α_S, α_b, p, α_r, τ_c and n are listed in Table 1, which is presented in section 2.3.

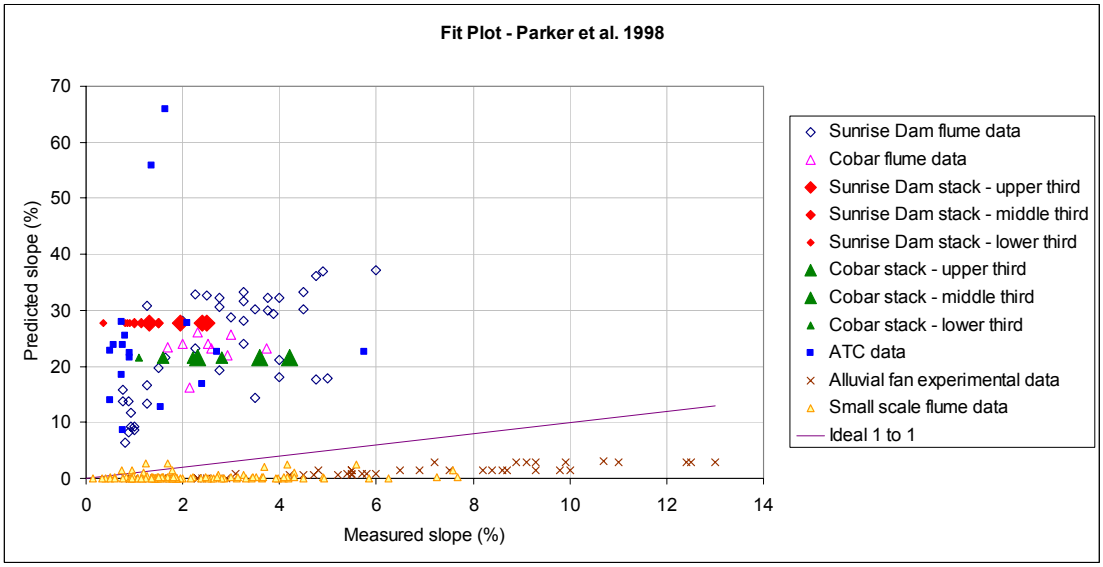

Figure 71. Fit plot of the Parker et al. 1998 model

The fit plot for the Parker et al. model is presented above as Figure 71. The predictions for all five data sets are very poor. The tailings slurry that Parker had calibrated the model parameters to was being discharged from a mine in the United States, and featured a very low concentration (3.3 % v/v) and a very high flow rate of about 7.7 m^3/s. These figures place Parker et al.'s data well outside the range of any of the other data sets featured here, so the poor fit of these 5 set of data to the Parker model is hardly surprising.

4.4.11 Parker et al. 1998 with Whipple et al. 1998 parameters

The same model presented by Parker et al. (shown immediately above in section 4.4.10 as equation 28) was also used by Whipple et al. in their analysis of small scale fluvial fan experiments. The experimental alluvial fan data generated by these workers to validate their model is the same data that has been utilised in this chapter for model validation. These workers used different values for the equation parameters α_S, α_b, p, α_r, τ_c and n, which are presented in section 2.3 in Table 1. As was done in the previous application of the Parker et al. model in section 4.4.10, an $\hat{r}$ value of 0.165 has been used once again in order to predict a slope that is representative of the upper third of the beach. The fit plot for this model is presented below in Figure 72.

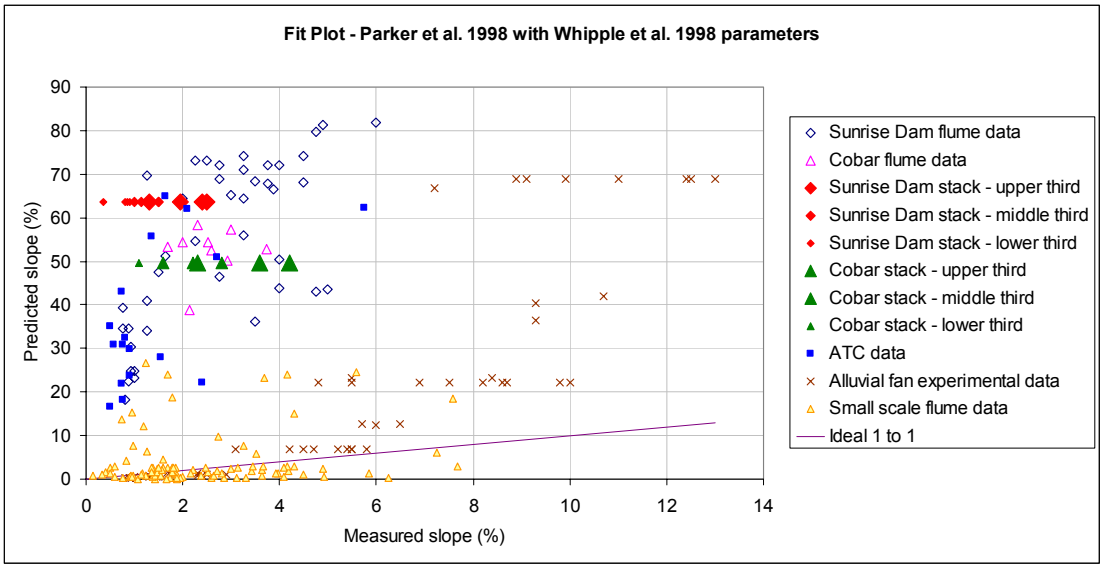

Figure 72. Fit plot of the Parker et al. 1998 model using the Whipple et al. 1998 parameters.

Figure 72 shows that the Parker et al. model with the Whipple et al. parameters predicts very poorly, with slopes of 50% and more being predicted in four of the data sets. This is an alarming result, particularly for the alluvial fan experimental data, which the parameters were developed to suit. One comment that must be made is that the numerous parameters required by the model are complex to derive in some cases, which precludes this model from being easily applied. The work presented here also demonstrates the sensitivity of the Parker et al. model when it is applied to different data sets that the parameters have not been adjusted to suit. On this basis it must be concluded that this model is overly sensitive to the parameters that it uses.

4.4.12 Parker et al. 1998 with Sun et al. 2002 parameters

The same model presented by Parker et al. (shown above in section 4.4.10 as equation 28) was also applied by Sun et al. (2002) to a large scale river delta. These workers derived another set of values for the equation parameters α_S, α_b, p, α_r, τ_c and n, which are presented in section 2.3 in Table 1. Once again an $\hat{r}$ value of 0.165 was used so that the predictions would be indicative of the slope in the upper third of the profile. The fit plot generated with this model is presented below in Figures 73and 74:

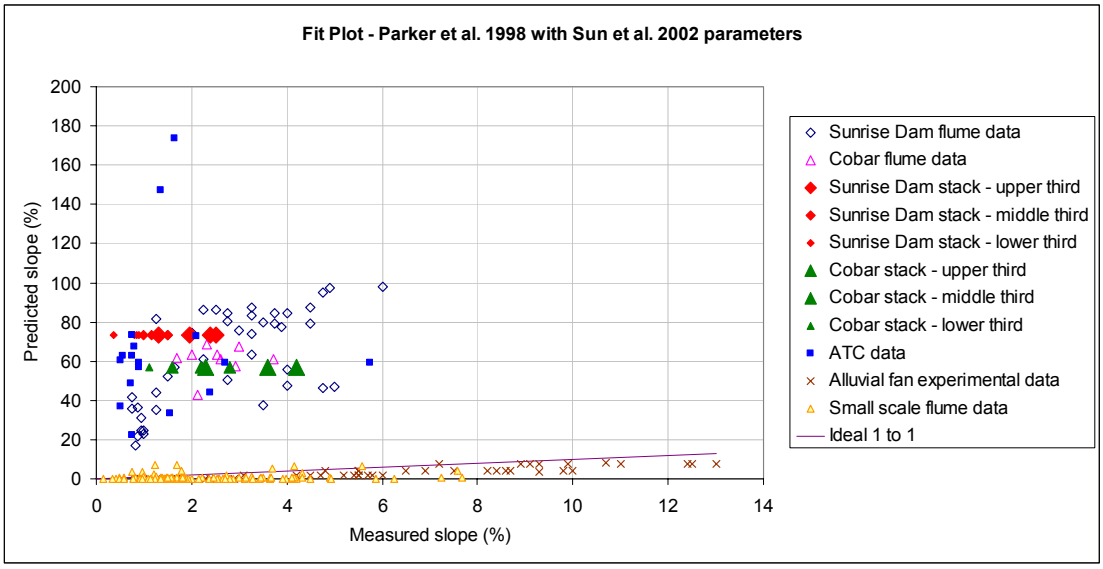

Figure 73. Fit plot of the Parker et al. 1998 model using the Sun et al. 2002 parameters

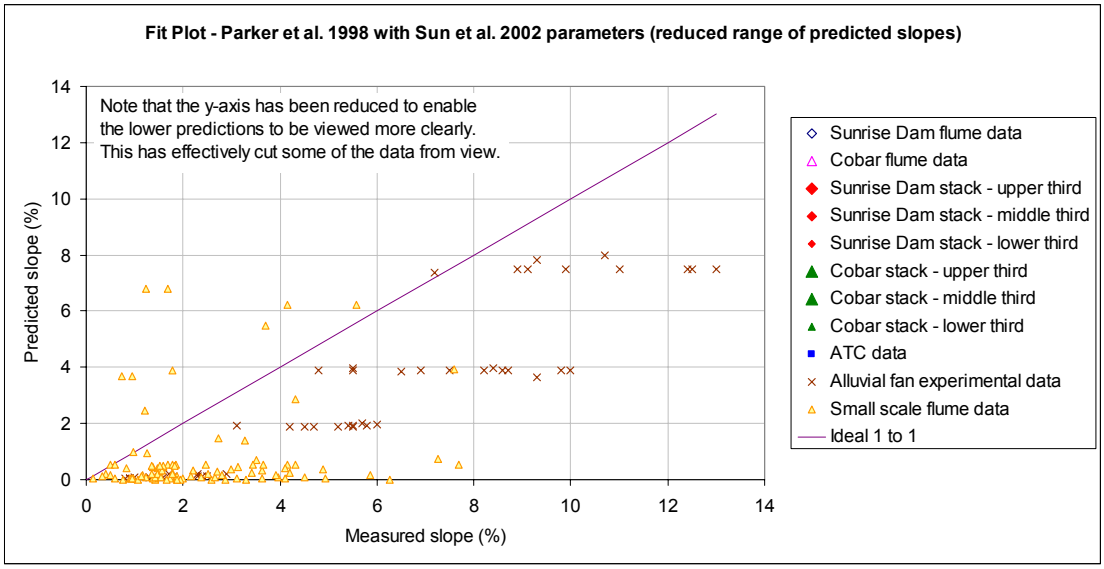

Figure 74. Fit plot of the Parker et al. 1998 model using the Sun et al. 2002 parameters, with the vertical scale reduced to provide a clearer view of the lower predictions. The excluded data points can be viewed in Figure 73 (above).

Figure 73 shows that the Parker et al. model with the Sun et al. parameters predicts very poorly for the thickened slurries that feature in the field flume data set, the stack data set and the ATC case history data set. These extremely high predicted slope values cause the lower slope predictions from the alluvial fan data set and the small scale flume data to be difficult to view, particularly in relation to the ideal 1 to 1 line, so a second fit plot has been presented as Figure 74 to enable these lower predicted points to be more easily viewable in relation to the ideal 1 to 1 line. From Figure 74 it is apparent that the alluvial fan data shows some resemblance to the ideal fit line, but the small scale flume data shows no alignment to the ideal line. The range of values used in Sun et al.'s analysis of an alluvial river delta is well outside the ranges of all five data sets used here. The flow rates range from 20 to 80 m^3/s, this lower value being well beyond the highest flow rate contained in any of the data sets presented here. The volumetric concentrations of the flows tested in Sun et al.'s analysis ranged from 0.05% to 0.2%, which are much lower than all of the concentrations featured in the validation data, with the exception of some of the corrected concentrations in the small flume data set. With these values in mind, it is surprising to see reasonable predictions made for some of the alluvial fan data points, considering that the alluvial fan data set has flow rates that are well below 20 m^3/s and concentrations that are well above 0.2% v/v.

The work presented in sections 4.4.10, 4.4.11 and 4.4.12 investigating the validity of the Parker et al. model with three different sets of empirical parameters would strongly suggest that this model is not applicable for predicting slopes on a tailings beach. In all three cases it was found that this model over-predicted the slopes for the data sets that featured tailings slurries. It is believed that the main reason for this failure is that the assigned empirical parameters were not derived with the purpose of predicting the slopes for fluids with such high concentrations as tailings. It is also suggested that the model itself was never intended to describe such concentrated slurries, particularly in describing the non-Newtonian properties of such fluids, since there are no apparent terms in equation 28 for describing viscosity or any other rheological aspects of the slurry.

4.4.13 Sofra & Boger 2000

The Sofra & Boger empirical equation is presented in section 2.4 as Equation 32, and is repeated below:

$$\theta = 2.667 \text{ x } 10^{6} \left(\frac{\tau_y \eta}{\rho^2 W^2 g v} \right) \tag{32}$$

where: θ is the angle of repose (in degrees)

τ_y is the yield stress (Pa)

η is the viscosity (Pa.s)

ρ is the slurry density (kg/m^3)

W is the width of the inclined plane (m)

g is the acceleration due to gravity (m/s^2)

v is the initial velocity of the flow (m/s)

The initial velocity of flow in their model is based on the release of a small volume of paste down an inclined ramp. This velocity is not directly comparable to the discharge velocity of tailings slurry from a spigot or the velocity of flow in a channel of tailings, but since Sofra & Boger proclaimed their model to be applicable for the prediction of beach slopes formed from the discharge of tailings slurry, it has

been tested here with the mean channel velocity used in place of their initial velocity term in the case of the flume data, whilst the mean spigot discharge velocity has been used for the stack data, with the spigot diameters assumed to be 200 mm at Cobar and 300 mm at Sunrise Dam. Another assumption was required in satisfying the input for the *W* term, the width of the inclined plane. The channel width, *b* was adopted for this parameter. For the non-flume data, it is assumed that the stream width, $b = 29.137Q + 116.07$, where Q is the flow rate in litres per second. This empirical equation is based on a linear fit to the self formed channel data presented by Pirouz (2006), with the fitting exercise presented in Figure 55 of section 4.4.1. For both sets of flume data, the width has been calculated from depth measurements and the known cross-sectional shapes of the channels used. For τy, the Bingham yield stress value has been used. For η, an apparent viscosity value has been calculated based on the approach of Wasp et al. (1977), it which the shear rate in a pipe was expressed as $8V/D$, where V is the average velocity of flow and D is the pipe internal diameter. Haldenwang & Slatter (2002) used the equivalent diameter $D = 4R_H$ (with R_H being the hydraulic radius), making the shear rate in a channel equal to $2V/R_H$. Therefore, for a Herschel-Bulkley fluid flowing in a channel we can present the following equation for the effective viscosity, η:

$$\eta = \frac{\left(\tau_y + K\left[\frac{2V}{R_H} \right]^n \right)}{\left[\frac{2V}{R_H} \right]} \qquad (61)$$

where τ_y is the yield strength of the fluid, K is the consistency index and n is the Herschel-Bulkley power. Applying this equation to calculate the effective viscosity generated the following fit plot:

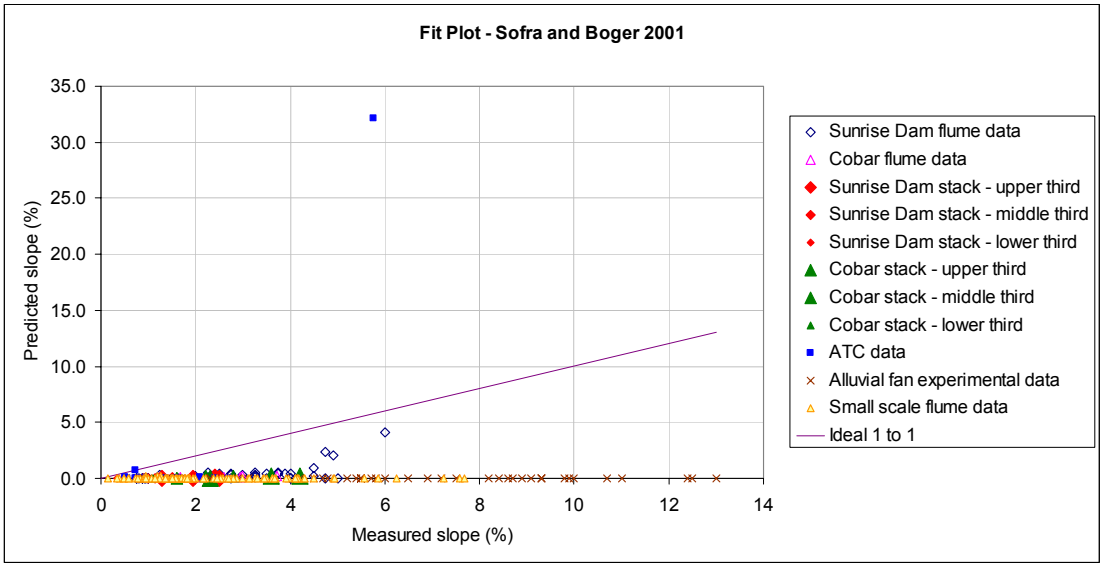

Figure 75. Fit plot of the Sofra & Boger 2001 empirical model

Figure 75 shows that the Sofra & Boger model fails is predicting the slopes from any of the five data sets. For the alluvial fan data, consistently flat slopes were predicted because the yield strength was assumed to be zero for all of the slurries tested in the alluvial fan experiments. The sand-water mixtures tested in the alluvial fan experiments had volumetric concentrations of 6% or less, so it was deemed reasonable to assume that these slurries should have zero yield stress values. Most of the fluids used in the small scale flume experiments exhibited zero yield stress values when they were tested in a rheometer (see Table 3 in section 3.4.7), so that explains why these points gained zero predictions in the Sofra & Boger model. The few data points that indicate significant predicted slopes all had yield stress values above 10 Pa, which shows that the Sofra & Boger model is highly sensitive to yield stress. The remaining data points featured in the other data sets all had yield stress values, but the reason for the unrealistic slope predictions rests on the incompatibility of Sofra & Boger's experimental approach in comparison to a channel flow scenario. Sofra & Boger did not run a continuous flow of slurry down their flume. Instead they released a small discrete volume of tailings paste (about 10 to 20 litres) down an inclined ramp to watch it run some 50 to 100 cm down the ramp and then stop, forming a tongue-like deposit. The yield stress values that were used by these workers in their experiments ranged from 17 to 210 Pa, which is higher than most of the data contained in the five validating data sets used here. This type of experiment is so very different to the flume experiments presented in Chapter 3 or the physical processes inherent in any of the other 3 data sets. The assumptions that have been made here

in order to apply this model to the validating data have deviated so significantly from the concept of Sofra & Boger's work, particularly in replacing Sofra & Boger's initial velocity term with the mean velocity of flow in a continuously flowing channel. The Sofra & Boger model predicts the slump angle of a small quantity of tailings paste released down an inclined ramp, which does not relate to a continuously flowing channel. However, this model was included in this chapter because of Sofra & Boger's claim that it could be used to predict beach slopes. The work presented here shows that it can not predict beach slopes.

4.4.14 Pinto & Barrera 2002

This empirical equation is presented as Equation 4 in section 2.1.1:

$$i = 0.009(s-1)^{15.6}\frac{C_W^{1.38}}{P^{0.86}} \qquad (4)$$

where i is the average slope of the beach (%), s is the ratio of the specific gravity of the solids to that of the water in the slurry, C_W is the solids concentration by weight (fraction), and P is the dry tonne production rate (kt per day).

The Pinto & Barrera model was easy to apply, with the input parameters being easily derived without the need to make any assumptions. The fit plot for this model is presented below as Figures 76 and 77.

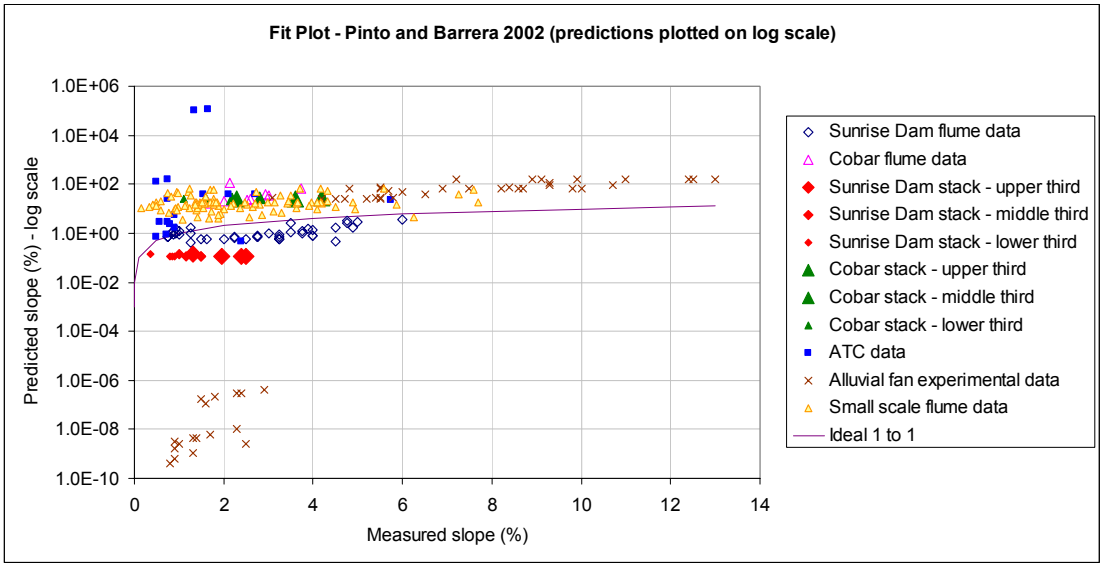

Figure 76. Fit plot of the Pinto & Barrera 2002 empirical model (predictions presented on a log scale due to significant spread in the magnitudes of the predicted slopes)

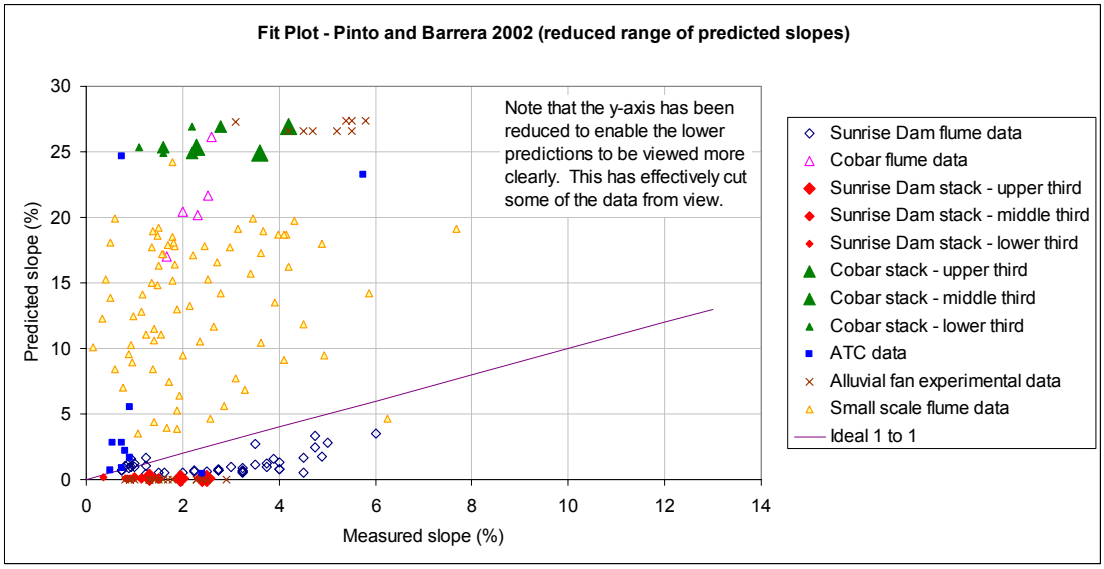

Figure 77. Fit plot of the Pinto & Barrera 2002 empirical model with the vertical scale reduced to provide a clearer view of the lower predictions. The excluded data points can be viewed in Figure 76 (above).

Figures 76 and 77 show that the Pinto & Barrera model (equation 4) predicts very poorly for most of the data, with some predicted slopes in the thousands (effectively predicting vertical slopes) and other predictions being very flat. The exception to this trend is that most of the segregating slurry points from the Sunrise Dam field flume data set have been predicted well. The poor predictions arise from

the power of 15.6 that is featured in this model, making it extremely sensitive to the specific gravity of the slurry particles and decant water. The Pinto & Barrera model is purely empirical, with the calibrating data featuring only 7 tailings beaches from copper mines in Chile. The range of values in this limited data set were as follows; P: 13 – 165 kt/day; G: 2.67 – 2.80; C_W: 20 – 53% w/w; i: 0.18 – 0.60%; median grain size: 10 – 119 μm. The narrow range of values in the specific gravity ratio (G) data provides some explanation as to how the power of 15.6 was derived by Pinto and Barrera during their least squares fitting exercise. The relatively low concentration values would suggest that most, if not all, of the tailings slurries tested were segregating. The very flat beach slopes that were measured tend to confirm this suggestion. It is also noted that the correlation observed by these workers between the median grain size data and the beach slope data was very poor, which is why they dropped this parameter from their model.

The good performance of the Pinto & Barrera model for some of the segregating slurries tested in the field flume at Sunrise Dam would seem reasonable on the basis of the calibration data of Pinto & Barrera being somewhat similar to that of the Sunrise Dam slurry; both are segregating, both have solid specific gravity values around 2.8, and both had flat beach slopes. However, this good performance was a mathematical fluke brought about by coincidence, which can be explained as follows: firstly, Sunrise Dam slurry contained very saline decant water, giving it a G ratio of 2.4, which is outside the range of Pinto & Barrera's model calibration data. Secondly, the range of flow rates tested in the field flume with segregating slurries at Sunrise Dam went from 1.9 to 11.7 litres per second, and the range of concentrations ranged from 25.8 to 50.9% w/w, which gives an equivalent dry production rate range of 0.23 to 1.3 kt/day. These production values were also well outside the range of values measured by Pinto & Barrera (13 – 165 kt/day). These two factors effectively cancelled each other out, so the end result was that 11 of the 16 segregating Sunrise Dam data points were predicted well by coincidence. It is noted that the alluvial fan data and the small scale flume data consist of segregating slurries, yet the predictions for this data were poor. Also, the segregating slurry monitored in the field flume at the Cobar mine was also predicted poorly. In conclusion, the Pinto & Barrera model is too sensitive to the specific gravity ratio G to be able to predict beach slopes in most situations, with this parameter raised to the power of 15.6.

4.4.15 Fitton et al. 2006

This semi-empirical equation appears as equations 13 and 14 in section 2.1.3, which are restated below:

$$d = 12.2Q^{0.6} \tag{13}$$

where d is the depth of flow in the channel (expressed in millimetres), and Q is the flow rate in litres per second.

$$i = 100 \tan \arcsin \left(\frac{0.073V^2}{\left[\frac{8\rho V^2}{\tau_y + K\left[\frac{2V}{R_H}\right]^n} \right]^{0.25} 2R_H g} \right) \tag{14}$$

where i is the beach slope (%), V is the mean velocity of flow in a channel of tailings slurry (m/s), ρ is the slurry density (kg/m^3), R_H is the hydraulic radius of the channel (m) and g is the acceleration due to gravity (m/s^2). τ_y, K and n are rheological parameters of the slurry as determined through the fit of the Herschel-Bulkley model to rheological data measured for the slurry experimentally, where τ_y is the yield stress of the slurry (Pa), K is the consistency index (Pa.s) and n is a power with no units.

The hydraulic radius was calculated from the depth value predicted by equation 13, using a new empirical equation shown below as equation 62:

$$R_H = 0.0008d^{0.9308} \tag{62}$$

This equation was generated as a fit to the depth vs hydraulic radius data that was measured at Sunrise Dam during the field flume experimental work, which is plotted below in Figure 78 with an inscribed curve of best fit. This equation calculates a very close approximation of the hydraulic radius value for a channel shaped as a segment of a circle of radius 170 mm, as can be seen from the fit of the curve inscribed in Figure 78 with its corresponding coefficient of determination equal to 0.9997. However, this approach subtly differs from that suggested by Fitton et al., since it was stated by these workers that the channel geometry should be "similar in magnitude and shape to the half-pipes used" in the field flume. This statement carried the implication that the hydraulic radius would be calculated geometrically from the predicted depth using a channel shaped as a circular segment of radius 170 mm. Though equation 62 does calculate values that are very close to this for the range of depth values that are presented in Figure 78, it does not do this via a fundamental geometric approach. This deviation was introduced deliberately, as it was seen that predicted depth values greater than 340 mm would exceed the diameter of a 170 mm radius pipe, thereby disabling the Fitton et al. model because of the inability to calculate a sensible hydraulic radius to put into equation 14. A less extreme point, but a relevant one none the less, is that it was also seen that predicted depths above 100 mm would cause the channel shape to be deeper and narrower than what was intended when the flume was designed to emulate the self-formed channel shapes found on a tailings beach (see Figure 12 in section 3.3.3 for a plot of channel shapes considered in the design of the flume). Such channel shapes would arguably violate the channel shape edict stated by Fitton et al. anyway, so it could actually be argued that the development of Equation 62 fulfils the intent of the channel shape assumption that was set forth by Fitton et al. more soundly than a geometric approach, while additionally enabling the extrapolated predictions of hydraulic radii for much larger flow rates.

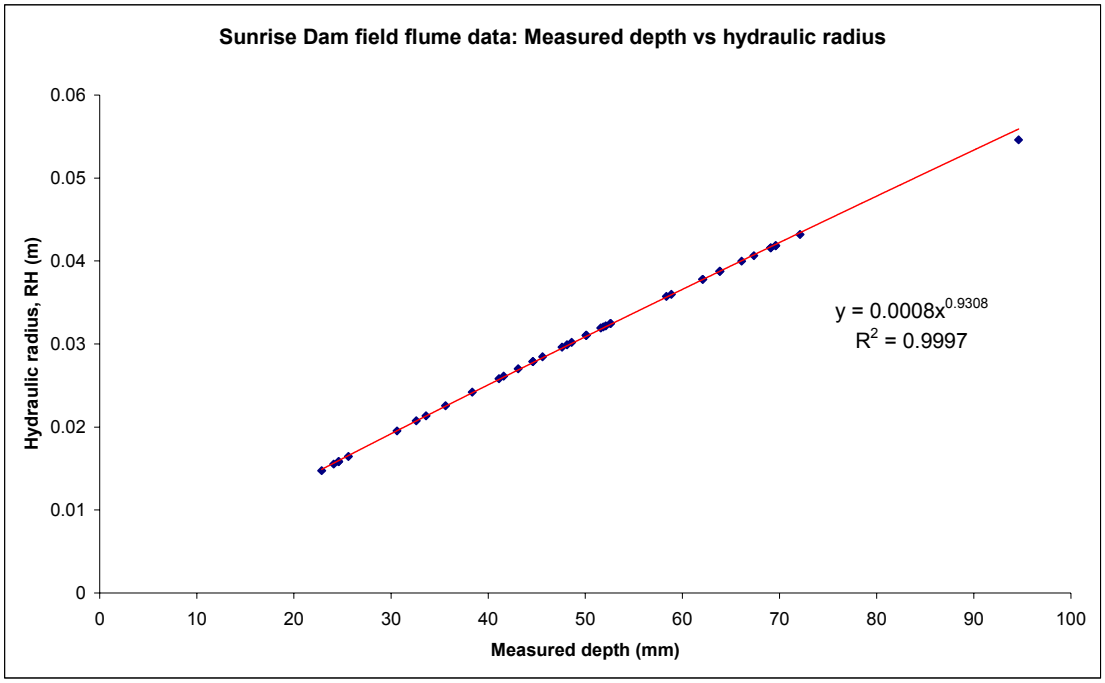

Figure 78. Plot of measured depths from the Sunrise Dam field flume data against the hydraulic radius values that had been calculated from these depths.

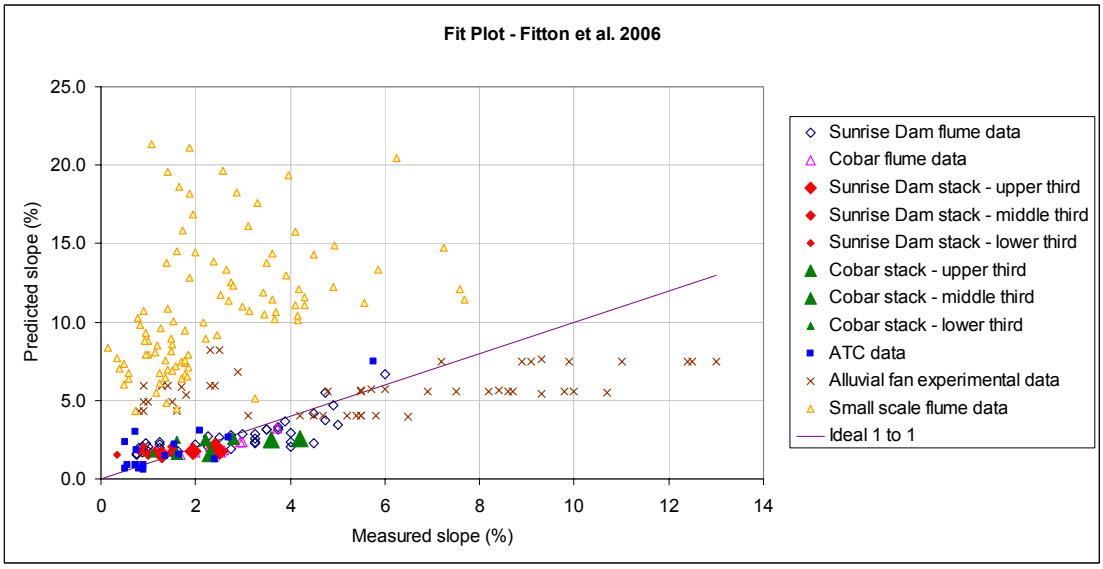

Figure 79. Fit plot of the Fitton et al. 2006 semi-empirical model

Figure 79 shows that the Fitton et al. model predicts well for the field flume data, the ATC data and the stack data from the two mines. The Fitton et al. model predicted moderately well against the alluvial fan data, but poorly against the small scale flume data. The good fit to the field flume data can largely be attributed to the fact that equations 13 and 62 were calibrated from the field flume data set.

However, equation 14 was not calibrated with any of the data collected by these workers, so the good slope predictions of the model from the depths and hydraulic radii predicted by equations 13 and 62 must be attributed to the good performance of the constituent equations that were combined to give equation 14 (those being the empirical Blasius equation, the Haldenwang-Slatter Reynolds number equation and the Darcy-Weisbach equation). The good predictions that were made by the Fitton et al. model against the ATC data and the stack data would suggest that the assumptions contained within equations 13 and 61 (depth being a factor of the flow rate, and the implications on channel shape) were realistic compared to the processes occurring on a tailings beach.

The Fitton et al. model predicted poorly in relation to the small flume data set. The cause of this poor prediction stems from flow rates in the 50 mm diameter pipe of the small flume that created channel shapes of high depth to width ratios that were not of similar proportions to those formed in the field flume, nor to those formed on a tailings beach. This effect resulted in the Q-d equation (equation 13) under-predicting the depth by factors of about 3 to 5 in every case, which in turn caused equation 62 to predict hydraulic radii that were about a quarter of that actually occurring in the small flume, finally causing equation 14 to predict slopes that were about 4 times steeper than those observed. It is concluded that the channel cross sections formed in the small flume, defined by the relatively high depth to width ratios, were not representative of those found on tailings beaches, while the Fitton et al. model is focused on modelling such channel shapes. Therefore, it can be said that the Fitton et al. model is not able to predict equilibrium slopes in channels that are narrower than those found on a tailings beach.

4.4.16 Chryss et al. 2006

This semi-empirical model, discussed in section 2.1.3, comprises some 7 equations as follows:

$$x = y_0(h_0(y/y_0)^{0.5} + h_1(y/y_0)^{1.5} + h_2(y/y_0)^{2.5}) \quad (6)$$

$$h_0 = (2/\mathrm{t}^2 - 2)^{0.5} \quad (7)$$

$$h_1 = 1/6(2/t^2 - 2)^{0.5}(-1/t^2 - (t^2 - 1)/(4t^2))/(1/(2t^2) - 1/2) \quad (8)$$

$$h_2 = 1/5(2/t^2 - 2)^{0.5}((0.5(1/(2\ t^2) - (3 + t^2)/(8t^2))/(1/(2t^2) - 0.5) \ldots$$
$$-(-1/t^2 - (t^2 - 1)/(4t^2))^2/(8(-0.5 + 1/(2 * t^2))^2))) \quad (9)$$

$$t = \frac{\tau_y}{(\rho g y_0)} \quad (10)$$

$$v(y) = V + 1/\chi(gR_hS_0)^{1/2}(1 + \ln(y/y_0)) \quad (11)$$

$$V = \frac{1}{n} R_h^{2/3} S_0^{1/2} \quad (12)$$

The first 4 equations define a channel shape, where x and y are Cartesian co-ordinates for channel cross-sectional profile, h_0, h_1 and h_2 are geometric constants, and y_0 is the total depth of flow in the channel. t is the non-dimensional mass yield stress of the bed material, τ_y is the yield stress of the bed material, ρ is the density of the bed material, and g is gravitational acceleration. Equation 11 is a velocity distribution equation, in which $v(y)$ is the axial velocity in a channel at a depth y metres above the channel bed, V is the mean axial velocity, χ is the Von Karman constant, R_h is the hydraulic radius, and S_0 is the slope of the channel. Equation 12 is the Manning equation, in which n is the Manning roughness coefficient.

The Chryss et al. beach slope model is complex and difficult to apply in comparison to the others tested in this chapter. A particularly difficult aspect of its application comes in defining τ_y, the yield stress of the bed material. For the alluvial fan data this was not attempted, since not enough was known about the bed formed in those experiments. Likewise, this model was not applied to the small scale flume data either, because of the difficulty in assigning a bed yield stress. Since no method was provided for

calculating this parameter, and with an absence of relevant experimental data available for approximating a value, it was assumed that the concentration of the bed tailings was 70% w/w, since this value was used by Chryss et al. in their work. As suggested by Chryss et al, a Manning's *n* value of 0.0081 $s/m^{1/3}$ was assumed, which was based on an empirical fit calibrating flume data. An χ value was determined from the graph presented by Chryss et al. The fit plot generated through this work is presented below as Figure 80.

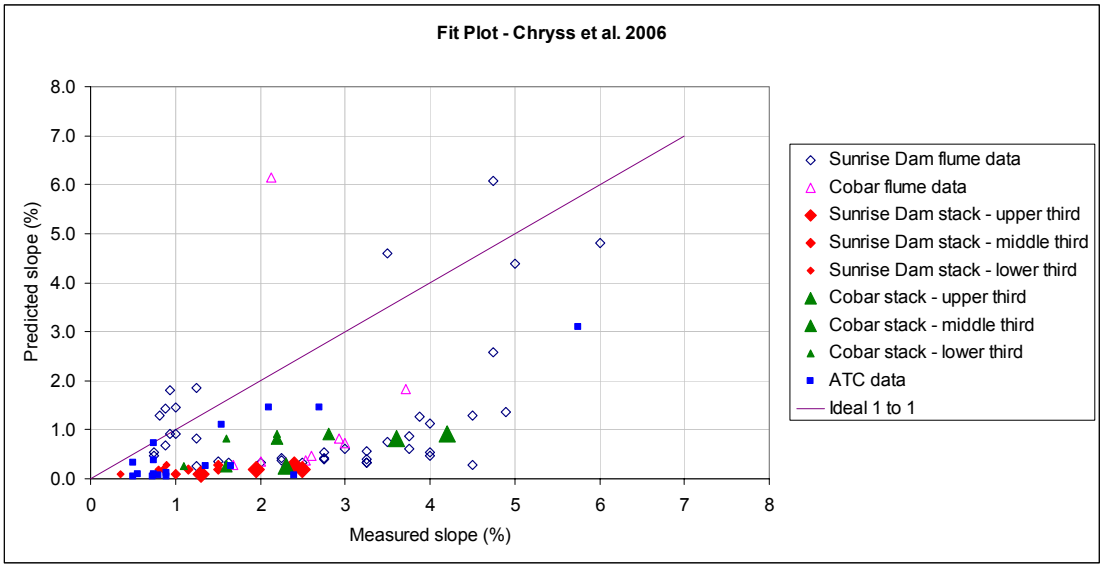

Figure 80. Fit plot of the Chryss et al. 2006 model

The fit plot presented above as Figure 80 shows that the Chryss et al. model generally predicts poorly for the 3 data sets that were tested. Given the lack of information regarding the bed yield stress, it is felt that this model is generally not practical to apply in the prediction of beach slopes until more research is conducted on the characterisation of channel beds on a tailings beach. The assumed value for Manning's *n* is also seen as an oversimplification that deserves more attention if this model is to be seriously presented for predicting beach slopes.

4.5 Statistical analysis of the accuracy of the predictions

In order to objectively quantify the accuracy of the predictions made by each model, several commonly used indicative statistics were considered (Willmott 1982):

- Mean squared error (MSE) $$MSE = \frac{1}{N}\sum_{i=1}^{N}(x_i - \hat{x}_i)^2 \quad (63)$$
- Residual Sum of Squares (RSS) $$RSS = \sum_{i=1}^{N}(x_i - \hat{x}_i)^2 \quad (64)$$
- Mean absolute error (E_{MAE}) $$E_{MAE} = \frac{1}{N}\sum_{i=1}^{N}\left|x_i - \hat{x}_i\right| \quad (65)$$

where N is the number of points in a data set, x_i is the estimated value and $\hat{x}_i$ is the true value.

All three of these statistics provide an objective indication of the accuracy of fit of the data to the ideal prediction line, though the respective values that each will take can be quite arbitrary in some cases, and possibly misleading in others. For example, it is expected that the residual sum of squares will appear to be very large when presented for a data set with 20 values when compared to a data set with 5 values, which might mislead the viewer to believe that the large data set has a poorer fit than the smaller data set. The mean squared error will avoid this problem because the size of the data set will no longer have an impact on its value, but the value itself will not carry any meaning in relation to the data. Alternatively, the mean absolute error will also avoid the effect of data set size, but with the added benefit that its value will be of a magnitude that is directly comparable to the original data in real terms. For these reasons, the mean absolute error has been chosen as the representative indicator of the predictive accuracy of the slope models.

The use of either Pearson's coefficient or the Coefficient of determination (R^2, equal to the square of the Pearson coefficient) have been considered here instead of these other statistics, but neither of these two statistics are appropriate in this case because they are only applicable for indicating how well a line (or curve) of fit can be imposed on a field of data points. In the work done here, we are looking at how closely the data points fall to an arbitrarily defined line, rather than looking at how well a fitted line describes the field of data points. In every case, though we are hoping that the data falls close to the

ideal line, we know that the line is not a fit to the experimental data, because each model that we are testing was created independently of the data sets that were used to validate it (with the exception of the depth and hydraulic radius equations in the Fitton et al. 2006 model (equations 13 and 62), which were empirically calibrated with the field flume data.

The mean absolute error has been calculated for each of the data sets tested in this chapter. These error statistics are presented in Table 8 to enable a comparison of the predictive accuracy of the slope models tested here.

Model	Field flume	Stack data	ATC data	Alluvial fan	Small flume
Melent'ev et al. 1973	0.9	1.5	1.8	3.2	1.5
Robinsky 1978	1.2	1.9	1.3	4.4	1.4
Blight and Bentel 1983 (corrected 1985)	2.6	1.5	1.3	5.6	2.4
Williams and Meynink 1986	1.8	1.1	4.6	1.3	3.3
Wates et al. 1987	1.2	1.0	0.94	3.3	2.4
Boldt 1988	1.7	2.2	7.4	4.0	1.2
Winterwerp et al. theoretical 1990	2.2	1.0	2.1	2.8	1.8
Winterwerp et al. empirical 1990	4.2	3.0	4.4	19.6	28.3
Kupper 1991	4.0	5.1	3.0	2.7	1.7
Parker et al. 1998	20.6	25.2	24.0	4.5	2.2
Parker et al. 1998 with Whipple et al. 1999	51.3	59.6	35.5	15.1	3.4
Parker et al. 1998 with Sun et al. 2002	58.8	68.8	65.7	2.7	2.2
Sofra and Boger 2001	2.4	1.5	2.6	5.6	2.4
Pinto and Barrera 2002	8.1	5.2	13091	49.3	18.2
Fitton et al. 2006	0.7	0.7	0.65	2.8	8.5
Chryss et al. 2006	1.9	1.3	0.88	-	-

Table 8. Statistical evaluation of the prediction accuracy of the models tested, showing the mean absolute deviation for each data set. Low figures indicate good agreement between predictions and the measured data.

The data presented above in Table 8 enables the predictive performance from the 16 tested models to be compared. To make the comparison clearer, a series of bar graphs are presented in Figures 81 to 85, with each graph presenting the best performing models for each of the five data sets tested:

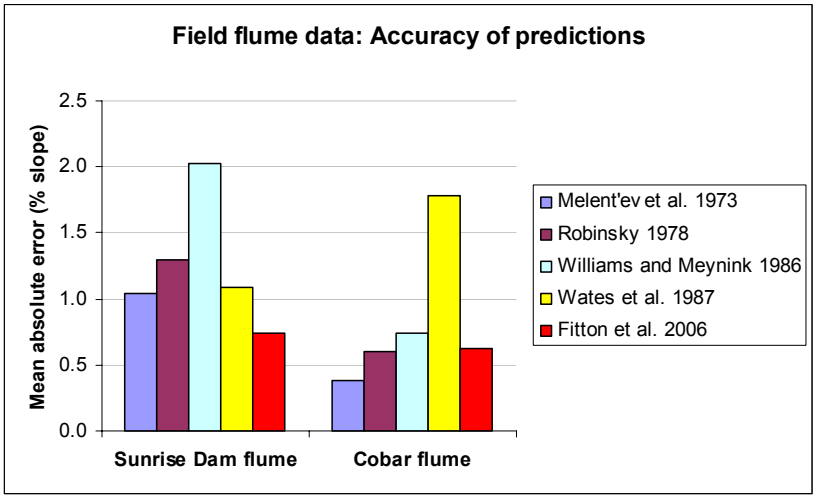

Figure 81. Statistical comparison of the best predictions made against the field flume data set, showing the mean absolute deviation for each data set. Low figures indicate good agreement between predictions and the measured data.

Figure 81 shows that the Fitton et al. model predicted well for both sets of flume data with a mean absolute error below 1% slope in both cases, but was out-performed on the Cobar flume data by the Melent'ev et al. model and the Robinsky graph fit equation.

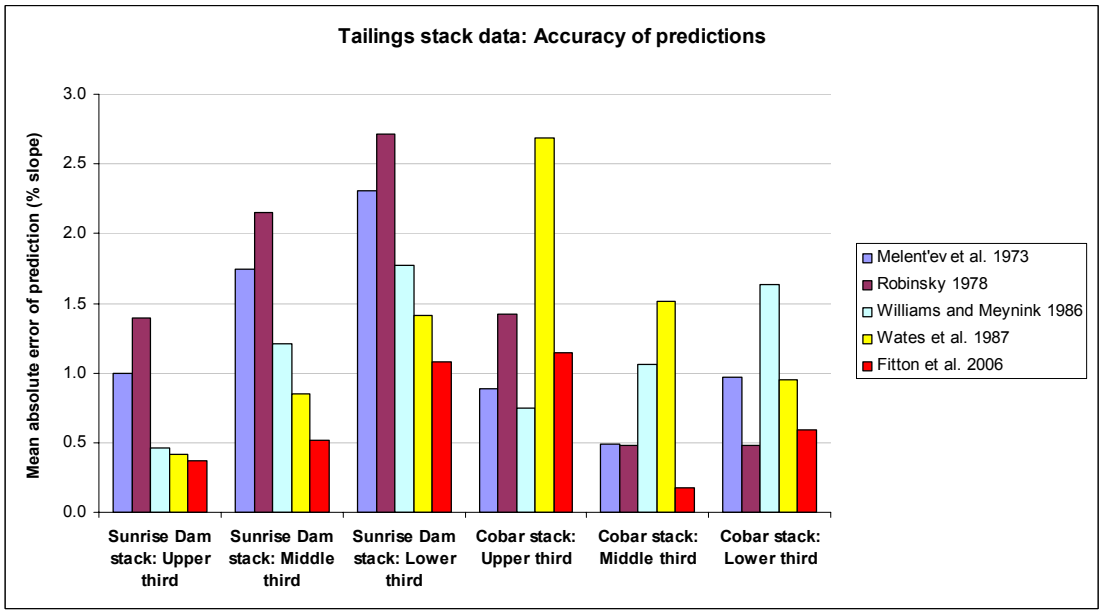

Figure 82. Statistical comparison of the best predictions made against the tailings stack data sets, showing the mean absolute deviation for each data set. Low figures indicate good agreement between predictions and the measured data.

Figure 82 shows that the Fitton et al. model predicted better than the other models against the Sunrise Dam stack data, but the results for the Cobar stack were mixed, with the Williams & Meynink model predicting better than the others in the upper third of the stack, the Fitton et al. model performing best

over the middle third and the Robinsky graph fit equation doing the best on the lower third of the stack. Overall, the Fitton et al. model performed better than the others with the tailings stack data, with the lowest overall mean absolute error.

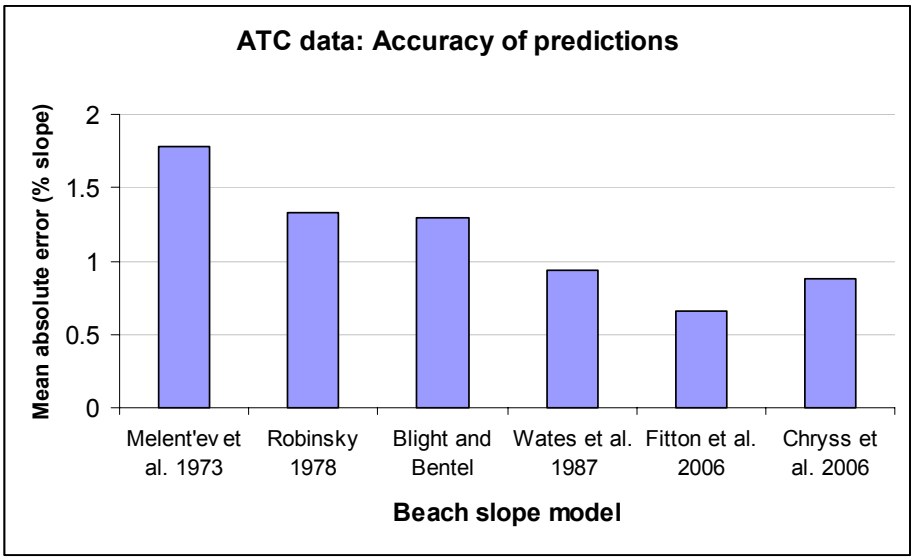

Figure 83. Statistical comparison of the best performing models against the Australian Tailings Consultants (ATC) data set, with the mean absolute deviation shown for each data set. Low figures indicate good agreement between predictions and the measured data.

Figure 83 shows that the Fitton et al. model predicted better against the ATC data than the other models, with the Chryss et al. and Wates models following with the nearest performance statistics.

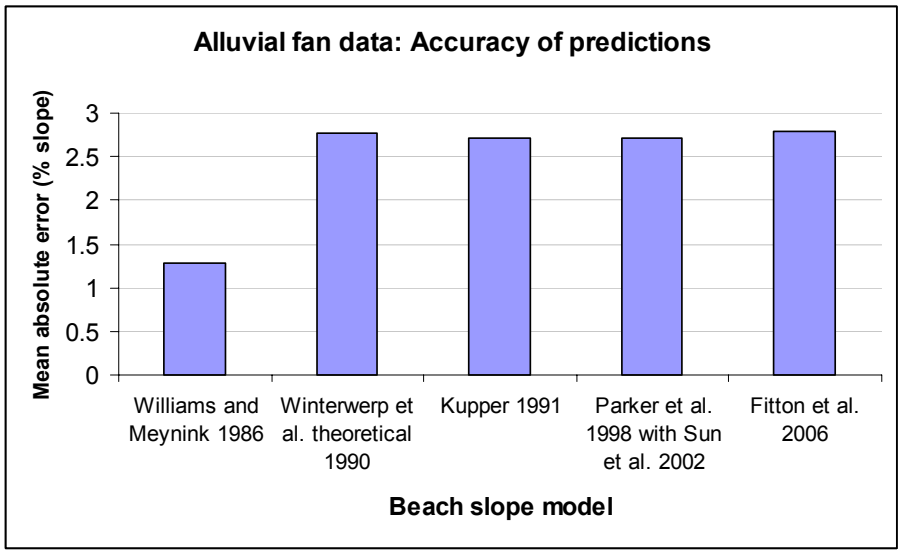

Figure 84. Statistical comparison of the best performing models against the Alluvial fan experimental data set, with the mean absolute deviation shown for each data set. Low figures indicate good agreement between predictions and the measured data.

Figure 84 shows that the Williams & Meynink model performed considerably better than any of the other beach slope models in predicting the slopes observed in the alluvial fan experiments. The next four models shown are the Williams & Meynink model, the Winterwerp et al. semi-emprical model, the Kupper model, the Parker et al. model with Sun et al. parameters and the Fitton et al. model, all of which performed relatively poorly with mean average errors around 2.7% slope.

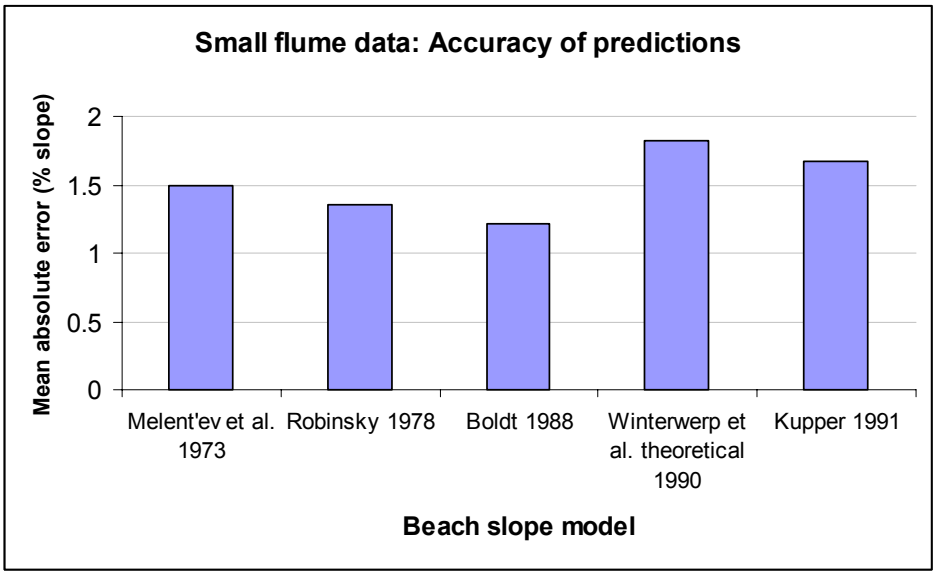

Figure 85. Statistical comparison of the models that performed best against the small scale laboratory flume experimental data set, with the mean absolute deviation shown for each data set. Low figures indicate good agreement between predictions and the measured data.

Figure 85 shows that the Boldt model predicted better against the small flume data than the other models, with a mean average error of 1.2% slope. However, this figure also exposes an interesting aspect of this statistical comparison exercise, since the Boldt model uniformly predicted slopes of 1.95% for every point in the small flume data set (shown in Figure 66), and the Robinsky model also predicted uniform slopes of about 1.3% for the entire data set (Figure 61), yet both of these models gained mean absolute error values that were lower than any of the others. This result occurred because the other models went to the opposite extreme in being too sensitive to the data in the small flume set, predicting slopes that were even further from the measured slopes (on average). Though this finding could be argued to expose a practical limitation of the type of statistical approach that has been adopted here, it is asserted that such results do have merit in showing how good a model is in the context of applying it to predict tailings beach slopes. From this, we can say that none of the models actually

predicted well against the small flume data set. Instead it should be said that the Boldt model predicted poorly and the others fared even worse. From this it must be recognised that the small scale flume experiments presented a significant deviation from tailings beaches in terms of scale, the fluids used, the concentration range tested, the channel shapes formed, the range of flow rates, the channel roughness and the particle sizes tested.

4.6 Discussion of beach slope model validation

Of the models found in the literature, the Fitton et al. model has yielded the best predictions against 3 of the 5 sets of data. In the case of the field flume data this is hardly surprising, since this model was empirically calibrated with this data. The stack data was also predicted best by the Fitton et al. model, though it is conceded that the stack data reports on the same slurries as those used in the flume tests, so the Fitton et al. model is also at an advantage in this respect over the other models. However, the Fitton et al. model predicted best against the Australian Tailings Consultants (ATC) data set, which does provide strong and completely independent validation for this model. The Williams & Meynink model performed better than the other models against the alluvial fan data set. Finally, the small scale flume data was seen to be best predicted by the Boldt model.

The majority of the models tested here were created for the prediction of beach slopes, so the independently collected data contained in the ATC set is seen as the most applicable data set of the five presented here for the validation of these models. Some of the models were not developed with a channel mechanism approach, so flume data does not suit such models conceptually. Models such as the Blight & Bentel model and the Sofra & Boger model fit into this category, since these two models were developed with a completely different approach towards the formation of a tailings beach. The small scale and low concentration range of the alluvial fan data makes it of less value and relevance than the ATC data. For these reasons, the performance of the beach slope models against the ATC data set is seen as the most critical test in this exercise. With the Fitton et al. model making the closest predictions against this data set, it is evidently the best beach slope prediction model of those tested from the literature.

Chapter 5: Development of new beach slope models

In this chapter three new tailings beach slope models are presented:

- A simple empirical model
- An a priori model
- A hybrid semi-empirical model

The presentation of three models (instead of one) is justified on the basis that each one has its own advantages and purpose relative to the other two. This will be clarified as each one is presented.

5.1 The simple empirical beach slope model

A simple equation that enables engineers to make a quick and reasonable estimate of a beach slope is a desirable and useful tool. Ideally, such a model would have very few input parameters, thereby minimising the amount of experimental measurement and other data collection that is required for its application, yet make reasonably accurate slope predictions. An equation is presented here for this purpose, which is based on an empirical fit to the experimental field flume data.

It was observed during the field flume experimental work (in section 3.3.7) that the flow rate had the greatest effect on the resultant equilibrium slope, with low flow rates resulting in steep equilibrium slopes. The slurry concentration was also observed to have an effect on equilibrium slopes. Very low concentrations had a dramatic effect, with segregation of the slurry particles occurring in the flume while the concentration was below the segregation threshold of the slurry. These very low concentrations resulted in equilibrium slopes that were very flat. However, for slurries above the segregation threshold, this trend occurred on a much weaker basis, with low concentrations still resulting in low slopes, but with many cases defying the trend due to the effect of a low flow rate overriding the effect caused by the low concentration. The new simple model is based on the trends noted between these two variables and the equilibrium slope of the flume, which are each plotted separately against the equilibrium slope in Figures 86 and 87.

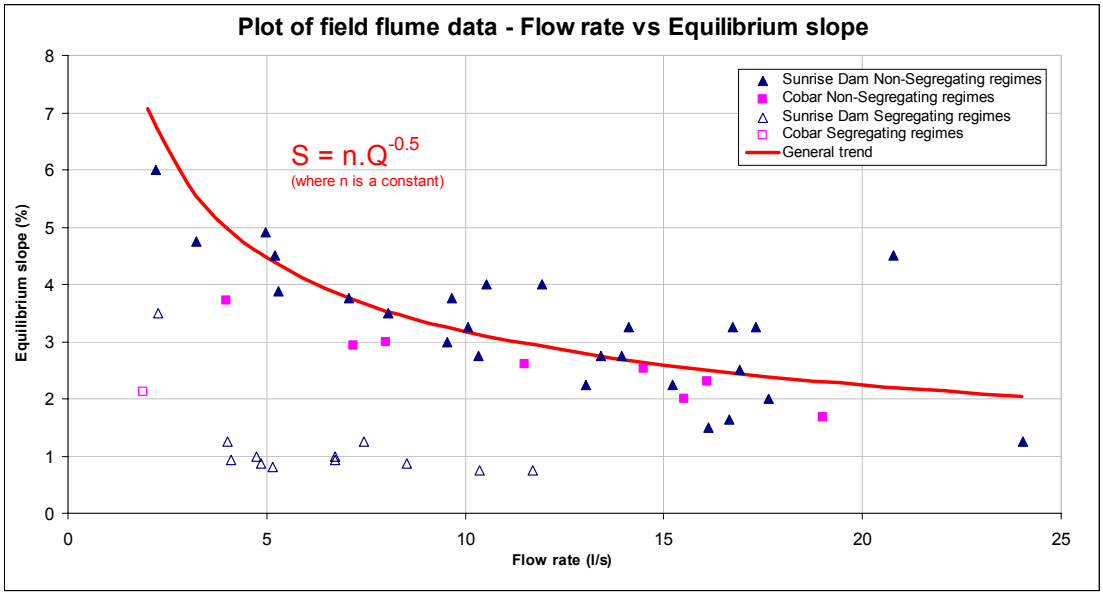

Figure 86. Plot of flow rate against equilibrium slope for the field flume data

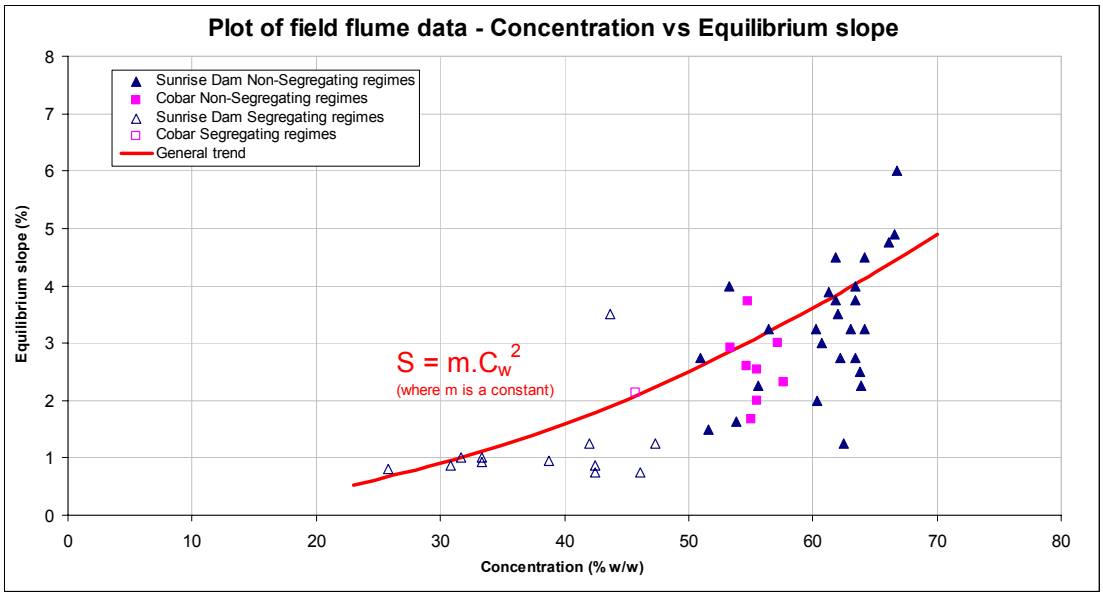

Figure 87. Plot of concentration against equilibrium slope for the field flume data

An equation based on these two trends was formulated with an empirical constant that was calibrated to fit the field flume data, which appears as follows:

$$i = \frac{26.6 C_W{}^2}{\sqrt{Q}} \qquad (66)$$

where C_W is the slurry concentration (fraction w/w) and Q is the flow rate from a spigot (l/s).

5.1.1 Validation of the simple empirical model

For the validation of the simple empirical model, the usual five sets of validation data (field flume data, stack data, ATC data, alluvial fan experimental data and small flume data) have been used, but in addition, an extra three groups of data (labelled "Seddon beach data (max slopes); (mean slopes) and (min slopes)") have been added to the usual five. These three new groups have been cited from the Seddon data set, which features tailings beach slope data from 30 different mines around the world that have appeared in various papers and reports between 1996 and 2006. A copy of the Seddon data set is presented in Appendix M. This data set is not complete, due to the omission of various data in the literature that it is based upon. Furthermore, no rheological data is provided for any of the 30 tailings slurries reported in the set, which is why it was not used as a general validation data set for the validation of other tailings beach slope models. However, since this new simple empirical model only requires the flow rate and concentration as input parameters, the Seddon data set can be applied in validating it. The three groups of Seddon data refer to "max slopes", "mean slopes" and "min slopes", which respectively represent the maximum beach slope reported from a mine; the calculated mean beach slope (if a range of slopes was quoted); and the minimum slope reported. The fit plot of the simple empirical model is presented in Figure 88.

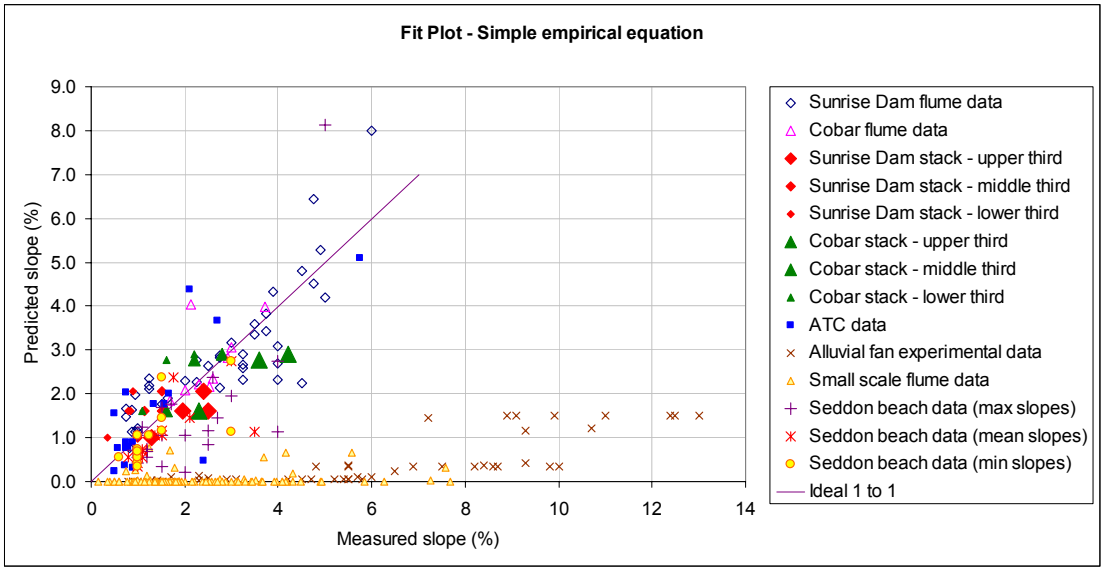

Figure 88. Fit plot of the Fitton simple empirical equation

Figure 88 shows that the simple empirical model predicts well against the field flume data (to which it was calibrated), the stack data, the ATC data and the Seddon data set. The model predicted very poorly against the small scale flume data and the alluvial fan data. The poor performance of the simple empirical model against these two small scale data sets is due to the sensitivity of the model to the low concentrations featured in these data sets. The power of two applied to the concentration (which is expressed as a fraction) results in very small slope predictions when the concentration is small, even if the slurry is flowing at a low flow rate. However, in defence of the simple empirical model, the concentrations (by weight) featured in the small flume data set range from 0.003% and 13%, and the alluvial fan experimental data set range between 1.0 and 15%. Both of these ranges of concentration are well below the slurry concentrations that are typically seen on tailings beaches. Even stronger defence of the simple empirical model is provided by its good predictive performance against the stack data, the ATC data and the Seddon data set. These three sets all contain full scale tailings beach slope data, with the latter 2 featuring a combined total of 47 full sized tailings beaches from around the world.

5.1.2 Discussion of the simple empirical model

It is acknowledged that the simple empirical model is crude. There is a complete ignorance of the rheology of a tailings slurry, with the outdated assumption that knowledge of the concentration of a

slurry is sufficient in this regard (see section 3.3.13 for discussion of this topic). There is an absence of consideration for particle size or density, carrier fluid density, or for the channel geometry. However, it can be seen in Figure 88 that the predictions made with this simple equation against the beach slope data compare favourably with the models presented earlier. Furthermore, this model does serve its purpose well, since it enables a rough prediction of beach slope to be made when there is a lack of rheology or particle size data (or any of the other parameters required in the more complex models presented in this work), plus it is easy to apply. It can be utilised to make a quick beach slope prediction without the use of a computer, where many of the other beach slope models can not. On this basis, the simple empirical model presented here presents a useful tool to engineers and mine operators when a rough slope prediction is needed quickly in the absence of detailed data.

For application of the simple empirical model without using its equation (equation 66), a chart is presented in Figure 89 that enables a beach slope to be predicted on the basis of the flow rate and concentration of slurry. To use the chart, first calculate the effective flow rate from each discharge point. (if the slurry is being discharged from 4 spigots, then divide the total flow rate by 4 to get the effective flow rate) Draw a vertical line from the x-axis from the value of the effective flow rate until the applicable concentration contour is hit. From there, draw a horizontal line to the y-axis to read off the predicted beach slope. It is important that the total tailings flow rate is divided by the number of open spigots in order to determine an effective flow rate. If the spigots are not of equal diameter, or if some of them are partially closed compared to others, it will be necessary to determine the flow rate from each spigot if a resultant beach slope is to be predicted. The experimental flume data points have been presented on the chart to show how well this data coincides with the model.

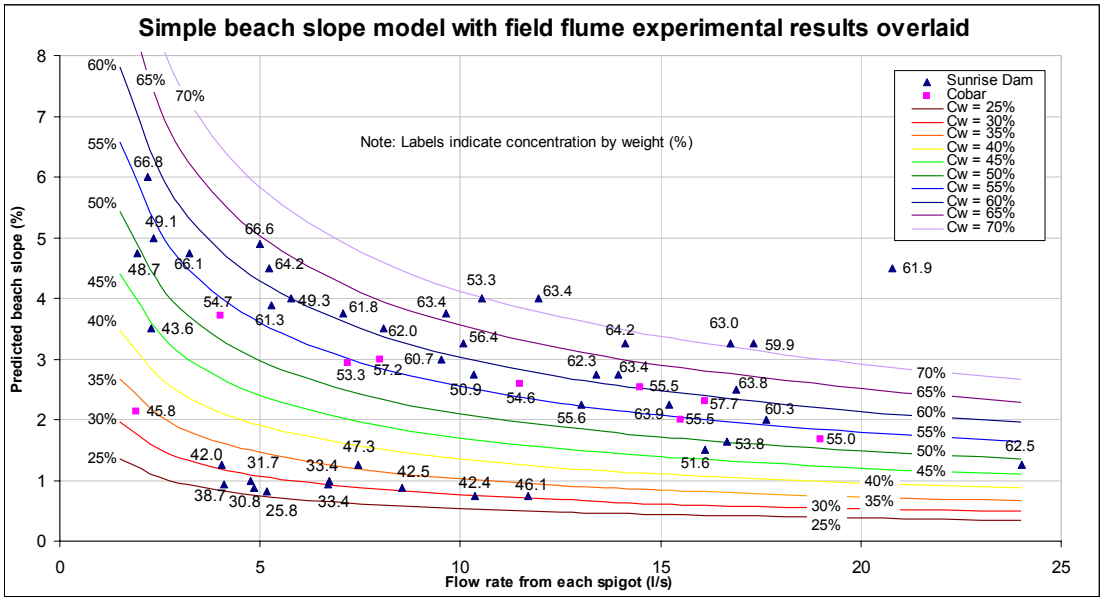

Figure 89. Chart based on the simple empirical model.

The prediction quality statistics for the simple empirical model are presented in Table 12 (section 5.7) along with the fit statistics for the better performing models tested from the literature in Chapter 4 and the other new models presented in Chapter 5, to show how it compared with those models.

5.2 Development of an a priori model

The Latin term "a priori" is defined by the Oxford dictionary as "from what is before". It describes the application of previous knowledge to reach a conclusion.

It is desirable to construct a beach slope prediction model that dispenses the empirical reliance on the field flume data. This would allow the field flume data to be used as a powerful data set for validating the model, instead of being spent on calibrating an empirical model

The ideal outcome here would be to construct a new model with fully theoretical existing equations, but this ideal is sorely compromised by the relative difficulty of modelling turbulent fluid dynamics, as history has demonstrated. (Slatter 2006) It is fair to say that the progressive efforts of various workers in this field have enabled some significant advances in the degree of incorporation of theory into the

current state of the art, but there is no fully theoretical model currently in existence to meet this challenge.

In light of this predicament, a pragmatic approach will be applied here to work towards the development of an a priori model that predicts well and is relatively easy to use.

Existing empirical equations will be methodically tested for their fitness to be incorporated into this new a priori model. Such existing empirical equations are seen to hold more credibility than the Fitton et al. model or the simple empirical model on the basis that they have been calibrated from independently gathered data that has been collected by impartial workers in a variety of other practical contexts. Many of these existing empirical equations have been built on larger or more diverse sets of data than the Fitton et al. model and the simple empirical model, which also adds to their credibility.

The ease of application of this new a priori model is also a consideration here. It is desirable that the model can be utilised by practical engineers who are equipped with only a calculator or modest computer. It is therefore intended that this new model will be as simple as possible, without significantly compromising its predictive capability.

5.2.1 Flume design approaches

A useful place to start in this quest for an a priori slope prediction model is to consider some flume design approaches that have already been presented in the literature. It is reasoned that such approaches should be able to model the processes that were observed within the experimental field flume, though it is expected that any safety factors and other conservative approximations contained within these flume design approaches to avoid solids deposition may cause the slope predictions to be higher than the experimentally observed flume slopes.

Faddick proposed a flume design method based on the Froude number and a minimum required horizontal velocity. (Faddick 1986) He postulated that a Froude number less than 1.25 would

introduce unstable fluctuations in depth and velocity in the flume and allow solids to settle on the flume bed, so he adopted this minimum permissible Froude number as a design criterion. He presented the following equation for the Froude number, *Fr*:

$$Fr = \frac{V}{\sqrt{gy}} \tag{67}$$

where V is the mean velocity of the flow, g is the acceleration due to gravity and y is the depth of flow. This form of the Froude number equation assumes that the open channel is wide, with the definition for "wide" entailing a width to depth ratio of at least 30, but Faddick assumes that wall effects will be negligible in a narrow flume.

Faddick's proposed design method also contained a minimum velocity criterion, based on an empirical relationship between the unhindered settling velocity of a large particle in the carrier fluid and the horizontal velocity of the fluid at a particular depth. The minimum velocity equation is as follows:

$$u_{0.1} = 35V_S \tag{68}$$

where $u_{0.1}$ is the axial velocity at a depth of 10% of the total depth of flow, and V_S is the unhindered settling velocity of the largest particle in the slurry. The Prandtl velocity distribution equation for wide channels was adopted as a means for modelling the velocity profile of the flow, which appears as follows:

$$u = V + \frac{1}{\chi}\sqrt{gR_H S_0}\left[1 + \ln\left(\frac{y'}{y}\right)\right] \tag{69}$$

where u is the axial velocity at a depth y' from the channel bed, χ is the Von Karman universal constant, R_H is the hydraulic radius of the channel (equal to the ratio of the cross-sectional area of flow and the wetted cross-sectional perimeter), and S_0 is slope of the hydraulic gradeline (assumed to run parallel to the bed slope). Again, Faddick assumed that his narrow channel would cause negligible

effects on the accuracy of this velocity profile model. He also assumed a value of 0.2 for the Von Karman constant for slurries.

Faddick's method used the Manning equation for estimating for the flow resistance in the channel:

$$V = \frac{1}{n} R_H^{2/3} S_0^{1/2} \tag{70}$$

where n is the empirical Manning roughness coefficient. Finally, the flow continuity equation was also used in Faddick's flume design method for determining the depth of flow:

$$V = \frac{Q}{A} \tag{71}$$

where Q is the flow rate of a fluid and A is the cross-sectional area of flow.

The Faddick flume design method was applied to the experimental field flume data to evaluate its accuracy for predicting the experimentally observed equilibrium slopes. One deviation was made from Faddick's method in an attempt to better suit the geometry of our flume, which was the adoption of a more general form of the Froude number equation as follows (Chow 1959):

$$Fr = \frac{V}{\sqrt{gD_m}} \tag{72}$$

where D_m is the hydraulic depth (equal to the ratio of the cross sectional area of flow and the width of the fluid surface). This equation enables the Froude number to be calculated for non-rectangular cross sections, and avoids the assumption of negligible wall effects. Other assumptions that were made by Faddick have been applied here. A Manning's n value of 0.012 $s/m^{1/3}$ has been used, based on the correlation presented by Chryss et al. (2006). The fit plot of this test is presented below:

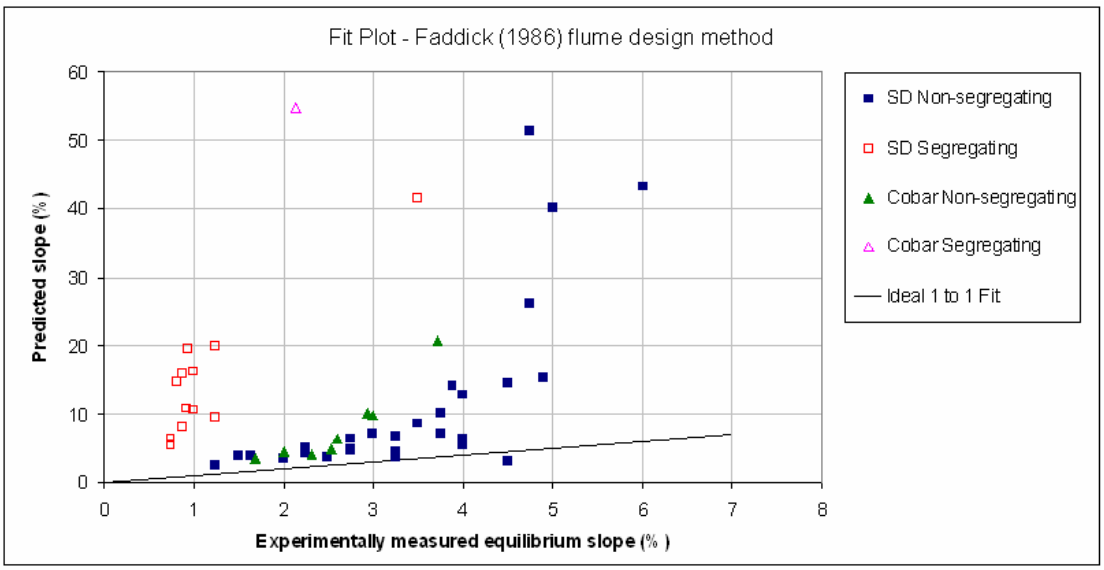

Figure 90. Fit plot of slopes predicted by the Faddick 1986 flume design method.

The fit plot shows that Faddick's design method has over-predicted the slope of the flume in almost all cases, but for some points, this over-prediction was much greater than was expected. This deviation between the predicted slope and the experimentally observed slope has been plotted against the applicable flow rate of each point to yield Figure 91, which shows a strong connection between prediction error and low flow rates. It is suspected that this is due to non-Newtonian effects that become much more apparent at low flow rates, which are not covered by the basic form of the Manning equation used here in the estimation of flow resistance. However, for large flow rates (which are generally the case in industrial flume applications), it can be said that the Faddick flume design method works quite well on the basis of the analysis presented here.

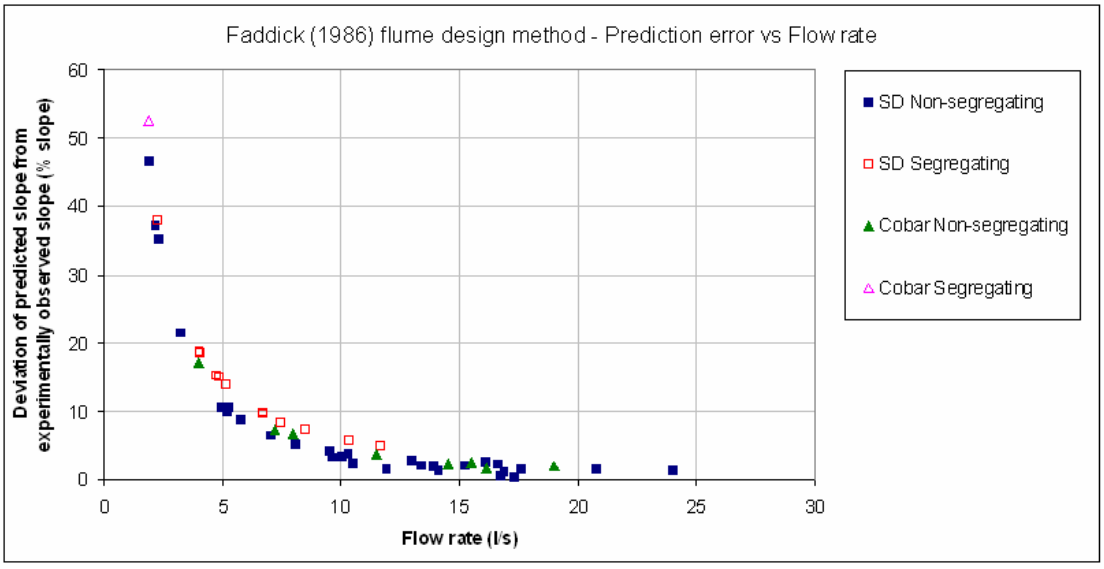

Figure 91. Plot of prediction error vs flow rate for the Faddick 1986 flume design method.

Wilson 1991 (homogeneous slurry flume design method)

Wilson (1991) presented a homogeneous slurry flume design method that was based on the design criterion of Faddick, proposing that the Froude number of the flow be equal to 1.2. The method is abbreviated to the following equation:

$$D_e = k_1 Q^{0.4} \tag{73}$$

where D_e is the equivalent diameter of the cross-section of the channel (equal to $4R_H$), and k_1 is a coefficient that is calculated by substitution of the various geometric parameters of the nominated cross-section. Wilson suggested the application of the Manning equation once again for determining the flume slope. This method was applied to the field flume data, using the originally observed flume depths as input parameters, yielding the fit plot Figure 92. It is noted that Wilson's model has under-predicted the flume slope in every case, implying that a flume designed by this method would suffer from particles depositing on its bed and ultimately causing the slurry to overflow. Also, the predicted slopes are almost the same in every case. This can be attributed to the insensitivity of the Manning equation to the viscous effects of the concentrations of the slurries tested, as well as the requirement that the Froude number be equal to 1.2 in every case. Wilson later states that this model suffers from its insensitivity to the slurry rheology, and goes on to present a rheologically active model.

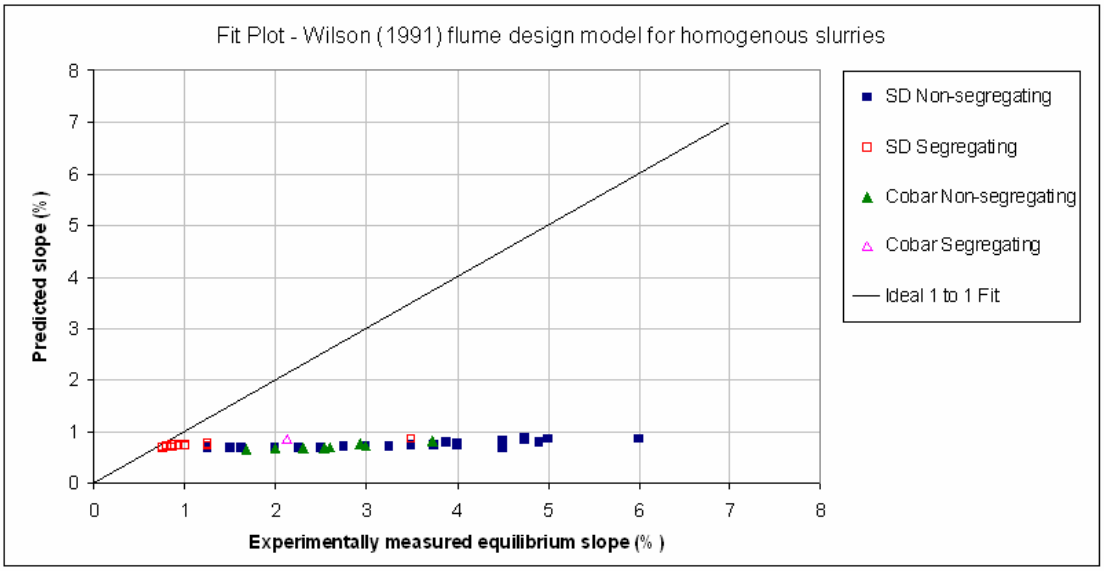

Figure 92. Fit plot of the Wilson 1991 homogeneous slurry flume design method.

Wilson 1991 (homogeneous slurry flume design method with rheological modification)

This rheologically modified flume design method essentially replaced the Manning equation with the Colebrook-White equation, which contains a viscosity term. (Wilson 1991) Once again, Wilson maintained the same Froude number design value of 1.2. The presented form of the Colebrook-White equation is as follows:

$$\frac{V}{U*} = -2.43\ln\left(\frac{e}{3.7D_e} + \frac{0.89\mu_f}{\rho_f U* D_e}\right) \qquad (74)$$

where $U*$ is the shear velocity equal to $(gR_{Hj})^{0.5}$, e is the boundary roughness (m), μ_f is the slurry viscosity and ρ_f is the slurry density. For calculating the effective viscosity, equation 61 (section 4.4.13) was used.

A fit plot of this rheologically modified flume design method is presented in Figure 93. As before, the experimentally observed depth values were used, and once again it is found that the design method under-predicts the slope of the flume.

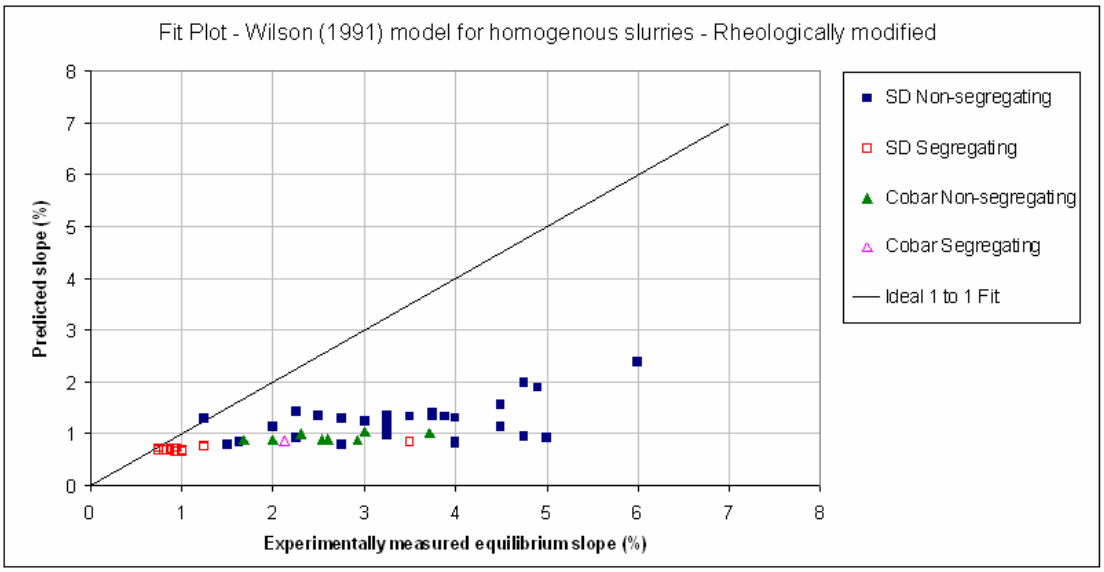

Figure 93. Fit plot of the Wilson 1991 rheologically sensitive flume design model.

Wilson (1991) also presented a coarse particles slurry flume design method, for which he defines "coarse" as being of coarse sand size and larger. The particles in the tailings slurries tested in the field flume were generally much smaller than coarse sand, so for this reason no application of Wilson's coarse particle design method is shown here.

In conclusion to this investigation of flume design methods as a means of predicting the equilibrium slope in the field flume, it has been found that none of the methods tested provided an accurate result against the experimental data, although the Faddick model predicted better against the data featuring larger flow rates. For channels carrying flows greater than 25 l/s, the results presented here would suggest that the Faddick model would predict equilibrium slopes accurately. However, the results of this exercise do not provide a reasonable model for the prediction of the flume data, so it is therefore necessary to consider another approach.

5.2.2 A sediment transport approach

The term "equilibrium slope" and its definition as described by Winterwerp et al. (1990) draws many parallels to the concept of "minimum transport" presented by several workers in the field of sediment transport. (Durand 1953; Gillies & Shook 1991; Wasp et al. 1977) In this chapter, it is postulated that the two concepts are essentially the same. This theory will be tested through the adoption of the minimum transport velocity concept as part of a channel slope model.

In a similar fashion to the flume design models considered above, this model will also be based on some well established aspects of open channel fluid dynamics and rheology. To test the proposed theory that equilibrium flow conditions in a channel are the same as the minimum transport conditions as defined in numerous sediment transport works, a minimum transport velocity equation will be used to calculate V_C, the minimum transport velocity. The trial depth will then be adjusted until the mean velocity is equal to the minimum transport velocity. Finally, a flow resistance equation will be used to determine a channel slope on the basis of this mean velocity. At this point it is asserted that an equilibrium slope is reached.

5.2.3 Selection of a flow resistance equation

There are a number of commonly used flow resistance equations available in the literature, all of which enable the prediction of the head loss of flow in open channels. It is of interest to compare these equations and determine which one best suits the prediction of head loss of tailings slurry in open channel flow. The applicable models will be tested against the experimental flume data by using them to predict the depth of flow in the flume and then comparing the predictions with the observed depth values.

Manning's equation provides the most popular means for predicting the depth of uniform flow in an open channel. Though it was developed for modelling the flow of water in an open channel, it has since been applied to other non-Newtonian fluids flowing in open channels, such in the slurry flume model proposed by Faddick. (presented in section 5.2.1) The Manning equation was been presented in section 5.2.1 as equation 58, and is restated below:

$$V = \frac{1}{n} R_H^{2/3} S_0^{1/2} \tag{75}$$

where V is the mean velocity of the flow, n is the empirical Manning roughness coefficient, R_H is the hydraulic radius of the channel (equal to the ratio of the cross-sectional area of flow and the wetted cross-sectional perimeter), and S is slope of the hydraulic gradeline (which runs parallel to the bed slope during uniform flow). Of particular interest here is the Manning roughness coefficient, which is a purely empirical number that accounts for the friction losses incurred by the channel boundaries. Manning's equation is simple to use, but is dependant on the accuracy of the empirical roughness coefficient, n. Much research has been done to present values of n for commonly encountered channel boundaries such as concrete or grass lined channels, but these published values for n are only suited to water in open channels.

Experimental work by Strickler in the 1920's led to a modified form of the Manning equation that enabled the determination of n for flows with granular beds. Strickler's 1923 equation appears as follows (Morris 2006):

$$n = \frac{1}{A} d_{50}^{1/6} \qquad (76)$$

Where A is a dimensional coefficient equal to 21.1 $m^{1/2}/s$, and d_{50} is the median particle diameter of the grains forming the channel bed. If the slurry particle median diameter from the field flume experiments is used for this term, the following fit plot is generated when using equations 75 and 76 to predict the depths observed in the field flume:

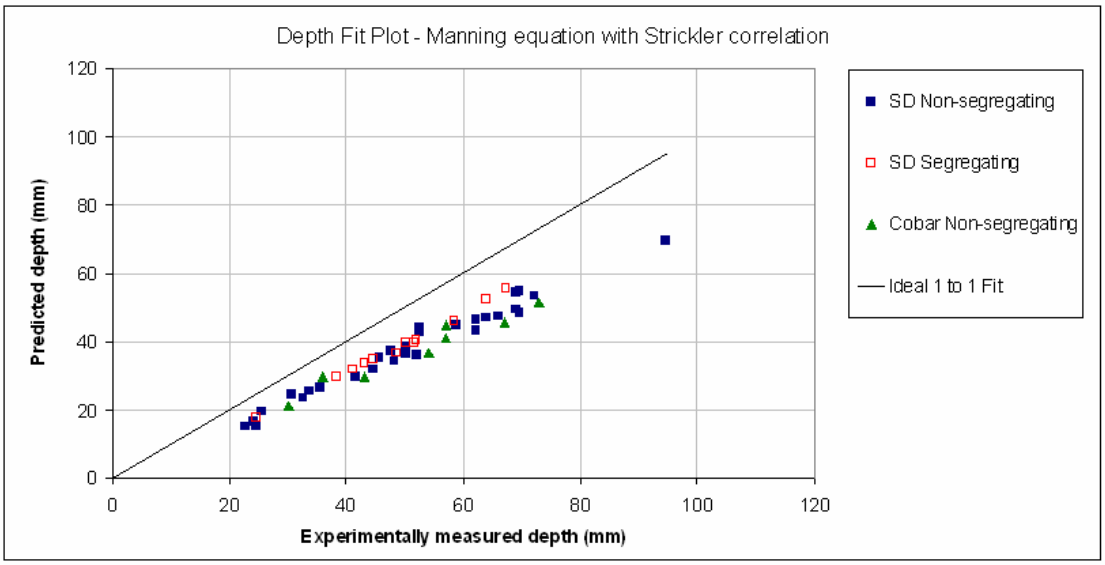

Figure 94. Depth prediction fit plot of the Manning equation with the Strickler 1923 correlation

In 1946 Lacey proposed an empirical value of 11.8 $m^{1/2}/s$ for the A term in the Manning-Strickler equation to predict the head losses of "Lacey regime flows", defined as flows in which no long term scour or deposition takes place. (Morris 2006) A fit plot using this A value follows:

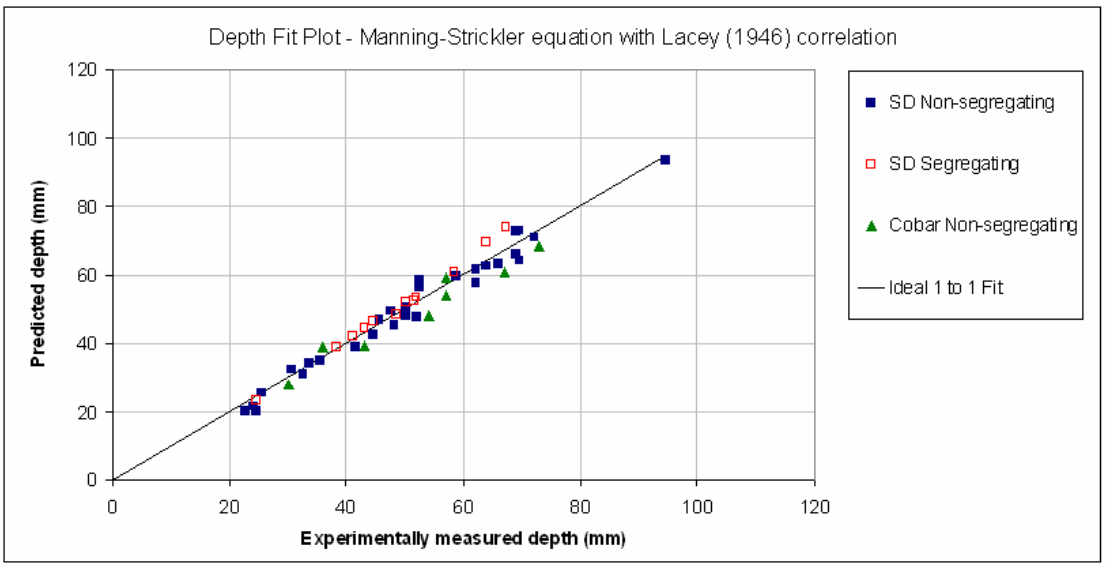

Figure 95. Depth prediction fit plot of the Manning-Strickler equation with the Lacey 1946 correlation

It is evident from Figure 95 that the Manning-Strickler equation with the Lacey correlation fits the flume data very well. This suggests that "Lacey regime flows" and their definition would coincide with the concept of equilibrium slopes that was presented by Winterwerp et al. (1990)

Morris presented another correlation for flows in self-formed channels on tailings beaches, where the d_{50} value used was the median particle diameter in the slurry and not the bed. His correlation returned an A value of 4.7 $m^{1/2}/s$. (Morris 2006) A fit plot of the Morris correlation follows:

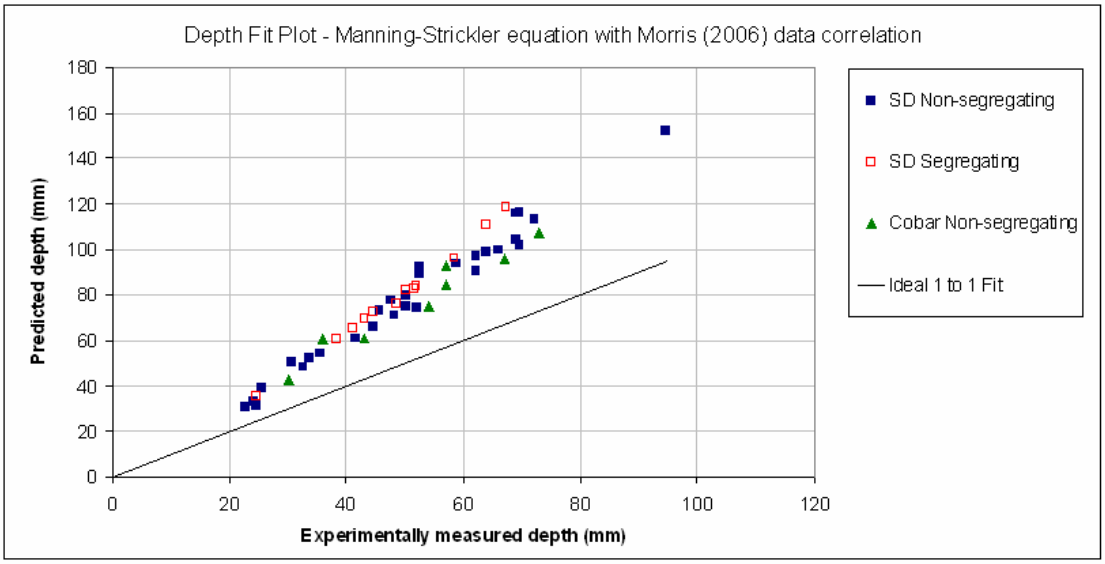

Figure 96. Depth prediction fit plot of the Manning-Strickler equation with the Morris 2006 correlation

Morris then proposed a new equation for predicting the value of A, based on a correlation to the gravimetric solids concentration of the particles in the fluid, C_W, which is as follows (Morris 2006):

$$A = 3.950 + 18.08\exp(-17.91C_W) \quad (77)$$

A fit plot arising from the application of Morris' model is presented below:

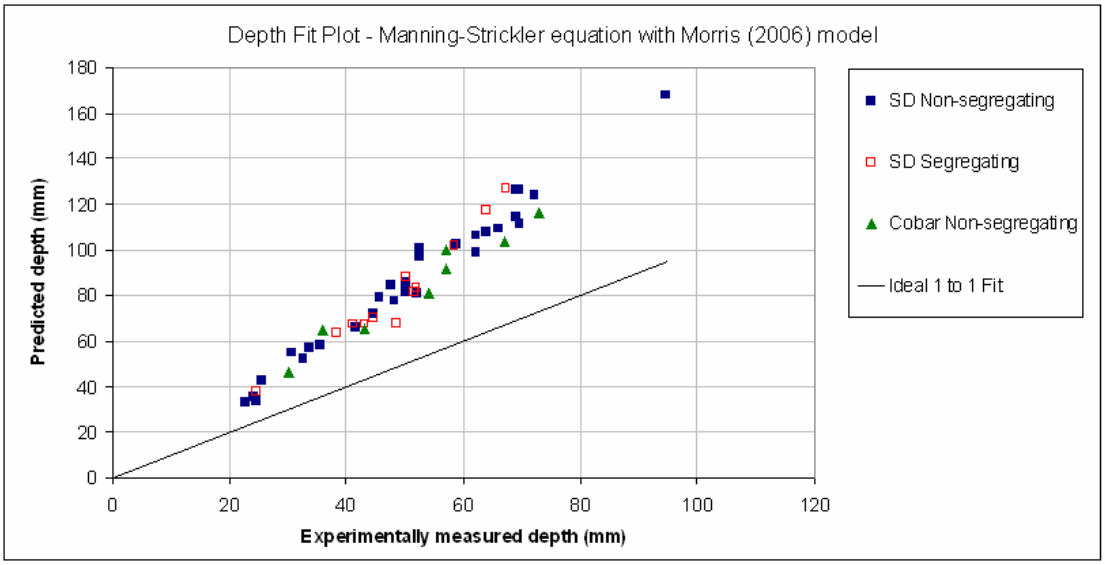

Figure 97. Depth prediction fit plot of the Manning-Strickler equation with the Morris 2006 concentration correlation

Figures 96 and 97 show that Morris' experimentally derived correlations do not fit the field flume data as well as Lacey's correlation (in Figure 95), even though Morris' experimental work was specifically focused on tailings slurries, where Lacey's was not.

The Chezy equation provides another open channel friction loss model (Chadwick et al. 2004):

$$V = C\sqrt{R_H S_0} \quad (78)$$

where C is the Chezy friction factor. The Chezy equation is very similar to the Manning equation, with the only real difference being the power of ½ being applied to the hydraulic radius, R_H, instead of the 2/3 featured in Manning's equation. As a result, the Chezy roughness coefficient, C, can be related to

Manning's n with the following equation, which is derived by equating the Manning and Chezy equations:

$$C = \frac{R_H^{1/6}}{n} \tag{79}$$

Due to this similarity of the Chezy and Manning equations, the Chezy equation has largely fallen into disuse in favour of the more popular Manning equation.

The Darcy-Weisbach equation was developed for determining the head loss in pipe flow, but can be readily adapted to open channel calculations. Unlike the Manning and Chezy equations, the Darcy-Weisbach equation is theoretically derived from first principles. It applies to both turbulent and laminar flow conditions. The common form of the Darcy-Weisbach equation is as follows (Douglas et al. 1983):

$$h_f = f_D \cdot \frac{L}{D} \cdot \frac{V^2}{2g} \tag{80}$$

where h_f is the head loss in a pipe of length L and diameter D. V is the mean velocity of flow, g is the acceleration due to gravity and f_D is defined as the Darcy friction factor. This is the pipe flow form of the equation, but it can be adapted to open channel flow using the following geometric relationship (Chadwick et al. 2004):

$$D = 4R_H \tag{81}$$

Another equation that further simplifies the application of the Darcy-Weisbach equation to open channel flow is the geometric relationship (Chadwick et al. 2004):

$$S_0 = \frac{h_f}{L} \tag{82}$$

Equations 80, 81 and 82 can be combined to yield the following open channel form of the Darcy-Weisbach equation:

$$f_D = \frac{8gR_H S_0}{V^2} \tag{83}$$

Like its Manning and Chezy counterparts, the head loss predictions of the Darcy-Weisbach equation are also affected by the value chosen for the friction factor. It is noted that the Darcy friction factor, f_D, is the only non-dimensional one of the three. A significant amount of experimental research has been done in an effort to predict the value of f_D, n or C for various scenarios; the most relevant of all of the various research studies was that done by Nikuradse in the early 1930's, in which he conducted pipe flow experiments with the inside surface of the pipe coated with sand grains of a uniform diameter, k_s. He discovered that the pressure loss in a pipe was not affected by the roughness of the pipe at relatively low pressure gradients, despite the flow being fully turbulent. Conversely, he also discovered that the viscosity of the fluid had no effect when the pressure gradient was very high, but in between these two extremes, he found that the viscosity and the roughness both had an effect on the friction losses in the pipe. In the mid 1930's Colebrook and White further investigated the findings of Nikuradse. In 1937 they presented a paper in which they combined the two correlations observed by Nikuradse, thereby introducing the empirical Colebrook-White equation for enabling the determination of an f_D value for a given turbulent flow of a Newtonian fluid in a pipe (Colebrook & White 1937). Colebrook and White then presented some typical k_s values for commonly used pipe materials. Various other workers have since published more k_s values for other surfaces (Abulnaga 2002).

The common pipe flow form of the Colebrook-White equation is shown below (Chadwick et al. 2004):

$$\frac{1}{\sqrt{f_D}} = -2\log_{10}\left[\frac{k_s}{3.7D} + \frac{2.51}{\mathrm{Re}\sqrt{f_D}}\right] \tag{84}$$

It can be seen that this equation is implicit of f_D, and so is not simple to apply. It can be used iteratively to determine an f_D value that will be accurate to a few decimal places after 4 or 5 iterations, but to do

this manually is a tedious process. For this reason, the Colebrook-White equation is often applied in a chart form in the popular Moody diagram, which enables the determination of a value for f_D for a pipe if the pipe roughness, k_s, and the Reynolds number, Re, are known. For pipe flow calculations the Moody diagram is very popular and convenient. However, with the recent widespread use of computers, the iterative work involved in calculating a value of f_D can be easily managed.

The Colebrook-White equation can be applied to open channel flow using the conversion (equation 69), which gives the following (Yen 2002):

$$\frac{1}{\sqrt{f_D}} = -2\log_{10}\left[\frac{k_s}{14.8R_H} + \frac{2.51}{\mathrm{Re}\sqrt{f_D}}\right] \tag{85}$$

For Newtonian fluids in open channel flow, the Reynolds number is calculated by (Haldenwang 2003):

$$\mathrm{Re} = \frac{4\rho V R_H}{\mu} \tag{86}$$

where μ is the viscosity of the fluid. For non-Newtonian fluids in open channel flow, Haldenwang et al. (2002) presented the following equation for calculating the Reynolds number, with the rheological properties of the fluid expressed in terms of the three Herschel-Bulkley fitting parameters τ_y, K and n:

$$\mathrm{Re}_{HB} = \frac{8\rho V^2}{\tau_y + K\left[\frac{2V}{R_H}\right]^n} \tag{87}$$

It can be seen that equation 87 can easily be derived with the substitution of equation 61 into equation 86, which is how Haldenwang et al. generated it.

Of key interest in this work is the k_s parameter from the Colebrook-White equation, which represents the roughness of the pipe or channel walls (expressed in meters). In Nikuradse's experiments the k_s

values were defined by the diameter of the sand glued to the pipes. Further research was done by Colebrook & White (1937) and others in defining k_s values for pipes and channels made of specific materials such as steel and concrete pipes (Abulnaga 2002). However, in a self formed open channel that has been eroded into a deposit of tailings, the roughness of the channel boundaries must be defined by the size of the grains in the underlying bed material. Ikeda et al. (1988) presented an approximation for k_s being equal to 1.5 x d_{90}. Abulnaga (2000) states that k_s in an open channel "is often taken to be equal to twice the grain diameter", but then goes on to say that there is very little published to support this. In this work with slurries of non-uniform grain size, the following six values were tested for k_s in this apparent absence of a generally accepted convention:

- d_{50}
- 2 x d_{50}
- d_{85}
- 2 x d_{85}
- 1.5 x d_{90}
- 2 x d_{90}

All six of the tested k_s values were found to generate good depth predictions upon comparison with the flume data, though the 2 x d_{90} option yielded the best predictions. The fit plot generated using k_s = 2 x d_{90} has been presented here as Figure 98, while the fit plot for $k_s = d_{50}$ has been presented as Figure 99 to show the relative difference between the best and worst performing of these values.

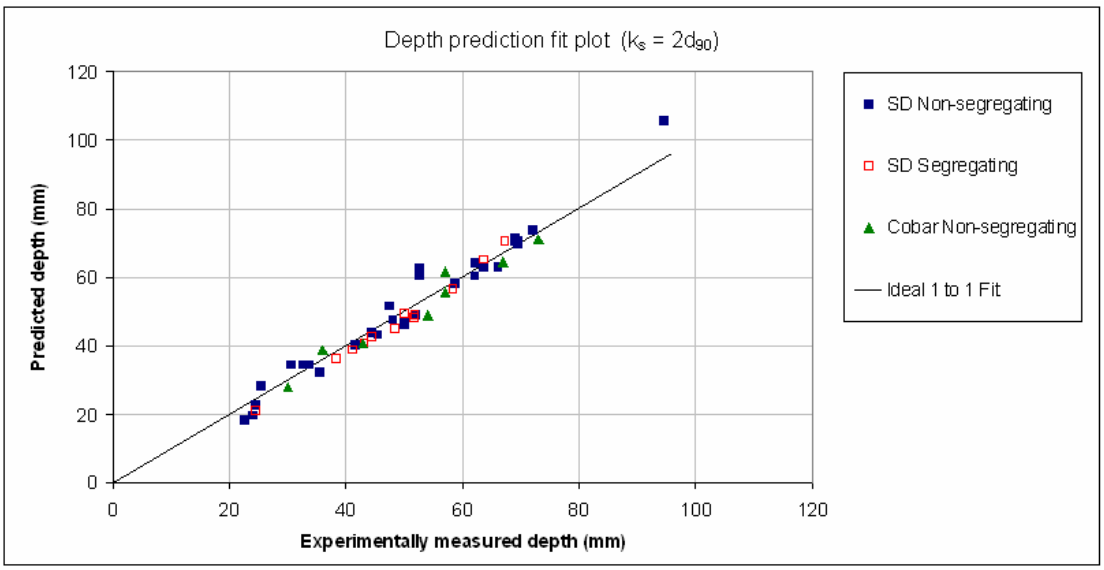

Figure 98. Depth prediction fit plot with k_s equal to $2d_{90}$

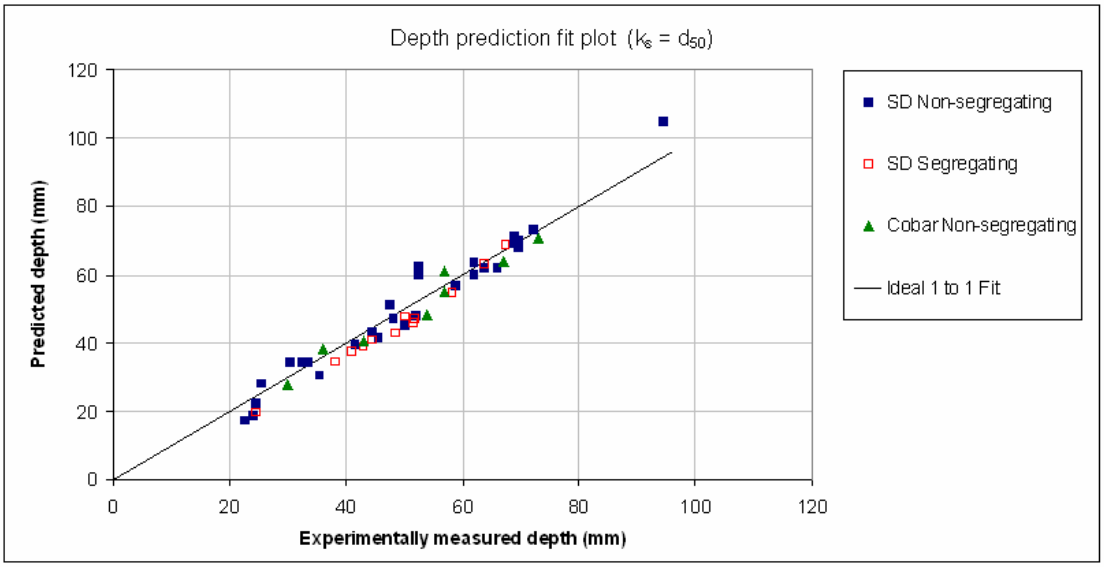

Figure 99. Depth prediction fit plot with k_s equal to d_{50}

Figures 98 and 99 demonstrate that the Colebrook-White equation, though empirically developed for pipe flows, works very well for open channel flows as well.

The statistical comparison of the predicted depth values against the experimentally measured depth values for each flow regime is presented in Table 9, with the mean absolute deviation for each group of data presented as the descriptive statistic of the quality of the prediction.

k_s value used	Mean absolute deviation (expressed in mm)				
	Sunrise Dam		Cobar	Non-seg.	Overall
	Non-seg.	Seg.	Non-seg.	Overall	
d50	3.3	3.7	3.0	3.3	3.4
2 x d50	3.3	3.6	3.0	3.2	3.3
d85	3.2	3.0	2.9	3.1	3.1
2 x d85	3.1	2.6	2.6	3.0	2.9
1.5 x d90 (Ikeda et al 1988)	3.1	2.7	2.6	3.0	2.9
2 x d90	3.0	2.5	2.8	3.0	2.9

Figures indicate the mean absolute deviation between the experimentally measured depth and the predicted depth (mm)

Table 9. Comparison of the accuracy of depth predictions using different k_s values in the Colebrook-White equation

This exercise has demonstrated that all of the six proposed k_s values will enable a good depth prediction, indicating that the Colebrook-White equation is robust in relation to the k_s value, and will competently predict the Darcy friction factor for the turbulent flow of slurries with such fine particles. This finding would suggest that the Colebrook-White equation is insensitive to such small k_s values as those tested here, but this insensitivity only occurs with relatively viscous fluids when the Reynolds number of the flow is in the transition turbulent region, such as in the non-segregating flows observed in the field flume. In such flows the k_s /(14.8R_H) roughness term in the Colebrook-White equation is about 30 to 300 times larger than the 2.51/(Re$\sqrt{f_D}$) viscous term, depending on the k_s value used. However, when segregating slurries were run in the field flume, the Colebrook-White equation was more sensitive to the bed roughness. Such slurries had lower viscosities and higher Reynolds numbers, causing the ratio of the roughness term to the viscous term in the Colebrook-White equation to drop to a range of 1.5 to 20, depending on the k_s value used. This finding relates closely to the observations of Nikuradse (discussed above). For the segregating flows it was found that this flow resistance model under-predicted the depth when smaller values of k_s were used. This would suggest that the channel boundaries are lined with larger particles in the case of segregating slurries, which would make sense on the basis that segregating slurries drop large particles preferentially, whilst non-segregating slurry particles tend to settle indiscriminately of their size. This reflects the experimental observations, as well as the findings of several others who noted that the large particles settle first in segregating slurries (Blight 1994; Fan & Masliyah 1990).

The Colebrook-White equation is used to calculate the Darcy friction factor for turbulent fluids in a pipe or channel, but it is not applicable to laminar flows. The equation for calculating the Darcy

friction factor for laminar flows follows, which is reduced from equating the Darcy-Weisbach equation with the theoretically derived Hagen-Poiseuille laminar equation (Chadwick et al. 2004):

$$f_D = \frac{64}{\mathrm{Re}} \tag{88}$$

A significant problem encountered in open channel flows is in defining the point of transition between laminar and turbulent flows. Much confusion exists over the transition point in channel flows, with many workers defining it as the Reynolds number value of 2000, which is the generally accepted transition figure for pipe flows, while some others define it at other Reynolds numbers of 500, 1000 or 2100. (Lowe 2003) Deeper analysis of the issue has found that the transition point in channels occurs at different Reynolds numbers, depending on the rheology of the fluid and other factors. (Haldenwang et al. 2002) A method for predicting the point of transition in open channels was presented by Haldenwang, which contained a group of empirical equations that were calibrated on experimental flume data gathered by the author. (Haldenwang 2003) The application of this method was quite complex. In this work a new simple method of predicting the point of transition in an open channel is presented.

5.2.4 A new method for predicting laminar/turbulent transition in open channels

An new method is presented here for predicting the point of laminar/turbulent transition in an open channel that can be applied to all fluids, both Newtonian and non-Newtonian. This method utilises the Hagen-Poiseuille equation (equation 88) and the Colebrook-White equation (equation 85). It is necessary to know the fluid rheology, density and flow rate, as well as the channel slope, geometry and roughness. The method is described in the following steps:

1. Guess an initial value of the depth in the channel

2. Calculate the cross sectional area of flow, A, and the wetted perimeter, P, as a function of the geometry of the flume channel

3. Calculate R_H, the ratio of A/P

4. Calculate V, the average velocity in the channel (equal to Q/A)

5. Calculate the Reynolds number for the flow using equation (equation 87)

6. Calculate f_D using the Hagen-Poiseuille equation (equation 88)

7. Calculate f_D using the Colebrook-White channel flow equation (equation 85)

8. Adjust the initially guessed depth value until the two values for f_D calculated in steps 6 and 7 equate. This is the point of laminar/turbulent transition.

A transition point between transition-turbulent and fully turbulent flow has also been proposed previously (Haldenwang 2003), but such a point is not defined here, because the empirical Colebrook-White equation used here is effective in calculating the Darcy friction factor over both the transition-turbulent and fully turbulent regions, thereby alleviating the need to consider this extra complication.

5.2.5 Identifying the state of flow in open channels

A closely related subject to the prediction of laminar/turbulent transition in open channels is the identification of the state of flow in an open channel (ie. whether the flow is laminar or turbulent). The conventional approach to determining the state of flow is to calculate the Reynold's number for the flow and then declare the flow to be laminar if the Reynolds number is below the point of transition, or turbulent if the Reynolds number is above the transition point.

From the work presented in section 5.2.4, the act of identifying the state of flow can be undertaken in a more direct way: Calculate f_D using the Hagen-Poiseuille equation (equation 88), and then calculate f_D using the Colebrook-White equation (equation 85). If the Hagen-Poiseuille equation calculates a bigger f_D value than the Colebrook-White equation, the flow is laminar. If the Colebrook-White equation calculates a bigger f_D value than the Hagen-Poiseuille equation, the flow is turbulent.

The work presented here in sections 5.2.4 and 5.2.5 is unproven, so some effort is made here to provide it with some scientific validation. This will be done by applying the method of flow state identification

in predicting the depth of flow in open channels for a range of experimentally measured channel flow data. Four independently collected sets of data have been run through this depth prediction method:

1. The first data set will be the field flume data that is presented in Appendix A, which contains a total of 49 points of data.

2. The second data set, containing 623 data points, was presented by Haldenwang (2003). He used 3 tilting flumes of rectangular cross section, with respective widths of 75 mm, 150 mm and 300 mm. With slopes varying from 0.01 to 0.05, he ran 4 different non-Newtonian fluids in his flumes:

- Kaolin slurry with volumetric concentrations ranging from 3% to 10% (240 points)
- Bentonite slurry of 3% and 6% concentration by volume (117 points)
- CMC solution volumetric concentrations ranging from 1% to 3.8% (232 points)
- Carbopol solution of 1% concentration by volume (34 points)

Haldenwang's apparatus was fitted with an in-line tube viscometer for measuring the rheological parameters of each fluid at the same time that the fluid was circulated through his flume. The flume was also fitted with digital depth gauges for measuring the fluid depth accurately.

3. The third data set, containing only 9 data points, was reported by Seckin et al. (2006) This data was collected in a 22 metre long tilted rectangular flume with a width of 398 mm. All 9 runs were done with water, with the flume fixed at a slope of 2.024×10^{-3}.

4. The fourth data set, containing 95 data points, will be the small scale laboratory flume data that was presented in Appendix H. This data set contains Carbopol and CMC solutions of various concentrations (described rheologically in section 3.4.7) and water.

The depth of flow for each of these experimentally measured flows will be predicted using the measured slopes, flow rates, rheology, and density data reported in their respective source literature. The roughness value (k_s) of all four channels was assumed to be 50 μm, which is deemed to be a reasonable estimate of the roughness of a laboratory flume, though values of 5 μm and 500 μm were also tested and found to have very little effect. The most sensitive data to this change in the k_s values was the Seckin data, which had much higher Reynolds numbers than the other data. When k_s was

assumed to be 50 μm, the mean absolute error in the depth prediction for the Seckin data set was equal to 0.7 mm. When k_s was changed to 5 μm, the mean absolute error went up to 1.5 mm, while a k_s value of 500 μm resulted in a mean absolute error of 4.8 mm. This depth plot is presented below as Figure 100.

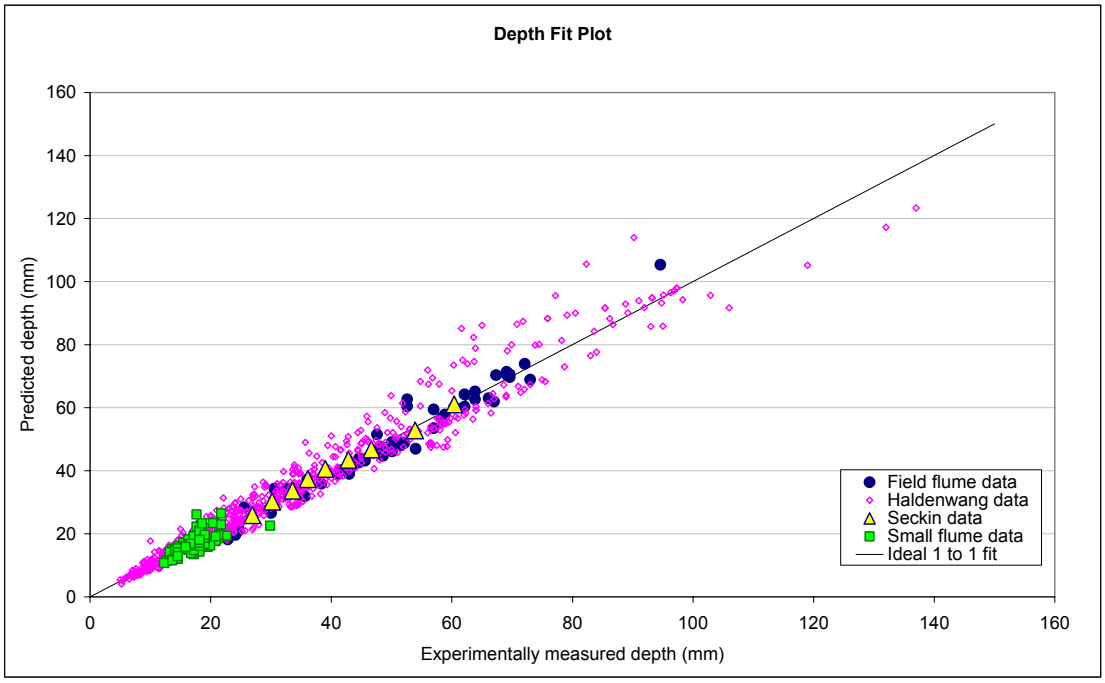

Figure 100. Fit plot featuring 776 points from 4 experimental data sets.

Figure 100 shows that this new method of identifying the state of flow is effective for non-Newtonian fluids and slurries over a wide range of channel geometries, flow rates and concentrations (including clear water flows), since the depth predictions for some 776 open channel flows shows good accuracy compared to the measured depths. In terms of Reynolds number values, 378 of the Haldenwang points were found to be flowing in the laminar regime, with the corresponding Reynolds numbers for these points ranging from 0.06 to 1002. The remaining 245 points from Haldenwang's data set were found to be in the transition and turbulent regimes, with corresponding Reynolds numbers ranging from 996 to 124000. The maximum laminar Reynolds number of 1002 and the minimum transition Reynolds number of 996 are both reasonable values in relation to those reported in the literature. (Haldenwang 2003; Lowe 2003) Further evidence of the correct identification of the flow state is provided by the accuracy of the depth predictions presented in Figure 100. If the laminar Hagen-Poiseuille equation was applied to a flow that was fully turbulent, the predicted depth would be much lower than the

observed depth. Conversely, if the Colebrook-White equation was applied to predict the depth in a laminar flow, the predicted depth would be greater that the observed depth. The predicted depths presented in Figure 100 all show a strong semblance to the measured depths, which proves that the state of flow identification method presented here works well.

The work presented here demonstrates that an open channel flow resistance model based on the Darcy-Weisbach / Colebrook-White / Haldenwang-Slatter equations presents some excellent advantages over the other models tested here. Its ability to handle non-Newtonian fluids with its rheologically descriptive Reynolds number is the main advantage, which suggests that the model would have uses in predicting head losses for a much broader range of applications, such as sludge flow, processing of food products or other viscous liquids in open channels. The other advantage of this model is its ability to model granular boundaries, representing potential applications in the modelling of alluvial channels, mudflows and hydraulic land reclamation operations.

The Manning-Strickler equation with the Lacey correlation also presented excellent depth predictions, and it enjoyed the advantage of being relatively easy to apply. The basis upon which Lacey generated his correlation is also of significant interest to this work, as it would appear that the definition of a Lacey flow regime coincides with that of the equilibrium flows, which is of prime interest in this study. However, the Lacey approach is not explicitly rheologically sensitive by way of its lack of any viscosity or rheological input parameters, which is a disadvantage in the current context.

On this basis, the Darcy-Weisbach / Colebrook-White / Haldenwang-Slatter open channel flow resistance model with a k_s value of 2 x d_{90} has been adopted for estimating head losses for the remainder of this work.

5.2.6 Selection of a minimum transport velocity equation

From numerous experimental studies into the transport of sediments in turbulent flows, there are many equations presented in the literature that enable the prediction of the minimum mean velocity required

to keep particles in suspension in a pipe, but not so many are presented for channel flows. This particular velocity appears in the literature under several names, with the most common ones being "minimum transport velocity", "deposition velocity" and the "critical velocity".

In order to test each of these minimum transport velocity equations an iterative method was adopted to arrive at a channel depth that produces a channel velocity that is equal to the minimum transport velocity as calculated by the respective minimum transport velocity equation from the literature. The Darcy-Weisbach / Colebrook White / Haldenwang-Slatter flow resistance model was then used to calculate the slope of the channel, which would effectively become the predicted equilibrium slope.

Some 18 minimum transport velocity models from the literature were tested in this work, but only those that yielded reasonable predictions are presented here. All of the minimum transport velocity models (except for one) have been formulated for application to pipe flow, so wherever this has been the case, the geometric conversion equation (equation 81) has been applied to allow the equation to be applied to open channel flow situations. The testing of these models is based on predicting the equilibrium slope of the slurry flows observed in the field flume and the small laboratory flume, with the experimental data used to evaluate the accuracy of each prediction. The open channel model is presented first, followed by the adapted pipe flow models, which are presented in alphabetical order.

Dominguez et al. (1996)

The Dominguez et al. (1996) equation is the only minimum transport velocity equation found in the literature that was specifically developed for open channel flows. It appears as:

$$V_C = 1.833\left[\frac{8gR_H(\rho_s - \rho_m)}{\rho_m}\right]^{1/2}\left(\frac{d_{85}}{R_H}\right)^{0.158} \qquad (89)$$

where R_H is the hydraulic radius of an open channel flow, d_{85} is the diameter of the 85th percentile particle, ρ_s is the density of the particles and ρ_m is the density of the mixture. This equation was

experimentally calibrated using slurries with concentrations ranging from 20% to 50% by weight, mean particle diameters ranging from 30 to 400 micron, solids densities ranging from 2000 to 36,500 kg/m3 and flow rates ranging from 40 to 100 l/s. These data ranges are comparable to those used in the field flume experiments, though the median particle diameters and flow rates used by Dominguez et al. are about double those used in the field flume. The range of flow rates is well beyond those tested in the small scale flume.

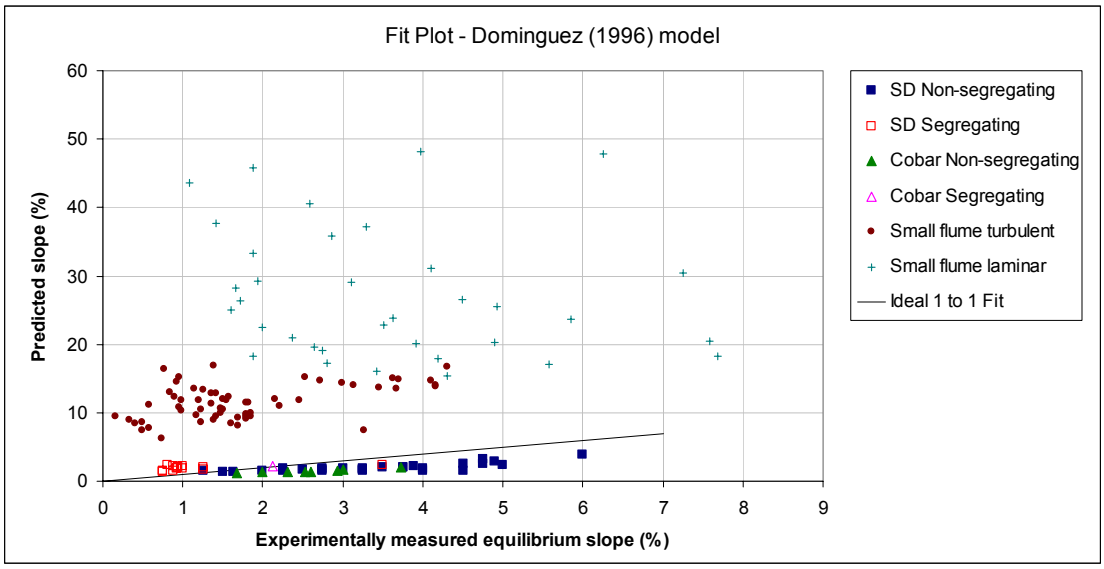

Figure 101. Fit plot of the Dominguez et al. (1996) model

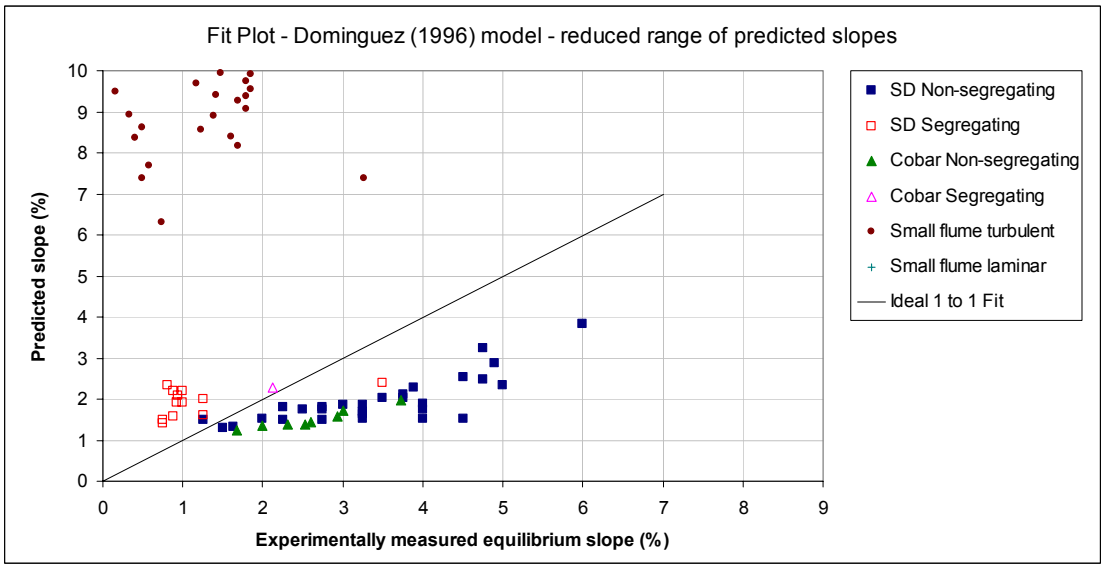

Figure 102. Fit plot of the Dominguez et al. (1996) model, with the range of predicted slopes reduced to improve the clarity of the field flume data in the ideal fit region

Figures 101 and 102 show that the Dominguez et al. model predicted very poorly against the small flume data, nor that it did not predict the slopes in the field flume very well. It was found that the predictions against the field flume data improved when larger flow rates were considered. This trend has been presented in Figure 103.

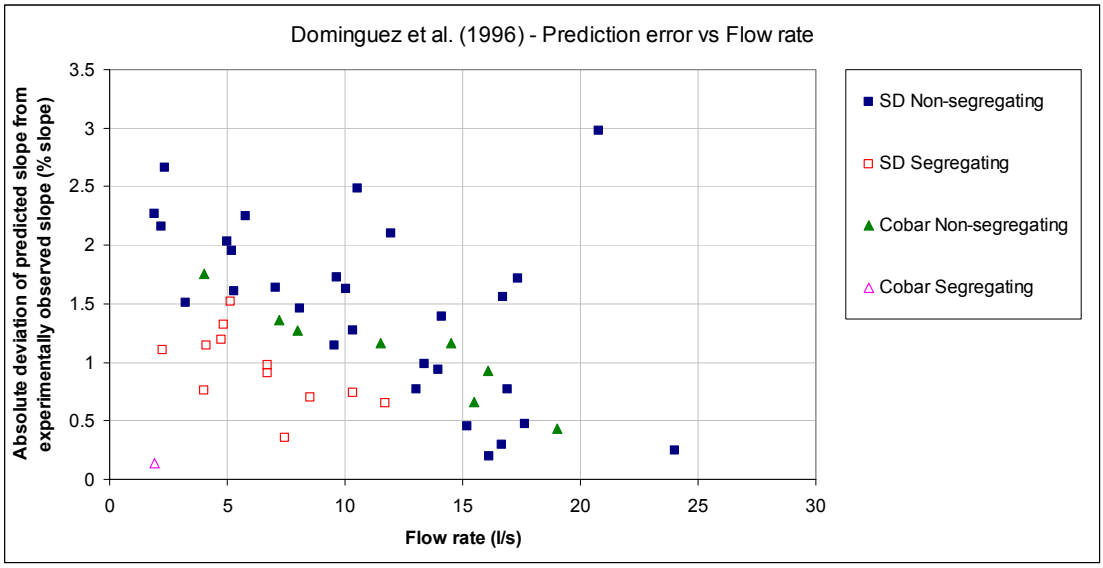

Figure 103. Plot of flow rate against the absolute deviation between the slopes predicted with the Dominguez model and the experimentally observed slopes.

Figure 103 indicates that the Dominguez et al. model predicted better against the larger flow rates observed in the field flume than it did against the low flow rates, thereby suggesting that the Dominguez et al. model would be effective for flow rates larger than 30 l/s.

Durand 1953 with the Wilson and Judge (1976) correlation

The Durand (1953) equation with the Wilson and Judge (1976) correlation appears as follows (Gillies et al. 2000):

$$V_C = 2.0 + 0.3\log_{10}((d/D)C_D)\sqrt{2gD(s-1)} \qquad (90)$$

where d is the diameter of the particle, D is the pipe diameter, C_D is the particle drag coefficient and s is the ratio of the particle density to the fluid density.

Two methods were employed in applying this equation. In the first the particle drag coefficient (C_D) was calculated using the following form of the drag equation (Baker & Jacobs 1979):

$$C_D = (4/3)dg(s-1)/V_S^{\,2} \qquad (91)$$

where V_S is the settling velocity of a single particle in the carrier fluid. V_S was determined experimentally (see sections 3.3.15 and 3.4.6), and found to be 0.028 m/s for a coarse Cobar slurry particle, 0.04 m/s for a "fine" glass particle and 0.1 m/s for a "coarse" glass particle (the latter two used in the small scale flume). For the tailings particle, the method used to select a slurry particle for the settling test was based on diluting the slurry and pouring off the light fraction, leaving the coarser particles behind. One of the coarse particles was then used in the settling tests. The particle diameter was assumed to be equal to the measured d_{85} value of 51 μm (see section 3.3.12 for particle sizing). For the glass particles, the d_{50} value was assumed to be the applicable particle size for each of the two populations, yielding 335 μm for the "fine" particle and 1400 μm for the "coarse" particle. (see section 3.4.5 for particle sizing) These values were used in equation 91 to calculate drag coefficients of 1.5 for the Cobar particle (which was adopted for both of the tailings slurries), 4.5 for the "fine" glass particle and 3.0 for the "coarse" particle. The fit plot generated by the Durand-Wilson-Judge model is presented below in Figures 104 and 105.

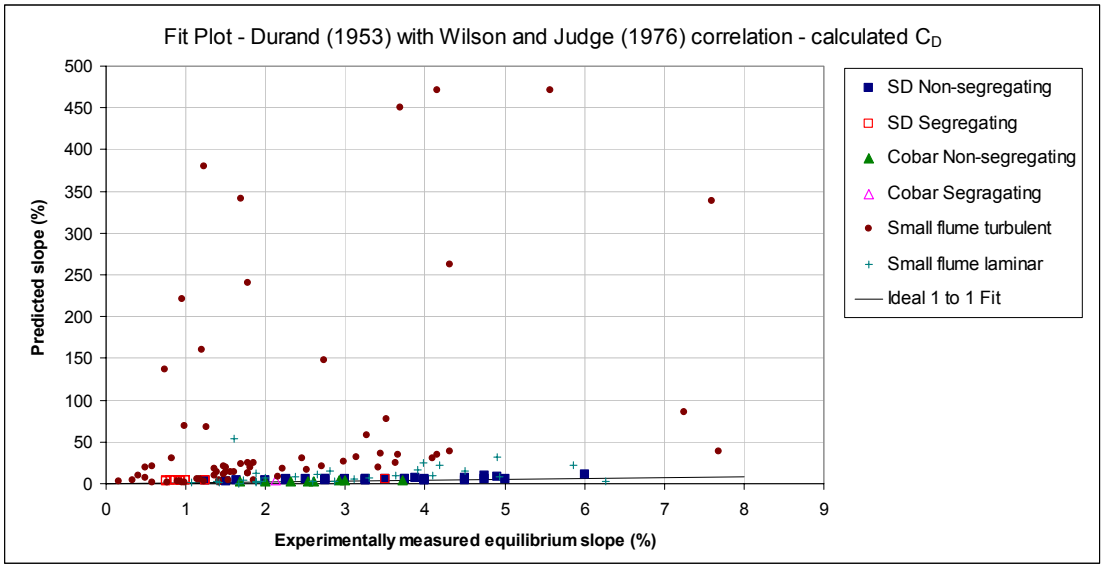

Figure 104. Fit plot of the Durand (1953) equation with the Wilson and Judge (1976) correlation, with a calculated particle drag coefficient

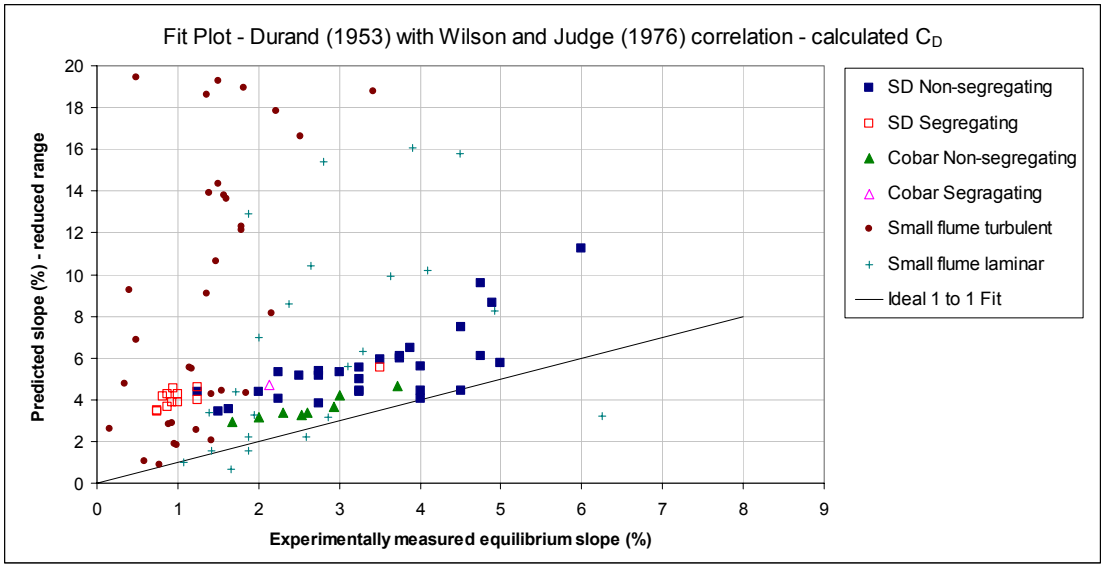

Figure 105. Fit plot of the Durand (1953) equation with the Wilson and Judge (1976) correlation, with a calculated particle drag coefficient. Vertical axis reduced for clarity in the ideal fit region.

Figures 104 and 105 show that the Durand model with the Wilson and Judge correlation has over-predicted most of the slopes observed in the two flumes. The predictions for the small flume data are particularly poor. In the case of the field flume data, it is thought that the over-prediction is due to the calculated value of the drag coefficient being too high, because it has been suggested that a value of 0.45 is more typical for a sediment particle such as those found in mineral slurries. (Ishii & Zuber 1979; Walton 1995). Due to the discrepancy between the calculated drag coefficient and those values cited in the literature, it was decided to try the same Durand-Wilson-Judge model, except with an assumed drag coefficient of 0.45 instead of the calculated one. The fit plot from this exercise is presented below as Figures 106 and 107:

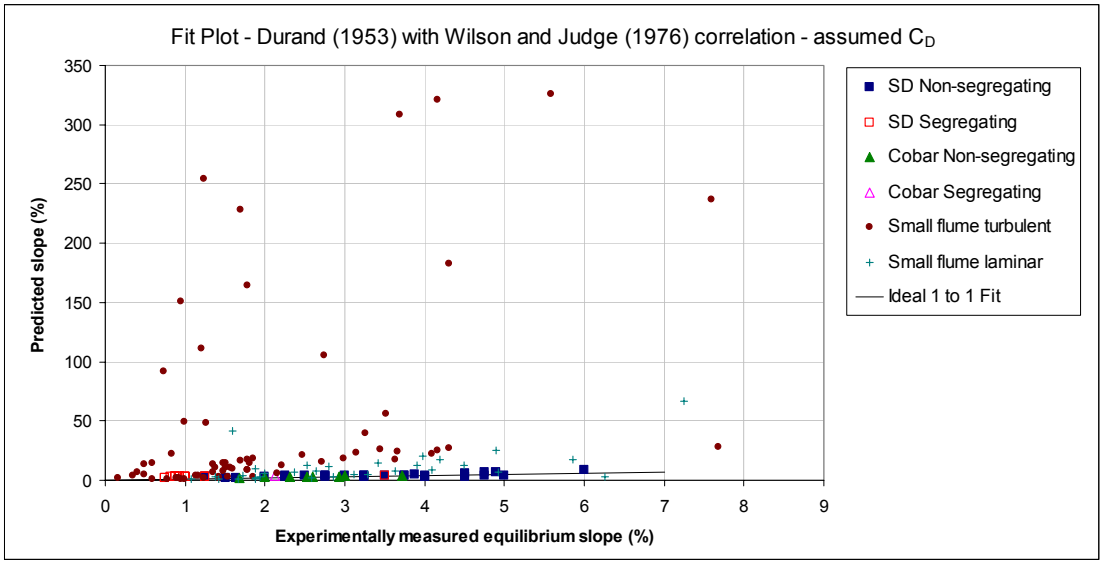

Figure 106. Fit plot of the Durand (1953) equation with the Wilson and Judge (1976) correlation, assuming a particle drag coefficient of 0.45

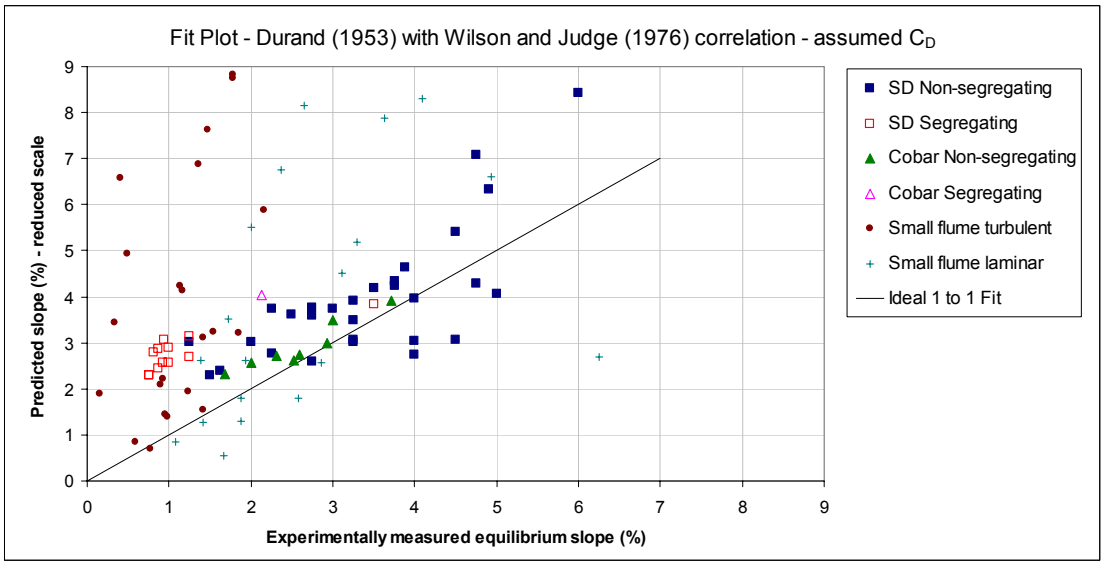

Figure 107. Fit plot of the Durand (1953) equation with the Wilson and Judge (1976) correlation, assuming a particle drag coefficient of 0.45. The vertical scale has been reduced for clarity in the ideal fit region.

For the field flume data, Figures 106 and 107 with the assumed drag coefficient show better predictions than Figures 104 and 105 with the calculated drag coefficient. This would suggest that the calculated drag coefficient of 1.5 is too high. It is thought that the reason for this is the assumed diameter of the particle used in the unhindered settling tests. If the assumed diameter of the selected particle had been 15 μm in diameter, the calculated drag coefficient would have been 0.45. This uncertainty suggests that an accurate method of sizing the individual particle is required if an unhindered particle settling

test is to be used to calculate a drag coefficient. For the small flume data, the predictions are still uselessly large.

Oroskar & Turian (1980)

Oroskar & Turian (1980) developed a theoretical transport velocity equation that was based on a turbulent energy dissipation approach. It appears as follows:

$$V_C = \sqrt{gd(s-1)}\left\{5C_V(1-C_V)^{2n-1}\left(\frac{D}{d}\right)\left(\frac{D\rho_l\sqrt{gd(s-1)}}{\mu}\right)^{1/8}/x\right\}^{8/15} \quad (92)$$

where C_V is the volume fraction of solids, n is the hindered settling exponent (which is a function of the particle Reynolds number), ρ_l is the density of the carrier fluid, x is the fraction of eddies with a vertical velocity component greater than the hindered settling velocity of the particles, and μ is the viscosity of the carrier fluid.

In Oroskar & Turian's paper, a graph was presented for the determination of n, which was based on a previously presented correlation of particle Reynold's number against n.

The determination of the fraction x is based on the assumption that the distribution of eddie velocities is similar to the distribution of molecular velocities that was derived by Kennard (1938) in his kinetic theory of gases. On this basis, the following equation is presented for the determination of x:

$$x = \frac{2}{\sqrt{\pi}}\left\{\frac{2}{\sqrt{\pi}}\gamma\exp(-4\gamma^2/\pi) + \int_{\gamma}^{\infty}\exp(-4\gamma^2/\pi)d\gamma\right\} \quad (93)$$

where γ is the ratio of the hindered settling velocity to the critical velocity of the slurry, which was said to be "usually close to unity (>0.95)".

For the testing of this model a value of 0.975 was assumed for γ, and a value of 3.0 was determined for n that was based on a calculated particle Reynolds number of 1.25.

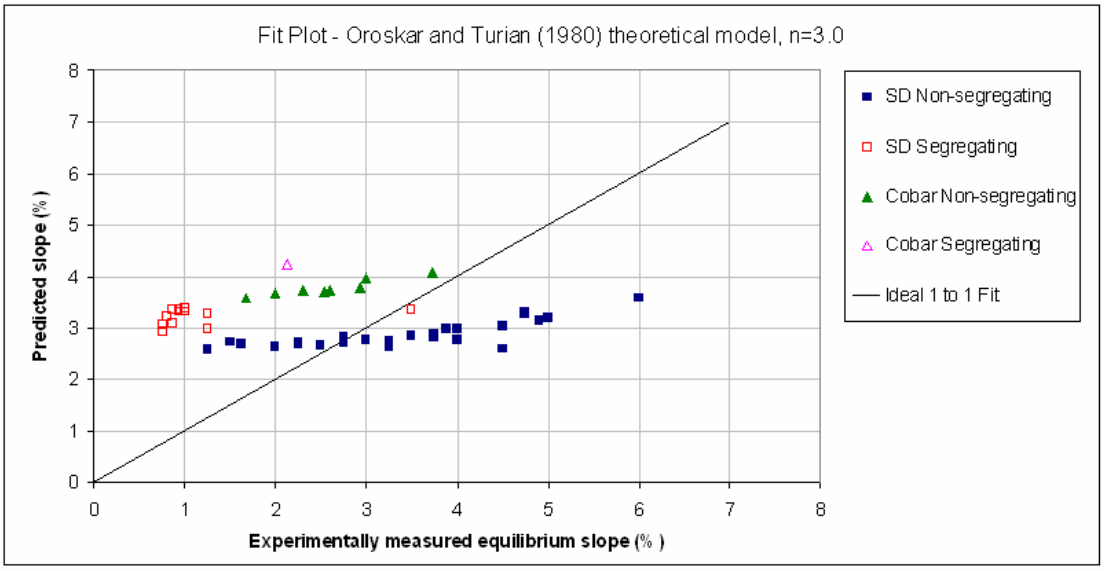

Figure 108. Fit plot of the Oroskar & Turian (1980) theoretical model

Figure 108 only presents the field flume data, against which the Oroskar & Turian theoretical model predicted poorly. The small flume data was run through the model, but for more than 90% of the cases tried, the model failed to predict depths that were less than the diameter of the pipe used in the laboratory flume (50 mm), so values for the hydraulic radius were not calculable.

Oroskar & Turian also presented an empirically calibrated version of their model which was based on a fit of the relevant parameters to a data set of some 357 points of experimental pipe data, with solids concentrations ranging from 1 - 50% v/v, solids densities ranging from 1300 – 5245 kg/m^3, fluid densities ranging from 900 – 1350 kg/m^3, fluid viscosities ranging from 0.47 – 38 mPa.s and flow rates ranging from 0.3 – 200 l/s. The field flume data is covered by most of these ranges except for the fluid viscosity range, since the effective viscosities observed in the field flume were as high as 500 mPa.s for the higher concentrations observed at Sunrise Dam. The data from the laboratory flume featured effective concentrations below 1% v/v and flow rates ranging from 0.08 – 0.4 l/s, both of which are outside Oroskar & Turian's ranges. The apparent viscosities tested in the laboratory flume ranged from 1 mPa.s to about 50 mPa.s, which is largely covered by Oroskar & Turian's range of calibrating data. The fluid and solid densities used in both the field flume and the laboratory flume are within the limits of Oroskar & Turian's data.

The empirically calibrated Oroskar & Turian equation appears as follows:

$$V_C = \sqrt{gd(s-1)}1.85C_V^{\,0.1536}(1-C_V)^{.3564}\left(\frac{d}{D}\right)^{-0.378}\tilde{N}_{\mathrm{Re}}^{\,0.09}x^{0.30} \qquad (94)$$

where $\tilde{N}_{Re}$ is a modified Reynolds number which is given by:

$$\tilde{N}_{\mathrm{Re}} = \frac{D\rho_l\sqrt{gd(s-1)}}{\mu} \qquad (95)$$

The fit plot generated with this equation is presented below as Figure 109:

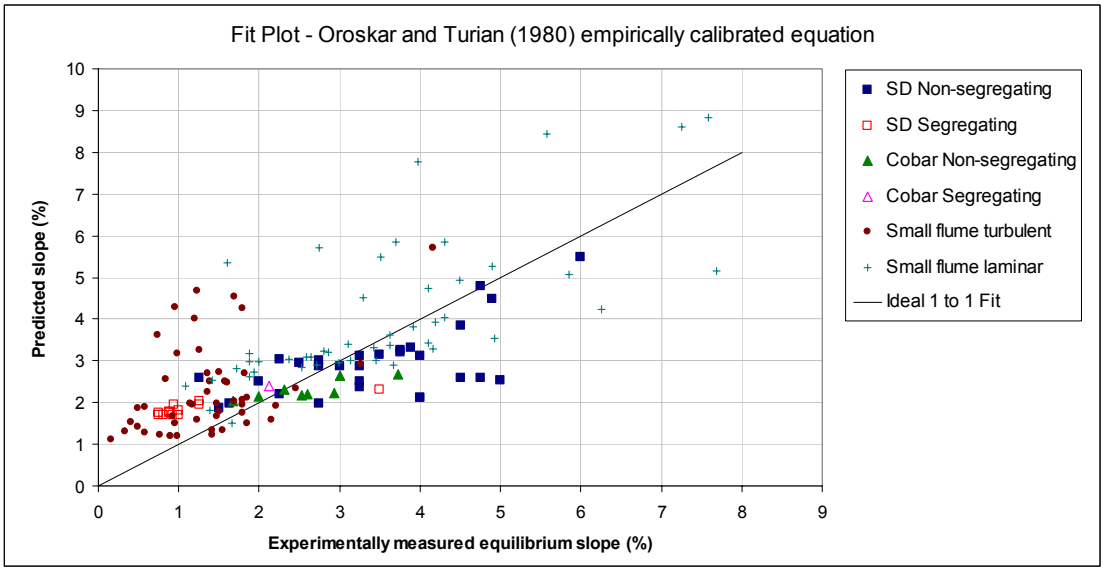

Figure 109. Fit plot of the Oroskar & Turian empirically calibrated equation

Figure 109 shows that the Oroskar & Turian empirically calibrated model is competent in predicting the equilibrium slopes observed in both the field flume and the laboratory flume. It is of interest to note that the very concentrated slurry flows tested at Sunrise Dam were predicted well, despite the apparent viscosities of these flows being well outside the range of data used by Oroskar & Turian to calibrate their model. It is also interesting to note the slope predictions for the laminar flow data measured in the laboratory flume, which are generally more accurate than the turbulent data predictions for the small flume data. The theoretical basis of Oroskar & Turian's model was in modelling the turbulent eddies that kept particles suspended in a flow. However, in the laminar flows no such eddies existed, and the particles were observed to slide along the flume bottom. This finding

suggests that some of Oroskar & Turian's calibrating data may have been taken from laminar flows. Otherwise, their model appears to predict particle transport in laminar flows well by mere coincidence.

Thomas 1979 equation

The Thomas (1979) equation as presented in Gillies et al. (2000):

$$V_{C\delta}\sqrt{\frac{f_N}{2}} = 1.1\left[\frac{g\mu(s-1)}{\rho}\right]^{1/3} \tag{96}$$

where $V_{C\delta}$ is the deposition velocity for particles that are smaller in diameter than δ_L, the thickness of the viscous sublayer, which is calculated with the following equation:

$$\delta_L = 5\frac{\mu}{\rho V\sqrt{\frac{f_N}{2}}} \tag{97}$$

where μ is the viscosity of the carrier fluid including the fine particles, and f_N is the Fanning friction factor, which is equal to one quarter of the Darcy friction factor. Since the particles in our slurries were less than the determined value of δ_L, it was decided that the viscosity would be calculated using the following equation (Baker & Jacobs 1979):

$$\eta = \frac{4\rho R_H V}{\mathrm{Re}_{HB}} \tag{98}$$

where Re_{HB} is the Herschel-Bulkley Reynolds number, calculated using equation 87. The predictions made with the Thomas model can be seen below:

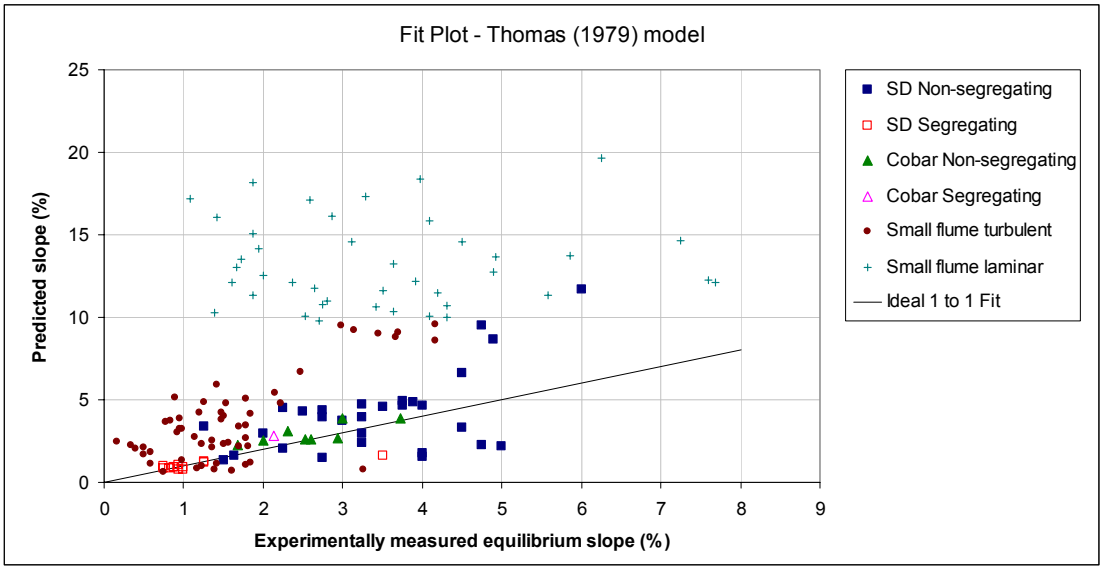

Figure 110. Fit plot of the Thomas (1979) model

Figure 110 shows that the Thomas model predicted the field flume data well, but not well for the laminar small flume data. What is of particular interest in this plot is that the model has predicted the segregating flows in the field flume very well. This suggests that the model would be good in predicting flows for segregating slurries in the design of flumes.

Wasp et al. 1977

Wasp et al. (1977) presented a graph for the prediction of the minimum transport velocity, which is presented below as Figure 111:

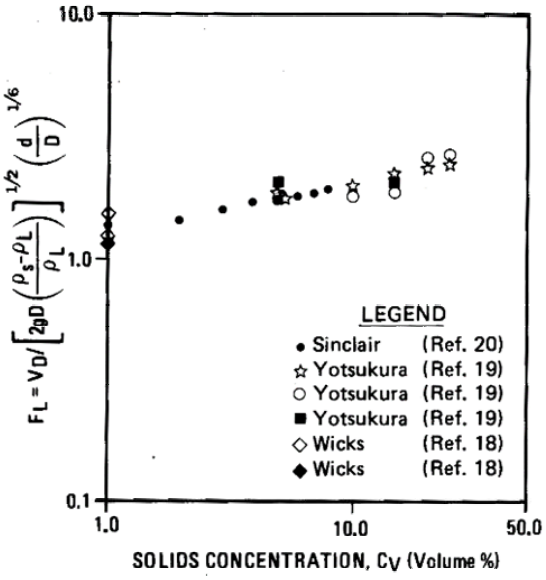

Figure 111. Transport velocity graph presented by Wasp et al. (1977)

An equation of best fit to the Wasp et al. graph yielded the following equation:

$$V_C = 3.8 C_V^{1/4} \left(\frac{d}{D}\right)^{1/6} \left[\frac{2gD(\rho_s - \rho_l)}{\rho_l}\right]^{1/2} \quad (99)$$

The experimental data presented in the Wasp et al. graph was all generated in pipes, covering the following range of flow rates: 0.06 – 48 l/s; and concentration: 1 – 25% v/v. Fluids used were water, diesel oil and kerosene, while the particles used were sand, coal and iron. It was noted by Wasp et al. that approximately 20% of these flows were laminar. A fit plot of the Wasp et al. model is presented below:

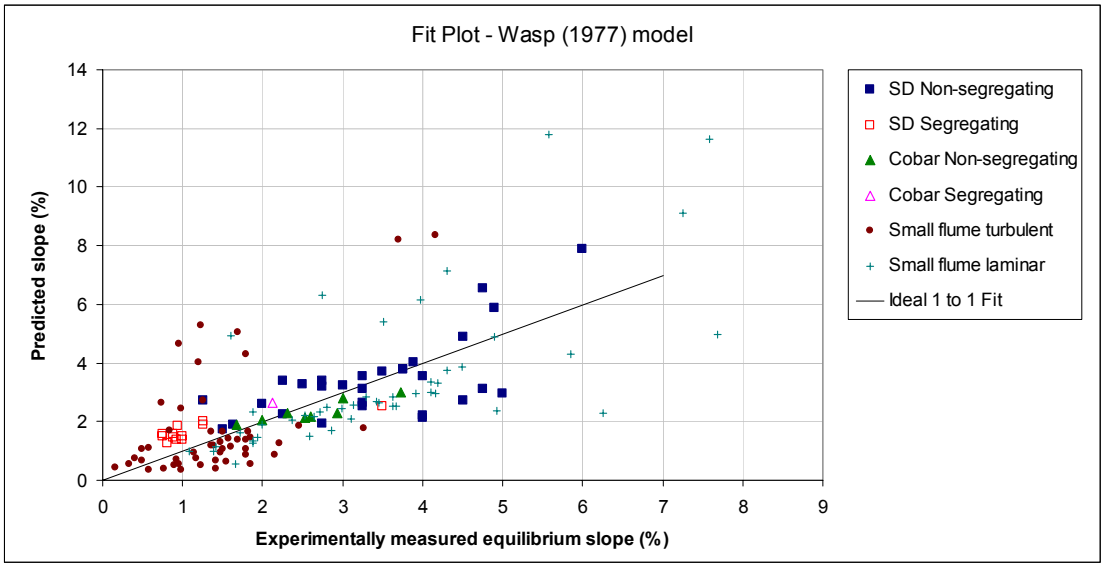

Figure 112. Fit plot of the Wasp et al. (1977) model

From Figure 112 it is evident that the Wasp model has predicted the equilibrium slopes for the experimental data from both flumes well. The fact that the model has been calibrated with laminar and turbulent data explains why it predicts the laminar data from the small flume well.

5.2.7 Evaluation of the minimum transport velocity models tested

Some 18 sediment transport models from the literature were tested, but only 6 of them were presented here. The Walton (1995), Spells (1955), Dominguez (1996) model with Vega (1988) viscosity modification, Zandi & Govatos (1967), Neill (1967), Zanke (1977) equations produced irrational results in their presented forms. Further efforts were made to find other literature to check the accuracy of the printed forms of these equations. Some of them were confirmed to be correctly presented by other texts, which leads to the conclusion that these models are simply not applicable to the characteristics of the slurries tested here.

Other models were more obviously not applicable to the characteristics found in the flume data. The Neill (1967) equation was one example of this. It consistently appeared in the same form in several texts, but since it was stated in one text (Raudkivi 1990) that the Neill equation applied only to "coarse particles (gravel)", it became apparent that it was simply not applicable to fine grained slurries.

The accuracy of the equilibrium slope predictions made by each of the 6 successfully applied models from the literature was evaluated by calculating the mean absolute deviation between the experimentally measured equilibrium slope and the predicted equilibrium slope for each group of data. (some discussion of this statistic is presented in section 4.5) The accuracy figures are presented in summary form in Table 10.

Model	Sunrise Dam		Cobar		Non-seg.	Seg.	Small flume		Overall
	Non-seg.	Seg.	Non-seg.	Seg.	Overall	Overall	Turbulent	Laminar	
Durand-Wilson-Judge 1976	2.1	3.0	1.0	2.6	1.9	2.9	48.2	8.1	34.3
Durand-Wilson-Judge 1976, assumed CD	0.9	1.6	0.3	1.9	0.8	1.6	69.0	8.3	23.4
Dominguez 1996	1.5	0.9	1.1	0.1	1.4	0.9	24.0	9.8	15.0
Oroskar and Turian 1980 theoretical model	0.9	2.1	1.2	2.1	1.0	2.1	N/A	N/A	N/A
Oroskar and Durian 1980 empirical model	0.8	0.9	0.4	0.3	0.7	0.8	1.0	1.0	0.9
Thomas 1979	1.6	0.2	0.4	0.7	1.4	0.3	2.3	9.8	4.0
Wasp 1977	0.8	0.7	0.3	0.5	0.7	0.7	1.0	1.3	1.0

Figures indicate the mean absolute deviation between experimental data and predictions (% slope)

Table 10. Summary of the fit of the successfully tested minimum transport velocity models

From Table 10 it can be seen that the Oroskar & Turian model gave the best overall fit to the flume data with the lowest mean absolute deviation between the experimental and predicted slopes of 0.9 % slope. The Wasp et al. model was just behind with a mean absolute deviation value of 1.0% slope. The Thomas model was next with a mean error of 4.0% slope, but it is noted that this model predicted most accurately against the segregating data observed in the field flume, with an average deviation of 0.3%

slope. The remaining minimum transport velocity models presented in Table 10 received considerably higher overall error figures because of their poor performance against the small flume data.

From this exercise, the Oroskar & Turian empirical model is recommended as the most suitable minimum transport velocity equation for application to tailings flows for the following reasons:

- The theoretical approach that the formulation of the equation was based upon
- Its ability to perform well against the small flume data, which demonstrates a capacity to handle a wide range of particle transport scenarios.
- The number of experimental data points that it was calibrated on (357)
- The range of solids concentrations represented in the calibration data (1 - 50% v/v)
- The range of solids densities represented in the calibration data (1300 – 5245 kg/m^3)
- The range of fluid densities represented in the calibration data (900 – 1350 kg/m^3)
- The range of fluid viscosities represented in the calibration data (0.47 – 38 mPa.s)
- The range of flow rates represented in the calibration data (0.3 – 200 l/s)

5.3 Homogeneous slurry flow models

In many texts there are two distinct categories for classifying slurry flows; heterogeneous flows, where the solids concentration in the flow varies with depth; and homogeneous flows, where the concentration profile is essentially uniform over the depth of flow. Other terms are often used in place of these, such as settling flows and non-settling flows, but this can be misleading because all slurries settle at sufficiently low velocities. In this section such approaches are tested against the field flume data, because the tailings slurries tested during the Cobar experimental work showed consistently uniform concentration profiles across their depths, with the exception of the lowest 10% of the depth, where the measured concentration was higher. (see Figure 21 in section 3.3.10). In section 5.2 sediment transport equations were considered, many of which are applied to heterogeneous flow modelling. In this section, homogeneous flow models will be tested. It is noted that one such homogeneous model has already been presented in section 5.1 under the Wilson 1991 flume design method.

Wasp et al. 1977

Wasp et al. (1977) presented the following homogeneous pipe flow equation for flows with an effective Reynolds number of 3000:

$$V_C = \frac{1500\eta}{D\rho}\left[1+\sqrt{1+\frac{D^2\tau\rho}{4500\eta}}\right] \quad (100)$$

where η is the effective viscosity of the flow, D is the diameter of the pipe, τ is the shear stress and ρ is the slurry density. The shear stress is calculated from the Bingham Plastic rheological fit parameters for the slurry, using the following equation (Wasp et al. 1977):

$$\tau = \tau_y + K\left(\frac{8V}{D}\right) \quad (101)$$

where τ_y is the slurry yield stress, and K is the Bingham plastic viscosity. The ratio $8V/D$ gives the shear rate in a pipe. For both of these equations, the pipe diameter D can be replaced with 4 R_H to enable them to be applied to channel flow situations. On this basis, the following fit plot was generated:

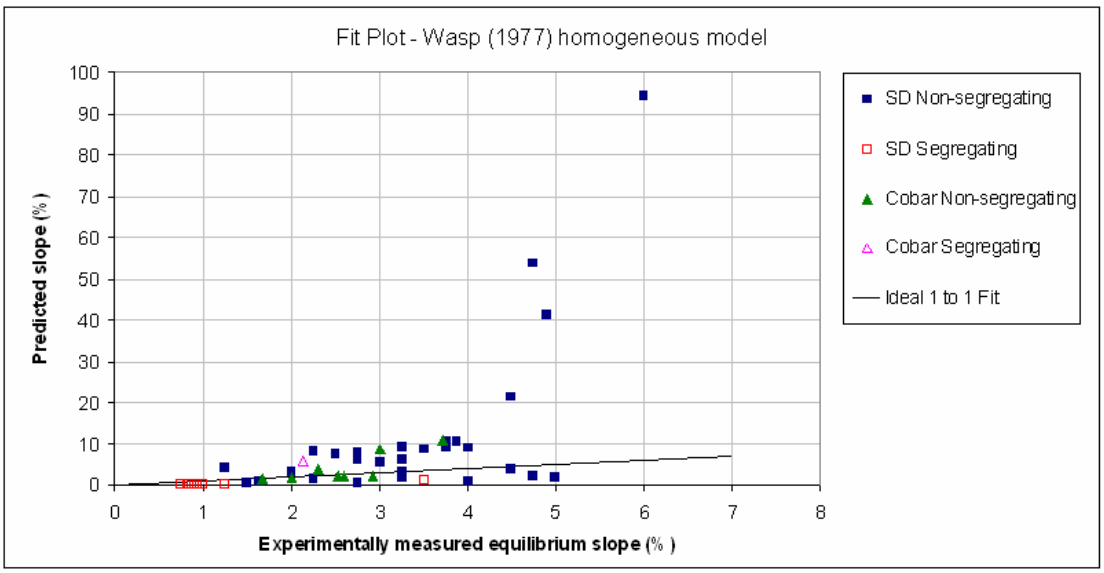

Figure 113. Fit plot of the Wasp et al. 1977 homogeneous model

Faddick 1982

From the context of the pipeline transport of coal slurries, Faddick (1982) presented the following equation, which was referred to as the Traynis equation some years later by Henderson (1988):

$$i_m = i_w\left[1+\frac{C_V(\rho_s-\rho_l)}{\rho_l}\right]+\left[\frac{\sqrt{gD}}{kC_DV}\times\frac{C_{VC}(\rho_s-\rho_{hm})}{\rho_l}\right] \quad (102)$$

where i_m is the hydraulic gradient of the slurry, i_w is the hydraulic gradient of clear water, C_V is the volumetric solids concentration, ρ_s is the solids density, ρ_l is the carrier fluid density, ρ_{hm} is the density of the heavy medium produced by fines, D is the diameter of the pipe, k is a transport constant for coarse coal (equal to 1.9), C_D is the drag coefficient for the coarse fraction of coal (with the coarse fraction defined as particles of diameter >150μm), V is the mean slurry velocity, and C_{VC} is the coarse solids volumetric concentration. From this same paper, Faddick presented the following equation for predicting the deposition velocity:

$$V_d = \sqrt{gD}\times\sqrt[3]{\frac{(\rho_c-\rho_{hm})}{\rho_c kC_D f_D}} \quad (103)$$

where ρ_c is the density of the coarse coal solids and f_D is the Darcy friction factor. A fit plot was generated using this equation, with the adoption of Faddick's k constant in the absence of any other information.

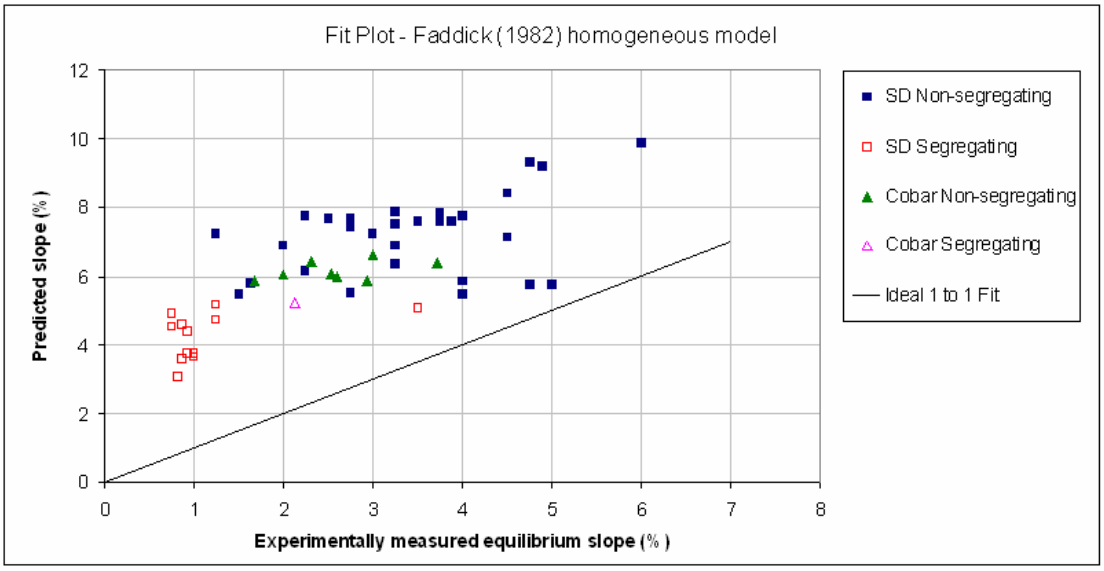

Figure 114. Fit plot of the Faddick 1982 homogeneous slurry model.

5.3.1 Discussion of homogeneous slurry models

The analysis presented in this section has raised some interesting findings about the application of homogeneous slurry models for predicting particle transport in tailings channels. On the basis of the definition of homogeneous flows found in the literature, the experimental data would definitely fit the description of homogeneous slurry, but on the basis of this analysis, the sediment transport models tested in section 5.2 performed better. It should be noted that while many of the sediment transport models have been calibrated on experimental data using fairly low concentrations of particles, some of them have been calibrated on slurries with volumetric concentrations well into the range of the experimental data gathered in the field flume. The Oroskar & Turian empirical model was calibrated with experimental data with concentrations up to 50% by volume, which exceeds the highest concentration tested in the field flume (45.2%). Since the field flume data showed that all of the slurry flows in the flume were homogeneous in terms of concentration profile, it is expected that slurries of 50% volumetric concentration are homogeneous when flowing under turbulent conditions. This would thereby suggest that the Oroskar & Turian empirical model would apply to homogeneous flows too. The Wasp et al. graphical model and the Durand models were calibrated on data with concentrations of 25% by volume, but their good performance against high concentration flows in section 5.2 would also suggest that they too may be of use in modelling homogeneous flows. This work therefore leads to the

conclusion that the analysis of particle transport in homogeneous slurry flows is better achieved using a sediment transport approach than with those homogeneous slurry approaches tested here.

5.4 Channel shape and prediction of beach slope

So far it has been shown that existing sediment transport, rheology and open channel hydraulics theory enables channel equilibrium slope and head loss predictions to be made for slurries flowing in a flume that has a fixed channel cross-section of known dimensions. However, it is noted that these methods can not yet be directly applied to predict beach slopes, because the shape of the channels found on a tailings beach have not been considered thus far. If the model were to assume that the self formed channel cross-section is the same as the flume cross-section, it would suffer from major problems if the flow rate from a spigot were to be much larger than the capacity of the flume cross-section. It is also not yet known how important the geometry of the channel shape is from the perspective of making an accurate slope prediction.

Due to these issues, the following questions are posed:

1. What channel shape does the tailings actually adopt in nature?
2. How can the model be modified to allow for this?
3. How does this affect the predictive ability of the model?
4. How sensitive is the model to different channel shapes?

The cross-sectional shape of a channel that forms when hydraulically discharged tailings erodes the underlying deposited material can be related to other similar processes that occur naturally, such as river morphology, alluvial erosion processes, mud flows, lava flows and even in ice flows. A considerable amount of research has been made into the nature of these flows, with significant attention going towards the prediction of the channel shape formed. Parker (1979) presented an equation for predicting the cross-sectional shape of a particular type of self-formed alluvial river with a gravel bed, termed a “threshold canal”, which took the form of the trough of a sinusoidal wave. His defining criterion for a threshold canal was one with bed material that was essentially at the threshold of being

transported by the river water (Parker 1979). His equation was based on the vector addition of forces acting on a gravel particle, but it was then demonstrated that there were some fundamental errors in the defining tenets of this approach, resulting in a paradox where it is possible for a so-called threshold channel to be stable with fluctuations in flow velocity, and likewise, for a so-called stable channel to be susceptible to erosion. (ASCE Task Committee on Hydraulics 1998) Other workers have tried other approaches to avoid this paradox, but it is concluded that the prediction of river bed shapes is still not fully understood.

Recently Chryss et al. (2006) presented a shape prediction method for tailings channels that was based on equating the forces at work at the channel boundary. The shape presented had a curved base and vertical sides, due to the mathematical collapse of the model in the region of the channel banks, forcing the adoption of straight vertical surfaces to enable its application. The resultant shape is unrealistic when compared to the self formed channel shapes that occur in nature. Furthermore, for this model to be applied, the concentrations of the slurry and the underlying bed material are required as input parameters. Since the bed concentration is not known, it is not possible to apply the Chryss et al. model in this work without making some further study into the bed density of settled tailings. To complicate this, it is noted that the bed concentration will be constantly increasing as a result of the slow settlement of the underlying tailings during the time that follows the channel formation. In theory, this will cause the shape of the channel to gradually change over time to reflect this change in bed density. Further research is needed in this area if channel shape in a tailings beach is to be better understood.

The experimental measurement of self formed channel shapes found on tailings beaches revealed that the cross-sectional shape of such channels was highly irregular and quite random. Even when only one channel was considered, the cross-sectional shape varied considerably from one point to another only a meter or so downstream. Some of these measured cross-sectional shapes are presented in Figure 115.

It is felt that a more progressive approach at this point might allow this matter to be addressed in another way: Rather than trying to predict a shape that appears to be quite random in nature, an analytical investigation of the effect that various shapes have on the predicted slope will be undertaken.

Several simple geometric shapes will be tested with a width to depth ratio based on the actual shapes measured on naturally formed channels in tailings. This will enable a quantitative comparison between the various shapes to ascertain what effect each one has on the predicted slope. Figure 115 shows three natural channel shapes superimposed over four simple geometric shapes; those being 2 parabolas, a rectangle and a circular arc. Of the four artificial shapes, the circular arc section is based on the actual dimensions of the flume used during the Cobar experiments.

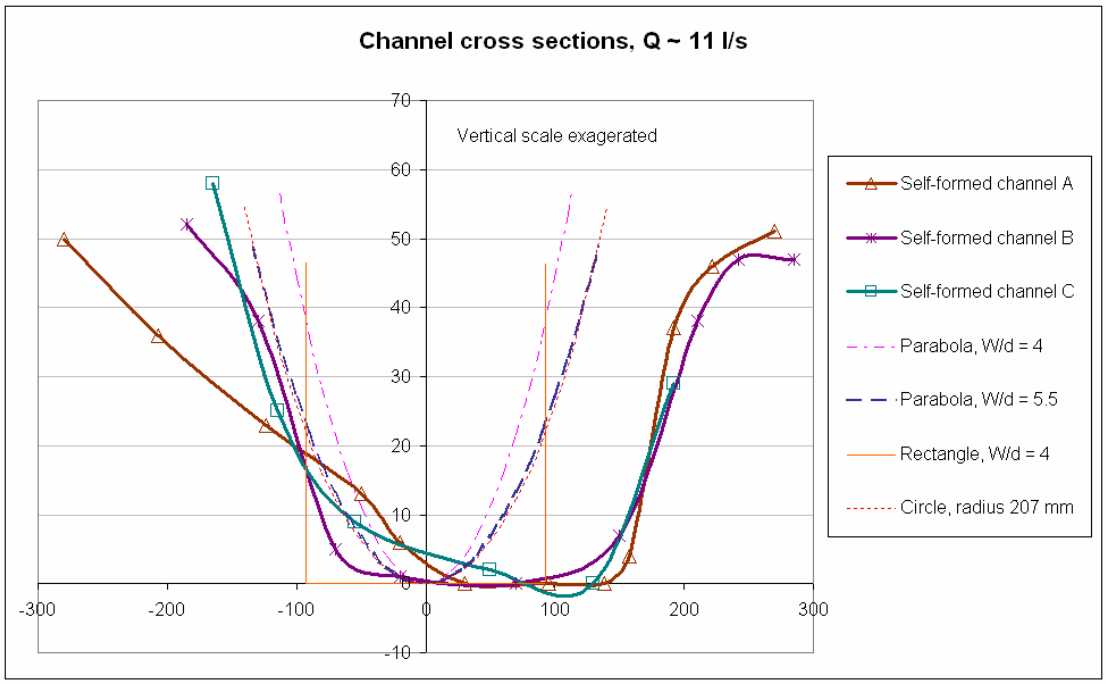

Figure 115. Four artificial channel shapes superimposed over 3 self-formed channel shapes that were measured in one channel. In all cases, the flow rate, Q, is approximately equal to 11 l/s.

Each of these four shapes (as well as two others listed in Table 11) were tested with the Oroskar and Turian model. In each case, the geometry of the simple shape was used to calculate the cross sectional area and wetted perimeter as a function of the depth in the same way as was done for the circular cross section. Equilibrium slope predictions were made using the same flow rates and slurry characteristics that were recorded in the 145 flow regimes from the field flume and small flume data sets, so that the predicted slopes could be compared to those measured experimentally in the flume. The results of these tests are presented in Table 11, with the sum of the absolute deviations between the measured and predicted points once more being adopted as the criteria used to quantify the quality of the fit.

Channel shape	Sunrise Dam		Cobar		Non-seg.	Seg.	Small flume		Overall
	Non-seg.	Seg.	Non-seg.	Seg.	Overall	Overall	Turbulent	Laminar	
Circular channel as used in flume	0.8	0.9	0.4	0.3	0.7	0.8	1.0	1.0	0.9
Parabolic cross-section, W = 4d	0.8	0.8	0.5	0.1	0.7	0.8	1.0	1.2	1.0
Parabolic cross-section, W = 5.5d	0.8	0.9	0.4	0.1	0.7	0.8	1.1	1.6	1.1
Parabolic cross-section, W = 7d	0.7	0.9	0.4	0.2	0.7	0.9	1.2	2.1	1.3
Rectangular cross-section, W = 4d	0.8	0.9	0.4	0.1	0.7	0.8	1.1	1.4	1.1
Rectangular cross-section, W = 7d	0.7	0.9	0.4	0.2	0.7	0.9	1.2	2.1	1.3

Figures indicate the mean absolute deviation between experimental data and predictions (% slope)

Table 11. Statistical comparison of the effect of channel shape on the predicted equilibrium slope

Table 11 provides some interesting findings:

- For both sets of flume data, the cross-sectional shape had a minor effect on the prediction, which suggests that the model is robust with regards to channel shape. The small flume data experienced a greater amount of prediction error when wider channel shapes were tested. This was due to the cross-sectional shape in the small flume being closer to a semi-circle, with a significantly narrower aspect ratio than 7 to 1. The fluid depths were typically around 15 to 20 mm above the pipe invert, but the pipe diameter was only 50 mm by comparison. For both sets of flume data it was found that the aspect ratio had a greater impact than the change in geometric shape.
- Predictions tended to deviate from the field flume data more at flatter slopes. This makes sense on the basis that most of the flat equilibrium slopes were observed at high flow rates in the field flume, where the circular cross section of the flume forced the flow to be unrealistically narrow compared to real channel shapes.

From this exercise, an important step has been taken to enable the model to be applied to the prediction of tailings beach slopes rather than just equilibrium slopes in channels, with the experimental data providing strong support for the validity of this approach. It is interesting to note that the findings of this analytical exercise reflect the experimental findings of Haldenwang et al. (2004) after these workers conducted open channel laminar flow experiments with non-Newtonian fluids in channels of triangular, rectangular and circular cross-sections. They also concluded that the channel shape had a negligible effect on the head loss, since it was only the hydraulic radius that was of relevance.

The findings of this work indicate that the aspect ratio is more important than the channel shape. For modelling the channels that form on tailings beach slopes, it is recommended that the best shape approximation to be applied is a parabola with a width 5.5 times the depth, because this aspect ratio is similar to those of the measured self-formed channels (presented in Figure 115).

5.5 The new a-priori beach slope prediction model

This chapter has provided some very useful findings to enable the construction of an a priori beach slope prediction model. On the basis of these findings, it is decided that the best model will result from the adoption of the following equations and shape geometry:

- The Darcy-Weisbach / Colebrook White / Haldenwang Slatter open channel flow resistance model with a k_s value of 2 x d_{90}
- The Oroskar and Turian empirically calibrated minimum transport velocity equation
- A cross-section shaped as a parabola with a width 5.5 times the depth

5.5.1 Required input parameters

To make a slope prediction with the new a priori model the following input data must be defined:

- Q, the flow rate (m^3/s)
- C_V, the concentration of the tailings slurry in terms of volume (fraction)
- d_{50}, the median particle diameter of the tailings slurry (m)
- d_{90}, the 90th percentile particle diameter of the tailings slurry (m)
- ρ_w, the density of the carrier fluid of the tailings slurry (kg/m^3)
- ρ_s, the density of the solid particles in the tailings slurry (kg/m^3)
- τ_y, K and n (Rheological parameters for a Herschel-Bulkley model fit for the slurry)

5.5.2 Prediction sequence

The following method is recommended for the application of this new beach slope model within a spreadsheet program, with the following steps taken to make each prediction:

1. Guess an initial value of the depth
2. Calculate the cross sectional area of flow, A, and the wetted perimeter, P, as a function of the geometry of the channel cross-section
3. Calculate R_H, the ratio of A/P
4. Calculate V, the mean velocity in the channel (equal to Q/A)
5. Calculate V_C, the minimum transport velocity, using the Oroskar & Turian empirical equation (equation 94):

$$V_C = \sqrt{gd(s-1)}\,1.85 C_V^{\,0.1536}(1-C_V)^{.3564}\left(\frac{d}{4R_H}\right)^{-0.378}\left(\frac{D\rho_l\sqrt{gd(s-1)}}{\mu}\right)^{0.09} x^{0.30}$$

6. Repeat steps 1 to 5, adjusting the depth value (in step 1) until V and V_C in steps 4 and 5 equate.
7. Calculate Re_{HB} using the Haldenwang Slatter Reynolds number equation (equation 87):

$$\mathrm{Re}_{HB} = \frac{8\rho V^2}{\tau_y + K\left[\frac{2V}{R_H}\right]^n}$$

8. Calculate f_D using the Colebrook White equation, using Re_{HB} for the Re term (equation 85):

$$\frac{1}{\sqrt{f_D}} = -2\log_{10}\left[\frac{k_s}{14.8R_H} + \frac{2.51}{\mathrm{Re}\sqrt{f_D}}\right]$$

9. Calculate S_0 using the Darcy-Weisbach equation (equation 83):

$$S_0 = \frac{f_D V^2}{8gR_H}$$

At this point, the slope predicted in step 9 will be the equilibrium slope.

5.5.3 Validation of the a priori model

The new a priori model will now be tested against the ATC data, the stack data and the alluvial fan experimental data in the same manner as the other beach slope prediction models were in Chapter 4. The fit plot follows as Figure 116:

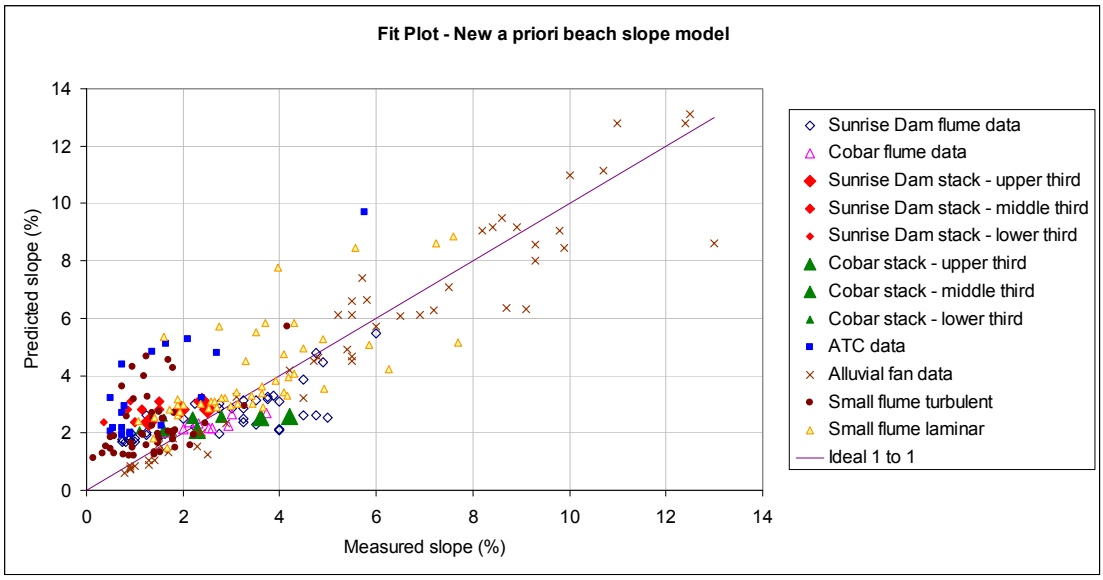

Figure 116. Fit plot of the new a priori model

Figure 116 shows that the a priori model is not predicting so well against the ATC data, with the predicted slopes generally about 1 to 3% steeper than those observed. The model predicted well against the stack data and the alluvial fan data.

The prediction quality statistics are presented in Table 12 in section 5.7 with those of the better performing beach slope models from the literature and the other new models.

5.6 A new semi-empirical beach slope model

The two new models introduced in sections 5.1 and 5.5 both offer significant benefits relative to one another, and each has a clear purpose; the simple empirical model enables quick easy predictions, and the a priori model offers proven reliability on the basis of the previously presented and tested work that

it was based upon. In this section a new semi-empirical beach slope model is presented with the sole objective of achieving the best possible predictive accuracy against beach slope data.

Due to the vastly different behaviour of the segregating slurries to the non-segregating slurries in the field flume (see Figure 15 in section 3.3.7), it was seen that a semi-empirical model that treats each of these two categories separately could provide more accurate beach slope predictions. The sediment transport aspect of the priori model described in section 5.2 presents an opportunity for the creation of a new semi-empirical beach slope model that is based on the same sediment transport approach as the a priori model, but featuring two new empirical minimum transport velocity equations; one created by fitting a curve to the non-segregating slurry data that was gathered at Cobar and Sunrise Dam; and the other by fitting a curve to the segregating data.

5.6.1 An empirical minimum transport velocity equation for the non-segregating data

After plotting various experimentally measured parameters against the observed mean velocity in the flume, it was found that the Bingham Reynolds number exhibited the strongest correlation with the slopes observed for the non-segregating data. The equation for the Bingham Reynolds number is presented below:

$$\mathrm{Re}_{Bingham} = \frac{\rho V R_H}{K_{BP}} \tag{104}$$

A plot of this trend is presented below in Figure 117:

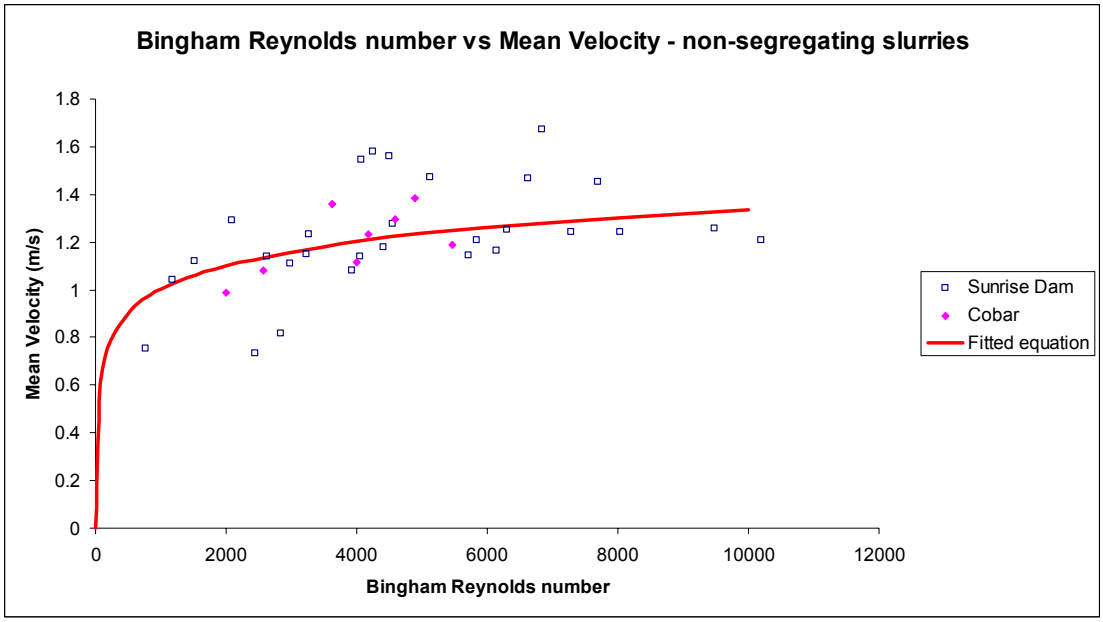

Figure 117. Plot of Bingham Reynolds number against the mean velocity for the non-segregating data in the field flume

The equation for the fitted curve in Figure 117 is as follows:

$$V_{CNon-segregating} = 0.145 \ln\left(\frac{\rho V R_H}{K_{BP}}\right) \quad (105)$$

This equation forms the non-segregating slurry modelling aspect of the new semi-empirical model.

5.6.2 An empirical minimum transport velocity equation for the segregating data

The mean velocity of the segregating data did not exhibit any strong correlation with any of the individual parameters tested. There were generally too few points, with little difference between them (relative to the parameters tested), so all of the plots showed the data bunched up in a small cloud with no obvious elongation in any direction to suggest a trend. Due to this small number of data points available, it was decided to use one of the minimum transport velocity equations from the literature for handling segregating slurries in the new model. Upon reviewing the findings of section 5.2.6, the Thomas model provided excellent predictions against the field flume segregating slurries, but it performed poorly against the small flume data. Since the predictive performance displayed by the

Wasp model (equations 99) against both the segregating slurries and the small flume data in section 5.2.6 was better than any of the other models, it was decided that this model would be adopted to serve in predicting the minimum transport velocities for segregating slurries in the new semi-empirical model.

A fit plot generated by applying the new semi-empirical model to the flume data appears below in Figure 118:

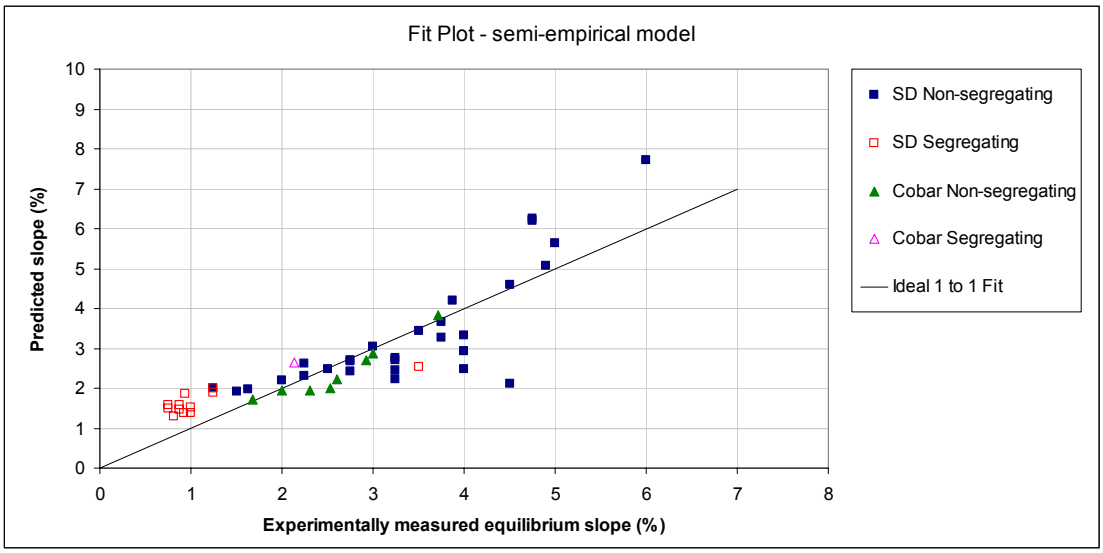

Figure 118. Fit plot of the semi-empirical model against the field flume data

Figure 118 shows that the new semi-empirical model offers good predictive performance against the field flume data, which is expected in the case of the non-segregating data that was used to calibrate the non-segregating aspect of the model.

5.6.3 Validation of the semi-empirical model

The new semi-empirical model was applied to the 5 sets of validating data, but in doing this, it was necessary to define each slurry as being either segregating or non-segregating. For the field flume data this was already established, and since the stack data was from the same two mines, the segregation status of this data was also known already. However, for the other 3 sets of data, the following assumptions were made: The slurries in the ATC data set were all assumed to be non-segregating. The

slurries in the other two data sets (the small flume data and the alluvial fan experimental data) were assumed to be segregating. It was felt that that these assumptions were reasonable for the latter two data sets because of their very low concentrations. The fit plot generated from this model with these assumptions appears below as Figure 119:

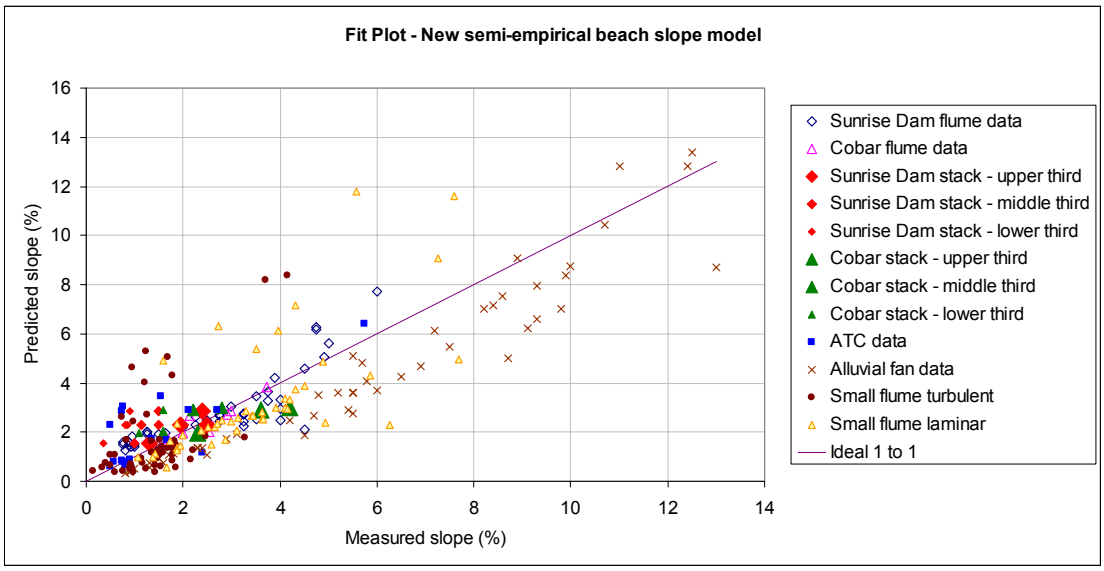

Figure 119. Fit plot of the new semi-empirical beach slope model

Figure 119 shows that the new semi-empirical beach slope model predicts well against all five data sets. The model does under-predict for most of the alluvial fan data, but the data points in this set do show good alignment with the ideal fit line.

5.6.4 Discussion of the semi-empirical model

The semi-empirical model offers a more accurate method of beach slope prediction than any of the other models tested in this work, as will be demonstrated in section 5.7 when the performance of the new models is evaluated and compared to the best models from the literature.

One of the obvious limitations of this semi-empirical model is the requirement for the segregation status of a slurry to be known before the correct equation can be applied. This does not mean that the segregation threshold of the slurry needs to be determined, but it is necessary to classify the slurry as

either segregating or non-segregating. However, the Wasp et al. minimum transport velocity model that forms the segregating slurry part of the model offers some relief in the event that the segregation status of the slurry is not known, since it performs reasonably well over the entire range of data (see Table 11 for statistics). Therefore, if the segregation status of a slurry is not known, the segregating model can be applied as a default. It was for this reason that the Wasp et al. minimum transport velocity model was selected for the segregating slurry component of this model instead of the Thomas model.

5.7 Evaluation of the accuracy of the new models

For quantitative comparison of the 3 new models with the other tested beach shape models, a table of descriptive statistics is presented below. Only the better performing beach slope models from the literature are included in the table. The figures represent the mean absolute deviation between the measured slopes and the predicted slopes for each data group, so low values indicate good predictions. A discussion of this descriptive statistic is presented in section 4.5.

Model	Field flume	Stack data	ATC data	Alluvial fan data	Small flume
Melent'ev et al. 1973	0.9	0.9	1.8	3.2	1.5
Robinsky 1978	1.2	1.4	1.3	4.4	1.4
Wates et al. 1987	1.2	1.4	0.9	3.3	2.4
Fitton et al. 2006	0.7	0.7	0.7	2.8	8.5
Chryss et al. 2006	1.9	2.2	0.9	-	-
Simple empirical model	0.6	0.7	0.6	5.2	2.4
a priori model	0.7	0.8	2.1	0.8	1.0
Semi-empirical model	0.6	0.5	0.7	1.1	1.4

Figures indicate the mean absolute deviation between experimental data and predictions (% slope)

Table 12. Statistical comparison of the predictions of the new models with those of the better performing models tested in Chapter 4.

The results from Table 12 are presented graphically below in Figure 120:

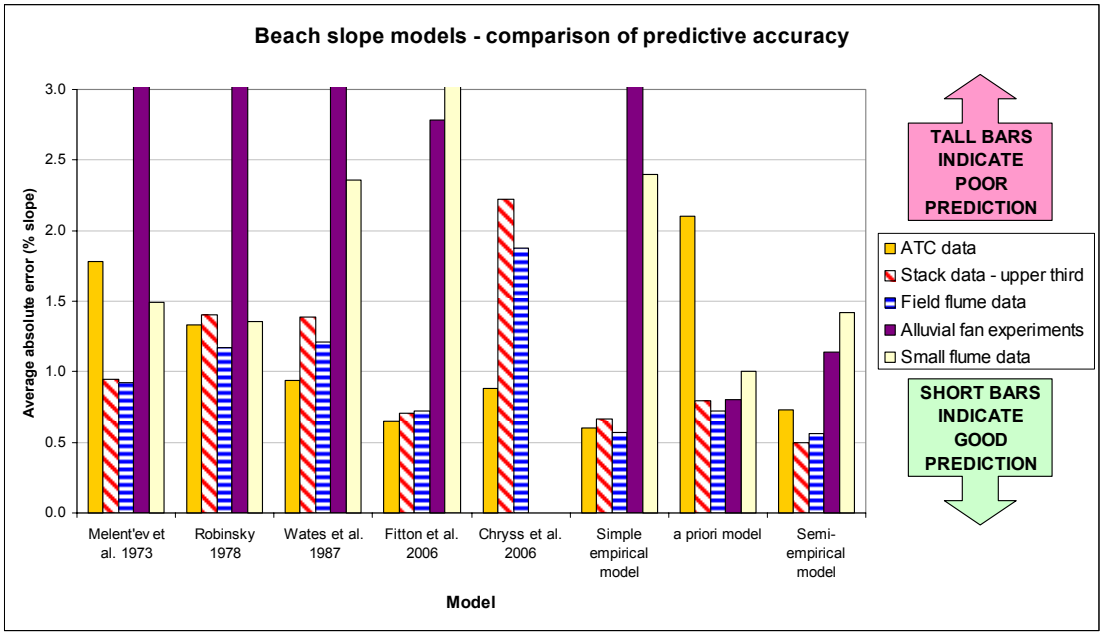

Figure 120. Bar graph comparing the predictive accuracy of the 3 new beach slope models with the 5 best performing models from the literature against each of the 5 validating data sets.

Figure 120 shows that the 3 new models offer specific advantages against one another, and also over the other models tested in the literature. For the prediction of beach slopes, the most relevant data sets to consider are the ATC data set and the Stack data set. Figure 120 shows that the new semi-empirical model, the new simple empirical model and the Fitton et al. model offer the best performance against these two beach slope data sets. The new simple empirical model offers better performance against the ATC data than any of the other models, but its poor performance against the small flume data and the alluvial fan data suggests that the simple empirical model will be limited in its predictive ability against slurries of lower concentrations or significantly different rheological characteristics. The new a priori model fared poorly against the ATC data, but predicted more accurately than any of the other models against the small flume data and the alluvial fan data.

This chapter is concluded by recommending the new semi-empirical model as the best beach slope model available amongst those presented here for the prediction of tailings beach slopes.

Chapter 6: Three dimensional beach shape modelling

The focus of this work so far has been the modelling of beach slopes, with some discussion of two-dimensional beach profiles as well. In this chapter, the overall three-dimensional shape of the deposited tailings within the perimeter confines of the tailings storage facility will be considered. Predicting the overall shape of the deposited tailings as it develops over time is the ultimate objective that drives the modelling of tailings beach slopes and profiles, so that the containment structures, discharge spigots, surface drainage systems and other related infrastructure can be progressively raised to safely and efficiently contain future tailings. In a tailings stack for example, if the tailings should deposit at the outer reaches, a raise of the perimeter bund may be necessary in time. In an extreme case where the tailings is beaching at much flatter slopes than originally thought, it may be necessary to construct a completely new bund at a larger radius, thereby abandoning the original bunds and perimeter drainage system to be buried in new tailings. Alternatively, if the stack is building up steeper than previously planned, it will be necessary to raise the discharge spigots first. If access to the spigots is to be maintained, this could include a raise of the access causeway too, and if it is preferred that the tailings pipeline remains above the deposited tailings, then it too will require raising. These activities all require the allocation of resources that can impact on the cash flow and operation of the mine, so it is of significant value to be able to predict such outcomes and plan for them.

A couple of approaches for modelling the three-dimensional shape of tailings beaches have been presented in the literature, whilst other models have been commercially marketed as software packages.

Robinsky presented a linear beach shape concept in his landmark paper of 1975. Consistent with his claim that thickened tailings would beach with a linear slope, he presented a three-dimensional drawing of a conical shaped tailings stack with a linear beach profile. Figure 121 shows the three-dimensional drawing that Robinsky presented of a tailings stack. The linear profile of his forecast is fairly evident.

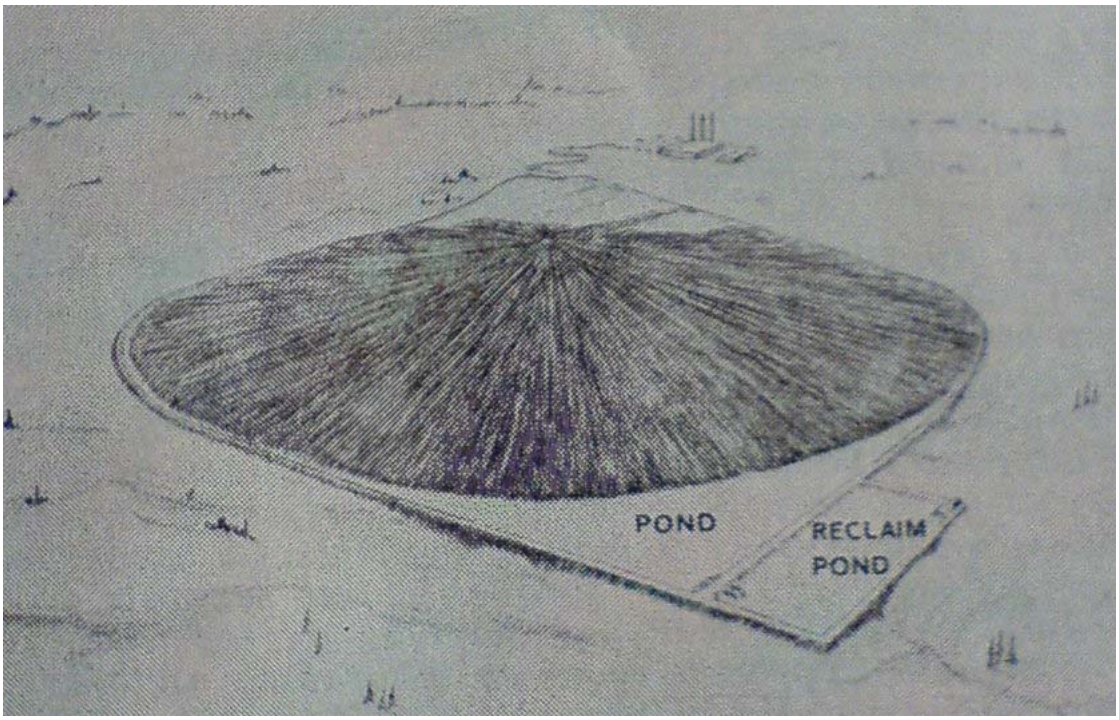

Figure 121. Robinsky's drawing of a tailings stack with a linear beach profile (Robinsky 1975)

It is well documented that tailings beaches always exhibit concavity (Blight et al. 1985, Melent'ev et al. 1973), with the degree of concavity varying from one beach to the next. The prediction of the curvature of tailings beach profiles has been the subject of a number of studies, some of which have been discussed in section 2.1.6. An example of a three-dimensional concave beach shape was presented recently by Williams et al. (2006) as a forecast of a large down-valley discharge thickened tailings storage facility in Iran. The three-dimensional contour plan of the facility is presented below in Figure 122. It can be seen that the contour interval of the predicted beach shape is larger at the lower reaches of the deposit and smaller nearer to the discharge spigots, clearly indicating concavity of the beach profile.

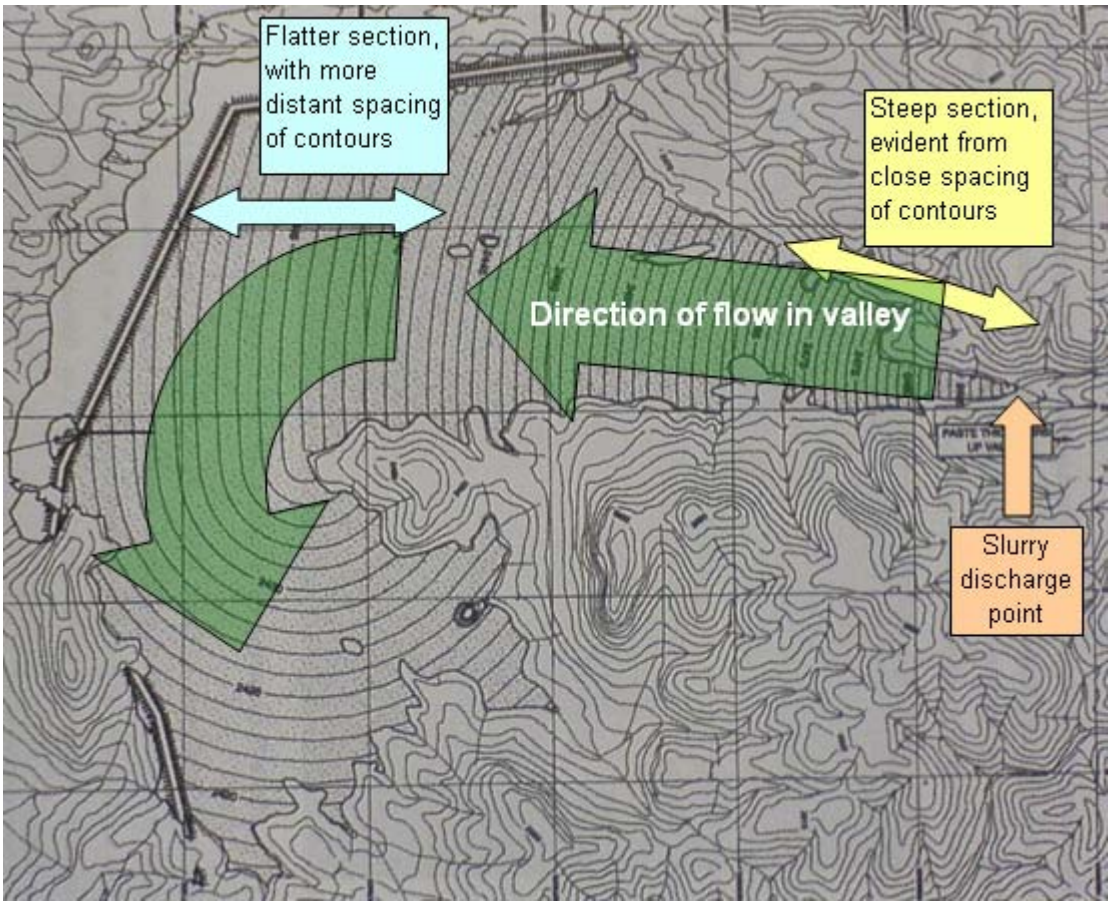

Figure 122. Forecast beach shape of a down-valley discharge scheme, with surface contours indicating profile concavity (Williams et al. 2006). The slurry is discharged from a single point at the right side of the drawing and flows down the valley. Note the embankments at the bottom of the valley (left side of the drawing), which are retaining the tailings.

Figure 122 shows that a two dimensional profile model has been used to generate the three-dimensional shape of the predicted tailings beach. A similar approach has been observed in software packages that specifically perform three-dimensional tailings shape modelling, in which the 2-dimensional beach profile is used to generate a three dimensional beach. (Rift TD, 2006; Mine Solutions, 2006) The first of these two software packages employed the Melent'ev et al. "Master Profile" model in defining the concavity of the beach profile (this equation has been previously discussed in section 2.1.6 and presented as equation 23). The other fitted a mathematical equation to survey data of an actual beach profile to define the concavity.

All of the three-dimensional shape prediction models discussed here assume a particular beach profile in order to generate a three-dimensional beach shape. This characteristic compromises the accuracy of the predicted shape if the discharge should change. A change in the discharge rate or the slurry

concentration or rheology would cause a change in beach slope, which should cause a change in the deposition location of the altered tailings. This effect is not considered in these models. Such a simplification will not allow variation in concavity that will occur if the discharge fluctuates heavily one week and hardly the next.

6.1 A new three dimensional tailings beach shape model

A new model for predicting the shape of a 3 dimensional tailings stack formed by the sub-aerial discharge of a non-segregating tailings slurry is presented here.

The beach shape model presented here requires a slope prediction model to be used to generate the input data to construct an overall shape. The Fitton et al. (2006) beach slope model has been used here for this purpose (because the three new models presented in Chapter 5 had not been created at the time that this shape model was created), but alternatively, any other tailings beach slope model could be used instead.

6.2 Modelling the growth of a linear beach:

In modelling the formation of a 3 dimensional tailings beach it is logical to begin by looking at the geometrically simplest scenario first, which would be that of a straight beach, typically like that seen in an impoundment with one or more straight sides. We will consider a straight beach of infinite length with discharge spigots spaced every x meters. Initially it is assumed that x is sufficiently small to allow the assumption that there is no transverse curvature of the beach. This effectively reduces the problem to a 2 dimensional one for developing the model.

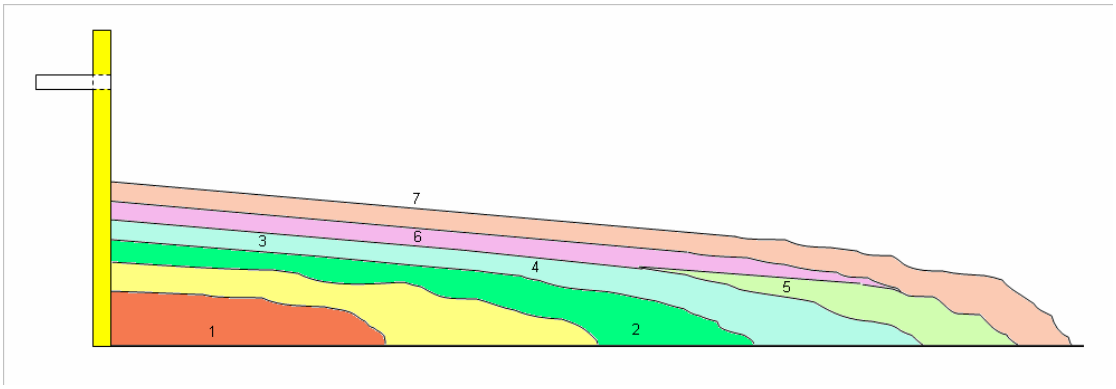

Figure 123. Cross-section of a simplified tailings build-up scenario, in which tailings are discharged from the spigot running through the wall to form a beach on the flat surface below. For meaning of numbers see text.

To simplify the approach further the underlying beach will be neglected for the moment, but instead it will be assumed that the discharge spigots protrude through a vertical wall a meter above a flat surface. The following sequence of events is illustrated in Figure 123: When a steady stream of homogeneous non-segregating slurry starts flowing out of the spigot, it will initially form a large blob beneath the spigot [1], growing in size [2]. This enlargement of the initial blob will be referred to as "sheet flow" from now on. After some time the viscous nature of the tailings presents significant resistance to further sheet flow occurring, and suddenly the newly arriving tailings slurry forms its own channel that rides on top of the deposited sheet flow [3]. At this point the force needed to form the channel is less than the force required to spread the extents of the deposited sheet flow further. This channel runs away from the wall until it gets near to the distant edge of the deposited sheet flow [4], where it suddenly reverts to sheet flow once again because of the reduction in resistance to sheet flow at this location. No particles are depositing in the channel, so eventually the fresh outer deposit will build up to a height that presents a significant resistance to the channel [5]. When this occurs, the channel will stop flowing at its outer reaches, and the slurry will instead overflow the banks of the channel at some point upstream to deposit particles higher up the beach [6]. This point could be anywhere along the path of the channel, even at the beginning near the wall. This process will endlessly repeat itself while the steady homogeneous discharge continues, causing the beach to grow in all areas at the slope dictated by the channel. [7]

A series of time lapse photographs of slurry deposition provides some illustration of the amount of time that passes during the first 4 stages of this tailings deposition process. (Pirouz et al. 2005) These

photos were taken on an actual tailings beach with a length of about 500 meters, and they showed a self formed channel riding over a sheet flow deposit approximately 5 minutes after it had arrived. It was evident that the channel advanced in length by some 40 – 50 meters during a 9 minute period. It is believed that the advance of the channel is made possible by two factors: 1). the freshly deposited sheet flow material has completely stopped, and 2). it presents sufficient depth for the channel to form.

It has been shown that the slope of the beach is dictated by the discharge parameters. (Fitton et al. 2006) We can now consider the dimensions of the beach by calculating the volume of tailings that has been discharged with the simple relationship:

$$V = Qt \tag{106}$$

where V is the volume discharged from each spigot (m^3), Q is the flow rate from each spigot (m^3/s) and t is the time (s). Over time, a greater part of the overall beach shape will be linear. For our modelling purposes we will assume that the beach length is sufficiently large for it to be considered linear. From this we can state that the horizontal length of the beach (from the spigot to the toe) can be calculated with the following geometric equation:

$$l = \sqrt{\frac{2V}{ix}} \tag{107}$$

where l is the length of the beach in meters and i is the channel equilibrium slope as a decimal (equal to the vertical rise divided by the horizontal run). The height at the top of the beach, h, can then be calculated with the following expression:

$$h = li \tag{108}$$

If we now consider the above scenario with an underlying beach instead of the assumed flat surface, it can be seen that the physical process would essentially be the same but with less material forming the initial blob. On this basis, the vertical wall in Figure 123 becomes irrelevant, since it only serves to

provide lateral support to the initial build-up of slurry. Assuming that the entire surface of the underlying beach is buried in the freshly deposited tailings, the equation for calculating the length of the beach would become:

$$l = \sqrt{\frac{2(V+P)}{ix}} \tag{109}$$

where P is the volume contained within the previously deposited beach that can be attributed to the spigot of interest. So far, the concavity of the beach is being ignored, but this will be addressed as the model is further developed.

6.3 Modelling a 3-dimensional conical stack

Once again the modelling begins with a simplified scenario: consider the constant discharge (Q) of a slurry from a small distance above flat ground over a finite period of time (t). This will initially form a sheet flow that will grow radially in all directions until suddenly the resistance to further growth will be greater than the force required for the incoming slurry to form a channel that runs across the top of the blob in some random direction, and the slurry will then be transported to the outer reaches of the blob via this channel. Over time this channel will adopt numerous paths and directions as the compounding deposits periodically present obstruction to the course of the channel. Ultimately this process will form a cone with height h and radius r. Such a scenario is depicted in Figure 124.

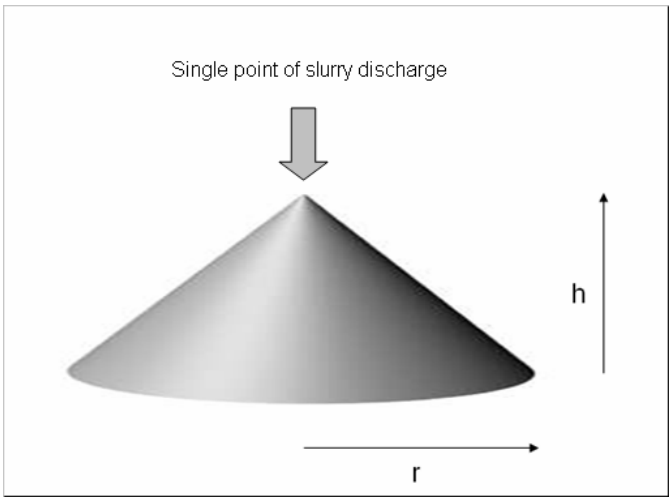

Figure 124. Simplified formation of a conical stack

Using equation 106 we can calculate the volume of tailings that has been discharged to the stack. Then in combining the following geometric equation relating the height, radius and slope of the cone:

$$h = ri \tag{110}$$

with the equation for calculating the volume of a cone:

$$V = \frac{1}{3}\pi.r^2 h \tag{111}$$

we can determine the radius of the cone by using the following equation:

$$r = \sqrt[3]{\frac{3V}{\pi.i}} \tag{112}$$

This is the simplest scenario for this model. Effort will now be devoted to considering changes in the slurry discharge, and how the shape of the deposit formed is affected by this compounding of successively varied slurry discharges.

6.4 The truncated cone model

The compound model must calculate a cone shape that has slopes corresponding to the respective discharge parameters of each flow regime, with each flow regime having its own discrete duration (*t*), a constant flow rate (Q) and constant rheological characteristics. If either the flow rate or the rheology of the slurry should change, this signifies the end of one flow regime and the beginning of the next. If we consider what would happen in the simplified stack scenario shown in Figure 124 if we were to change the flow parameters or rheology to produce a steeper channel equilibrium slope, we would find that the fresh tailings would deposit at the top of the cone to form a steeper conical 'cap' on top. Alternatively, if we changed the slurry to one with a flatter channel equilibrium slope, we would expect the slurry to form a channel that runs all the way down the side of the underlying cone to the toe, and then start depositing around the lower part of the stack. These two outcomes are illustrated in Figure 125.

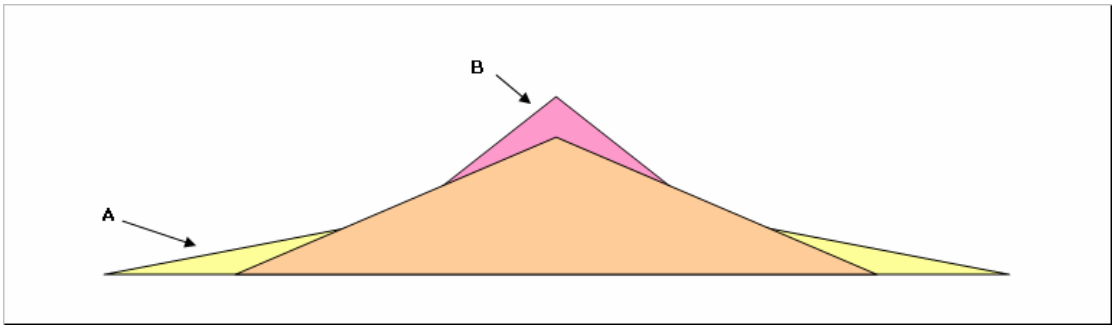

Figure 125. Cross-section of a conical tailings stack subjected to two fresh deposits of tailings; 'A' came from a slurry with a flatter channel equilibrium slope than that of the underlying beach, conversely 'B' came from a slurry with steeper equilibrium slope than the slope of the underlying beach.

The more complex shapes of these recent deposits can still be calculated using the same conical geometry approach as that above, but with the added complication of taking the underlying stack geometry into account. Consider the same stack some time later, after four more flow regimes have left deposits:

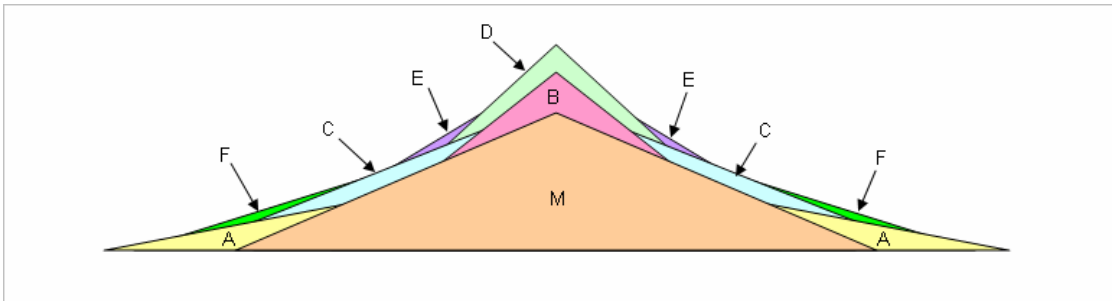

Figure 126. Cross-section of a 7 stage compound stack.

If we consider deposit C in Figure 126, it can be seen that it arrived after deposits A, B and M. We therefore need to take the overlapping portions of deposits A, B and M out of the envelope of the projected cone of deposit C. These overlapping portions are shown below:

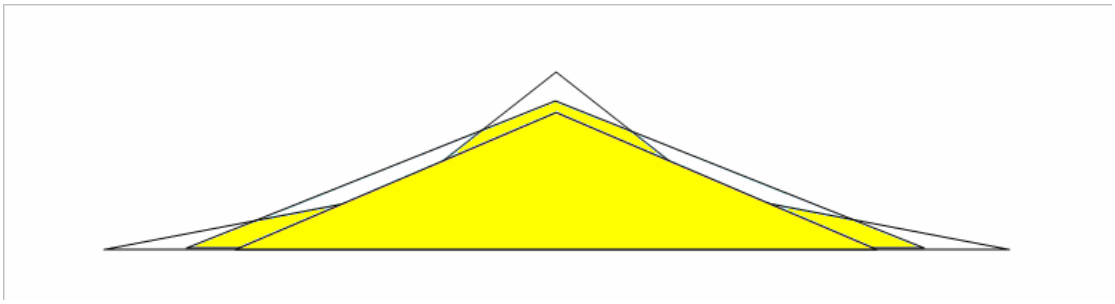

Figure 127. The shaded area represents the relevant portions of previously deposited tailings that fall within the projected cone of deposit C in Figure 126.

We can consider the shaded area of Figure 127 as a stack of 4 concentric truncated cones topped with a simple cone. The equation for calculating the volume of a truncated cone is:

$$V = \frac{1}{3}\pi H(R^2 + Rr + r^2) \tag{113}$$

where R is the upper radius of the frustum, r is the base radius and H is the height. The equation for the volume of a plain circular cone has been presented earlier (equation 111).

The actual volume of deposited tailings for each flow regime is calculated by the $Q.t$ relationship (equation 106). We use this discharged volume to determine the size of the new deposit by subtracting

the volume of underlying tailings from the volume contained within the projected cone of each deposit.

The challenge is to be able to define h, H, R and r as the stack gets more complex with the compounding of different flow regimes. As the stack grows with more regimes of tailings discharge, it is likely that the determination of the shape of each deposit will get even more complex, but as can be seen in Figure 126, the new deposits eventually build up so much that some of the previous deposits no longer have any contact with another new deposit, so they no longer need to be considered.

To efficiently tackle this challenge, a computer aided iterative approach was used to determine the size of the projected cone of each deposit, firstly by nominating an arbitrary value for the height of the projected cone and then calculating the resulting volumes of the projected cone and the underlying tailings, and comparing the difference between the two to the discharged volume. This process would then be iterated with the nomination of other heights for the projected cone until the trapped volume was calculated to be equal to the discharged volume of tailings, at which point the correctly sized projected cone had been found. This process is presented in Figure 128 as a flow chart:

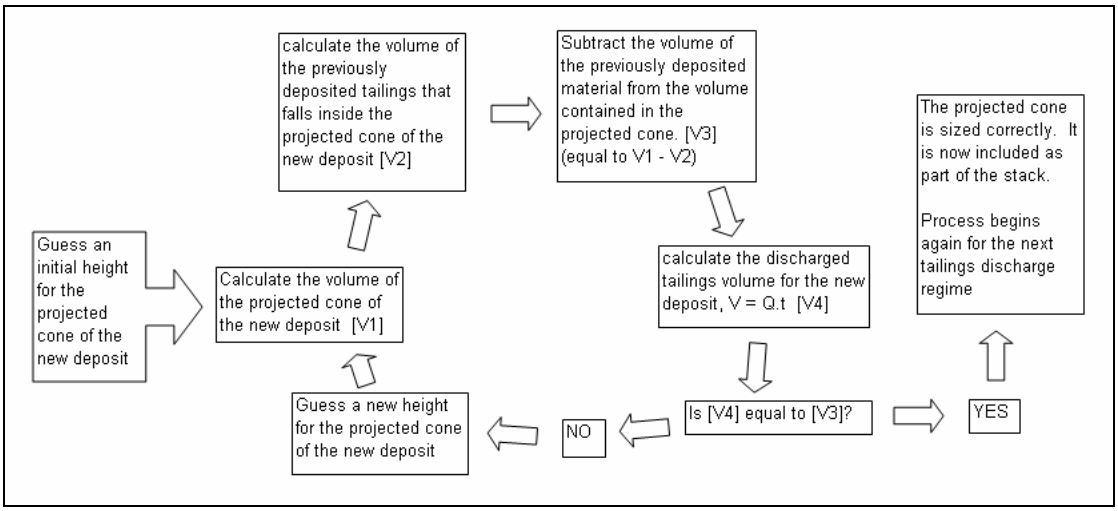

Figure 128. Flow chart for the truncated cone model

6.4.1 Testing of the truncated cone model against real stacks:

The truncated cone model was tested against two real tailings stacks: the 2000 meter diameter circular stack at the Sunrise Dam Gold Mine in Western Australia (Figure 129) and the 1000 meter long stack at the Peak Gold Mine in New South Wales, Australia (Figure 3). Aerial survey data was made available for analysis, as well as tailings discharge figures for the same timeframe. This information can be found in Appendices D and E.

Figure 129. Aerial photograph the Sunrise Dam tailings stack, taken from Google Earth ©.

The testing of the model involved simulating the growth of these two stacks over the timeframe covered by the two respective sets of supplied survey data, which amounted to about 2 years of growth at the Peak stack and 3 years of growth at the Sunrise Dam stack. The simulated beach shapes were built on top of the underlying stacks as described in the initial aerial surveys, and then compared to the actual measured beach shapes that were surveyed at the end of each term.

The simulation of the Peak stack was limited due to a lack of detailed discharge data, with having access only to averaged discharge history over intervals of 6 to 12 months. While this enabled the model to be applied with relative ease, it oversimplified the tailings discharge by forcing the assumption that the discharge parameters were constant over these very long periods. In the case of the

Sunrise Dam stack, daily averaged discharge data was made available for each day of the 3 year period. Other limitations of the simulation were the assumptions both stacks having flat underlying terrain, and both stacks being circular in plan view. In the case of the Sunrise Dam stack, neither of these limitations imposed a significant deviation from the actual situation, but for the Peak stack this did make a considerable simplification from the complex geometry and terrain found there (see Appendix D for a layout plan).

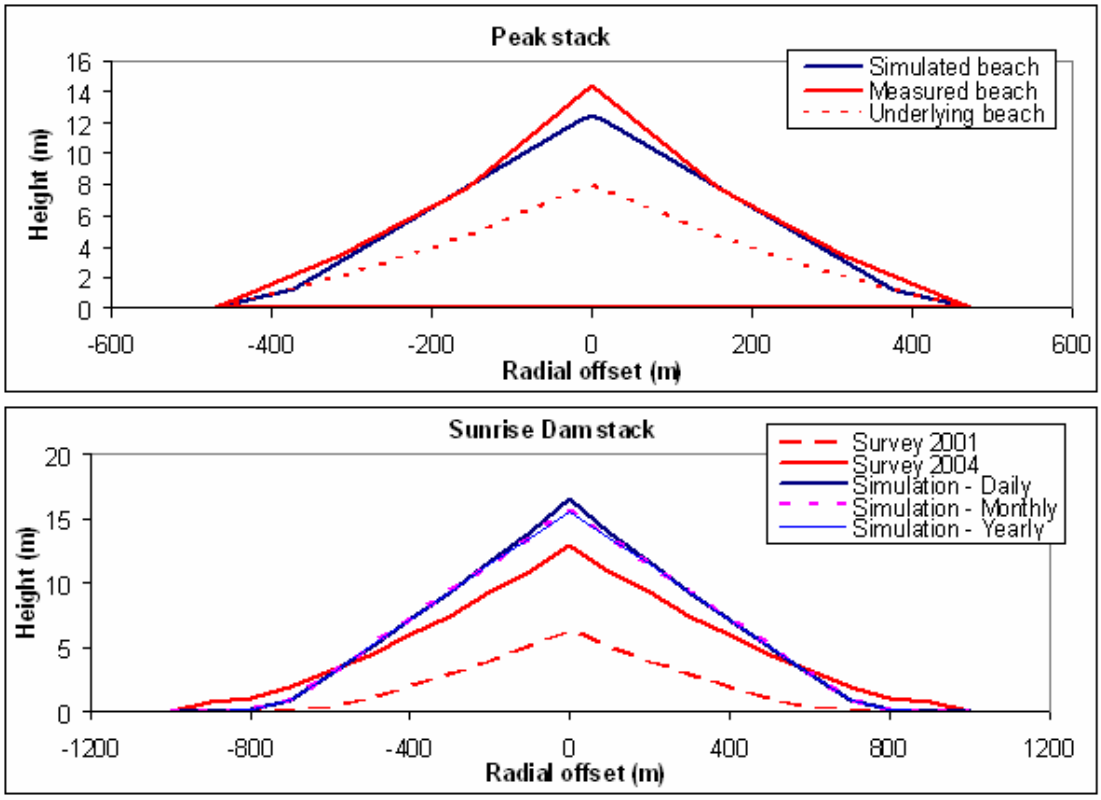

Figure 130. Comparisons between cross-section plots of simulated and actual tailings stacks for Peak (top) and Sunrise Dam (bottom). The Sunrise Dam simulation has been run 3 times to show the effect of data averaging with respect to time.

The above plots of Figure 130 present some interesting insight into the practical limitations of the simulation process employed here. In the case of the Peak stack, the simulated stack turned out to be a simple cone with only one beach slope apparent on the surface. This occurred because the final stage of simulated discharge lasted with constant discharge parameters for about 6 months, completely covering the previously deposited material with a thick layer of tailings that beached all over at one constant slope. If more detailed discharge data had been available (featuring smaller discharge intervals with some variation in flow rate and rheology), this may have resulted in more concavity in

the simulated stack, producing a result more closely resembling the measured beach. This effect has been demonstrated with the three simulations run for the Sunrise Dam stack. Daily averaged data was supplied, and was used in the first simulation. In the next simulation this data was grouped into month long blocks, with the flow rate and concentration averaged over each of the months. Finally in the third simulation of the Sunrise Dam stack, the data was further summarised on a yearly basis. It can be seen that the monthly and yearly data produced almost identical simulated beach profiles, which both resembled the Peak stack simulation in their lack of concavity.

This result raises some question over the original daily averaged data. As can be seen here, any form of averaging reduces the amount of concavity in the simulated beach, because any short-lived flow regimes with extremely high or low flow rates or concentrations that would cause steep deposits at the crown of the stack or flat deposits at the toe have been blended with other data. It is therefore noted that daily averaged data may be much better than monthly or yearly averaged data, but it still leaves significant doubt over the accuracy of the predicted beach shape.

It should also be noted that in the case of the Peak stack simulation, it appears that the supplied discharge figures were short in terms of the total volume of slurry discharged, because of the simulated beach showing a cross-sectional profile beneath that of the measured beach surface at the end of the term.

6.4.2 Frequently varying discharge parameters and large stacks

So far the model has considered a stack to grow as a series of concentric cones. This has been shown to be a manageable approach, and indeed it would be quite accurate if the discharge parameters (flow rate and rheology) remained constant for long periods like a month or more. However, tailings discharge typically varies on a daily (or even hourly) basis, due to reasons such as changing ore type from the mining face, breakdowns in the processing plant, wet weather causing dilution of the slurry etc. The result of this varying discharge on the proposed model is that the individual deposits become extremely thin if the same rationale is to be applied. Consider deposit A in Figure 126. In 3 dimensions it would resemble the shape drawn in Figure 131 (below):

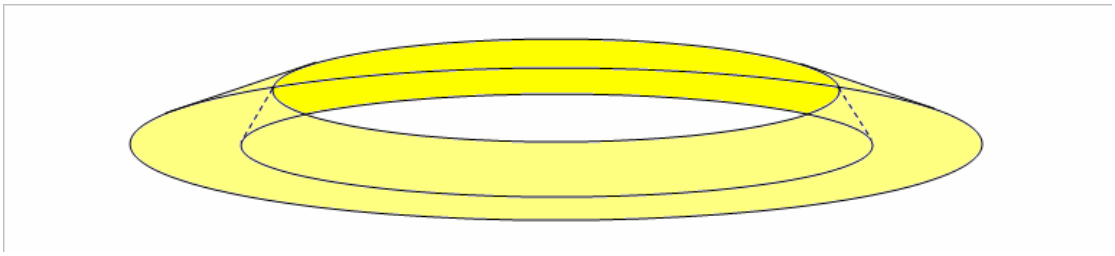

Figure 131. A 3-dimensional representation of the outermost deposit from Figure 126.

If this deposit had been created on the basis of 30 minutes of uniform discharge instead of 60 days, the assumptions of the model would cause it to look more like the shape in Figure 132 (below):

Figure 132. A 3-dimensional representation of a widely dispersed deposit.

In reality the tailings does not spread itself so thinly like this. Instead, the self-formed channel of tailings slurry will deposit in one area of the stack in a local deposit as shown in Figure 133:

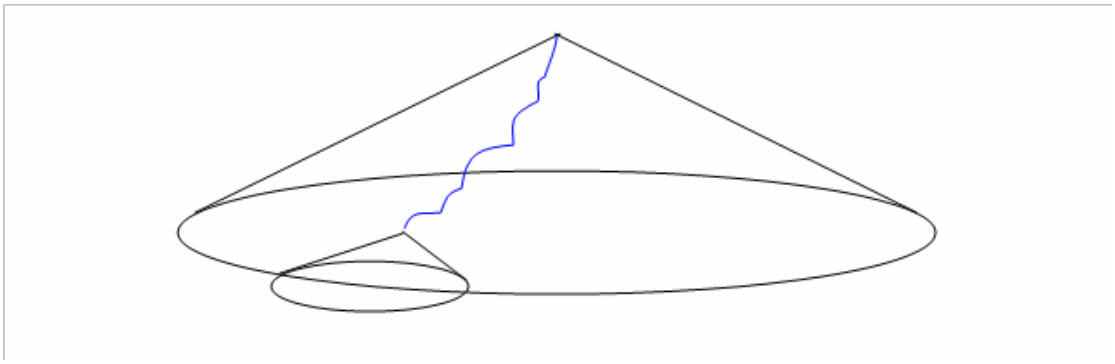

Figure 133. A small deposit formed by a channel meandering to the outer reaches of a large stack.

If the steady discharge were to continue for another month or two, the self formed channel of tailings would meander along different routes radiating from the centre of the stack, and the deposit would

continue to grow around the base of the stack, eventually to form a shape that more closely resembles Figure 131 in an ideal scenario.

However, if we continue to pursue the more challenging reality of constantly changing discharge, we need to model a stack as the build up of numerous small conical deposits as shown below in Figure 134:

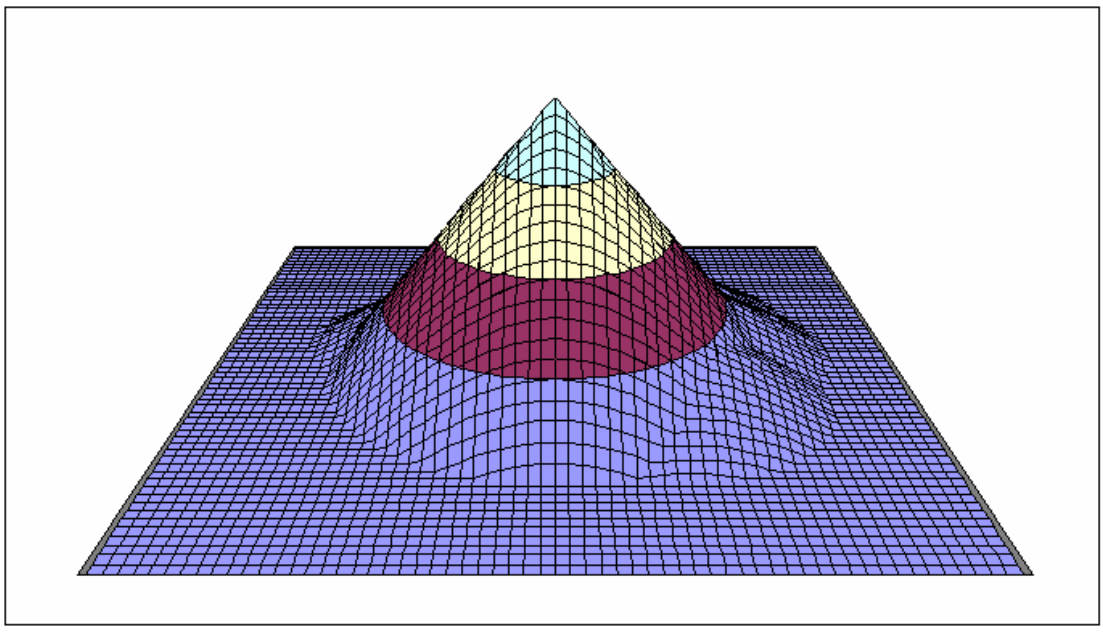

Figure 134. A compound stack formed by the accumulation of 4 small deposits on a larger underlying cone.

This rationale of small local deposits of tailings requires a new approach for the modelling of the growth of the stack. New challenges are introduced with the need to define both the location and the shape of each deposit. The former has to consider the path of the meandering channel that supplies tailings to each new deposit, and then nominate the point where the channel stops and the deposit gets placed. In addressing the latter challenge, consideration must be made for the geometry of the underlying material as well as the surface geometry of the freshly deposited material.

6.5 The local deposit model

For developing a local deposition model as described above to simulate the Sunrise Dam tailings stack, each channel path has been assumed to run as a straight line that heads radially outward from the top of the stack in a random direction. A random number generator has been used to define the direction of the channel for each regime in the form of a compass bearing. Straight channels do not form on a real tailings stack, but the random direction of each channel will ensure that the location of each deposit occurs in a realistically random location on the stack's surface.

By applying a numerical analysis approach, this new concept uses a computer to define the surface of a stack with a 100 meter grid of 3 dimensional Cartesian co-ordinates, and then conduct numerous trial and error calculations to determine where each new deposit will lie. A closer spaced grid would have been better, but this would require more processing power from the computer.

Each new deposit is initially shaped as a cone with a side slope equal to the prevailing beach slope. The beach slope was calculated with the Fitton et al. (2006) beach slope model (equations 13,14 and 62). The volume of each deposit was calculated using the Q.t relationship (equation 106).

There are two possible outcomes for locating for the apex of each cone onto the stack: either along the path of the prevailing channel, or otherwise above the apex of the stack. Only one of these two outcomes is possible. If the prevailing channel equilibrium slope is significantly steeper than the slopes found on the tailings stack, the new deposit will form on top of the stack as a crown. If the prevailing channel equilibrium slope is much flatter than the slopes found on the tailings stack, the new deposit will be located at the toe of the stack in a position dictated by the compass bearing direction of the channel. In either case, the volume trapped between the surface of the new cone and the underlying stack is equal to the discharged volume of that deposit. The discharged volume and the prevailing beach slope of each deposit mathematically enable only one of the two outcomes to be possible for the location of each deposit. The computer model started this analysis for each deposit by calculating the "critical volume" for each deposit, which is defined as the volume trapped between the stack surface and a cone with the an apex coinciding with the stack apex that has a side slope equal to the prevailing

beach slope. An "IF" statement was then used to determine which of the two location outcomes was appropriate, depending on whether the "critical volume" is bigger or smaller than the discharge volume for the prevailing flow regime. If the critical volume is smaller than the discharge volume, the flow regime creates a crown type deposit on top of the stack apex. If the critical volume is larger than the discharge volume, the new deposit is located somewhere on the side of the stack. In either case, an iterative exercise ensued to determine exactly where the new deposit should be placed so that the volume trapped between the new cone and the existing stack surface is equal to the discharge volume. For the crown type deposit, the iterative trial and error approach searched for the particular vertical distance between the stack apex and the new cone apex that would result in the trapped volume being equal to the discharge volume. For the channel fed deposit, the iterative approach searched for the particular channel length that would enable the trapped volume to be equal to the discharged volume.

Once the appropriate location was found for the new deposit, the vertical co-ordinates of the respective new shape were superimposed over the grid co-ordinates of the underlying stack, thereby becoming part of the new stack surface.

A flow diagram outlining this sequence is presented below as Figure 135:

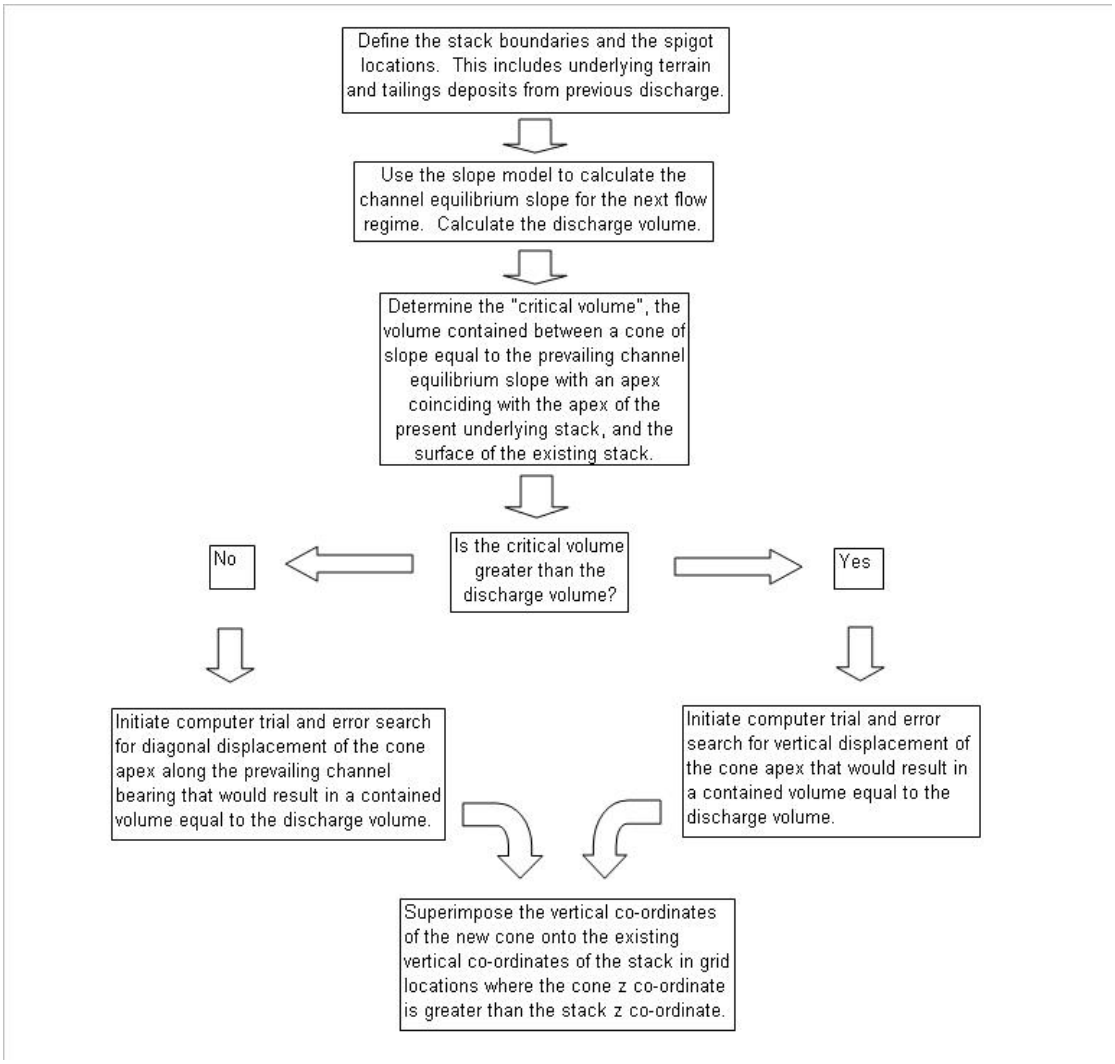

Figure 135. Flow chart of the logic steps of the local deposit stack model

A series of deposits from one of the simulations that was conducted on the Sunrise Dam tailings stack is presented in Figure 136. The numbers in the grid boxes represent elevations of points on the surface of the tailings stack. The coloured regions show the final locations for 11 consecutive deposits.

Immediately below Figure 136 is an aerial photograph of the Sunrise Dam tailings stack (Figure 137).

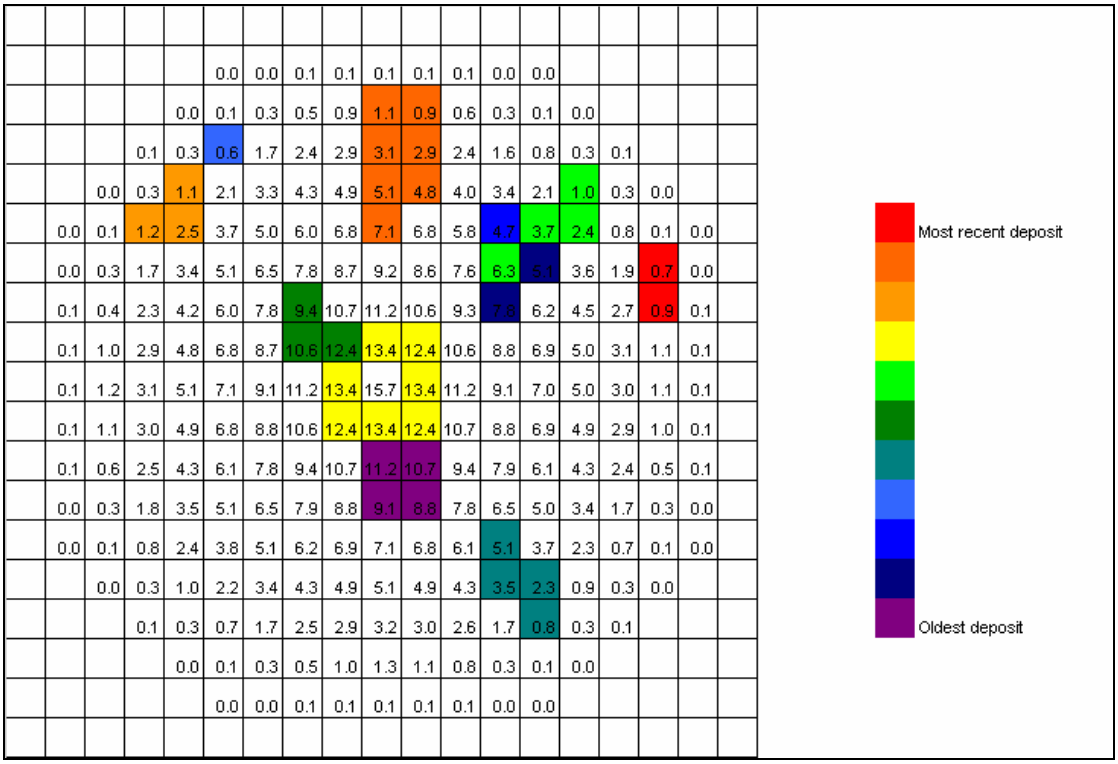

Figure 136. A series of 11 consecutive deposits (each indicated by a different colour) that were placed on the surface of the simulated Sunrise Dam stack.

Figure 137. An aerial photograph of the Sunrise Dam stack. The dark areas on the stack surface show the locations of recently deposited tailings. (Picture provided by Google Earth ©)

Figures 136 and 137 show that the individual tailings deposits that have been placed by the new model bear some resemblance to the real tailings deposits that can be seen in the aerial photograph. The shapes and locations of the simulated deposits have been determined using the procedure described in Figure 135. The comparison of the aerial photograph with the simulation grid suggests that the new shape model is offering a realistic mechanism for modelling the tailings deposition process on a tailings stack.

A three-dimensional plot of the simulated stack is presented below in Figure 138:

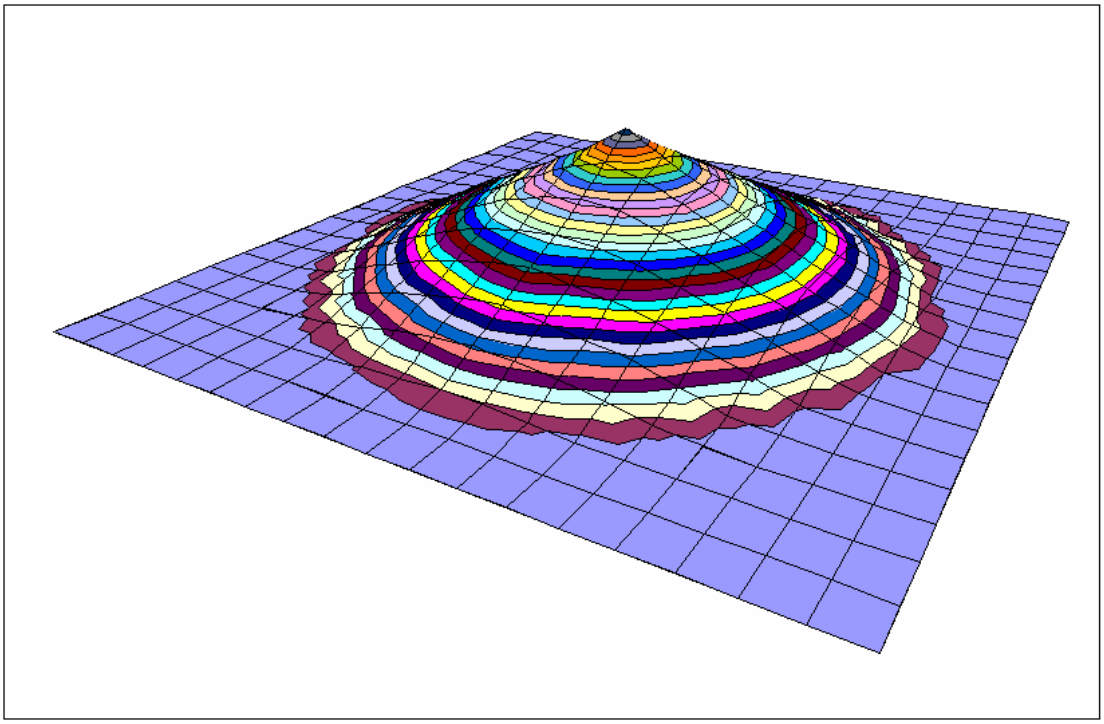

Figure 138. A 3 dimensional plot of a simulated stack generated by the local deposit stack model. The grid spacing is 100 m, and the contour interval is 0.5 m. Vertical scale exaggerated.

Figure 138 presents a realistic stack shape compared to the oblique aerial photograph of the Sunrise Dam stack presented in Figure 129. This general resemblance is also seen as positive confirmation of the model's ability to emulate the development of a tailings stack.

Some 15 simulations were performed with this new local deposit stack model, which are summarised in Table 13. The first two simulations used the daily averaged tailings discharge data that was supplied

by the Sunrise Dam gold mine as input data. This discharge data is presented in Appendix E. It can be seen that the flow rate and the concentration figures that were reported on a daily basis all demonstrated some variation from one day to the next. The standard deviation for each of these two columns of data were calculated, and found to be 21.2 l/s for the flow rate data and 2.35 % w/w for the concentration data. The input data for the next 11 regimes was generated artificially by introducing two new parameters; standard deviation in flow rate, and standard deviation in concentration. Using these new parameters together with nominated values of mean flow rate and mean concentration, a random number generator was employed to create 3 columns of data for describing each discharge regime: Channel direction, Flow rate and Concentration. The Fitton et al. (2006) beach slope model then used the flow rate and concentration figures to determine a prevailing channel equilibrium slope for each regime. This predicted slope was then fed into the beach shape model. In the last two simulations the real discharge data was used once more, but it was averaged over longer time intervals, similar to the simulations performed with the truncated cone model.

The criterion that defined the start and end of each flow regime was the chronological duration of each flow regime. For the daily averaged date supplied by the mine, this meant that each flow regime had a duration of 24 hours. For the last two simulations the flow regime durations were set by the chosen intervals of 1 month and 6 months respectively. However, if the discharge rate and slurry concentration were to remain constant for a period of (say) a year, then the model's approach in sending all of this slurry down one randomly defined channel would be unrealistic. To address this issue, another "IF" statement would be included into the model that would cut this long running regime into any number of smaller ones (as defined by some nominated time duration such as 1 day or 1 hour), with the same flow rate and concentration, but with new channel directions assigned to each new short regime to reflect the channel morphology that takes place on tailings beaches.

6.5.1 Water losses

It was necessary to consider the loss of volume that results from water bleeding out of the tailings slurry and evaporating from the slurry. Observation of real tailings discharge has shown that decant water can be seen to run off the top of the deposited tailings slurry after it stops. Much of this water

evaporates before it runs to the edge of the stack, while more moisture is evaporated from the deposited tailings during the long term process of desiccation. These processes all have a direct impact on the contained volume in the stack, so it is necessary to account for this loss of water in trying to model the build up of a tailings beach.

6.5.1.1 Water loss adjustment method # 1

This adjustment method attempted to account for bleed water runoff only. The static settlement tests that were conducted at RMIT University (see section 3.3.16) were used as a basis for estimating the amount of bleed water that would leave the deposited tailings. It was observed during these tests that less concentrated slurries yielded more bleed water. This data was used to create a simple empirical equation for predicting the water loss from a slurry as a function of the initial concentration. A plot of the water losses as a factor of slurry concentration is presented below as Figure 139, with a line of best fit inscribed.

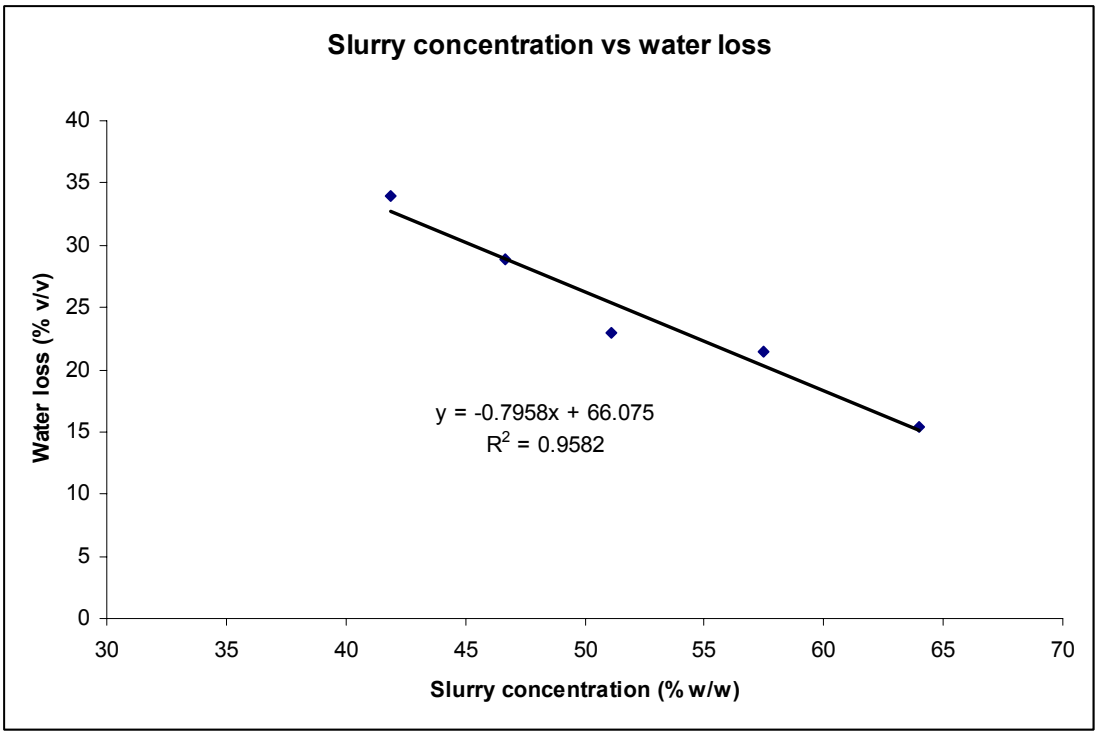

Figure 139. Plot of the experimentally observed water loss through static settlement of slurries of various concentrations. (data presented in Table 2 in section 3.3.16)

The empirical equation of the linear fit presented in Figure 139 appears below:

$$W.L. = -0.798\ Cw + 66.206 \quad (114)$$

Where W.L. is the water loss (expressed as a percentage of the total volume), and C_W is the initial concentration of the slurry (% w/w) This equation was then applied to each flow regime to adjust the discharge volume. The channel slope was still calculated on the basis of the raw discharge data though, since it is assumed that this water loss occurs after the slurry has deposited on the tailings beach.

6.5.1.2 Water loss adjustment method # 2

Another more direct water loss correction method was developed after it was found that there was still a substantial discrepancy between the volume contained in the surveyed Sunrise Dam stack (6.57 Mm^3) and the discharged volume of tailings (9.49 Mm^3). This method simply calculated a ratio between these two respective volumes, which has been named the "Volume Reduction Ratio" (VRR), and calculated to be 0.692. This new water loss compensation was applied by simply multiplying the discharged amount of each regime by the VRR. As before, the equilibrium channel slope was still calculated on the basis of the raw discharge data.

This second water loss compensation method deserves some comparison with the first to rationalise the implication of the VRR in respect to the experimental findings presented in Figure 139. Equation 114 would require an input slurry concentration of 44.3% w/w in order to calculate a water loss of 30.8% v/v, which is the necessary reduction in volume required in order to calculate a VRR of 0.692. This input concentration of 44.3% w/w is much lower than the mean concentration reported by the mine (61.7% w/w). There are numerous possible causes for this discrepancy. The most obvious one is that water loss method #1 does not consider evaporation, which would further reduce the volume of the deposited tailings. This issue of volume reduction by evaporation will not be pursued further here, but it is noted as an area that needs further investigation.

It is noted that the concept of the shrinkage limit (Lambe & Whitman, 1979) would be of value here in describing these water loss effects in a manner that is already established within the industry, but this concept has not been considered here for the sake of focusing on this model without digressing into the field of soil mechanics. In the application of this model to other tailings facilities however, it is thought that the shrinkage limit would present a very useful means by which the VRR could be rationalised with some simple laboratory experiments.

It is acknowledged that this water loss adjustment method would be more accurate if it took the respective concentration of each regime into account (like the previous method), but the error will be small in light of the relative uniformity of the regime concentrations.

It is noted from observation of tailings beaches that the desiccation (cracking) that occurs over the days following the deposition of tailings causes the beach to contain air in the resultant cracks. This reduction in density does not effectively register in terms of volume as detected by aerial survey, since the surface levels are not affected so much. It is therefore important to note that the new water loss calculations will not take these air voids into account.

As a general note, it is felt that the shape models presented here would benefit from further research of water losses from deposited tailings. This could involve dry weights analysis of in-situ samples of "dry" tailings dug from tailings beaches. This might also involve some quantification of the effect of a salt crust forming on the tailings surface, a phenomena evident at Sunrise Dam.

For the 15 simulations presented here, Water Loss Method #2 was used for all except the second one, which used Water Loss Method #1.

6.5.2 Testing of the local deposit beach shape model against actual beach shapes

The new stack shape model was applied to simulate the Sunrise Dam tailings stack. The same aerial survey data that was used in the previous stack simulation work (in section 6.4.1 with the truncated cone model) was again used here. As before, a survey done on the 29th December 2001 was adopted to mark the initial stack shape. The simulated growth of the stack began from the stack shape that was presented in that survey data. Three years' worth of discharge data was then fed into the model, generating a simulated shape for the stack that had evolved with three years of development from the initial stack shape. The aerial survey data that was gathered on the 31st December 2004 was then used to compare to the final simulated shape to the final surveyed shape.

In the first of these simulations, the historic discharge data was fed into the model. This list contained 1028 flow regimes, with each regime consisting of the averaged flow rate and concentration for each day of the 3 year period. This simulation employed the second water loss adjustment method. In the second simulation, the same historic discharge data was fed into the model, but in this simulation the first water loss adjustment method was used. As discussed in section 6.5.1, it was found that the deposited volume was not correct, so the remaining simulations employed the second water loss adjustment method.

Another 13 simulations were run to study the effects of the input parameters of this local deposit stack model, and also to determine what input parameters must be entered into the model to arrive at a simulated stack that closely resembles the measured stack at Sunrise Dam. A tabulated listing of the input parameters and key results of these 15 simulations is presented in Table 13, and the averaged profiles for a selection of these simulations have been presented graphically in Figure 140. It was found that simulations 9, 12 and 13 offered similar averaged profiles to the actual surveyed profile.

The "averaged profile" of a stack is calculated by averaging each of the four profiles of the stack in the directions of the four compass points. This is discussed in section 4.1.1.

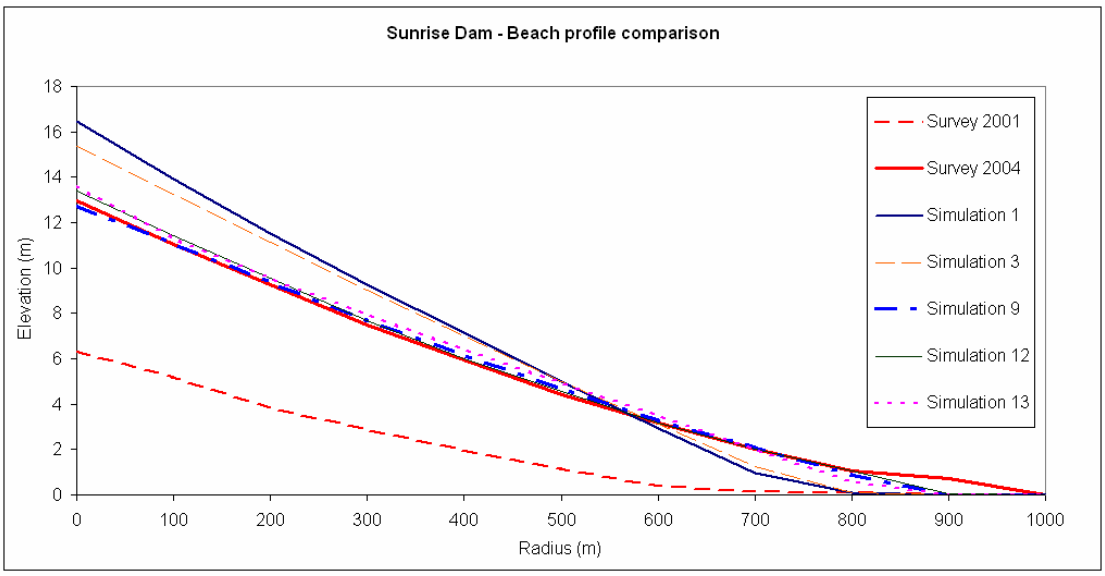

Figure 140. Averaged profiles of some simulations of the Sunrise Dam stack generated by the local deposit model.

Figure 140 shows that simulations 9, 12 and 13 resulted in final stack shapes that resembled the real stack. In order to achieve these shapes it was found that lower slurry concentrations were needed that those reported by the mine. Simulation 1 was created using the discharge data that was reported from the mine. It can be seen that the averaged profile from this simulation is much steeper than the actual averaged profile. One explanation for this discrepancy is the effect of rainfall, which is discussed in section 6.6.

Simulation Number	Mean Flow rate lt/s	Flow SD lt/s	Mean Cw %	Cw SD %	Stored Volume Mm^3	Slopes Upper %	Middle %	Lower %	Con-cavity Ratio*	Water loss method	Comments
1	100.1	21.2	61.7	2.35	6.57	2.43	2.13	1.53	1.14	2	Actual discharge data.
2	100.1	21.2	61.7	2.35	7.88	2.45	2.13	1.85	1.15	1	Actual discharge data.
3	100.1	21.2	61.7	2.35	6.57	2.11	2.01	1.58	1.05	2	Artificial data.
4	100.1	40.0	61.7	2.35	6.57	2.22	2.02	1.59	1.10	2	Artificial data.
5	100.1	21.2	61.7	6.00	6.57	2.76	2.27	1.44	1.22	2	Artificial data.
6	120.0	21.2	61.7	2.35	7.87	2.07	1.95	1.79	1.06	2	Artificial data.
7	100.1	21.2	55.0	2.35	6.57	1.59	1.52	1.43	1.04	2	Artificial data.
8	100.1	21.2	55.0	5.00	6.57	1.91	1.68	1.34	1.14	2	Artificial data.
9	100.1	21.2	52.0	5.00	6.57	1.68	1.48	1.21	1.13	2	Artificial data.
10	100.1	21.2	52.0	6.00	6.57	1.80	1.53	1.15	1.18	2	Artificial data.
11	100.1	21.2	50.0	6.00	6.57	1.65	1.41	1.08	1.17	2	Artificial data.
12	100.1	21.2	50.0	8.00	6.57	1.89	1.50	0.99	1.26	2	Artificial data.
13	100.1	50.0	55.0	2.35	6.57	1.91	1.50	1.47	1.27	2	Artificial data.
14	100.1	5.3	61.7	1.67	6.57	2.15	2.10	1.56	1.02	2	Monthly averaged real discharge data.
15	100.1	1.25	61.7	1.62	6.57	2.12	2.12	1.55	1.00	2	Half-yearly averaged real discharge data.
Survey	100.1	21.2	61.7	2.35	6.57	1.67	1.37	1.29	1.22		Final beach profile as surveyed in Dec 04
Initial					2.53	1.19	0.88	0.46	1.34		Initial beach profile as surveyed in Dec 01
*Concavity ratio is defined by Upper third slope / Middle third slope.											

Table 13. Simulations of the Sunrise Dam stack run with the local deposit stack model.

Table 13 shows the input parameters for the 15 simulations and the summarised characteristics of the simulated stack. It is noted that the artificial data used in simulations 3 – 13 was generated using a random number generator, with the mean values and standard deviations of this artificial flow rate and concentration data presented in the 2nd, 3rd, 4th and 5th columns of the table as marked. Simulation 1, 2, 14 and 15 all used the original data, but it can be seen that the averaging of the data over longer periods (for simulations 14 and 15) caused the standard deviations of the flow rate and concentration to drop because the data had less variation from one period to the next. For simulations 1 and 2, the reported mean and standard deviation figures can be seen in Appendix E. A comparison of the effects of changing each of the 4 key input parameters (mean flow rate, mean concentration, flow rate standard deviation and concentration standard deviation) is shown below, in a graph that is based on the results of simulations 3 to 7, between which only one parameter varies:

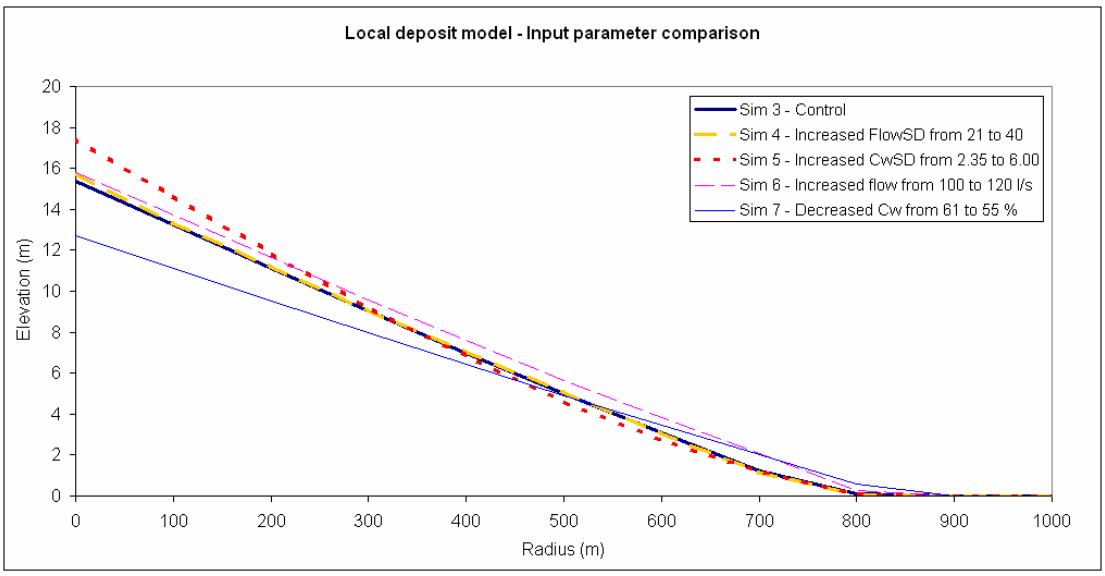

Figure 141. Averaged profiles of 5 simulations of the Sunrise Dam stack generated by the local deposit stack model, each showing the effect of changing a single input parameter.

Figure 141 shows that the change in the mean flow rate standard deviation (flow SD) from 21 l/s to 40 l/s had a small effect on the concavity of the beach, increasing the concavity ratio (the ratio of the upper slope to the middle slope) from 1.05 to 1.10.

The increase in the concentration standard deviation (Cw SD) from 2.35% to 6% had a considerable impact on the resultant stack shape, giving more concavity to the beach, with steeper slopes at the top of the stack and flatter slopes near the toe. The apex of the stack is considerably higher, but the toe radius remains about the same. The concavity ratio increased from 1.05 to 1.22.

Increasing the mean flow rate from 100 l/s to 120 l/s produced a larger volume of tailings, which is reflected in the higher and longer profile of the beach. The beach slopes decreased slightly along most of the length of the beach, but the concavity ratio remained about the same.

The change in the mean concentration from 61% to 55% also had a notable effect, with the apex getting lower and all the beach slopes becoming flatter. The length of the beach increased slightly, but the concavity ratio remained almost identical.

Time averaging of the data has shown the same effect here as that which was observed previously with the truncated cone model. The daily averaged data showed more concavity than the monthly or semesterly averaged data that was generated in simulations 14 and 15 (see Table 13). It can also be noted that the standard deviation in the flow rate decreased considerably with further time averaging of the data. On this basis the data would suggest that the actual non-averaged discharge at Sunrise Dam for the 3 year period would have a larger flow rate standard deviation than the 21 l/s calculated from the daily average data, thereby causing the model to predict a profile more like Simulation 4.

In referring to Figure 140 it was noted that the 13th simulation bears a good resemblance to the actual surveyed beach shape, but it had an input mean concentration of only 55% w/w, a significant drop from the 61% reported by the mine. In some of the other simulations, mean concentrations of only 52% and even 50% were found to predict shapes resembling the survey data. One possible cause of this discrepancy is the effect of rainfall, something that has not been mentioned until now. This is discussed in section 6.6.

6.6 Rainfall effects

It is noted that some 407.5 mm of rain is reported to have fallen at the Sunrise Dam mine during the 2004 calendar year, while 180.6 mm was recorded for 2003, and 450 mm for 2002. This information was provided by the mine. If any of this rain water were to be absorbed into the tailings slurry, the rheological parameters of the slurry would be altered, resulting in a flatter equilibrium slope, and hence a flatter beach slope.

It is likely that rain water could enter the tailings slurry by a number of means; both upstream of the processing plant and downstream, as well as within the processing plant itself. However, it is expected that any introduction of rainwater upstream of the tailings discharge spigots (such as direct wetting the ore in the open pit or on the ROM pad, or dilution of the slurry within the leach tanks or thickeners for example) will not be of relevance, because the tailings concentration figures provided by the mine are understood to be read at the tailings pumps. Rain falling directly on the stack is seen to pose an impact on the water content of the slurry, with the potential for runoff from the vast surface area of the stack to

enter the tailings channels that meander down its slopes. There is also the potential for ponds to form near the perimeter bunds of the stack (the bund does not appear in the averaged profile for the survey data in figure 140, but it can be seen in the survey layout plan provided in Appendix D). If the channel should run into the pond, severe dilution will take place, with expected segregation and alluvial deposition of coarse particles taking place immediately, and the longer term suspension of fine particles in the pond, ultimately resulting in a significantly flatter beach in the area occupied by the pond after it finally evaporates. There is also the question of water that is absorbed into the surface of the tailings beach without running off. Gauging the actual amount of water to enter the tailings in such scenarios would be of benefit to this investigation.

It is calculated that the Sunrise Dam stack has a catchment surface area of some 314 hectares. Over the 3 year period this would have collected some 3.26 Mm^3 of rainwater on the basis of the figures shown above. Compared to the 9.49 Mm^3 of discharged tailings, this is a significant volume of water, and when compared to the 6.57 Mm^3 of deposited tailings calculated from the survey data, the rainfall becomes even more significant. With this in mind, it is possible that the effective concentration of discharged tailings could be much lower than the 61 % reported, bringing simulations 9 and 13 with their respective concentrations of 55% and 50% into the realms of plausibility, depending on how spread out the rainfall events were. The effects of evaporation would need to be considered in this investigation too, but such work is beyond the scope of this modelling exercise.

6.7 Beach profile concavity

Beach profile concavity has been discussed on numerous occasions in past literature, with a review of this literature presented in section 2.1.6. Numerous causes for concavity have been asserted; for segregating slurries, concavity has been previously claimed to be the result of segregation of particles as they deposit along a tailings beach, with the larger particles coming to rest near the discharge outlets (and hence producing a steep beach slope) and the smaller particles travelling further down the beach to produce a flatter beach slope near the toe. (Robinsky 1978) For non-segregating slurries, beach profile concavity has been attributed to a decrease in viscosity over distance, due to a gradual increase in water content in the slurry as a result of consolidation of the underlying tailings (Robinsky 1978); particle

size, with larger particles causing more concavity than small ones (Blight & Bentel 1983); a decrease in concentration of the slurry as it progressively loses solid particles during its journey down the beach (Wates et al. 1987); seepage of water through the deposited tailings from the steep areas of the beach to the flatter areas (Kupper 1991); a variation in density of the underlying tailings from the point of view of the stability of the channels that form on top (Chryss et al. 2006); and through variation in the slurry discharge parameters (Fitton et al. 2006).

The work presented in this chapter presents a strong case to support the theory that the variation in the slurry discharge parameters is the cause of concavity in a beach formed with non-segregating tailings slurry.

This new model presents a means by which concavity is generated without any "concavity factor" being required. Providing the input data exhibits variation in either the flow rate or the rheology, the simulated stack will exhibit concavity.

6.8 Discussion

Two models have been presented in this chapter for the simulation of the growth of a tailings stack formed by the deposition of non-segregating tailings slurry, with the second of these models providing a more realistic basis for beach development and some realistic shapes in comparison to a real tailings stack. This exercise has not only introduced a plausible explanation for the concavity typically observed on a tailings beach created by the sub-aerial discharge of a non-segregating tailings slurry, but a means by which this concavity can be modelled.

The local deposit model presented here could be further developed to suit more complex tailings stacks with multiple points of discharge on undulating underlying terrain. It could also be adapted to perform beach growth simulations in impoundment type tailings storage facilities.

This new beach shape model presents a superior approach to any of the other shape models discussed in section 6.1. Not only does this model produce more realistic surface contours than those generated by the other models, but it also has the ability to handle detailed input data and react to the input data. For example, if one day should find that the water content of the tailings shoots up unexpectedly, the resultant deposited material on that day will form a flatter beach somewhere far from the discharge spigot. Likewise, if an unexpected drop in the tailings flow rate should occur (perhaps as a result of a mill break-down), then the deposited tailings during this time will form a steep build-up near the spigot. The other models will not react in such a manner. They will simply build up the entire TSF surface on the basis of the input slope and concavity factors that the user defines. Longer term effects such as the gradual changing of the ore mined, increasing production, or upgrades in processing technology can be handled rationally by the local deposit model by reacting to the input data fed into it.

Strong anecdotal support is provided for this model by some examples of the management of the tailings storage facilities at the Sunrise Dam gold mine and the Peak gold mine in Cobar. The operating personnel at the Sunrise Dam gold mine have exploited the channel flow behaviour of tailings slurry to control the deposition that occurs on their tailings stack. By adjusting the flow rate from individual discharge spigots with valves, they could control how far the tailings would deposit from the discharge spigot; if they wanted to build up the upper region of the beach they would cut back the discharge rate on the applicable spigot, while if they wanted to send the tailings out to the far reaches of the stack they would increase the flow from a spigot. At the Peak gold mine in Cobar this channel flow behaviour of tailings slurry was exploited in a different way in an effort to develop steeper beach slopes; more discharge spigots were fitted to the end of the tailings supply line. By splitting the discharge into about 8 streams, the beach became significantly steeper, providing that the streams could be prevented from merging into one another on the beach. This reflects the findings of the operators of the Kidd Creek stack, who also split the slurry flow to achieve steeper beach slopes. (Robinsky 1975) Such anecdotal observations of tailings deposition behaviour provide strong support to the notion of the channel slope dictating the beach slope, which in turn presents some good support to the new beach slope models and beach shape model presented in this work.

Chapter 7: Conclusions and Recommendations

7.1 Conclusions

This work has made some valuable contributions to the state of the art of tailings beach slope prediction, tailings deposition modelling, and the modelling of open channel flows.

Strong evidence has been presented to suggest that the equilibrium slope of an open channel of tailings dictates the resultant beach slope that forms. The models that predict channel equilibrium slopes well when compared to open channel flume data also predict beach slopes accurately upon comparison with industrial beach slope data. Further evidence of this phenomenon is provided by anecdotal reports from two mines where this channel flow behaviour is exploited to control the beach that is formed.

Some 16 tailings beach slope prediction models from the literature have been applied to predict beach slopes against some 5 sets of relevant experimental and industrial data, with the predictive accuracy of each model statistically evaluated and compared. It was found that the Fitton et al. (2006) model was the only one that predicted tailings beach slopes reasonably well in comparison to industrial beach slope data, with the other models failing to do so.

Experimental findings suggest that the open channel flow of tailings slurry in self-formed channels on tailings beaches is always turbulent within the range of rheology and flow rates tested.

Segregation does not occur in a flowing channel of tailings slurry when the concentration of the slurry is above its effective segregation threshold. Below this segregation threshold, the channel adopts a relatively flat equilibrium slope. In such segregating slurry flows, the segregation of particles occurs at channel slopes flatter than equilibrium, with the larger particles settling to the channel bed.

It was found that sheared segregation threshold tests should supersede the static segregation threshold tests that are currently used to determine the slurry segregation threshold. Static tests appear to under-predict the effective segregation threshold in a flowing open channel of tailings slurry.

The flow rate has a major effect on the equilibrium slope of a channel, with low flow rates requiring steep slopes to avoid solids deposition from occurring on the channel bed, and high flow rates maintaining flatter slopes without deposition occurring.

The concentration has a less noticeable affect on the slope, but the experimental results suggest that low concentrations of slurry will drop particles at flatter slopes than high concentrations.

Particle size has been experimentally observed to affect the channel slope, with large particles causing steeper equilibrium slopes than small particles.

A comparison of some flow resistance equations has found that the Darcy-Weisbach equation works well with the Colebrook White equation being used to calculate the Darcy friction factor to model open channel flows.

It has been found that the Manning-Strickler flow resistance equation with the Lacey particle size correlation fits the flume data very well, therefore suggesting that the equilibrium flow criterion is equivalent to the Lacey regime flow criterion.

Investigation of the application of the Colebrook White equation for open channels with granular boundaries has found that the best results were gained by assuming that the channel surface roughness term k_s in the Colebrook White equation is equal to 2 x d_{90}.

The Oroskar & Turian (1980) minimum transport velocity equation is found to offer good predictions of the minimum velocity required to transport solid particles in tailings slurries upon comparison with some 17 other minimum transport velocity equations from the literature.

An analytical investigation of the cross-sectional shape of self formed tailings channels has found that the cross-sectional geometry has a negligible effect on the beach slope predictions made with the new a priori model and the new semi-empirical model.

Three new tailings beach slope models have been presented in this work:

- A new simple empirical equation is presented to enable tailings beach slope predictions to be made with ease and speed, with only the flow rate and concentration required as input parameters. A chart form of this new simple empirical model is also presented, which enables beach slopes to be predicted without the need for any calculations to be made.

- A new a priori tailings beach slope prediction model is presented here, which enjoys the major advantage of being founded on proven, previously established equations. This a priori model makes good predictions compared to previously presented beach slope models.

- A new semi-empirical beach slope model is presented, which yields more accurate beach slope predictions than the a priori model. This model is empirically calibrated with the field flume data, but validated with other independent data.

A method for predicting the laminar/turbulent transition point in open channels for a non-Newtonian fluid is presented. This method can be used to determine the state of flow (whether the flow is laminar or turbulent), and can also be applied to predict the depth of flow in an open channel of non-Newtonian fluid, for both laminar and turbulent flows.

A new three-dimensional tailings stack shape prediction model provides realistic shape predictions upon comparison with a real stack. It is found that the new model breaks new ground in its ability to react to the input data with its shaping of the tailings beach surface.

The new models presented in this work lend further support to the semi-empirical model presented by Fitton et al. (2006). It is of interest to note the resemblance of the field flume data in the fit plots of the new models presented here to that in the fit plot presented in Fitton et al. (2006). For these new models, it can be seen that the outlying points appear to recur in the same manner as was observed in the Fitton et al. (2006) plot. This would suggest that the experimental data is the cause, with these points actually being outliers, as opposed to the model being the cause of their waywardness. This

exercise has therefore lent substantial support to the semi-empirical model put forth by Fitton et al. (2006).

This work has shown that the various physical principles at work in the deposition process of hydraulically discharged non-segregating tailings have already been extensively researched under a number of other related scientific fields. It brings the science of tailings beach slope prediction into the well established fields of rheology, sediment transport and hydraulics. Much work has been done in recent decades to empirically predict tailings beach slopes, to develop laboratory scale experimental procedures for predicting beach slopes, to explain the phenomena with the application of various theories, and create new ones. It is hoped that this work will provide some basis and direction for future research in the field of tailings beach slope prediction to build on.

It was found that the Parker et al. (1988) model with the Whipple et al. (1998) empirical constants performed quite poorly against all of the validation data used in this work, but more importantly, it performed poorly against the alluvial fan data that was presented by Whipple et al. This is a significant issue, because this model was deemed to be the most accurate and realistic by Whipple et al. Given the considerably better performance of some of the beach slope models reviewed and presented in this work, a significantly improved approach could be recommended to those wanting to model the slopes of alluvial fan deposits.

It can also be argued from this finding that the beach slope equations presented here present the potential for an advance in the prediction of river and natural channel bed slopes, since the Parker model visited here is often cited in the prediction of such processes. (Eaton et al. 2004; Kramer & Marden 1992)

7.2 Recommendations

The following recommendations are made, not only on the basis of what has been learned in this project, but also in terms of what could add further benefit in related fields:

- More flume tests in a larger flume that is able to run large flow rates of 30 ~ 150 l/s would be useful, since this is the magnitude of the discharge in many large mines.

- Further flume testing of tailings slurries with different rheology and particle characteristics to those tested in this research should be carried out. It has already been noted that the rheology of the two tailings slurries of Sunrise Dam and Cobar was remarkably similar as a function of the respective concentration of each slurry. It is also noted that both slurries contained particles of almost identical density.

- More research with the self-formed channel style of flume would be of value. This would add further support to the link between equilibrium slopes and beach slopes.

- The installation of a Coriolis flowmeter in the slurry supply line of the flume would improve the flow and concentration measurement techniques significantly. A Coriolis flowmeter is able to measure both flow rate and fluid density with accuracy and reliability. Spikes or fluctuations would be noticed immediately. The time taken to make these measurements would be virtually instant, compared to 5 minutes for flow and 3 minutes for concentration using the methods described in Chapter 3. With the Coriolis flowmeter feeding a constant stream of measurements to a computer, the further installation of actuated valves in the water and slurry feed lines would allow the computer to constantly adjust the incoming flows of tailings and water to eliminate fluctuations.

- The installation of a pair of differential pressure transducers into the tailings feed line to the flume would enable in-line rheological measurement of the slurry as it enters the flume. This would present a significant advance on the present method, since all assumptions about the slurry rheology could then be replaced with a constant stream of measured rheology data.

- Further research into the segregation threshold of a slurry would be useful. In particular, it is felt that some form of empirical or theoretical relationship between the static segregation threshold value and the effective sheared segregation threshold would be of significant value.

- Development of a sheared segregation testing apparatus with simpler geometry would be of value, so that the effective shear rate can be more easily determined.

- Conduct more flume tests at the low flow rate region to further investigate the phenomenon of low concentrations reaching steep slopes. This also has potential implications for the interpretation of results from small scale flume experiments.

References

Abulnaga, BE 2002, *Slurry Systems Handbook*, McGraw-Hill Professional Publishing.

ASCE Task Committee on Hydraulics, BM, and Modeling of River Width Adjustment 1998, 'River Width Adjustment. II: Modeling', *J. Hydr. Engrg.*, vol. 124, no. 9, pp. 903-17.

Baker, P & Jacobs, B 1979, *A guide to slurry pipeline systems*, BHRA fluid engineering.

Bhagoria, JL, Saini, JS & Solanki, SC 2002, 'Heat transfer coefficient and friction factor correlations for rectangular solar air heater duct having transverse wedge shaped rib roughness on the absorber plate', *Renewable Energy*, vol. 25, pp. 341–369

Blight, GE 1987, 'The concept of the master profile for tailings dam beaches', paper presented to The International Conference on Mining and Industrial Waste Management, Johannesburg, South Africa.

Blight, GE 1994, 'The master profile for hydraulic fill tailings beaches', *Trans. Instn civ engrs geotech engng*, vol. 107, pp. 27-40.

Blight, GE & Bentel, GM 1983, 'The behaviour of mine tailings during hydraulic deposition', *Journal of the South African Institute of Mining and Metallurgy*, vol. 83, no. 4, pp. 73-86.

Blight, GE, Thomson, RR & Vorster, K 1985, 'Profiles of hydraulic-fill tailings beaches, and seepage through hydraulically sorted tailings', *Journal of the South African Institute of Mining and Metallurgy*, vol. 85, no. 5, pp. 157-61.

Boldt, CMK 1988, *Beach characteristics of mine waste tailings*, 9171, US Bureau of mines.

Chadwick, A, Morfett, J & Borthwick, M 2004, *Hydraulics in civil and environmental engineering*, Fourth edn, Spon press.

Chow, VT 1959, *Open-channel hydraulics*, International student edition edn, McGraw-Hill, New York.

Chryss, AG & Pullum, L 2007, 'A new viscometric technique to successfully measure shear thickening behaviour, if and when it occurs', paper presented to HYDROTRANSPORT 17 The 17th International Conference on the Hydraulic Transport of Solids, Cape Town, South Africa, 7–11 May 2007.

Chryss, AG, Fitton, TG & Bhattacharya, SN 2006, 'Turbulent flow of non-Newtonian tailings in self-formed channels on tailings stacks', paper presented to Paste 2006, Limerick, Ireland, 3-7 April 2006.

Clayton, S, Grice, TG & Boger, DV 2003, 'Analysis of the slump test for on-site yield stress measurement of mineral suspensions', *International Journal of Mineral Processing*, vol. 70, no. 1-4, pp. 3-21.

Colebrook, C & White, C 1937, 'Experiments with Fluid Motion in Roughened Pipes', *Proc. R. Soc. London, Ser. A*.

Cooke, R 2002, 'Laminar flow settling: the potential for unexpected problems.' paper presented to British Hydromechanics Research Group 15th International Conference on Slurry Handling and Pipeline Transport HYDROTRANSPORT 15, Banff, Canada, June 2002.

Coussot, P, Proust, S & Ancey, C 1996, 'Rheological interpretation of deposits of yield stress fluids', *J. Non-Newtonian Fluid Mech.*, vol. 66, pp. 55-70.

Davies, MP & Rice, S 2001, 'An alternative to conventional tailings management–"dry stack" filtered tailings', paper presented to Tailings and Mine Waste'01, Fort Collins, USA.

de Hoog, FR & Anderssen, RS, 2005, 'Approximate solutions for the Couette viscometry equation', *Bulletin of the Australian Mathematical Society*, vol. 72, no. 3, pp. 461-470.

Delft 2006, *Delft Hydraulics Instruments*, viewed 30th December 2006 <http://www.wldelft.nl/inst/intro/index.html>.

Dominguez, B, Souyris, R & Nazer, A 1996, 'Deposit velocity of slurry flow in channels', paper presented to Hydrotransport 13.

Douglas, J, Gasiorek, J & Swaffield, J 1983, *Fluid Mechanics*, Pitman Publishing.

Durand, R 1953, 'Basic relationships of the transportation of solids in pipes - experimental research', paper presented to Minnesota International Hydraulics Convention, Minnesota, USA.

Ehm, G 2005, *Anglogold Ashanti country report Australia for 2005*.

Engels, J 2006, *Tailings Storage Guidelines and Standards*, viewed November 11 2006, <http://www.tailings.info/guidelines.htm>.

Faddick, RR 1982, 'Technical aspects of shiploading coal slurries', paper presented to Seventh International Technical Conference on Slurry Transportation, March 23-26, 1982.

Faddick, RR 1986, 'Slurry flume design', paper presented to 10th International Conference on the Hydraulic Transport of Solids in Pipes.

Fan, X & Masliyah, J 1990, 'Laboratory Investigation of Beach Profiles in Tailings Disposal', *Journal of Hydraulic Engineering*, vol. 116, no. 11, pp. 1357-73.

Fitton, TG, Chryss, AG & Bhattacharya, SN 2006, 'Tailings beach slope prediction: A new rheological method', *Int. J. Surface Mining, Reclamation and Environment*, vol. 20, no. 3, pp. 181-202.

Fourie, AB 1988, 'Beaching and Permeability Properties of Tailings', paper presented to Hydraulic Fill Structures.

Fourie, AB 2006, 'Liquefaction Potential for Surface Deposits of High-Density Thickened Tailings', paper presented to Paste 2006, Limerick, Ireland.

Gillies, RG & Shook, CA 1991, 'A Deposition Velocity Correlation for Water Slurries', *Can. J. Chem. Eng.*, vol. 69, pp. 1225-7.

Gillies, RG, Schaan, J, Sumner, RJ, McKibben, MJ & Shook, CA 2000, 'Deposition Velocities for Newtonian Slurries in Turbulent Flow', *Can. J. Chem. Eng.*, vol. 78, pp. 704-8.

Glenister, D & Abbott, T 1989, 'Dewatering and Disposal of Fine Bauxite Residue', paper presented to Dewatering Technology and Practice, Brisbane, Australia.

Graham, L, Hamilton, R, Rudman, M, Strode, P & Pullum, L 2002, 'Coarse solids concentration profiles in laminar pipe flows', paper presented to British Hydromechanics Research Group 15th International Conference on Slurry Handling and Pipeline Transport HYDROTRANSPORT 15, Banff, Canada, June 2002.

Haldenwang, R 2003, 'Flow of non-Newtonian fluids in open channels', D.Tech. thesis, Cape Technikon, Cape Town.

Haldenwang, R, Slatter, P & Chhabra, R 2002, 'Laminar and Transitional flow in Open Channels for non-Newtonian Fluids', paper presented to 15th International Conference on Hydrotransport., Banff, Canada.

Haldenwang, R, Slatter, P, Vanyaza, S & Chhabra, R 2004, 'The effect of shape on laminar flow in open channels for non-Newtonian fluids', paper presented to 16th International Conference on Hydrotransport, Santiago, Chile, 26–28 April, 2004.

Henderson, ME 1988, 'Slurry pipelines: Present and Future', paper presented to Hydraulic Fill Structures.

ICMM, ICoMaM 2005, *ICMM PRELIMINARY COMMENTS ON THE DRAFT FRAMEWORK FOR RESPONSIBLE MINING*, <http://www.frameworkforresponsiblemining.org/pubs/ICMMComments.pdf>.

Ikeda, S, Parker, G & Kimura, Y 1988, 'Stable width and depth of straight gravel rivers with heterogeneous bed materials', *Water Resources Research*, vol. 24, no. 5, p. 713–22.

Ishii, M & Zuber, N 1979, 'Drag coefficient and relative velocity in bubbly, droplet or particulate flows', *AIChE J.*, vol. 25, pp. 843-55.

Jeyapalan, J, Michael Duncan, J & Bolton Seed, H 1983a, 'Analyses of flow failures of mine tailings dams', *ASCE J Geotec Eng*, vol. 109 / 2, no. 2, pp. 172-89.

Jeyapalan, J, Michael Duncan, J & Bolton Seed, H 1983b, 'Investigation of flow failures of tailings dams', *ASCE J Geotec Eng*, vol. 109, no. 2, pp. 172-89.

Kupper, AAG 1991, 'Design of hydraulic fill', PhD thesis, University of Alberta.

Lambe, TW & Whitman, RV 1979, 'Soil Mechanics, SI Version', John Wiley & Sons, Inc., New York.

Lowe, S 2003, 'Omission of Critical Reynolds Number for Open Channel Flows in Many Textbooks', *J. Profl. Issues in Engrg. Educ. and Pract.*, vol. 129, no. 1, pp. 58-9.

Malvern Instruments 2007, *Mastersizer 2000 datasheet*, viewed 29 March 2007 <http://www.malvern.com/LabEng/products/Mastersizer/ms2000/ms2k_datasheet.htm>.

McPhail, GI 1994, 'Prediction of the beaching characteristics of hydraulically placed tailings', PhD thesis, University of Witwatersrand.

McPhail, GI & Blight, GE 1998, 'Predicting tailings beach profiles using energy and entropy', paper presented to 5th Int conf Tailings and Mine Waste 1998.

Melent'ev, BA, Kolpashnikov, HP & Volnin, BA 1973, *Alluvial hydraulically engineered constructions*, Energy, Moscow.

Mine Solutions 2006, *Tailings Manual*, viewed 12th Sep 2006 <http://www.minesolutions.com/help/tailings/index.html>.

Morris, PH 1993, 'Two-dimensional model for sub-aerial deposition of mine tailings slurry', *Trans. Instn Min. Metall. (Sect. A: Min. Industry)*, vol. 102, pp. A181-7.

Morris, PH 2006, 'Flow resistance on mine waste beaches', *Int. J. Surface Mining, Reclamation and Environment*, vol. 20, no. 3, pp. 203-8.

Morris, PH & Williams, DJ 1996, 'Prediction of Mine Tailings Delta Profiles', *Transactions of the Institution of Mining and Metallurgy, Section A - Mining Industry*, vol. 105, pp. A63-A8.

Morris, PH & Williams, DJ 1997a, 'Hydraulic conditions leading to exponential mine tailings delta profiles', *Transactions of the Institution of Mining and Metallurgy, Section A - Mining Industry*, vol. 106, pp. A34-A7.

Morris, PH & Williams, DJ 1997b, 'Co-disposal of washery wastes at Jeebropilly colliery, Queensland, Australia', *Transactions of the Institution of Mining and Metallurgy, Series A.*, vol. 106, pp. 25-9.

Morris, PH & Williams, DJ 1997c, 'Hydraulic sorting of co-disposed coarse and fine coal wastes', *Transactions of the Institution of Mining and Metallurgy, Series C*, vol. 106, pp. 21-6.

Morris, PH & Williams, DJ 1999, 'Worldwide correlations for subaerial aqueous flows with exponential longitudinal profiles', *Earth Surf. Process. Landforms*, vol. 24, pp. 867-79.

Newman, P, Cadden, A & White, R 2001, 'Paste, The Future of Tailings Disposal?' paper presented to International Conference on Mining and the Environment, Skelleftea, Sweden, June 25-July 1, 2001.

Nguyen, QD & Boger, DV 1998, 'Application of rheology to solving tailings disposal problems', *International Journal of Mineral Processing*, vol. 54, no. 3-4, pp. 217-33.

Oroskar, AR & Turian, RM 1980, 'The critical velocity in pipeline flow of slurries', *AIChE J.*, vol. 26, pp. 550-8.

Parker, G 1979, 'Hydraulic geometry of active gravel rivers', *J. Hydr. Div. ASCE*, vol. 105, pp. 1185-201.

Parker, G, Paola, C, Whipple, K & Mohrig, D 1998, 'Alluvial fans formed by channelized fluvial and sheet flow. I: Theory', *Journal of Hydraulic Engineering*, vol. 124, no. 10, pp. 985-95.

Parker, G, Paola, C, Whipple, K, Mohrig, D, Toro-Escobar, C, Halverson, M & Skoglund, T 1998, 'Alluvial Fans Formed by Channelized Fluvial and Sheet Flow. II: Application', *J. Hydr. Engrg.*, vol. 124, no. 10, pp. 996-1004.

Pashias, N, Boger, DV, Summers, J & Glenister, DJ 1996, 'A fifty cent rheometer for yield stress measurement', *Journal of Rheology*, vol. 40, no. 6, pp. 1179-89.

Paterson, A 2004, 'High density slurry and paste tailings, transport systems.' paper presented to International Platinum Conference 'Platinum Adding Value'.

Pinto, M & Barrera, S 2002, 'Tailings beach slope forecasting - copper tailings', paper presented to 9th Int conf Tailings and Mine Waste 2002.

Pirouz, B 2006, 'Beach slope forecasting', PhD thesis, K. N. Toosi University of Technology.

Pirouz, B, Kavianpour, MR & Williams, MPA 2005, 'Thickened Tailings Beach Deposition. Field Observations and Full-Scale Flume Testing.' paper presented to Paste 2005, Santiago, Chile.

Pirouz, B, Kavianpour, MR & Williams, MPA 2006, 'Sheared and un-sheared segregation and settling behavior of fine sand particles in hyperconcentrated homogeneous sandwater mixture flows', *Journal of Hydraulic Research*, vol. In press.

Rade, L & Westergren, B 1990, *Beta mathematics handbook (Second Edition)*, Studentlitteratur, Lund.

Raudkivi, AJ 1990, *Loose Boundary Hydraulics (Third Edition)*, Pergamon Press.

Ribeiro, LFM & Assis, AP 1999, 'Experimental simulation of the hydraulic deposition process in tailings dams', Masters thesis, Federal University of Ouro Preto.

Rift TD software package, viewed 3rd July 2006, <http://www.riftxone.com/>.

Robinsky, EI 1975, 'Thickened discharge - A new approach to tailings disposal', *CIM Bulletin*, vol. 68, pp. 47-53.

Robinsky, EI 1978, 'Tailings Disposal by the Thickened Discharge Method for Improved Economy and Environmental Control', paper presented to Tailings Disposal Today, Proceedings of the 2nd International Tailing Symposium, Denver, Colorado, USA, May 1978.

Seckin, GS, N; Yurtal, R 2006, 'Boundary shear stress analysis in smooth rectangular channels', *Canadian Journal of Civil Engineering*, vol. 33, no. 3, p. 336.

Shenoy, AV & Mashelkar, RA 1983, 'Engineering Estimate of Hydrodynamic Entrance Lengths In Non-Newtonian Turbulent Flow', *Ind. Eng. Chem. Process Des. Dev*., 22, 165-168

Slatter, P 2004, 'The hydraulic transportation of thickened sludges', paper presented to Water Institute of South Africa (WISA) Biennial Conference, Cape Town, South Africa, 2-6 May 2004.

Slatter, P 2006, 'Particulate systems rheology', paper presented to Paste 06 Rheology workshop, Limerick, Ireland.

Smith, GM, Abt, SR & Nelson, JD 1986a, 'Profile prediction of hydraulically deposited tailings', *Transaction of the Society of Mining Engineers of AIME*, vol. 280, pp. 2024-7.

Smith, GM, Abt, SR & Nelson, JD 1986b, 'A prediction procedure for hydraulically placed tailings', paper presented to Geotechnical and Geohydrological aspects of waste management, Fort Collins, USA.

Sofra, F & Boger, DV 2000, 'Exploiting the rheology of mine tailings for dry disposal', paper presented to 7th Int conf Tailings and Mine Waste 2000.

Sofra, F & Boger, DV 2001, 'Slope prediction for thickened tailings and pastes', paper presented to 8th Int conf Tailings and Mine Waste 2001.

Sofra, F & Boger, DV 2002, 'Environmental rheology for waste minimisation in the minerals industry', *Chemical Engineering Journal*, vol. 86, no. 3, pp. 319-30.

Sun, T, Paola, C, Parker, G & Meakin, P 2002, 'Fluvial fan deltas: Linking channel processes with large-scale morphodynamics', *Water Resources Research*, vol. 38, no. 8, pp. 26-1 to -10.

Theriault, JA, Frostiak, J & Welch, D 2003, 'Surface Disposal of Past Tailings at the Bulyanhulu Gold Mine, Tanzania', paper presented to Sudbury Mining and Environment conference, Sudbury, Ontario, Canada, May 25th-28th, 2003.

UNEP, UNEP 2005, *Chronology of major tailings dam failures*, viewed 26 September 2005 <http://www.wise-uranium.org/mdaf.html>.

Walton, IC 1995, 'Eddy diffusivity of solid particles in a turbulent liquid flow in a horizontal pipe', *AIChE J.*, vol. 41, no. 7, pp. 1815-20.

Wasp, EJ, Kenny, JP & Gandhi, RL 1977, *Solid-liquid flow slurry pipeline transportation*, First edn, Trans Tech Publications, Germany.

Wates, JA, Stevenson, C & Purchase, AR 1987, 'The effect of relative densities on beaching angles and segregation on gold and uranium tailings dams', paper presented to International Conference on Mining and Industrial Waste Management, Johannesburg.

Whipple, K, Parker, G, Paola, C & Mohrig, D 1998, 'Channel Dynamics, Sediment Transport, and the Slope of Alluvial Fans: Experimental Study', *Journal of Geology*, vol. 106, no. 6, pp. 677-93.

Williams, DJ & Morris, PH 1989, 'Comparison of Two Models for Subaerial Deposition of Mine Tailings Slurry', *Transactions of the Institution of Mining and Metallurgy, Section A - Mining Industry*, vol. 98, pp. A73-A7.

Williams, MPA 2001, 'Tailings beach slope forecasting, A review', paper presented to High density and thickened tailings conference, Pilanesberg, South Africa.

Williams, MPA 2005, *Private communication*.

Williams, MPA & Meynink, WJC 1986, 'Tailings beach slopes', paper presented to Workshop on Mine Tailings Disposal, The University of Queensland.

Williams, MPA & Seddon, KD 1999, 'Thickened tailings discharge: A review of the Australian experience', paper presented to 6th Int conf Tailings and Mine Waste 1999.

Williams, MPA, Murphy, SD, MacNamara, L & Khoshniaz, N 2006, 'The Miduk Copper Project: Down-Valley Discharge of Paste Thickened Tailings, Design and Early Operating Experience', paper presented to Paste 2006, Limerick, Ireland.

Willmott, CJ 1982, 'Some comments on the evaluation of model performance', *Bull. Amer. Meteorol. Soc.* vol. 63, pp.1309-1313.

Wilson, KC 1991, 'Slurry transport in flumes', in NP Brown & NI Heywood (eds), *Slurry handling design of solid-liquid systems*, Elsevier applied science, pp. 167-80.

Winterwerp, JC, de Groot, MB, Mastbergen, DR & Verwoert, H 1990, 'Hyperconcentrated sand-water mixture flows over flat bed.' *Journal of Hydraulic Engineering*, vol. 116, pp. 36-54.

Yen, BC 2002, 'Open channel flow resistance', *Journal of Hydraulic Engineering*, vol. 128, no. 1, pp. 20-39.

Yen, BC 2003, 'On establishing uniform flow with tail gate', *ASCE J Water and Maritime Eng*, vol. 156, no. 3, pp. 281-283.

Appendix A: Field flume experimental data

This appendix contains the detailed log of measurements made during the Sunrise Dam experimental campaign, which took place from 22nd February 2005 to 18th March 2005. The Cobar detailed data is not presented here, as it has already been presented in the thesis of Behnam Pirouz (Pirouz 2006), but a summary table of the equilibrium slopes recorded at both mine sites is presented below as Table 14.

Flow, Q	Concentration, C_{vw}	Channel Radius	Depth	Eq' Slope	d_{50}	d_{85}	ρ_s	ρ_w
l/s	% w/w	mm	mm	%	μm	μm	kg/m^3	kg/m^3
Sunrise Dam								
1.935	48.7	170	23	4.8	16	140	2800	1150
2.205	66.8	170	25	6.0	16	140	2800	1150
2.27	43.6	170	25	3.5	16	140	2800	1150
2.33	49.1	170	24	5.0	16	140	2800	1150
3.245	66.1	170	26	4.8	16	140	2800	1150
4.03	42.0	170	38	1.3	16	140	2800	1150
4.095	38.7	170	41	0.9	16	140	2800	1150
4.755	31.7	170	43	1.0	16	140	2800	1150
4.86	30.8	170	45	0.9	16	140	2800	1150
4.985	66.6	170	33	4.9	16	140	2800	1150
5.165	25.8	170	49	0.8	16	140	2800	1150
5.22	64.2	170	31	4.5	16	140	2800	1150
5.295	61.3	170	34	3.9	16	140	2800	1150
5.785	49.3	170	36	4.0	16	140	2800	1150
6.71	33.4	170	52	0.9	16	140	2800	1150
6.735	33.4	170	52	1.0	16	140	2800	1150
7.06	61.8	170	42	3.8	16	140	2800	1150
7.455	47.3	170	50	1.3	16	140	2800	1150
8.075	62.0	170	45	3.5	16	140	2800	1150
8.54	42.5	170	58	0.9	16	140	2800	1150
9.54	60.7	170	52	3.0	16	140	2800	1150
9.65	63.4	170	48	3.8	16	140	2800	1150
10.07	56.4	170	50	3.3	16	140	2800	1150
10.34	50.9	170	50	2.8	16	140	2800	1150
10.36	42.4	170	64	0.8	16	140	2800	1150
10.53	53.3	170	46	4.0	16	140	2800	1150
11.695	46.1	170	67	0.8	16	140	2800	1150
11.94	63.4	170	48	4.0	16	140	2800	1150
13.025	55.6	170	59	2.3	16	140	2800	1150
13.405	62.3	170	62	2.8	16	140	2800	1150
13.95	63.4	170	53	2.8	16	140	2800	1150
14.12	64.2	170	53	3.3	16	140	2800	1150
15.22	63.9	170	70	2.3	16	140	2800	1150
16.115	51.6	170	70	1.5	16	140	2800	1150
16.65	53.8	170	69	1.6	16	140	2800	1150
16.735	63.0	170	62	3.3	16	140	2800	1150
16.9	63.8	170	69	2.5	16	140	2800	1150
17.33	60.3	170	64	3.3	16	140	2800	1150
17.625	60.3	170	72	2.0	16	140	2800	1150
20.78	61.9	170	66	4.5	16	140	2800	1150
24.03	62.5	170	95	1.3	16	140	2800	1150
Cobar								
1.9	45.8	180	----	2.13	7.8	51	2800	1000
4	54.7	180	30	3.72	7.8	51	2800	1000
7.2	53.3	180	36	2.93	7.8	51	2800	1000
8	57.2	207	43	3	7.8	51	2800	1000
11.5	54.6	207	54	2.6	7.8	51	2800	1000
14.5	55.5	207	57	2.53	7.8	51	2800	1000
15.5	55.5	207	57	2	7.8	51	2800	1000
16.1	57.7	180	67	2.31	7.8	51	2800	1000
19	55.0	207	73	1.68	7.8	51	2800	1000

Table 14. Summary table of equilibrium slopes observed in the field flume experiments

Upon close inspection of the logged data (Table 15) it will soon become apparent that the equilibrium slopes summarised in Table 14 do not stand out amongst all the other recorded information. This epitomised the nature of the flume experiments, where a constant vigilance was maintained in an attempt to determine whether the slope of the flume was above or below the elusive equilibrium slope at any given moment. This makes the results highly subjective to the experimenter's judgement, which is a common and often lamented trait of sediment transport experiments. The frequent monitoring of the upstream surface level (USL), downstream surface level (DSL) and the regular searching for deposition was done in an effort to test for the presence of depositing sediment in the flume bed, the criteria which indicated that the flume slope flatter than equilibrium. A period of 20 minutes in which no deposition was observed in the channel led to the conclusion that the prevailing flume slope was steeper than equilibrium. Due to occasional unexpected fluctuations in slurry discharge from the process plant, regular monitoring of the flow and concentration were necessary. The bob measurements were a rough indicator of the flow rate, which worked by means of a buoy floating in the plunge box, where weir principles dictated that the elevation of the buoy would be a function of the flow rate. These bob readings were useful as an "early warning" indicator that the flow had unexpectedly changed, or possibly that deposition was occurring in the flume, thereby elevating the upstream depth.

On numerous occasions many hours worth of logged data (and work) was forfeited due to an unexpected change in the flow rate or slurry concentration. This data has remained in the log.

Table 15. Detailed log of chronologically recorded data from the Sunrise Dam campaign

Date	Time	Flow	Marcy	Slope	USL	DSL	Bob	Vel	Deposition	Location dep'n	Other comments
22-Feb-05	10:20		61.7	3							
	10:40	5.71									
	10:44				220	226					
	11:35				208	224					
	11:36			4							
	11:44				230	232					
	11:48		63								
	11:52	5.71									
	12:01				229	231					
	12:19				227	232					
	12:34				225	233					
	12:37		63								
	12:39	5.71									
	12:41			4.5							
	12:46				231	235					
	13:02				231	233					
	13:04			4.25							
	13:12				231	234					
	14:27				225	225					
	14:29	5.22									
	14:30								10		
	14:32			4.5							
	14:38				233	233					

	15:00				231	234					
	15:05		63								
	15:13				230	234					
	15:15								1	6 to 8	
	15:30				230	234					
	15:35	5.22									
	15:46				229	234					
	15:50							?			?
	16:30				228	234					
23-Feb-05	08:45										Slurry temp 39 deg
	09:00		59.1								
	09:02	7.41									
	09:05			3.25							
	09:08				219	226					
	09:18		60								
	09:24				215	225					
	09:25								5	7	
	09:30	7.95									
	09:44				219	225					
	10:45				203	220					
	10:48	9.23									
	10:52		61.3								
	10:55								15	6 to 8	
	10:58			3.75							
	11:04				218	224					
	11:12	8.63									
	11:31				217	224					
	11:53				217	224					
	11:58		59.9								
	12:01	8									
	12:10				217	224					
	12:11								2	7.5	
	12:30				214	224					
	12:33		59.7								
	12:38	8.57									
	12:55				212	225					
	13:00								5	7.5	
	13:06				217	225					
	13:28				216	225					
	14:42				206	228					
	14:43								15	7.5	
	14:46	7.06									
	14:48		61.4								
	15:11				221	229					
	15:30							0.81			Position 6
	15:45				216	228					
	15:46							0.88			
	15:48							0.82			
	15:49							0.86			
	15:49							0.81			
	15:50							0.85			
	15:50							0.82			
	15:54				214	228					
	16:10										Velocity profile x section at 6
	16:33		61.5								
	16:38				210	228					
24-Feb-05	07:10		64.5								
	07:12										Decant marcy = 9%
	07:20										Potable water marcy = -8%
	07:32										Air temp = 22 deg
	07:34										Slurry temp at downstream 35.5
	07:35										Slurry temp upstream 36
	07:35		65.8								
	07:40	3.5									
	07:45			6							
	07:55				233	234					
	08:08		63.7								
	08:13	4.48									
	08:20				234	234					
	08:38				233	234					
	08:40										Velocity profile x section at 6.1
	08:58	4.2									
	09:00		62.8								
	09:03				235	235					
	09:06	4									
	09:07								0		?
	09:08			5.25							
	09:16				236	235					
	09:21							1.2			CL d10 pos6.1
	10:57				234	234					
	11:18							1.29			
	11:20	5.24									
	11:25				230	231					

	11:26							1.35			
	11:26		64								
	12:00								0		
	12:02			4.9							
	12:02							1.21			
	12:07				231	231					
	12:10		65								
	12:13	5.31									
	12:16							1.26			
	12:17										Velocity profile x section at 6.1
	13:06										Air temp = 41.5 deg
	14:30				229	231					
	14:32	4.67									
	14:34							1.26			CL d10 pos6.1
	14:35		65.2								
	14:38								1	7	
	14:39			4.5							
	14:40							1.5			CL d10 pos6.1
	14:44							1			
	14:47	4.58									
	14:47							0.95			
	14:52				224	224					
	15:08				233	231					
	15:08							0.5			
	15:08		66								
	15:12										Run aborted. Mill trouble.
	15:13	0.3									
	15:20										Density probe proven useless
	15:30										Air temp = 39 deg
	15:35							0.01			
	15:40	0.1									
	15:46										Mill conc. 69%
	15:46							0.05			
25-Feb-05	07:00			3							
	07:30	2.86									
	07:45	2.14									
	08:15	4.92									
	08:16			4.5							
	08:20		62.8								
	08:40	2.38									
	08:41			6							
	08:45				243	240					
	08:47										Air temp = 33.5 deg
	08:48										Slurry temp = 39.5 deg
	10:10										Supply trouble. Flow reduced.
	10:15	2									
	10:15		67.5								
	10:20				238	241					
	10:30		64.2								
	10:32										Supply trouble. Flow reduced.
	10:33							0.7			CL d10 pos4.7
	10:39										Opened valve
	10:42							1.2			
	10:42	2.65									
	10:49				237	239					
	10:50							1.15			
	10:53		64.2								
	10:55							1.25			
	10:57				237	239					
	10:58							1.14			
	11:00	1.76									
	11:00							1.18			
	11:07							1.26			
	11:08				234	237					
	11:11								1	5 to 8	
	11:15							1.2			
	11:16				236	238					
	11:17	2.3									
	11:17							1.16			
	11:20		65.2								
	11:25										Velocity profile x section at 4.7
	11:57				244	242					
	11:57	1.26									
	12:00		64.5								
	15:00	4.62									
	15:05		63.2								
26-Feb-05	07:00			7							
	07:45	1.33									
	07:48				249	245					
	07:52		62.2								
	08:06	0.16									
	08:08										Opened valve
	08:15	5.5									
	12:14	3.8			240						

	08:55		64								
	08:59				240						
	09:00	3.9									
	09:04										Closed valve 30 deg
	09:10	3.34									
	09:11				242						
	09:15			5.25							
	09:18				239	239					
	09:21		64								
	09:23	3.32									
	09:28				239	239					
	09:45	3.11									
	09:48				240	239					
	09:51		64.2								
	10:00				240	239					
	10:06	3.29									
	10:12		64.5								
	10:13				240	239					
	10:15			5							
	10:17				239	239					
	11:03				239	239					
	11:06	3.2									
	11:10		65								
	11:15			4.75							
	11:25				238	238					
	11:30	2.98									
	11:36				238	238					
	11:42		64.2								
	11:51				238	237					
	11:54	3.14									
	11:59				237	237					
	12:01		64.2								
	12:03										Velocity profile x section at 4.7
	12:48										Velocity profile x section at 7.5
	12:57							0.83			CL d10 pos8.7
	13:03	3.35									
	13:04		64.3								
	13:05				234	237					
	13:07								3	2 to 3	
	14:50			2.25							
	14:52		64								
	14:55				205	215					
	14:58	7.36									
	15:08				201	214					
	15:10										Filmed hydraulic jumps
	15:20				195	211					
	15:25	10.3									
	15:26								10	0 to 9	
	15:29			2.75							
	15:30										Air temp = 41 deg
	15:32										Slurry temp = 43 deg
	15:50	9.09									
	15:56				216	224					
	16:00		64.9								
	16:09				217	225					
	16:11	8.89									
	16:30										Mill changed flow
	16:42				222	228					
	16:45	5.91									
	16:47										Opened valve. No good.
27-Feb-05	07:05		61								
	07:07			1.2							
	07:25				172	182					
	07:32	19.9									
	07:53				167	184					
	07:56		61								
	08:06	19.1									
	08:15				159	186					
	08:17								8	8	
	08:35			2							
	08:36				186	195					
	08:40		60.5								
	08:46	17.6									
	08:55				184	197					
	09:50				180	200					
	09:56	17.7									
	10:10										Vert. vel profile x section pos?
	11:10				177	198					
	11:15		62								
	11:25										Drew deposition profile
	11:25								17	7.6	
	11:50	18.1									
	12:05				190	201					
	13:25				181	203					

	13:30		63								
	13:45	17.4									
	14:00				183	200					
	14:08				181	200					
	14:08								5	8	
	14:19				183	201					
	14:25				185	202					
	14:30	16.5									
	14:38		62.5								
	14:40				187	204					
	14:45	16.6									
	14:45						11				
	14:53				183	203					
	15:15										Eratic flow
28-Feb-05	06:40			4							
	06:45	12.2									
	06:58		62.5								
	07:00				213	220					
	07:04						12.5				
	07:15	11.9									
	07:30				211	219					
	07:30						12.5				
	07:30		62.5								
	07:35								0		
	07:45	11.6									
	07:50						13				
	08:00				211	219					
	08:02								1	6.5 to 7.5	
	08:05			3.75							
	08:08										Slurry temp = 42.5 deg
	08:10										Air temp = 24 deg
	08:15	11.5									
	08:21				211	218					
	08:22		62								
	08:30								3	7.5	
	08:33						13.5				
	08:35				214	220					
	08:42	9.65									
	08:57				211	218					
	08:57		62.5								
	08:59								3	6	
	09:03			3.25							
	09:10				207	213					
	09:15	11.8									
	09:18						12.5				
	09:22				207	213					
	09:30										Opened valve
	09:33						11.5				
	09:37	13.6									
	09:43				202	210					
	09:48						11.7				
	09:48		62.5								
	10:43				198	210					
	10:43						11.7				
	10:46		63.5								
	10:51	14.1									
	10:54								4	5.5 to 7.5	
	10:55			2.75							
	11:06				206	214					
	11:22	14.3									
	11:28				204	214					
	11:28		62.5								
	11:41				205	213					
	11:43								3	7.5	
	11:58	13.6									
	12:02				206	214					
	12:02		62.5								
	12:08						12.2				
	12:10								5	6 to 8	
	12:11										Bob = 19.5 cm @ 0 flow 7% slope
	12:12										Windy and rainy. Retired
01-Mar-05	07:00						13.3				
	07:15			3.75							
	07:32				214	222					
	07:36		61								
	07:42				214	222					
	07:43						13.4				
	07:44								0		
	07:46			3							
	07:50				211	218					
	07:51						13.2				
	07:56		61								
	08:00				210	217					

	08:01						13.2				
	08:03										Air temp = 19.5 deg
	08:05										Slurry temp = 40.5 deg
	09:33				204	218					
	09:33						13.2				
	09:37		60.5								
	09:44	9.54									
	09:49				203	218					
	09:50						13.2				
	10:20				201	215					
	10:20						12.5				
	10:22		61.3								
	10:27	11.8									
	10:32				200	216					
	10:45						12.5				
	10:46				200	216					
	10:48		61.2								
	10:55	10.8									
	10:56						12				
	11:08				202	217					
	11:09						12.9				
	15:10	11									
	15:11								20	7 to 9	
	15:12				180						
	15:13		62.1								
02-Mar-05	09:15										Opened slurry valves max
	09:30			2.25							
	09:46				187	199					
	09:50	17									
	09:53		63.1								
	10:03				189	201					
	10:04						10.2				
	10:10	15.4									
	10:16				189	201					
	10:16						10.5				
	10:19		62.6								
	10:37				189	203					
	10:38						10.9				
	10:45	14.6									
	10:48						10.9				
	10:52				187	202					
	10:57		62.8								
	11:04				186	202					
	11:04						10.9				
	11:20	15.2									
	11:23						10.8				
	11:28				184	200					
	12:00						11				
	12:05	14.2									
	12:08						11				
	12:10				185	201					
	12:13		63								
	13:36				158	200					
	13:36								20	6	
	13:36						9.8				
	13:44	17.8									
	13:44						9.5				
	13:54		63								
	13:59				182	200					
	14:01						9.7				
	14:20						8.3				
	14:26				178	193					
	14:30	22.2									
	14:33						8.5				
	14:41				177	191					
	14:43		62.8								
	14:44						7.7				
	14:48	23.2									
	14:50						7.7				
	14:54				173	190					
	14:56						7.7				
	15:08		61.5								
	15:12				174	192					
	15:14						7.5				
	15:17	22.5									
	15:23								3	6.5 to 9	
	15:25						8				
	15:30				177	192					
	15:39			1.75							
	15:42		61.7								
	15:46				173	185					
	15:48						7.8				
	15:55				173	185					
	15:59			1.25							

	16:02				166	177					
	16:04						7.4				
	16:11							1.39			cl depth15 pos?
	16:15				166	177					
	16:18	24									
	16:19						7.4				
	16:22		62								
	16:26				165	175					
	16:27						7.4				
	16:31				163						
	16:31						7.2				
	16:37	24.2									
	16:37						7.2				
	16:39				162	174					
	16:41		62								
	17:20				159	172					
	17:20						7.1				
	17:22		61.8								
	17:30	23.9									
	17:36				158	175					
	17:36						7.1				
03-Mar-05	07:00			3.25							
	07:00				197	208					
	07:01						10				
	07:04		62.5								
	07:20	16.5									
	07:24				196	207					
	07:24						10				
	07:25										7 fluid samples collected
	07:50				194	207					
	07:50						9.8				
	07:59										Air temp = 21.5 deg
	07:59										Slurry temp = 38 deg
	08:08	17									
	08:09						9.8				
	08:13				193	207					
	08:16		62								
	08:37				193						
	08:38						9.8				
	08:39		61.5								
	08:41				193	208					
	08:42						10				
	08:45	17.6									
	08:46						10				
	08:52			2.25							
	08:56				188	198					
	08:58						9.8				
	09:00							1.2			CL pos8 d20
	09:05							1.37			CL pos6.5 d20
	09:10				188	199					
	09:10						10				
	09:14							1.49			CL pos4.9 d20
	09:20										Mill changed flow
	09:24							1.51			CL pos3.1 d20
	09:28				192	203					
	09:29						11.2				
	09:31		62.2								
	09:37	13.4									
	09:38						11.2				
	09:41				192	205					
	10:50				181	204					
	10:55								10	5 to 8	
	11:00			2.75							
	11:10				198	208					
	11:10						11.4				
	11:13		62								
	11:23	13.2									
	11:27						11.4				
	11:29				197	208					
	11:39							1.21			CL pos8.1 d20
	11:42						11.4				
	11:44		62								
	11:46							1.42			CL pos6.5 d20
	11:49						11.4				
	11:51							1.57			CL pos4.8 d20
	11:55						11.4				
	11:56				194	208					
	11:58							1.66			CL pos3.1 d20
	12:05						11.4				
	12:10							1.61			CL pos3.9 d20
	12:14				193	208					
	12:15						11.4				
	12:16							1.52			CL pos 5.4 d20
	12:20										Recorded long section profile

	12:32								6	5 to 6	
	12:32						11.4				
	12:36		61.5								
	12:43	13.6									
	12:47						11.4				
	12:51				191	209					
04-Mar-05	06:35			3.5							
	06:40	8.05									
	06:47		62								
	06:53				217	223					
	06:54						14.5				
	07:08				215	224					
	07:09						14.5				
	07:12		61.2								
	07:22	8.05									
	07:25						14.5				
	07:25							1.41			CL pos5.65 d20
	07:31				214	223					
	07:31						14.5				
	07:37							1.51			CL pos4.87 d20
	07:42				213	223					
	07:42						14.5				
	07:47		62								
	07:49							1.51			CL pos4.26 d20
	08:00				212	224					
	08:01						14.5				
	08:05							1.58			CL pos3.30 d20
	08:06										Recorded long section profile
	08:12						14.5				
	08:16	8.27									
	08:18							1.31			CL pos6.60 d20
	08:19						14.5				
	08:21				210	225					
	08:28								4	4	
	08:30							1.51			CL pos5.20 d20
	08:32		61.5								
	08:37							1.11			CL pos8.30 d20
	08:38				214	224					
	08:39						14.7				
	08:43	7.88									
	08:45						14.7				
	08:46				213	225					
	08:47							1.33			CL pos7.50 d20
	08:47		61.6								
	08:50										7 fluid samples collected
	09:08		62								
	10:40										Closed slurry valve
	10:48	5.5									
	10:50		61.2								
	11:00			3.88							
	11:04						16.5				
	11:05				228	232					
	11:16						16.5				
	11:16				227	233					
	11:42						16.5				
	11:44				225	233					
	11:46		61								
	11:50								3	6 to 8	
	11:54										Recorded long section vel profile
	12:20	5.09									
	12:22						16.5				
	12:24				222	233					
	12:27								6	6.3	
	12:33										3 fluid samples collected
	12:42						16.5				
05-Mar-05	06:25										Opened water valve
	06:32	2.08									
	06:38										Opened slurry valve
	06:40		55.5								
	06:53	11.7									
	06:57		55.5								
	07:05			2							
	07:10										Air temp = 17 deg
	07:13										Slurry temp = 39 deg
	07:16				205	210					
	07:17						13.8				
	07:25		54.5								
	07:30				203	209					
	07:33						13.6				
	07:40				208	211					
	07:41						14.2				
	07:45				204	207					
	07:45						14				

	07:48		61.7								
	07:50	10.8									
	07:54										Water shut off. Aborted run.
	10:50										Opened water valve
	10:52	3.7									
	10:55										Opened slurry valve
	11:00		55								
	11:08	16									
	11:10		54								
	11:15			1.5							
	11:21				192	197					
	11:23		55								
	11:25						11.5				
	11:30				191	196					
	11:32						11.5				
	11:33										Recorded vel profile section 4.2
	12:05				190	196					
	12:05						11.5				
	12:07		55.5								
	12:21		55								
	12:29				191	197					
	12:29						11.8				
	12:42				190	196					
	12:42						11.7				
	12:52		55.7								
	12:53				190	196					
	12:54						11.5				
	12:56								5	8 to 9	
	13:05				189	196					
	13:05						11.2				
	13:07		55.9								
	13:15	16									
	13:16						11.2				
	13:23				186	195					
	13:25								8	8 to 9	
	14:31				189	195					
	14:31						11.2				
	14:45	16.2									
	14:45		55.5								
	14:50										4 fluid samples collected
	15:00						11.2				
	15:10			1.63							
	15:15				191	196					
	15:15						11.2				
	15:17		56.1								
	15:26				192	196					
	15:27						11.1				
	15:30	16.4									
	15:35		56.7								
	15:36				192	196					
	15:42	16.5									
	15:45		56								
	15:46				191	196					
	15:47						11.1				
	15:49								0		
	15:55	16.9									
	16:00				192	196					
	16:01								0		
	16:07	16.3									
	16:10										4 fluid samples collected
	16:20										Graham Ehm visited site
	17:05	16.5									
	17:06								0		
	17:11				192	195					
	17:12						11.1				
	17:15		56								
06-Mar-05	06:30		45								
	06:36	6.72									
	06:41		43.5								
	06:45			1							
	06:48				214	209					
	06:49						15.5				
	06:52		42.5								
	06:58				213	209					
	06:59						15.2				
	07:05	6.75									
	07:09						15.2				
	07:14				212	208					
	07:15						15.2				
	07:17								0		
	07:19		43.5								
	07:22				212	208					
	07:26						15.2				
	07:35	6.5									

	07:37						15.2				
	07:40				212	208					
	07:43		43.5								
	07:52			0.88							
	07:54				213	203					
	07:56						15.2				
	07:59							1			CL pos8 d10
	08:01							0.92			CL pos7 d10
	08:03							0.98			CL pos6 d10
	08:05							1.05			CL pos5 d10
	08:07							0.87			CL pos4 d10
	08:09							0.76			CL pos3 d10
	08:11							0.67			CL pos2 d10
	08:13							0.71			CL pos1 d10
	08:13				212	179					
	08:15										Calm surface from 1 to 3
	08:22								30	1.5	
	08:28			0.93							
	08:31				214	209					
	08:32		43.5								
	08:40	6.71									
	08:43						15.2				
	08:44				213	208					
	08:46							0.89			CL pos8 d10
	08:47							1.03			CL pos7 d10
	08:48							1.03			CL pos6 d10
	08:49							1.06			CL pos5 d10
	08:50							1.01			CL pos4 d10
	08:51							1.03			CL pos3 d10
	08:52							1			CL pos2 d10
	08:53							0.95			CL pos1 d10
	08:56				213	208					
	08:58		43.9								
	09:00						15.2				
	09:01										7 fluid samples collected
	09:18		44								
	11:59										New flow rate
	12:00			1.5							
	12:07				207	209					
	12:09		50								
	12:12	8.89									
	12:14						14				
	12:21				206	209					
	12:32				206	209					
	12:48				205	209					
	12:50						14				
	14:05				205	210					
	14:20	9.12									
	14:25		49								
	14:27						14.1				
	14:28				206	210					
	14:50										Andrew measured velocities
	15:04				206	209					
	15:05						14.2				
	15:07		49.6								
	15:40			1.38							
	15:43				206	209					
	15:43		49								
	15:46			1.25							
	15:48				205	208					
	15:48						14.2				
	15:54	8.87									
	15:58				205	208					
	16:00		49								
	16:01						14.1				
	16:13				205	208					
	16:15								0		
	16:25				205	208					
	16:26								0		
	16:30		50								
	16:35	8.57									
	16:39				206	208					
	16:41			1.1							
	16:43				205	207					
	16:43						14.1				
	16:49				205	206					
	16:50										Andrew measured velocities
	16:59				206	206					
	17:11				206	206					
	17:19				206	206					
	17:21			0.88							
	17:24				205	204					
	17:24						14.1				
	17:30	8.54									

	17:31				206	204					
	17:34		49.3								
	17:40				206	203					
	17:41						14				
	17:49				205	203					
	17:51						13.9				
	17:52			0.75							
	17:53										Called ROM. Same blend.
	17:55		49.5								
	17:58				205	200					
	17:59						13.8				
	18:03	9.36									
	18:04				205	199					
	18:05						13.8				
	18:08								4	0.3	
07-Mar-05	06:30			2							
	06:40										Drew plumbing system diagram
	07:10		50.5								
	07:13	5.45									
	07:25		48.5								
	07:33	3.75									
	07:39		49								
	07:43	3.95									
	07:45				232	227					
	07:46						17				
	07:54		48								
	08:04	3.74									
	08:09				231	227					
	08:10						17.1				
	08:21				232	228					
	08:22						17.1				
	08:27								0		
	08:30			1.5							
	08:33				230	226					
	08:34						17.1				
	08:37		47								
	08:41	3.56									
	08:54				229	225					
	08:54						17				
	10:20				229	225					
	10:20		50								
	10:21						16.9				
	10:27	3.74									
	10:32			1							
	10:34				227	223					
	10:35						16.8				
	10:47				226	223					
	10:48						16.8				
	10:52		50.3								
	10:54				225	223					
	10:55								3	9	
	10:56										Andrew measured velocities
	11:06				225	223					
	11:06						16.8				
	11:12								9	8.7	
	11:28	3.77									
	11:30		49.7								
	11:43						14.8				
	11:43								30	9.3	
	11:55	3.89									
	12:00										3 fluid samples collected
	12:05										Mill reduced water flow
	12:40		49								
	12:50	3.91									
	12:52			1.25							
	12:56				225	224					
	12:57						17.1				
	12:59		49								
	14:03		49								
	14:06				225	224					
	14:07						17				
	14:12	4.15									
	14:17								0		
	14:20										Measured gate leakage rates
	14:25										New flow regime
	14:50		55								
	15:00	11.1									
	15:08			1.9							
	15:13				206	210					
	15:14						13.5				
	15:21				207	210					
	15:22						13.6				
	15:30		53.8								
	15:32				207	210					

	15:33						13.7				
	15:45				206	210					
	15:46						13.7				
	15:33				206	210					
	15:57								0		
	16:00			1.5							
	16:02				203	208					
	16:02						13.3				
	16:06	10.4									
	16:06		53.9								
	16:10										Measured gate leakage rates
	16:17				204	207					
	16:19						13.4				
	16:22								0		
	16:28				203	208					
	16:28						13.3				
	16:30			1.25							
	16:31				201	204					
	16:32						13.2				
	16:36	10.4									
	16:40		54								
	16:45				201	204					
	16:45						13.1				
	16:51			1							
	16:53				200	203					
	16:53						13.1				
	17:00				201	203					
	17:08	10.1									
	17:10		53.3								
	17:18				201	202					
	17:19								0		
08-Mar-05	07:30	10.2									
	07:32		54.5								
	07:35			1							
	07:37						13.9				
	07:38				202	204					
	07:40				199	204					
	07:41						13.9				
	07:50		54.5								
	07:59				196	203					
	08:00						13.8				
	08:03								12	8.8	
	08:09	10.5									
	08:10						13.5				
	08:12		55								
	08:14			1.75							
	08:23				205	210					
	08:24						13.8				
	08:25										Called ROM. Same blend.
	08:37				203	210					
	08:38						13.7				
	08:40								5	8.6	
	08:43			2							
	08:51				207	212					
	08:52						13.8				
	08:54	10.2									
	08:57		55								
	09:00						14				
	09:11				207	212					
	09:11						14				
	09:20				206	211					
	09:21						13.9				
	10:10				198	211					
	10:11						13.7				
	10:13		56								
	10:14								13	8.8	
	10:17	10.7									
	10:20			2.25							
	10:30				208	214					
	10:30						13.9				
	10:41				208	214					
	10:44						13.8				
	10:53				205	213					
	10:54						13.7				
	10:56		56.4								
	11:02	10.7									
	11:07				204	213					
	11:08						13.8				
	11:12								3	8.5	
	11:14			2.5							
	11:24				206	212					
	11:25						13.6				
	11:26										5 fluid samples collected
	11:37				207	213					

	11:38						13.8				
	11:47				207	215					
	11:48						14				
	12:05				207	214					
	12:06						14				
	12:07								3	8.6	
	12:08			2.75							
	11:55	10.5									
	12:16				209	215					
	12:17						14.1				
	12:21		56								
	12:24				209	215					
	12:25						14				
	12:25								2	8.6	
	12:26			3							
	12:49				210	217					
	12:49						14.2				
	12:50								2	8.6	
	12:52			3.25							
	12:56		56.5								
	15:04		56								
	15:08	10.5									
	15:09								2	8.6	
	15:11			4							
	15:15				215	219					
	15:15						14.7				
	15:44				215	219					
	15:45						14.8				
	15:52								0		
	16:01								0		
	16:02			2.25							
	16:07				208	215					
	16:07						14.1				
	16:55				205	215					
	16:55						14.1				
	17:00								3	8.6	
	17:03		55.7								
09-Mar-05	06:10										Opened water valve full
	06:12										Opened slurry valve partially
	06:15	14.5									
	06:20		59								
	06:21										Aborted run. Reset valves
	06:22	5.13									
	06:28		45.5								
	06:30			1.5							
	06:33				225	220					
	06:34						17.1				
	06:40	4.94									
	06:45		42								
	06:47				224	220					
	06:47						16.8				
	06:48								0		
	06:55		43								
	06:59				224	220					
	07:00						16.8				
	07:00								0		
	07:01			1							
	07:03				222	217					
	07:04						16.8				
	07:25							1.01			CL pos5.9 d16 (tot d @ 5.9 = 42)
	07:28				222	217					
	07:28						16.7				
	07:28		42.5								
	07:30								0		
	07:35	4.57									
	07:36						16.7				
	07:38				222	217					
	07:39								0		
	07:40							0.99			
	07:41			0.75							
	07:44				219	215					
	07:45						16.7				
	07:46							0.92			
	07:55				219	218					
	07:56								4	1	
	07:57							0.91			
	07:58						16.6				
	08:02	4.87									
	08:05		42.5								
	08:07				219	219					
	08:07								7	1.2	
	08:08						16.5				
	08:10							0.91			

	08:11										Sandy deposit. Not slimy.
	08:15			0.88							
	08:16										Difficult to scrape channel deposit
	08:22				220	215					
	08:23						16.4				
	08:26	4.86									
	08:36							0.96			
	08:37		43								
	08:39				220	215					
	08:39						16.3				
	08:45				221	216					
	08:46						16.6				
	08:47		42.5								
	08:49							0.95			
	09:39				220	216					
	09:39						16.5				
	09:40								0		
	09:43		42								
	09:45										New flow regime
	10:30	15.9									
	10:33		60								
	10:40										Closed tailings valve slightly
	10:43	14.3									
	10:44		59								
	10:45										Reduced tailings further
	10:50	12.9									
	10:52		57.5								
	10:56			2.25							
	10:59				201	206					
	10:59						12.7				
	11:00							1.45			
	11:12				201	207					
	11:12						12.6				
	11:13							1.45			
	11:15		57.5								
	11:28				201	207					
	11:29						12.5				
	11:30								0		
	11:31							1.46			
	11:33			2							
	11:34				199	205					
	11:34						12.5				
	11:36										Air temp = 37 deg
	11:37										Slurry temp = 40 deg
	11:40	13.2									
	11:46				198	205					
	11:47						12.1				
	11:49							1.43			
	11:50		57.5								
	11:50								0		
	12:03				195	203					
	12:04						12				
	12:06								2	8.7	
	12:07							1.45			
	12:10		58								
	12:15										New flow regime
	12:21	2.3									
	12:26		15								
	12:28										More slurry, less water
	12:34	3.87									
	12:37		35.5								
	12:40										Reduce water further
	12:45	3.43									
	12:50		36.5								
	12:52										Reduce water further
	12:55	1.76									
	12:58		51								
	13:03		53								
	13:08		54								
	13:10			3.5							
	13:12		54								
	13:14				242	240					
	13:15						19.9				
	14:17				242	240					
	14:17										Air temp = 40 deg
	14:18						18.4				
	14:22	1.87									
	14:23		55								
	14:25								12	9.7	
	14:26			3.75							
	14:31				242	240					
	14:32						19.8				
	14:42				242	240					

	14:43						19.8				
	14:44								2	9	
	14:45										Scraped out channel
	14:55								2	9	
	14:58			4.25							
	15:05							1.28			CL pos5.9 d12 (tot d @ 5.9 = 24)
	15:10	1.87									
	15:12										Measured gate leakage rates
	15:18		54.5								
	15:20							1.27			
	15:21								2	9	
	15:23			4.75							
	15:30				243	241					
	15:32						20				
	15:34							1.33			
	15:47				243	240					
	15:47						19.9				
	15:48								1	8.8	
	15:49			5.25							
	15:51				243	240					
	15:52						20.1				
	15:53							1.4			
	15:59	1.89									
	16:03				244	241					
	16:04						20.1				
	16:04		55.5								
	16:05							1.4			
	16:15								1	8.8	
10-Mar-05	06:28		50								
	06:33	1.6									
	06:40										Opened tailings valve
	06:43	2.7									
	06:45										Closed tailings valve
	07:25	2.05									
	07:28		53.5								
	07:30			6							
	07:33				245	241					
	07:35						20				
	07:39							1.4			CL pos5.9 d10 (tot d @ 5.9 = 21)
	07:43				245	241					
	07:44						20.1				
	07:45							1.41			
	07:47		53.5								
	07:54				245	241					
	07:55						20.2				
	07:58	1.82									
	08:00		53.5								
	08:03							1.37			
	08:09				246	242					
	08:09						20.3				
	08:10								0		
	08:11			3.5							
	08:13				244	240					
	08:13						20				
	08:14							1.17			
	08:15										Photographed channel on stack
	08:34				244	240					
	08:35						19.7				
	08:35								5	9.3	
	08:41	1.46									
	08:43		51.5								
	08:45							1.09			
	08:46										Low flow rate evidently blocks up
	08:50										New flow regime
	08:55	9.23									
	08:56		52.5								
	08:59										Closed slurry valve partially
	09:03	7.59									
	09:05		50								
	09:07										Closed water valve partially
	09:10	7.57									
	09:14		50								
	09:16										Closed water valve further
	09:20	7.32									
	09:22		52								
	09:25			1.5							
	09:29		52								
	09:32				215	214					
	09:33						15.1				
	09:45							1.24			CL pos5.9 d10 (tot d @ 5.9 = 48)
	09:56				213	214					

	09:56						14.8				
	10:03	7.45									
	10:05		50.5								
	10:05							1.29			
	10:06								0		
	10:08				210	212					
	10:09						14.2				
	11:06				213	214					
	11:06						14.9				
	11:08								0		
	11:15	7.48									
	11:20		52								
	11:31								0		
	11:36			1.25							
	11:40				209	211					
	11:41						14.3				
	11:44							1.21			
	11:50										Air temp 40 deg, very windy
	11:57				202	203					
	11:58						14.7				
	12:04							1.21			
	12:08	7.43									
	12:10		52								
	12:11							1.21			
	12:20				212	213					
	12:21						14.8				
	12:23								0		
	12:26							1.21			
	12:34				213	214					
	12:34						14.9				
	12:35								0		
	12:38			1							
	12:44				210	211					
	12:45						14.8				
	12:46							1.14			
	12:53	7.65									
	12:56		52.5								
	12:58							1.15			
	13:04								1	8.7	
	14:00										Site ravaged by storm
	14:48								3	8.6	
	14:50							1.15			
	15:00										Site hit by another storm
	15:31										New flow regime
	15:35	2.98									
	15:40		29								
	15:42										Closed water valve partially
	15:44	2.69									
	15:50										Opened both valves more
	16:03		56								
	16:05	13									
	16:07										Further adjusted valves
	16:20	10									
	16:21		54								
	16:25			2							
	16:30				209	211					
	16:30						14				
	16:38	9.73									
	16:40		53.5								
	16:45				210	212					
	16:45						14				
	16:54				211	212					
	16:54						14.1				
	16:57								0		
	17:07				211	212					
	17:07						14.2				
	17:12	9.1									
	17:14		53								
	17:15								0		
	17:16			1.5							
	17:19				209	209					
	17:20						14.1				
	17:29				208	210					
	17:29						14				
	17:30								0		
11-Mar-05	06:05	8.5									
	06:10		63								
	06:30										Water supply out. Pond empty.
	07:05	17.2									
	07:10										Plant gate valve broken. Water on.
	07:35	16.2									
	07:36		56.5								
	07:50	13.8									

	07:53		55								
	08:07	10.3									
	08:10		51								
	08:12						13.6				
	08:14			1.5							
	08:17				204	204					
	08:18						13.1				
	08:30							1.26			CL pos5.9 d10 (tot d @ 5.9 = 59)
	08:32				204	205					
	08:33						13.1				
	08:37	10.6									
	08:41							1.26			
	08:44		51								
	08:56				206	205					
	08:56						13.1				
	08:57								0		
	09:00			1							
	09:03				201	200					
	09:03						13.1				
	09:05		49								
	09:25				202	201					
	09:25						13.2				
	10:23				198	197					
	10:23						12.3				
	10:27	12									
	10:29		52								
	10:31							1.19			
	10:33								0		
	10:35			0.75							
	10:37				195	194					
	10:37						12.5				
	10:37							1.15			
	10:47				196	195					
	10:47						12.7				
	10:49								0		
	10:50							1.11			
	11:03				196	195					
	11:04						12.7				
	11:06								0		
	11:09							1.14			
	11:15	11.4									
	11:17						12.7				
	11:17		51								
	11:20							1.12			
	11:23				196	195					
	11:23						12.7				
	11:24								0		
	11:25			0.5							
	11:27				193	165					
	11:27						12.7				
	11:28					163					
	11:30								5	2.3	Sandy deposit, not slimy
	11:32		51								
	11:33							1.04			
	11:43			0.63							
	11:44				194	191					
	11:44						12.7				
	11:45							1.07			
	11:49	11.3									
	11:50		51								
	11:52						12.7				
	11:53							1.08			
	11:54				194	187					
	11:54						12.7				
	11:55								6	1	
	11:56							1.09			
	12:00			0.75							
	12:03				194	194					
	12:04						12.7				
	12:07							1.12			
	12:15	11.6									
	12:16		50.5								
	12:18						12.7				
	12:19							1.12			
	12:20				194	194					
	12:21						12.7				
	12:23								0		
	12:24										New flow regime
	12:31	10.3									
	12:32		50.5								
	12:34			1.5							
	12:36				201	205					
	12:37						13.4				

	12:38							1.25			
	13:37	9.9									
	13:39		49								
	13:42				203	206					
	13:43						13.8				
	13:44								0		
	13:45			1							
	13:46				200	202					
	13:47						13.7				
	13:48							1.08			
	13:54				199	201					
	13:54						13.6				
	13:55							1.12			
	13:57								0		
	14:05				200	200					
	14:05						13.3				
	14:05		49.5								
	14:06							1.12			
	14:07								0		
	14:09			0.75							
	14:10				199	198					
	14:11						13.2				
	14:12							1.05			
	14:15	10.5									
	14:17		49								
	14:19							1.05			
	14:21				200	197					
	14:21						13.3				
	14:23								0		
	14:31				200	198					
	14:31						13.4				
	14:33								0		
	14:34			0.5							
	14:35				198	170					
	14:36						13.3				
	14:37								6	1.2	
	14:38							0.94			
	14:42			0.63							
	14:44				199	194					
	14:45						13.3				
	14:45							0.97			
	14:48	10.2									
	14:49		50								
	14:51							1.02			
	14:53				199	194					
	14:53						13.3				
	14:55								5	0.6	Sandy deposit, not slimy
	14:56							1.04			
	15:02			0.69							
	15:05				200	196					
	15:06						13.4				
	15:06							1.05			
	15:08	10.2									
	15:09		51								
	13:10							1.01			
	15:14				198	196					
	15:15						13.4				
	15:16								1	0.2	
	15:19										Photographed channel d/s end
	15:20			2							
	15:23										Photographed channel d/s end
12-Mar-05	07:05		44.5								
	07:08	7.25									
	07:10										Opened slurry valve more
	07:16	9									
	07:19		49								
	07:25										Closed slurry valve partially
	07:35	8.38									
	07:40		48.5								
	07:45										Closed slurry valve partially
	07:50	5.4									
	07:54		39.5								
	08:00			0.75							
	08:03				216	210					
	08:03						16.5				
	08:05				216	205					
	08:05								5	1	
	08:13			1.25							
	08:16				220	216					
	08:16						16.7				
	08:23	5.17									
	08:25		39.5								
	08:27				220	216					
	08:28						16.7				

	08:44				220	216					
	08:45						16.7				
	08:45							1.09			CL pos5.9 d10 (tot d @ 5.9 = 47)
	08:48			1							
	08:50				219	215					
	08:51						16.8				
	08:52							1.05			
	08:58	5.04									
	09:00		38.5								
	09:06				218	214					
	09:06						16.6				
	09:07							1.03			
	09:15				218	214					
	09:15						16.6				
	09:15								0		
	09:16							1.04			
	09:18			0.88							
	09:19				217	213					
	09:19						16.6				
	09:20							1.03			
	09:28	5.21									
	09:29		39								
	09:34				218	213					
	09:34						16.4				
	09:35							1			
	09:45				217	213					
	09:45						16				
	09:47							0.99			
	09:48								0		
	09:50			0.81							
	09:52				216	211					
	09:53						16				
	09:53							0.98			
	10:39				216	212					
	10:40						15.9				
	10:43							0.97			
	10:45								2	0.6	
	10:52	5.12									
	10:54		39.5								
	10:56							0.97			
	10:59										New flow regime
	11:01			3							
	11:07	5.03									
	11:11		42								
	11:14										Closed both valves partially
	11:20	2.36									
	11:22		48								
	11:25			1.5							
	11:28				233	231					
	11:28						18.6				
	11:32							0.98			CL pos5.9 d10 (tot d @ 5.9 = 30)
	11:34		48.5								
	11:39				234	231					
	11:40						17.8				
	11:44	2.36									
	11:45							1			
	11:45						17.3				
	11:49				237	231					
	11:50						16.7				
	11:52								20	9.5	
	11:54							1			
	11:57			2							
	12:01				235	233					
	12:02						18.6				
	12:03							1.06			
	12:06	2.32									
	12:08		50								
	12:10				236	233					
	12:11						18				
	12:11							1.07			
	12:13								12	9.1	
	12:15			3							
	12:19				238	235					
	12:20						19.2				
	12:20							1.19			
	12:23	2.3									
	12:25		50								
	12:29				239	235					
	12:30						18.8				
	12:30							1.2			
	12:34								5	9	
	12:35							1.2			
	12:37			4							

	12:41				239	236					
	12:42						19.4				
	12:42							1.33			
	12:49				239	237					
	12:50						19.4				
	12:50							1.32			d ~ 5 highly turbulent
	12:57	2.29									
	12:59		50								
	13:01				240	237					
	13:02						19.2				
	13:02							1.35			
	13:07				240	237					
	13:07						19				
	13:08							1.34			
	13:08								0		
	13:11			3.75							
	13:12				239	236					
	13:13						18.8				
	13:13							1.31			
	14:13	2.27									
	14:15		50								
	14:23				239	237					
	14:24						19				
	14:24							1.3			
	14:25								0		
	14:27			3.5							
	14:30							1.25			
	14:33				239	237					
	14:33						18.9				
	14:43								2	8.8	
	14:48										New flow regime
	14:54	2.59									
	14:57		54								
	15:00			3							
	15:02				235	235					
	15:03						18.4				
	15:04		53.5								
	15:06							1.3			
	15:23				235	236					
	15:23						18.4				
	15:24							1.29			
	15:25								8	9.1	
	15:27			3.5							
	15:30				237	236					
	15:31						18.6				
	15:32							1.37			
	15:34	2.61									
	15:35		54.5								
	15:38							1.36			
	15:40				237	236					
	15:40						18.6				
	15:41							1.38			
	15:43								2	8.6	
	15:45			4							
	15:48				238	235					
	15:48						18.8				
	15:49							1.44			
	15:54				238	236					
	15:54						18.8				
	15:55							1.44			
	15:57	2.63									
	15:58		54.2								
	16:03										Air temp = 34.5 deg
	16:04										Slurry temp = 42 deg
	16:06				239	237					
	16:07						19				
	16:08								2	8.6	
	16:10			4.5							
	16:14				239	237					
	16:15						19.7				
	16:16							1.47			
	16:20	2.3									
	16:23		54								
	16:25				240	237					
	16:25						19.6				
	16:26								1	8.7	
	16:30			5							
	16:32				241	238					
	16:33						19.7				
	16:34							1.47			
	16:41				241	238					
	16:43						19.6				
	16:46	2.36									
	16:48		52.7								

	16:49							1.53			
	16:50				240	237					
	16:51						19.4				
	16:51								0		
13-Mar-05	06:25	4.42									
	06:30		42								
	06:38										Closed water valve partially
	06:45	3.96									
	06:48		46								
	06:54			1.5							
	06:57				228	223					
	06:58						17.2				
	07:08							1.06			CL pos5.9 d10 (tot d @ 5.9 = 37)
	07:09				227	222					
	07:10						16.9				
	07:14								0		
	07:15							1.06			
	07:20	4.29									
	07:22		47.5								
	07:25							1.05			
	07:26				226	222					
	07:26						16.9				
	07:27								0		
	07:29			1							
	07:30				224	218					
	07:31						16.8				
	07:31							0.99			
	07:41				224	219					
	07:42						16.8				
	07:42							0.97			
	07:47	4.13									
	07:49		47.3								
	07:52				224	219					
	07:53						16.8				
	07:55								0		
	07:57			0.5							
	07:58				221	191					
	07:59						16.8				
	07:59							0.66			
	08:01								25	7.5 to 0	
	08:02							0.45			
	08:06			0.75							
	08:08				223	214					
	08:09						16.8				
	08:11								8	0.7	
	08:12							0.87			
	08:18			0.88							
	08:19				224	218					
	08:20						16.9				
	08:20							0.93			
	08:26	4.01									
	08:28		47								
	08:30							0.91			
	08:31				224	219					
	08:31						16.9				
	08:33								4	0	
	08:39			0.94							
	08:40							0.96			
	08:41				224	219					
	08:42						16.9				
	08:43							0.95			
	08:47							0.97			
	08:49				224	219					
	08:49						16.9				
	08:53	4.18									
	08:55		47								
	08:58				224	219					
	08:58						16.8				
	08:59							0.96			
	09:00								0		
	09:56				224	219					
	09:56						19.9				?
	09:57								0		
	10:00										New flow regime
	10:05	2.08									
	10:07		49.5								
	10:11			2							
	10:15				237	233					
	10:16						18.7				
	10:21							1.08			CL pos5.9 d10 (tot d @ 5.9 = 28)
	10:24				237	234					
	10:24						18.6				
	10:28	2.04									

	10:29		51								
	10:31							1.09			
	10:32								8	9	
	10:34			4							
	10:38				242	237					
	10:38						19.1				
	10:39							1.29			
	10:50				242	237					
	10:51						19.9				
	10:52							1.28			
	10:56	1.91									
	10:58		51.5								
	11:00							1.31			
	11:01				241	237					
	11:01						19.6				
	11:02								2	8.9	
	11:05			5							
	11:06							1.4			
	11:10				242	238					
	11:10						20.1				
	11:20				242	238					
	11:20						19.9				
	11:25	2.15									
	11:27		53.2								
	11:29							1.41			
	11:30				241	238					
	11:31						19.7				
	11:32								0		
	11:35			4.5							
	11:36				241	238					
	11:36						19.6				
	11:37							1.37			
	11:38		53								
	11:46				241	239					
	11:47						19.5				
	11:48								1	8.8	
	11:52			4.75							
	11:54				242	238					
	11:55						20.1				
	11:55							1.38			
	11:58	1.97									
	11:59		53.2								
	12:01							1.39			
	12:04				242	238					
	12:04						20				
	12:05								1	8.9	
	12:11										Velocity profile x section at 9.35
	12:30										Velocity profile x section at 9.5
	12:55	1.9									
	12:56		54								
	12:57							1.33			CL pos5.9 d10
14-Mar-05	07:10	8.32									
	07:12		56.5								
	07:14										Closed slurry valve partially
	07:19	5.84									
	07:21		54								
	07:25			2.5							
	07:28				223	223					
	07:28						16.2				
	07:39							1.36			CL pos5.9 d10 (tot d @ 5.9 = 40)
	07:41				223	223					
	07:41						16.2				
	07:42								4	8.5	
	07:45			3.5							
	07:51				226	225					
	07:51						16.8				
	07:52							1.53			
	07:54	5.63									
	07:58		53.7								
	08:00							1.46			
	08:01				227	225					
	08:01						16.8				
	08:03								2	8.6	
	08:05			4.5							
	08:07				229	228					
	08:08						17.4				
	08:09							1.64			
	08:13	5.5									
	08:15		53								
	08:18				229	228					
	08:18						17.2				
	08:20								0		
	08:22							1.66			

	08:27				230	228					
	08:28						17.3				
	08:50								0		
	08:51							1.65			
	08:52			4							
	08:53				228	227					
	08:54						17.1				
	08:55							1.58			
	09:00	5.49									
	09:02		53								
	09:03				228	227					
	09:04						16.9				
	09:04							1.6			
	09:11				227	226					
	09:11						16.7				
	09:24								0		
	09:25			3.75							
	09:26				225	225					
	09:27						16.7				
	09:28							1.58			
	09:31	6.08									
	09:33		54								
	09:34						16.8				
	09:36				225	226					
	09:37						16.8				
	09:37							1.56			
	09:40								1	8.5	
	09:41										New flow regime
	09:45	10.5									
	09:47		59								
	09:49										Opened water valve slightly
	09:55	10.7									
	09:57		58								
	10:00			2.5							
	10:02				205	212					
	10:02						13.5				
	10:05							1.43			CL pos5.9 d10 (tot d @ 5.9 = 51)
	11:22	10.6									
	11:25		58.5								
	11:28				196	212					
	11:29						13.5				
	11:29							1.45			
	11:30								10	8	
	11:35			3.5							
	11:37				208	215					
	11:38						13.6				
	11:39							1.62			
	11:48				207	214					
	11:49						13.3				
	11:50							1.6			
	11:55	10.8									
	11:56						14				
	11:56		59.5								
	11:59							1.59			
	12:02				212	218					
	12:03						14.7				
	12:04				215	220					
	12:04						15				
	12:05								0		
	12:06			3							
	12:08				214	218					
	12:08						15				
	12:09							1.5			
	12:18				222	216					
	12:19						14.5				
	12:23	10.1									
	12:25		57.5								
	12:30							1.53			
	12:31				207	214					
	12:32						13.7				
	12:33								4	8.4	
	12:36			3.25							
	12:38				209	215					
	12:39						13.9				
	12:40							1.6			
	12:48				210	215					
	12:48						14.1				
	12:49							1.57			
	12:54	10									
	12:56		58								
	13:00				211	217					
	13:00						14.1				
	13:01							1.59			

	13:02								2	8.5	
	13:05										New flow regime
	13:12	10.9									
	13:14		56								
	13:16			3.25							
	13:20				209	213					
	13:21						13.7				
	13:22							1.58			
	13:32				209	213					
	13:32						13.7				
	13:33							1.63			
	13:39	10.7									
	13:41		55.5								
	13:42							1.62			
	13:43				211	214					
	13:44						14.1				
	13:45								2	8.5	
	13:48			3.75							
	13:51				211	216					
	13:51						14				
	13:52							1.66			
	15:06				218	219					
	15:06						15.1				
	15:08							1.69			
	15:09								0		
	15:13	9.86									
	15:15		53								
	15:19			3.5							
	15:20				214	216					
	15:21						14.4				
	15:22							1.61			
	15:32				214	215					
	15:33						14.4				
	15:33								0		
	15:36							1.62			
	15:40	9.99									
	15:42		53.5								
	15:44				213	215					
	15:45						14.4				
	15:45							1.63			
	15:52				214	216					
	15:52						14.4				
	15:53							1.61			
	15:54								0		
	15:54			3							
	15:56				213	213					
	15:56						14.4				
	16:03	9.82									
	16:05		53								
	16:08				212	214					
	16:09						14.3				
	16:10							1.55			
	16:18				214	215					
	16:18						14.5				
	16:20								0		
	16:21							1.5			
	16:22			2.5							
	16:23				211	212					
	16:24						14.4				
	16:24							1.49			
	16:27	9.82									
	16:29		52.5								
	16:31							1.47			
	16:35				211	213					
	16:36						14.1				
	16:36								0		
	16:40							1.47			
	16:44				212	214					
	16:45						14.3				
	16:45								1	8.5	
	16:46			2.75							
	16:47				212	214					
	16:48						14.3				
	16:48							1.52			
	16:56				212	213					
	16:56						14.2				
	16:57							1.52			
	17:00	10.3									
	17:02		54.5								
	17:05				211	213					
	17:06						14.1				
	17:07							1.52			
	17:15				212	214					
	17:16						14.1				

	17:18							1.53			
	17:19								0		
	17:25								0		
15-Mar-05	06:50	19.1									
	06:55		59								
	07:03			2							
	07:07				185	197					
	07:08						10				
	07:20							1.4			CL pos5.9 d10 (tot d @ 5.9 = 72)
	07:25				186	197					
	07:26						10				
	07:28								6	8	
	07:32			2.5							
	07:42	19.2									
	07:44		59								
	07:50				190	200					
	07:51						10.1				
	07:55							1.52			
	08:00				190	200					
	08:00						10.1				
	08:10				190	199					
	08:11						10				
	08:14								1	7.9	
	08:20			2.75							
	08:25				192	202					
	08:25						10.5				
	08:27							1.47			
	08:34	17.5									
	08:36		60								
	08:39							1.52			
	08:41				193	203					
	08:41						10.2				
	08:43								1	7.8	
	08:46			3							
	08:52				198	203					
	08:53						10.6				
	08:55							1.65			
	09:58				192	203					
	09:59						10.5				
	10:00								2	7.9	
	10:02			3.25							
	10:05	17.3									
	10:07		60.5								
	10:13				194	205					
	10:13						11				
	10:19							1.59			
	10:26				194	205					
	10:26						11				
	10:34							1.58			
	10:36				193	203					
	10:37						10.7				
	10:39								0		
	10:50										New flow regime
	10:56	2.58									
	11:00		60								
	11:25										Water cut off
	11:40										Surveyed levels of flume. OK
	13:32	19.8									
	13:34		61								
	13:37			1.5							
	13:41				171	184					
	13:42						8.7				
	13:55							1.31			CL pos5.9 d20 (tot d @ 5.9 = 90)
	13:59				171	184					
	14:00						8.7				
	14:00							1.3			
	14:03								3	7	
	14:04			1.75							
	14:12				175	188					
	14:13						8.8				
	14:13							1.31			
	14:16	23.5									
	14:18		62								
	14:23				175	188					
	14:24						8.8				
	14:25							1.31			
	14:27								2	7	
	14:30			2							
	14:35				179	192					
	14:35						8.9				
	14:36							1.38			
	14:43	21									
	14:51				178	193					

	14:51						9				
	14:52							1.32			
	14:55								4	7	
	14:59			2.5							
	15:07				181	197					
	15:08						9				
	15:09							1.48			
	15:13	21.7									
	15:17		61								
	15:22				180	197					
	15:23						9.4				
	15:23							1.4			
	15:25								2	7.8	
	15:28			3.5							
	15:31				184	198					
	15:32						9.6				
	15:32							1.43			
	15:36	20									
	15:39		61.5								
	15:42				185	201					
	15:43						9.7				
	15:44								1	7.9	
	15:47			4							
	15:50				186	203					
	15:50						9.9				
	15:52							1.58			Probe lowered 10 mm more
	15:55	20.9									
	15:57		61								
	16:00							1.6			
	16:01				185	201					
	16:02						10				
	16:20				185	200					
	16:20						10				
	16:22								1	7.8	
	16:23			4.5							
	16:31				187	204					
	16:31						10.1				
	16:32							1.65			
	16:34	20.8									
	16:35		61.5								
	16:43						10.5				
	16:43				188	205					
	16:44							1.62			
	16:53				188	206					
	16:53						10.5				
	16:55							1.63			
	16:56								0		
16-Mar-05	06:22	6.37									
	06:30		63.5								
	06:32			4							
	06:35										Air temp 16 deg
	06:38				222	217					
	06:38						16				
	06:51				222	217					
	06:51						16.1				
	07:01				222	217					
	07:01						16.1				
	07:10								0		
	07:14			3.5							
	07:17				219	224					
	07:17						16				
	07:19	6.47									
	07:21		63.5								
	07:28				218	224					
	07:28						15.9				
	07:41				216	223					
	07:41						15.9				
	07:43								3	5	
	07:45			3.75							
	07:53				223	227					
	07:53						16.4				
	07:56	6.02									
	07:57		62.5								
	08:04				223	227					
	08:04						16.6				
	08:18							1.33			CL pos5.9 d10 (tot d @ 5.9 = 40)
	08:22				223	228					
	08:22						16.7				
	08:25								3	5	
	08:30			3.88							
	08:39				225	228					
	08:39						16.9				
	08:43	5.37									

	08:44		63								
	08:45							1.33			
	08:50				224	228					
	08:50						16.8				
	08:50							1.26			
	09:05				223	227					
	09:05						16.7				
	09:07								1	4	
	09:10			4.25							
	09:18				226	228					
	09:18						16.9				
	09:19							1.36			
	09:26		62								
	09:29	5.36									
	10:41				226	229					
	10:42						17.1				
	10:44							1.38			
	10:47								0		
	10:52	5.06									
	10:54		63.5								
	11:05										New flow regime
	11:12	2.48									
	11:13		64.5								
	11:20			6							
	11:21				239	238					
	11:22						19.5				
	11:23							1.43			CL pos5.9 d10 (tot d @ 5.9 = 23)
	11:35				239	238					
	11:35						19.5				
	11:37							1.4			
	11:47				239	238					
	11:47						19.6				
	11:48							1.42			
	11:49								0		
	11:51			5							
	11:53				237	236					
	11:54						19.2				
	11:54							1.27			
	11:58	2.74									
	11:58						19.2				
	11:59		64								
	12:00										Checked u/s vs d/s marcy. Same.
	12:12				237	236					
	12:12						19.3				
	12:13							1.27			
	12:14							1.23			
	12:23				237	236					
	12:23						19.4				
	12:24							1.24			
	12:25								0		
	12:28	2.76									
	12:29		63.5								
	12:30							1.28			
	12:31			4							
	12:33				235	233					
	12:33						19.1				
	12:34							1.04			
	12:48				234	233					
	12:49						19.2				
	12:50							1.02			
	13:05				232	231					
	13:06						19.3				
	13:10								0		Viscous slow sublayer
	13:15							0.96			
	13:16										Velocity profile x section at 5.9
	15:00				220	223					
	15:00						19.1				
	15:05								15	1	Cresting behavior noted
	15:15			4.25							
	15:20				235	234					
	15:20						19.3				
	15:21							1.15			
	15:25	3.08									
	15:27		63.5								
	15:36				235	234					
	15:36						19.3				
	15:37							1.18			
	15:40										Measured gate leakage rates
	15:52				235	233					
	15:52						19.3				
	15:55								4	0.4	
	16:00			4.75							
	16:05	2.7									

	16:07		64.7								
	16:09				236	235					
	16:09						19.4				
	16:10							1.25			
	16:40				236	235					
	16:40						19.5				
	16:42								0		
	16:43			4.5							
	16:46				235	234					
	16:46						19.4				
	16:47							1.21			
	16:56	2.79									
	16:58		63								
	17:00							1.21			
	17:08				235	234					
	17:08						19.2				
	17:10								1	1.4	
17-Mar-05	06:37	10.7									
	06:39		63.5								
	06:44			3.5							
	06:59				210	215					
	07:00						14.2				
	07:06							1.38			CL pos5.9 d10 (tot d @ 5.9 = 52)
	07:10						14				
	07:12							1.38			
	07:19	11									
	07:21		63.5								
	07:23							1.42			
	07:24				207	213					
	07:24						13.8				
	07:28								1	5.5 to 2	
	07:34			4							
	07:41				209	215					
	07:41						14				
	07:42							1.53			
	07:57				210	216					
	07:57						14.1				
	07:58							1.52			
	08:03	10.6									
	08:06		64								
	08:07							1.49			
	08:09				211	217					
	08:09						14.2				
	08:11								0		
	08:12			3.75							
	08:14				210	216					
	08:14						14.1				
	08:15							1.42			
	08:30				209	215					
	08:30						14				
	08:31							1.46			
	08:43	10.7									
	08:45		63								
	08:47							1.45			
	08:48				209	215					
	08:48						14				
	08:50								0		
	08:53										New flow regime
	08:56	9.07									
	08:58		64								
	09:01										Closed slurry valve partially
	09:03	7.19									
	09:07			4.5							
	09:15				222	225					
	09:16						16.3				
	09:17							1.38			CL pos5.9 d10 (tot d @ 5.9 = 41)
	10:35				221	224					
	10:35						16.1				
	10:38	7.03									
	10:41		64.5								
	10:46							1.4			
	10:48								0		
	10:49			4							
	10:52				218	221					
	10:53						16				
	10:54							1.33			
	11:05				218	221					
	11:06						15.9				
	11:07							1.37			
	11:13	7.17									
	11:15							1.37			
	11:17		65								
	11:19				218	221					

	11:20						16				
	11:25							1.35			
	11:27								0		
	11:29			3.5							
	11:33				216	218					
	11:33						15.8				
	11:34							1.27			
	11:49				215	217					
	11:49						15.8				
	11:50							1.27			
	12:06				215	216					
	12:07						15.7				
	12:08							1.28			
	12:09								0		
	12:12			3							
	12:14				211	213					
	12:14						15.5				
	12:15							1.2			
	12:18	7.96									
	12:20		62.5								
	12:35				208	212					
	12:35						15.5				
	12:36							1.2			
	12:47				208	213					
	12:48						15.8				
	12:49							1.18			
	12:51								0		Viscous bed layer
	12:53			2.5							
	12:55				204	209					
	12:55						15.8				
	12:56							1.06			
	12:59	6.61									
	13:01		65								
	13:05							1.03			
	13:15				202	208					
	13:15						16.1				
	13:18								5	1	Viscous bed layer
	13:21			2.75							
	13:27				213	216					
	13:28						16.1				
	13:28							1.11			
	14:33				202	206					
	14:33						15.7				
	14:38	7.37									
	14:39		65								
	14:40							1.04			
	14:42								4	1	Viscous bed layer
END OF SUNRISE DAM EXPERIMENTAL CAMPAIGN											

Table 17. Detailed log of chronologically recorded data from the Sunrise Dam campaign

Appendix B: Field flume experimental results - Particle size data

This appendix contains all of the particle size distribution data that was generated from the Cobar and Sunrise Dam experimental work.

Cobar Sample Register (with associated plots following)

Q (l/s)	x	Depth	Date	Time
1.93	0	Top of flow	04-Jun-04	11:00
1.93	0	Bottom of flow	04-Jun-04	11:00
1.93	4.5	Top of flow	04-Jun-04	11:00
1.93	4.5	Bottom of flow	04-Jun-04	11:00
1.93	9	Top of flow	04-Jun-04	11:00
1.93	9	Bottom of flow	04-Jun-04	11:00
7.3	0	Top of flow	03-Jun-04	14:15
7.3	0	Bottom of flow	03-Jun-04	14:15
7.3	4.5	Top of flow	03-Jun-04	14:15
7.3	4.5	Bottom of flow	03-Jun-04	14:15
7.3	9	Top of flow	03-Jun-04	14:15
7.3	9	Bottom of flow	03-Jun-04	14:15
15	0	Top of flow	31-May-04	15:15
15	0	Bottom of flow	31-May-04	15:15
15	4.5	Top of flow	31-May-04	15:15
15	4.5	Bottom of flow	31-May-04	15:15
15	8	Top of flow	31-May-04	15:15
15	8	Bottom of flow	31-May-04	15:15
16.1	0	Top of flow	02-Jun-04	11:10
16.1	0	Bottom of flow	02-Jun-04	11:10
16.1	4.5	Top of flow	02-Jun-04	11:10
16.1	4.5	Bottom of flow	02-Jun-04	11:10
16.1	9	Top of flow	02-Jun-04	11:10
16.1	9	Bottom of flow	02-Jun-04	11:10
19	0	Top of flow	30-May-04	17:30
19	0	Bottom of flow	30-May-04	17:30
19	4.5	Top of flow	30-May-04	17:30
19	4.5	Bottom of flow	30-May-04	17:30
19	9	Top of flow	30-May-04	17:30
19	9	Bottom of flow	30-May-04	17:30

x = Distance from downstream end of flume (m)

Table 16. Summary of fluid samples extracted from the flume during the Cobar experimental campaign for particle size distribution analysis

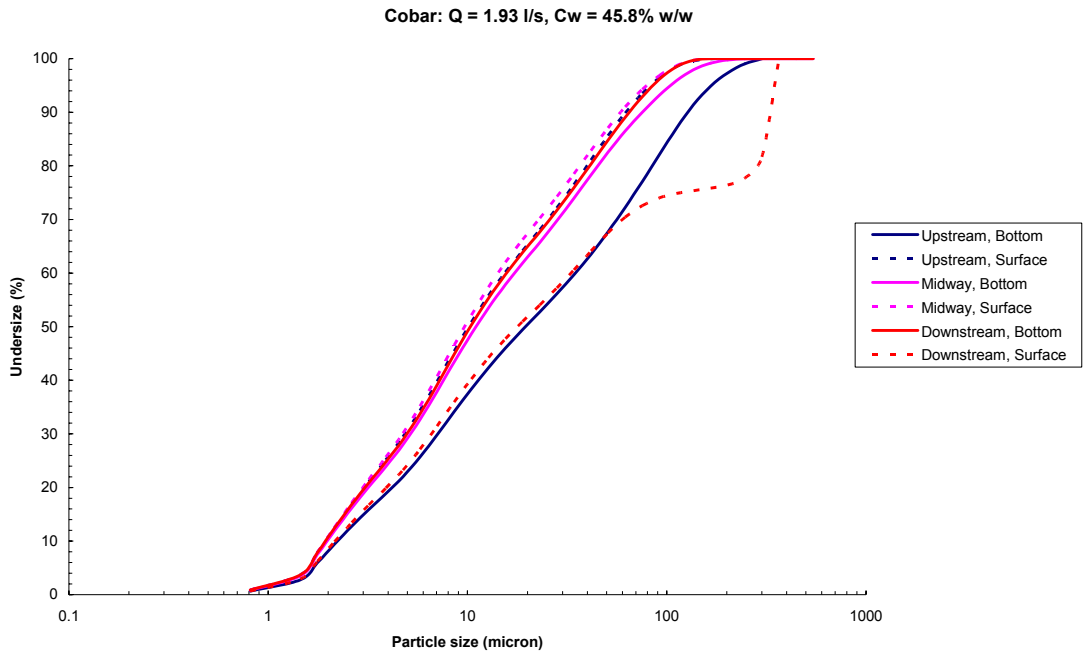

Figure 142. Particle size distribution curves for 6 fluid samples extracted from various points in the field flume during the Cobar experiments, with a flow rate of 1.93 l/s and concentration of 45.8% w/w

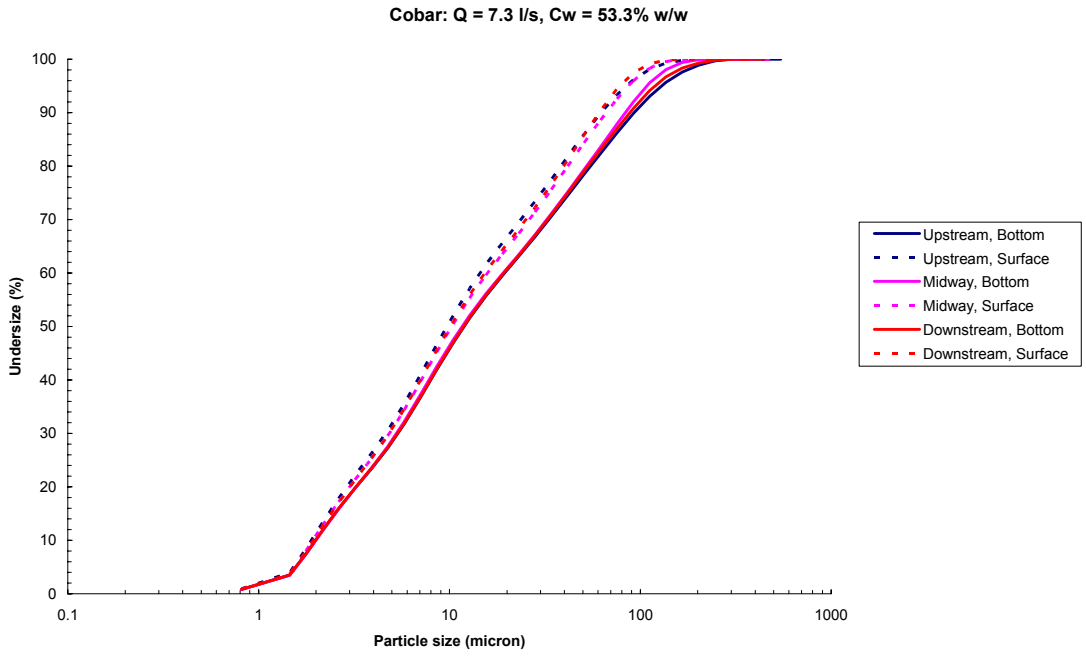

Figure 143. Particle size distribution curves for 6 fluid samples extracted from various points in the field flume during the Cobar experiments, with a flow rate of 7.3 l/s and concentration of 53.3% w/w

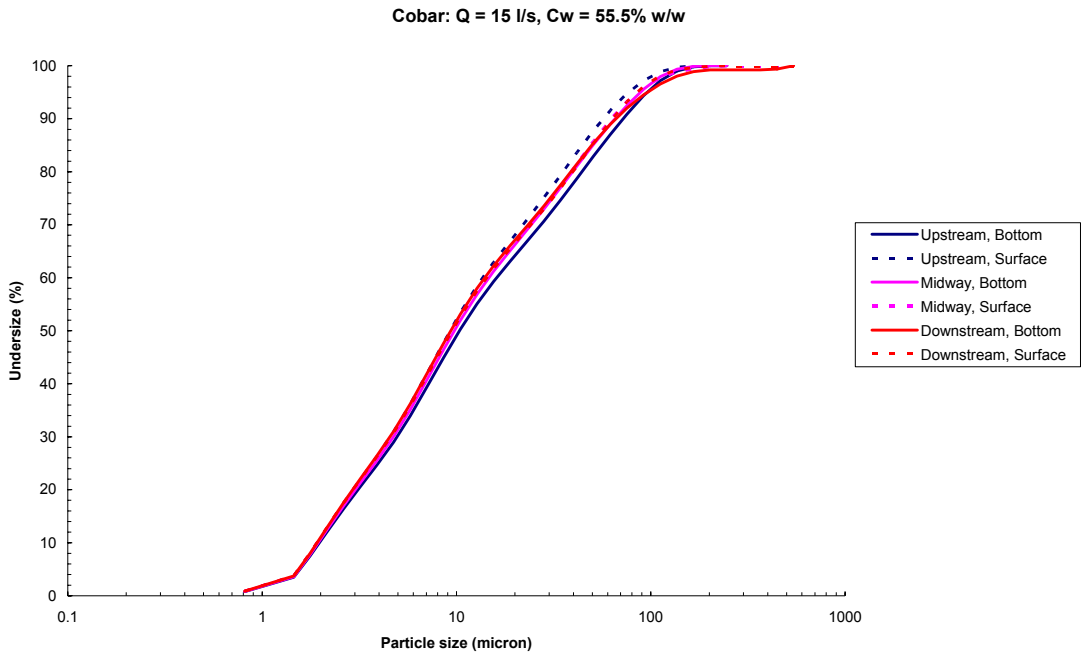

Figure 144. Particle size distribution curves for 6 fluid samples extracted from various points in the field flume during the Cobar experiments, with a flow rate of 15 l/s and concentration of 55.5% w/w

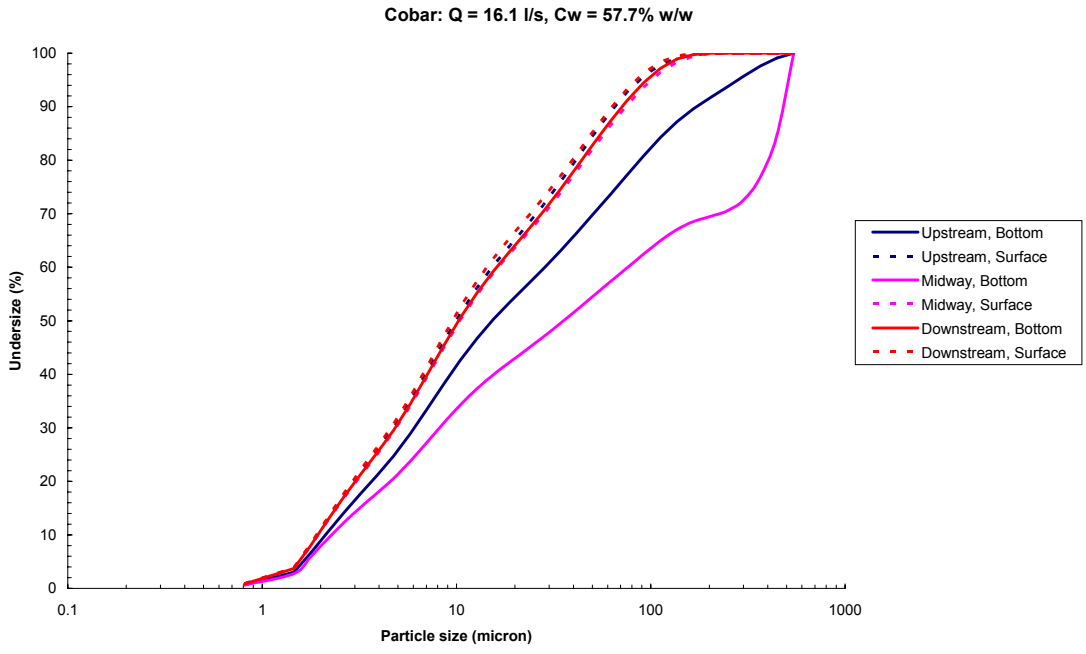

Figure 145. Particle size distribution curves for 6 fluid samples extracted from various points in the field flume during the Cobar experiments, with a flow rate of 16.1 l/s and concentration of 57.7% w/w

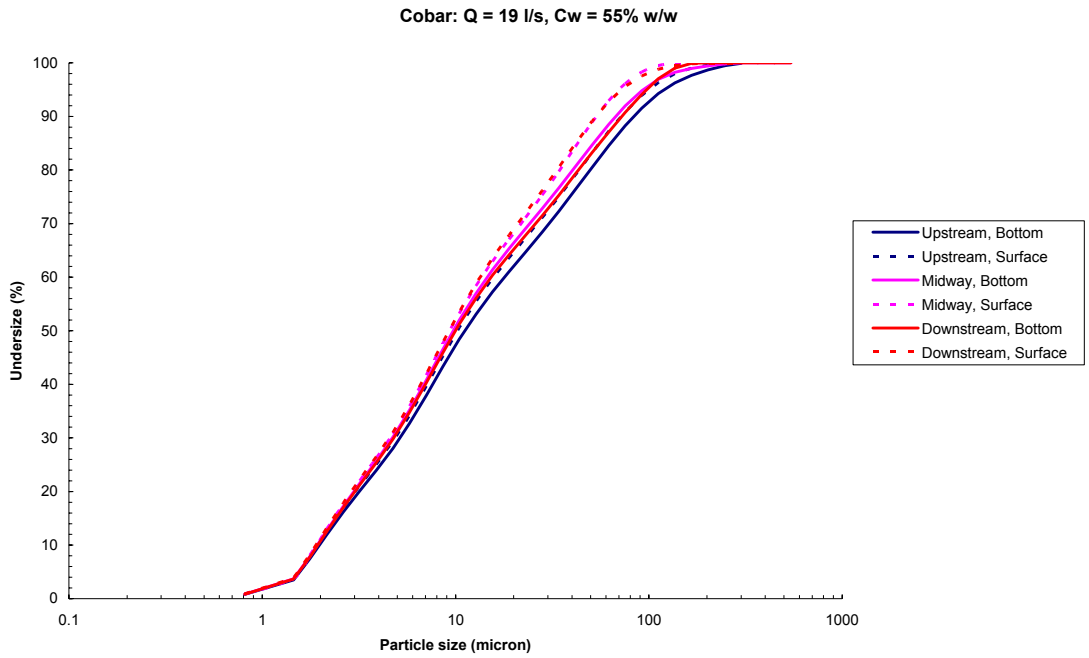

Figure 146. Particle size distribution curves for 6 fluid samples extracted from various points in the field flume during the Cobar experiments, with a flow rate of 19 l/s and concentration of 55% w/w

Sunrise Dam particle size distribution data

Sample No.	Position	Depth	Date	Time	Comments
1	Plunge Box	-	03-Mar-05	07:25	Flow 16.5 l/s, Slope 3.25%, Conc. 62.5%
2	8.2	75	03-Mar-05	07:25	
3	8.2	10	03-Mar-05	07:25	
4	4.9	10	03-Mar-05	07:25	
5	4.9	65	03-Mar-05	07:25	
6	1.6	65	03-Mar-05	07:25	
7	1.6	10	03-Mar-05	07:25	
8	8.2	10	04-Mar-05	08:53	Flow 7.9 l/s, Slope 3.5%, Conc. 62%
9	8.2	Bottom	04-Mar-05	08:55	
10	4.9	10	04-Mar-05	08:57	
11	4.9	Bottom	04-Mar-05	08:59	
12	Plunge Box	-	04-Mar-05	09:01	
13	1.5	10	04-Mar-05	09:02	
14	1.5	Bottom	04-Mar-05	09:04	
15	Plunge Box	-	04-Mar-05	12:34	Flow 5 l/s, Slope 3.9%, Conc. 61%
16	5	10	04-Mar-05	12:36	
17	1	10	04-Mar-05	12:38	
18	8.2	10	05-Mar-05	14:50	Flow 16.2 l/s, Slope 1.5%, Conc. 55.5%
19	8.2	Bottom	05-Mar-05	14:53	
20	3.2	Bottom	05-Mar-05	14:56	
21	3.2	10	05-Mar-05	14:58	
22	8.2	10	05-Mar-05	16:00	Flow 16.3 l/s, Slope 1.63%, Conc. 56%
23	8.2	Bottom	05-Mar-05	16:00	
24	3.2	10	05-Mar-05	16:00	
25	3.2	Bottom	05-Mar-05	16:00	
26	Plunge Box	-	06-Mar-05	08:59	Flow 6.7 l/s, Slope 0.93%, Conc. 44%
27	8.2	10	06-Mar-05	09:00	
28	8.2	Bottom	06-Mar-05	09:01	
29	5.5	10	06-Mar-05	09:04	
30	5.5	Bottom	06-Mar-05	09:05	
31	3.2	10	06-Mar-05	09:08	
32	3.2	Bottom	06-Mar-05	09:10	
33	Plunge Box	-	07-Mar-05	12:02	Flow 3.9 l/s, Slope 1.0%, Conc. 50%
34	8.2	10	07-Mar-05	12:04	
35	8.2	Bottom	07-Mar-05	12:05	
36	Plunge Box	-	08-Mar-05	11:24	Flow 10.7 l/s, Slope 2.5%, Conc. 56%
37	8.2	10	08-Mar-05	11:26	
38	8.2	Bottom	08-Mar-05	11:28	
39	3.2	10	08-Mar-05	11:30	
40	3.2	Bottom	08-Mar-05	11:32	

"Position" indicates the distance from the downstream end of the flume (m)

Table 17. Summary of fluid samples extracted from the flume during the Sunrise Dam experimental campaign for particle size distribution analysis

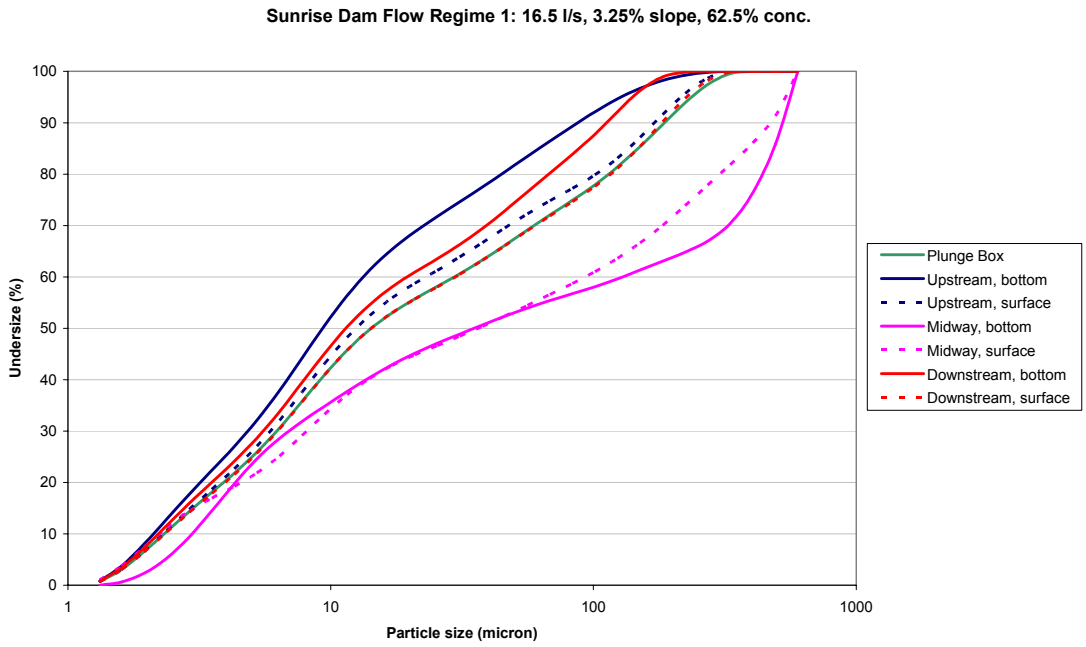

Figure 147. Particle size distribution curves for 7 fluid samples extracted from various points in the field flume during "Flow regime 1" of the Sunrise Dam experiments

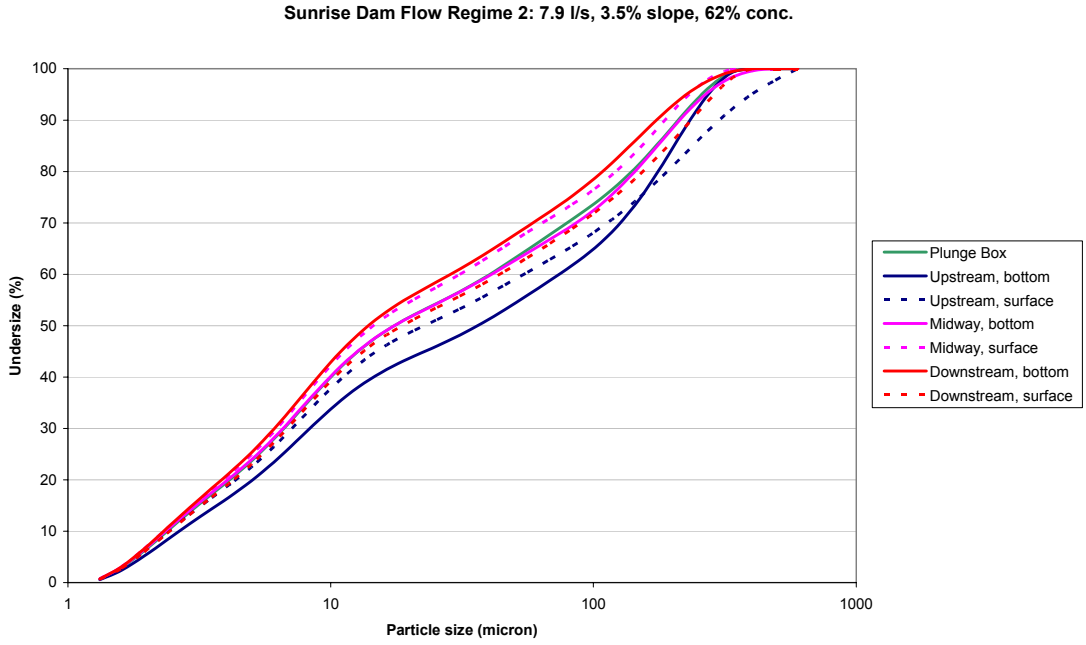

Figure 148. Particle size distribution curves for 7 fluid samples extracted from various points in the field flume during "Flow regime 2" of the Sunrise Dam experiments

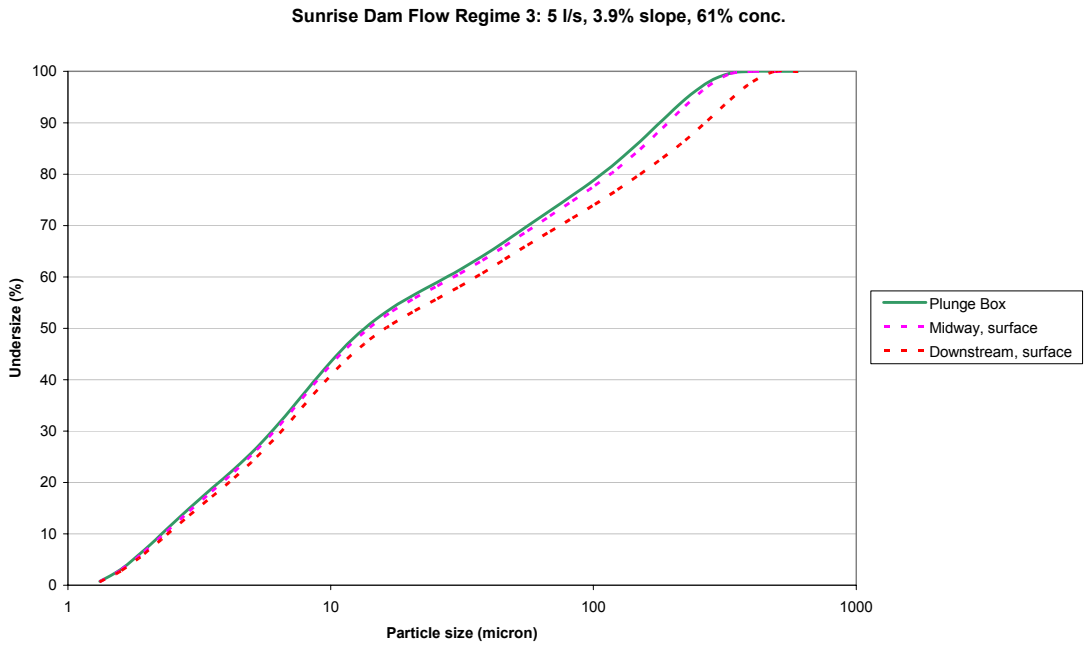

Figure 149. Particle size distribution curves for 3 fluid samples extracted from various points in the field flume during "Flow regime 3" of the Sunrise Dam experiments

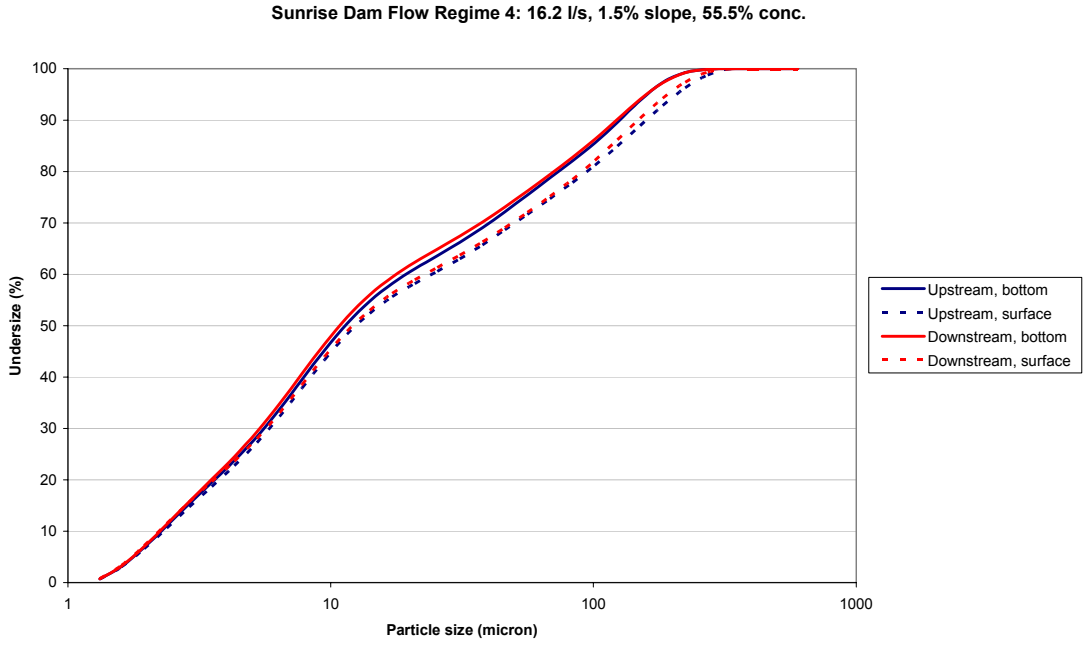

Figure 150. Particle size distribution curves for 4 fluid samples extracted from various points in the field flume during "Flow regime 4" of the Sunrise Dam experiments

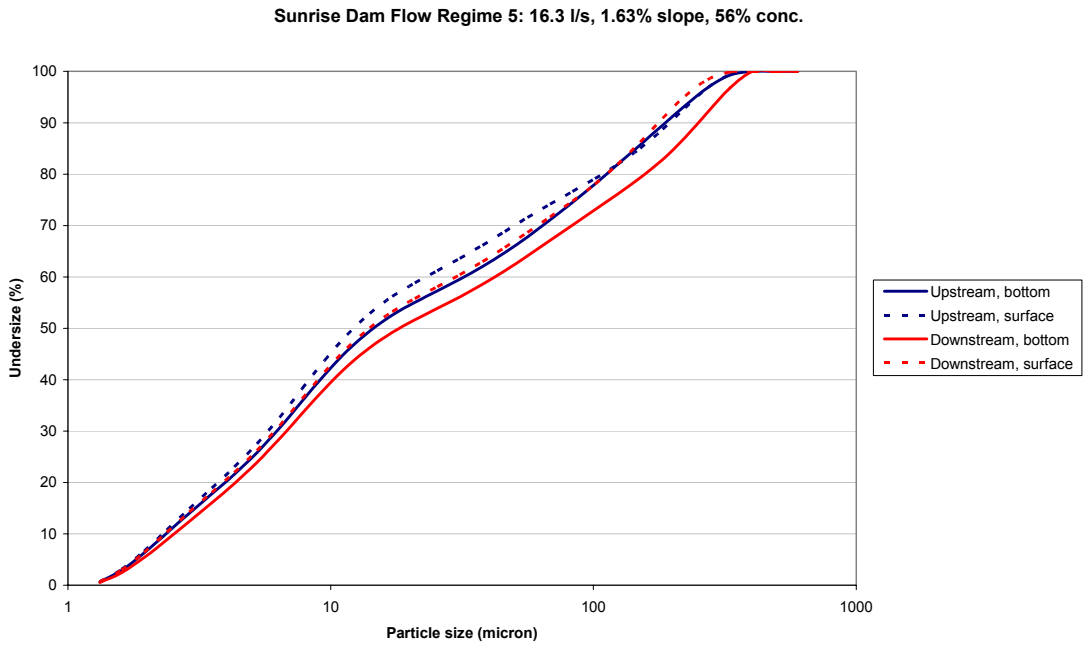

Figure 151. Particle size distribution curves for 4 fluid samples extracted from various points in the field flume during "Flow regime 5" of the Sunrise Dam experiments

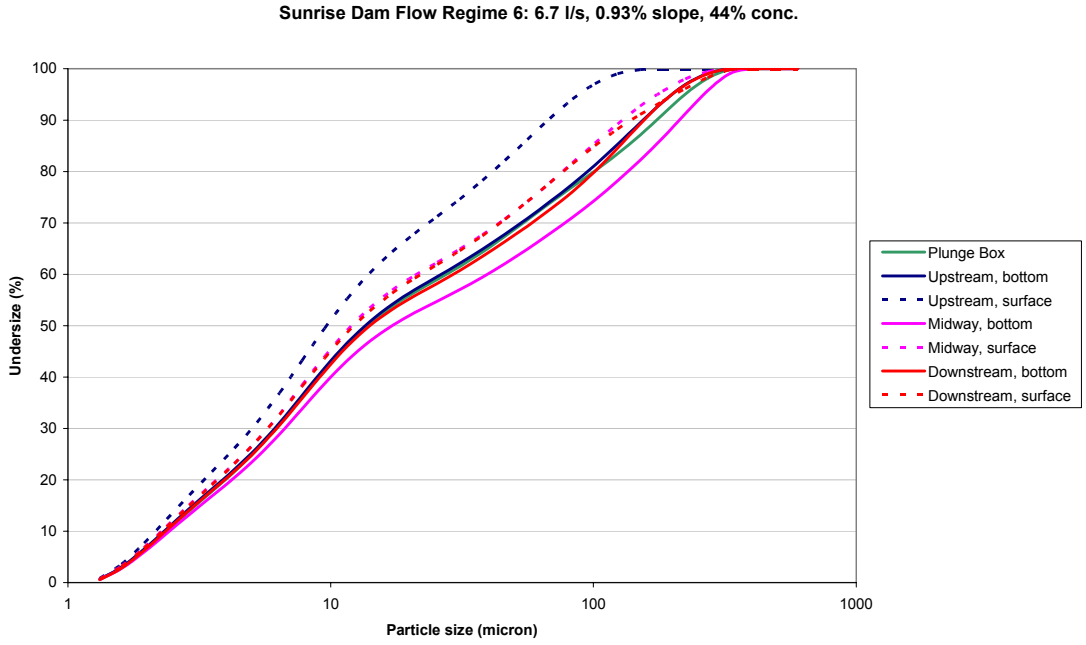

Figure 152. Particle size distribution curves for 7 fluid samples extracted from various points in the field flume during "Flow regime 6" of the Sunrise Dam experiments

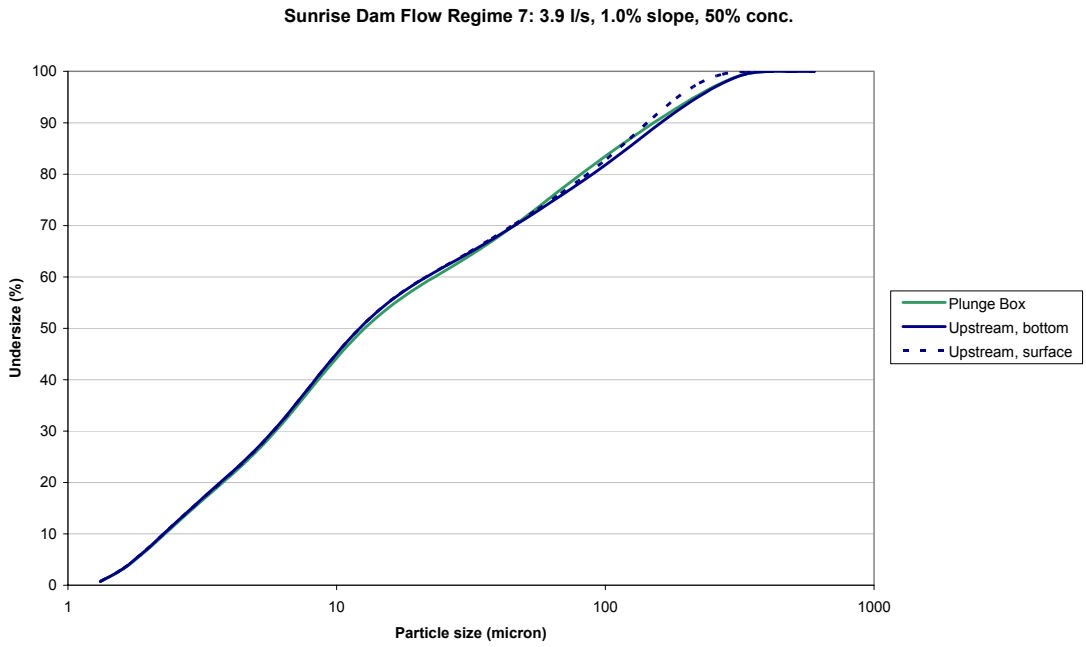

Figure 153. Particle size distribution curves for 3 fluid samples extracted from various points in the field flume during "Flow regime 7" of the Sunrise Dam experiments

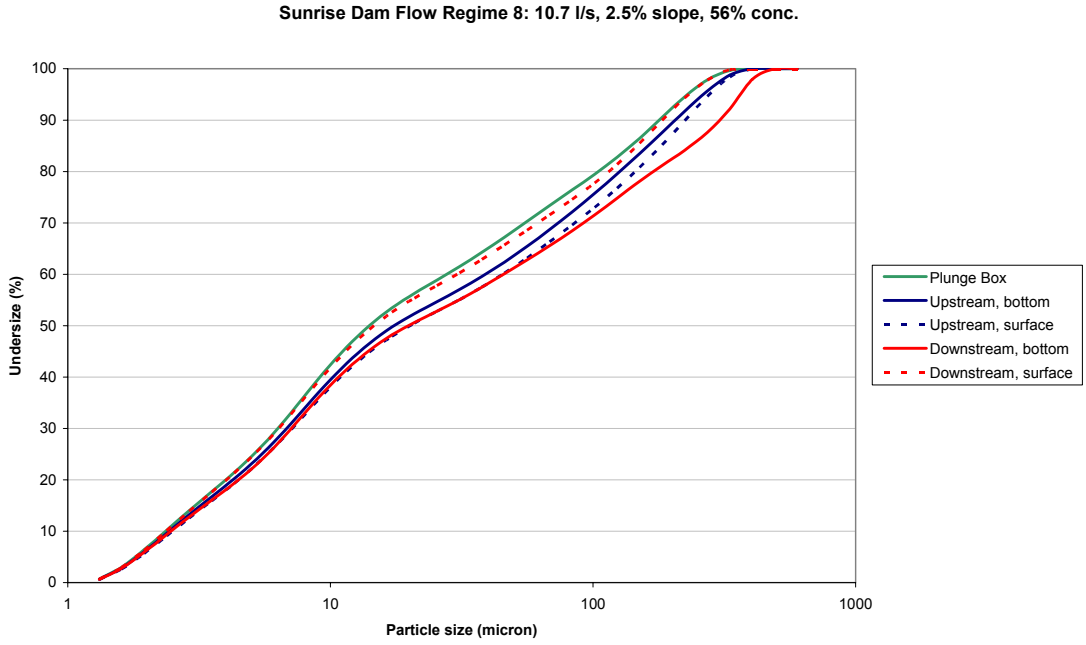

Figure 154. Particle size distribution curves for 5 fluid samples extracted from various points in the field flume during "Flow regime 8" of the Sunrise Dam experiments

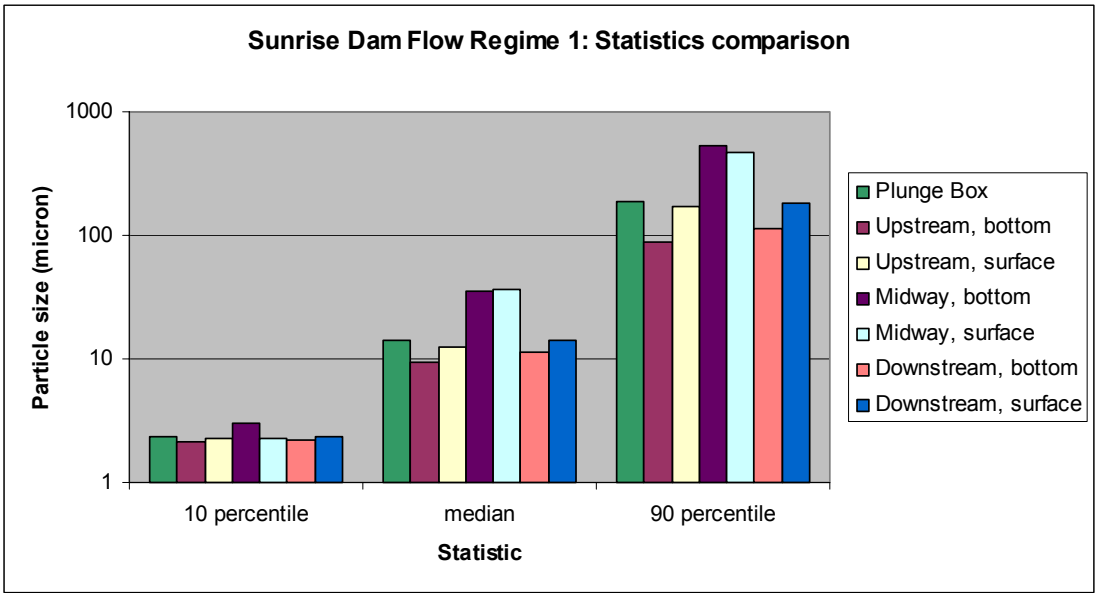

Figure 155. Comparison of 3 particle size statistics at various points in the flume during "Flow regime 1" of the Sunrise Dam experiments

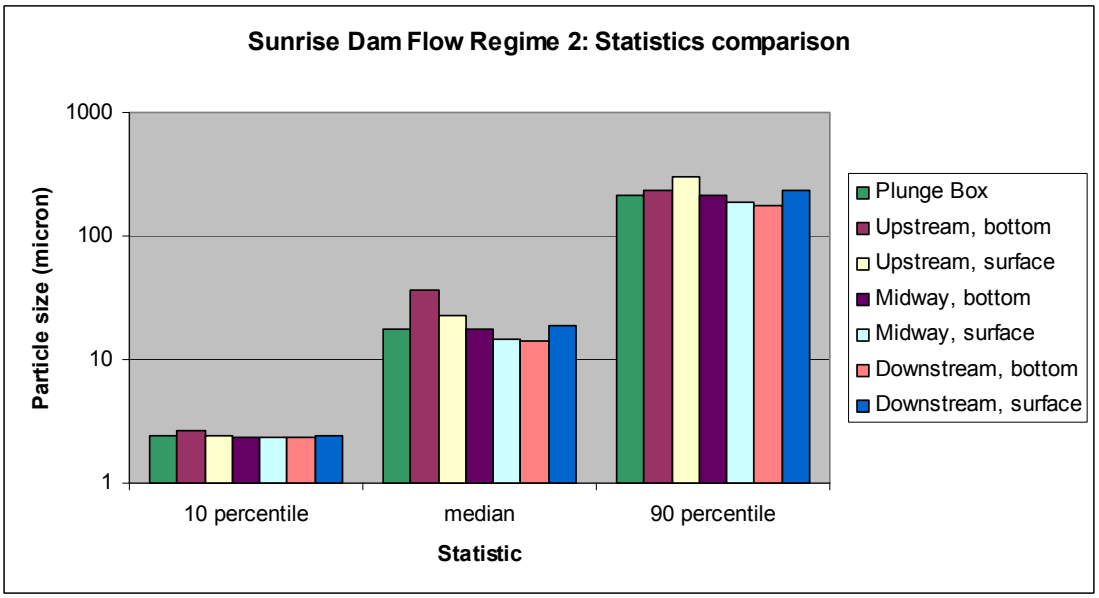

Figure 156. Comparison of 3 particle size statistics at various points in the flume during "Flow regime 2" of the Sunrise Dam experiments

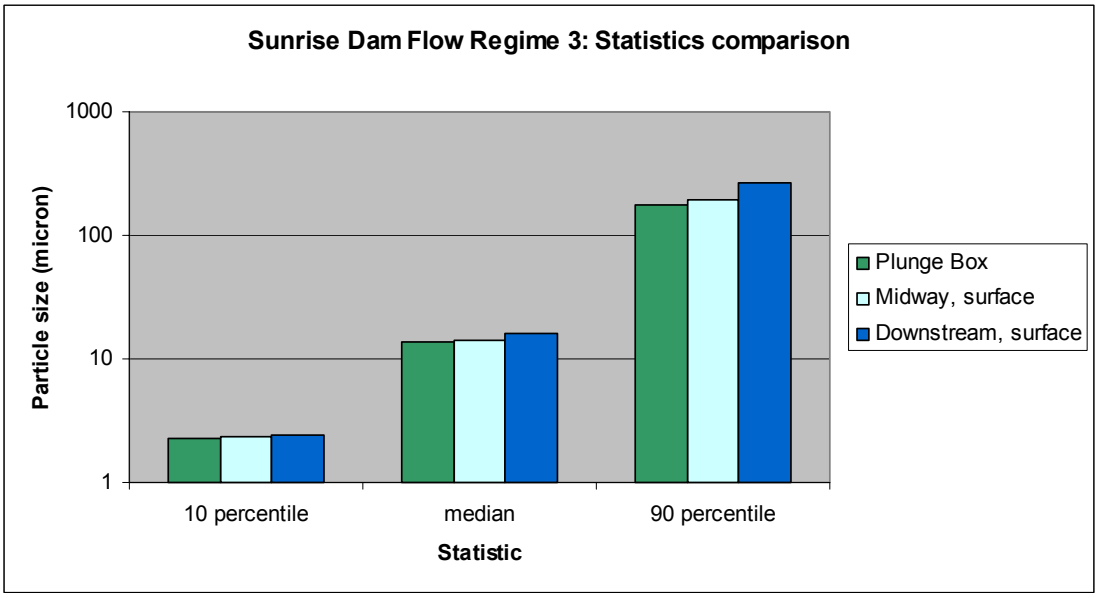

Figure 157. Comparison of 3 particle size statistics at various points in the flume during "Flow regime 3" of the Sunrise Dam experiments

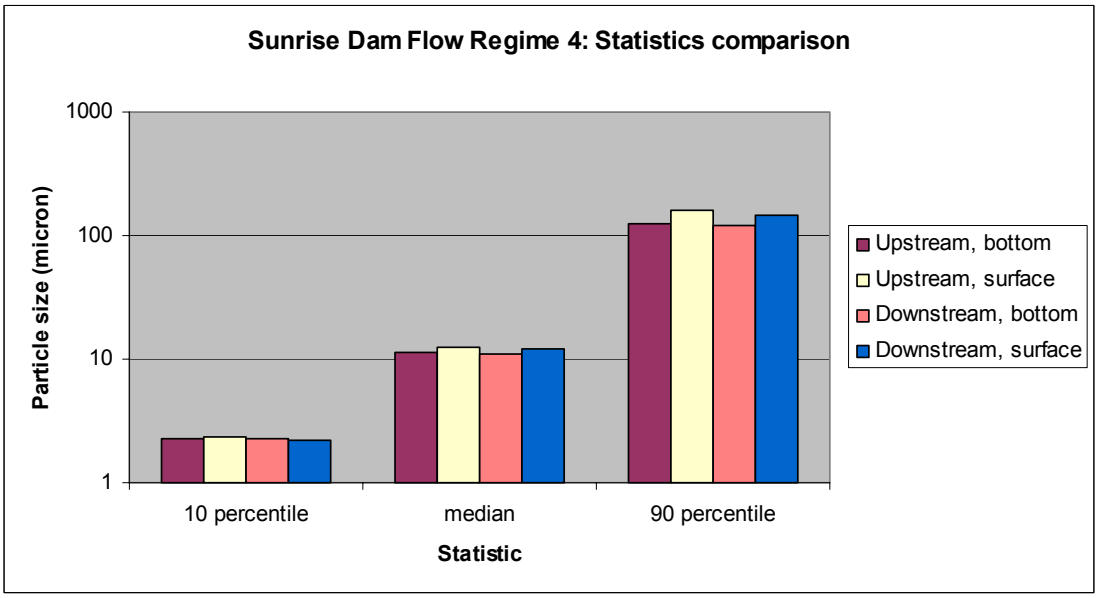

Figure 158. Comparison of 3 particle size statistics at various points in the flume during "Flow regime 4" of the Sunrise Dam experiments

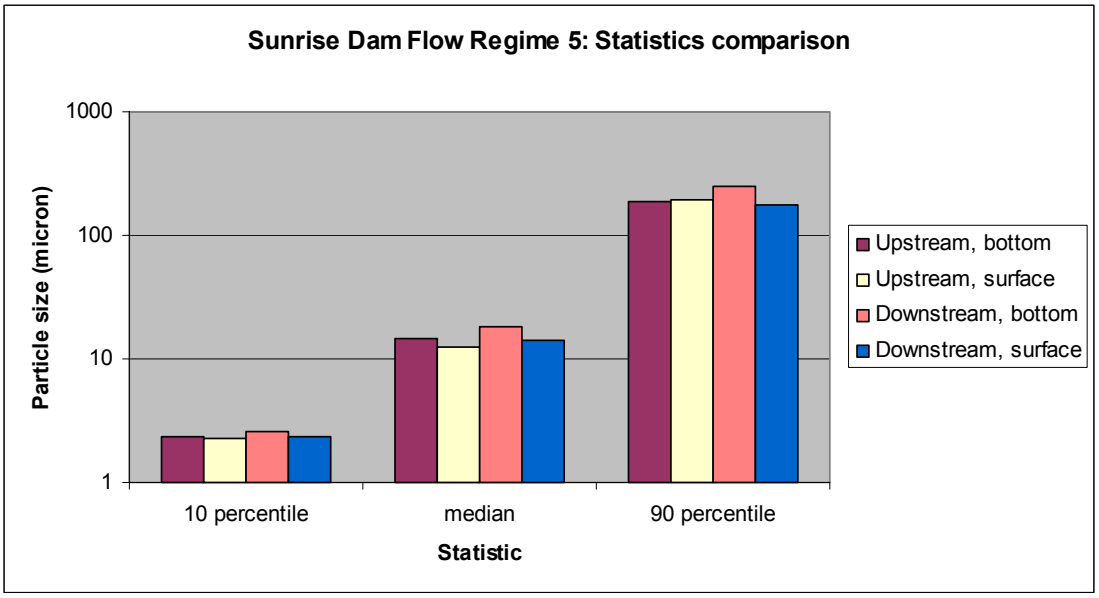

Figure 159. Comparison of 3 particle size statistics at various points in the flume during "Flow regime 5" of the Sunrise Dam experiments

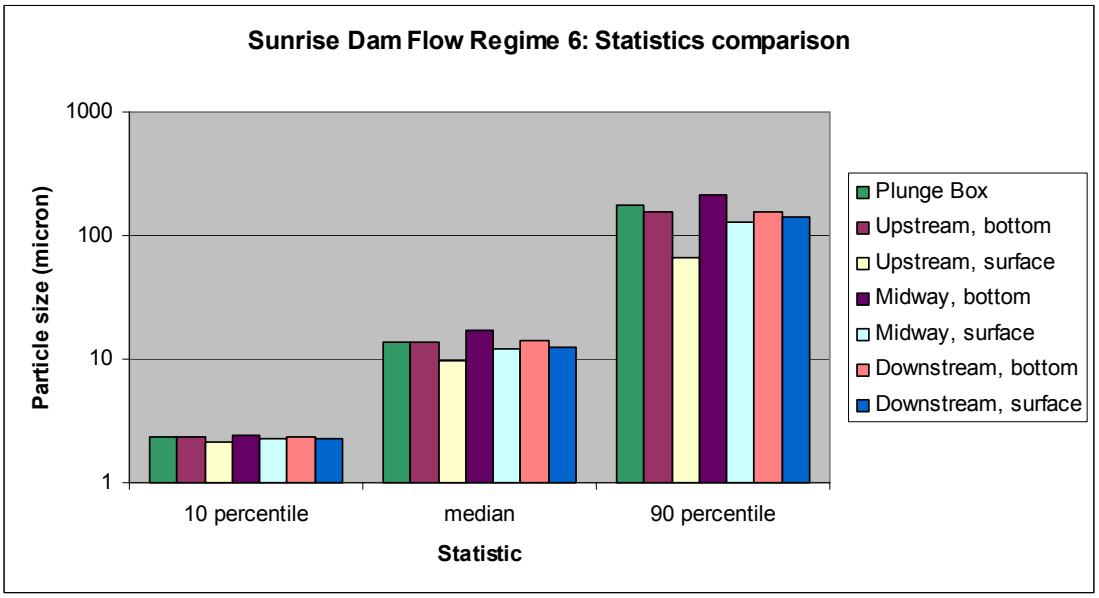

Figure 160. Comparison of 3 particle size statistics at various points in the flume during "Flow regime 6" of the Sunrise Dam experiments

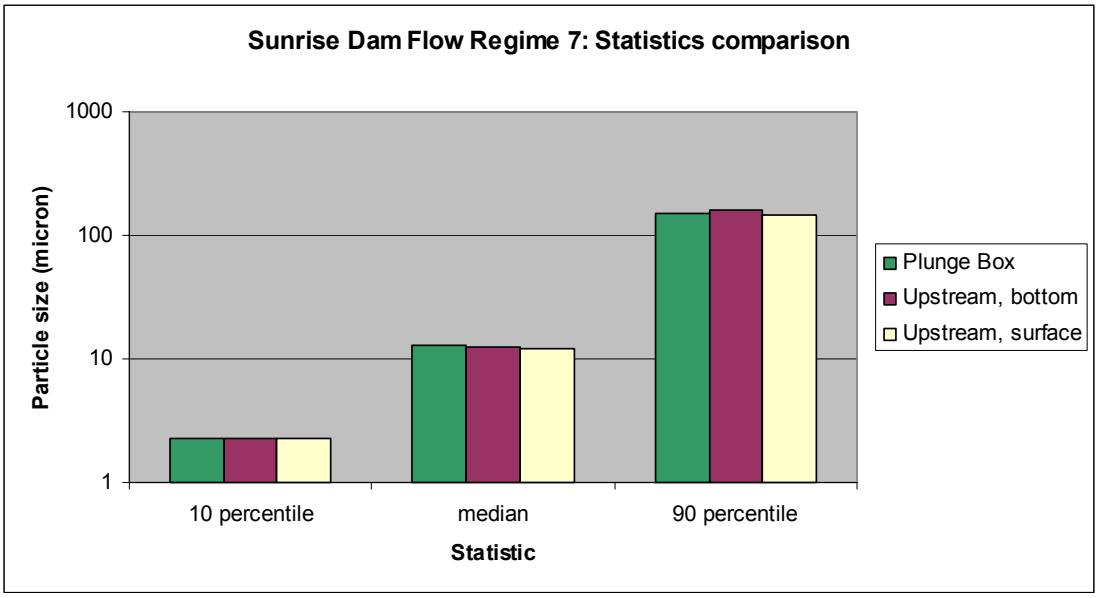

Figure 161. Comparison of 3 particle size statistics at various points in the flume during "Flow regime 7" of the Sunrise Dam experiments

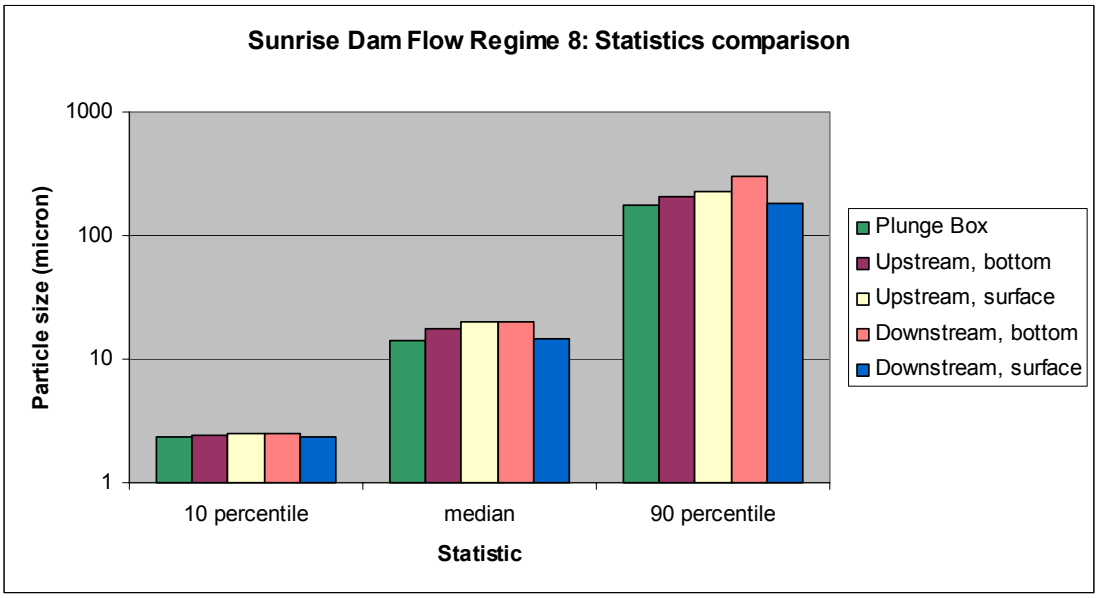

Figure 162. Comparison of 3 particle size statistics at various points in the flume during "Flow regime 8" of the Sunrise Dam experiments

Appendix C: Field flume experimental results – Velocity and concentration profiles

The following profiles are based on data that was recorded at Sunrise Dam. No profiles are presented here from the Cobar experimental campaign, as they are already presented in Behnam Pirouz's thesis (Pirouz 2006).

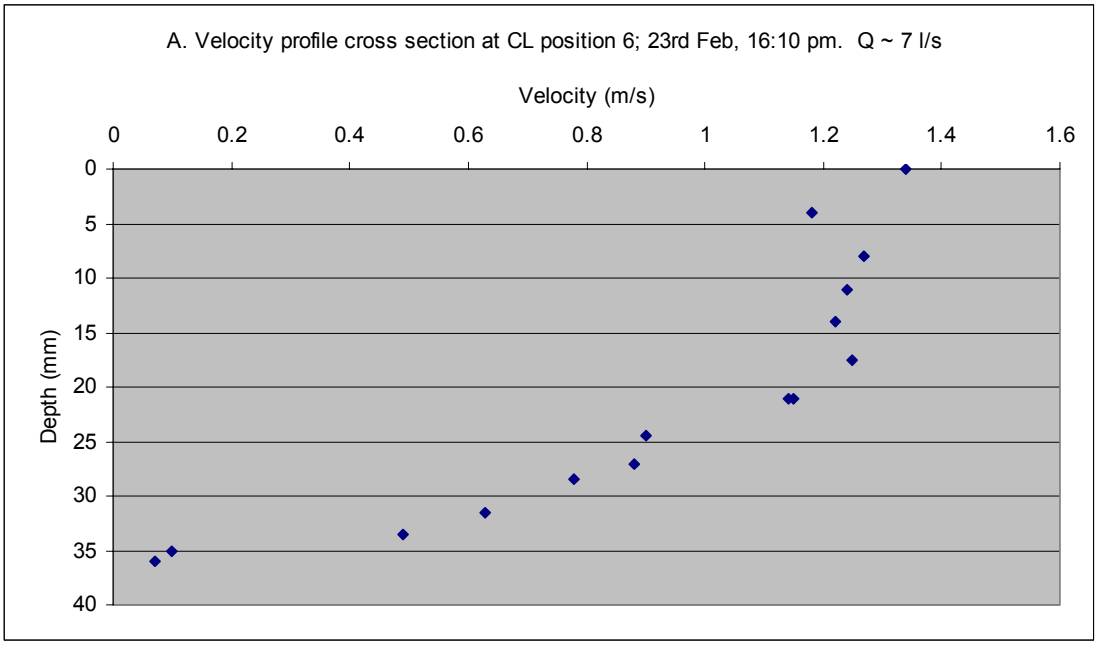

Figure 163. Velocity profile cross section at CL position 6; 23rd Feb, 16:10 pm. Q ~ 7 l/s

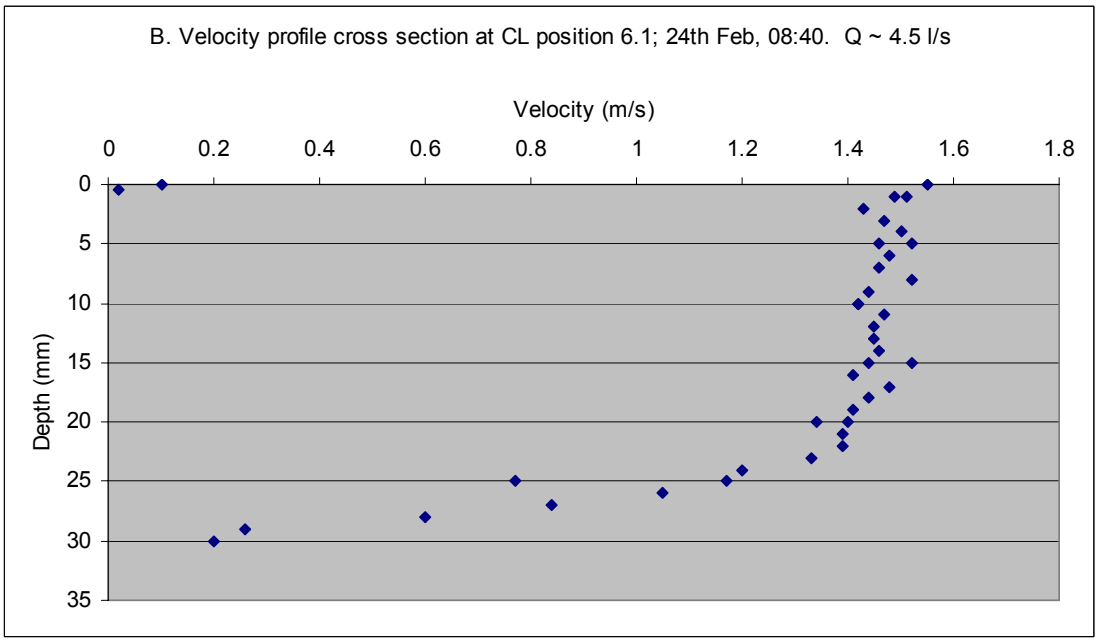

Figure 164. Velocity profile cross section at CL position 6.1; 24th Feb, 08:40. Q ~ 4.5 l/s

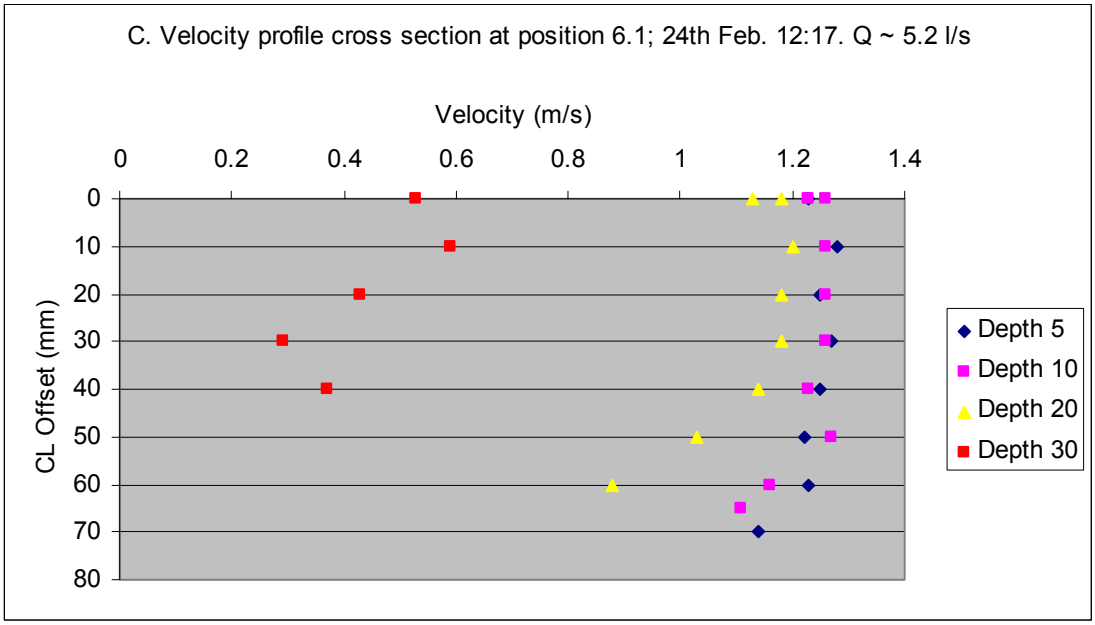

Figure 165. Velocity profile cross section at position 6.1; 24th Feb. 12:17. Q ~ 5.2 l/s

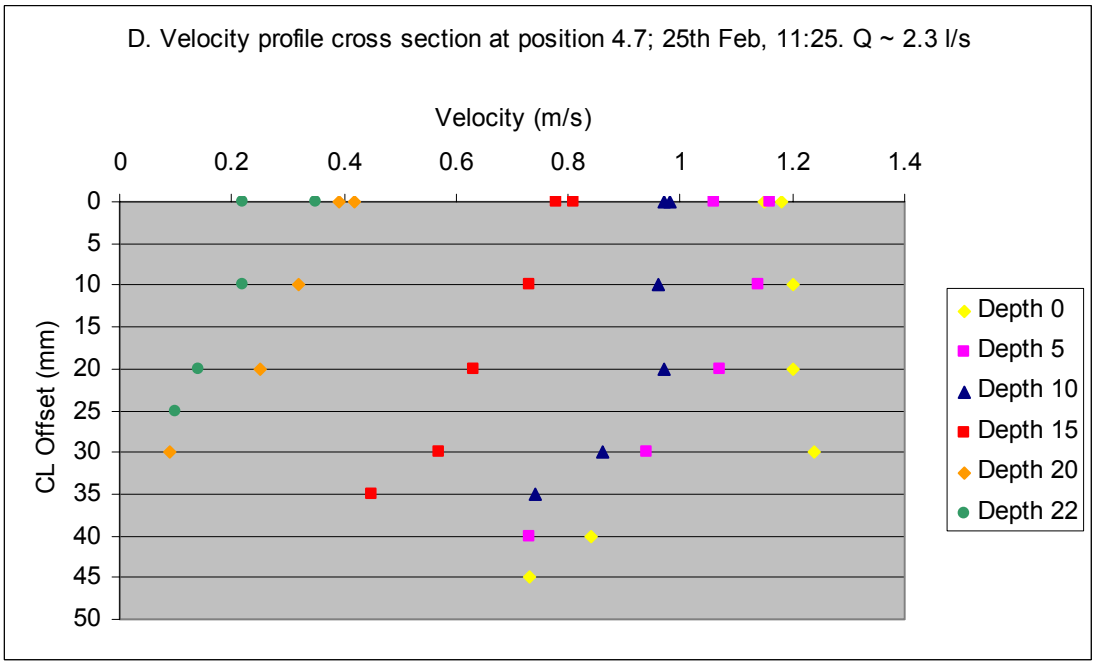

Figure 166. Velocity profile cross section at position 4.7; 25th Feb, 11:25. Q ~ 2.3 l/s

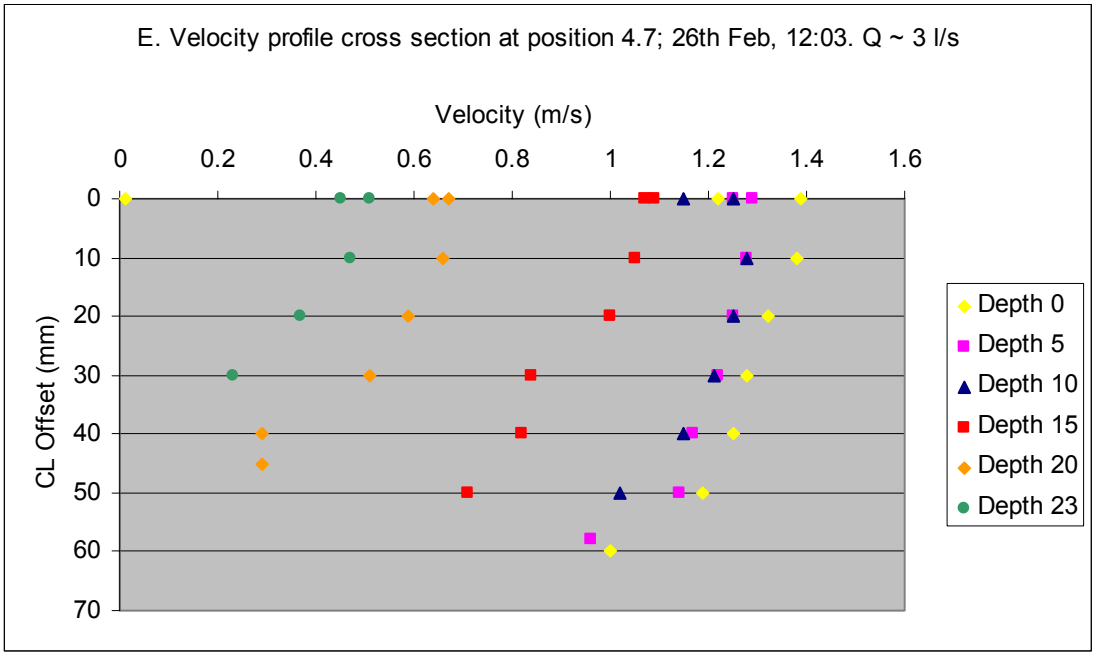

Figure 167. Velocity profile cross section at position 4.7; 26th Feb, 12:03. Q ~ 3 l/s

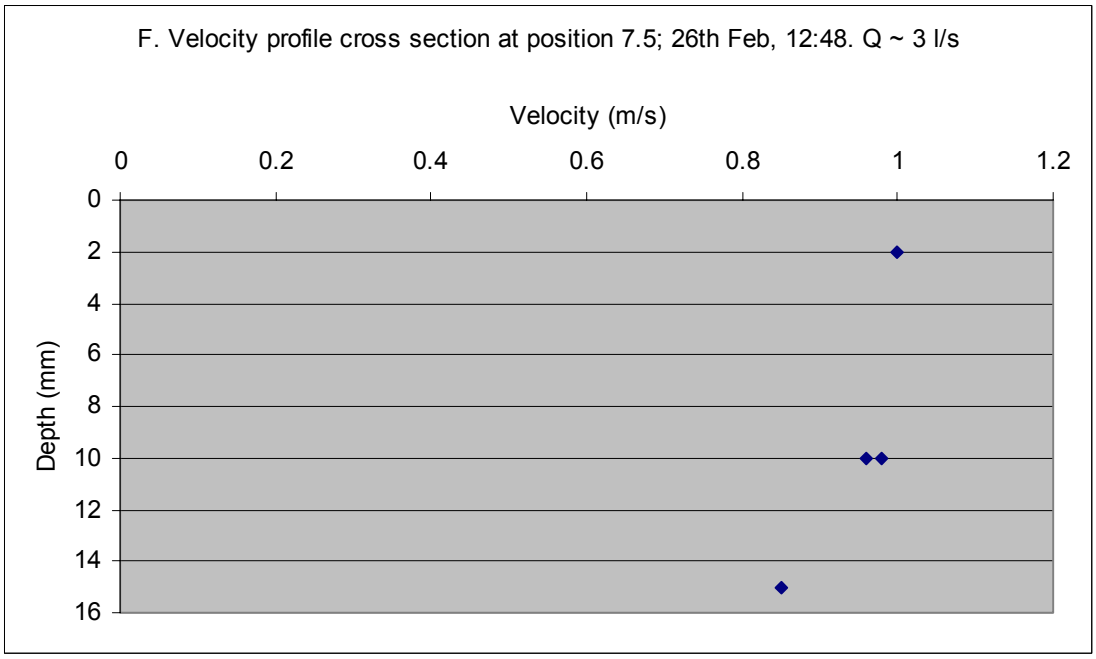

Figure 168. Velocity profile cross section at position 7.5; 26th Feb, 12:48. Q ~ 3 l/s

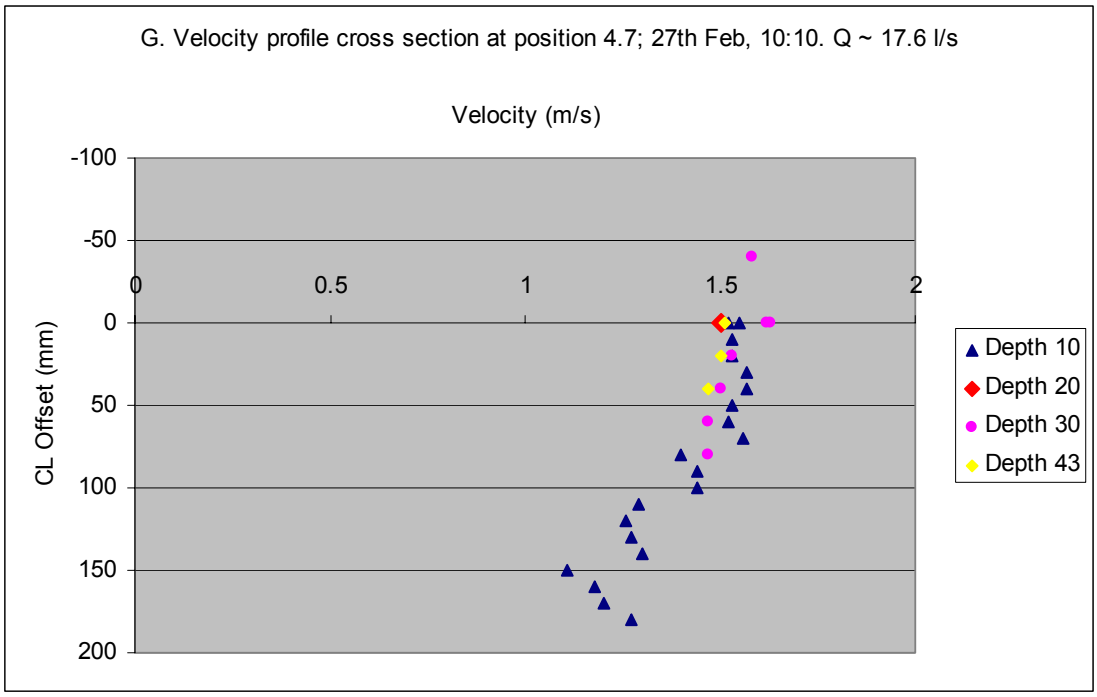

Figure 169. Velocity profile cross section at position 4.7; 27th Feb, 10:10. Q ~ 17.6 l/s

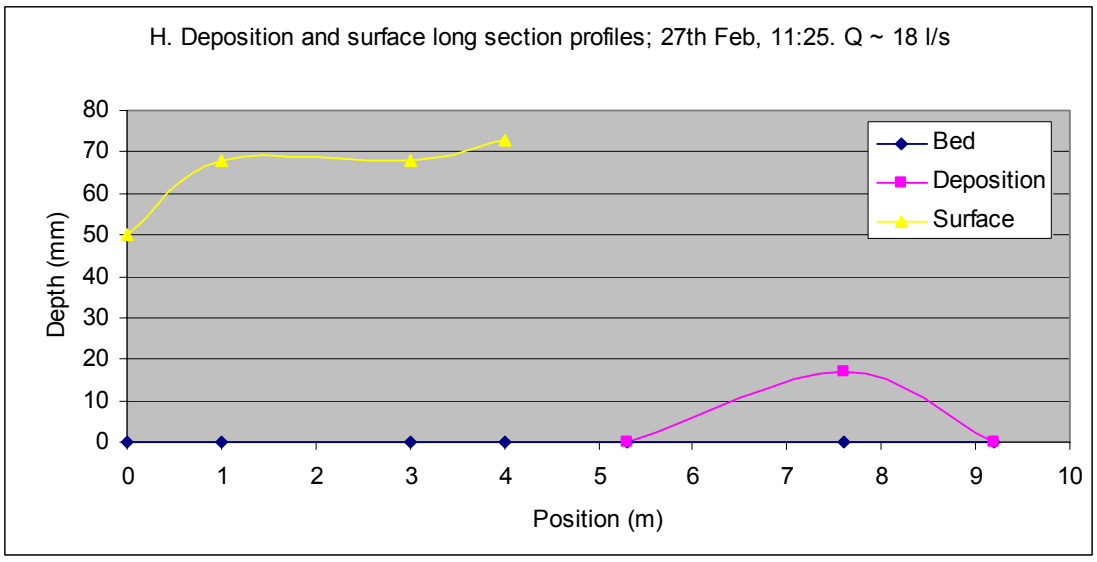

Figure 170. Deposition and surface long section profiles; 27th Feb, 11:25. Q ~ 18 l/s. "Position" denotes the distance from the downstream end of the flume (in metres)

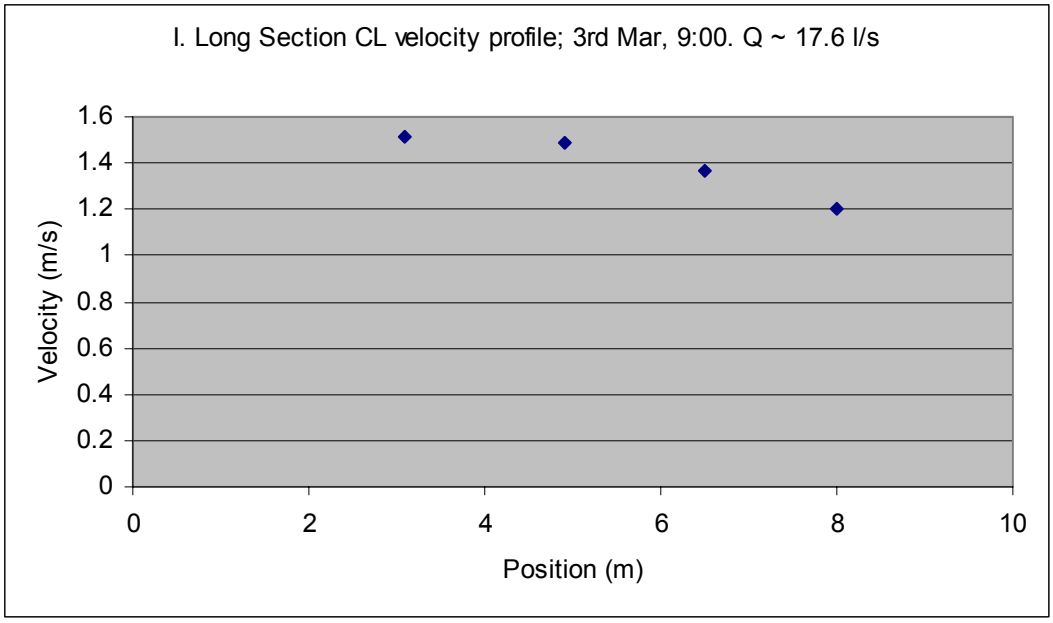

Figure 171. Long Section CL velocity profile; 3rd Mar, 9:00. Q ~ 17.6 l/s. "Position" denotes the distance from the downstream end of the flume (in metres)

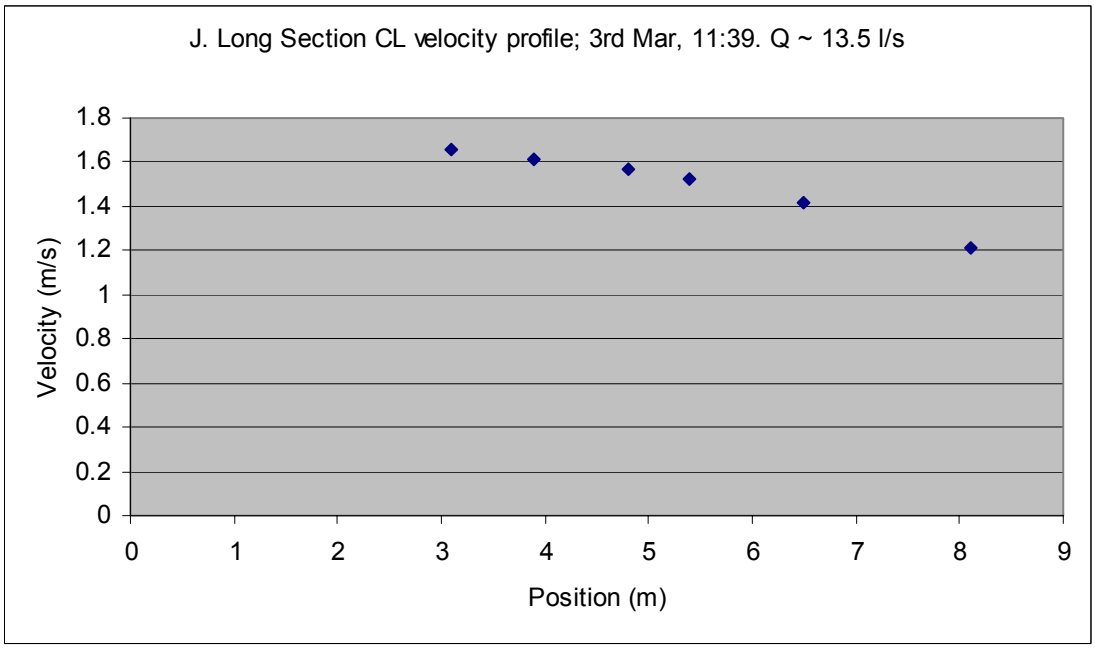

Figure 172. Long Section CL velocity profile; 3rd Mar, 11:39. Q ~ 13.5 l/s. "Position" denotes the distance from the downstream end of the flume (in metres)

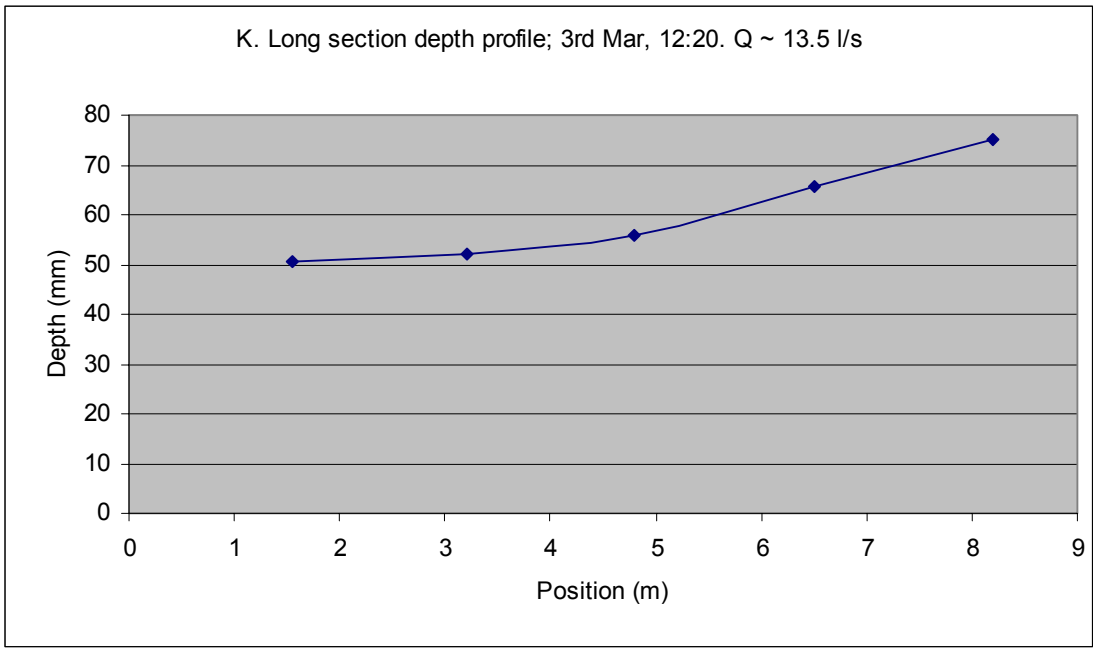

Figure 173. Long section depth profile; 3rd Mar, 12:20. Q ~ 13.5 l/s. "Position" denotes the distance from the downstream end of the flume (in metres)

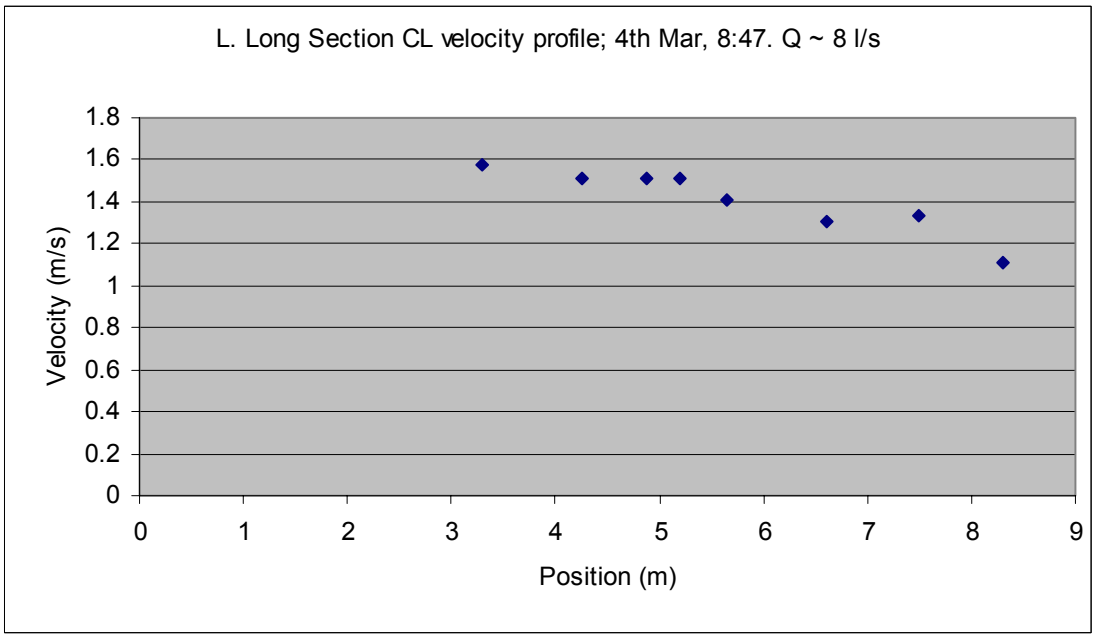

Figure 174. Long Section CL velocity profile; 4th Mar, 8:47. Q ~ 8 l/s. "Position" denotes the distance from the downstream end of the flume (in metres)

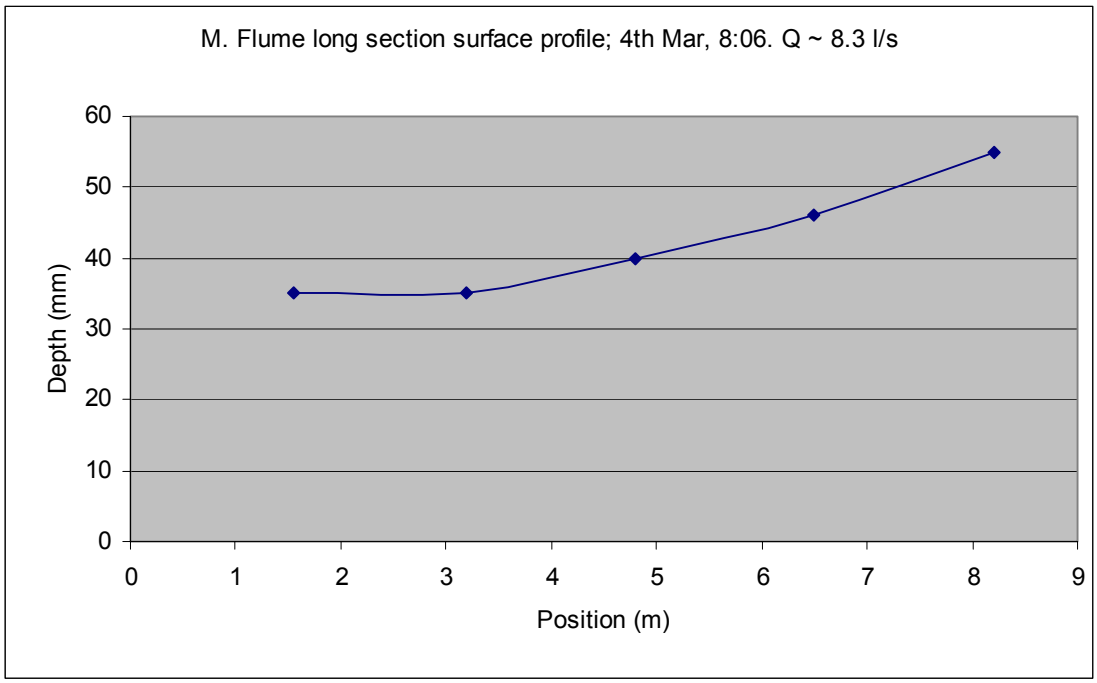

Figure 175. Flume long section surface profile; 4th Mar, 8:06. Q ~ 8.3 l/s. "Position" denotes the distance from the downstream end of the flume (in metres)

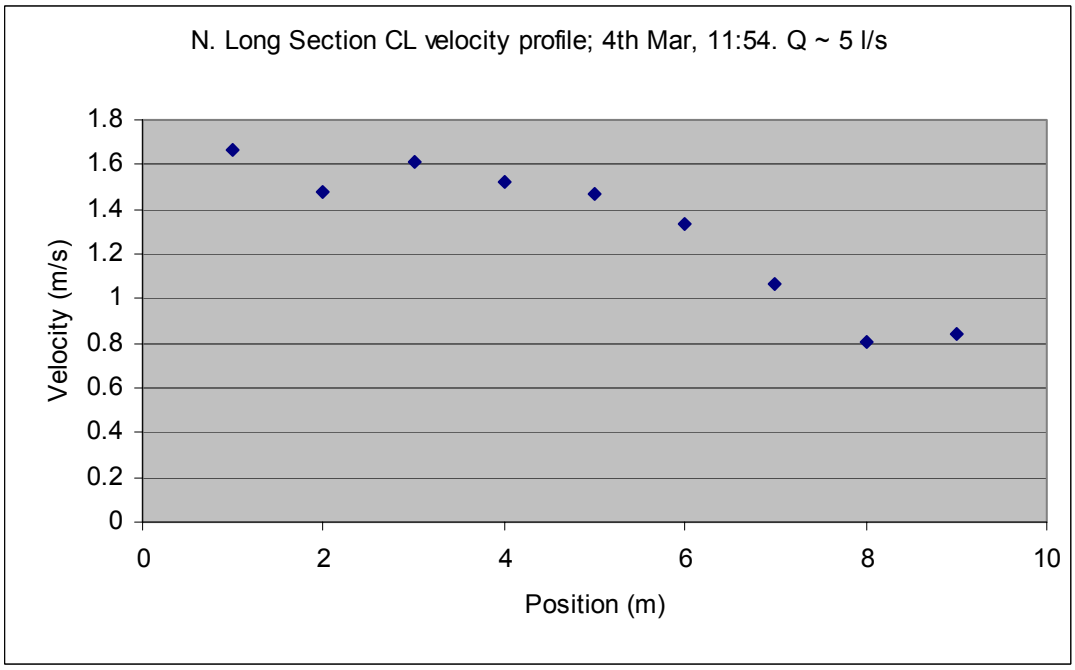

Figure 176. Long Section CL velocity profile; 4th Mar, 11:54. Q ~ 5 l/s. "Position" denotes the distance from the downstream end of the flume (in metres)

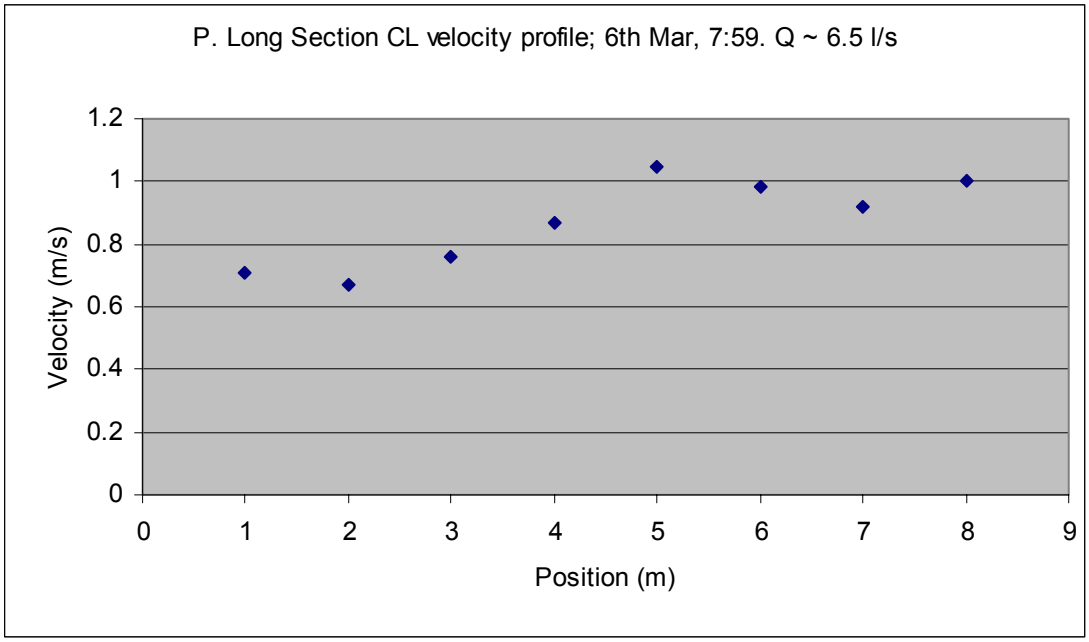

Figure 177. Long Section CL velocity profile; 6th Mar, 7:59. Q ~ 6.5 l/s. "Position" denotes the distance from the downstream end of the flume (in metres)

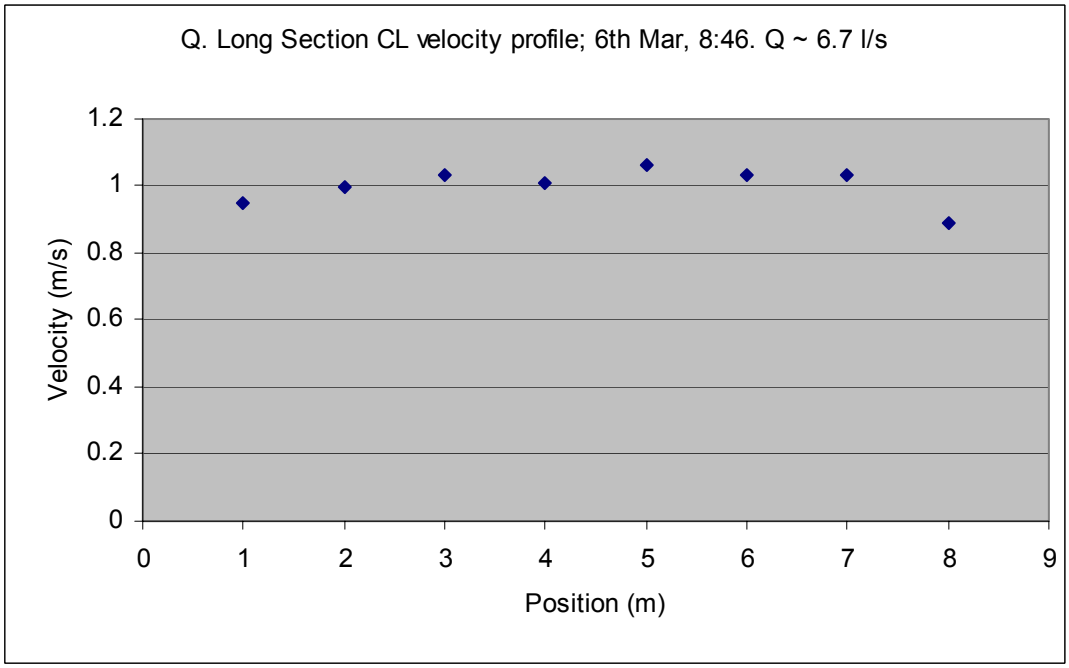

Figure 178. Long Section CL velocity profile; 6th Mar, 8:46. Q ~ 6.7 l/s. "Position" denotes the distance from the downstream end of the flume (in metres)

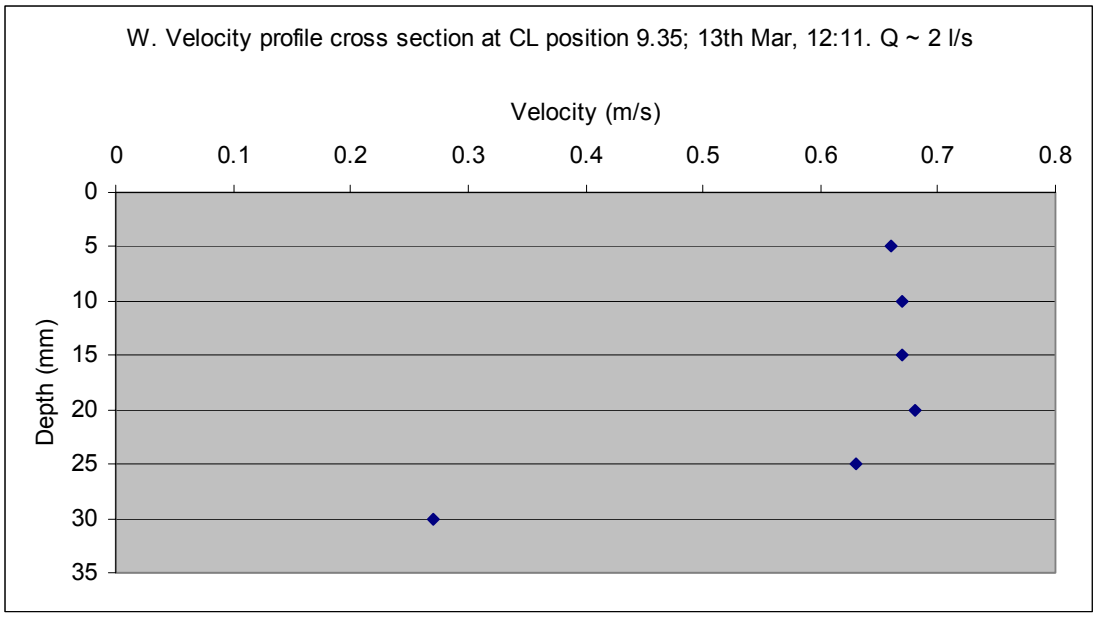

Figure 179. Velocity profile cross section at CL position 9.35; 13th Mar, 12:11. Q ~ 2 l/s

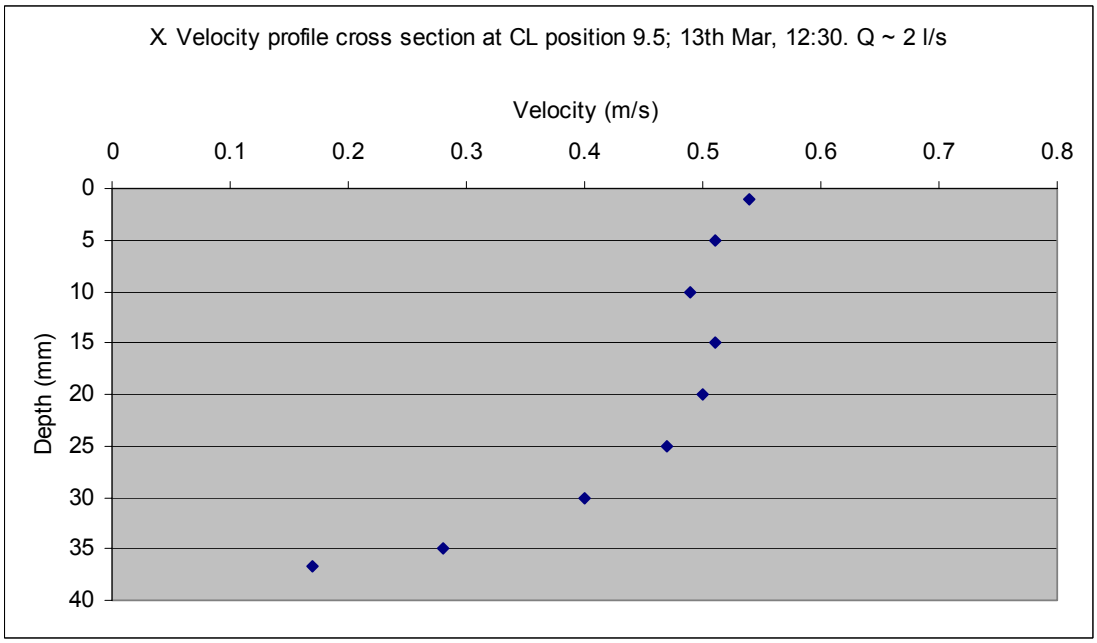

Figure 180. Velocity profile cross section at CL position 9.5; 13th Mar, 12:30. Q ~ 2 l/s

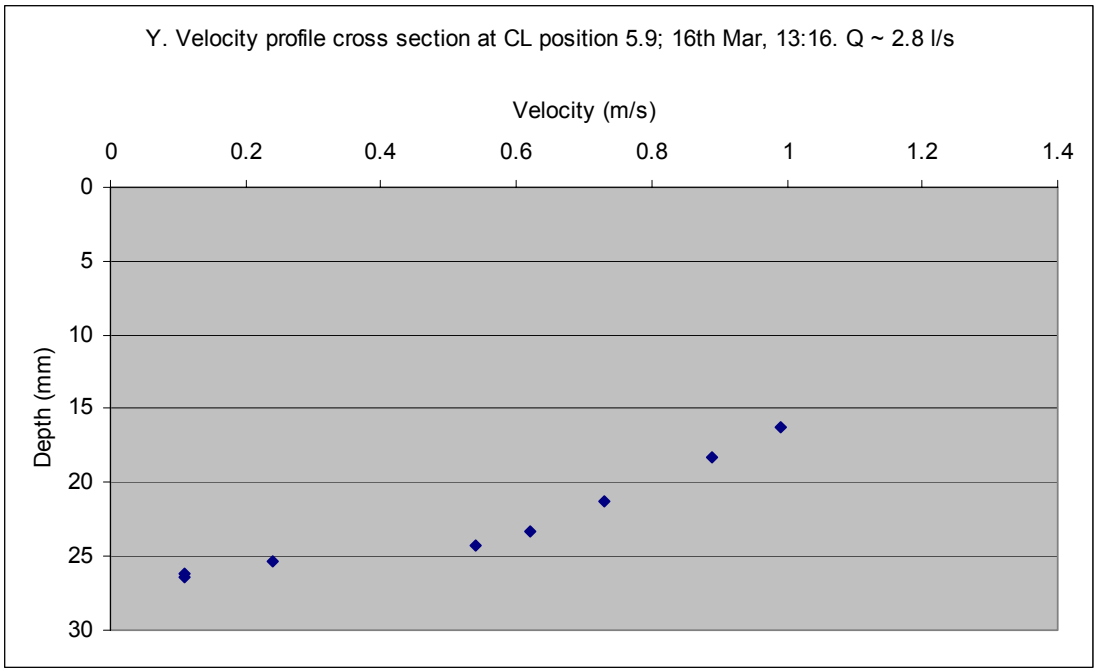

Figure 181. Velocity profile cross section at CL position 5.9; 16th Mar, 13:16. Q ~ 2.8 l/s

Appendix D: Aerial survey data

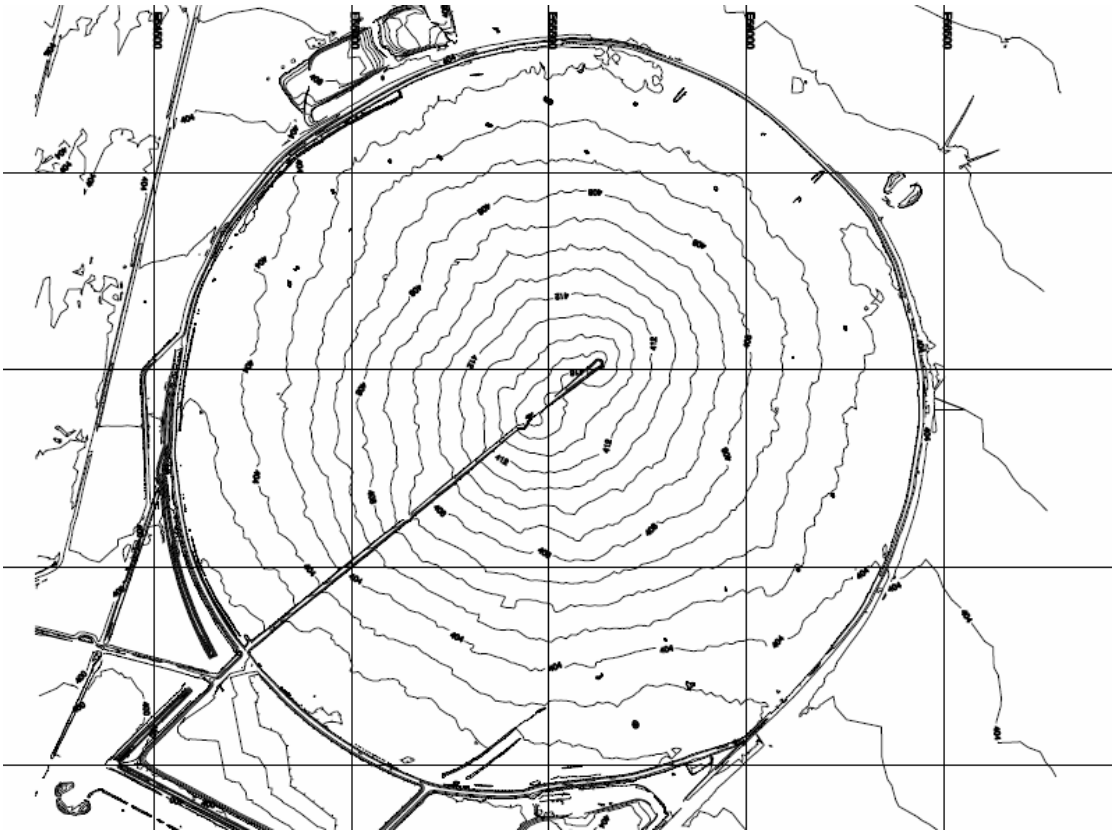

Figure 182. Sunrise Dam stack contour plan, based on survey done on 31st December 2004.

Appendix E: Historic tailings discharge data for Sunrise Dam stack

The following table of data was provided by AngloGold Ashanti, the operators of the Sunrise Dam gold mine. It contains the daily total number of dry tonnes of ore that has been processed by the mill, and the average tailings slurry concentration for every day between the 1st December, 2001 and the 31st December, 2004. On both of these dates an aerial survey of the stack was conducted.

Table 18. Historic daily averaged tailings discharge data for the Sunrise Dam stack

Date	Dry Tonnes	TAILS % Solids by weight	Tails Flowrate (mean t/h of slurry)	Tails density (t/m^3)	Tails Flowrate (mean m^3/h of slurry)	Q (l/s)
01-Dec-01	9716	60	675	1.769401	381.3141	105.9206
02-Dec-01	9415	61	648	1.778754	364.0848	101.1347
03-Dec-01	9768	59	685	1.760565	388.8416	108.0116
04-Dec-01	9675	58	690	1.743729	395.8716	109.9643
05-Dec-01	9211	59	648	1.756828	368.8812	102.467
06-Dec-01	9780	60	685	1.761298	388.8457	108.0127
07-Dec-01	9679	60	674	1.767368	381.121	105.8669
08-Dec-01	9601	58	686	1.742149	393.8535	109.4038
09-Dec-01	8995	58	652	1.729613	376.8573	104.6826
10-Dec-01	9644	59	682	1.751816	389.3719	108.1589
11-Dec-01	8337	58	601	1.734292	346.5337	96.25936
12-Dec-01	3782	58	273	1.734292	157.2186	43.67183
13-Dec-01	8486	59	597	1.756828	339.8371	94.39918
14-Dec-01	9780	58	698	1.743992	399.9982	111.1106
15-Dec-01	7998	61	547	1.784177	306.6971	85.19365
16-Dec-01	9339	60	646	1.773027	364.4511	101.2364
17-Dec-01	9365	61	644	1.779823	361.5711	100.4364
18-Dec-01	9455	63	625	1.819633	343.663	95.46194
19-Dec-01	9515	61	650	1.785834	363.9464	101.0962
20-Dec-01	9498	62	634	1.810117	350.1265	97.25736
21-Dec-01	9439	63	629	1.811839	347.0378	96.39938
22-Dec-01	9942	60	692	1.767775	391.2055	108.6682
23-Dec-01	9568	58	688	1.736001	396.5623	110.1562
24-Dec-01	9393	60	650	1.772664	366.7534	101.876
25-Dec-01	9327	58	676	1.729613	390.7609	108.5447
26-Dec-01	8853	60	619	1.762195	351.4663	97.62953
27-Dec-01	9196	59	655	1.745311	375.2891	104.247
28-Dec-01	9632	58	689	1.740922	395.9406	109.9835
29-Dec-01	9842	57	717	1.724442	415.992	115.5533
30-Dec-01	8522	58	616	1.73117	356.1098	98.91938
31-Dec-01	9858	57	717	1.725732	415.7533	115.487
01-Jan-02	9770	59	690	1.753268	393.5318	109.3144

02-Jan-02	9581	59	675	1.754868	384.9117	106.9199
03-Jan-02	9742	59	693	1.746192	396.9765	110.2712
04-Jan-02	9676	59	689	1.745311	394.8667	109.6852
05-Jan-02	9725	58	698	1.738736	401.2322	111.4534
06-Jan-02	9759	58	700	1.738855	402.5664	111.824
07-Jan-02	9717	56	725	1.704066	425.5265	118.2018
08-Jan-02	9879	58	707	1.74136	405.7935	112.7204
09-Jan-02	9577	61	659	1.77895	370.2616	102.8504
10-Jan-02	9776	62	662	1.794166	369.1678	102.5466
11-Jan-02	9663	62	653	1.796451	363.6256	101.0071
12-Jan-02	9871	63	657	1.812486	362.5726	100.7146
13-Jan-02	9937	63	659	1.816768	362.7163	100.7545
14-Jan-02	9856	61	669	1.792493	373.1477	103.6521
15-Jan-02	9839	60	679	1.776211	382.0071	106.1131
16-Jan-02	9856	59	693	1.758077	393.9294	109.4248
17-Jan-02	9964	59	699	1.759686	397.2014	110.3337
18-Jan-02	9544	63	633	1.816196	348.6652	96.85144
19-Jan-02	9761	64	640	1.82925	349.8345	97.17626
20-Jan-02	9914	62	670	1.79696	372.7684	103.5468
21-Jan-02	9833	63	654	1.813911	360.448	100.1244
22-Jan-02	9790	62	659	1.800887	365.9227	101.6452
23-Jan-02	8432	62	563	1.808934	311.361	86.48918
24-Jan-02	10502	61	719	1.784177	402.7168	111.8658
25-Jan-02	10471	61	714	1.787494	399.4785	110.9662
26-Jan-02	9738	61	661	1.792493	368.675	102.4097
27-Jan-02	9679	61	662	1.784177	371.1542	103.0984
28-Jan-02	9898	57	720	1.726507	416.899	115.8053
29-Jan-02	9098	63	602	1.819633	330.6801	91.85559
30-Jan-02	1923			1.14	0	0
31-Jan-02	8065	66	510	1.870775	272.6359	75.73221
01-Feb-02	9835	63	655	1.812771	361.1274	100.3132
02-Feb-02	10095	61	687	1.789157	384.1531	106.7092
03-Feb-02	10047	62	674	1.804113	373.6936	103.8038
04-Feb-02	9992	61	681	1.788207	380.7938	105.776
05-Feb-02	10161	60	707	1.767775	399.8266	111.063
06-Feb-02	10057	60	698	1.769401	394.729	109.6469
07-Feb-02	9638	59	682	1.751272	389.4844	108.1901
08-Feb-02	7857	59	560	1.745311	320.6484	89.06901
09-Feb-02	9918	58	707	1.744592	405.2184	112.5607
10-Feb-02	9719	58	699	1.736001	402.8184	111.894
11-Feb-02	9792	59	693	1.751937	395.2773	109.7992
12-Feb-02	9914	60	694	1.762031	393.7151	109.3653
13-Feb-02	9528	62	645	1.794927	359.3806	99.82794
14-Feb-02	9788	60	685	1.762031	388.7032	107.9731
15-Feb-02	9964	59	700	1.758613	397.8791	110.522
16-Feb-02	9910	60	691	1.76534	391.4704	108.7418
17-Feb-02	9821	61	674	1.781697	378.0684	105.019
18-Feb-02	9424	62	637	1.796261	354.7244	98.53454
19-Feb-02	9799	61	670	1.784453	375.6038	104.3344
20-Feb-02	9699	60	670	1.775342	377.1132	104.7537
21-Feb-02	9831	58	701	1.744592	401.6795	111.5776
22-Feb-02	9841	61	671	1.787217	375.6035	104.3343
23-Feb-02	9857	62	665	1.799202	369.3602	102.6001

24-Feb-02	9900	62	663	1.805653	367.3837	102.051
25-Feb-02	9492	60	656	1.773853	369.9374	102.7604
26-Feb-02	9929	59	701	1.753268	399.9501	111.0973
27-Feb-02	9742	59	688	1.753268	392.4218	109.0061
28-Feb-02	9628	59	681	1.751816	388.7533	107.987
01-Mar-02	9347	60	649	1.769401	366.8361	101.8989
02-Mar-02	9770	62	659	1.798361	366.5982	101.8328
03-Mar-02	9645	62	649	1.80104	360.4137	100.1149
04-Mar-02	9772	61	669	1.784328	374.6551	104.0709
05-Mar-02	9749	60	682	1.762913	386.6066	107.3907
06-Mar-02	9517	61	652	1.782523	365.8773	101.6326
07-Mar-02	8618	61	589	1.785834	329.6299	91.56387
08-Mar-02	9819	62	658	1.805961	364.2177	101.1716
09-Mar-02	9760	60	679	1.768046	383.8928	106.6369
10-Mar-02	9876	62	661	1.807659	365.3901	101.4972
11-Mar-02	9913	61	680	1.781322	381.8367	106.0658
12-Mar-02	9974	63	663	1.814482	365.3005	101.4724
13-Mar-02	9768	62	658	1.800887	365.0981	101.4161
14-Mar-02	9505	63	632	1.813393	348.659	96.84974
15-Mar-02	9777	64	639	1.832243	348.8881	96.91335
16-Mar-02	9780	65	628	1.853111	338.7651	94.10141
17-Mar-02	10043	63	668	1.813911	368.138	102.2606
18-Mar-02	10051	62	675	1.802575	374.7151	104.0875
19-Mar-02	9987	61	686	1.780872	384.9501	106.9306
20-Mar-02	9943	60	685	1.776667	385.7808	107.1613
21-Mar-02	10117	61	686	1.793405	382.4788	106.2441
22-Mar-02	9914	60	684	1.775938	385.111	106.9753
23-Mar-02	8584	61	588	1.783468	329.5307	91.53631
24-Mar-02	10833	60	747	1.776211	420.6237	116.8399
25-Mar-02	10453	60	722	1.774299	407.0808	113.078
26-Mar-02	9167	64	600	1.831185	327.6237	91.00658
27-Mar-02	2861	60	199	1.769401	112.2869	31.1908
28-Mar-02	9587	59	674	1.757848	383.3169	106.4769
29-Mar-02	9252	60	644	1.766446	364.8462	101.3462
30-Mar-02	8627	62	578	1.806338	319.8193	88.8387
31-Mar-02	9276	62	623	1.802575	345.8351	96.0653
01-Apr-02	9185	61	629	1.783074	352.81	98.00277
02-Apr-02	9589	62	643	1.804113	356.6782	99.07729
03-Apr-02	9435	61	647	1.782523	362.7374	100.7604
04-Apr-02	9900	63	657	1.815338	362.1303	100.5918
05-Apr-02	9402	62	633	1.801168	351.2579	97.57164
06-Apr-02	9350	61	634	1.793405	353.4853	98.19037
07-Apr-02	9526	62	641	1.80104	355.9924	98.88677
08-Apr-02	9609	63	637	1.817913	350.1296	97.25821
09-Apr-02	9092	61	618	1.79138	344.7912	95.77534
10-Apr-02	5321	62	358	1.802575	198.3942	55.1095
11-Apr-02	9745	59	688	1.753268	392.5381	109.0384
12-Apr-02	9537	56	713	1.702055	419.1481	116.43
13-Apr-02	9063	59	640	1.753268	365.0706	101.4085
14-Apr-02	9357	55	711	1.688873	421.1299	116.9805
15-Apr-02	9329	57	679	1.725302	393.7302	109.3695
16-Apr-02	9249	58	664	1.737427	382.4353	106.232
17-Apr-02	9234	60	644	1.764762	365.1193	101.422

18-Apr-02	8805	59	618	1.758613	351.5901	97.66391
19-Apr-02	9287	60	643	1.772664	362.6182	100.7273
20-Apr-02	9304	60	649	1.764972	367.7395	102.1499
21-Apr-02	9464	60	662	1.762913	375.319	104.2553
22-Apr-02	9587	59	677	1.753268	386.1712	107.2698
23-Apr-02	9462	60	655	1.772367	369.6019	102.6672
24-Apr-02	9825	60	680	1.772367	383.8099	106.6139
25-Apr-02	8302	59	584	1.757274	332.2374	92.28816
26-Apr-02	9468	62	637	1.800887	353.8752	98.29867
27-Apr-02	9752	61	667	1.784328	373.886	103.8572
28-Apr-02	9897	59	700	1.751816	399.6082	111.0023
29-Apr-02	8458	60	583	1.776407	328.3105	91.19737
30-Apr-02	8736	60	610	1.764762	345.42	95.95001
01-May-02	8179	60	570	1.766151	322.6581	89.62725
02-May-02	9128	61	629	1.77758	353.6518	98.23661
03-May-02	9300	60	647	1.767078	366.3675	101.7688
04-May-02	8774	58	632	1.735684	363.8591	101.072
05-May-02	9457	58	674	1.744432	386.4874	107.3576
06-May-02	9983	58	718	1.736001	413.7843	114.9401
07-May-02	9935	60	688	1.772664	387.9254	107.7571
08-May-02	8353	59	589	1.755046	335.4859	93.19053
09-May-02	8754	58	626	1.742149	359.1355	99.75987
10-May-02	8626	56	645	1.702809	378.5864	105.1629
11-May-02	8438	59	594	1.756471	338.1017	93.91713
12-May-02	8195	61	563	1.780323	316.1659	87.82387
13-May-02	8412	60	581	1.774845	327.3272	90.92423
14-May-02	8409	62	563	1.806809	311.5245	86.53459
15-May-02	3692	58	267	1.732209	153.999	42.77749
16-May-02	9393	61	642	1.785834	359.2812	99.80034
17-May-02	8855	61	604	1.787679	337.7466	93.81849
18-May-02	9286	62	629	1.794927	350.2469	97.29079
19-May-02	9086	60	632	1.767594	357.623	99.33973
20-May-02	9599	61	660	1.779636	370.6986	102.9718
21-May-02	9557	60	669	1.761298	379.9606	105.5446
22-May-02	9585	59	677	1.753268	386.0975	107.2493
23-May-02	9814	57	719	1.720468	417.6373	116.0104
24-May-02	10008	61	688	1.77895	386.9348	107.4819
25-May-02	10101	60	697	1.775342	392.7396	109.0943
26-May-02	9451	60	653	1.773853	368.3283	102.3134
27-May-02	9286	61	637	1.782156	357.2043	99.22342
28-May-02	9782	59	690	1.754868	392.9766	109.1602
29-May-02	9533	60	666	1.7635	377.6906	104.9141
30-May-02	9179	60	636	1.771031	359.3272	99.8131
31-May-02	10188	61	701	1.778327	394.2759	109.5211
01-Jun-02	10245	61	698	1.788855	390.0504	108.3473
02-Jun-02	9914	62	670	1.796451	373.0792	103.6331
03-Jun-02	9502	60	661	1.768046	373.723	103.8119
04-Jun-02	9858	61	678	1.779225	380.9595	105.8221
05-Jun-02	9487	62	634	1.808225	350.7224	97.42288
06-Jun-02	10023	61	680	1.792772	379.2882	105.3578
07-Jun-02	9656	61	658	1.788855	367.5943	102.1095
08-Jun-02	9839	61	670	1.789157	374.3871	103.9964
09-Jun-02	10320	61	703	1.789157	392.719	109.0886

10-Jun-02	10694	62	723	1.796451	402.4187	111.783
11-Jun-02	10520	61	716	1.789157	400.3006	111.1946
12-Jun-02	10123	61	694	1.782824	389.0237	108.0621
13-Jun-02	10030	59	707	1.754723	403.0465	111.9574
14-Jun-02	9790	60	681	1.767594	385.3469	107.0408
15-Jun-02	9495	60	656	1.774299	369.7822	102.7173
16-Jun-02	9793	60	679	1.771031	383.3673	106.4909
17-Jun-02	9817	60	682	1.769401	385.2725	107.0201
18-Jun-02	9277	61	632	1.787679	353.8086	98.28018
19-Jun-02	9375	60	648	1.773481	365.5761	101.5489
20-Jun-02	10133	61	698	1.77758	392.5794	109.0498
21-Jun-02	9825	59	697	1.748919	398.5897	110.7194
22-Jun-02	9853	61	674	1.783993	377.9286	104.9802
23-Jun-02	9552	60	669	1.761298	379.765	105.4903
24-Jun-02	10321	59	726	1.757639	412.8045	114.6679
25-Jun-02	10462	62	708	1.795096	394.4983	109.5829
26-Jun-02	9988	61	681	1.787494	381.0601	105.85
27-Jun-02	9785	60	676	1.774299	381.0552	105.8487
28-Jun-02	10080	60	701	1.767594	396.7447	110.2069
29-Jun-02	9886	61	681	1.77758	383.0332	106.3981
30-Jun-02	10027	60	696	1.769401	393.5434	109.3176
01-Jul-02	9818	58	703	1.740922	403.6101	112.1139
02-Jul-02	9215	60	640	1.769401	361.6634	100.462
03-Jul-02	0			1.14	0	0
04-Jul-02	8826	61	608	1.77758	341.9392	94.98311
05-Jul-02	9403	59	661	1.757848	375.9605	104.4335
06-Jul-02	9376	59	665	1.749281	380.1273	105.5909
07-Jul-02	9005	61	618	1.781697	346.6471	96.29086
08-Jul-02	9014	61	616	1.785834	344.7871	95.77421
09-Jul-02	9240	61	627	1.793236	349.4078	97.05773
10-Jul-02	9505	61	652	1.782156	365.6286	101.5635
11-Jul-02	9693	59	681	1.758613	387.0731	107.5203
12-Jul-02	7363	61	501	1.78999	279.843	77.73417
13-Jul-02	9281	60	641	1.774065	361.5942	100.4428
14-Jul-02	9744	60	682	1.762195	386.8683	107.4634
15-Jul-02	9938	59	704	1.750077	402.3798	111.7722
16-Jul-02	10233	60	714	1.764972	404.4631	112.3509
17-Jul-02	9615	60	663	1.775938	373.498	103.7494
18-Jul-02	10762	60	754	1.761298	427.8925	118.859
19-Jul-02	3940	54	307	1.669543	183.8054	51.05705
20-Jul-02	10121	59	711	1.758077	404.5129	112.3647
21-Jul-02	10067	59	705	1.760565	400.7189	111.3108
22-Jul-02	9590	59	673	1.759283	382.5252	106.257
23-Jul-02	9708	58	693	1.743333	397.48	110.4111
24-Jul-02	9907	58	712	1.737427	409.6435	113.7899
25-Jul-02	10159	58	733	1.732953	423.2356	117.5654
26-Jul-02	8938	53	701	1.664382	421.0598	116.961
27-Jul-02	8726	58	628	1.735187	362.146	100.5961
28-Jul-02	9560	58	692	1.73117	399.4713	110.9642
29-Jul-02	10155	59	712	1.759686	404.7984	112.444
30-Jul-02	10179	57	744	1.721869	432.1343	120.0373
31-Jul-02	9811	59	693	1.753268	395.2009	109.778
01-Aug-02	9795	59	697	1.746032	399.2491	110.9025

02-Aug-02	10098	60	706	1.762195	400.9045	111.3624
03-Aug-02	10099	59	718	1.746632	411.2502	114.2362
04-Aug-02	10060	59	705	1.760565	400.4626	111.2396
05-Aug-02	8855	59	621	1.760146	352.7141	97.97613
06-Aug-02	10002	60	691	1.774845	389.1952	108.1098
07-Aug-02	9837	59	690	1.760402	391.6729	108.798
08-Aug-02	10098	60	703	1.766446	398.1875	110.6076
09-Aug-02	10133	61	695	1.782156	389.805	108.2792
10-Aug-02	9981	62	672	1.800465	373.2896	103.6916
11-Aug-02	9288	60	645	1.769401	364.537	101.2603
12-Aug-02	10030	60	698	1.767775	394.6602	109.6278
13-Aug-02	9699	60	675	1.766692	382.2885	106.1913
14-Aug-02	10026	60	692	1.774845	390.1235	108.3676
15-Aug-02	9677	58	701	1.729613	405.4072	112.6131
16-Aug-02	10020	60	691	1.776833	388.688	107.9689
17-Aug-02	6057	58	435	1.737427	250.4647	69.57352
18-Aug-02	9411	59	663	1.755269	377.8243	104.9512
19-Aug-02	10258	60	716	1.763991	406.103	112.8064
20-Aug-02	9221	60	641	1.767775	362.8561	100.7934
21-Aug-02	4335	56	323	1.706587	188.9873	52.49647
22-Aug-02	9694	60	673	1.769401	380.4559	105.6822
23-Aug-02	8769	62	589	1.802575	326.9263	90.81285
24-Aug-02	8248			1.14	0	0
25-Aug-02	4442			1.14	0	0
26-Aug-02	10485			1.14	0	0
27-Aug-02	10393	60	728	1.761298	413.2045	114.779
28-Aug-02	9974	61	681	1.785834	381.4801	105.9667
29-Aug-02	10184	60	710	1.76534	402.2915	111.7476
30-Aug-02	9973	60	693	1.769401	391.4051	108.7236
31-Aug-02	10357	60	719	1.769401	406.5029	112.9175
01-Sep-02	10232	60	711	1.769401	401.5961	111.5545
02-Sep-02	9472	62	639	1.797978	355.6193	98.78313
03-Sep-02	9454	62	640	1.794166	356.9822	99.16174
04-Sep-02	9689	61	659	1.790824	367.7544	102.154
05-Sep-02	9371	60	646	1.775938	364.0253	101.1181
06-Sep-02	9747	59	688	1.753268	392.5978	109.0549
07-Sep-02	9679	59	683	1.754723	388.9594	108.0443
08-Sep-02	8778	60	608	1.77173	343.2266	95.34073
09-Sep-02	9588	59	676	1.754868	385.2177	107.0049
10-Sep-02	9187	60	641	1.76534	362.915	100.8097
11-Sep-02	9463	56	703	1.708482	411.2066	114.2241
12-Sep-02	9373	58	675	1.734814	389.2604	108.1279
13-Sep-02	9549	58	687	1.735858	395.8682	109.9634
14-Sep-02	9551	59	676	1.751671	385.7189	107.1441
15-Sep-02	9393	59	668	1.746897	382.3356	106.2043
16-Sep-02	9040	58	655	1.729613	378.7555	105.2099
17-Sep-02	9523	60	661	1.769401	373.7648	103.8236
18-Sep-02	8344	61	572	1.782156	320.9879	89.1633
19-Sep-02	9646	61	662	1.780872	371.8134	103.2815
20-Sep-02	9859	60	686	1.767775	387.9461	107.7628
21-Sep-02	8135	64	528	1.839527	287.2591	79.79419
22-Sep-02	9979	61	683	1.784328	382.5806	106.2724
23-Sep-02	9435	63	626	1.816768	344.398	95.66612

24-Sep-02	9756	60	675	1.773481	380.4337	105.676
25-Sep-02	9859	60	680	1.776211	382.7987	106.333
26-Sep-02	10045	60	698	1.769401	394.2484	109.5134
27-Sep-02	9969	60	690	1.772119	389.5617	108.2116
28-Sep-02	9987	61	687	1.77895	386.0915	107.2477
29-Sep-02	9902	60	692	1.762643	392.861	109.1281
30-Sep-02	9877	58	716	1.729613	413.8171	114.9492
01-Oct-02	8937	56	670	1.70055	393.8267	109.3963
02-Oct-02	3467			1.14	0	0
03-Oct-02	10001	54	769	1.679486	457.9459	127.2072
04-Oct-02	10078	56	745	1.711651	435.4738	120.965
05-Oct-02	10006	57	729	1.724442	422.9139	117.4761
06-Oct-02	9705	58	696	1.739173	400.121	111.1447
07-Oct-02	9329	58	673	1.733511	388.2711	107.8531
08-Oct-02	9695	57	711	1.71879	413.7763	114.9379
09-Oct-02	9563	58	693	1.729613	400.6413	111.2892
10-Oct-02	9637	60	672	1.76534	380.6813	105.7448
11-Oct-02	9376	59	662	1.753268	377.662	104.9061
12-Oct-02	9777	60	679	1.769401	383.7158	106.5877
13-Oct-02	9943	60	694	1.763991	393.603	109.3342
14-Oct-02	6704	64	436	1.83848	237.0976	65.86045
15-Oct-02	6558	58	468	1.742675	268.7943	74.66509
16-Oct-02	6528	58	472	1.73091	272.8988	75.80522
17-Oct-02	8061	58	577	1.74136	331.1328	91.98133
18-Oct-02	9917	59	706	1.745311	404.7148	112.4208
19-Oct-02	9523	61	654	1.780323	367.3872	102.052
20-Oct-02	10401	59	737	1.750366	420.9507	116.9308
21-Oct-02	10140	61	694	1.784177	388.845	108.0125
22-Oct-02	9727	60	677	1.767922	382.656	106.2933
23-Oct-02	9798	59	690	1.75618	392.8043	109.1123
24-Oct-02	10269	59	725	1.753268	413.6424	114.9007
25-Oct-02	10040	59	710	1.751816	405.3683	112.6023
26-Oct-02	10717	57	778	1.728317	449.9963	124.999
27-Oct-02	10177	59	720	1.751816	410.9204	114.1445
28-Oct-02	9148	59	647	1.751816	369.3641	102.6011
29-Oct-02	9545	59	673	1.755269	383.221	106.4503
30-Oct-02	9795	59	691	1.754723	393.6152	109.3376
31-Oct-02	9866	58	705	1.741719	405.0484	112.5134
01-Nov-02	8398	61	575	1.783468	322.4012	89.55588
02-Nov-02	10021	59	714	1.745311	408.9356	113.5932
03-Nov-02	9800	60	676	1.776211	380.4893	105.6915
04-Nov-02	9538	63	627	1.826113	343.4033	95.3898
05-Nov-02	9812	62	658	1.804266	364.8827	101.3563
06-Nov-02	9772	63	643	1.825391	352.1967	97.83241
07-Nov-02	9825	61	674	1.781697	378.2358	105.0655
08-Nov-02	8968	61	613	1.785834	343.0237	95.28437
09-Nov-02	9337	61	640	1.782523	358.9702	99.71394
10-Nov-02	9508	63	629	1.819633	345.5744	95.99288
11-Nov-02	9129	61	621	1.790824	346.494	96.24834
12-Nov-02	9696	58	703	1.729613	406.2428	112.8452
13-Nov-02	9524	60	663	1.766446	375.5508	104.3197
14-Nov-02	10096	60	701	1.769401	396.2442	110.0678
15-Nov-02	10047	62	670	1.810289	370.2471	102.8464

16-Nov-02	10064	64	652	1.841815	354.2428	98.40078
17-Nov-02	9810	65	631	1.851165	340.7557	94.65436
18-Nov-02	9968	62	665	1.810117	367.4482	102.069
19-Nov-02	8567	61	585	1.785834	327.6813	91.02257
20-Nov-02	1656			1.14	0	0
21-Nov-02	9485			1.14	0	0
22-Nov-02	9278	63	610	1.825391	334.3781	92.8828
23-Nov-02	10021	65	645	1.849384	348.9715	96.93653
24-Nov-02	9858	63	648	1.825916	355.0257	98.61824
25-Nov-02	9620	63	641	1.812012	353.6116	98.22545
26-Nov-02	9283	64	608	1.831185	331.7565	92.15459
27-Nov-02	9398	62	636	1.795562	354.11	98.3639
28-Nov-02	9307	61	631	1.793236	351.951	97.76417
29-Nov-02	9659	59	681	1.754868	388.0313	107.7865
30-Nov-02	9842	64	646	1.828283	353.2284	98.119
01-Dec-02	9758	54	753	1.676823	449.0216	124.7282
02-Dec-02	9913	57	719	1.728749	415.931	115.5364
03-Dec-02	9206	53	725	1.661021	436.4708	121.2419
04-Dec-02	9286	55	707	1.687121	419.2752	116.4653
05-Dec-02	9471	62	637	1.801168	353.8394	98.28871
06-Dec-02	10129	63	673	1.813911	371.296	103.1378
07-Dec-02	10191	62	689	1.796451	383.4974	106.5271
08-Dec-02	10001	58	723	1.732209	417.1809	115.8836
09-Dec-02	9838	60	679	1.774845	382.7964	106.3323
10-Dec-02	9997	62	676	1.795841	376.5368	104.5936
11-Dec-02	9738	63	648	1.812486	357.6914	99.35871
12-Dec-02	10175	63	678	1.811064	374.536	104.0378
13-Dec-02	10207	63	678	1.814949	373.548	103.7633
14-Dec-02	10137	63	674	1.813393	371.8665	103.2963
15-Dec-02	9986	62	672	1.800887	373.2433	103.6787
16-Dec-02	5996	62	404	1.799202	224.6911	62.41419
17-Dec-02	9430	63	627	1.813911	345.6476	96.01322
18-Dec-02	10056	62	679	1.797978	377.5347	104.8708
19-Dec-02	10191	63	675	1.818199	371.2001	103.1111
20-Dec-02	9570	61	656	1.782156	368.1286	102.2579
21-Dec-02	10341	63	689	1.811064	380.6561	105.7378
22-Dec-02	10138	63	667	1.825391	365.3714	101.4921
23-Dec-02	9774	63	647	1.817913	356.1561	98.93225
24-Dec-02	9083	63	600	1.8212	329.3658	91.49051
25-Dec-02	9601	63	637	1.816507	350.5717	97.38103
26-Dec-02	9589	64	625	1.835555	340.5602	94.60005
27-Dec-02	9189	61	628	1.785834	351.4547	97.6263
28-Dec-02	9287	62	627	1.797978	348.6551	96.84863
29-Dec-02	10005	60	698	1.764972	395.437	109.8436
30-Dec-02	9878	63	655	1.816196	360.8445	100.2346
31-Dec-02	10105	62	681	1.799508	378.4751	105.132
01-Jan-03	9023	62	611	1.794166	340.7079	94.64107
02-Jan-03	10047	64	651	1.842885	353.0894	98.08038
03-Jan-03	10245	64	663	1.844063	359.46	99.85001
04-Jan-03	10354	61	707	1.785834	396.0221	110.0061
05-Jan-03	10816	59	768	1.747956	439.4896	122.0805
06-Jan-03	10405	62	704	1.795562	392.0769	108.9103
07-Jan-03	9990	63	661	1.819633	363.0974	100.8604

08-Jan-03	10027	61	680	1.792772	379.4591	105.4053
09-Jan-03	10495	60	729	1.769401	411.8967	114.4157
10-Jan-03	11024	62	743	1.799508	412.9216	114.7005
11-Jan-03	10605	64	694	1.831185	379.0144	105.2818
12-Jan-03	11078	61	756	1.787343	422.7277	117.4244
13-Jan-03	10533	61	719	1.785834	402.8869	111.913
14-Jan-03	10387	62	702	1.796451	390.8783	108.5773
15-Jan-03	10380			1.14	0	0
16-Jan-03	8650	62	583	1.799202	324.135	90.03751
17-Jan-03	9884	62	664	1.802575	368.5147	102.3652
18-Jan-03	11161	61	761	1.787494	425.7895	118.2749
19-Jan-03	10703	61	729	1.789157	407.2824	113.134
20-Jan-03	10924	60	761	1.766151	430.9701	119.7139
21-Jan-03	9569	61	650	1.79138	362.8931	100.8036
22-Jan-03	3340			1.14	0	0
23-Jan-03	8344	62	559	1.805396	309.7597	86.04435
24-Jan-03	9558	64	627	1.829074	342.6402	95.17784
25-Jan-03	10086	63	663	1.825916	363.2254	100.8959
26-Jan-03	9907	61	682	1.77758	383.856	106.6267
27-Jan-03	9755	60	678	1.768046	383.6793	106.5776
28-Jan-03	10177	60	704	1.773481	396.853	110.2369
29-Jan-03	9794	63	649	1.817722	356.9928	99.16468
30-Jan-03	8015	58	573	1.74136	329.2175	91.44929
31-Jan-03	9993	62	669	1.807195	369.9836	102.7732
01-Feb-03	10472	58	753	1.736001	434.0369	120.5658
02-Feb-03	8876	66	562	1.868755	300.8674	83.57429
03-Feb-03	9262	64	600	1.842885	325.4979	90.4161
04-Feb-03	9344	65	602	1.848253	325.8838	90.52327
05-Feb-03	9748	63	650	1.811064	358.84	99.67779
06-Feb-03	6972	60	484	1.769401	273.6174	76.00482
07-Feb-03	10011	62	678	1.794927	377.6098	104.8916
08-Feb-03	9983	65	643	1.848791	347.9344	96.64844
09-Feb-03	9486	60	660	1.767775	373.2474	103.6798
10-Feb-03	9765	61	665	1.789157	371.5739	103.215
11-Feb-03	9161	62	617	1.80104	342.3188	95.08856
12-Feb-03	10181	62	682	1.805961	377.6481	104.9022
13-Feb-03	10547	61	724	1.781322	406.253	112.8481
14-Feb-03	9966	62	669	1.804113	370.6793	102.9665
15-Feb-03	10382	60	722	1.767594	408.645	113.5125
16-Feb-03	8814	61	604	1.782156	339.0622	94.18394
17-Feb-03	11159	60	778	1.765791	440.4788	122.3552
18-Feb-03	10140	61	690	1.789527	385.6463	107.124
19-Feb-03	9237	60	637	1.776833	358.284	99.52335
20-Feb-03	9521	63	627	1.824341	343.6913	95.46981
21-Feb-03	9388	65	605	1.848051	327.5142	90.97616
22-Feb-03	10361	62	699	1.798828	388.4695	107.9082
23-Feb-03	10433	61	716	1.781322	401.8576	111.6271
24-Feb-03	9953	61	682	1.782156	382.8531	106.3481
25-Feb-03	9015	62	610	1.794927	340.0307	94.45297
26-Feb-03	7886	61	536	1.790824	299.3078	83.14105
27-Feb-03	949			1.14	0	0
28-Feb-03	6897	58	499	1.73032	288.5905	80.16404
01-Mar-03	7709	61	529	1.781697	296.7733	82.43704

02-Mar-03	8716	61	591	1.793405	329.5101	91.53059
03-Mar-03	9326	62	624	1.806809	345.4736	95.96489
04-Mar-03	8528	61	581	1.788855	324.6799	90.18886
05-Mar-03	1413			1.14	0	0
06-Mar-03	9082	62	611	1.80104	339.3978	94.27716
07-Mar-03	9390	62	627	1.808934	346.7514	96.31985
08-Mar-03	9714	62	651	1.806338	360.1293	100.0359
09-Mar-03	10443	61	719	1.778493	404.0352	112.232
10-Mar-03	10469	59	738	1.754868	420.5995	116.8332
11-Mar-03	10463	63	689	1.824813	377.434	104.8428
12-Mar-03	5750	61	393	1.785834	219.9479	61.09665
13-Mar-03	9436	60	655	1.769401	370.3264	102.8685
14-Mar-03	9951	61	681	1.784177	381.5991	105.9998
15-Mar-03	9694	60	670	1.773481	378.007	105.002
16-Mar-03	9523	57	696	1.721869	404.277	112.2992
17-Mar-03	8946			1.14	0	0
18-Mar-03	9388	61	640	1.788207	357.7828	99.3841
19-Mar-03	9017	60	625	1.771031	352.9818	98.05049
20-Mar-03	9510	59	673	1.751816	383.9792	106.6609
21-Mar-03	9495	60	663	1.763991	375.8995	104.4165
22-Mar-03	9263	63	617	1.812283	340.3458	94.5405
23-Mar-03	7690	57	564	1.71879	328.2154	91.17096
24-Mar-03	9663	60	672	1.767368	380.4753	105.6876
25-Mar-03	9704	62	656	1.795841	365.5197	101.5333
26-Mar-03	9802			1.14	0	0
27-Mar-03	9176	62	619	1.797978	344.4759	95.68774
28-Mar-03	9509	62	637	1.805396	353.0189	98.06082
29-Mar-03	9744	60	674	1.773027	380.2472	105.6242
30-Mar-03	9956	60	687	1.775938	386.7117	107.4199
31-Mar-03	9989	61	679	1.79138	378.8213	105.2281
01-Apr-03	9740	58	697	1.74136	400.1086	111.1413
02-Apr-03	9573	58	689	1.736001	396.7525	110.209
03-Apr-03	10089	60	698	1.772664	393.9203	109.4223
04-Apr-03	10005	61	680	1.790369	380.0155	105.5599
05-Apr-03	10064	62	673	1.807659	372.3712	103.4364
06-Apr-03	8390	60	580	1.774299	326.7528	90.76467
07-Apr-03	10141	62	685	1.79752	380.9999	105.8333
08-Apr-03	10124	60	701	1.772119	395.6142	109.8928
09-Apr-03	9628	63	639	1.816196	351.7078	97.69662
10-Apr-03	9850	63	655	1.814482	360.7476	100.2077
11-Apr-03	10073	61	690	1.782824	387.1011	107.5281
12-Apr-03	9980	59	705	1.753268	401.9754	111.6598
13-Apr-03	10183	61	700	1.779225	393.5188	109.3108
14-Apr-03	10236	62	694	1.794166	386.545	107.3736
15-Apr-03	9425	60	660	1.761298	374.7348	104.093
16-Apr-03	2223			1.14	0	0
17-Apr-03	10115	60	698	1.776211	392.7493	109.097
18-Apr-03	9291	61	633	1.788603	353.8382	98.28838
19-Apr-03	9591	63	637	1.814949	351.0177	97.50493
20-Apr-03	9863	62	659	1.80936	363.9759	101.1044
21-Apr-03	9859	64	647	1.828283	353.8377	98.28825
22-Apr-03	10396	60	717	1.776833	403.2608	112.0169
23-Apr-03	9862	60	684	1.770883	386.1336	107.2593

24-Apr-03	10434	55	797	1.684837	473.0703	131.4084
25-Apr-03	10634	56	796	1.701553	467.7674	129.9354
26-Apr-03	10867	57	800	1.716106	465.9362	129.4267
27-Apr-03	10892	57	795	1.723271	461.2815	128.1337
28-Apr-03	10237	60	710	1.770883	400.8302	111.3417
29-Apr-03	10660	60	743	1.766151	420.5383	116.8162
30-Apr-03	9970	60	690	1.772367	389.4678	108.1855
01-May-03	10596	61	728	1.780323	408.7682	113.5467
02-May-03	10687	59	757	1.750366	432.5355	120.1488
03-May-03	10475	59	741	1.751494	423.1703	117.5473
04-May-03	10587	60	732	1.773853	412.6003	114.6112
05-May-03	10819	57	787	1.726084	455.9806	126.6613
06-May-03	10545	62	713	1.796451	396.8277	110.2299
07-May-03	10018	62	674	1.800887	374.4429	104.0119
08-May-03	10068	62	682	1.794166	380.1873	105.6076
09-May-03	10357	59	734	1.750366	419.157	116.4325
10-May-03	10334	60	716	1.771031	404.5318	112.3699
11-May-03	10518	59	741	1.755937	421.8285	117.1746
12-May-03	10552	61	720	1.787343	402.6742	111.8539
13-May-03	10104	61	686	1.792493	382.5201	106.2556
14-May-03	4526			1.14	0	0
15-May-03	9972			1.14	0	0
16-May-03	9719	61	660	1.79138	368.5845	102.3846
17-May-03	9484	64	622	1.82925	339.9111	94.41976
18-May-03	8506	57	617	1.728502	357.023	99.17305
19-May-03	10201	61	695	1.789157	388.1797	107.8277
20-May-03	9293	61	631	1.79138	352.4214	97.89483
21-May-03	9486	61	651	1.781322	365.3643	101.4901
22-May-03	9525	60	667	1.761298	378.7089	105.1969
23-May-03	9641	58	694	1.735858	399.6694	111.0193
24-May-03	9138	57	663	1.728906	383.3038	106.4733
25-May-03	9825	58	708	1.734577	408.1821	113.3839
26-May-03	9486	59	665	1.760565	377.6212	104.8948
27-May-03	8077	63	538	1.812283	296.7751	82.43752
28-May-03	9159	63	603	1.825391	330.1103	91.69732
29-May-03	9576	60	663	1.772664	373.8872	103.8576
30-May-03	10562	59	745	1.754723	424.4436	117.901
31-May-03	10599	60	737	1.768046	416.8761	115.7989
01-Jun-03	10564	58	753	1.744432	431.729	119.9247
02-Jun-03	10216	56	758	1.708482	443.9351	123.3153
03-Jun-03	10519	59	745	1.750608	425.5663	118.2129
04-Jun-03	9678	59	687	1.748919	392.6284	109.0634
05-Jun-03	10510	61	723	1.779225	406.1556	112.821
06-Jun-03	10466	61	715	1.785834	400.3076	111.1965
07-Jun-03	10564	62	713	1.79752	396.8964	110.249
08-Jun-03	9566	62	639	1.808225	353.6397	98.23326
09-Jun-03	9686	62	650	1.804266	360.2161	100.06
10-Jun-03	8792	63	583	1.816196	321.1749	89.21525
11-Jun-03	9003	61	620	1.778327	348.4214	96.78374
12-Jun-03	9511	59	676	1.747474	386.7456	107.4293
13-Jun-03	9822	58	701	1.743154	402.2838	111.7455
14-Jun-03	10313	59	725	1.757639	412.4778	114.5772
15-Jun-03	10001	61	681	1.789157	380.5656	105.7127

16-Jun-03	10461	61	718	1.781322	402.95	111.9305
17-Jun-03	9287	65	596	1.853246	321.6313	89.34202
18-Jun-03	8723	64	568	1.837017	309.1519	85.87553
19-Jun-03	9003	63	599	1.813911	330.0081	91.66891
20-Jun-03	9349	63	619	1.818069	340.5975	94.61042
21-Jun-03	9336	62	623	1.80936	344.534	95.70388
22-Jun-03	10132	59	716	1.753268	408.0968	113.3602
23-Jun-03	9931	60	693	1.76534	392.3012	108.9726
24-Jun-03	9628	62	649	1.799508	360.6182	100.1717
25-Jun-03	9527	62	637	1.807195	352.7442	97.98449
26-Jun-03	9869	64	645	1.833125	351.731	97.70305
27-Jun-03	9768	63	647	1.818069	355.8368	98.84356
28-Jun-03	9644	63	639	1.818069	351.3388	97.59412
29-Jun-03	9471	62	636	1.802575	353.0982	98.08282
30-Jun-03	10007	60	692	1.773853	389.9839	108.3289
01-Jul-03	10352	60	717	1.771439	404.9772	112.4937
02-Jul-03	9088	62	611	1.802575	338.8328	94.12024
03-Jul-03	10049	62	675	1.802575	374.6624	104.0729
04-Jul-03	9841	62	659	1.805653	365.2146	101.4485
05-Jul-03	9777	62	654	1.807659	361.7221	100.4784
06-Jul-03	9484	62	643	1.794166	358.1406	99.48349
07-Jul-03	9360	62	628	1.804266	348.085	96.69027
08-Jul-03	9412	61	645	1.782824	361.6865	100.4685
09-Jul-03	1783			1.14	0	0
10-Jul-03	10071	59	711	1.753268	405.64	112.6778
11-Jul-03	10073	61	693	1.779225	389.2599	108.1278
12-Jul-03	9648	60	674	1.7635	382.2478	106.1799
13-Jul-03	10054	59	716	1.745311	410.3152	113.9764
14-Jul-03	10386	59	738	1.746897	422.7317	117.4255
15-Jul-03	9844	56	731	1.70785	428.2187	118.9497
16-Jul-03	9067	57	658	1.728502	380.5741	105.715
17-Jul-03	9340	57	677	1.728749	391.8709	108.853
18-Jul-03	9121	58	661	1.729613	382.1274	106.1465
19-Jul-03	9742	60	672	1.775342	378.7749	105.2153
20-Jul-03	9553	63	628	1.825916	344.0448	95.568
21-Jul-03	9783	63	647	1.819633	355.5705	98.7696
22-Jul-03	9945	61	685	1.77758	385.313	107.0314
23-Jul-03	9599	61	656	1.785834	367.1666	101.9907
24-Jul-03	9480	61	648	1.784453	363.3749	100.9375
25-Jul-03	9788	61	672	1.780323	377.5995	104.8887
26-Jul-03	10386	60	716	1.776833	402.8481	111.9023
27-Jul-03	9831	60	683	1.769401	385.8523	107.1812
28-Jul-03	9607	60	663	1.775938	373.1903	103.664
29-Jul-03	9203	62	620	1.799508	344.696	95.74889
30-Jul-03	8881	62	594	1.808225	328.3099	91.19718
31-Jul-03	9321	62	622	1.810289	343.5039	95.41776
01-Aug-03	8462	64	551	1.837017	299.8785	83.29957
02-Aug-03	8946	64	585	1.831185	319.7241	88.81225
03-Aug-03	8982	62	600	1.809643	331.353	92.04251
04-Aug-03	9102	61	622	1.785834	348.1446	96.70684
05-Aug-03	9512	60	661	1.769401	373.3086	103.6968
06-Aug-03	8927	60	616	1.775938	346.773	96.32584
07-Aug-03	10092	59	714	1.751937	407.3847	113.1624

08-Aug-03	9347	63	622	1.813393	342.8833	95.24536
09-Aug-03	8828	62	593	1.802575	329.1316	91.42543
10-Aug-03	9740	63	640	1.826547	350.4371	97.34365
11-Aug-03	9869	62	658	1.810289	363.7202	101.0334
12-Aug-03	10019	62	675	1.800465	374.7275	104.091
13-Aug-03	4360	60	303	1.769401	171.1242	47.53451
14-Aug-03	9099	62	611	1.802575	339.2292	94.23032
15-Aug-03	10228	62	686	1.804113	380.4476	105.6799
16-Aug-03	9928	62	669	1.799202	372.0479	103.3467
17-Aug-03	10588	62	713	1.8007	395.8773	109.9659
18-Aug-03	10512	64	683	1.839527	371.2272	103.1187
19-Aug-03	11085	62	745	1.802575	413.2636	114.7954
20-Aug-03	10007	64	654	1.833513	356.4367	99.01019
21-Aug-03	9783	65	630	1.850274	340.2426	94.51183
22-Aug-03	10192	62	682	1.807659	377.0732	104.7426
23-Aug-03	10177	65	653	1.853111	352.5482	97.93004
24-Aug-03	9446	65	605	1.856363	325.7427	90.48407
25-Aug-03	10152	63	675	1.813393	372.3965	103.4435
26-Aug-03	9759	62	651	1.809643	360.0065	100.0018
27-Aug-03	10071	59	715	1.748919	408.568	113.4911
28-Aug-03	10414	59	732	1.757274	416.7637	115.7677
29-Aug-03	10384	60	721	1.769401	407.5569	113.2102
30-Aug-03	10844	61	735	1.793405	409.9814	113.8837
31-Aug-03	10226	62	690	1.798361	383.7033	106.5842
01-Sep-03	10364	61	713	1.778327	401.0716	111.4088
02-Sep-03	10274	60	710	1.773853	400.3983	111.2217
03-Sep-03	10950	64	717	1.830023	392.0133	108.8926
04-Sep-03	9563	62	643	1.802575	356.5417	99.03937
05-Sep-03	10825	62	726	1.804113	402.652	111.8478
06-Sep-03	10963	62	740	1.797978	411.5646	114.3235
07-Sep-03	9840	62	659	1.805961	364.9821	101.3839
08-Sep-03	10420	62	702	1.799508	390.2799	108.4111
09-Sep-03	10401	61	710	1.785834	397.8305	110.5085
10-Sep-03	10254	62	689	1.802575	382.2929	106.1925
11-Sep-03	10989	62	740	1.801168	410.5693	114.047
12-Sep-03	10501	62	710	1.795841	395.5203	109.8668
13-Sep-03	10339	61	707	1.784177	396.4775	110.1326
14-Sep-03	10287	61	699	1.79138	390.1301	108.3695
15-Sep-03	10355			1.14	0	0
16-Sep-03	10217			1.14	0	0
17-Sep-03	1078			1.14	0	0
18-Sep-03	10123	62	683	1.797978	380.0425	105.5674
19-Sep-03	10280	62	688	1.807195	380.6006	105.7224
20-Sep-03	10034	63	664	1.819633	364.6937	101.3038
21-Sep-03	9739	62	654	1.802575	363.0817	100.856
22-Sep-03	10014	62	669	1.808741	369.8853	102.7459
23-Sep-03	9736	62	654	1.802575	362.9724	100.8257
24-Sep-03	10298	62	689	1.807195	381.2769	105.9103
25-Sep-03	10537	63	702	1.811839	387.43	107.6194
26-Sep-03	10326	60	712	1.776211	400.9492	111.3748
27-Sep-03	10869	61	743	1.784453	416.6029	115.723
28-Sep-03	11066	60	773	1.763991	438.0732	121.687
29-Sep-03	11210	61	763	1.788855	426.7721	118.5478

30-Sep-03	11107	62	753	1.794166	419.4328	116.5091
01-Oct-03	10615	63	700	1.822507	384.2076	106.7243
02-Oct-03	10446	62	699	1.807195	386.7531	107.4314
03-Oct-03	11074	62	740	1.808225	409.3756	113.7154
04-Oct-03	11453	63	757	1.819633	416.2783	115.6328
05-Oct-03	10552	62	706	1.807659	390.4098	108.4472
06-Oct-03	10688	61	729	1.787343	407.856	113.2933
07-Oct-03	11041	61	752	1.788603	420.5082	116.8078
08-Oct-03	10130	62	679	1.805653	375.9071	104.4186
09-Oct-03	10786	62	729	1.796451	405.8847	112.7458
10-Oct-03	11522	64	750	1.837017	408.3403	113.4279
11-Oct-03	10552	63	695	1.824341	380.8846	105.8013
12-Oct-03	10908	63	723	1.816768	398.1587	110.5996
13-Oct-03	11336	62	758	1.808225	419.0549	116.4042
14-Oct-03	10017	61	679	1.793236	378.802	105.2228
15-Oct-03	10603	62	713	1.802575	395.3064	109.8073
16-Oct-03	11516	62	775	1.80104	430.3428	119.5397
17-Oct-03	11020	63	727	1.822507	398.8566	110.7935
18-Oct-03	10110	62	681	1.799508	378.675	105.1875
19-Oct-03	10324	62	695	1.80104	385.8101	107.1695
20-Oct-03	10237	62	688	1.802575	381.6654	106.0182
21-Oct-03	8203	64	531	1.842885	288.2828	80.07854
22-Oct-03	3534			1.14	0	0
23-Oct-03	10014	59	703	1.758613	399.8662	111.0739
24-Oct-03	10629	64	690	1.840533	374.7956	104.1099
25-Oct-03	10659	64	699	1.829733	381.7557	106.0432
26-Oct-03	10705	63	714	1.811064	394.0727	109.4646
27-Oct-03	10763	62	720	1.807195	398.5006	110.6946
28-Oct-03	11440	61	781	1.785834	437.5703	121.5473
29-Oct-03	10513	61	715	1.790824	399.0426	110.8452
30-Oct-03	10923	61	748	1.782824	419.7323	116.5923
31-Oct-03	11365	58	820	1.733811	472.7697	131.3249
01-Nov-03	10432	60	724	1.769401	409.4165	113.7268
02-Nov-03	10329	62	690	1.808934	381.411	105.9475
03-Nov-03	11381	61	772	1.792772	430.6998	119.6388
04-Nov-03	11190	61	768	1.781697	430.7803	119.6612
05-Nov-03	10227	61	698	1.787217	390.3261	108.4239
06-Nov-03	9564	63	633	1.818199	348.358	96.76612
07-Nov-03	10844	60	749	1.775342	421.6359	117.1211
08-Nov-03	10906	60	756	1.770759	427.111	118.6419
09-Nov-03	11183	60	783	1.761298	444.6318	123.5088
10-Nov-03	10484	60	728	1.769401	411.4669	114.2963
11-Nov-03	10447	61	715	1.784328	400.506	111.2517
12-Nov-03	10706	63	711	1.815338	391.6054	108.7793
13-Nov-03	10090	60	697	1.774845	392.6128	109.0591
14-Nov-03	11238	59	789	1.758613	448.7576	124.6549
15-Nov-03	9788	60	680	1.769401	384.1343	106.704
16-Nov-03	9108	64	590	1.842885	320.0904	88.914
17-Nov-03	9300			1.14	0	0
18-Nov-03	10444	64	679	1.838969	369.0985	102.5274
19-Nov-03	9861	64	641	1.838969	348.5097	96.80824
20-Nov-03	11130	66	705	1.869489	376.8748	104.6874
21-Nov-03	10767	65	687	1.859861	369.4578	102.6272

22-Nov-03	10993	65	701	1.860118	377.081	104.7447
23-Nov-03	10922	66	690	1.871281	368.9379	102.4828
24-Nov-03	10162	65	655	1.848051	354.5169	98.47692
25-Nov-03	9492	63	629	1.816768	346.4591	96.23865
26-Nov-03	3887	62	260	1.806809	143.9821	39.99503
27-Nov-03	10766	66	684	1.86523	366.7125	101.8646
28-Nov-03	10677	66	679	1.863724	364.431	101.2308
29-Nov-03	10623	66	675	1.864545	362.1636	100.601
30-Nov-03	10302	64	672	1.835555	365.8747	101.6319
01-Dec-03	10697	62	717	1.805961	396.7836	110.2177
02-Dec-03	10611	64	689	1.840213	374.3346	103.9818
03-Dec-03	10310	65	662	1.853246	357.0744	99.18733
04-Dec-03	10527	65	676	1.853246	364.603	101.2786
05-Dec-03	10511	63	698	1.814949	384.6749	106.8541
06-Dec-03	10682	63	707	1.818069	389.1377	108.0938
07-Dec-03	10534	62	710	1.799202	394.7312	109.6476
08-Dec-03	10546	63	693	1.827318	379.0368	105.288
09-Dec-03	10602	64	686	1.844063	371.983	103.3286
10-Dec-03	10605	66	665	1.880431	353.7958	98.27661
11-Dec-03	10614	66	667	1.877788	355.3597	98.71103
12-Dec-03	10661	65	684	1.852948	369.4004	102.6112
13-Dec-03	10671	65	681	1.860718	365.7618	101.6005
14-Dec-03	10600	64	686	1.843421	372.2504	103.4029
15-Dec-03	10721	64	694	1.842885	376.7972	104.6659
16-Dec-03	8956			1.14	0	0
17-Dec-03	4264	63	283	1.813911	156.2872	43.4131
18-Dec-03	9712	63	643	1.818199	353.7466	98.26293
19-Dec-03	10692	65	686	1.853111	370.3879	102.8855
20-Dec-03	10342	64	675	1.834096	368.0737	102.2427
21-Dec-03	10669	63	701	1.826836	383.7082	106.5856
22-Dec-03	10657	64	697	1.832243	380.2769	105.6325
23-Dec-03	10576	64	689	1.837017	374.8196	104.1166
24-Dec-03	10659	62	719	1.798361	399.9196	111.0888
25-Dec-03	10664	64	696	1.833513	379.843	105.5119
26-Dec-03	10619	63	707	1.811839	390.4386	108.4552
27-Dec-03	10576	62	706	1.809643	390.1386	108.3718
28-Dec-03	10563	63	698	1.821356	382.9759	106.3822
29-Dec-03	10714	62	721	1.800887	400.4724	111.2423
30-Dec-03	10782	64	698	1.843421	378.6263	105.174
31-Dec-03	10635	63	705	1.816768	388.1851	107.8292
01-Jan-04	10788	65	692	1.854736	372.8463	103.5684
02-Jan-04	10862	66	690	1.86523	369.9736	102.7705
03-Jan-04	10942	65	703	1.851489	379.9046	105.529
04-Jan-04	10864	66	690	1.86619	369.5647	102.6569
05-Jan-04	9892	62	667	1.799508	370.4939	102.915
06-Jan-04	10902	62	729	1.807195	403.6423	112.1229
07-Jan-04	10630	64	698	1.828283	381.518	105.9772
08-Jan-04	10839	64	705	1.838613	383.2637	106.4621
09-Jan-04	10807	63	716	1.818199	393.637	109.3436
10-Jan-04	10167	64	660	1.840213	358.6667	99.62963
11-Jan-04	9801	64	643	1.82925	351.256	97.57112
12-Jan-04	10826	61	744	1.780323	417.6369	116.0102
13-Jan-04	10687	61	729	1.787494	407.7009	113.2503

14-Jan-04	10666	61	726	1.788855	406.0803	112.8001
15-Jan-04	10566	62	715	1.795096	398.4083	110.669
16-Jan-04	10066	63	667	1.818069	366.7081	101.8634
17-Jan-04	10350	62	698	1.798361	388.3331	107.8703
18-Jan-04	10871	61	743	1.785834	415.808	115.5022
19-Jan-04	10431	62	707	1.794166	393.9097	109.4193
20-Jan-04	9599	64	629	1.829526	343.8738	95.52051
21-Jan-04	4354			1.14	0	0
22-Jan-04	10366			1.14	0	0
23-Jan-04	10346	62	701	1.794166	390.6923	108.5256
24-Jan-04	9595	65	616	1.852502	332.6668	92.40744
25-Jan-04	10684	62	722	1.79696	401.7124	111.5868
26-Jan-04	10859	62	727	1.807195	402.0343	111.6762
27-Jan-04	10948	62	735	1.804266	407.1379	113.0939
28-Jan-04	10639	64	698	1.829074	381.3926	105.9424
29-Jan-04	10723	63	710	1.817722	390.8299	108.5639
30-Jan-04	10786	61	737	1.785834	412.5345	114.5929
31-Jan-04	10856	61	739	1.789157	413.0966	114.749
01-Feb-04	10743	63	713	1.815814	392.6676	109.0743
02-Feb-04	10870	63	723	1.812771	399.1086	110.8635
03-Feb-04	10808	62	730	1.79696	406.3893	112.8859
04-Feb-04	10773	61	735	1.787494	410.9824	114.1618
05-Feb-04	10511	61	720	1.783468	403.525	112.0903
06-Feb-04	9597	63	638	1.814482	351.4874	97.63538
07-Feb-04	10820	63	714	1.821356	392.2666	108.9629
08-Feb-04	10378	64	678	1.83264	370.1388	102.8163
09-Feb-04	10747	64	697	1.840925	378.7502	105.2084
10-Feb-04	10041	63	659	1.827494	360.7802	100.2167
11-Feb-04	10295	65	664	1.846818	359.8013	99.94479
12-Feb-04	10468	62	704	1.801168	391.1078	108.641
13-Feb-04	10804	62	729	1.798361	405.3607	112.6002
14-Feb-04	9752	61	666	1.785834	373.0198	103.6166
15-Feb-04	9150	64	596	1.837017	324.2805	90.07793
16-Feb-04	8528	63	568	1.812012	313.4795	87.07765
17-Feb-04	10447	64	683	1.832243	372.7843	103.5512
18-Feb-04	10562	65	674	1.860718	362.0004	100.5557
19-Feb-04	10850	65	699	1.848791	378.1367	105.038
20-Feb-04	10403	66	661	1.864728	354.5776	98.49379
21-Feb-04	10244	65	658	1.853246	354.7885	98.55235
22-Feb-04	10613	65	685	1.847311	370.6413	102.9559
23-Feb-04	10794	65	692	1.854736	373.0536	103.626
24-Feb-04	10020	65	644	1.852183	347.546	96.54055
25-Feb-04	2147			1.14	0	0
26-Feb-04	9295	62	621	1.808225	343.597	95.44361
27-Feb-04	10094	63	673	1.811064	371.5826	103.2174
28-Feb-04	9858	64	642	1.837017	349.3772	97.04922
29-Feb-04	9945	62	664	1.810117	366.5989	101.833
01-Mar-04	10249	61	697	1.790369	389.2644	108.129
02-Mar-04	10181	60	705	1.772367	397.7201	110.4778
03-Mar-04	9618	59	681	1.750608	389.0954	108.082
04-Mar-04	9980	63	662	1.816768	364.2877	101.191
05-Mar-04	10211	65	655	1.854736	352.9034	98.02872
06-Mar-04	10939	65	702	1.852948	379.0077	105.2799

07-Mar-04	10715	65	688	1.853111	371.1676	103.1021
08-Mar-04	10868	65	702	1.845834	380.3636	105.6566
09-Mar-04	10916	64	711	1.837017	386.8611	107.4614
10-Mar-04	9783	62	654	1.808225	361.6316	100.4532
11-Mar-04	10828	63	713	1.824341	390.8653	108.5737
12-Mar-04	11196	62	751	1.803984	416.5146	115.6985
13-Mar-04	11364	60	795	1.762643	450.8633	125.2398
14-Mar-04	10723	57	780	1.726084	451.9745	125.5485
15-Mar-04	11703	64	766	1.831185	418.2498	116.1805
16-Mar-04	11559	60	801	1.771031	452.4847	125.6902
17-Mar-04	10470	65	671	1.854736	361.8596	100.5165
18-Mar-04	11729	64	768	1.831185	419.2019	116.445
19-Mar-04	11424	65	735	1.851165	396.8241	110.2289
20-Mar-04	11658	65	747	1.854736	402.9312	111.9253
21-Mar-04	11554	65	745	1.848253	402.9626	111.934
22-Mar-04	11648	65	750	1.850274	405.0894	112.5248
23-Mar-04	11624	64	752	1.844358	407.6617	113.2394
24-Mar-04	11063	64	720	1.837017	392.0894	108.9137
25-Mar-04	11765	63	773	1.826547	423.2952	117.582
26-Mar-04	10858	64	707	1.837017	384.8043	106.8901
27-Mar-04	10153	64	660	1.83848	359.0677	99.74102
28-Mar-04	10846	59	765	1.754868	435.7379	121.0383
29-Mar-04	10730	60	743	1.772664	418.9658	116.3794
30-Mar-04	10906	58	778	1.743992	446.0202	123.8945
31-Mar-04	10714	63	713	1.813393	393.0124	109.1701
01-Apr-04	10540	60	727	1.775938	409.4204	113.7279
02-Apr-04	10616	61	726	1.784328	406.9839	113.0511
03-Apr-04	11106	59	778	1.760565	442.107	122.8075
04-Apr-04	9475	61	650	1.781697	364.7399	101.3166
05-Apr-04	11010	65	702	1.860718	377.3562	104.8212
06-Apr-04	10594	64	686	1.842885	372.3083	103.419
07-Apr-04	3578	61	246	1.780323	138.0165	38.3379
08-Apr-04	10460	64	680	1.838613	369.8672	102.7409
09-Apr-04	9890	66	624	1.8728	333.3932	92.60922
10-Apr-04	9537	65	615	1.847607	332.9456	92.48488
11-Apr-04	9857	63	647	1.827318	354.2715	98.40876
12-Apr-04	10624	63	707	1.813393	389.7412	108.2614
13-Apr-04	10862	63	718	1.819633	394.7996	109.6666
14-Apr-04	10562	64	690	1.83264	376.6866	104.6352
15-Apr-04	10577	63	704	1.813393	387.9919	107.7755
16-Apr-04	10181	63	670	1.825391	366.9282	101.9245
17-Apr-04	2914	63	193	1.819633	105.9058	29.41827
18-Apr-04	0			1.14	0	0
19-Apr-04	0			1.14	0	0
20-Apr-04	0			1.14	0	0
21-Apr-04	0			1.14	0	0
22-Apr-04	0			1.14	0	0
23-Apr-04	6299	65	405	1.852183	218.494	60.69278
24-Apr-04	9721	65	621	1.859628	333.6818	92.68938
25-Apr-04	10498	62	701	1.808741	387.7788	107.7163
26-Apr-04	10747	58	767	1.743729	439.738	122.1495
27-Apr-04	10110	62	684	1.794927	381.3447	105.9291
28-Apr-04	9573	63	635	1.816196	349.7025	97.1396

29-Apr-04	10280	64	672	1.832243	366.845	101.9014
30-Apr-04	9733	65	628	1.847311	339.9194	94.42206
01-May-04	10619	64	696	1.829074	380.6597	105.7388
02-May-04	11343	64	744	1.829074	406.6324	112.9534
03-May-04	10761	63	708	1.825391	387.8579	107.7383
04-May-04	10209	64	660	1.84485	357.7948	99.38746
05-May-04	9782	63	652	1.811064	360.0749	100.0208
06-May-04	9693	65	625	1.848253	338.0866	93.91295
07-May-04	10219	65	656	1.853111	353.997	98.33249
08-May-04	10187	63	679	1.811064	375.0038	104.1677
09-May-04	10319	65	667	1.845834	361.1244	100.3123
10-May-04	10445	64	677	1.841815	367.626	102.1183
11-May-04	10429	63	692	1.816196	380.9874	105.8298
12-May-04	9388	63	621	1.819633	341.2142	94.78172
13-May-04	9801	63	646	1.822769	354.6147	98.50409
14-May-04	9383	62	626	1.809643	346.1463	96.15175
15-May-04	9772	63	645	1.822507	353.6945	98.24847
16-May-04	10346	67	640	1.898008	337.165	93.65694
17-May-04	10136	67	627	1.89744	330.5741	91.82614
18-May-04	9936	65	636	1.856526	342.557	95.15472
19-May-04	9930	66	625	1.876862	332.9013	92.47258
20-May-04	10443	68	645	1.900566	339.1857	94.21824
21-May-04	10557	64	688	1.835555	374.9178	104.1438
22-May-04	9947	65	638	1.853246	344.4974	95.69374
23-May-04	10439	64	676	1.843421	366.5904	101.8307
24-May-04	11159	64	724	1.840533	393.4939	109.3039
25-May-04	10598	66	674	1.864545	361.3277	100.3688
26-May-04	10148	65	651	1.853246	351.4473	97.62426
27-May-04	10552	64	684	1.841415	371.6124	103.2257
28-May-04	10667	63	702	1.825391	384.4627	106.7952
29-May-04	9453	63	623	1.823083	341.8331	94.95363
30-May-04	10419	65	667	1.856363	359.278	99.79943
31-May-04	11253	65	722	1.852948	389.9133	108.3092
01-Jun-04	9658	64	625	1.844063	338.8435	94.12319
02-Jun-04	10489	64	683	1.837017	371.715	103.2542
03-Jun-04	10877	63	724	1.812012	399.8169	111.0602
04-Jun-04	11769	64	762	1.842885	413.6132	114.8926
05-Jun-04	10917	65	705	1.845834	382.0755	106.1321
06-Jun-04	11511	65	737	1.856363	396.9299	110.2583
07-Jun-04	11698	65	748	1.857994	402.4566	111.7935
08-Jun-04	11698	66	735	1.877788	391.6592	108.7942
09-Jun-04	10986	66	693	1.874321	369.5681	102.6578
10-Jun-04	11296	64	731	1.844063	396.3148	110.0874
11-Jun-04	11735	65	758	1.845834	410.6928	114.0813
12-Jun-04	11026	64	713	1.844358	386.6951	107.4153
13-Jun-04	10671	65	686	1.851759	370.365	102.8792
14-Jun-04	10156	63	669	1.824341	366.6047	101.8346
15-Jun-04	9603	64	625	1.837017	340.3158	94.53216
16-Jun-04	0			1.14	0	0
17-Jun-04	7780	65	503	1.845834	272.2871	75.6353
18-Jun-04	10815	66	683	1.8728	364.5835	101.2732
19-Jun-04	11041	64	718	1.838613	390.3841	108.44
20-Jun-04	10807	66	685	1.867838	366.7709	101.8808

21-Jun-04	9916	66	628	1.868755	336.107	93.36304
22-Jun-04	9991	63	658	1.824341	360.6368	100.1769
23-Jun-04	10472	63	688	1.826836	376.6181	104.6161
24-Jun-04	10087	64	655	1.840213	355.8694	98.85262
25-Jun-04	10316	63	680	1.823083	373.0432	103.6231
26-Jun-04	10587	63	697	1.823948	382.3784	106.2162
27-Jun-04	10708	64	695	1.840533	377.6053	104.8904
28-Jun-04	10599	64	691	1.835423	376.497	104.5825
29-Jun-04	10657	64	695	1.835423	378.5687	105.158
30-Jun-04	10663	65	686	1.849869	371.0392	103.0665
01-Jul-04	10406	65	670	1.849384	362.3674	100.6576
02-Jul-04	10640	64	690	1.841415	374.7189	104.0886
03-Jul-04	10429	64	684	1.828283	374.3037	103.9732
04-Jul-04	10519	64	689	1.830657	376.2368	104.5102
05-Jul-04	10536	64	689	1.832243	375.9886	104.4413
06-Jul-04	10446	65	673	1.848253	364.3445	101.2068
07-Jul-04	10061	65	645	1.854736	347.7363	96.5934
08-Jul-04	10504	64	687	1.831185	375.3908	104.2752
09-Jul-04	10662	66	678	1.863724	363.9141	101.0873
10-Jul-04	10623	68	654	1.904845	343.0913	95.30314
11-Jul-04	10532	66	662	1.877371	352.8421	98.01171
12-Jul-04	10296	65	657	1.859628	353.4111	98.16974
13-Jul-04	9842	65	634	1.849384	342.7167	95.1991
14-Jul-04	10433	64	678	1.838773	368.8089	102.4469
15-Jul-04	10733	64	696	1.841415	377.9929	104.998
16-Jul-04	9970	64	649	1.837017	353.3327	98.14798
17-Jul-04	10791	63	710	1.825391	388.9125	108.0313
18-Jul-04	10837	63	719	1.816507	395.709	109.9192
19-Jul-04	10355	64	670	1.844063	363.3233	100.9231
20-Jul-04	10381	66	656	1.871281	350.6776	97.41044
21-Jul-04	10536	66	667	1.869489	356.7801	99.10557
22-Jul-04	10486	66	662	1.8728	353.4937	98.19269
23-Jul-04	10413	67	647	1.892771	341.6919	94.91441
24-Jul-04	10083	67	623	1.899712	327.8402	91.06672
25-Jul-04	8820	68	540	1.910005	282.9462	78.59617
26-Jul-04	10004	66	632	1.8728	337.2372	93.67699
27-Jul-04	9923	67	615	1.894947	324.6893	90.19148
28-Jul-04	10021	67	622	1.894325	328.1539	91.15386
29-Jul-04	10091	65	644	1.860718	345.867	96.07417
30-Jul-04	9727	65	627	1.848253	339.244	94.23444
31-Jul-04	10595	63	699	1.822507	383.4601	106.5167
01-Aug-04	10703	66	680	1.86523	364.5657	101.2683
02-Aug-04	10546	64	683	1.842297	370.9577	103.0438
03-Aug-04	9764	62	653	1.808225	360.9348	100.2597
04-Aug-04	3863	61	266	1.77758	149.651	41.56971
05-Aug-04	10559	62	706	1.807195	390.9246	108.5902
06-Aug-04	10592	63	701	1.819633	384.9916	106.9421
07-Aug-04	10146	62	680	1.805961	376.3529	104.5425
08-Aug-04	10285	63	681	1.818199	374.599	104.0553
09-Aug-04	10257	64	664	1.844063	359.8879	99.96885
10-Aug-04	9849	64	645	1.829733	352.7486	97.98573
11-Aug-04	10109	64	656	1.840213	356.6227	99.06187
12-Aug-04	9855	65	628	1.861919	337.2131	93.67031

13-Aug-04	9939	63	663	1.811064	365.8621	101.6284
14-Aug-04	10524	64	683	1.840925	370.903	103.0286
15-Aug-04	9992	65	641	1.853111	346.1299	96.14719
16-Aug-04	10246	61	700	1.785834	391.9073	108.8631
17-Aug-04	10024	65	647	1.847607	349.9207	97.2002
18-Aug-04	10094	65	652	1.846639	352.875	98.02083
19-Aug-04	10269	64	671	1.833513	365.7753	101.6043
20-Aug-04	10815	65	690	1.860718	370.6711	102.9642
21-Aug-04	10837	65	696	1.852502	375.7095	104.3637
22-Aug-04	10866	65	699	1.851165	377.4247	104.8402
23-Aug-04	10771	65	689	1.856526	371.3381	103.1495
24-Aug-04	10735	64	704	1.829074	384.8465	106.9018
25-Aug-04	10447	64	684	1.831185	373.3763	103.7157
26-Aug-04	9346	63	615	1.825391	336.8282	93.5634
27-Aug-04	10517	62	704	1.807195	389.3955	108.1654
28-Aug-04	10643	62	714	1.804113	395.8848	109.968
29-Aug-04	10361	62	698	1.799508	388.0964	107.8046
30-Aug-04	10760	63	707	1.827318	386.7267	107.4241
31-Aug-04	10590	63	705	1.812771	388.8328	108.0091
01-Sep-04	7675			1.14	0	0
02-Sep-04	316			1.14	0	0
03-Sep-04	7388	61	501	1.792971	279.4951	77.63752
04-Sep-04	10249	63	681	1.813911	375.679	104.3553
05-Sep-04	10718	63	711	1.815814	391.7543	108.8206
06-Sep-04	10729	63	710	1.819633	389.9664	108.324
07-Sep-04	10502	62	707	1.8007	392.6355	109.0654
08-Sep-04	9367	63	621	1.817483	341.548	94.87443
09-Sep-04	10380	62	693	1.810289	382.5403	106.2612
10-Sep-04	10160	61	696	1.782824	390.417	108.4492
11-Sep-04	9556	60	669	1.761298	379.9575	105.5438
12-Sep-04	9801	64	640	1.834513	348.6092	96.83588
13-Sep-04	9206	64	604	1.828283	330.3868	91.7741
14-Sep-04	8923	64	578	1.842297	313.8375	87.17709
15-Sep-04	9636	63	638	1.818069	351.0514	97.51429
16-Sep-04	9326	64	605	1.841815	328.2646	91.1846
17-Sep-04	10484	64	688	1.828283	376.2832	104.5231
18-Sep-04	10703	63	707	1.821356	388.0426	107.7896
19-Sep-04	9863	64	641	1.83848	348.8076	96.891
20-Sep-04	10129	66	640	1.870978	342.3116	95.08656
21-Sep-04	10500	64	679	1.845029	367.8898	102.1916
22-Sep-04	9688	63	641	1.819633	352.1161	97.81003
23-Sep-04	9841	65	636	1.845834	344.4217	95.67269
24-Sep-04	9796	64	635	1.841815	344.7888	95.77466
25-Sep-04	9895	64	641	1.842885	347.7394	96.59428
26-Sep-04	8993	64	586	1.835263	319.5345	88.75957
27-Sep-04	9295	63	617	1.815814	339.7453	94.3737
28-Sep-04	10195	62	685	1.802575	380.0767	105.5769
29-Sep-04	10592	61	726	1.782824	407.0234	113.0621
30-Sep-04	10920	61	741	1.791886	413.809	114.9469
01-Oct-04	11069	61	762	1.77758	428.8547	119.1263
02-Oct-04	10726	62	716	1.810117	395.3853	109.8293
03-Oct-04	10879	63	717	1.823083	393.4198	109.2833
04-Oct-04	9942	64	651	1.831185	355.317	98.69917

05-Oct-04	9225	63	608	1.823467	333.4322	92.62007
06-Oct-04	10075	62	673	1.80936	371.8308	103.2863
07-Oct-04	10379	63	687	1.818069	378.1026	105.0285
08-Oct-04	10483	62	700	1.80936	386.8784	107.4662
09-Oct-04	10767	63	714	1.816507	393.1355	109.2043
10-Oct-04	10878	63	716	1.824341	392.6575	109.0715
11-Oct-04	10868	64	707	1.838613	384.2911	106.7475
12-Oct-04	10935	63	727	1.814482	400.4682	111.2412
13-Oct-04	10830	65	692	1.85872	372.2158	103.3933
14-Oct-04	10892	66	689	1.871143	368.0037	102.2232
15-Oct-04	10409	65	669	1.852502	360.8651	100.2403
16-Oct-04	10187	64	660	1.842297	358.3254	99.53483
17-Oct-04	8751	65	563	1.850769	304.129	84.48026
18-Oct-04	10559	62	712	1.799508	395.4898	109.8583
19-Oct-04	10895	63	716	1.826836	391.8494	108.8471
20-Oct-04	10665	64	695	1.835423	378.8413	105.2337
21-Oct-04	10800	64	699	1.843421	379.2529	105.348
22-Oct-04	11084	62	744	1.804266	412.2017	114.5005
23-Oct-04	11421	63	756	1.818069	416.0619	115.5727
24-Oct-04	11283	63	749	1.815338	412.7223	114.6451
25-Oct-04	11107	61	763	1.780323	428.496	119.0267
26-Oct-04	10268	63	679	1.819633	373.2004	103.6668
27-Oct-04	3326			1.14	0	0
28-Oct-04	11413	66	724	1.867344	387.616	107.6711
29-Oct-04	11274	64	733	1.838613	398.627	110.7297
30-Oct-04	11017	63	729	1.819633	400.444	111.2345
31-Oct-04	9893	64	642	1.840213	349.0035	96.94541
01-Nov-04	10048	64	654	1.837017	356.0952	98.91534
02-Nov-04	10244	63	673	1.826547	368.5729	102.3814
03-Nov-04	10077	65	650	1.846818	352.1947	97.83187
04-Nov-04	10272	67	635	1.898008	334.7552	92.98757
05-Nov-04	10050	67	629	1.882802	334.2288	92.84132
06-Nov-04	10047	64	659	1.829526	359.9325	99.98125
07-Nov-04	10023	63	667	1.812283	368.2958	102.3044
08-Nov-04	10087	63	669	1.816507	368.3141	102.3095
09-Nov-04	10502	65	670	1.859628	360.503	100.1397
10-Nov-04	10211	66	648	1.865985	347.4565	96.5157
11-Nov-04	10349	65	662	1.857994	356.0402	98.90004
12-Nov-04	10129	62	681	1.802575	377.6223	104.8951
13-Nov-04	10808	62	729	1.799202	405.022	112.5061
14-Nov-04	10575	62	709	1.805653	392.4554	109.0154
15-Nov-04	10844	62	727	1.805653	402.4226	111.7841
16-Nov-04	10587	63	704	1.813911	388.0836	107.801
17-Nov-04	10749	62	718	1.808741	397.0596	110.2943
18-Nov-04	10664	63	701	1.826547	383.698	106.5828
19-Nov-04	9847	64	644	1.832016	351.4851	97.63474
20-Nov-04	9996	63	664	1.814482	366.1001	101.6945
21-Nov-04	10807	63	718	1.814482	395.8028	109.9452
22-Nov-04	10358	64	677	1.832016	369.7302	102.7028
23-Nov-04	10665	64	696	1.834825	379.1569	105.3214
24-Nov-04	10574	63	699	1.819633	384.346	106.7628
25-Nov-04	9945	64	651	1.831767	355.1341	98.64835
26-Nov-04	11015	65	706	1.854736	380.7039	105.7511

27-Nov-04	11476	64	751	1.831185	410.1501	113.9306
28-Nov-04	11165	64	723	1.843421	392.0986	108.9163
29-Nov-04	10252	64	669	1.834096	364.8488	101.3469
30-Nov-04	10555	63	694	1.826547	379.7705	105.4918
01-Dec-04	10298	65	665	1.845834	360.4032	100.112
02-Dec-04	9897	65	635	1.852948	342.9224	95.25622
03-Dec-04	10813	64	704	1.837017	383.2133	106.4481
04-Dec-04	10010	64	649	1.841815	352.3282	97.86895
05-Dec-04	9650	61	654	1.793236	364.91	101.3639
06-Dec-04	10002	65	645	1.847311	349.3037	97.02882
07-Dec-04	9693	62	647	1.80936	357.7277	99.36879
08-Dec-04	3729	65	241	1.845834	130.5114	36.25317
09-Dec-04	9784	65	629	1.851165	339.8384	94.39955
10-Dec-04	10085	64	662	1.828283	361.9352	100.5376
11-Dec-04	9057	63	599	1.819633	329.1824	91.43956
12-Dec-04	7739	65	493	1.862903	264.4334	73.45372
13-Dec-04	8161	64	530	1.839527	288.1943	80.05398
14-Dec-04	9198	65	592	1.849638	320.1893	88.94147
15-Dec-04	8991	63	592	1.824813	324.3125	90.0868
16-Dec-04	9032	66	568	1.877371	302.5726	84.04796
17-Dec-04	8564	64	561	1.830657	306.2879	85.07998
18-Dec-04	8792	64	576	1.830657	314.4469	87.34636
19-Dec-04	11265	62	754	1.806809	417.3304	115.9251
20-Dec-04	10847	59	763	1.756828	434.4065	120.6685
21-Dec-04	10221	63	676	1.819633	371.4878	103.1911
22-Dec-04	10965	64	716	1.833831	390.401	108.4447
23-Dec-04	11291	63	751	1.813911	413.8908	114.9697
24-Dec-04	11610	62	783	1.798361	435.6054	121.0015
25-Dec-04	11403	65	734	1.849869	396.7971	110.2214
26-Dec-04	11641	64	761	1.833125	414.8844	115.2457
27-Dec-04	10748	64	699	1.838773	379.9377	105.5383
28-Dec-04	10156	64	661	1.837017	359.9395	99.98319
29-Dec-04	10308	64	675	1.831185	368.403	102.3342
30-Dec-04	10326	64	676	1.830657	369.3267	102.5907
31-Dec-04	10394	63	686	1.8212	376.9132	104.6981

mean	61.690	669.257	1.777	360.557	100.155
sd	2.3456	67.33056	0.122065	76.20373	21.1677

Table 18. Historic daily totalled tailings discharge data for the Sunrise Dam stack

Appendix F: Model sensitivity analysis

In this appendix, sensitivity analyses are presented for the three new models presented in Chapter 5. The sensitivity analyses were conducted by changing each of the input parameters of a model by 10% and 35% in either direction of a control value. Only one parameter was changed at a time, with all of the other input parameters left on their control values. The predicted beach slope was calculated after each change was made, and then a percentage change in predicted slope was calculated.

Sensitivity analysis of the Simple empirical model

Parameter	-35%	-10%	Control	+10%	+35%
Q	**13**	**18**	**20**	**22**	**27**
result	2.75	2.33	2.21	2.11	1.90
% change	24.03	5.41	0	-4.65	-13.93
Cw	**39.65**	**54.9**	**61**	**67.1**	**82.35**
result	0.94	1.79	2.21	2.68	4.03
% change	-57.75	-19.00	0	21.00	82.25

Table 19. Sensitivity analysis figures generated with the Simple empirical model

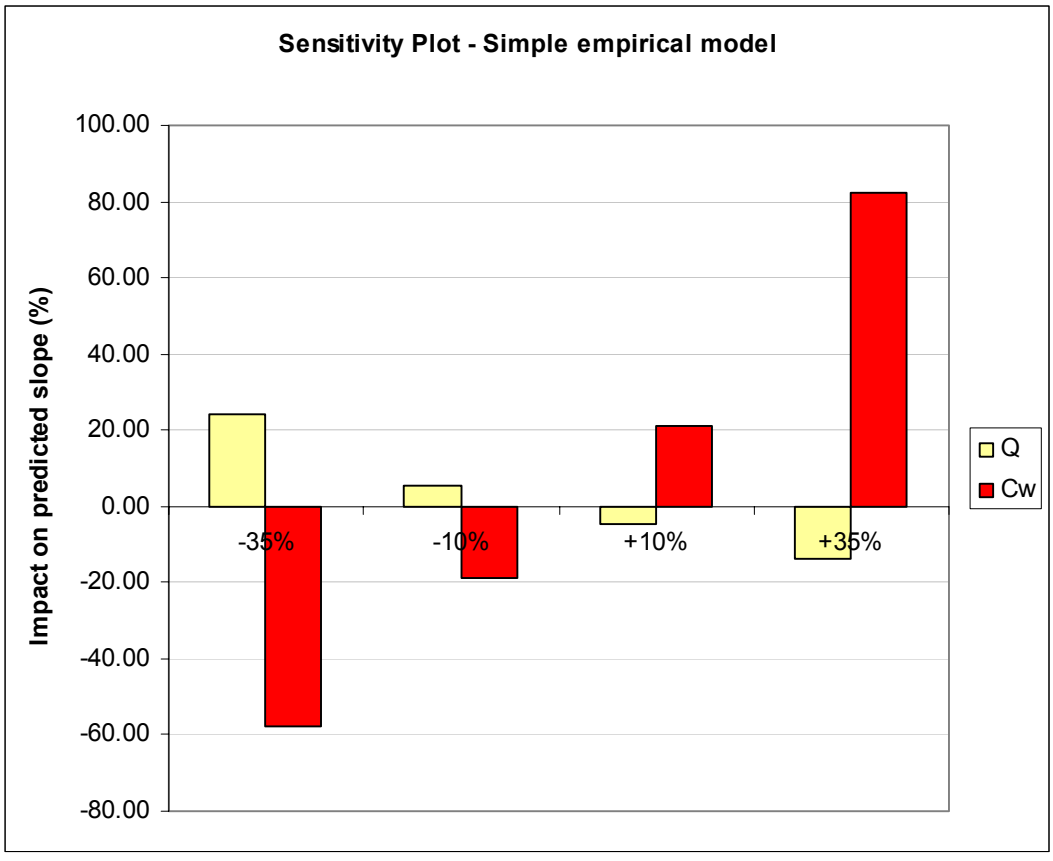

Figure 183. Sensitivity plot for the Simple empirical model

Sensitivity analysis of the a priori beach slope model

Parameter	-35%	-10%	Control	+10%	+35%
Q	**13**	**18**	**20**	**22**	**27**
result	2.73	2.56	2.51	2.47	2.38
% change	8.76	1.99	0	-1.59	-5.18
Cw	**39.65**	**54.9**	**61**	**67.1**	**82.35**
result	1.47	1.98	2.51	3.40	9.58
% change	-41.43	-21.12	0	35.46	281.67
Radius	**110.5**	**153**	**170**	**187**	**229.5**
result	2.45	2.50	2.51	2.53	2.57
% change	-2.39	-0.40	0	0.80	2.39
d50	**10.4**	**14.4**	**16**	**17.6**	**21.6**
result	2.23	2.44	2.51	2.58	2.73
% change	-11.16	-2.79	0	2.79	8.76
ρ_{solids}	**1.82**	**2.52**	**2.8**	**3.08**	**3.78**
result	1.23	2.17	2.51	2.85	3.68
% change	-51.00	-13.55	0	13.55	46.61
ρ_{fluid}	**0.7475**	**1.035**	**1.15**	**1.265**	**1.5525**
result	4.68	2.97	2.51	2.14	1.44
% change	86.45	18.33	0	-14.74	-42.63
τ_y	**4.6608**	**6.4535**	**7.1705**	**7.8876**	**9.6802**
result	2.31	2.46	2.51	2.59	2.69
% change	-7.97	-1.99	0	3.19	7.17
K	**0.1234**	**0.1709**	**0.1899**	**0.2089**	**0.2563**
result	2.45	2.50	2.51	2.53	2.57
% change	-2.39	-0.40	0	0.80	2.39
n	**0.39**	**0.54**	**0.6**	**0.66**	**0.81**
result	2.41	2.48	2.51	2.56	2.74
% change	-3.98	-1.20	0	1.99	9.16

Table 20. Sensitivity analysis figures generated with the a priori model

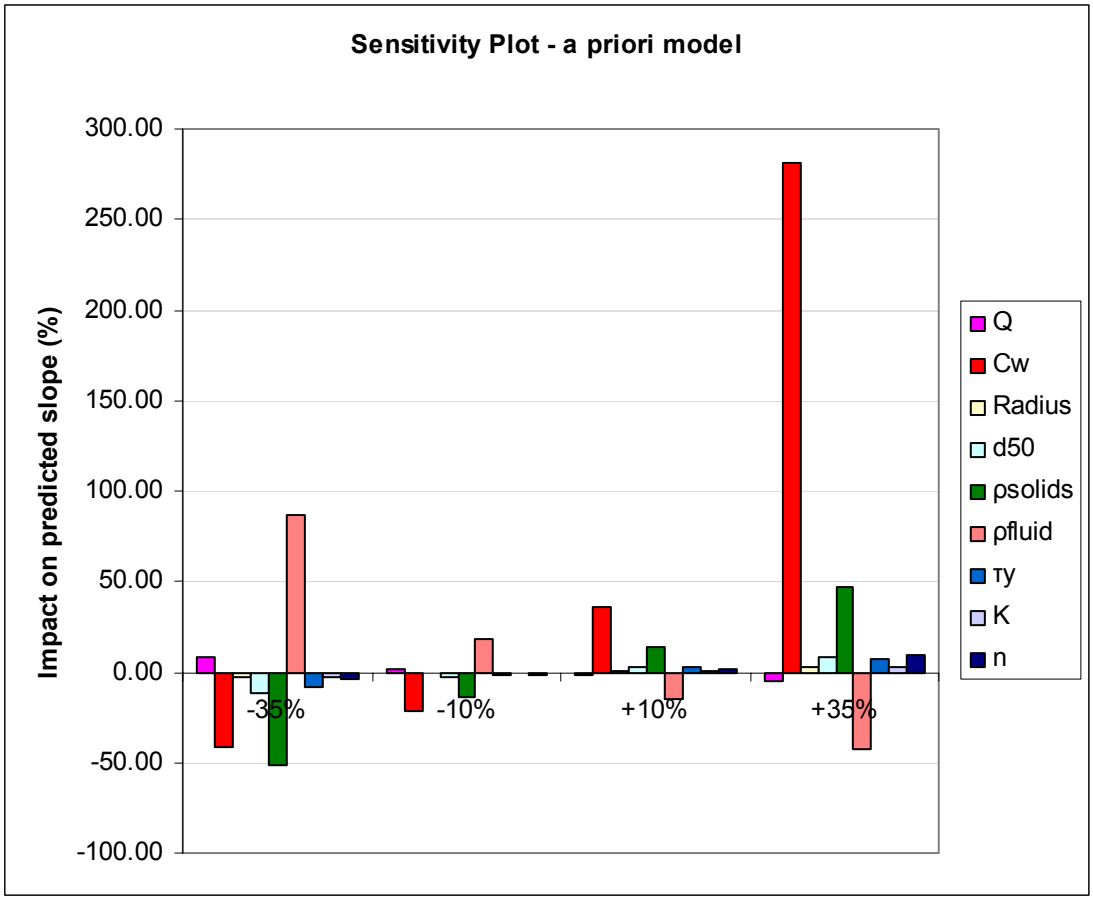

Figure 184. Sensitivity plot for the a priori model

Sensitivity analysis of the semi-empirical model

Parameter	-35%	-10%	Control	+10%	+35%
Q	**13**	**18**	**20**	**22**	**27**
result	2.77	2.47	2.38	2.29	2.12
% change	16.39	3.78	0	-3.78	-10.92
Cw	**39.65**	**54.9**	**61**	**67.1**	**82.35**
result	0.43	2.18	2.38	2.57	2.39
% change	-81.93	-8.40	0	7.98	0.42
Radius	**110.5**	**153**	**170**	**187**	**229.5**
result	2.27	2.34	2.38	2.41	2.48
% change	-4.62	-1.68	0	1.26	4.20
d50	**10.4**	**14.4**	**16**	**17.6**	**21.6**
result	2.37	2.37	2.38	2.38	2.38
% change	-0.42	-0.42	0	0.00	0.00
ρ_{solids}	**1.82**	**2.52**	**2.8**	**3.08**	**3.78**
result	2.31	2.36	2.38	2.38	2.41
% change	-2.94	-0.84	0	0.00	1.26
ρ_{fluid}	**0.7475**	**1.035**	**1.15**	**1.265**	**1.5525**
result	2.28	2.35	2.38	2.39	2.43
% change	-4.20	-1.26	0	0.42	2.10

τ_y	**4.6608**	**6.4535**	**7.1705**	**7.8876**	**9.6802**
result	2.16	2.32	2.38	2.43	2.56
% change	-9.24	-2.52	0	2.10	7.56
K	**0.1234**	**0.1709**	**0.1899**	**0.2089**	**0.2563**
result	2.31	2.36	2.38	2.39	2.44
% change	-2.94	-0.84	0	0.42	2.52
n	**0.39**	**0.54**	**0.6**	**0.66**	**0.81**
result	2.27	2.34	2.38	2.42	2.60
% change	-4.62	-1.68	0	1.68	9.24
K_{BP}	**0.0106**	**0.0147**	**0.0163**	**0.0179**	**0.022**
result	2.86	2.49	2.38	2.27	2.07
% change	20.17	4.62	0	-4.62	-13.03

Table 21. Sensitivity analysis figures generated with the semi-empirical model

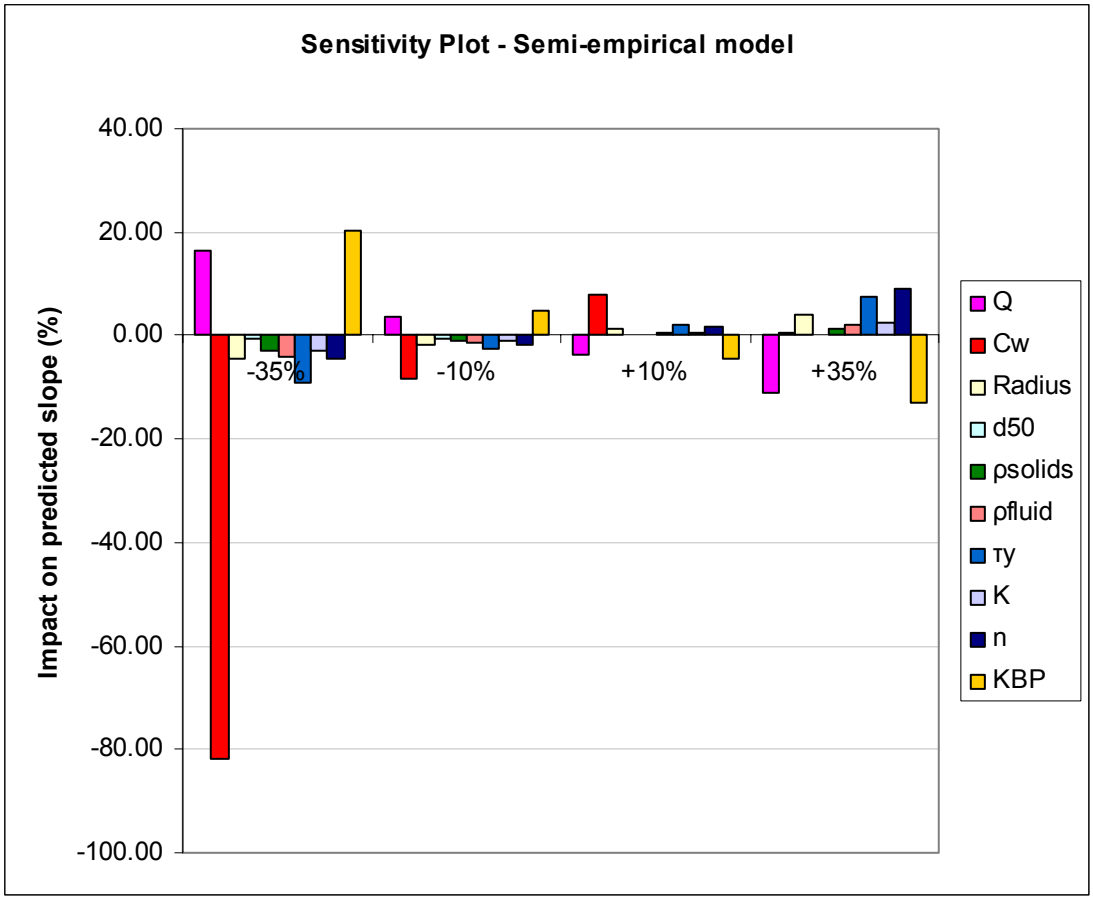

Figure 185. Sensitivity plot for the semi-empirical model

Appendix G: Experimental error analysis

Random Error Analysis

Statistical analysis is presented here to determine the random error in the following 4 variables that were measured in the field flume and small flume experiments:

- Flow rate
- Concentration
- Particle size
- Rheology

The analysis will be presented for the field flume data first, then for the small scale flume data. For all of these variables the random error is calculated in terms of a confidence interval:

$$\bar{x} \pm P\left(\frac{\sigma}{\sqrt{n}}\right)$$

where: $\bar{x}$ = sample mean

P = area under a normal distribution curve, equal to 1-α, where

α = 1 – the confidence interval

σ = standard deviation of the sample

n = the number of data points in the sample

The P value corresponding to a confidence interval of 95% is 1.96, and for a confidence interval of 90%, P is equal to 1.6449. (Rade & Westergren 1990)

Field flume: Statistical estimation of random errors in flow measurements

Tables 22, 23 and 24 present three series of flow measurements that were recorded in the field flume on 3 different days of experimentation. Each series contains data that was recorded during a single flow regime, implying that the valves in the slurry feed line were not disturbed during that period.

Date	Time	Elapsed	Fill time s/240 l	Flow rate l/s			
						Descriptive statistics	
28-Feb-05	06:45	00:00	19.5	12.3			
	06:45	00:00	19.4	12.4		Mean	11.5019289
	06:45	00:00	19.9	12.1		Standard Error	0.18324196
	07:15	00:30	20.4	11.8		Median	11.7647059
	07:15	00:30	19.7	12.2		Mode	12.0603015
	07:15	00:30	20.2	11.9		Standard Deviation	0.83972015
	07:45	01:00	19.9	12.1		Sample Variance	0.70512994
	07:45	01:00	21	11.4		Kurtosis	1.67658138
	07:45	01:00	20.4	11.8		Skewness	-1.5944093
	07:45	01:00	21.3	11.3		Range	2.92231512
	07:45	01:00	19.9	12.1		Minimum	9.4488189
	07:45	01:00	21.2	11.3		Maximum	12.371134
	08:15	01:30	20.9	11.5		Sum	241.540506
	08:15	01:30	21.4	11.2		Count	21
	08:15	01:30	20.2	11.9		Confidence Level(95.0%)	0.38223603
	08:42	01:57	25.4	9.4			
	08:42	01:57	24.4	9.8			
	08:42	01:57	24.8	9.7			
	09:15	02:30	20.5	11.7			
	09:15	02:30	20.2	11.9			
	09:15	02:30	20.1	11.9			
Duration of measurements:				02:30			

Table 22. Random error analysis on flow rates measured in the field flume (first sample of data)

Date	Time	Elapsed	Fill time s/240 l	Flow rate l/s			
						Descriptive statistics	
06-Mar-05	06:36	00:00	35.2	6.82		Mean	6.78209978
	06:36	00:00	36	6.67		Standard Error	0.0389521
	06:36	00:00	36	6.67		Median	6.73213105
	07:05	00:29	35.8	6.70		Mode	6.66666667
	07:05	00:29	34.6	6.94		Standard Deviation	0.13493403
	07:05	00:29	36.3	6.61		Sample Variance	0.01820719
	07:35	00:59	34.5	6.96		Kurtosis	-1.1439841
	07:35	00:59	34.9	6.88		Skewness	0.55954469
	07:35	00:59	34.2	7.02		Range	0.40597361
	08:40	02:04	36	6.67		Minimum	6.61157025
	08:40	02:04	35.7	6.72		Maximum	7.01754386
	08:40	02:04	35.6	6.74		Sum	81.3851974
						Count	12
Duration of measurements:				02:04		Confidence Level(95.0%)	0.08573299

Table 23. Random error analysis on flow rates measured in the field flume (second sample of data)

Date	Time	Elapsed	Fill time s/240 l	Flow rate l/s		
					Descriptive statistics	
15-Mar-05	14:16	00:00	10.3	23.3	Mean	21.3453524
	14:16	00:00	10.3	23.3	Standard Error	0.35755579
	14:16	00:00	10.1	23.8	Median	20.8695652
	14:43	00:27	11.9	20.2	Mode	23.3009709
	14:43	00:27	11.7	20.5	Standard Deviation	1.38480761
	14:43	00:27	11.3	21.2	Sample Variance	1.91769212
	14:43	00:27	10.8	22.2	Kurtosis	-1.0789191
	15:13	00:57	12	20.0	Skewness	0.59432469
	15:13	00:57	12.3	19.5	Range	4.25018112
	15:13	00:57	11.5	20.9	Minimum	19.5121951
	15:13	00:57	10.5	22.9	Maximum	23.7623762
	15:36	01:20	12	20.0	Sum	320.180287
	15:55	01:39	11.5	20.9	Count	15
	16:34	02:18	11.4	21.1	Confidence Level(95.0%)	0.76688089
	16:34	02:18	11.7	20.5		
Duration of measurements:				02:18		

Table 24. Random error analysis on flow rates measured in the field flume (third sample of data)

The analysis presented above in Tables 22 to 24 has been summarised below in Table 25.

Mean Q	95% CL	CL/Mean
11.5	0.382236	0.0332
6.78	0.085733	0.0126
21.3	0.766881	0.0359
Take error as 3.6% of Q		

Table 25. Summary of field flume flow rate random errors.

Table 25 shows that the random error for the flow rate can be described as being Q±3.6%, which covers all 3 samples tested here. This confidence interval was used in generating the error bars presented in Figure 48 in section 3.5.1.

Field flume: Statistical estimation of random errors in concentration measurements

The random error analysis for the variation in concentration in the field flume followed the same method as was used for analysing the flow rate. Table 26 presents three series of concentration measurements that were recorded in the field flume on 3 different days of experimentation. Each series contains data that was recorded during a single flow regime, implying that the valves in the slurry feed line were not disturbed during that period. Table 27 presents the descriptive statistics for each of the 3 samples of concentration data.

Date	Time	Elapsed time	Marcy reading (% solids w/w)
01-Mar-05	07:36	00:00	61
	07:56	00:20	61
	09:37	02:01	60.5
	10:22	02:46	61.3
	10:48	03:12	61.2
	15:13	07:37	62.1
12-Mar-05	07:54	00:00	39.5
	08:25	00:31	39.5
	09:00	01:06	38.5
	09:29	01:35	39
	10:54	03:00	39.5
16-Mar-05	06:30	00:00	63.5
	07:21	00:51	63.5
	07:57	01:27	62.5
	08:44	02:14	63
	09:26	02:56	62
	10:54	04:24	63.5

Table 26. Samples of concentration data measured in the field flume on three different days

	Sample date		
	01-Mar	12-Mar	16-Mar
Mean	61.18333	39.2	63
Standard Error	0.215123	0.2	0.258199
Median	61.1	39.5	63.25
Mode	61	39.5	63.5
Standard Deviation	0.526941	0.447214	0.632456
Sample Variance	0.277667	0.2	0.4
Kurtosis	2.162378	0.3125	-0.78125
Skewness	0.903081	-1.25779	-0.88939
Range	1.6	1	1.5
Minimum	60.5	38.5	62
Maximum	62.1	39.5	63.5
Sum	367.1	196	378
Count	6	5	6
Confidence Level(95.0%)	0.552991	0.555289	0.663721

Table 27. Descriptive statistics for each of the three samples of concentration data

Mean Cw	95% CL	CL/Mean
61.2	0.55	0.0090
39.2	0.555289	0.0142
63.0	0.663721	0.0105

Take error as 1.5% of concentration

Table 28. Summary of field flume concentration random errors

From Table 28 the largest error as a percentage of the mean was found to be 1.42%. From this, a value of 1.5%of the mean concentration has been adopted as the random error for all the field flume concentration measurements, and has been used to define the length of the error bars presented in Figure 50 in section 3.5.1.

Field flume: Statistical estimation of random errors in particle size measurements

Table 29 presents median particle diameters that were measured in the Malvern Particle Sizer at RMIT University for 4 samples of tailings slurry that were extracted from the field flume. Sample 11 was tested 4 times, but the other 3 samples were only tested 3 times each. The descriptive statistics for this data are also presented in Table 29.

	Measured d_{50} values			
	sample 11	**sample 19**	**sample 16**	**sample 25**
run 1	9.8	8	6.72	8.54
run 2	7.59	6.79	7.67	9.37
run 3	7.47	5.31	6.49	9.34
run 4	7.09			
	Descriptive Statistics			
	sample 11	**sample 19**	**sample 16**	**sample 25**
Mean	7.9875	6.7	6.96	9.0833333
Standard Error	0.6134924	0.7778389	0.3611556	0.2718047
Median	7.53	6.79	6.72	9.34
Standard Deviation	1.2269848	1.3472565	0.6255398	0.4707795
Sample Variance	1.5054917	1.8151	0.3913	0.2216333
Skewness	1.8153475	-0.299269	1.472364	-1.724142
Range	2.71	2.69	1.18	0.83
Minimum	7.09	5.31	6.49	8.54
Maximum	9.8	8	7.67	9.37
Sum	31.95	20.1	20.88	27.25
Count	4	3	3	3
Confidence Level(90.0%)	1.4437706	2.2712783	1.054569	0.7936657
CL/Mean	0.1807537	0.3389968	0.1515185	0.087376
Take error as 34% of d50				

Table 29. Median particle size data from tailings slurry used in the field flume

Field flume: Statistical estimation of random errors in rheological measurements

Tables 30 to 35 present rheometric data that was measured in the Contraves Rheomat 115 rheometer at RMIT University for 6 samples of tailings slurry that were extracted from the field flume. Each sample was tested twice. The 90% confidence limit is presented at the bottom of each table for the respective sample. Red figures indicate experimental artefact in the data that results from changing gears in the rheometer between low and high speeds of bob rotation. The shear stress measured at a shear rate of 100/s was chosen as the test statistic from the rheometric data, because the shear stresses measured at shear rates of greater interest (around a value of 30/s, which was more representative of the typical shear rates experienced by the slurry flowing in the field flume) were often affected by this artefact.

Test:	tf2809_01	tf2809b_01
Cw (% w/w):	65.9	
D(1/s)	Tau(Pa)	Tau(Pa)
0.1	3.966	3.554
0.16	3.975	4.263
0.25	3.966	4.292
0.4	3.746	4.244
0.63	3.889	4.665
1	4.646	5.614
1.6	6.763	5.594
2.5	9.876	6.418
4	10.68	8.861
6.3	13.81	15.31
10	19.7	18.81
16	12.7	14.53
25	21.64	4.435
40	22.39	3.966
63	23.19	14.18
100	24.24	23.11
250	28.42	27.48
400	32.36	31.11
Mean tau	23.68	23.68
90% CL		3.567

Table 30. Rheometric data for tailings slurry of 65.9% solids by weight

Test:	tf2809c_01	tf2809d_01
Cw (% w/w):	60.6	
D(1/s)	Tau(Pa)	Tau(Pa)
0.1	0.7089	1.178
0.16	0.7472	0.8909
0.25	0.7472	0.8813
0.4	0.7664	0.958
0.63	0.9484	1.197
1	1.475	1.887
1.6	2.701	3.008
2.5	3.966	4.215
4	5.776	6.16
6.3	7.041	6.897
10	7.319	7.098
16	6.131	4.454
25	7.913	7.51
40	8.219	7.846
63	8.583	8.248
100	9.235	8.89
250	11.43	11.06
400	13.77	13.36
Mean tau	9.06	9.06
90% CL		1.089

Table 31. Rheometric data for tailings slurry of 60.6% solids by weight

Test:	tf2809e_01	tf2809f_01
Cw (% w/w):	56.7	
D(1/s)	Tau(Pa)	Tau(Pa)
0.1	0.958	0.5556
0.16	0.5939	0.3544
0.25	0.5843	0.3736
0.4	0.6514	0.4694
0.63	0.8622	0.6801
1	1.619	1.427
1.6	2.682	2.567
2.5	3.056	2.864
4	3.238	2.998
6.3	3.353	3.075
10	3.362	3.161
16	2.836	2.031
25	3.659	3.516
40	3.889	3.746
63	4.177	4.062
100	4.569	4.454
250	6.102	5.939
400	7.989	7.826
Mean tau	4.51	4.51
90% CL		0.363

Table 32. Rheometric data for tailings slurry of 56.7% solids by weight

Test:	tf2809g_01	tf2809h_01
Cw (% w/w):	52.0	
D(1/s)	Tau(Pa)	Tau(Pa)
0.1	0.6035	0.7376
0.16	0.4119	0.6514
0.25	0.4311	0.6993
0.4	0.5269	0.7951
0.63	0.8334	1.054
1	1.312	1.418
1.6	1.437	1.485
2.5	1.485	1.485
4	1.504	1.533
6.3	1.523	1.581
10	1.533	1.619
16	1.351	0.9867
25	1.772	1.667
40	1.973	1.868
63	2.184	2.088
100	2.443	2.318
250	3.592	3.458
400	6.303	6.035
Mean tau	2.38	2.38
90% CL		0.395

Table 33. Rheometric data for tailings slurry of 52.0% solids by weight

Test:	tf2809i_01	tf2809j_01
Cw (% w/w):	47.2	
D(1/s)	Tau(Pa)	Tau(Pa)
0.1	0.2682	0.364
0.16	0.1916	0.2778
0.25	0.2395	0.297
0.4	0.3449	0.3928
0.63	0.5652	0.5939
1	0.6418	0.7185
1.6	0.6706	0.7185
2.5	0.6706	0.7185
4	0.6801	0.7376
6.3	0.7185	0.7664
10	0.7664	0.8143
16	0.4886	0.4598
25	0.9196	0.9101
40	1.092	1.073
63	1.236	1.188
100	1.447	1.389
250	2.654	2.596
400	5.163	5.02
Mean tau	1.42	1.42
90% CL		0.183

Table 34. Rheometric data for tailings slurry of 47.2% solids by weight

Test:	tf2809k_00	tf2809l_01
Cw (% w/w):	44.9	
D(1/s)	Tau(Pa)	Tau(Pa)
0.1	0.4886	0.3161
0.16	0.5748	0.4311
0.25	0.5748	0.4311
0.4	0.5748	0.4311
0.63	0.5748	0.4311
1	0.5748	0.4311
1.6	0.5748	0.4311
2.5	0.5939	0.4502
4	0.6227	0.479
6.3	0.6418	0.479
10	0.6706	0.5269
16	0.4311	0.6993
25	0.7951	0.8334
40	0.958	0.958
63	1.073	1.035
100	1.293	1.245
250	2.606	2.519
400	4.886	4.608
Mean tau	1.27	1.27
90% CL		0.152

Table 35. Rheometric data for tailings slurry of 44.9% solids by weight

From Tables 24 to 29, the ratio of the 90% confidence limit to the mean shear stress measured at 100/s has been calculated. This is presented in Table 36:

Slurry Cw	Mean tau at 100/s	95% CL	CL/Mean
65.9	23.68	3.57	0.151
60.6	9.06	1.089	0.120
56.7	4.51	0.363	0.080
52	2.38	0.39	0.166
47.2	1.42	0.18	0.129
44.9	1.27	0.15	0.119
Take error as 17% of shear stress value			

Table 36. Summary of mean shear stress and confidence limit statistics for the six concentrations of slurry tested.

Laboratory flume: Statistical estimation of random errors in flow measurements

Tables 37, 38 and 39 present three series of flow measurements that were recorded in the small scale laboratory flume on 3 different days of experimentation. Each series contains data that was recorded during a single flow regime, implying that the pump and the valves in the slurry feed line were not disturbed during that period.

Date	Time	Elapsed	Flow rate l/min			
					Descriptive statistics	
08-Feb-07	13:39	00:00	10.5			
	13:41	00:02	10.6		Mean	10.225
	13:44	00:05	10.5		Standard Error	0.05439056
	13:46	00:07	10.5		Median	10.2
	13:49	00:10	10.4		Mode	10.5
	13:50	00:11	10.3		Standard Deviation	0.21756225
	13:54	00:15	10.2		Sample Variance	0.04733333
	13:57	00:18	10.2		Kurtosis	-1.1525709
	14:02	00:23	10.2		Skewness	0.3440353
	14:05	00:26	10.1		Range	0.7
	14:07	00:28	10.1		Minimum	9.9
	14:09	00:30	10.1		Maximum	10.6
	14:10	00:31	10		Sum	163.6
	14:14	00:35	10		Count	16
	14:17	00:38	9.9		Confidence Level(95.0%)	0.11593074
	14:20	00:41	10			

Table 37. Flow measurements recorded in the laboratory flume (first sample of data)

Date	Time	Elapsed	Flow rate l/min			
					Descriptive statistics	
12-Feb-07	14:45	00:00	14.1			
	14:48	00:03	14.2		Mean	14.1125
	14:49	00:04	14.1		Standard Error	0.0125
	14:51	00:06	14.1		Median	14.1
	14:53	00:08	14.1		Mode	14.1
	14:55	00:10	14.1		Standard Deviation	0.03535534
	14:58	00:13	14.1		Sample Variance	0.00125
	15:00	00:15	14.1		Kurtosis	8
					Skewness	2.82842712
					Range	0.1
					Minimum	14.1
					Maximum	14.2
					Sum	112.9
					Count	8
					Confidence Level(95.0%)	0.0295578

Table 38. Flow measurements recorded in the laboratory flume (second sample of data)

Date	Time	Elapsed	Flow rate l/min			
					Descriptive statistics	
14-Feb-07	14:37	00:00	21.1			
	14:42	00:05	21.5		Mean	21.425
	14:44	00:07	21.5		Standard Error	0.11086779
	14:47	00:10	21.6		Median	21.5
					Mode	21.5
					Standard Deviation	0.22173558
					Sample Variance	0.04916667
					Kurtosis	3.26457914
					Skewness	-1.719868
					Range	0.5
					Minimum	21.1
					Maximum	21.6
					Sum	85.7
					Count	4
					Confidence Level(95.0%)	0.35283079

Table 39. Flow measurements recorded in the laboratory flume (third sample of data)

From Tables 37 to 39, a summary of the mean flow rates and confidence limits is presented below in Table 40, with the ratio of the confidence limit to the mean calculated for each of the three samples. The largest ratio was 1.65%, so a value of 1.7% was adopted as the random error for the flow rate measured in the small flume. This error value has been used to size the error bars presented in Figure 52 of section 3.5.1.

Mean Q	95% CL	CL/Mean
10.2	0.115931	0.0113
14.1	0.029558	0.0021
21.4	0.352831	0.0165
Take error as 1.7% of Q		

Table 40. Summary of flow rate random error statistics

Laboratory flume: Statistical estimation of random errors in fluid specific gravity measurements

Table 41 presents 4 samples of specific gravity data that were measured during the small flume experiments, along with the descriptive statistics for each sample group. The coriolis meter used in this flume displayed a specific gravity reading, so this value was used in this analysis.

Date	Time	Elapsed time	Specific Gravity	Mean
08-Feb-07	10:17	00:00	0.998	0.998
	13:41	03:24	0.997	0.998
09-Feb-07	12:06	00:00	1.000	1.000
	12:28	00:22	1.000	1.000
12-Feb-07	14:20	00:00	0.998	0.998
	14:34	00:14	0.998	0.998
21-Feb-07	10:55	00:00	0.998	0.999
	11:36	00:41	1.000	0.999

	08-Feb	*09-Feb*	*12-Feb*	*21-Feb*
Mean	0.9975	1	0.998	0.999
Standard Error	0.0005	0	0	0.001
Median	0.9975	1	0.998	0.999
Standard Deviation	0.000707107	0	0	0.001414214
Sample Variance	5E-07	0	0	0.000002
Range	0.001	0	0	0.002
Minimum	0.997	1	0.998	0.998
Maximum	0.998	1	0.998	1
Sum	1.995	2	1.996	1.998
Count	2	2	2	2
Confidence Level(95.0%)	0.006353102	0	0	0.012706205

Table 41. Concentration measurements from the small flume experiments, with the descriptive statistics presented below.

From Table 41 a summary of the relevant statistics has been presented below in Table 42 to determine the applicable error for the data population.

Mean SG	95% CL	CL/Mean
1.00	0.01	0.0064
1	0	0.0000
0.998	0	0.0000
0.999	0.012706	0.0127

Take error as 1.3% of concentration

Table 42. Summary of the statistics applicable to the specific gravity data recorded in the small flume

Table 42 shows that the maximum ratio of the confidence limit to the mean recorded specific gravity was 0.0127, so a random error value of 1.3% has been adopted for this variable. This error value has been used to size the error bars presented in Figure 54 of section 3.5.1.

Laboratory flume: Statistical estimation of random errors in particle size measurements

Figure 186 presents 3 particle size curves that were generated by performing sieve analysis on 3 samples of crushed glass particles from the same "mid" population of particles.

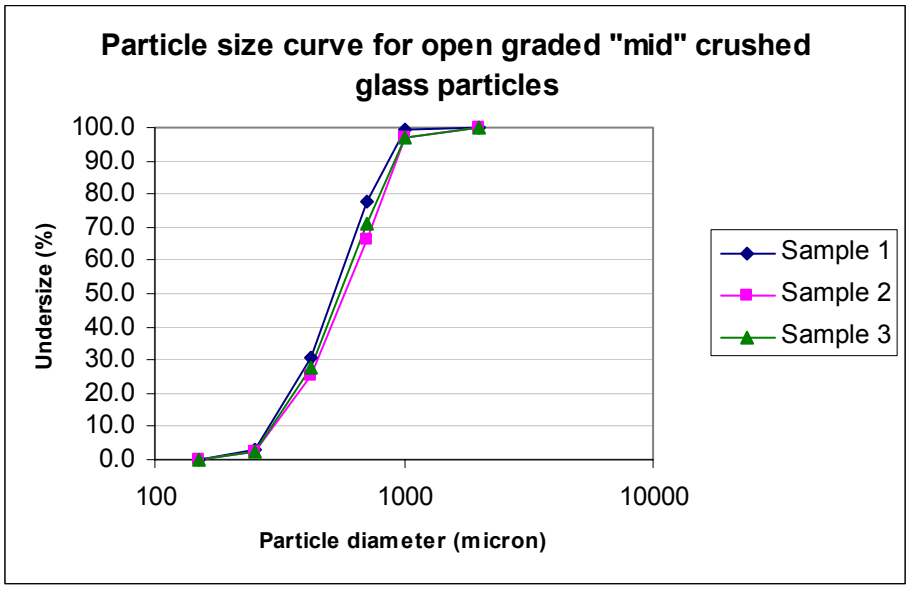

Figure 186. Particle size curves for 3 samples of the "mid" crushed glass particles used in the small scale laboratory flume.

The d_{50} value was selected as the most relevant statistic to analyse for random error from this data. The respective d_{50} values of the 3 samples are displayed more clearly in Figure 187, where the horizontal axis is presented as a normal scale and the domain of interest is zoomed in.

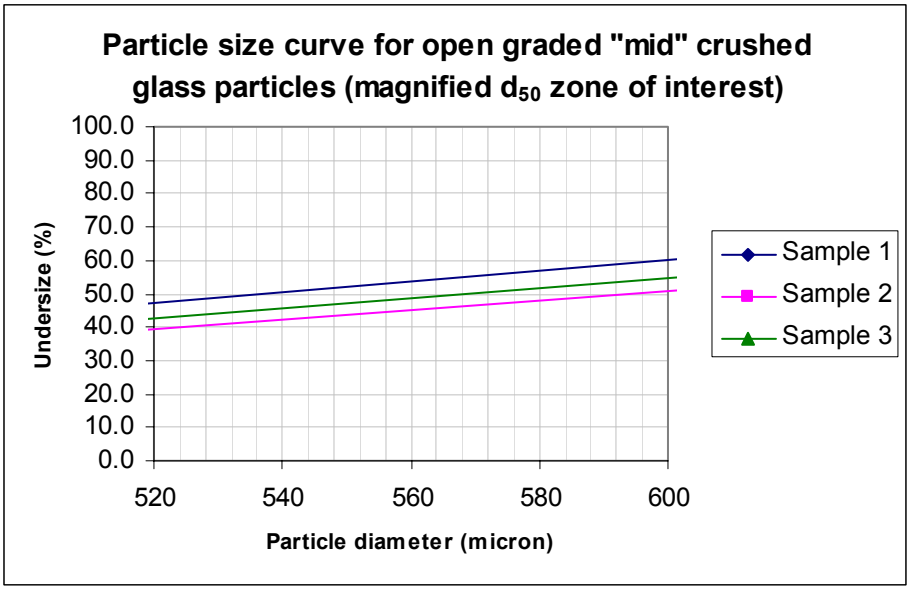

Figure 187. Particle size data from Figure 186, presented with the d_{50} region in clearer view

From Figure 187, the d_{50} values for samples 1, 2 and 3 respectively are found to be 535 μm, 592 μm and 567 μm. The mean and 95% confidence limit were calculated for this sample of 3 data points, and are presented below in Table 43.

Mean d_{50}	95% CL	CL/Mean
564.6	70.97566	0.125
Take error as 13% of d_{50}		

Table 43. Summary of random error statistics for d_{50} in the small flume experiments

The random error of ±13% has been used in Figure 53 in section 3.5.1 for sizing the 95% confidence interval error bars.

Laboratory flume: Statistical estimation of random errors in rheology measurements

Table 44 presents shear stress measurements for 4 non-Newtonian fluids that were run in the small scale laboratory flume. Each fluid was tested 3 times in a Contraves rheometer. The selected statistic for analysis is the shear stress at a shear rate of 146/s.

Fluid	Carbopol		
Test no.	070207a	070207b	070207c
D(s-1)	Tau(Pa)	Tau(Pa)	Tau(Pa)
146	1.341	1.245	1.293
Mean tau	1.29	1.29	1.29
95% CL			0.119239
Fluid	CMC		
Test no.	090207a	090702b	090702c
D(s-1)	Tau(Pa)	Tau(Pa)	Tau(Pa)
146	6.418	6.37	6.37
Mean tau	6.39	6.39	6.39
95% CL			0.068842
Fluid	CMC diluted		
Test no.	120207a	120207b	120207c
D(s-1)	Tau(Pa)	Tau(Pa)	Tau(Pa)
146	3.88	3.832	3.928
Mean tau	3.88	3.88	3.88
95% CL			0.119239
Fluid	CMC2 xxd		
Test no.	190207a	190207b	190207c
D(s-1)	Tau(Pa)	Tau(Pa)	Tau(Pa)
146	2.634	2.634	2.634
Mean tau	2.63	2.63	2.63
95% CL			0

Table 44. Rheometric data for 4 fluids used in the laboratory flume, each tested 3 times.

Fluid	Mean tau at 146/s	95% CL	CL/Mean
Carbopol	1.29	0.12	0.0922
CMC	6.39	0.069	0.0108
CMC diluted	3.88	0.119	0.0307
CMC2 xxd	2.63	0.00	0.0000
Take error as 9.3% of shear stress value			

Table 45. Summary of statistics for the rheometric measurement of fluids from the small flume.

Table 45 shows that the largest ratio of the confidence limit to the mean shear stress at 146/s was 0.0922. This value has been used to adopt a random error in rheology data as ±9.3%. This error value was then used in sizing the error bars presented in Figure 55 in section 3.5.1.

Field flume measurement error analysis

The following exercises were undertaken to determine the worst possible logged value for a measured variable in the field flume, within the limitations of the estimated accuracy associated with each individual measurement that contributed to the logged measurement for that variable. Table 5, presented in section 3.5.2, contains estimates of the accuracy of each measurement made in the experimental work. In such cases where only one measurement was required to log of a variable (such

as recording the slurry temperature with a thermometer), a worst-case scenario analysis was not made because that logged measurement would be equal to the measured temperature plus or minus the accuracy of the thermometer. However, for the measurement of the flow rate, the slope of the flume, and the concentration of the slurry, more than one measurement was required in order to log a final value. This work calculates the maximum possible error that could occur in the logging of each of these three variables.

Flow rate measurement

For the measurement of the flow rate in the field flume, the time taken for the flow measuring box to be filled had to be measured. This introduced 4 sources of measurement error:

- the accuracy of a hand-held digital stopwatch (± 0.1 s)
- the human reaction time in starting a stopping the watch (± 0.14 s)
- the measurement of the dimensions of the flow measuring box with a tape measure (± 0.01 m)
- the effect of waves on the fluid surface level (± 0.01 m for flows less than 12 l/s, ± 0.02 m for flows greater than 12 l/s)

The human reaction time in starting and stopping the stopwatch was determined through a series of simple experiments. The person operating the stopwatch was asked to start the instrument and then stop it on the 5 second mark. This was done 8 times, with the following recorded data being logged:

Reaction time exercise Try to stop stopwatch on 5.0s		
Trial time	Mean	St Dev
5.1	5.08	0.07
5.1		
5.0		
5.2		
5.0		
5.0		
5.1		
5.1		

Table 46. Human reaction time in operating a stopwatch

From Table 46 it was found that the human error involved in stopping the stopwatch was ±0.07 s. It was reasoned that such a reaction time would also apply in starting the stopwatch to coincide with the

filling of the flow measuring box. This equates to an estimated human error of ±0.14 s with every flow measurement. Adding the resolution of the stopwatch of ±0.1 s to this, the worst possible error in the recorded time would be ±0.24 s.

The plan dimensions of the flow measuring box were 1.2 x 1.0 m. For most measurements a depth of 0.2 m was used, giving a capacity of 240 litres to the box. The largest flow rate recorded was 24 l/s, so the expected time to fill would be 10 s. With the estimated accuracy of the tape measure at 1 cm, and the wave effect in the tank making the level measurement accurate to 2 cm for a flow greater than 12 l/s, in the worst case, the volume would be measured at a minimum of 1.19 x 0.99 x 0.18 m, or a maximum of 1.21 x 1.01 x 0.22 m.

There are 4 foreseeable worst case scenarios that can be drawn from this combination of errors:

Scenario A: Actual flow rate = 24 l/s.

Tank dimensions: 1.19 x 0.99 x 0.18

Time = 10.24s

Calculated flow rate = 20.7 l/s

Error = -3.3 l/s or -13.7%

Scenario B: Actual flow rate = 24 l/s.

Tank dimensions: 1.21 x 1.01 x 0.22

Time = 9.76 s

Calculated flow rate = 27.5 l/s

Error = +3.5 l/s or 14.6%

Scenario C: Actual flow rate = 12 l/s.

Tank dimensions: 1.19 x 0.99 x 0.18

Time = 20.24s

Calculated flow rate = 10.5 l/s

Error = -1.5 l/s or -12.5%

Scenario D: Actual flow rate = 12 l/s.

Tank dimensions: 1.21 x 1.01 x 0.22

Time = 19.76 s

Calculated flow rate = 13.6 l/s

Error = +1.6 l/s or 13.4%

The worst of these 4 scenarios suggest that the flow measurement is accurate to ±14.6 %.

Concentration measurement

The measurement of concentration in the field flume was done with a Marcy balance. The dial of the balance could be read to a resolution of ±0.1 % w/w. The plastic bucket was estimated to hold 1000 ± 5 ml. It was assumed that the spring in the balance exhibited linear elasticity, and that the empty bucket registers a reading of 0% w/w. From these two sources of error, the following 4 worst case scenarios were tested:

Scenario A: Actual slurry concentration = 66 % w/w.

Volume of sample: 995 ml

Scale registers 66 x 99.5% = 65.7% w/w

Dial reading error of -0.1% w/w

Dial reading: 65.6 % w/w

Error = -0.4 % w/w or 0.6% abs

Scenario B: Actual slurry concentration = 66 % w/w.

Volume of sample: 1005 ml

Scale registers 66 x 100.5% = 66.3% w/w

Dial reading error of +0.1% w/w

Dial reading: 66.4 % w/w

Error = +0.4 % w/w or 0.6% abs

Scenario C: Actual slurry concentration = 25 % w/w.

Volume of sample: 995 ml

Scale registers 25 x 99.5% = 24.9% w/w

Dial reading error of -0.1% w/w

Dial reading: 24.8 % w/w

Error = -0.2 % w/w or 0.8% abs

Scenario D: Actual slurry concentration = 25 % w/w.

Volume of sample: 1005 ml

Scale registers 25 x 100.5% = 25.1% w/w

Dial reading error of +0.1% w/w

Dial reading: 25.2 % w/w

Error = +0.2 % w/w 0.8% abs

The worst of these 4 scenarios suggest that the concentration measurement is accurate to ±0.8 %.

Slope measurement

The measurement of a slope in the field flume was done optically by sighting a mark on the A-frame relative to the position of the flume. The marks on the A-frame were drawn on with a texta marker, in locations decided with the use of a surveyor's automatic level. This presents 3 sources of error:

- Parallax error in reading the mark on the A-frame (±2 mm)
- Making the initial marks on the A-frame (±2 mm)
- Accuracy of the automatic level (±1 mm)

The accuracy of the level was checked with a standard 3 point test. The base of the levelling staff was kept clean and free from mud or other material that could corrupt its height.

With these 3 sources of error all being of the same units, it makes the worst scenario analysis easy. The three of them are added together to give a maximum error of ±5 mm. Only one scenario needs to be calculated from this:

5 mm maximum compounded error in height at the downstream end of the flume

over 10 m horizontal length of flume

0.005/10= 0.0005

This is a 0.05% slope error

The findings of this measurement error analysis have been summarised in Table 5 in section 3.5.2.

Small scale laboratory flume measurement errors

In the small scale laboratory flume the measurement of the relevant variables was made much easier with the use of the coriolis meter. It was able to record the flow rate, concentration and temperature of the slurries to high accuracies in a single measurement. The accuracies presented by the manufacturer of the coriolis meter have been presented in Table 5 in section 3.5.2.

Slope measurement

The only variable in the small scale flume experiments that was susceptible to the compounding of errors from more than one measurement was the slope. The measurement of a slope in the small scale flume was done optically by measuring the gap between the flume and the building structure with a tape measure. The elevation of the structure relative to the pivotal point of the flume was measured with a laser level. This presented 2 sources of error:

- Accuracy of measuring the gap between the flume and the structure (±2 mm)
- Accuracy of the laser level (±2 mm)

The accuracy of the level was checked with a standard 3 point test. With these 2 sources of error being of the same units, this gives a maximum error of ±4 mm. Only one scenario needs to be calculated from this:

4 mm maximum compounded error in height at the downstream end of the flume

over 5.4 m horizontal length of flume

0.004/5.4= 0.000741

This is a 0.07% slope error

The findings of this measurement error analysis have been summarised in Table 5 in section 3.5.2.

Appendix H: Small scale flume equilibrium slope data

Table 47. Summary of equilibrium slope data observed in the small scale flume

Date	Time	Fluid	Particles	Flow rate (l/min)	Slope (fraction)	Depth (mm)
31-Jan-07	12:05	Water	Crushed glass	9.4	0.014	14
02-Feb-07	11:30	Water	Crushed glass	7.2	0.010	13
02-Feb-07	12:00	Water	Crushed glass	9.0	0.018	12
02-Feb-07	12:31	Water	Crushed glass	17.6	0.033	15
06-Feb-07	10:53	Water	Crushed glass	10.3	0.018	14
07-Feb-07	11:01	Water	Crushed glass	24.0	0.007	22
07-Feb-07	14:20	Carbopol	Crushed glass	21.1	0.010	30
07-Feb-07	14:49	Carbopol	Crushed glass	18.1	0.012	23
07-Feb-07	15:14	Carbopol	Crushed glass	14.3	0.013	18
08-Feb-07	12:05	Carbopol diluted	Crushed glass	20.9	0.012	21
08-Feb-07	12:16	Carbopol diluted	Crushed glass	23.8	0.017	21
08-Feb-07	12:26	Carbopol diluted	Crushed glass	17.5	0.018	18
08-Feb-07	13:38	Carbopol diluted	Crushed glass	12.5	0.010	16
08-Feb-07	14:20	Carbopol diluted	Crushed glass	10.0	0.008	14
09-Feb-07	15:23	CMC	Crushed glass	11.9	0.072	17
09-Feb-07	15:33	CMC	Crushed glass	17.9	0.076	18
09-Feb-07	15:58	CMC	Crushed glass	6.7	0.040	17
09-Feb-07	16:20	CMC	Crushed glass	21.0	0.056	20
12-Feb-07	10:35	CMC diluted	Crushed glass	11.7	0.035	18
12-Feb-07	10:40	CMC diluted	Crushed glass	16.6	0.043	17
12-Feb-07	10:54	CMC diluted	Crushed glass	21.5	0.042	20
12-Feb-07	14:07	CMC diluted	Crushed glass	10.5	0.016	19
12-Feb-07	14:41	CMC diluted	Crushed glass	19.4	0.037	17
12-Feb-07	15:01	CMC diluted	Crushed glass	14.1	0.027	17
13-Feb-07	11:16	CMC2	Fine crushed glass	6.0	0.063	15
13-Feb-07	11:29	CMC2	Fine crushed glass	21.1	0.077	19
13-Feb-07	11:54	CMC2	Fine crushed glass	15.1	0.059	19
13-Feb-07	14:16	CMC2	Fine crushed glass	18.3	0.049	21
13-Feb-07	14:31	CMC2	Fine crushed glass	13.0	0.045	19
13-Feb-07	14:44	CMC2	Fine crushed glass	10.5	0.041	19
13-Feb-07	15:02	CMC2	Fine crushed glass	8.3	0.033	19
14-Feb-07	11:07	CMC2 diluted	Fine crushed glass	10.8	0.049	17
14-Feb-07	11:13	CMC2 diluted	Fine crushed glass	20.3	0.043	21
14-Feb-07	11:29	CMC2 diluted	Fine crushed glass	16.8	0.042	19
14-Feb-07	11:32	CMC2 diluted	Fine crushed glass	14.5	0.039	19
14-Feb-07	11:37	CMC2 diluted	Fine crushed glass	11.7	0.036	18
14-Feb-07	11:42	CMC2 diluted	Fine crushed glass	9.1	0.031	17
14-Feb-07	11:45	CMC2 diluted	Fine crushed glass	7.0	0.029	16
14-Feb-07	11:51	CMC2 diluted	Fine crushed glass	6.0	0.026	16
14-Feb-07	12:06	CMC2 diluted	Fine crushed glass	5.2	0.019	16
14-Feb-07	14:48	CMC2 further diluted	Fine crushed glass	21.6	0.042	19
14-Feb-07	14:59	CMC2 further diluted	Fine crushed glass	18.9	0.041	18
14-Feb-07	15:07	CMC2 further diluted	Fine crushed glass	17.7	0.036	18
14-Feb-07	15:11	CMC2 further diluted	Fine crushed glass	16.4	0.034	19
14-Feb-07	15:16	CMC2 further diluted	Fine crushed glass	15.1	0.028	19
14-Feb-07	15:22	CMC2 further diluted	Fine crushed glass	14.0	0.019	19

14-Feb-07	15:31	CMC2 further diluted	Fine crushed glass	12.8	0.026	18
14-Feb-07	15:35	CMC2 further diluted	Fine crushed glass	11.8	0.024	18
14-Feb-07	15:39	CMC2 further diluted	Fine crushed glass	10.8	0.020	19
14-Feb-07	15:52	CMC2 further diluted	Fine crushed glass	8.9	0.017	18
14-Feb-07	15:57	CMC2 further diluted	Fine crushed glass	7.8	0.019	17
14-Feb-07	16:04	CMC2 further diluted	Fine crushed glass	6.7	0.019	17
14-Feb-07	16:09	CMC2 further diluted	Fine crushed glass	5.7	0.014	17
14-Feb-07	16:18	CMC2 further diluted	Fine crushed glass	4.8	0.011	16
15-Feb-07	10:50	CMC2 xd	Fine crushed glass	21.3	0.037	19
15-Feb-07	10:53	CMC2 xd	Fine crushed glass	20.1	0.034	19
15-Feb-07	10:56	CMC2 xd	Fine crushed glass	19.3	0.031	19
15-Feb-07	11:01	CMC2 xd	Fine crushed glass	18.1	0.030	18
15-Feb-07	11:07	CMC2 xd	Fine crushed glass	17.1	0.027	19
15-Feb-07	11:11	CMC2 xd	Fine crushed glass	16.0	0.025	18
15-Feb-07	15:40	CMC2 xxd	Fine crushed glass	22.9	0.025	19
15-Feb-07	16:09	CMC2 xxd	Fine crushed glass	9.8	0.014	17
15-Feb-07	16:25	CMC2 xxd	Fine crushed glass	5.3	0.017	14
19-Feb-07	14:02	CMC2 dd	Fine crushed glass	22.9	0.018	17
19-Feb-07	14:17	CMC2 dd	Fine crushed glass	17.6	0.022	15
19-Feb-07	14:31	CMC2 dd	Fine crushed glass	15.9	0.018	15
19-Feb-07	14:54	CMC2 dd	Fine crushed glass	14.2	0.022	14
19-Feb-07	15:03	CMC2 dd	Fine crushed glass	11.9	0.014	15
20-Feb-07	10:44	CMC2 ddd	Fine crushed glass	22.7	0.017	17
20-Feb-07	10:54	CMC2 ddd	Fine crushed glass	21.9	0.018	17
20-Feb-07	11:05	CMC2 ddd	Fine crushed glass	18.8	0.015	16
20-Feb-07	11:14	CMC2 ddd	Fine crushed glass	16.9	0.015	15
20-Feb-07	11:23	CMC2 ddd	Fine crushed glass	15.6	0.015	15
20-Feb-07	12:04	CMC2 ddd	Fine crushed glass	12.3	0.015	14
20-Feb-07	12:21	CMC2 ddd	Fine crushed glass	10.9	0.009	15
20-Feb-07	14:21	CMC2 d4	Fine crushed glass	22.5	0.005	22
20-Feb-07	14:28	CMC2 d4	Fine crushed glass	19.9	0.006	20
20-Feb-07	14:41	CMC2 d4	Fine crushed glass	16.0	0.004	19
20-Feb-07	14:50	CMC2 d4	Fine crushed glass	14.8	0.005	18
20-Feb-07	15:01	CMC2 d4	Fine crushed glass	13.4	0.003	18
20-Feb-07	15:15	CMC2 d4	Fine crushed glass	11.4	0.002	18
21-Feb-07	11:41	Water	Coarse crushed glass	23.2	0.016	18
21-Feb-07	11:55	Water	Coarse crushed glass	19.5	0.014	18
21-Feb-07	12:01	Water	Coarse crushed glass	15.3	0.012	16
21-Feb-07	12:15	Water	Coarse crushed glass	12.5	0.012	15
21-Feb-07	12:27	Water	Coarse crushed glass	10.0	0.006	15
21-Feb-07	13:53	CMC w	Coarse crushed glass	21.9	0.018	18
21-Feb-07	14:00	CMC w	Coarse crushed glass	18.0	0.016	17
21-Feb-07	14:07	CMC w	Coarse crushed glass	14.1	0.011	16
21-Feb-07	14:14	CMC w	Coarse crushed glass	11.8	0.009	15
21-Feb-07	14:25	CMC w	Coarse crushed glass	8.6	0.008	13
21-Feb-07	14:36	CMC w	Coarse crushed glass	22.4	0.014	19
21-Feb-07	14:53	CMC w	Coarse crushed glass	19.7	0.015	18
21-Feb-07	14:57	CMC w	Coarse crushed glass	16.1	0.014	16
21-Feb-07	15:06	CMC w	Coarse crushed glass	10.5	0.010	14

Table 16. Summary of equilibrium slope data observed in the small scale flume

Appendix I: Small scale flume experiments - Refractive error correction

The refractive error in the glass pipe of the small flume was quantified via a series of optical experiments. A small vertical scale was set up inside the glass pipe, with a steel ruler used outside the pipe to measure the apparent depth in relation to the actual depth shown by the small scale inside the pipe. The steel ruler was used on both the near and far sides of the pipe repeatedly for each measurement to avoid parallax errors. Photos of this operation are presented below:

Figure 188. Photographs of optical experiments conducted to overcome the refractive errors in the pipe, which were based on relating the actual depth inside the pipe to outside measurements.

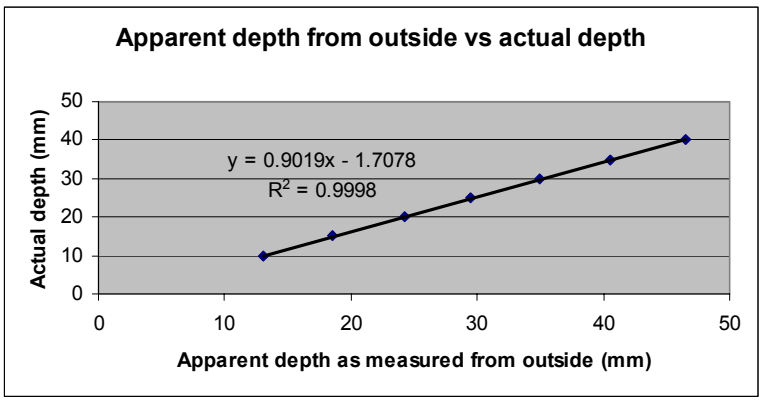

Figure 189. Plot of observed data with fitted line.

The mathematical expression of the fitted line was adopted throughout the data analysis for determining the actual depth as a function of the apparent depth measured from outside the pipe with the steel ruler.

Appendix J: Small scale flume experiments - Rheological data and model fitting

This appendix contains all of the rheograms that were recorded for the 13 non-Newtonian fluids used in the small scale laboratory flume at RMIT University, along with the rheological model curve that has been fitted. The rheological analysis was performed in a Contraves Rheomat 115 rheometer, which is described in some detail in section 3.3.13. Each of the 13 fluids was tested 3 or more times in the rheometer at the same temperature that it was under in the laboratory flume. The parameters for the rheological model fits are presented in Table 3 in section 3.4.7.

Many of these rheograms exhibit a turbulent vortice artefact, where the measured shear stress was seen to climb dramatically from a certain shear rate value, in an apparent display of shear thickening. The rheogram for the Carbopol solution, presented immediately below as Figure 190, provides a good example of this artefact, where it can be seen that the shear stress data suddenly climbed away from the fitted curve at a shear rate of about 290/s. This artefact has been discussed in more detail in section 3.4.7.

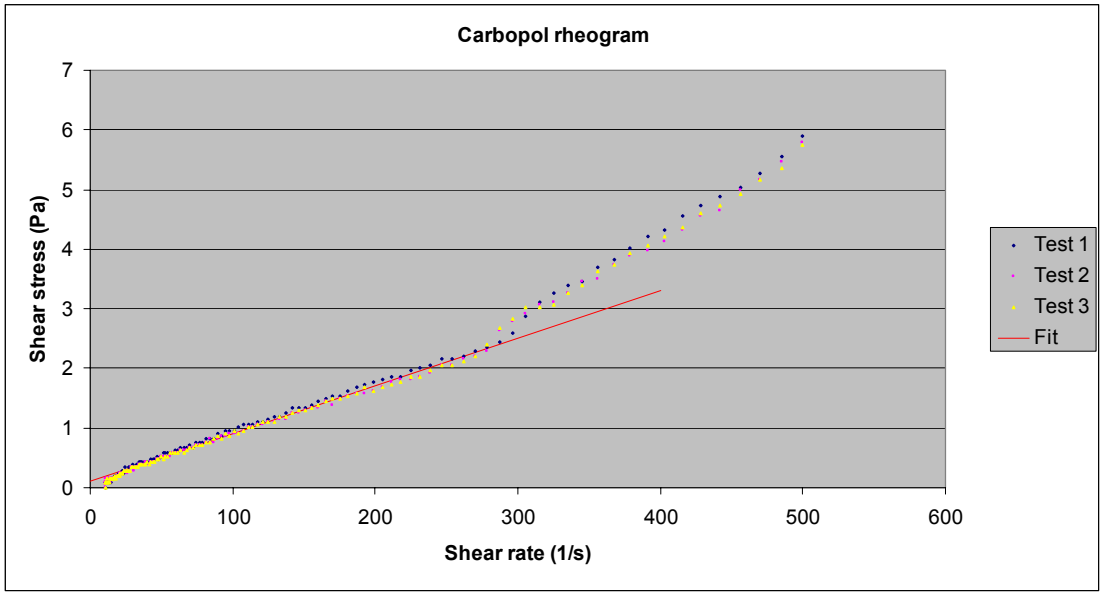

Figure 190. Rheograms with model fit for the Carbopol fluid used in the small flume

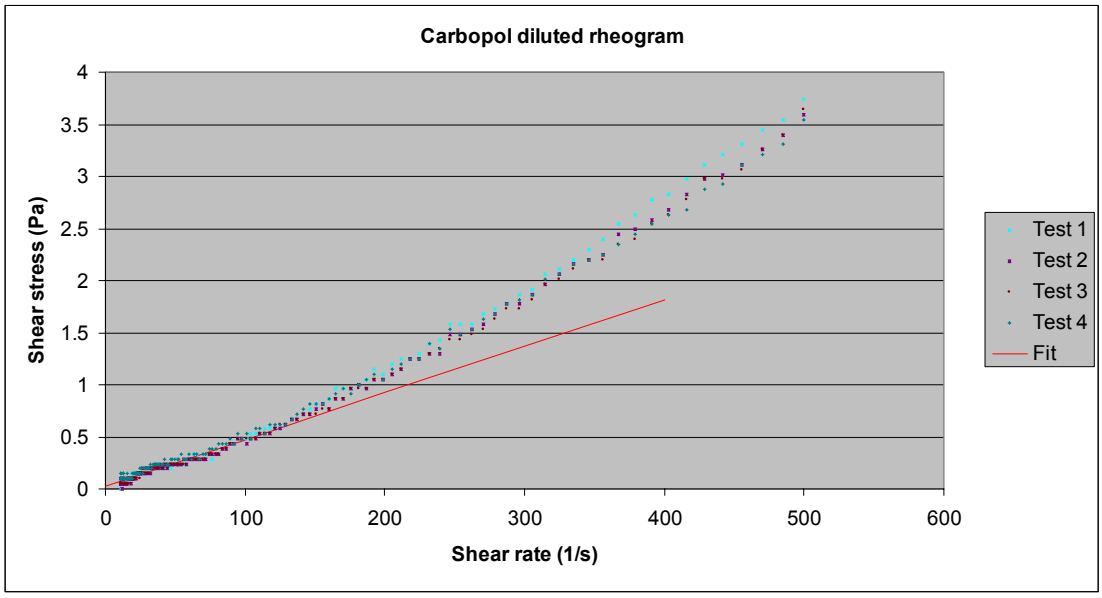

Figure 191. Rheograms with model fit for the "Carbopol diluted" fluid used in the small flume

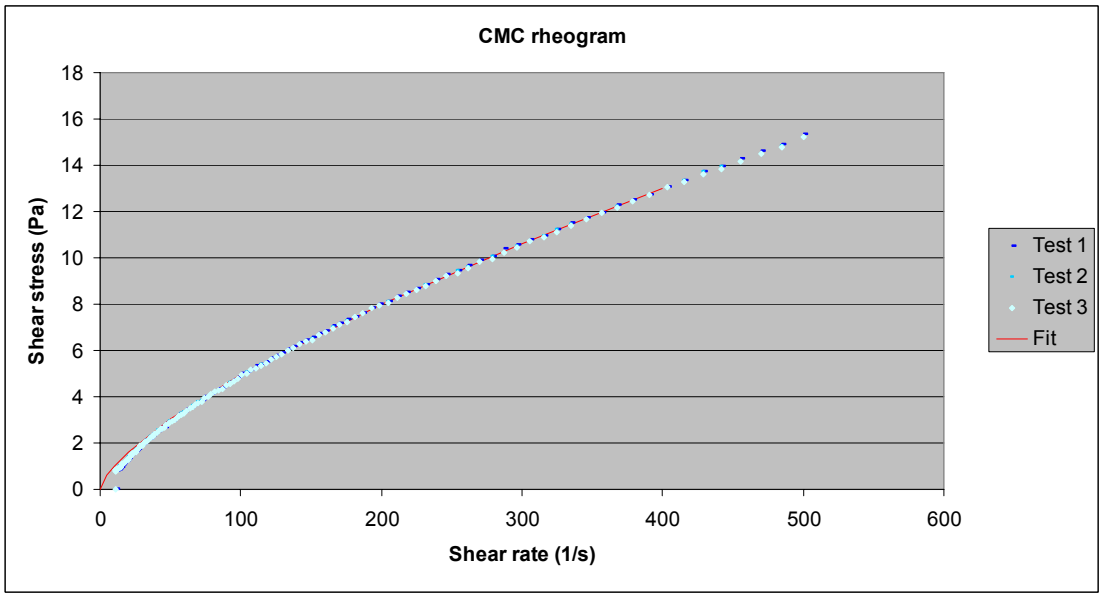

Figure 192. Rheograms with model fit for the "CMC" fluid used in the small flume

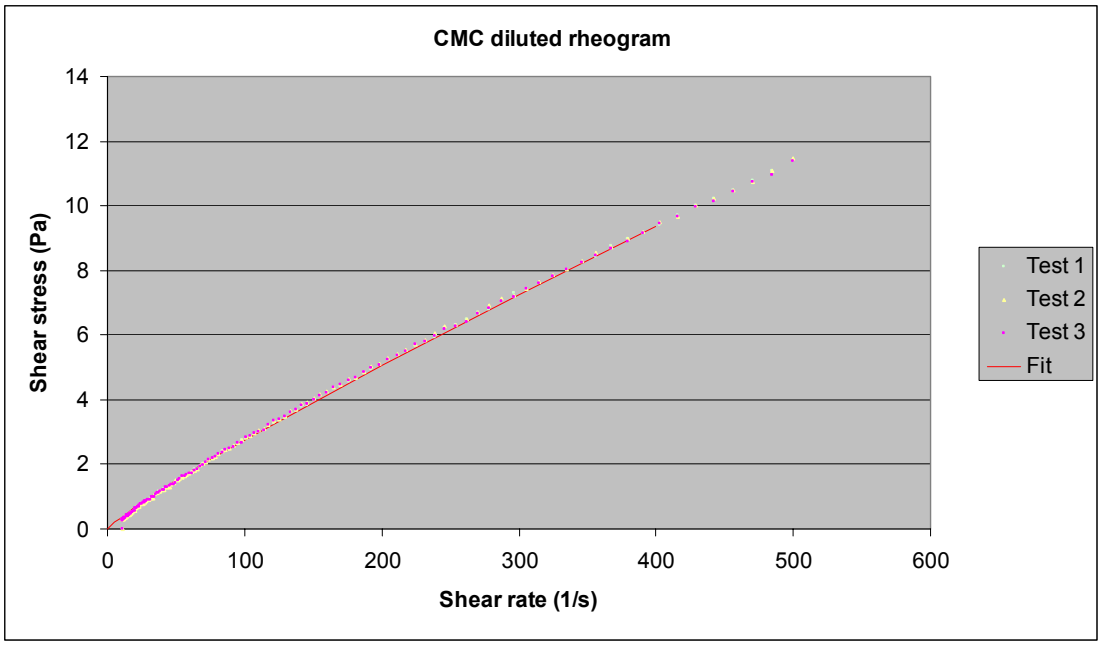

Figure 193. Rheograms with model fit for the "CMC diluted" fluid used in the small flume

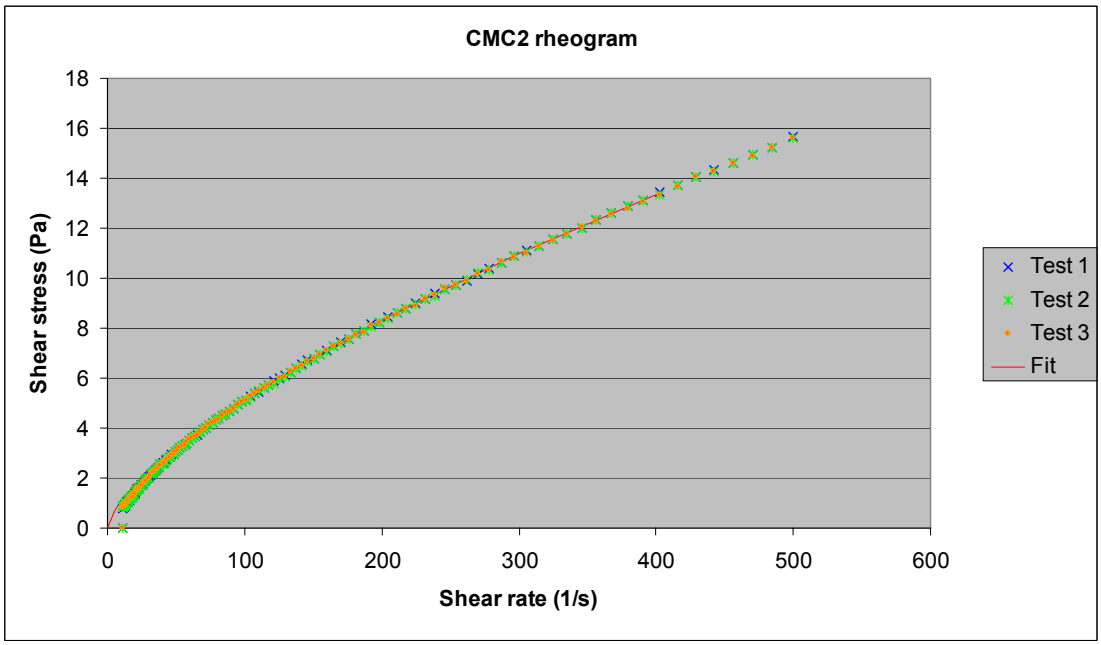

Figure 194. Rheograms with model fit for the "CMC2" fluid used in the small flume

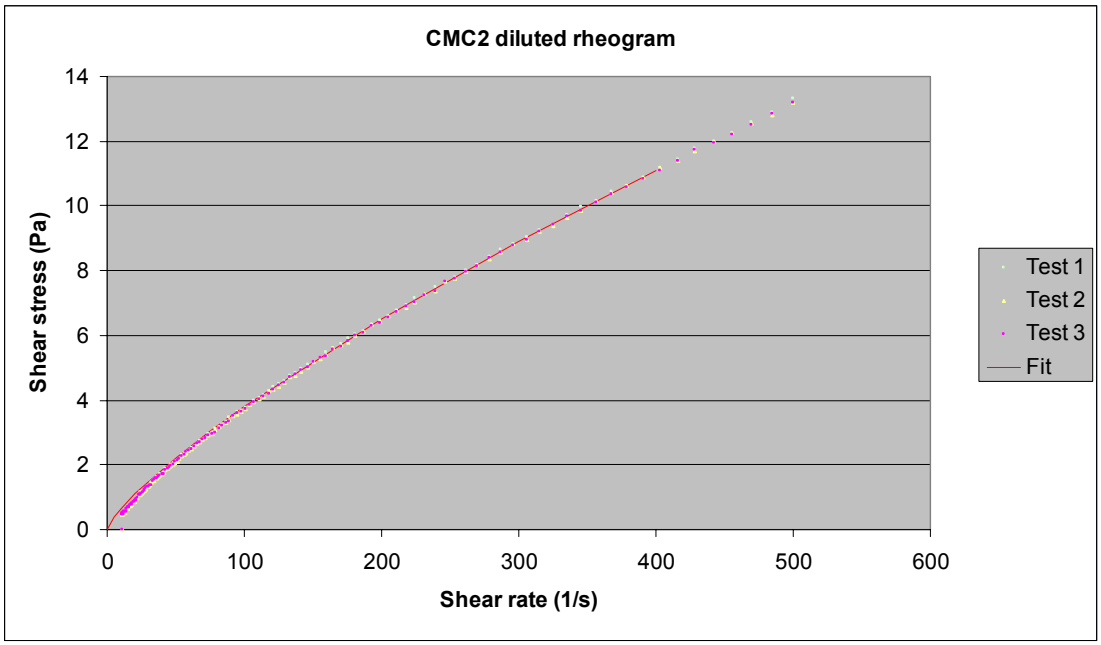

Figure 195. Rheograms with model fit for the "CMC2 diluted" fluid used in the small flume

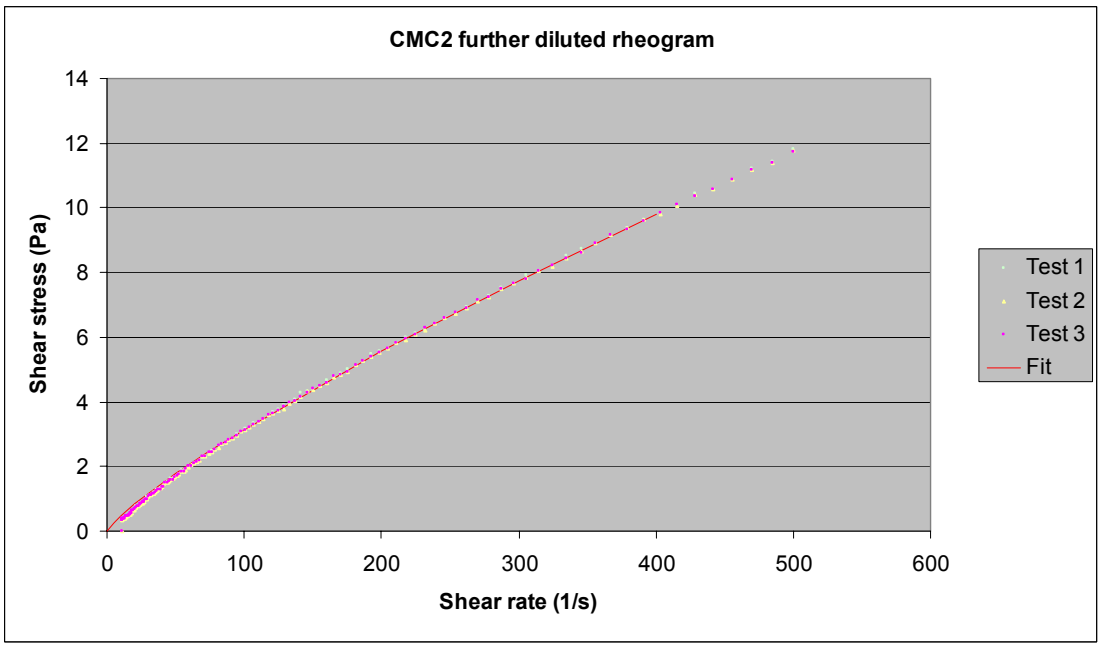

Figure 196. Rheograms with model fit for the "CMC2 further diluted" fluid used in the small flume

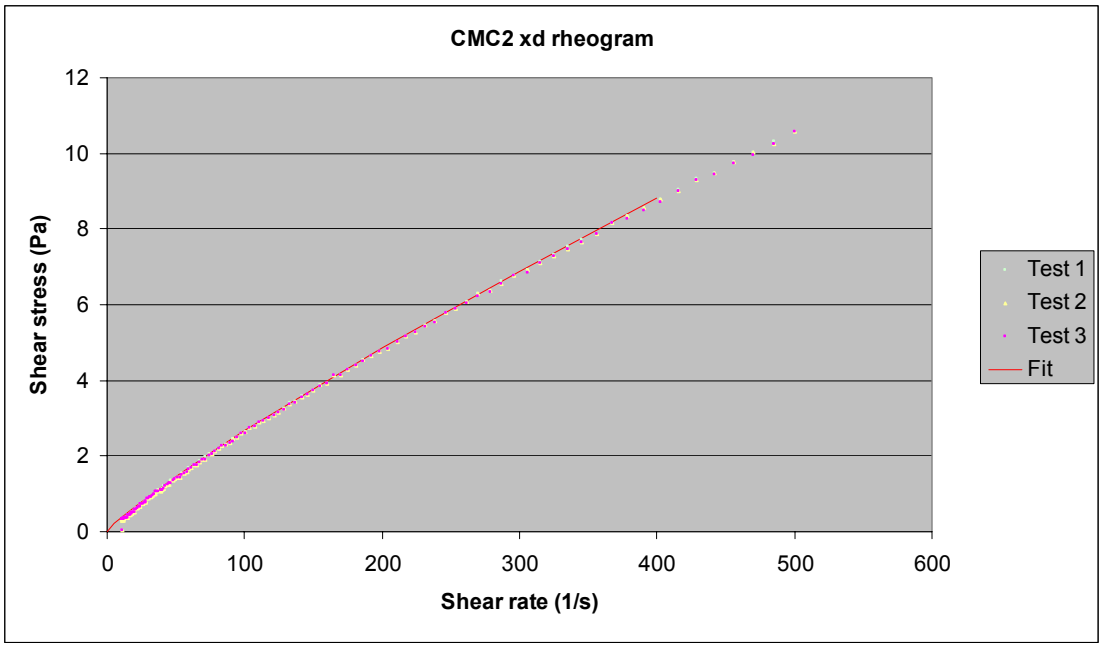

Figure 197. Rheograms with model fit for the "CMC2 xd" fluid used in the small flume

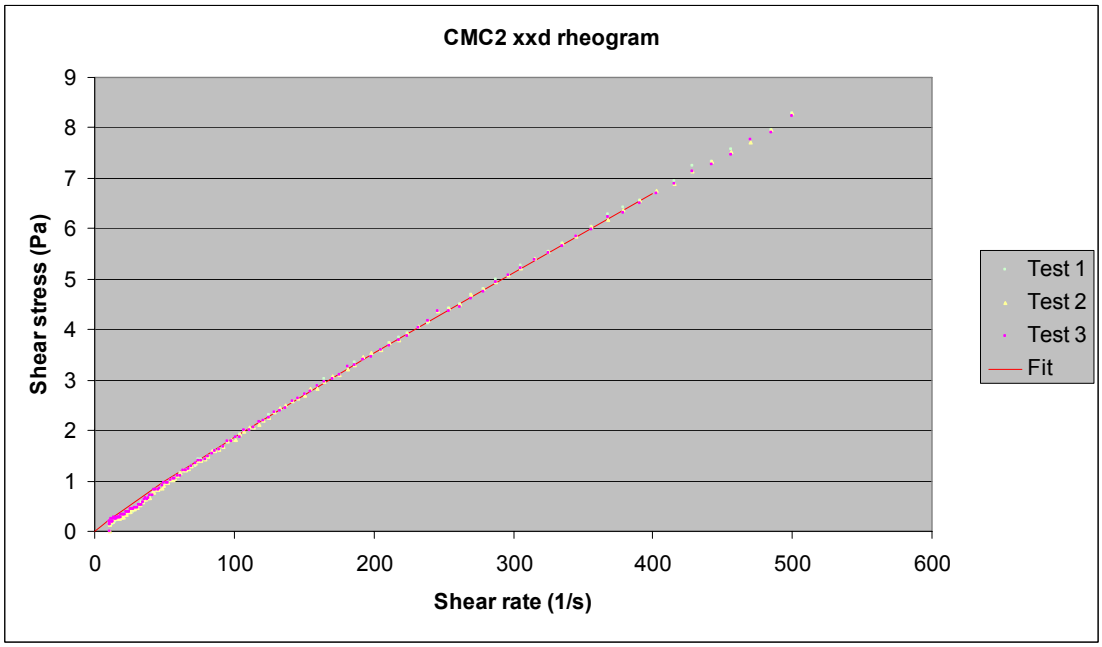

Figure 198. Rheograms with model fit for the "CMC2 xxd" fluid used in the small flume

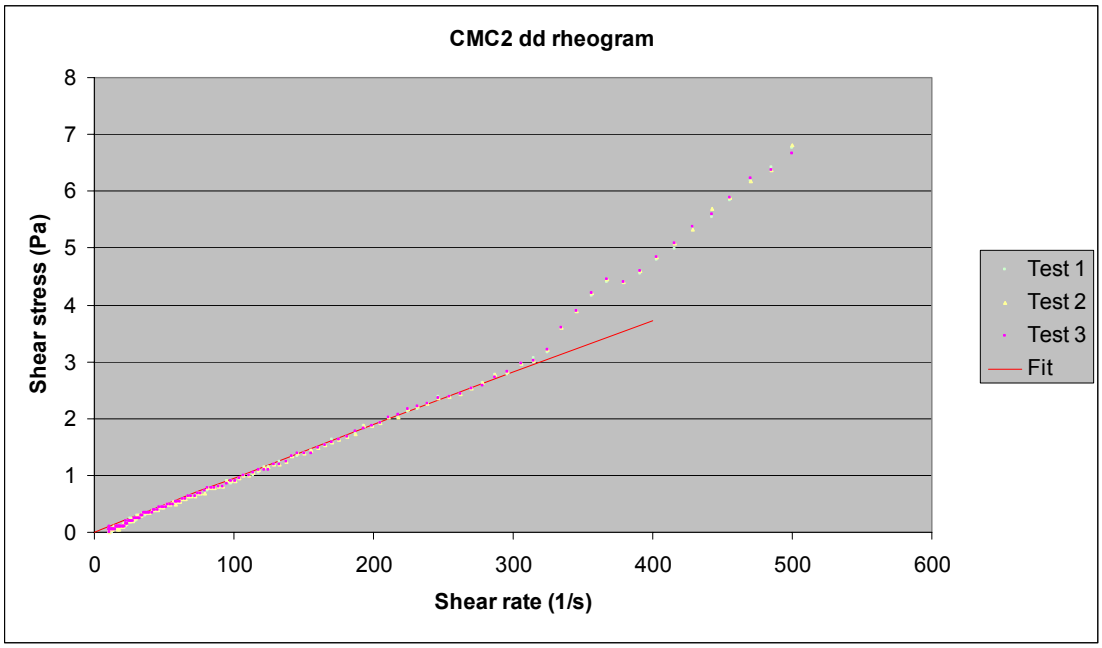

Figure 199. Rheograms with model fit for the "CMC2 dd" fluid used in the small flume

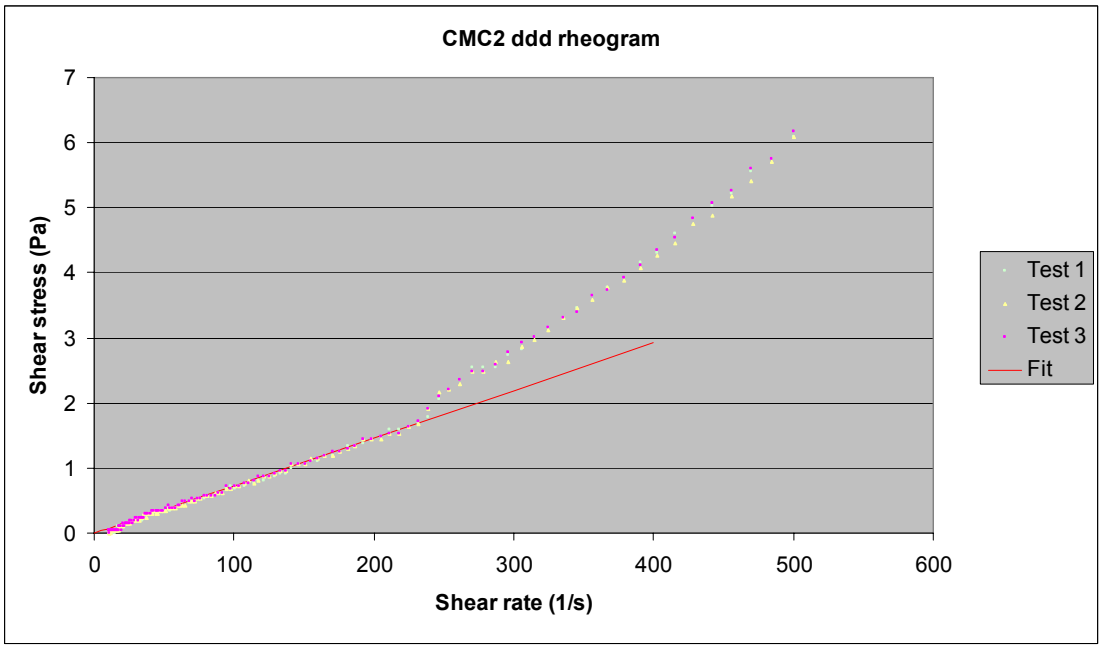

Figure 200. Rheograms with model fit for the "CMC2 ddd" fluid used in the small flume

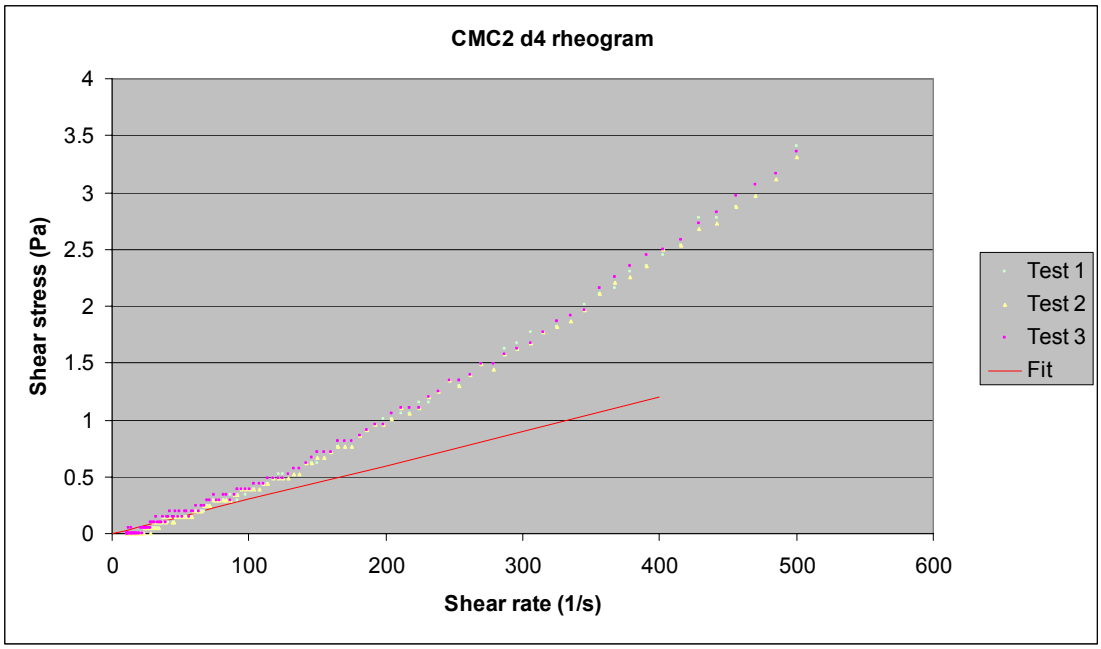

Figure 201. Rheograms with model fit for the "CMC2 d4" fluid used in the small flume

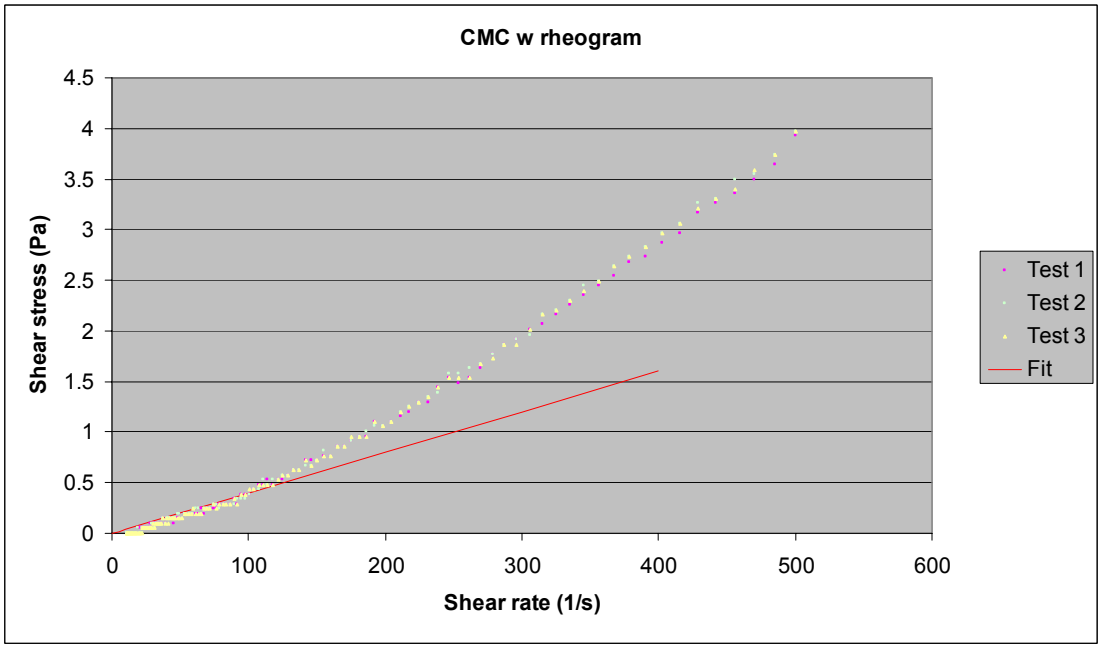

Figure 202. Rheograms with model fit for the "CMC w" fluid used in the small flume

Appendix K: Water density adjustment for temperature

The following density data, presented by W.L. Switzer of the North Carolina State University, was accessed on the internet on the 8th March 2007 from the following URL: http://www.ncsu.edu/chemistry/resource/H2Odensity_vp.html

Density of Water

Temperature	Density	Empirical fit
°C	g/mL	g/mL
15	0.999103	0.999096154
16	0.998946	0.998937179
17	0.998778	0.998767949
18	0.998599	0.998588462
19	0.998408	0.998398718
20	0.998207	0.998198718
21	0.997996	0.997988462
22	0.997774	0.997767949
23	0.997542	0.997537179
24	0.9973	0.997296154
25	0.997048	0.997044872
26	0.996787	0.996783333
27	0.996516	0.996511538
28	0.996237	0.996229487
29	0.995948	0.995937179
30	0.99565	0.995634615

W. L. Switzer
Department of Chemsitry - 8204
North Carolina State Unversity
Raleigh NC 27695
(919) 515-2945

Table 48. Water SG at various temperatures, with the Switzer data in the "Density" column and the empirically fitted data in the "Empirical fit" column.

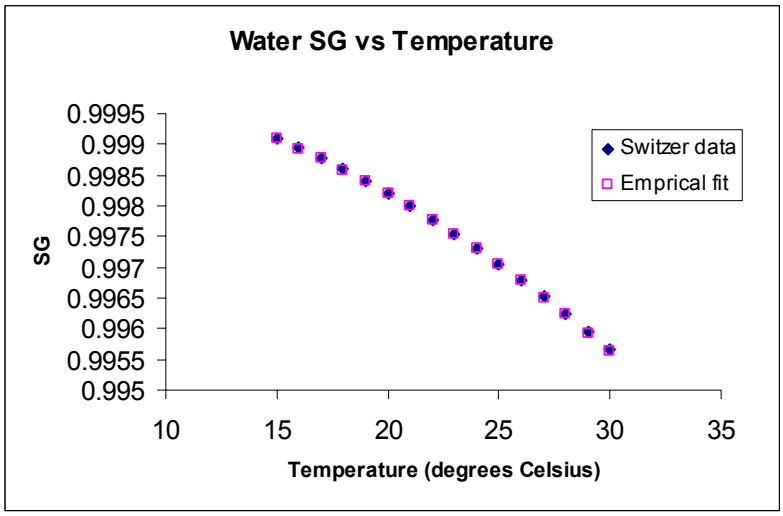

Figure 203. Plot of the Switzer data with the empirically fitted data overlaid to demonstrate the good fit of the empirical fit equation, presented below.

The equation for the empirical fit is as follows:

$$SG_{water} = 1.00025 - \frac{T^2}{195000}$$

Appendix L: Private communication from A. Chryss

Tim,

In reference to your request for the equations used to calculate the *h* coefficients in the channel shape equation (shown below):

$$x = y_0(h_0(y/y_0)^{0.5} + h_1(y/y_0)^{1.5} + h_2(y/y_0)^{2.5})$$

These coefficients were derived with the use of a Taylor series expansion. The first 3 terms in this series are sufficient to define a channel shape that serves in the slope predictions. These 3 terms are as follows:

$$h_0 = (2/t^2 - 2)^{0.5}$$

$$h_1 = 1/6(2/t^2 - 2)^{0.5}(-1/t^2 - (t^2 - 1)/(4t^2))/(1/(2t^2) - 1/2)$$

$$h_2 = 1/5(2/t^2 - 2)^{0.5}((0.5(1/(2\ t^2) - (3 + t^2)/(8t^2))/(1/(2t^2) - 0.5) \ \ldots$$

$$-(-1/t^2 - (t^2 - 1)/(4t^2))^2/(8(-0.5 + 1/(2 * t^2))^2)))$$

$$t = \frac{\tau_y}{(\rho g y_0)}$$

where t is the dimensionless mass yield stress of the bed material, τ_y is the yield stress of the bed material, ρ is the density of the bed material, and g is gravitational acceleration.

Regards,

Andrew.

Appendix M: Seddon data set

The Seddon data set was presented at the Paste 07 conference on Paste and Thickened Tailings in Perth in March 2007 by its editor, Keith Seddon, Technical Manager of Australian Tailings Consultants. The data set consists of tailings discharge and beach slope data from some 30 mines around the world, most of which has been dredged from published literature.

Mine	Location	Ore Type	Year Commenced	Status	Typical Throughput
					Mtpa
Kidd Creek	Canada	Copper/zinc	1973	Active	2.92
Elura (Endeavour)	NSW, Australia	Zinc	1981	Active	1.0
Argyle	WA, Australia	Diamond	1985	Decommissioned	3.3-6.5
Peak	NSW, Australia	Gold	1992	Active	0.4
Union Reefs	NT, Australia	Gold	1995	Closed 2001	2.0-3.0
McArthur River	NT, Australia	Lead	1995	Active	2.4
Cluff Lake	Saskatchewan	Uranium	1995	Closed 2002	0.32
Ernest Henry	Qld, Australia	Copper	1997	Active	7.0
Mount Keith	WA, Australia	Nickel	1997	Active	10.5
Blendevale (Pillara)	WA, Australia	Lead	1998	Closed	1.5
Warkworth #2_ Redbank	NSW, Australia	Ash	1998	Active	0.1
Ekati	Canada	Diamond	1998	Active	1.6
Strathcona.	Canada	Nickel	1998	Active	0.5
Century	Qld, Australia	Zinc	1999	Active	4.3
Sunrise Dam	WA, Australia	Gold	2000	Active	3.6
Bulyanhulu	Tanzania	Gold	2000	Active	0.7
Myra Falls	Canada	Copper/zinc	2003	Active	
Osborne	Qld, Australia	Copper / gold	2004	Active	1.34
Cobriza	Peru	Copper	2004	Active	1.8
Miduk	Iran	Copper	2005	Early operations	4.8
Sar Cheshmeh	Iran	Copper		Design Stage	32
					32
In-Pit Disposal Schemes:					
EKAPA	S.Africa	Diamond	2002	Active	0.8
Pajingo	Australia	Gold	2002	Active	0.73
Kimberley	S.Africa	Diamond	2003	Active	8.6
Gove	NT, Australia	Bauxite	1972	Active	
Vaudreuil (Jonquiere)	Canada	Bauxite	1987	Active	0.45
Alcoa Kwinana	WA, Australia	Bauxite	1989	Active	1.9
Alcoa Pinjarra	WA, Australia	Bauxite	1987	Active	3.3
Alcoa Wagerup	WA, Australia	Bauxite	1991	Active	2.2
Aughinish	Ireland	Bauxite	1993	Active	1.7

Figure 204. The Seddon data set (sheet 1 of 4)

Mine	Tailings Properties					
	SG	Particle Size			Plasticity	
		d_{85}	d_{50}	d_{10}	LL	PI
Kidd Creek						
Elura (Endeavour)						
Argyle		8000	1000	6		
Peak						
Union Reefs		75	55	25		
McArthur River						
Cluff Lake	2.7					
Ernest Henry	3.3	170	45	14	24	0
Mount Keith						
Blendevale (Pillara)						
Warkworth #2_ Redbank						
Ekati	2.7					
Strathcona.	2.9	~40				
Century	2.82	50	9	<1	26	11
Sunrise Dam						
Bulyanhulu		80	25	5		
Myra Falls						
Osborne	3.5	200	70	20		
Cobriza	3.73		<35			
Miduk		120	35	1		
Sar Cheshmeh		130	45	2	28	10
In-Pit Disposal Schemes:						
EKAPA	2.65					
Pajingo		~50				
Kimberley		400	75	~2		
Gove						
Vaudreuil (Jonquiere)	~3.0					
Alcoa Kwinana	~3.1					
Alcoa Pinjarra	~3.1	<50	4	<2		
Alcoa Wagerup	~3.1					
Aughinish						

Figure 205. The Seddon data set (sheet 2 of 4)

Mine	Thickener Details				Flocculent Type	Flocculent Rate
	Type	Number	Diameter	Unit Loading		
			m	$t/m^2.hr$		g/t
Kidd Creek	High Compression	1	35	0.37	Percol445+Lime	20 to 25
Elura (Endeavour)						
Argyle						
Peak	High rate	1	8	0.97		10 to 15
Union Reefs	High rate	1				
McArthur River						
Cluff Lake	HD	1	26	0.02		
Ernest Henry	High Compression	1	70	0.22		
Mount Keith						
Blendevale (Pillara)						
Warkworth #2_ Redbank						
Ekati	High rate, deep cone (Ecat)	2	12	0.86		
Strathcona.	High rate, deep cone (Ecat)	1	10	0.23	MF351+lime	20
Century	High rate	1	45	0.33		32 to 38
Sunrise Dam	High rate	1	24	0.97	Nalco 83370	19
Bulyanhulu	Other, refer text					
Myra Falls	Paste	1	25			
Osborne	High rate	1	9	0.77		
Cobriza	Paste	1	14	0.43		35
Miduk	Paste	4	16	0.73	Percol 727	25 to 30
Sar Cheshmeh	Paste	12	25	0.66		
		6	40	0.52		
In-Pit Disposal Schemes:						
EKAPA	Paste	1	15	0.17		80-100
Pajingo	Paste	1	14	0.17		
Kimberley	Paste	5	15	0.36		<50
Gove						
Vaudreuil (Jonquiere)	Paste	1	12	0.49		
Alcoa Kwinana	High Compression	1	50	0.12		60
Alcoa Pinjarra	High Compression	1	90	0.06		50-80
Alcoa Wagerup	High Compression	1	70	0.07		60
Aughinish	Other, refer text					

Figure 206. The Seddon data set (sheet 3 of 4)

Mine	Slurry Density	Disposal Scheme	Beach Slope		Reference
			Max	Range or Typical	
	% Solids		%	%	
Kidd Creek	63	Stack	2.5	1.5	Lord, 2003
Elura (Endeavour)	60	Segmented stack	1.7		Williams & Seddon, 1999
Argyle	72(??)	Segmented stack	10 target		McMahon et al, 1996
Peak	55-62	Stack	2.5 +	1.5-2.0	Williams & Seddon, 1999; ATC Internal
Union Reefs	<55	Down valley	0.9		Williams & Seddon, 2003
McArthur River	60	Stack	1.0		Williams & Seddon, 1999
Cluff Lake	52	Down valley	3.0		Lord,2003
Ernest Henry	75	Stack	1.1		Williams & Seddon, 1999
Mount Keith	44	Multiple stack	2.0		Williams & Seddon, 1999
Blendevale (Pillara)	65	Stack	1.5		Williams & Seddon, 1999
Warkworth #2_ Redbank	70	Side hill	5.0		ATC Internal
Ekati	40	Surface	1.0	1	Lord,2003
Strathcona.	45		1.5	1.25 - 1.5	Paste,2006
Century	52-58	Down valley	1.0	0.6-1.0	Murphy,2006
Sunrise Dam	64	Stack	2.0	1.0-2.0	Williams & Seddon, 2004
Bulyanhulu			10 max		Landriaut, 2000
Myra Falls	65-68		3.0		Lord,2003
Osborne	72-76	Stack	4.0	3	McPhail et al 2004, Brent and Dobb, 2006
Cobriza	77	Valley / side hill			V.Gonzales (D.O.E) Paste 2005, p261+
Miduk	63	Down valley	2.5		ATC Internal
Sar Cheshmeh	60+	Down valley			ATC Internal
In-Pit Disposal Schemes:					
EKAPA	53-57	In Pit			Hohne et al, 2004
Pajingo	59-61	In Pit			Gregory, 2003
Kimberley	44-57	In Pit	1.5	1	Houman & Johnson, 2003
Gove					
Vaudreuil (Jonquiere)	45		4.0	3.0-4.0	Lord,2003
Alcoa Kwinana	50	Dry Stacking	1.2	1.0 - 1.2	Cooling, 2000
Alcoa Pinjarra	50	Dry Stacking	1.2	1.0 - 1.2	Cooling, 2000
Alcoa Wagerup	50	Dry Stacking	1.2	1.0 - 1.2	Cooling, 2000
Aughinish	63	Dry Stacking	2.7	1.5 - 2.7	Paste 2006

Figure 207. The Seddon data set (sheet 4 of 4)

Appendix N: Rheometric correction

This appendix reports on the application of rheometric correction methods to the Couette rheometry data for one of the Sunrise Dam tailings slurry samples. The need for such corrections arises from both the fluid properties and the rheometer geometry differing from the assumed uniform shearing that occurs between two parallel flat planes. It has been noted that non-Newtonian fluids with high yield stresses can stick to the surface of the cup in a Couette rheometer due to the yield stress of the fluid being greater than the shear stress experienced in the fluid at some distance from the rotating bob, causing the sheared zone to be reduced to a distance less than the gap between the bob and the cup. This effect is increased in a rheometer with a large gap in relation to the diameter of the bob, since the shear rate experienced by the fluid at the bob surface becomes increasingly greater than that experienced at the outer wall of the rheometer.

Some attempt was made to apply corrections to the rheometric data gathered for a sample of Sunrise Dam tailings in the Contraves Rheomat rheometer at a concentration of 60.6 % w/w (see section 3.3.13 for details of the rheometry). Two rheometric correction methods for Couette geometry were used to adjust the shear rate of the rheometric data; the Krieger Maron method and the Power Law method.

The equation for the Krieger Maron correction method follows as an infinite series (de Hoog & Anderssen 2005):

$$f(\sigma) = 2\sum_{j\geq 0} s^{2j}\Omega'(s^{2j}\,\sigma) \qquad , \quad \Omega' = \frac{d\Omega}{d\sigma}$$

where Ω is the angular velocity of the bob, and σ is the local shear stress in the fluid, given by (de Hoog & Anderssen 2005):

$$\sigma = \frac{M}{2\pi {R_b}^2 L}$$

where M is the torque applied to the bob, R_b is the radius of the bob, and L is the length of the bob.

The Power Law correction method (de Hoog & Anderssen 2005):

$$\gamma(\sigma) = \frac{2\lambda\Omega(\sigma)}{1 - s^{-2\lambda}} \quad , \quad \lambda = \sigma\frac{\Omega'(\sigma)}{\Omega(\sigma)}$$

The adjusted data from the application of these two correction methods is presented graphically in Figure 208 alongside the uncorrected rheometer output data to provide some comparison between them.

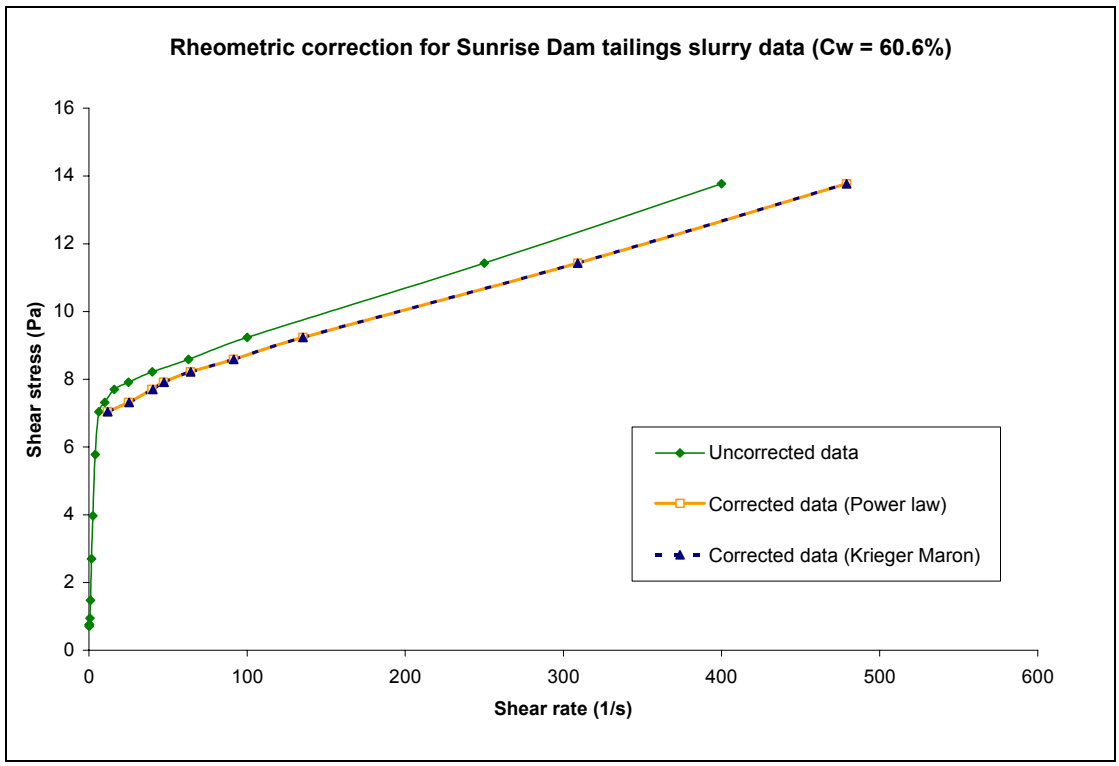

Figure 208. Graph comparing raw Couette rheometer data to geometrically corrected data, with the Krieger Maron and Power law correction methods applied.

From Figure 208 it can be seen that the Krieger Maron correction is almost identical to that yielded by the Power Law method. Using either method, the amount of correction equates to less than the experimental noise inherent in the raw data, which was calculated at ±17% of the measured shear stress within 95% confidence limits. (see Appendix G for experimental error analysis). Due to this relative insignificance, it was recognised that any effort to correct the rheometric data would add no value to the data, so rheometric corrections were not applied to any other rheometric data.

Appendix O: Shear rate investigation

This appendix investigates the range of shear rates that occurred in the open channel flow experiments that were reported in Chapter 3 of the thesis.

The shear rate for each experimental flow was calculated using the same approach as that discussed in section 4.4.13 of the thesis; Wasp et al. (1977) asserted that the shear rate in a pipe flow is equal to $8V/D$, where V is the average velocity of flow and D is the pipe internal diameter. Consistent with the work of Haldenwang & Slatter (2002), the equivilant diameter D of an open channel is equal to $4R_H$, where R_H is the hydraulic radius of the channel. Multiplying these two equations, we find that the shear rate in an open channel is equal to $2V/R_H$.

The shear rate was calculated with this equation for the 49 runs recorded in the field flume and the 95 runs recorded in the small lab scale flume. A plot of the resulting shear rates follows:

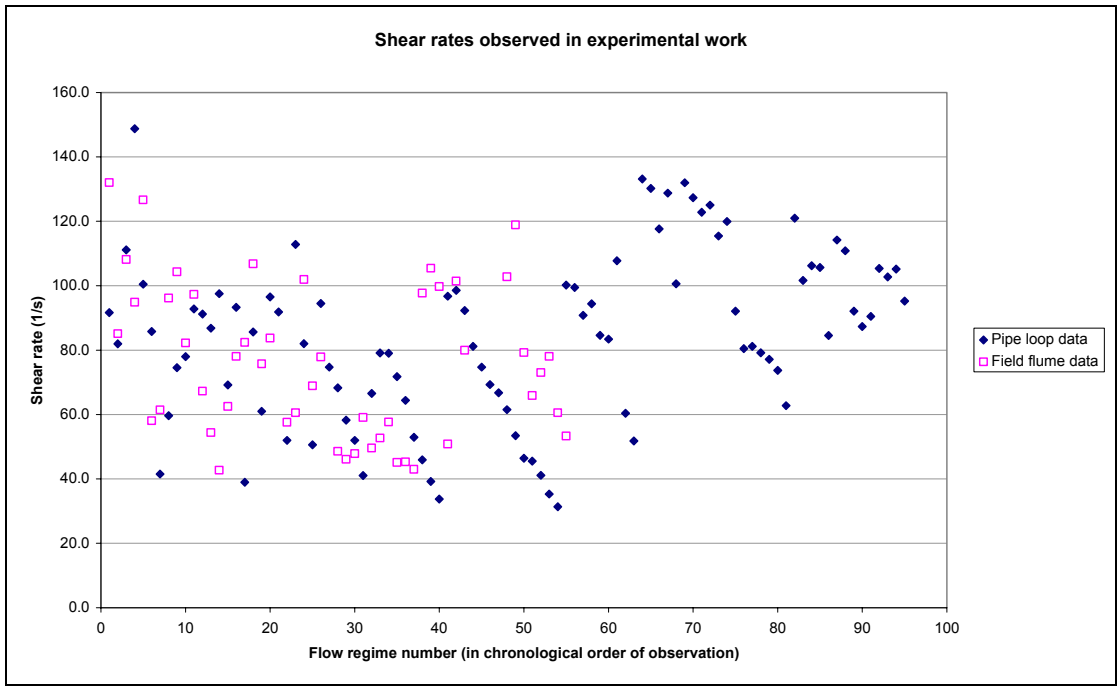

Figure 209. Plot of the shear rates observed in the flume experiments described in Chapter 3.

Figure 209 suggests that the typical shear rates found in the type of open channel flows that occur on a tailings beach range between 40/s and 140/s.